THE INFLUENCE OF CHLORIDE ON THE THAUMASITE FORM OF SULFATE ATTACK IN MORTARS CONTAINING CALCIUM CARBONATE

by

SANDRO MARDEN TORRES

A THESIS PRESENTED FOR THE DEGREE OF DOCTOR OF PHILOSOPHY

DEPARTMENT OF CIVIL AND STRUCTURAL ENGINEERING
CENTRE FOR CEMENT AND CONCRETE
FACULTY OF ENGINEERING
THE UNIVERSITY OF SHEFFIELD

AUGUST 2004

Acknowledgements

I should like to thank CAPES (Coordenação de aperfeiçoamento de Pessoal de Nível Superior-Ministério da Educação – Brasil) for the provision of my scholarship for the development of this research.

I should also like to thank Dr Cyril Lynsdale, Prof. R.N. Swamy and Prof. J.H. Sharp for offering me the conditions to work in a highly multidisciplinary environment of research. I could not be more grateful for all the encouragement, scientific advices and guidance, which helped me to be enthusiastic about researching on important issues concerning the durability of Portland cement all the way throughout the course of this research.

I would like to acknowledge and thank the dedication of all technical and clerical staff of the Department of Civil and Structural Engineering, Department of Mechanical Engineering and Department of Engineering Materials at the University of Sheffield, which provided the conditions for a high quality and effective working environment.

To all my fellow PhD students, thanks for your friendship and companionship.

I am thankful to Dr. Normando Perazzo Barbosa for all the dedication and effort towards my work.

Finally, I should thank to my parents, relatives and friends in Brazil. There are those who may not have a chance to read these acknowledgements, but their invisible contribution to this work will not be forgotten.

Abstract

Chlorides have been reported to be present in several field cases where thaumasite attack has occurred. However, no published systematic research dealing with the role of chloride in the thaumasite form of sulfate attack could be found in the literature. This research project has been designed through a comprehensive experimental programme to address this issue. This investigation studies the following: the formation of thaumasite in long-term exposure of carbonated systems to sulfate environment; whether or not the presence of chloride affects the thaumasite form of sulfate attack (TSA); the effect of long-term and short-term carbonation on the precipitation of thaumasite; the composition of thaumasite formed in chloride containing solutions; the chloride binding capacity of thaumasite-affected cement matrix; and the use of metakaolin to prevent TSA in carbonated mortar.

Mortar samples were cast using siliceous sand and Portland cement replaced by different amounts (0, 5 and 15%) of limestone filler, and by 10% metakaolin. Mortar cubes were subsequently stored in deionised water, magnesium sulfate solution, combined sulfate and sodium chloride solution and simulated seawater at 5°C and 20°C. Long-term specimens consisted of Portland cement mortars containing 15% limestone filler, which were exposed to atmospheric carbonation at 5 and 20°C for 5 years, were also immersed in these salt solutions at both temperatures. The mortar cubes were examined regularly every month, and the results of visual assessment recorded. The mineralogy of the deteriorated products was determined by x-ray diffraction (XRD), infrared spectroscopy (IRS). The pH of the solutions was also measured periodically. The composition of the thaumasite and the deteriorated cement matrix was assessed by means of the determination of the unit cell parameters of the crystal, by quantitative infrared spectroscopy (IRS); scanning electron microscopy (SEM); backscattered electron image (BEI) and chemical analyses by energy dispersive X-ray and quantitative x-ray microanalyses.

The results indicate that the effect of chloride on sulfate attack is affected by temperature, because it affects the solubility of some minerals and increases the activity of carbonates. At 20°C, the presence of chlorides appears to mitigate sulfate attack by combining with the aluminates of the cement forming Friedel's salt. At this temperature, the main carbonate phases were calcite and aragonite, whereas thaumasite was predominant in all samples at 5°C, which caused damage that increased with increase in the chloride concentration in solution and the carbonate content, as evidenced by increased loss of mass and pH. Because of the demand for an alkaline environment, thaumasite did not precipitate within the long-term carbonated surface areas, but immediately underneath. The formation of thaumasite was not prevented in carbonated specimens after short-term. In the presence of chloride, thaumasite precipitated with lower lattice parameter *c*, indicative of a higher carbonate to sulfate ratio, and its composition shifted towards the thaumasite end-member of the solid-solution series. Thus, chloride does not seem to enter into thaumasite crystal structure. In addition, the chloride binding capacity of thaumasite-affected areas of the cement is reduced as the residual CSH phase both decalcifies and loses its silicon to give place to the deposition of thaumasite. The performance of metakaolin containing mortars in salt solutions was improved by the pozzolanic effect, but also by an increase in the chloride binding capacity, which reduced the deleterious effect of the chloride on the formation of thaumasite. However, metakaolin-containing samples in magnesium sulfate developed some signs of damage that were detected after 18 months.

The interaction between chloride and other ionic species on thaumasite formation in the cement matrix is very complex, and can have some implications to the $CaCO_3$ threshold for durable concretes under TSA prone environments and also to the steel corrosion of concrete reinforcement.

Table of Contents

List of Figures

List of Tables

Cement Chemistry Notations

Oxides

C=CaO	S=SiO_2	H=H_2O	$\overline{S}$=SO_3
A=Al_2O_3	M=MgO	$\overline{C}$=CO_2	F=Fe_2O_3

Portland cement and some other main phases

Formula	Phase name
C_3S	Tricalcium silicate (Alite)
C_2S	Dicalcium silicate (Belite)
C_3A	Tricalcium aluminate (Celite)
C_4AF	Tetracalcium alumino ferrite
CSH	Calcium silicate hydrate
CH	Calcium hydroxide (Portlandite)
$C\overline{C}$	Calcium carbonate (Calcite, Aragonite)
MH	Brucite
$C\overline{S}H_2$	Gypsum
$C_3A3C\overline{S}H_{32}$	Ettringite
$C_3A.C\overline{S}H_{12}$	Monosulfate
$C_3A.C\overline{C}_{0.5}H_{12}$	Hemi-Carboaluminate hydrate
$C_3S\overline{C}\,\overline{S}H_{15}$	Thaumasite
$C_3A.CCl_2.H_{10}$	Friedel's salt (Monochloride)
C_3AH_6	Calcium aluminate hydrate (Hydrogarnet)
NaCl	Halite
$M\overline{S}$	Epsom salt
AH_3	Aluminate hydrate (Gybbsite, bohemite)

Nomenclatures

OPC	Ordinary Portland Cement
PLC	Portland Limestone Cement
AFm	Calcium (Aluminium-Ferrite) Mono- Sulfate phases, such as monosulfate and Friedel's salt
AFt	Calcium (Aluminium-Ferrite) Tri-Sulfate phases, such as ettringite
MAC	Minor Additional Constituent
TSA	The Thaumasite form of Sulfate Attack
TF	Thaumasite formation
XRD	X-ray Diffraction
IRS	Infrared Spectroscopy
EDX	Energy Dispersive X-ray
QXMA	Quantitative X-ray Micro-Analyses

Chapter One

INTRODUCTION

1.1. Background

The thaumasite form of sulfate attack (TSA) is a chemical interaction between concrete and sulfate ions that can causes severe durability problems in practice. This form of attack has been receiving great attention from both academics and practising engineers in the past decade. Indeed, more than 100 papers have been published in the past five years, which account for mechanisms, durability of binders and field cases.

The main reason for such increased interest in TSA can be attributed to the recent discovery of thaumasite being responsible for the deterioration of important underground structures, such as columns in the Canadian Arctic in 1995 [1], the foundations of bridges on the M5 motorway in the UK in 1998 [2], and several tunnels around Europe [3, 4]. In the past, the incidences of thaumasite were restricted to grouts[5], renders[6], brick mortars and historic buildings [7]. There have been some reports of thaumasite in concrete structures under seawater [8]. These past experiences appeared not to be sufficient to generate the current level of concern and interest.

The aggressiveness of TSA is caused by the fact that not only are portlandite and aluminate hydrate phases attacked, but also all the hydrated and unhydrated cement clinker phases take part in the reaction to form thaumasite [9-11]. Portlandite and aluminate hydrates, such as monosulfates, are common hydrated phases of the cement matrix that react with sulfate ions coming from groundwater to form gypsum and ettringite; both of these are detrimental to concrete for destroying binding properties, and being expansive during crystallization [12]. The type of attack involving these phases is often called convetional sulfate attack. Nevertheless, cements that were designed to resist convetional sulfate attack, such as sulfate-resisting Portland cement (SRPC), are no longer assured to perform well in conditions susceptible to TSA. The TSA affected concrete totally loses its integrity, as the phase responsible for the binding properties of the concrete, the calcium silicate hydrate (C-S-H), is consumed during the

reaction to form thaumasite. The end product is then a white, incohesive, loose mushy material that can be removed with bare hands.

However, not all environments lead to TSA. The main risk factors leading to TSA have been reported by the Thaumasite Expert Group (TEG), composed of scientists, engineers and members from the concrete industry, and set up by the UK Ministry for Construction [2]. By examining field cases and research up to 1999, it was concluded that the primary risk factors are: (i) sources of carbonate, silicate, and sulfate; (ii) wet environment and cold temperature, below 15°C.

Research reported after 1999 mostly agree with such risk assessment. However, the mechanism of thaumasite formation is not completely understood, for there are several aspects that have not been adequately investigated. For instance, it is not known whether ettringite, which can occur as a result of conventional sulfate attack, turns into thaumasite via a topochemical or through solution mechanism. Also, there are reports where thaumasite has occurred at temperatures above 15°C. Moreover, it has been pointed out that using an internal source of carbonates in the cement in structures exposed to sulfate-containing underground environment adversely affects the long-term durability of concretes [11, 13], although the European standard EN 197:2000 allows the replacement of clinker by up to 5% in several Portland cements, and allows between 2 to 10% of the aggregate by calcium carbonates in the SD-1 [14].

Another uncertain aspect of TSA is whether chlorides play any role in the interaction process. The detrimental role that chlorides play in inducing corrosion of steel reinforcement is well known and established. In TSA-affected concrete, it has been reported that the concentration of chloride around the reinforcement has negatively affected the overall damage of the structure due to corrosion. Indeed, chloride species have been identified in the most severe cases of TSA [15, 16], which originated predominantly from deicing salts, but also, from seawater in some cases [16, 17]. Nevertheless, the current view reported by the TEG, which is reflected in the standards for concrete under aggressive environment, is that the presence of chloride mitigates sulfate attack [14].

A literature survey reveals that although extensive work has been done on the mechanisms of thaumasite formation, field occurrences of TSA, and engineering performance of cementitious binders exposed to TSA, no systematic studies on the role of chlorides on TSA have been reported. An experimental programme has therefore

been designed to address some of the principal questions that have arisen from such a review. The main objectives of this study are:

1. To investigate changes in the microstructure of Portland cement mortars immersed in magnesium sulfate solution at 5°C for 5 years;

2. To evaluate whether or not chloride plays any role in the formation of thaumasite;

3. To investigate the extent to which atmospheric carbonation affects the formation of thaumasite;

4. To study the effectiveness of metakaolin in Portland limestone cements exposed to sulfates, and combined chloride and sulfate solutions at different temperatures;

5. To assess whether or not the chemical composition of thaumasite is affected by the presence of chlorides;

6. To analyse the effect of thaumasite on the chloride binding capacity of the cement matrix in cement, containing limestone filler.

1.2. Structure of the thesis

The thesis is organised in general terms to follow the main objectives of this project. The literature review is presented in Chapter 2. The overall experimental programme is described in Chapter 3. The following chapters are presented in the format of journal papers; some repetition may therefore be expected in the introduction and in the description of some test methodology details reported in each chapter. All the conclusions reached are fully self-supported within each chapter, as individual pieces of research. However, in order to give a full account of all the observations and experimental details, these chapters are generally longer than typical journal papers.

Chapter 4 is entitled *Microstructure of Portland-limestone cement mortars damaged by formation of thaumasite*, which addresses objective 1 of this thesis. In this chapter, features of the microstructure of limestone containing mortar exposed, long-

term, to cold sulfate solution have been examined. The evolution of the attack was discussed and analysed elsewhere [13, 18].

In Chapter 5, entitled *Performance of Limestone filler and metakaolin containing Portland cement mortar under combined chloride and sulfate exposure,* objectives 2 to 4 are discussed, as well as other aspects affecting the mechanisms, such as the solubility of some minerals and pH. Objectives 5 and 6 are studied in Chapter 6, which is entitled *Effect of Combined Chloride and Sulfate on TSA: Microstructure and Micro-analytical results.*

An overall discussion of the whole research is presented in Chapter 7, and the overall conclusions derived from this study are reported in Chapter 8. These two last chapters are not written in paper format, but they account for the main features of the findings some of which are reported in the various chapters.

Chapter Two

LITERATURE REVIEW

2.1 Introduction

Portland cement concrete is one of the largest used materials worldwide due chiefly to its ability to conform to most modern architectural concepts whilst at the same time being able to endure the exposure to various aggressive environments. However, modern society, more aware of the impact that mismanagement of natural resources can have on a global scale, not only demands extended serviceability of constructions by compliance of technical engineering requirements, but also the environmentally friendliness of processing the materials.

Indeed, such modern demands have been affecting the production and use of Portland cement in several ways. Firstly, the emission of industrial green house gases to the atmosphere, which is intrinsic to cement production, has become the subject of discussion internationally such as the Kyoto agreement of 1997. The production of Portland cement releases greenhouse gases during its production process, during grinding, fuel burning and the calcinations of its raw material. Secondly, along with the adverse effect on the climate, the prospect of other world oil crises, such as that experienced during the seventies, demands austere energy resource management. Thirdly, the emergence of common markets also brings the need for the unification of different standards for Portland cements, and the code of practice for safe construction. Indeed, different countries allow different limits for cement replacement materials, as well as different codes of practice, which can potentially hinder the advantages generated by a free commerce of services and commodities.

In this context, the beneficial impact that the use of some cement replacement materials has on energy saving, durable construction as well as the environment has been shared by researchers, cement manufacturers and engineers. This is confirmed by several examples of the successful use of industrial by-products such as ground granulated blast furnace slag, fly ash, silica fume, calcined clays (metakaolinite), and natural pozzolans in constructions throughout the world.

Indeed, these modern issues have also brought about the need to review and adapt old concepts such as restrictions on the use of non-cementitious (inert) material in 'pure' ordinary Portland cement (OPC), or minor additional constituents (*MAC*). In the past, the first British and American standards issued in 1904 regarded clinker replacement materials with great care, and considered, for instance, that any limestone filler in Portland cement should be treated as an adulterant in OPC [19]. This consideration prevailed in most countries as the amount of minor additional constituents in OPC was prohibited or limited to less than 5% in some European countries, for instance [20]. The modern approach is rather different. For instance, the standard ENV 197:1992 and the recently published BS EN 197:2001- Part 1 , which is currently used in European countries, allow the replacement of clinker by up to 5% as *MAC* and up to 35% limestone filler as Portland limestone cements [21].

2.2 The use of limestone filler in Portland cement

Indeed, the use of limestone filler replacing clinker has been differently recommended by independent standards in different countries: For instance, the amount of limestone filler in Portland cement could reach up to 35% for general use, and up to 5% for sulfate resisting cements in France , but in practice the use was usually smaller than 21% for strength class 32.5 [22]. In other European countries, before the publication of the unified EN 197:1992, filler was allowed to replace clinker as a minor additional constituent up to 5% in Ordinary Portland cement (OPC) [20]. In some countries such as France, Greece and Luxembourg limestone was allowed up to 3% replacement of OPC. In the UK, OPC could not contain *MAC* until the introduction of the EN 197:1992.

In Canada, the use of *MAC* has been limited to 5%, which since can be comprise of limestone filler, according the standard CAN3-A5-M83 [23]. However, the current American Standards do not allow such replacement in OPC (ASTM C 150-95) [19].

In Brazil, the standard (NBR-5732:1991) allows up to 5% of limestone filler in CP I (CEM I) and up to 10% in CPIIF32 (BS EN CEM II-L/A). In some areas such as the North and Northeast, where low industrial activity makes the use of industrial by-products very cost ineffective, the Brazilian cement industry operates mostly with CPIIF32 and CPZ32 (BS EN CEM IV/A), which can contain up to 10% and 14% of limestone and pozzolanic material, respectively.

However, it appears that higher use of limestone filler content in Portland cement will spread to other countries, following the European initiative [23].

2.2.1 Advantages of limestone filler in Portland cement

A. Environmental point of view

Among several favourable aspects, it has been reported that limestone is easily accessible to cement manufacturers, as it is usually available at the site of the cement plant quarries. Also, limestone requires less energy to grind than clinker, which improves the energy use in the production of cement [22]. Indeed, it has been found that the grinding time of cement production was reduced by up to 26% when 7.5% of the clinker was replaced by limestone filler [24].

Moreover, not only less energy is used to produce 1 ton of cement with the same performance of OPC, but also CO_2 emission is significantly reduced. Indeed, in conjunction with other indirect CO_2 emissions, the process of cement production such as fuel and grinding, the total CO_2 emission can reach about 85% to 100% ton per ton of clinker [25-27]. In this context, the replacement of clinker by fillers leads to an immediate reduction in CO_2 emission without any changes in the production process.

B. Limestone filler-cement interactions

Nevertheless, although its use appears to be comprehensibly favourable on the one hand, the effect of *MAC* or filler on the performance of concretes is not entirely understood. Indeed, limestone filler is not chemically inert in Portland cement, and its effect on the microstructure and durability of cement is still not completely known. There appears to be some uncertainties about how this type of filler affects the microstructure of Portland cement, especially with regard to long-term durability properties, which may partially explain the reason for such conservative use of higher quantities of limestone in cement.

Limestone filler interacts with the cement matrix by a combination of physical and chemical processes: by (i) filling the pores of the matrix and increasing density and tortuosity of the pore structure; (ii) improving hydration by offering sites for nucleation of hydrated products; and also (iii) reactions at the limestone-cement interface.

C. Effect of limestone filler on engineering properties

Soroka and Setter [28, 29], who investigated mortars containing up to 40% filler by mass of cement replacing the equivalent amount of sand, found that higher compressive

strength developed in filler systems than in plain OPC mortar. Because the performance of limestone filler was superior to that of other fillers at early ages, but virtually the same after 90 days, they attributed the development in strength to the 'filler effect' in which fine particles filled the pores of the cement matrix, and increased the density of the mortars, but not due to the formation of calcium carboaluminate hydrate ($C_3A.C\overline{C}H_{12}$) However, no technique was used to detect the presence of carboaluminte, which is a highly crystalline phase. Nonetheless, carboaluminate was assumed to have precipitated in the very fine limestone containing mortar, because the samples that developed higher strength showed lower bound water content, which seems unexpected since compressive strength increases as the hydration of cement increases according to Powers equation [30]. They concluded that such discrepancies could be explained by retardation of the hydration of C_3A, caused by the presence of the very fine limestone filler reacting to form carboaluminate. Indeed, carboaluminate hydrate contains less water than the monosulfate (Afm) or ettringite (Aft) phases. Hence, the chemical and physical effects of limestone filler could not be distinctly evaluated.

Capiteli and Florindo [24] found that there was a nominal decrease in the density of paste of approximately 1.9% when clinker was replaced by 15% of limestone. If only the difference in densities between clinker and limestone is considered, the reduction in density should be around 4.1%. Hence, this finding supports the view of a positive effect of limestone filler replacement on density as concluded by Soroka and Setter [28, 29] .

Hartshorn et al [31] performed tests on mortars containing up to 35% limestone filler. The water to binder (cement + limestone) ratio was kept constant in these experiments. It was found that replacements up to 15% did not present significant differences in the compressive strength, dynamic modulus of elasticity and ultrasonic pulse velocity when compared to the control OPC after one year in air at both 5 and 20°C. However, there were concerns with respect to the durability of limestone filler in sulfate environments.

D. Chemical reactions between limestone and clinker phases

The formation of reaction products at the filler particle-cement interface has also been considered as another factor concerning the improvements that limestone filler brings to the system.

For instance, Kakali et al. [32] found the precipitation of monocarboaluminate hydrate in limestone filler containing sample, with specific surface of approximately half of that of Soroka and Setter [28, 29]. Moreover, the extent of the chemical activity of limestone filler depends on the C_3A content and $CaSO_4/C_3A$ ratio [33, 34]. With low C_3A or high $CaSO_4/C_3A$ ratio, limestone appears to be inert with respect to its chemical activity with aluminates.

In a microstructure investigation in systems without C_3A, Monteiro and Mehta [35] identified that the formation of a smaller structure of $Ca(OH)_2$-$CaCO_3$ compound at the interface of limestone-cement matrix can be responsible for such potential increase in strength, since the smaller structure of this mineral would have a higher positive effect on strength than that of highly ordered crystals such as calcium hydroxide and carboaluminate hydrates.

As far as the interaction with the silicate phases is concerned, Pera et al. [36] investigated the effect of limestone contents up to 50% on the compressive strength of cement paste mini-cylinders. It was found that no significant difference in compressive strength occurred between the OPC control and OPC replaced with up to 20% $CaCO_3$ after 60 days. Also, it was reported that the compressive strength of binders containing replacement levels higher than 30% developed approximately 90% of OPC control strength after 60 days, despite higher water/cement ratio (~0.48 compared to 0.28 in OPC). Because carbosilicate hydrate phases precipitated in both $CaCO_3$-C_3S and $CaCO_3$-OPC with significant improvement in strength, it was concluded that the precipitation of such phases positively affected the mechanical performance of samples, particularly when the filler content was higher than 30%. This observation was more evident in C_3S paste samples, most likely because of the negative effect of $CaSO_4$ on the reactivity of calcite as identified by Ohba et al [33], which was present in OPC but not in alite-carbonate paste.

The chemical interaction of limestone filler through solution was also investigated by Tasong et al [37]. It was found that limestone released approximately 1% of its mass after 1 day under water and also that sodium and sulfate ions were consumed when limestone was diluted in cement solution. Limestone aggregate was then considered as chemically more stable than basalt, because there was no crystallisation of products due to chemical interaction with cement. This conclusion was based on X-Ray diffraction data, but it is pertinent to emphasise that the system was kept at 70° C in order to

accelerate the hydration of cement. At this temperature, it is known that some products such as monocarboaluminate can suffer changes to their crystal structures [38].

2.2.2 Durability of limestone filler containing concrete

In the case of reactivity at the interface of fine particles of filler and in the pore structure of cements, general improvement with respect to porosity and diffusion of ionic species should also be observed. However, there are different views with respect to the improvements of limestone to the pore system of cement.

On the one hand, Hormain et al. [39] had found that 20% limestone increased the total porosity in cement paste. This view was also shared by Zelic et al. [40] who reported that 20% limestone replacement increased the total porosity of mortars. Again, Irassar et al. [41] also reported that limestone increased porosity due to the formation of non-binding product during hydration. On the other hand, Heilkal et al [42] found that 20% filler reduced the total porosity when compared to OPC paste. Tsivilis et al. [43] also reported that the total porosity was reduced at all replacement levels, between 5 and 35%, in comparison to OPC mortar after 9 months.

These discrepancies are also reflected on the chloride diffusion properties of limestone filler cements, and published data show conflicting results.

Hornain et al [39] studied the chloride-binding capacity of cement paste and mortar containing 20% limestone filler replacing cement. It was reported that the limestone filler enhanced the chloride permeability in both the paste and mortar by contributing to the formation of indirectly connected pores. By studying chloride charge through a diffusion cell, Tsivilis et al. [43] found that a smaller chloride ionic charge was found in cements containing up to 20% limestone filler than in OPC. Despite this charge being significantly reduced, all mixes were considered as high-chloride permeable cements. This permeability was attributed to the high water to cement ratio used. Because the dissolution of calcium carbonates also generates negatively charged species such as carbonates and bicarbonates in solution, it becomes difficult to differentiate the contribution of chloride or carbonates to the total charge if both species diffuse to the cell when calcium carbonate concentration increases in the cement. Therefore, it is not clear whether this high chloride charge can be entirely associated to chloride diffusion. In addition, the mass loss of the reinforcement steel bar was ca. 60% smaller in 20 and 35% limestone cements than in pure OPC. On the other hand, Matthews [44] identified that although the rebar mass loss due to corrosion was not significantly great in all

mixes, a 25% limestone mix developed the most intense corrosion, which was associated with a higher carbonation depth in this mix. This observation is different from that of Tsivilis et al. [43], who reported lower carbonation depths in limestone containing mixes. However, Bonvetti et al. [45] reported that the effect of limestone on chloride penetration can be either positive, when air curing is used, or negative, in the case of wet curing. This was explained by the positive contribution of limestone toward cement hydration when water is absent in early ages of curing.

2.2.3 Sulfate attack in limestone filler containing concrete

As previously discussed, the chemical activities of calcium carbonate filler occur both at the surface and also in the cement pore solution; this is marked by an increase in the hydration of cement, and the formation of a refined transition zone filler-cement, in which cement hydration products precipitate. Hence, it is likely that sulfate ions can interact differently with these precipitated products around the interface depending on the stability of the precipitated products and the main mechanism governing this chemical attack.

Hooton [46] investigated the sulfate resistance of some commercial cements containing up to 4.7% limestone filler. Based on expansion tests in 5%Na_2SO_4, it was concluded that the presence of carbonates did not affect the performance of these cements (C_3A<10.4%) since no trend could be established with respect to carbonate content and expansion measurements, which was considered acceptable for a moderate sulfate resistance cement in most cases.

Matthews [44], who investigated the effect of the sulfate resistance of ifller cements at 20°C after 5 years, found no detectable difference in the performance of OPC and OPC containing 5% limestone filler in both sodium and magnesium sulfate solution (1.5% SO_3). It was found that the performance of these mixes was controlled by C_3A content of the cement. However, higher concentrations of carbonate filler in the cement (25%) performed either positively or negatively, depending on whether the concrete was immersed in sodium or in magnesium sulfate solutions. Interestingly, it was identified that some samples containing carbonate filler developed thaumasite, a different kind of sulfate product which is much more common in sulfate conditions at low temperature. It was also pointed out that the formation of thaumasite did not depend on carbonate content, as it was detected in both low and high carbonate content samples. Even OPC developed traces of this mineral, which lead to the conclusion that the carbonate sources

were likely to be either atmospheric carbonation or contamination from other carbonated samples inside the container.

Hartshorn et al. [31] identified a loss in strength of mortar samples containing limestone contents higher than 5% after one year in 1.8%$MgSO_4$ at 20°C. Hartshorn et al. [47] also found thaumasite in high carbonate content cement paste (35%) after 224 days in this solution.

Irassar et al. [41] presented similar findings for low carbonate filler content (<10%), in which no significant difference was observed after 9 months in 0.352M of Na_2SO_4 (~3.4% of SO_4^{2-}) at room temperature (about 20°C). However, it was found that even in the same conditions, the performance of 20% limestone replacement in low C_3A cement was worse than that of other mixtures after 90 days. This trend was explained by an increase in sulfate demand, due to a greater susceptibility of limestone cements to sulfate attack caused by abundant deposition of portlandite in the cement-filler transition zone, which is ultimately attacked by sulfate ions and forms gypsum.

Kakali et al. [32] found that limestone offered more stability to the ettringite, which was not converted into monosulfate in the calcium carbonate-cement systems. In fact, when in sulfate solution, monosulfate can be converted into secondary ettringite, which is accepted as a cause of expansion, and hence poses durability problems to the concrete. In that case, limestone would increase the durability of concrete exposed to such conditions.

2.3 Mechanisms of 'Conventional' Sulfate Attack

Sulfate attack is responsible for the loss of integrity of the cement matrix because hydration products of Portland cement undergo chemical changes in sulfate solutions. The term 'conventional' is used here to differentiate the attack caused by phases such as ettringite and gypsum rather than thaumasite.

In general, some hydration products of cement are not stable in sulfate solutions. For instance, in a simplistic way, when calcium silicate phases (C_3S and C_2S) of Portland cement hydrate, portlandite (CH) and calcium silicate hydrates ($C_3S_2H_3$) are generated, as can be seen in equations 2.1 and 2.2 . Both phases can be affected by sulfates according to equations 2.3 and 2.4 [48]. Gypsum ($C\bar{S}H_2$) and MSH are non-binding products, hence, the matrix loses its cohesiveness and disruption occurs. In the case of sodium or calcium sulfate, the end product would differ as neither brucite (MH)

nor M-S-H would precipitate, but sodium hydroxide would form instead. The formation of brucite has a two-fold effect. On the one hand, it reduces the pH below the stability of C-S-H, which leads to the total conversion of CSH into the non-binder MSH until completion [49], as shown in equation 2.4. On the other hand, the deposition of brucite at the surface helps to block the system, as reported by Buenfeld and Newman [50]. Indeed, it was found that high magnesium concentration altered the results of chloride diffusion in mortars in the diffusion cell test by blocking the surface with the formation of brucite.

Hydration of silicate phases:

$$2C_3S + 6H \rightarrow C_3S_2H_3 + 3CH \quad (2\text{-}1)$$

$$2C_2S + 4H \rightarrow C_3S_2H_3 + CH \quad (2\text{-}2)$$

Reaction with magnesium sulfate :

$$CH + M\bar{S}H_7 \rightarrow MH + C\bar{S}H_2 + 4H \quad (2\text{-}3)$$

$$C\text{-}S\text{-}H + M\bar{S}H_7 \rightarrow C\bar{S}H_2 + M\text{-}S\text{-}H \quad (2\text{-}4)$$

From the hydration of the aluminate phases present in Portland cement, ettringite ($C_3A.3C\bar{S}H_{32}$) is formed at early stages, but it is converted into monosulfate ($C_3A.C\bar{S}H_{12}$) at later stages. The overall reactions can be seen in equations 2.5 and 2.6. However, monosulfate converts into ettringite when the concentration of sulfates increases in the pore solution. This mechanism, as shown in equation 2.7, is expansive and causes disruption of the cement matrix. Although both monosulfate and ettringite can form from the hydration of tetracalcium aluminium ferrite (C_4AF) of the cement [51, 52], it is thought that the conversion of monosulfate into iron-rich ettringite is not as detrimental as the previous reaction. This explains why sulfate resistant Portland cement, which is rich in C_4AF and low in C_3A, performs well in sulfate environments [53].

The hydration of tricalcium aluminate occurs according to equations 2.5. The conversion of ettringite into monosulfate follows equation 2.6, and the formation of secondary ettringite due to sulfate attack occurs as shown in equation 2.7 [12, 54].

$$C_3A + 3C\bar{S}H_2 + 26H \rightarrow C_3A.3C\bar{S}H_{32} \quad (2\text{-}5)$$

$$C_3A3C\bar{S}H_{32} + 2C_3A + 4H \rightarrow 3C_3A.C\bar{S}H_{12} \quad (2\text{-}6)$$

$$C_4A\bar{S}H_{12} + 2C\bar{S}H_2 + 16H \rightarrow C_3A.3C\bar{S}H_{32} \quad (2\text{-}7)$$

As far as hydration and sulfate attack are concerned, the presence of carbonates in cement affects the system in several ways.

Firstly, in high C_3A cement, carbonate filler could improve the resistance to sulfate attack if the mechanism was governed by ettringite formation. This can be seen in equations 2.8 and 2.9, where:

(i) Carbonates increase hydration of the aluminate phases [32-34, 54, 55], and also;

(ii) Monosulfate is not stable but is replaced by ettringite and hemicarboaluminate hydrate [56], hence, the precipitation of the secondary ettringite due to sulfate attack would not occur.

$$3C_3A + 3C\bar{S}H_2 + 2H + \bar{C} + 48H \rightarrow C_3A.3C\bar{S}H_{32} + 2C_3A.C\bar{C}_{0.5}H_{12} \quad (2\text{-}8)$$

$$3C_3A.C\bar{S}H_{12} + \bar{C} + 2CH + 18H \rightarrow C_3A.3C\bar{S}H_{32} + 2C_3A.C\bar{C}_{0.5}H_{12} \quad (2\text{-}9)$$

Another effect of carbonates is that they appear to increase the stability of ettringite itself, at least with respect to dehydration in vacuum. Indeed, instead of being damaged by the action of the high vacuum in electron microscopy [57], carbonated ettringite increased its crystal stability as experienced by Lachovisky et al. [58], who could assess the lattice parameter in transmission electron microscopy of carbonated ettringite but not of pure ettringite. This technique uses high vacuum and voltage, which can cause damage in the water molecules of phases that can dehydrate such as ettringite. The significance of a more stable ettringite is that it would not convert into monosulfate and, subsequently, into secondary ettringite due to sulfate attack, hence, increasing durability.

Indeed, the reduced content of C_3A, which is replaced by ferrite (C_4AF), makes sulfate resisting Portland cement (SRPC) a very effective binder for concrete in most aggressive 'conventional' sulfate environments [59]. Osborne [60] reported the good performance of SRPC in very aggressive sodium and magnesium sulfates (1.5%SO_3) after 5 years at 20°C. It was pointed out that the good performance of this cement was irrespective of initial air curing, which was reported as beneficial due to the formation of a carbonated layer over the surface. Gollop and Taylor [61] pointed out from considerations of the microstructural features in strong magnesium solution that the unhydrated ferrite phase was largely found in areas where magnesium silicate hydrate had formed. Indeed, the ferrite phase remained unattacked even in much higher

concentrations of magnesium sulfate at 20°C as reported by Bonen and Cohen [48]. It was concluded that the amount of ferrite increased close to the surface, mainly when the concentration of magnesium in solution increased from 2.1 to 4.2%SO_4 at room temperature (about 20°C).

As for the nucleation of portlandite, carbosilicate and/or $Ca(OH)_2$-$CaCO_3$ compounds at the filler-matrix interface, some reactions can be expected to occur. Portlandite can be converted to gypsum according to equation 2.3. In this sense, limestone filler would be detrimental to the concrete in systems where gypsum prevails over ettringite, as in low C_3A cement [41], for instance. However, the stability of the carbosilicate [36] or $Ca(OH)_2$-$CaCO_3$ [35] compound in sulfate solutions has not been reported in any published research.

Perhaps the most important reason for the recent interest in the long-term performance of carbonates in concrete systems can be attributed to the involvement of carbonates and the presence of thaumasite.

2.4 Thaumasite form of Sulfate attack

2.4.1 Background

According to the mechanism of conventional sulfate attack, the restriction of C_3A content of the cement improves the performance of concrete in aggressive sulfate environments. However, not all sulfate mechanisms are necessarily controlled by this factor. This happens to be the case with the thaumasite form of sulfate attack (TSA). Thaumasite ($C_3S\overline{C}\,\overline{S}H_{15}$), which bears a strong structural similarity to ettringite ($C_3A3C\overline{S}H_{32}$), does not contain aluminium, or at least tolerates little aluminium, in its crystal structure [62].

In a recent review of TSA, Crammond [63] underlined that 95% of the 80 new cases of sulfate attack in the UK in the past 15 years are reported to be due to TSA, in which SRPC cement was used in some instances. The majority of UK cases occurred in highway bridges, in which sulfates and sulfide-bearing soils were present, and also with carbonates coming mostly from limestone aggregate.

However, the presence of thaumasite formation is not a new finding in concrete structures. In the United States, Erlin and Stark [64] reported the first case of thaumasite in concrete in sulfate bearing underground water, and several other field cases have

since been reported elsewhere in European countries, Canada, Africa and United States [63]. What seems unusual is that TSA occurred in several concretes of important structures, and there is also the question as to why this type of attack was not identified to the same extent in previous field cases. Crammond [9] attributes this fact to several factors:

(i) A deficiency of the current standard tests for the sulfate resistance of cements, in which tests are conducted at 20°C, which favours 'conventional' sulfate attack rather than TSA;

(ii) Routine inspections of buried concrete are rarely carried out;

(iii) The conditions on the site may change due to increase in sulfate levels, because of chemical reactions within the soil, which may also increase the chances of thaumasite development; and

(iv) The difficulties in differentiating thaumasite from ettringite, due to the use of less advanced techniques in the past.

Another aspect is that thaumasite composition can change towards that of ettringite, in a series of solid-solutions, which, again, increases the difficulties of a precise characterisation [65, 66].

Perhaps the most aggressive case of TSA deterioration in field concrete occurred in a Canadian Arctic structure, as reported by Bickley et al [67]. The concrete aggregate was made from a local gravel consisting of oolitic and dolomitic limestone as well as siliceous material. Some of the cement used appeared to be a sulfate resisting Portland cement (CSA type 50), and the concrete strength reached between 31.9 and 53.9MPa in its sound parts. The soil did not contain any sulfide-bearing minerals, and the concentration of maximum soluble sulfates was maximum at 84 ppm. This 2 year old concrete column was severely attacked, with the precipitation of thaumasite and gypsum at the expense of C-S-H and portlandite. Neither CSH nor Portlandite were identified among the corroded parts of the concrete. It was pointed out that the level of Cl^- was always high in the corroded areas attacked by thaumasite, although no distinct chloride-bearing mineral was detected.

The most severe case of the TSA affected UK structures is reported to have occurred in the foundations of a 30-year-old motorway M5 bridge in Tredington-Ashchurch, Gloucestershire. The concrete was designed to resist sulfate attack

according to the standard current at the time for concrete in sulfate containing ground water, where site classification was described as class 2 ($0.14\% SO_4^{2-}$). However, oxidation of the pyritic-rich back fill soil increased the sulfate content to class 3 ($0.3\% SO_4^{2-}$) during its service life [68]. The aggregate contained both oolitic and dolomitic limestone.

The occurrence of TSA in important structures led the UK government to set up the Thaumasite Expert Group (TEG). As a result of the current knowledge on site and laboratory investigations, the first TEG-1999 report identified the following primary risk factors affecting the performance of concretes to TSA, a sources of (i) sulfate; (ii) carbonate; (ii) silicate; (iii) water and (iv) low temperature (<15°C). The findings identified by the TEG led the current BRE SD 1:2001 to subdivide the BRE 363 sulfate class according to the mobility of the groundwater, pH and thresholds for the concentration of magnesium, as well as introducing restrictions to thresholds for carbonate coming from the aggregates used to make the concrete.

2.4.2 Mechanisms of thaumasite formation

A. Morphology of the attack

It has been reported that the formation of thaumasite can cause expansion, but its main characteristic is the formation of a white-mushy material with no cohesiveness [63, 69]. Figures 2.1 and 2.2 show some examples of deterioration caused by TSA. The attack is progressive from the surface inwards, in which the main cement binder (CSH) is consumed and turned into thaumasite [13].

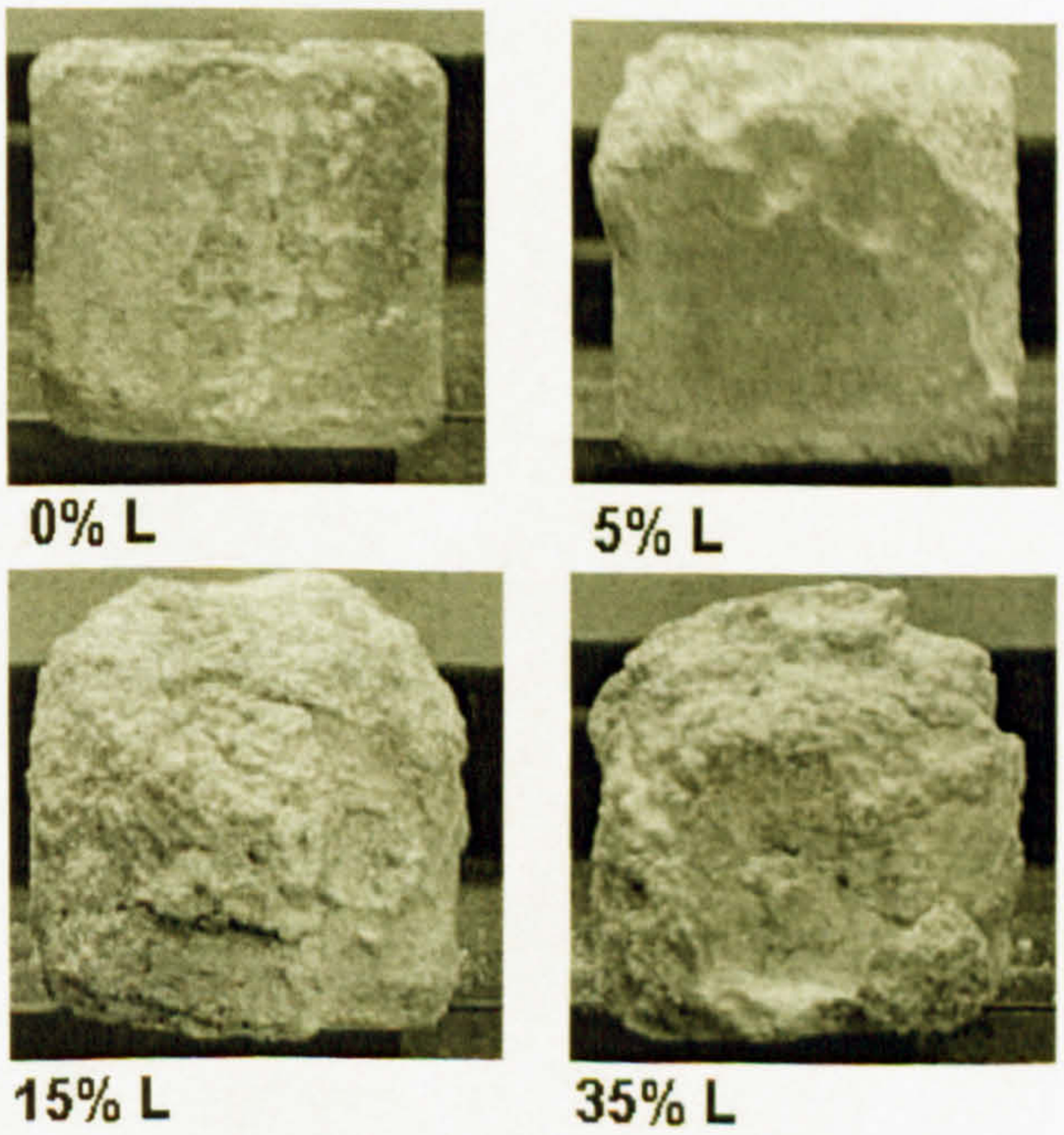

Figure 2.1: Example of different limestone filler containing cements after 5 years in 1.8%$MgSO_4$ at 5°C: Cross section view (Torres et al. [13], Appendix III).

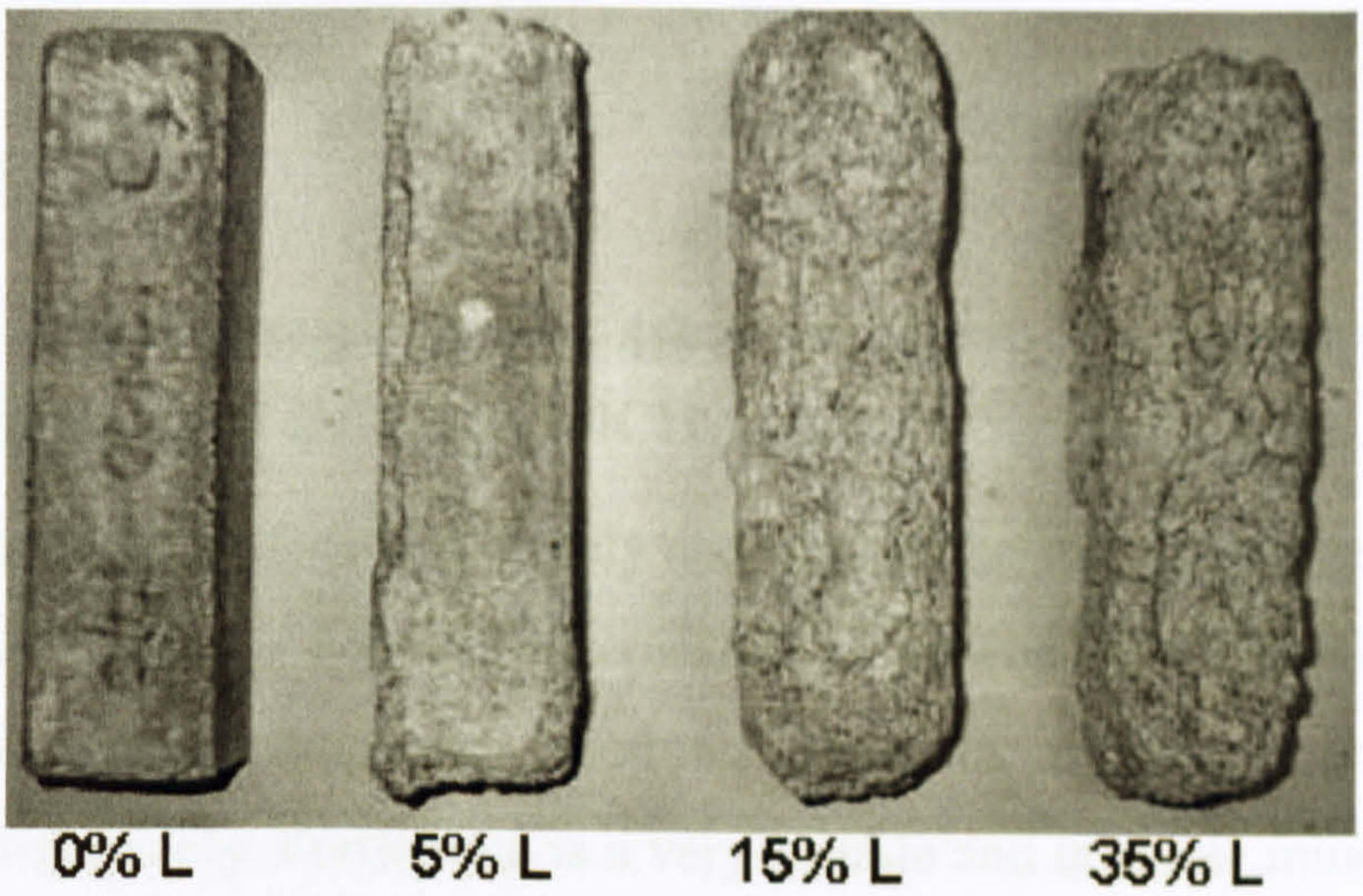

Figure 2.2: Example of different limestone filler containing cements after 5 years in 1.8%$MgSO_4$ at 5°C: lateral view (Torres et al. [13], Appendix III).

B. Chemical reactions

In general, published researches agree with respect to the postulated mechanisms of thaumasite formation. It has been suggested that thaumasite forms according to at least two main routes:

a. Direct route, in which CSH is consumed along with carbonate and sulfate in a through solution mechanism, as shown in equations 2.10 [11] and 2.11 [10];

Direct route:

$$C_3S_2H_3 + 4M\overline{S} + 2C\overline{C} + 3CH + 32H \rightarrow 2C_3S.\overline{C}\,\overline{S}\,H_{15} + 2C\overline{S}\,H_2 + 4MH \quad (2\text{-}10)$$

$$C_3S_2H_3 + 2M\overline{S} + 2C\overline{C} + CH + 28H \rightarrow 2C_3S.\overline{C}\,\overline{S}\,H_{15} + 2MH \quad (2\text{-}11)$$

b. The 'woodfordite' route, as shown in Equations 2.12 written in cement chemistry notation (from Bensted [11]), in which ettringite and CSH interact with calcium carbonate. The term woodfordite comes from the finding of a silicon-containing ettringite that was thought to be a new mineral. This term was later withdrawn from the international crystallographic powder diffraction database.

Woodfordite route:

$$C_3S_2H_3 + C_3A.3C\overline{S}H_{32} + 2C\overline{C} + 4H \rightarrow 2C_3S.\overline{C}\,\overline{S}H_{15} + C\overline{S}H_2 + AH_3 + 4CH \quad (2\text{-}12)$$

Although the attack on C-S-H is widely accepted as the main factor responsible for the severity of TSA, there are divergent opinions as to whether portlandite (CH) is a reactant or a product in the thaumasite reaction mechanism, as can be seen in equations 2-11 and 2-12, respectively. Portlandite is a very soluble and unstable mineral in sulfate solution, especially at low temperatures in which its solubility doubles [12]. It is argued that portlandite (product of the reaction 2.12) can form calcium carbonate by carbonation [10].

The 'woodfordite' route is the least understood. On the one hand, it is proposed to be a topochemical mechanism, in which the sulfates and water within ettringite are replaced by carbonates that results in a change of ettringite into thaumasite in a discontinuous series of minerals but it can also be through solution. Indeed, ettringite, which is readily formed during cement hydration, usually forms due to sulfate attack prior to the formation of thaumasite [11, 70]. However, the existence of a gap in this series gives rise to another possible hypothesis in which ettringite dissolves and recrystallises according to the local chemistry of the pore solution. Crammond [63] discusses this issue by recalling that the distribution of thaumasite in the cement matrix is uniform, meaning that it happens not only at previous sites of ettringite but also within the cement matrix.

C. Source of carbonates

It has been widely accepted that limestone, either as filler or as an aggregate, is a readily available ingredient for the thaumasite form of sulfate attack. Several field cases and laboratory work have confirmed this. Indeed, higher restrictions are now specified when carbonates from fines in addition to those from coarse aggregates are present [14].

When the source of carbonates is the aggregates, in a very aggressive condition, the amount of carbonates can reach between 2% and 10% of $CaCO_3$ equivalent to the total mass of the aggregate, whether it comes entirely from the fines or coarse aggregate, i.e., more than 5% by the weight of cement. As far as limestone filler as *MAC* in Portland

cements is concerned, there are different opinions with regards to the minimum amount required.

On the one hand, the findings of Harthsorn et al. [11, 31, 47] indicate that the use of 5% limestone filler in Portland cement can be detrimental, with respect to the durability to TSA. Also, further investigation after 5 years of exposure, Torres et al. [13] indicated that the damage increases progressively in all samples containing limestone filler (LF), and even in OPC containing 5% $CaCO_3$, in which ettringite and thaumasite were identified after one year. Indeed, no ettringite was found in the corroded area of any sample but thaumasite was readily identified. After further examination, Torres et al. [18] (Appendix IV) also identified a good correlation between the unit cell parameter of thaumasite and carbonate content in the samples, in which the higher the carbonate content, the closer the product to the thaumasite end member cell parameters.

Also, there are several studies pointing to the fact that cement containing 15% limestone filler is particularly susceptible to TSA, even after 1 year [71-74]. In all cases, cement containing about 15% to 20% limestone filler were attacked by sulfates after only one year, although differences in sulfate concentrations and cations do not allow simple comparisons. However, the mechanisms of attack were attributed to TSA in all cases containing calcium carbonate filler. For instance, taking the lowest sulfate concentration tested, Barker and Hobbs [71] found that samples containing 15% limestone filler did not perform differently from OPC mortar samples after one year in 0.42%SO_4 at 5°C. However, it was pointed out that the mode of attack in PLC was due to a formation of both thaumasite and ettringite, whereas the mode of attack in OPC was due to ettringite alone.

On the other hand, Hobbs [75] found that the observations in field cases and laboratory experiments are in agreement with respect to the primary risk factors leading to TSA. It was postulated that a Portland cement containing a total amount of more than 15% $CaCO_3$ would be adversely affected by TSA. Hooton and Thomas [23] also share a similar view that concentrations higher than 15% would be at risk of TSA, and also that 5% would not adversely affect the performance of Portland cements to TSA.

However, the source of carbonates can also be external as reported by Slater et al. [16], who pointed out that carbonates and bicarbonates in the groundwater would be enough to supply the amount needed to form the extent of thaumasite detected in the Tredington-Ashchurch bridge. Indeed, Collett et al. [76] concluded that thaumasite can

occur in concrete even without any internal source of carbonates, as carbonation and bicarbonates in the groundwater can also supply the source of carbonates necessary to form thaumasite. It was pointed out that the solubility of these species increases as the temperature decreases.

D. Source of silicate

The most common sources of silicon in Portland cement are: (i) calcium silicate phases of the clinker such as alite (C_3S) and belite (C_2S) and also (ii) their hydrated product C-S-H, which is the main binder and responsible for the properties of the Portland cement concretes [63].

Some interesting features of the hydration of belite at low temperatures have been reported. Brunauer and Kantro [77] observed that the rate of hydration of belite at 5°C is strongly reduced when compared with hydration at 25°C and 50°C, but the degree of hydration at 5°C was found to be equal to that at 25°C and higher than that at 50°C after 400 days. These observations have been broadly confirmed more recently by Escalante-Garcia and Sharp [78] working in the temperature range from 10 to 60°C. Also, Miller and Tang [79] reported that γ-$CaSO_4$ (soluble anhydrite) can be incorporated in silicate clinker phases. Yang and Sharp [80] identified clusters of ettringite within belite grains. However Taylor [81], who also detected sulfate in clinker phases, concluded that this source of sulfate should not affect the durability of concretes, at least with respect to delayed ettringite formation, which is also detrimental to concrete. The question that arises is whether the slow hydration of belite at lower temperatures, which can contain dissolved sulfate ions, would participate in the formation of thaumasite prior to the disruption of C-S-H, as it should be easier to supply silicon and calcium from this unhydrated phase than from a 'sound' C-S-H in the early stages of the attack.

Another source of silicate can be the aggregate itself. Tasong et al. [37] examined the chemical interaction between aggregates and cement paste. A selection of basalt, limestone, silica sand and quartzite was studied by means of the dissolution of several elements in water and cement solutions. It was identified that the chemical activity of these aggregates plays a more active role in the transition zone of the aggregate-cement paste than previously supposed. It was identified that basalt was the most reactive, followed by quartzite and silica sand, and finally limestone. A significant release of Si^{4+} was observed in quartzite and silica sand, which absorbed both Ca^{2+} and OH^- from the cement solution, that possibly crystallised as amorphous calcium silicate hydrates at the interface. Although the pH of the cement solution was not determined, it is likely to be

very alkaline. Indeed, the solubility of silicon increases dramatically when the pH is higher than ca. 10.5 [82]. This can be a possible explanation as to why depositions of thaumasite around silica grains are often identified [63]. Indeed, Hill et al. [83] identified the formation of thaumasite in SRPC concretes, where the aggregate was silica containing gravel, in BRE sulfate classes 2 and 4B after 5 months storage at 5°C. Although it is difficult to identify the source of silicon in this case, it is important to consider that a source of silica from the aggregate might offer an extra chance of weakening the aggregate-cement transition zone.

E. Temperature

Thaumasite formation is a slow process, even in conditions ideal for its precipitation. For that reason, the use of accelerated conditions to investigate such phenomena prevails in most researches. There seem to be several reasons for such delayed formation. Hartshorn et al. [11] have concluded that this delay is caused by the kinetics of cement hydration since the formation of thaumasite demands hydration products such as calcium hydroxide, C-S-H and ettringite. The hypothesis of a late hydration of belite could possibly be considered as a factor affecting such kinetics. It is also possible that the 'woodfordite' route triggers other routes, since ettringite is mostly found prior to thaumasite formation [11, 70] . It appears that the formation of thaumasite via ettringite is faster than the direct route, as reported by Bensted [84] in which the formation of thaumasite from ettringite was faster than from aluminium free systems. Bensted also postulates that carbonates should firstly act on the crystal structure of ettringite, during which carbonates promote a charge dislocation of the hydroxyl group to permit an increase in the coordination of silicon to 6. Thus, the kinetics of thaumasite nucleation appears to be more affected by temperature than by the presence of the ionic species alone.

Low temperature

Table 2.1 shows the time required for the formation of thaumasite at low temperature (<5°C) under laboratory conditions. The fastest thaumasite formation was found by Gaze [85], and Gaze and Crammond [70], who observed weak peaks of thaumasite by XRD after about a month. Hartshorn et al. [69] reported that thaumasite formed more quickly in mortar than in paste, possibly because the transition zone at the paste aggregate interface introduced more porosity, or the silica sand contributed some extra silicate to the system. A strong solution seems to increase the time as can be seen in Gaze and Crammond [70], Hartshorn [69] and Crammond and Nixon [86], who

found thaumasite after six months in mortar under 0.42% magnesium sulfate solution and predominantly gypsum and brucite at the same age for samples under 1.99% $MgSO_4$. There is a possibility that the deposition of a brucite coating, which derives from magnesium sulfate, might have caused such delay. Indeed, Bonen and Cohen [48] reported that by increasing its concentration the diffusion of sulfate ions was diminished due to a large deposit of brucite-gypsum double layer on the surface. The findings of Gollop and Taylor [87] that the amount of Mg^{2+} under the gypsum layer was as little as that found in the sound material, also seems to support this opinion.

Table 2-1: Time required for the formation of thaumasite in cement –based systems (Detection by XRD)

Reference	Mixture	Solution	Temp .(°C)	Age (Days)
Van Ardt and Visser [88]	hemihydrate:Portlandite $CaCO_3$:Amorphous SiO_2 1:1:1:1 moles	Water	5	$120^{(ms)}$
Ludwig and Mehr [89]	gypsum:calcium carbonate:Silica (from the binding) at 1:1:1: water/binder=0.71-3	Water	2	90
Crammond and Nixon [86]	Mortar 1:3:0.6-0.8	0.42% $MgSO_4$ 1.80% $MgSO_4$	5 5	180 nf<180
Gaze [85]	Crushed mortar (BS4551:1980): 22% gypsum 44% gypsum	Water Water	5 5	$42^{(sm)}$ $70^{(st)}$
Gaze and Crammond [70]	Crushed mortar (BS4551:1980): 1:1:5.5:1.1+25%limestone Cement:lime:sand:water	0.42% $MgSO_4$ 1.99% $MgSO_4$ 0.42% K_2SO_4 1.99% K_2SO_4	5 5 5 5	$29^{(w)};40^{(ms)}$ n.f<197 $50^{(t)}$ $50^{(ms)}$
Hartshorn et al, [11]	Paste 5% 15% 35% limestone 1:2.5:0.5 Mortar: 35% limestone	1.80% $MgSO_4$	 5 5 5 5	 280 196 196 126^{st}
Bensted [84]	C_3S:$CaCO_3$:$CaSO_4$ Ettringite:$CaCO_3$:C-S-H	Water	2	180^{t} 540^{sm} $365^{t}720^{sm}$

Intensity grade of XRD peaks:
nf-not found under; t-traces; w-weak; sm- small-moderate; ms- moderately strong; st-strong

Room temperature

The scarce examples of thaumasite formation at relatively high temperature may be attributed to a strong belief that it does not readily occur at temperatures above 15° C, although thaumasite formation at 20°C has been reported [69, 89-93]. Table 2-2 shows the conditions under which thaumasite precipitated at temperatures higher than 15°C. This mineral was not detected before 600 days in most cases, perhaps due to a kinetically faster deposition of calcite or aragonite, which might have yielded a lack of carbonate ions in solution. In this case, the sulfates precipitate as ettringite

predominantly, and ettringite could have slowly carbonated to form thaumasite at a later stage. The fastest formation was identified by Hartshorn et al. [69], who found it after 224 days as a material deposited in a cement mortar containing 35% calcium carbonate filler. Al-Almoudi et al. [94] identified only one thaumasite peak at 23.63° 2θ (16%) in OPC containing 60% ground granulated blast furnace slag (ggbs). It was not explained why the most intense 9.25° (100%) and 16.08° 2θ (40%) peaks were not detected, even among the background noise.

Table 2-2: The formation of thaumasite in cement –based systems at room temperature (Detection by XRD)

Reference	Mixture	Solution	Temp (°C)	Age (Days)
Ludwig and Mehr [89]	gypsum:calcium carbonate:silica (from cement) at 1:1:1 proportion by volume	Water	20	600$^{(NS)\ (50b)*}$
Morales [90]	66.6%type V:33.3% gypsum le-Chatelier/Ansttet test	Water	~20	1095
Knudsen [91]	NM	NM	~20	NM
Al-Almoudi [94]	40%OPC:60%slag:0.5(w/b)	2.1%(Mg+Na)	25	720$^{(VS23.63\ 2\theta)}$
Hartshorn [69]	1:2.5:0.5 Mortar: 35% limestone	1.80% $MgSO_4$	20	224$^{(50b)*}$
Collepardi [92]	Historic Building-Italy	NM	~20	NM
Irassar et al [93]	1:2.75:0.478 Mortar OPC+20%$CaCO_3$	5%Na_2SO_4	20	730

Intensity grade of XRD peaks:
NS-not shown; NM- not mentioned; vs- very strong; 50b- Peak intensity 50% of the background intensity

F. The effect of pH

The effect of pH on the formation of thaumasite has been investigated by Gaze and Crammond [70]. It was found that thaumasite did not form when the pH was below 10.5, but it readily formed in very alkaline pH solutions. In addition, thaumasite can be attacked by alkali carbonation, which results in the precipitation of calcite, at reduced pH of 9 or below.

In further studies on the effect of carbonate sources other than aggregate and filler, Collett et al. [76] pointed out that a reason for this pH threshold can be that the carbonate species in solution, such as CO_3^{2-} and HCO_3^{1-}, which take part in the reaction mechanism of thaumasite formation, are in equilibrium at the pH of 10.33. Indeed, this equilibrium is around 10.55 when the temperature drops from 25°C to 5°C, for instance. Below a pH of around 10.55, the concentration of HCO_3^{1-} is dramatically reduced to give rise to the concentration of carbonic acid, resulting in less carbonate species that would be free to react to form thaumasite [82].

However, Hill et al. [83] identified traces of thaumasite in a PLC concrete immersed in acidic solution after 5 months. It was argued that such an apparent contradiction could be explained because the high content of limestone in PLC would generate enough carbonates due to the dissolution of calcite in acid to allow the precipitation of some transient thaumasite. It was also pointed out that the formation of thaumasite in acid is not stable, as stated by Gaze and Crammond [70], and would undergo dissolution to form gypsum and silica and release CO_2 gas. The equilibrium between calcium bicarbonate ions that occurs at the pH as high as 10.55 at 5°C [82] could not only have increased the local pH to levels where thaumasite can form, but also carbonate ions could have been available long enough for thaumasite formation.

The need for alkaline environments is in agreement with findings of site investigations. Indeed, Slater et al. [16] identified that the pH increased towards the thaumasite affected concrete-soil interface, reaching around 10.0-11.5, whereas the pH of the groundwater was around 8.0-8.6.

Sibick et al. [17] investigated an occurrence of TSA in seawater. The structure was the steps of a harbour by the sea in south Wales, UK. The construction underwent several repair works during 5 years. In the worst cases, lime and OPC or SRPC binders were severely attacked by the seawater. The main minerals found were thaumasite, ettringite, gypsum, brucite, magnesium silicate hydrate, and calcite. It was reported that the attack was characteristic of magnesium intrusion in the C-S-H structure, and also thaumasite attack. Although the pH was not reported, seawater pH is often around 8.6 [82], which is below what is currently accepted for thaumasite to form. However, the precipitation of 'popcorn' calcite, lead to the conclusion that thaumasite may have been attacked by 'alkali carbonation' as described by Gaze and Crammond [70]. The aggressiveness of the kinetics of this type of attack was considerable, when compared to other mechanisms. However, those mortars contained significant amount of lime. As far as speed of attack is concerned, the attack of the Canadian Arctic concrete column occurred slightly faster. In both reported cases, excessive chlorides were identified within the corroded material, but not chloride-bearing phases. Perhaps they should not be expected, since such phases are sensitive to low pH (<11.7~11.9) [95]. Indeed, Hobbs and Taylor [96] and Eden [97], reported that the concentration of bound chloride in field cases of TSA were usually low at the attacked surface. Certainly, TSA is not commonly found in seawater, yet the temperature and presence of sulfate and magnesium ions favour it. The major mitigation factor is the absence of high pH.

2.4.3 Role of chloride ions on sulfate attack

A. Mechanism of chloride and sulfate attack

Sodium chloride

A mitigating role of chlorides on sulfate attack has been reported in some researches. Ben-Yair [98] identified that the presence of calcium chloroaluminate hydrate (Friedel's salt) increased the precipitation of ettringite, although less expansion was observed in Portland cement immersed in combined sulfate-chloride solutions than in pure sulfate solutions. Conjeau [99] also discussed the beneficial aspects of Friedel's salt formation in seawater. Indeed, Al-Almoudi et al. [94] showed that less expansion and strength reduction occurred in all systems combining Type I and V cements with silica fume, fly ash and ggbs in 2.1% (Mg+Na) and 15.7% NaCl after 1 year. In further investigations with the same binders, Al-Almoudi [100] confirmed the mitigating role that chloride plays in sulfate attack, but reported that this is more evident in sodium sulfate than in magnesium sulfate. Two factors were considered: chloride can mitigate the sulfate attack in cases in which ettringite is more favourable to precipitate, because monosulfate reacts with chlorides and forms Friedel's salt (Equations 2.13 and 2.14). Hence, the formation of the detrimental secondary ettringite does not occur, and less damage should be expected.

$$Ca(OH)_2 + 2NaCl \rightarrow CaCl_2 + 2NaOH \qquad (2\text{-}13)$$

$$C_3A + CaCl_2 + 10H \rightarrow C_3A.CaCl_2.H_{10} \qquad (2\text{-}14)$$

When considering the hydration of aluminates of the cement and the deleterious formation of secondary ettringite, it can be seen that the formation of Friedel's salt can be beneficial as it has formed with the reactions with aluminates, and reduces the chances of the formation of secondary ettringite (*see* equations 2.5-2.7). Friedel's salt can also form from the alumino-ferrite phases of the cement, but ettringite that is formed via alumino-ferrite does not seem to be harmful to the concrete as it appears to be amorphous, hence, the crystallisation pressure is reduced [101].

Because the concentration of sulfates in solution containing chloride were higher than in sulfate alone, Al-Almoudi [100] concluded that the solubility of both gypsum and ettringite increases with increase in concentration of chlorides. Hence, less gypsum and ettringite would be expected in these cases, and thus, less damage due to sulfate attack. However, it is possible that the reason why more sulfates were in solution can be

attributed to the chlorides bound with aluminates, hence, lessening the chances for the formation of ettringite. Nevertheless, Ben-Yair [98], reported that the presence of Friedel's salt increases the precipitation of ettringite, which appears to suggest a reduction in the solubility of ettringite. Indeed, Damidot and Glasser [102] using thermodynamic modelling predicted that ettringite, gypsum and Friedel's salt are stable in the presence of chlorides and sulfates at a series of compositions. It was also pointed out that ettringite and gypsum solubility reduces with increase of chloride concentration, and also that ettringite can be stable at pH as low as 9.5. These conflicting ideas are indicative that the effect of chlorides on the solubility of both ettringite and gypsum is complex, especially in cement systems where other ionic species, such as carbonates and aluminates, can react and influence the equilibrium.

Sea water

Although chloride and sulfate ions also occur together in seawater, the attack is more correlated with the disruption of the C-S-H by the action of the magnesium ions. Although this mechanism is extremely aggressive to concrete, the blocking effect of the deposition of brucite and aragonite reduces further diffusion of ionic species in both ways. Indeed, Conjeaud [99] reported that no leaching of portlandite was detected after a period of 3 years in synthetic seawater solution, due to the deposition of a double-layer of these two minerals. However, in the tidal zone, this layer can be broken due to strong waves, and further damage would occur. This blocking effect on the reduction of ionic diffusion of species has also been reported elsewhere [48, 50, 103, 104].

Mechanism of chloride, sulfate and carbonate interaction

When carbonates are added to chloride and sulfate in solutions, Friedel's salt ($C_3A.CaCl_2.H_{10}$) is no longer stable and converts to hydrogarnet (C_3AH_6), according to equations 2.15. Ultimately, hydrogarnet is also carbonated and turns into calcite and gibbsite or hydrous alumina (AH_3) as shown in equation 2.16 [105, 106].

Dissolution of Friedel's salt

$$C_3A.CaCl_2.H_{10} + CO_3^{2-} \rightarrow C_3AH_{6\,solid} + C\overline{C} + 4H + 2Cl^{-} \qquad (2\text{-}15)$$

Dissolution of HG

$$C_3AH_{6\,solid} + 3\overline{C} \rightarrow AH_3 + 3C\overline{C} + 3H \qquad (2\text{-}16)$$

The stability of Friedel's salt in carbonated concrete samples has been investigated by Suryavanshi and Swamy [107], who concluded that Friedel's salt is not stable in low pH carbonated zones. This can possibly explain why chloride diffusion was found to be higher in carbonated zones of concretes [108].

As discussed previously, sulfate attack is affected by the presence of carbonates. Indeed, the majority of studies in combined chloride and sulfate solutions were carried out at temperatures higher than 15°C. However, no research has been published on the combined effect of chlorides, sulfates and carbonates on the durability of Portland cements, in conditions prone to develop thaumasite, e.g. at lower temperatures.

B. Field case involving chloride and thaumasite

There are some examples in which the concrete suffered the thaumasite type of attack when chloride ions were present.

Thaumasite has been identified in seawater in a 125 year old dyke wall by Regourd et al. [8]. In laboratory conditions, Conjeau [99] examined the performance of mortars sand:cement (1:3) made with four type I cements (C_3A~13.5), one type V (C_3A=0) and alite (C_3A=2%) for 3 years at 20°C in synthetic seawater. Most cements lost ca. 25~20% of their strength compared to the control in water, except for two Type I cements of similar composition that lost 50% of their compressive strength after 3 years. It was concluded that the loss in strength was associated with the formation of Si ettringite (woodfordite), but not Friedel's salt or ettringite. Because of the amount of silicon (~5% by EDX) and the XRD pattern, this silicon-containing mineral was concluded to be different from thaumasite as reported by Lukas [109]. At that time, the extent of solid solution between ettringite and thaumasite was not known. As for the source of carbonates necessary for thaumasite solid solution, it has been reported that the samples were coated by a layer of calcite due to prior exposure to high humidity air, prior to the immersion in the salt solution. Walkeley and Roy [110] also detected the formation of 'woodfordite' in grouts containing carbonate from a local source exposed to a highly saline brine at 30°C.

Nevertheless, Brown and Doerr [111] reported that thaumasite, Friedel's salt, sodium chloride and a sodium-rich material occurred in regions as deep as 40 mm into an attacked concrete in South California. This concrete was made with a type V cement and water/cement ratio of 0.65-0.70. It was also reported that magnesium silicate hydrate, brucite, and a sodium-carbonate material were found in the inner parts. In this

region, temperature is usually above 15°C, which also makes this case relevant for hot climate countries. However, it is not clear whether the thaumasite found was formed when the temperature reached below 15°C in some months, as reported by Diamond [112].

The presence of chloride has been identified in many recent cases, with consequences of induced corrosion of the reinforcement around the TSA affected areas. Wimpenny and Slater [15] pointed out that the combined effect of sulfates and chlorides involved in TSA lead to chloride induced corrosion. In a recent review of the same findings reported in 1966, Stark [5] accounted for thaumasite formation in a grout that never hardened, which was near a sodium chloride mine. It is not clear whether there was any involvement of this salt with the observed formation of thaumasite. Hagelia et al. [113] investigated a series of sprayed concretes in 2 to 35 years old Norwegian tunnels. The concrete used was mostly good quality concrete, with low water cement ratio and the use of either SRPC or low C_3A OPC with silica fume ranging from 5 to 10% and Fly ash (20%). The source of carbonates was identified to be bicarbonates in the water, however some limestone aggregate was present in some concretes. The initiation time for TSA was estimated to be less than 13 years. In the most severe case, in a 5 km sub-sea tunnel made with rapid setting OPC (C_3A 8%-w/c=0.37-0.47 and 6-8% silica fume), this time was reduced to less than 5 years. The water analysis shows significant amounts of Cl (1.8%), sulfates (0.24%) and Mg (1.0%) among other species. The attack was characterised as TSA-TF with magnesium attack on the C-S-H, with formation of brucite and M-S-H. No chloride binding phases were reported, and nor a possible chemical interaction between chlorides and the cement matrix was discussed.

Nevertheless, there is no published research to establish the role of chloride in the thaumasite form of sulfate attack. In some researches, it appears that the mechanism of chloride attack in concrete is not clear. On the one hand, Monsoni et al. [114] reported that the main factor contributing to the deterioration of cement mortars was the leaching of calcium hydroxide, which was favoured at lower temperatures. On the other hand, Chatterji [115] questioned whether leaching of $Ca(OH)_2$ and formation of monochlorohydrate would explain the $CaCl_2$ deterioration. This question arose because, irrespective of the curing temperature (5, 20 and 40° C), all the portlandite was removed, monochlorohydrate was formed in all conditions, but the greater deterioration was associated with the formation of '*an unidentified needle shape biaxial crystal*' (principal diffraction lines at 9.56 and 5.46 Å). It was found that this mineral demands a high concentration of $CaCl_2$, the presence of $Ca(OH)_2$ and it preferentially forms at

temperatures below 20° C. More interestingly, the cement paste was turned completely white in colour after only a month. Such conditions are also critical for the formation of thaumasite. The X-ray powder diffraction lines mentioned above are also closely similar to those of thaumasite (9.56 and 5.52). Indeed, Chatterji's experiments were performed in crushed concrete samples that had been previously carbonated prior to exposure to the salt solution. Bertsson and Chandra [116] examined the damage in concrete slabs that had been exposed to calcium chloride salt. They concluded that the attack was similar to that observed by Chatterji, in which a needle-like phase (3μm length) was observed under the scanning electron microscope. This morphology is also characteristic of thaumasite. However, an important feature of TSA, the formation of a white mushy end product, was not reported in these researches. It is not possible to conclude definitely that thaumasite was present in any of theses cases, but the resemblances should be noted.

2.4.4 The use of metakaolin cement replacement to prevent TSA

Portland cement containing high levels of ggbs has been widely accepted as a good choice for the prevention of thaumasite, even when carbonate aggregates are present [117, 118].

However, conflicting results have been found with regard to fly-ash. Hill et al. [119] found that 20% pfa concrete developed ettringite rather than thaumasite after 5 months in sulfate solutions at 5°C. Norbst and Stark [120] identified thaumasite in ground mortar containing pfa after 280 days at 6°C in sulfate solution, and Mulenga et al. [121] reported that thaumasite developed after 84 days in pfa concrete immersed in 4.4% sodium sulfate, but the performance of 40%pfa in PLC gave satisfactory results after 1 year of exposure.

Recently, Smallwood et al. [122] reported a good performance with metakaolin (7%) containing OPC (C_3A=11%) with respect to thaumasite after 280 days in highly sulfate solution. Tsivilis et al. [73] also investigated the use of 10% metakaolin and 15% limestone filler replacing OPC (C3A=6.3%). After 1 year in 1.8% MgSO4 at 5°C, metakaolin system performed as well as 50% ggbs and 15% limestone filler systems.

Indeed, the mechanisms by which this pozzolan and other cement replacement materials control the formation of thaumasite are not completely understood. So far, no research has been carried out on the performance of metakaolin, or any other cement

replacement material, in systems where chlorides, sulfates and carbonates are all present, particularly with regard to susceptibility to thaumasite formation.

2.5 Concluding remarks

The main conclusions that can be drawn from this review are as follows:

- The replacement of Portland cement clinker by minor additional constituents, pozzolans, industrial by-products and natural and calcined clays represents a good alternative towards important issues such as atmospheric pollution, energy savings as well as durability and engineering properties of concrete.

- The use of limestone filler as a cement replacement material can be mostly justified not only by its environmental and production processing benefits, but also by several positive contributions to a better performance of concrete. However, limestone filler is not an inert material in concrete.

- Although the presence of limestone increases the hydration of the silicate and aluminate phases of the cement, the effect of limestone filler in the microstructure of cement is not totally understood. This can be identified from the different findings reported in the literature with respect to the performance of cementitious systems containing limestone filler.

- It can be concluded that the presence of limestone filler can cause durability problems for concretes in contact with underground waters containing aggressive species such as sulfates and chlorides and carbonates. However, the mechanisms by which carbonates affect the resistance of concretes in aggressive conditions vary according to the main mechanism of the attack.

    - On the one hand, carbonates can improve the durability when ettringite formation is the dominant mechanism, because of the formation of carboaluminate hydrates with the apparent increase in the stability of ettringite formed during the early periods of the cement hydration, for instance. This reduces the chances of secondary ettringite formation, which is an expansive phenomenon.

- However, limestone can be very detrimental to the concrete integrity when gypsum are especially thaumasite are the main reaction products of attack. Nevertheless, there are different views about the minimum amount of carbonates that can be deleterious to the concrete. This is still not clear, which demonstrates the lack of understanding and complexity of the several mechanisms involved.

- Not all environments lead to the thaumasite form of sulfate attack. The main risk factors contributing to TSA are a source of (i) silicate, (ii) carbonate, (iii) sulfate, and (iv) wet and cold environments.

- Although several field cases indicate that chloride might play a role in the formation of thaumasite, it has been reported that the role of chlorides is primarily to increase the chances for the corrosion of the steel reinforcement. Nevertheless, whether there are other effects involving chlorides and sulfates in the presence of the main risk factors affecting the formation of thaumasite is not known.

- As far as chloride and TSA is concerned, the current standard for concrete in aggressive environments BRE SD-1 states that:

> *'...Only in abnormally high concentrations does chloride affect unreinforced concrete. There is also considerable evidence, from seawater studies, that the presence of chloride generally reduces sulfate attack. ...' SD 1:2001: Part 1: section 2.6 Chloride ions, pp6.*

- However, it should be considered that the mechanism of seawater attack is different from, the use of deicing salts such NaCl alone, because seawater contains high concentration of magnesium ions from both magnesium sulfate and magnesium chloride. As discussed earlier, magnesium plays a two-fold role: (i) either blocking the pores by the precipitation of aragonite and brucite (positive effect), or (ii) by disrupting the CSH structure (negative effect).

- The mechanism by which some binders mitigate against thaumasite attack is also not known. Although, ggbs appears to be the best binder, less convincing results are presented with respect to fly ash. Also, although

studies of the use of metakaolin point to good performance under TSA conditions, it is not known whether the chloride binding capacity of this pozzolan would reduce the performance of such a binder in a combined action of chlorides and sulfates.

In the light of this review, it can be summarised that no significant discussion or systematic research has been carried out with respect to the potential role that chloride ions might play on TSA. Therefore, it is believed that the role of chloride on TSA should be investigated. A systematic research programme is necessary to address some of the main questions arising from this review, namely:

- Does chloride play any significant role on the formation of thaumasite, either mitigating or accelerating the process of attack?
- Does chloride affect the composition and structure of thaumasite?
- Is the chloride binding capacity of limestone containing mortars affected by the precipitation of thaumasite?
- Is the performance of metakaolin and *limestone* containing cement mortar affected in combined sulfate and chloride solutions?
- Is the effect of combined chloride and sulfates influenced by temperature?

Chapter Three

EXPERIMENTAL PROGRAMME

3.1 Introduction

In the literature review, it was found that several aspects of the thaumasite form of sulfate attack (TSA) have not yet been investigated systematically. Firstly, no systematic research has been cried out on the role of chlorides on TSA, although these ions were identified in many field cases. Secondly, the performance of metakaolin in repressing such chemical attack has not yet been investigated in combined chloride and sulfate ion containing systems. Finally, although the role of atmospheric carbonation on TSA has been investigated, there is no published literature on long-term carbonation of laboratory-controlled samples and its effect on TSA.

3.2 Experimental design

In order to achieve the objectives of this research described in Chapter 1, the chosen parameters were selected according to the main risk factors affecting the thaumasite form of sulfate attack, as well as others identified as unexplored from the literature review in Chapter 2: source of carbonate ions, source of sulfate ions, temperature and source of chloride ions, as shown in Table 3-1.

Table 3-1: Experimental parameters.

Primary risk factors						
Factors	Source	Units	Levels			
Source of Carbonate	Atmospheric carbonation	-	Not measured			
	Limestone filler	%(m/m$_{opc}$)[a]	0	5	15	
Temperature	-	°C	5	20		
Source of sulfates	Epsom salts	%(SO_4^{2-})	0.6			
	Seawater		0.279			
Wet environment	Deionised and demineralised water	l/kg[b]	~1.7			
New parameter						
Factors	Source	Units	Levels			
Source of Cl^-	NaCl	%(Cl^-)	0	0.5	1.0	2.0
	Seawater		2.7			

(a) mass of limestone/mass of OPC (b) litre of solution/weight of sample

This programme did not include all possible interactions within the parameters, which would amount to 144. Instead, the experimental programme consisted of 52 possible interactions, and these are outlined in Figure 3.1. The reduced number of interactions was because a pilot study was also carried out to identify the usefulness of a frequency response function and damping obtained at different excitation frequencies (cyclic load, at the resonance frequency and at ultrasonic frequency levels) on assessing damage caused by TSA. This was carried out in 64 prismatic mortar specimens (40x40x160mm). However, the data reported in this thesis refers to the analyses of the cubes specimens only.

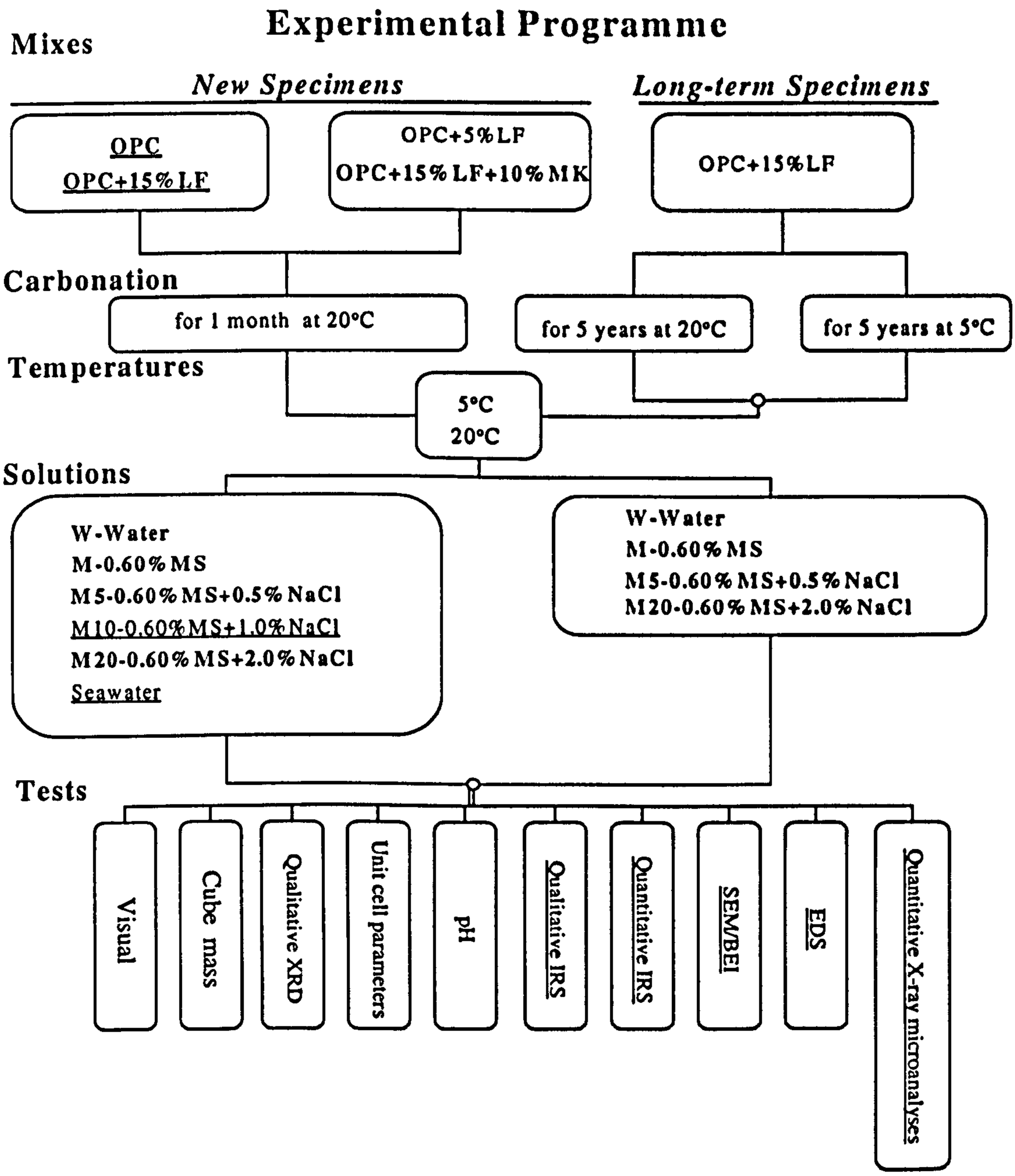

Figure 3.1: Schematic view of the experimental programme. (LF): amount of limestone filler in %; (MK): metakaolin; (MS): magnesium sulfate; (XRD) X-ray diffraction; (IRS): Infrared spectroscopy; (SEM/BEI): scanning electron microscopy/ backscattered electron image; (EDS): energy dispersive x-ray; underlined solutions and tests were applied to the underlined mixes.

3.3 Materials

Table 3-2 shows the selected materials for this investigation. The characterisations and proportions are shown in subsequent sections.

Table 3-2: materials selected

Component	Material
Fine aggregate	German Normensand (an European Standard quartzite sand)
Cement	BS12 OPC
Pozzolan	Metakolinite
Filler	Carboniferous limestone

3.1.2 Characterisation

The chemical and mineralogical composition of the Portland cements and limestone are shown in Table 3-3 and Table 3-4. The mineralogical composition of the cement was calculated by the Bogue method.

Table 3-3: Chemical and mineralogical composition of materials in Long-term specimens.

Oxides	Limestone (%)*	OPC (%)**	Phases	Content (%)
SiO_2	0.86	21.08	C_3S	48.70
Al_2O_3	0.08	5.13	C_2S	23.70
Fe_2O_3	0.34	3.00	C_3A	8.50
CaO	56.25	64.58	C_4AF	9.10
MgO	0.58	2.91		
SO3	0.22	2.93		
K_2O	0.05	0.74	Gypsum	6.30
Na_2O	0.08	0.32		
loss on ignition	42.01	1.36	Free CaO	1.70

* Supplied by the Dept. of Engineering Materials of the University of Sheffield;
** Supplied by the manufacturer.

Table 3-4: Chemical and mineralogical composition of materials in new specimens.

Oxides	Limestone*	OPC**	Metakaolin*	Phases	Content
	(%)	(%)	(%)		(%)
SiO_2	0.86	20.82	55.40	C_3S	49.41
Al_2O_3	0.08	5.30	40.50	C_2S	22.42
Fe_2O_3	0.34	2.08	0.65	C_3A	10.52
CaO	56.25	64.78	0.01	C_4AF	6.32
MgO	0.58	0.98	0.12		
SO3	0.28	3.28	-		
K_2O	0.05	0.57	2.17		
Na_2O	0.08	0.20	0.13	gyspum	7.05
LI	42.01	1.63	1.00	Free CaO	1.7

* Supplied by the Dept. of Engineering Materials of the University of Sheffield;
** Supplied by the manufacturer.

3.4 Mortar mixes and casting

A series of mortar prisms (40x40x160 mm^3) were cast according to the mixes shown in Table 3-5, in which a binder to sand ratio 1:2.5 was used for all mixes. The water to binder ratio was kept constant at 0.50, except for the metakolin containing mix in which the water to cement ratio was the same as that of the 15% limestone filler containing mix, in order to compensate for the effect of diluting the cement content by 25% (15%LF + 10%MK). Each mix was cast in one single batch. The limestone powder and the Portland cement were dry mixed prior to the inclusion of the other constituents, in order to guarantee an even mixture of the limestone filler with the cement. The same was done for the metakaolin containing mix. After the sand was added, further dry mechanical mixing was performed before adding the water. The specimens were mechanically mixed at low speed, poured into steel prismatic moulds in two layers. The mixes contained in the prism moulds were compacted in a vibrating table in two stages (one per layer) in order to remove any entrapped air bubbles. The mould edges were sealed with silicon sealant to avoid loss of water during the first day of curing. The moulds were then covered with plastic sheets, and wet Hessian bags for the first 24 hours at room temperature (~18-20°C).

Subsequently, the specimens were placed under water for 7 days, followed by 21 days in air at room temperature. Prior to submersion in the test solutions at the specific storage temperature, each prism was cut into 2 cm^3 cubes. The cubes were then placed in individual containers, with specific solutions, until required for testing. During the

period of this investigation, the containers were covered with Perspex lids and wrapt with cling film to avoid water evaporation.

Table 3-5: Mortar mixes of new specimens

Microstructure Mortar Samples							
Mix	Cement		Limestone	Metakaolin	Sand	Water	W/C
0	g/prism	192.86	0.00	0.00	482.14	96.43	0.50
	per wieght cement	1.00	0.00	0.00	2.50	0.50*	
5	g/prism	183.21	9.64	0.00	482.14	96.43	0.53
	per wieght cement	0.95	0.05	0.00	2.50	0.50*	
15	g/prism	163.93	28.93	0.00	482.14	96.43	0.59
	per wieght cement	0.85	0.15	0.00	2.50	0.50*	
MK	g/prism	147.54	28.93	16.39	482.14	86.79	0.59
	per wieght cement	0.77	0.15	0.09	2.50	0.45*	

* Considering replacement materials as binders.

3.5 Long term samples

Long-term mortar samples, which used the same limestone filler of this investigation as well as mix proportions and water to binder (w/b) ratio, were originally cast by Hartshorn [69]. In order to assess the effect of carbonation on TSA development, these mortar prisms (40x40x160cm), which were stored in air at 5°C and 20°C for 5 years, hereafter designated as 15LT5 and 15LT20, respectively, were cut in 2 cm^3 cubes. These mixes will be designated as long-term specimens LT. These cubes were stored in the selected solutions as shown in Table 3-6.

Table 3-6: Long-term Mortar Mixes

Mix	OPC (%)	Limestone (%)	w/b	T (°C)	Solution	
15LT5	85	15	0.5	5	M	0.6% SO_4
15LT20	85	15	0.5	20	M5	0.6% SO_4 + 2.0% Cl
					M20	0.6 % SO_4 + 2.0% Cl

3.6 Test Solutions

Six solutions were used in the experiments: High purity water, which was both deionised and demineralised (W), pure magnesium sulfate 0.60% SO_4 diluted in high purity water (M), and three combinations of chloride and sulfate (i) 0.60% SO_4 + 0.5%Cl (M5), (ii) 0.6%SO_4 + 1.0% Cl (M10) and (iii) 0.6% SO_4 + 2.0% Cl (M20), all in high purity water. The chemical compositions are shown in Table 3-7. Table 3-8 shows

the composition of the simulated seawater, designated as *sea* in some parts of this research. The salt solutions were renewed in two stages: In the first stage, no replenishment was made for a period of six months. This was used in order to investigate the variability of the pH with respect to the onset of thaumasite formation. In the second stage, the salt solutions were renewed once every three-months up to 12 months for all systems, and up to 18 months for MK to simulate field cases where natural underground water movement is continuously reloading the system with ions

Table 3-7: Solution compositions.

Solution	SO_4^{2-}	Cl^-	Mg^{2+}	Na^+
	g/l			
W	0.00	0.00	0.00	0.00
M	6.00	0.00	1.50	0.00
M5	6.00	5.00	1.50	3.24
M10	6.00	10.00	1.50	6.50
M20	6.00	20.00	1.50	12.97
Sea water	2.79	21.5	1.20	20.75

Table 3-8: Synthetic seawater composition.

Sea water					
Salt	g/l	SO_4^{2-} (g/l)	Cl^-(g/l)	K^+(g/l)	HCO_3^- (g/l)
NaCl	32.00		21.5		
$MgCl_2$	2.80				
Espom salt	5.00	2.79			
Gyspum	1.50				
$KHCO_3$	0.20			0.08	0.12

3.7 Visual inspection

Visual assessment of the specimens was made on a monthly basis, in which the cubes were scanned and any change in colour, expansion or precipitation of any material was recorded.

3.8 Mass change

In order to assess the damage in the mortar cubes, the mass of six replicas was determined after 12 months of immersion in solution. The samples were taken from their individual containers and surface dried. Any loose parts of the sample as well as any mushy material was removed by hand prior to weighing. However, it was not

possible to remove totally the mushy material, resulting in lower reproducibility of the results for the highly damaged samples.

3.9 X-ray diffraction and Infrared spectroscopy sample preparation

At the required testing date, two types of material were taken from each container: (i) the material that precipitated at the bottom of the containers, which was designated as corroded material, and (ii) the remaining cube, which were designated as bulk sample. The corroded material after 12 months consisted of all material deposited in the bottom of each container as a result of the attack in all cubes during the entire period of immersion. These samples were primarily crushed in a porcelain mortar and pestle. Secondly, the corroded material was gently sieved through a series of sieves, grading from 1200 to 150μm, in an attempt to reduce the amount of sand particles in the powder since the corroded material was easier to grind by hand than the silica sand. Subsequently, both sets of powder were mechanically ground in an agate grinder at low speed, for approximately 10 minutes. Acetone was also used during the mechanical grinding in order to stop hydration, provide a better distribution of particles and also as a cooling agent, which is necessary to avoid the destruction of phases such as ettringite and Friedel's salt, both sensitive to heat above 60°C. The temperature of the mechanically ground powder was occasionally checked, which was never higher than 35°C. After grinding, the samples were sieved through a 35μm sieve. In order to avoid contamination from another sample, the sieves were washed with acetone in between each sieving, as were the brush, the mortar and pestle and the mechanical agate grinder.

Finally, the powders were stored in small plastic bags. Before being tightly sealed, the bags were pressed by hands so that most of the air was removed. X-ray diffraction (XRD) and infrared spectroscopy (IRS) were performed immediately after the sample preparation. However, the powdered samples stayed in the plastic bags inside silica gel containing desiccators until completion of the analyses.

3.9.1 XRD

The analyses were performed either by a Philips 1710 diffractometer, with an automatic loading device, or by a Siemens D500 X-ray diffractometer. The powders were back-filled in an aluminium holder, to reduce the chances of preferred orientation. For qualitative analysis, all the X-ray readings followed the same set up: ($CuK\alpha$-40kV-35mA-step size: 0.02°-2°/min). The database of the Joint Committee for Powder

Diffraction Files (*JCPDF*) was used to identify the crystalline phases of the patterns, built in the *WinXpoe* software.

For unit cell parameter determinations, the testing time was increased to an overnight running (*CuKα*-40kV-35mA-step size: 0.02°2θ-speed: 0.056°2θ/min) either in the reflection Siemens D500 or in the transmission X-ray STOE. The advantages of the STOE over the Philips or Siemens are its monochromatic radiation and a built in position sensitive X-ray detector (PSD), which provide better resolution with respect to the full width at a half maximum (FWHM) of the peaks, which are expected to be around 0.05°θ rather than 0.15°θ, respectively. However, both reflection and transmission geometries can be used for unit cell parameter determination only, provided an accurate correction for zero peak shifts is performed, as these parameters are calculated using interplanar spaces (d_{hkl}) and Miller indices (h,k,l) and do not depend on peak shape, but peak position only. Unit cell parameters (a and c) of hexagonal minerals are calculated according to Equations 3.1 and 3.2. Peak shift is very common in XRD, which depends mostly on instrumental factors but also depends on sample preparation factors as well [123]. For such reasons, and also because the difference between thaumasite and ettringite XRD peaks can be as small as ~ 0.12°2θ, it is imperative to correct the patterns with respect to 2θ angle. The wave length λ depends on the radiation used. For copper radiation λ is equal to 1.540598Å.

$$d_{hkl} = \frac{\lambda}{2\sin(\theta_{hkl})} \tag{3.1}$$

$$\frac{1}{d_{hkl}^2} = \frac{4}{3}\left(\frac{h+hk+k}{a^2}\right) + \frac{l^2}{c^2} \tag{3.2}$$

The zero shift correction was performed by using the *WinXpoe/angle correction* built in software. In this procedure, all the peaks assigned to a known phase in the acquired XRD pattern, either calcite or quartz in this research, were compared to a standard powder diffraction of the same mineral from the JCPDF database. The raw data was then corrected using the polynomial with best parameters using least-square procedure. The aligned XRD pattern was then used for both qualitative analyses and lattice parameter determinations.

The error associated with unit cell parameters was estimated at ±0.005°2θ. An example of this estimation can be seen in Table 3-9, which was taken from a thaumasite detected in the corroded material of a 15%LF after 12 months.

Table 3-9: Estimation of error in unit cell parameter determinations.

Dobs	2Theta	I(rel)	I(abs)	FWHM	Miller indices			dcalc	dobs-dcalc
					h	k	l		
9.60	9.21	55.93	396.00	0.220	1	0	0	9.58	0.0172
5.53	16.03	36.85	261.00	0.083	1	1	0	5.53	-0.0066
4.35	20.38	5.36	38.00	0.083	2	0	1	4.35	-0.0003
3.80	23.37	37.71	267.00	0.220	1	1	2	3.80	0.0051
3.53	25.22	15.75	112.00	0.180	2	0	2	3.53	-0.0030
3.43	25.98	19.31	137.00	0.260	2	1	1	3.42	0.0053
3.28	27.17	7.20	51.00	0.083	1	0	3	3.27	0.0054
2.95	30.28	7.38	52.00	0.080	1	1	3	2.95	0.0020
2.73	32.82	25.27	179.00	0.200	3	0	2	2.73	0.0015
2.58	34.79	11.01	78.00	0.083	3	1	1	2.58	0.0009
2.51	35.75	23.91	169.00	0.280	2	1	3	2.51	-0.0009
2.37	37.94	10.09	71.00	0.040	3	1	2	2.37	0.0011
2.20	40.98	10.87	77.00	0.083	3	2	0	2.20	0.0026
2.18	41.43	14.26	101.00	0.083	4	0	2	2.18	0.0003
2.16	41.70	21.42	152.00	0.360	2	2	3	2.17	-0.0016
2.11	42.80	14.54	103.00	0.120	3	1	3	2.11	-0.0016
2.03	44.66	43.29	307.00	0.280	3	2	2	2.03	0.0013
1.91	47.45	20.50	145.00	0.240	2	0	5	1.92	-0.0011
1.81	50.23	9.89	70.00	0.180	3	3	1	1.82	-0.0010
1.74	52.59	7.77	55.00	0.120	3	3	2	1.74	-0.0001
								SD	0.0047
								Error 2thetha [Confidence Limit (95%)]	0.002

3.9.2 Infrared Spectroscopy (IRS)

Because thaumasite has a distinctive vibration wave band of 500cm^{-1}, IRS is a very powerful technique in the detection and characterisation of solid solutions between thaumasite and ettringite [124].

The Infrared spectroscopy analyses were performed alongside XRD, using the same powder samples. Pellets of 12 mm (diameter) were prepared by intergriding 2 mg of the sample with 198 mg of potassium bromide (KBr) until a homogeneous powder was produced. The balance was sensitive to ±0.01mg. The mixed powders were compressed in an appropriate die, under vacuum, for 2 minutes at 2MPa and 2 minutes at 20MPa. Subsequently, the pressure was slowly released to avoid breaking the discs. The pellets were then placed in a brass or cardboard holders in the Perkin Elmer Spectrum 200 FTIR spectrometer chamber. The equipment was set to scan the samples in the *Mid infrared* (MIR) range of 4800-370cm^{-1}. The spectra were acquired in a transmittance mode, as a ratio between the samples and a background, which were run prior to the analyses. The spectra were analysed in the software suite *Spectrum for Windows*.

In some samples, a quantitative approach was taken, as an attempt to correlate the damage associated with the formation of octahedron silicon, which is exclusive tothaumasite solid solution series, and (i) the intensity of 500cm^{-1} wave band and (ii) the ratio between this wave band and 855cm^{-1} wave band, which is assigned to Al-O-H as in ettringite. A more detailed description of these techniques is addressed in Chapter 6 of this thesis.

In order to estimate the accuracy of the quantitative approaches taken with IRS, a pure sample of gypsum was tested twice. Table 3-10 and Figure 3.1: show the raw net intensity IRS data of gypsum spectrum and relative intensity ratio standard errors within these peaks. It can be seen that the error varied with the magnitude of the IRS signal, but it was found to be below 12.5% for transmittance values higher than 5% and between 15% to 20% for values below 5%, in both approaches: (i) net intensity and (ii) intensity ratios.

Table 3-10: Raw data and error distribution in IR spectra of gypsum.

Number	Peak Cm-1	Replica 1 Transmittance (%)	Rreplica 2 Transmittance (%)	Mean	Sd	Rel Sd error
1	1141.600	53.120	53.350	53.235	0.163	0.379
2	1007.700	14.380	9.430	11.905	3.500	7.858
3	674.500	38.320	38.220	38.270	0.071	0.347
4	601.200	46.600	45.770	46.185	0.587	0.829
Peak ratios		Replica 1 Transmittance (%)	Replica 2 Transmittance (%)	Mean	Sd	Rel Sd error
1/2		3.694	5.657	4.676	1.388	12.600
1/3		1.386	1.396	1.391	0.007	2.968
1/4		1.140	1.166	1.153	0.018	5.847
2/3		0.375	0.247	0.311	0.091	48.469
2/4		0.309	0.206	0.257	0.073	52.328
3/4		0.822	0.835	0.829	0.009	5.724

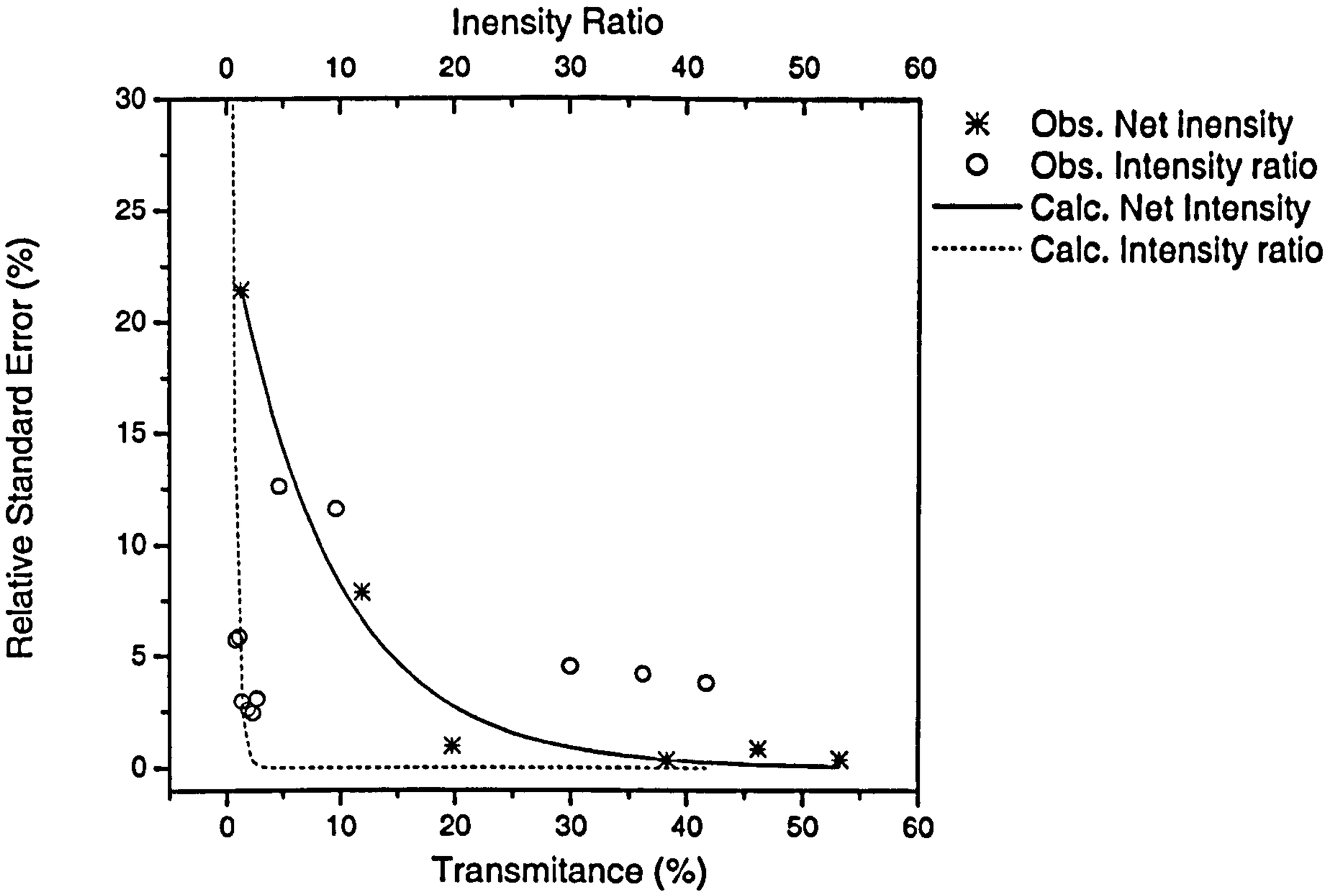

Figure 3.1: Distribution of error on the IRS gypsum spectrum.

The quantitative approach was used for the corroded material of Portland cement mortar samples with and without limestone filler after 12 months in salt solutions, but not for metakaolin containing samples.

3.10 Scanning Electron Microscopy and X-Ray Microanalysis

The samples containing 15% limestone filler were analysed by means of backscattered electron imaging (BEI-25kV) of a polished section and energy dispersive X-ray (EDS)/Link analytical software after 12 months in salt solutions at 5°C. Cubes ($8cm^3$) were taken from the appropriate storage containers and dried in desiccators for three days at room temperature. The samples were cut along the cross section using an oil-based cutting wheel, so that changes between surface and core could be detected, and impregnated with cold setting resin and left under vacuum for 24h. After hardening, the samples were manually ground using four grades of silicon carbide paper and oil-based solution. Subsequently, the samples were polished in four grades of diamond discs from 6μm to 1/4μm. After polishing, the samples were submitted to an ultrasonic bath in acetone for 15 minutes, in order to ensure clean a surface. They were then carbon coated and placed in a vacuum desiccator until required for testing. Long-term specimens were analysed using a Camscan Mk 2 SEM/Link (BEI/15kV). Lower voltage

was used in order to investigate a more superficial chemical composition of thaumasite solid solutions, as the interaction volume reduces with the reduction of the accelerating voltage [125]. The primary electron range, which determines the size of the volume, is affected by the atomic mass (A), atomic number (Z), the density of the material (ρ g/cm^3) and the electron beam (E_0 keV), and can be calculated by using Equation 3.3 [125]:

$$R = \frac{0.0276 A E_0^{1.67}}{\rho Z^{0.89}} (\mu m) \qquad (3.3)$$

As for X-ray microanalyses, the polished samples were analysed in a Phillips PSEM 500 microscope in backscattered electron (BSE) mode. The take off angle was 40°, and the acquisition time was 100 seconds. The EDS unit was set to detect Kα of the following elements: Na, Mg, Al, Si, P, S, Cl, K, Ca, Mn, Fe and Cr; O was calculated by stoichiometric calculations.

The atomic concentrations were calculated using the built in software, which performed the appropriate ZAF correction. The ZAF correction is a complicated computational routine, which takes into account the different interactions between the electron beam and atoms in the specimens, including the differences from a standard sample of known composition and the samples to be analysed. Basically, this method takes into account [125]:

(Z) The fact that the atomic number of the element in the standard and the mean atomic number of the matrix of the sample are different;

(A) The fact that the energy generated by the element in the standard and the same element in the specimen is differently absorbed, since this energy passes through different matrixes as they travel towards the detector;

(F) The fluorescence generated by the characteristic and continuum radiation in the interaction volume.

Basically, the intensity of the elements ($I_{SPECIMEN}^{ELEMENT}$) were normalised with respect to a standard sample ($I_{STANDARD}^{ELEMENT}$), with previously known composition, and the concentration of a certain element ($C^{SPECIMEN}$) determined by Equation 3.4 [125].

$$C^{SPECIMEN} = (ZAF)^{ELEMENT} \frac{I^{ELEMENT}_{SPECIMEN}}{I^{ELEMENT}_{STANDARD}} \quad (3.4)$$

After the corrections, atomic ratios were used to investigate changes in the cement matrix due to chemical attack, the chloride binding capacity of the matrix at the core and the surface and also the composition of thaumasite affected areas.

3.11 pH changes

The pH was measured at monthly intervals using a Hanna HI 931000 pH and temperature meter and H 1217D electrode. This equipment contains an accuracy of ±0.01 pH and automatically compensates the effect of temperature on pH. The pH meter was calibrated with buffer solutions at a pH of 10, 7 and 4, prior to each set experiment, meaning before each day in which half of the samples were analysed. The electrode, which was immersed about 4 cm inside the solution, was agitated until a constant reading was displayed for each reading. Subsequently, the electrode was dried with paper towels and washed in deionised water in between each reading to avoid contamination from one solution to another. The initial pH of each solution, before the contact with mortar sample, is shown in Table 3-11. The temperature of the solution was frequently checked immediately after removing the samples from the fridge, in order to identify whether the conditions were kept as designed. Little variation of temperature was detected for samples inside the fridge. Samples at room temperature were mostly around 20°C but occasionally around 18°C, on some winter days.

Table 3-11: Initial pH of solutions before contact with mortar samples.

Solution	pH
Water	7
M	7.28
M5	7.01
M10	6.78
M20	6.85
Sea	8.12

3.12 Statistical analysis

In order to evaluate the effects of the selected parameters and their interactions, a multivariate analysis and analysis of variances (ANOVA) were performed according to the experimental design shown in Table 3-12, for samples immersed in solutions for 12 months.

Table 3-12: Experimental design for samples after 12 months.

Effects	Units	Replicas			
Cube mass	g	6			
Unit *c*	Angstroms	1			
Unit *a*	Angstroms	1			
$\overline{S}$ /Ca	-	16			
Al/Ca	-	16			
Cl/Ca	-	16			
Si/Ca	-	16			
NetSi500	% Transm.	1			
Si_{moles}	Moles	1			
Factors	**Units**	**Levels**			
$CaCO_3$ filler replacing clinker	%	0		5	15
Cl concentration in solution	%	0	0.5	1.0	2.0
Temperature	°C	5		20	

For the polynomial statistical models, some effects were included as factors in order to estimate whether any significant correlation existed between these effects. The starting statistical model included all the factors and their interactions up to the third order orthogonal polynomial. After fitting by a non-linear least square procedure, the significance of each parameter of the polynomial was tested. The best models were chosen when all the parameters were statistically significant, as represented by t-student test of each parameter (Prob>t) and the multivariate correlation coefficient (R^2) and F distribution of the model. The multivariate statistics equations and table is according to Kleinbaum et al.[126].

Chapter Four

MICROSTRUCTURE OF 5-YEAR OLD MORTARS CONTAINING LIMESTONE FILLER DAMAGED BY THAUMASITE

4.1 Abstract

This paper presents the findings of a long-term study on the microstructure of Portland cement mortar specimens containing 5, 15 and 35% limestone filler, as cement replacement, after exposure to a solution of magnesium sulfate at a concentration of 1.44% SO_4, for 5 years at 5°C. The findings are compared to results reported earlier, obtained from the same systems but after one-year exposure. It was found that the deterioration due to thaumasite advanced with the increased exposure period and limestone content. Thaumasite solid solutions (Tss) formed as the dominant phases within the deteriorated cement matrix and at the paste-aggregate interface resulting in cracks and delamination. Thaumasite was also found as an inner product in various clinker grains. Interestingly, the control specimens, with no limestone filler, were found to exhibit cracks due to the formation of Tss, with atmospheric carbon dioxide being the most likely source for the carbonates.

4.2 Introduction

Composite cements make an effective contribution to sustainable construction and the energy efficiency of the concrete industry. There are extensive examples of successful utilisation of industrial by-products such as fly ash, ground granulated blastfurnace slag and silica fume, as well as natural pozzolans, in durable concrete structures. The use of cement replacement materials is also of great environmental importance, since Portland cement production is responsible for about 5-7% of the industrially emitted carbon dioxide to the atmosphere, and also nitrogen oxides, both of which are known to contribute to global warming and acid rain.

For environmental benefits and efficiency gains, composite cements incorporating limestone filler [21] were introduced in recent years. In these Portland-limestone cements, ordinary Portland cement (OPC) is partially replaced by limestone in the range from 6-35% by mass. The European standard (ENV 197-1) allows OPC to contain up to 5% filler by mass and usually limestone is used. Following the discovery of thaumasite in deteriorated bridge foundations in the UK, as reported in the Thaumasite Expert Group (TEG) [2] and Crammond et al [127], the durability of concrete incorporating limestone is currently being extensively investigated. In some of these foundations, the buried concrete was made using sulfate-resisting Portland cement (SRPC) and limestone aggregates. The involvement of limestone in the thaumasite form of sulfate attack (TSA) has been identified as a major factor responsible for the deterioration. Hitherto it had been widely believed that the amount of aluminate phases present in Portland cement controlled sulfate attack through the formation of secondary ettringite and gypsum. However, Hill et al. [119] have shown that restriction of the tri-calcium aluminate phase content in cement does not mitigate against the occurrence of TSA.

The incorporation of fine limestone as filler, partially replacing some of the Portland cement, is known to bring about even greater susceptibility to thaumasite formation than does limestone aggregate [2]. The onset and progress of deterioration in cement paste and mortar, due to TSA, was also found to increase with the increase in limestone filler content in prisms stored in magnesium sulfate solution at 5°C for a period up to 5 years [11, 13, 31, 47]. Furthermore, it was established that thaumasite forms as a solid solution rather than as the pure phase [18]. The solid solution is between thaumasite, $Ca_6[Si(OH)_6.12H_2O]_2(SO_4)_2(CO_3)_2$, and ettringite,

$Ca_6[Al(OH)_6.12H_2O]_2.(SO_4)_3.2H_2O$, and has a miscibility gap associated with a change in the crystallographic space group [65, 66].

The aim of this paper is to report the microstructural changes associated with the formation of thaumasite in mortars made from Portland cement incorporating various levels of limestone filler. The mortars had been stored for 5 years in magnesium sulfate solution at 5°C and are the same samples as those reported on previously [11, 13, 31, 47].

4.3 Experimental Work

The samples were obtained from test specimens, which were prepared about five years previously [6, 7]. Mortar prisms (40 x 40 x 160 mm) were made with a cement to aggregate ratio of 1:2.5 and a water to binder ratio of 0.5. The chemical and mineralogical composition of the Portland cement and limestone are shown in Table 1. The mineralogical composition of the cement was calculated by the Bogue method. Limestone powder replaced 5%, 15% and 35% of the Portland cement on a mass to mass basis. The test specimens were cured in water for 27 days after demoulding at one day, and were then submerged in 1.44% SO_4, as a solution of Epsom salt ($MgSO_47H_2O$), at 5°C. The solution was changed every 3 months in order to simulate mobile ground water. The prisms were kept in these conditions for a minimum of 4 years, after which the solution was allowed to evaporate, and the test specimens were exposed to a drying environment at 5°C for several months. The results reported in this work refer to an overall period of exposure of just over five years.

Table 4-1: Chemical composition of limestone filler and Portland cement.

Oxides	Limestone (%)	OPC (%)	OPC phase Composition	(%)
SiO_2	0.86	21.08	C_3S	48.70
Al_2O_3	0.08	5.13	C_2S	23.70
Fe_2O_3	0.34	3.00	C_3A	8.50
CaO	56.25	64.58	C_4AF	9.10
MgO	0.58	2.91		
SO_3	0.22	2.93	Gypsum	6.30
K_2O	0.05	0.74	Free CaO	1.70
Na_2O	0.08	0.32		
Loss on ignition	42.01	1.36		

The microstructure of the polished surface was examined using a CamScan scanning electron microscope (SEM) in backscattered electron image mode (BEI) with an accelerating voltage of 15kV. Cubes of 20mm size were cut from the edges of each

prism and dried in a dissector for 36 hours at room temperature. Subsequently, the samples were impregnated with a cold setting resin under vacuum. They were then polished down to 1μm and carbon coated. The chemical analysis was carried out by energy dispersive spectroscopy (EDS) equipped with Link analytical facilities.

4.4 Results and Discussion

4.2.1 Control OPC Mortar

Figure 4.1, obtained at low magnification, shows the features close to the edge of the control mortar, which contained no limestone filler. Expansion and cracks could be seen near the surface of the sample. A sub-surface parallel crack pattern had developed along the expanded part of the surface, as can be seen in the magnification of the detail 2 shown in Figure 4.2. The external layer was comprised of needle-like aragonite, calcite, a magnesium-containing hydrate region probably incorporating brucite, and thaumasite. Figure 4.3 shows the chemical composition of the thaumasite, which contained Ca, Si and S and also some Al that is probably indicative of solid solution, in accordance with the XRD data reported previously [18].

Figure 4.4 presents the magnified image of detail 1 from Figure 4.1. It shows an expanded dark-grey area close to the external surface, which is predominantly thaumasite. A closer look reveals another material, with a texture different from that of the dark-grey area, (a band of 60μm), which has crystallised adjacent to the surface of the quartz aggregate, and this can be seen at higher magnification in Figure 4.5. As shown in Figure 4.6, the EDS analysis of these needles shows Ca, Si and S. Since no aluminium was observed, the chemical composition of these needles is characteristic of thaumasite. The extent and distribution of the thaumasite within the matrix and interface suggest that the control OPC sample, is undergone TSA and not thaumasite formation (TF) as defined by the TEG Report [2].

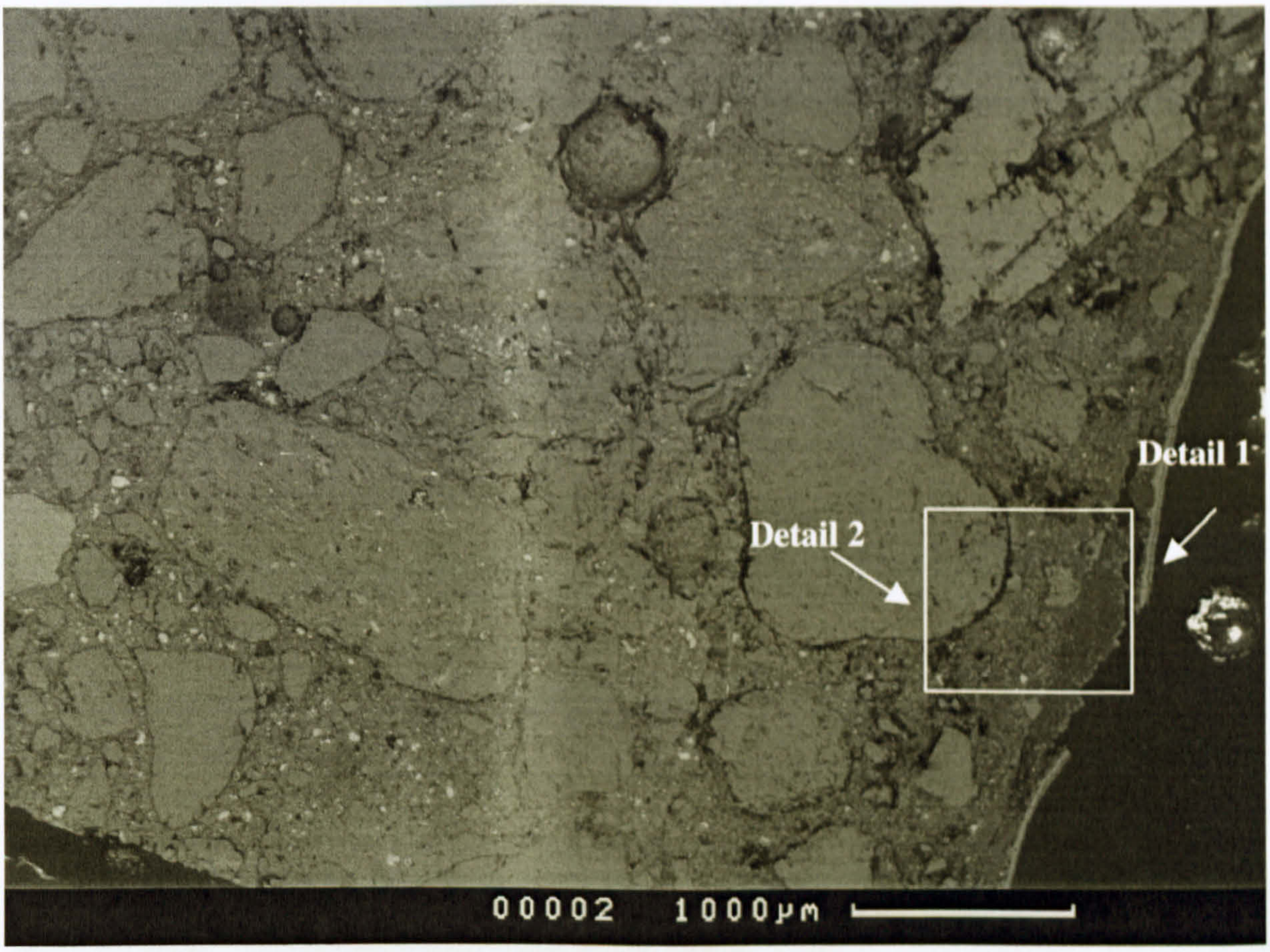

Figure 4.1: SEM of control OPC mortar after 5 years at 5°C in $MgSO_4$ solution.

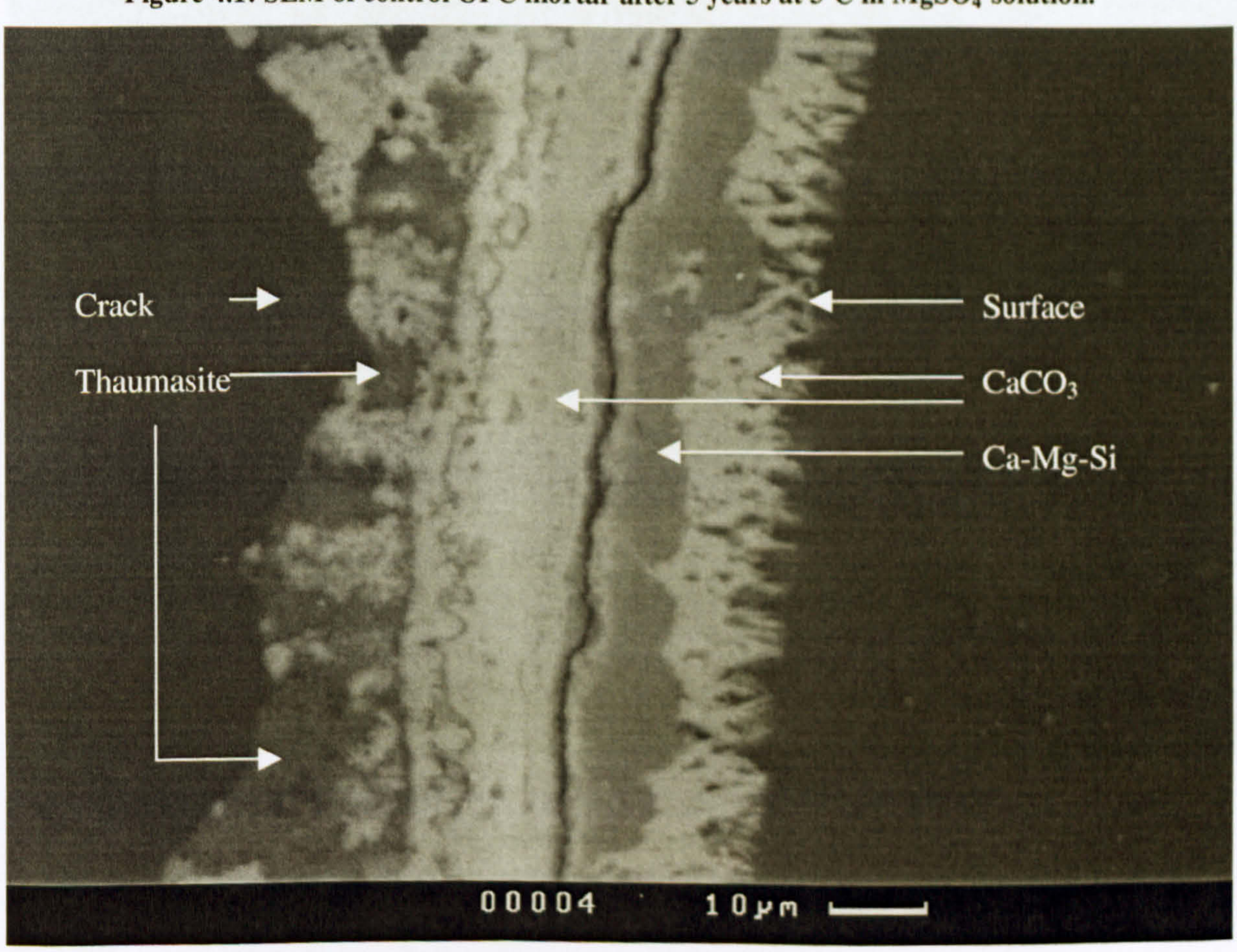

Figure 4.2: Control OPC, detail 1 of Figure 4.1.

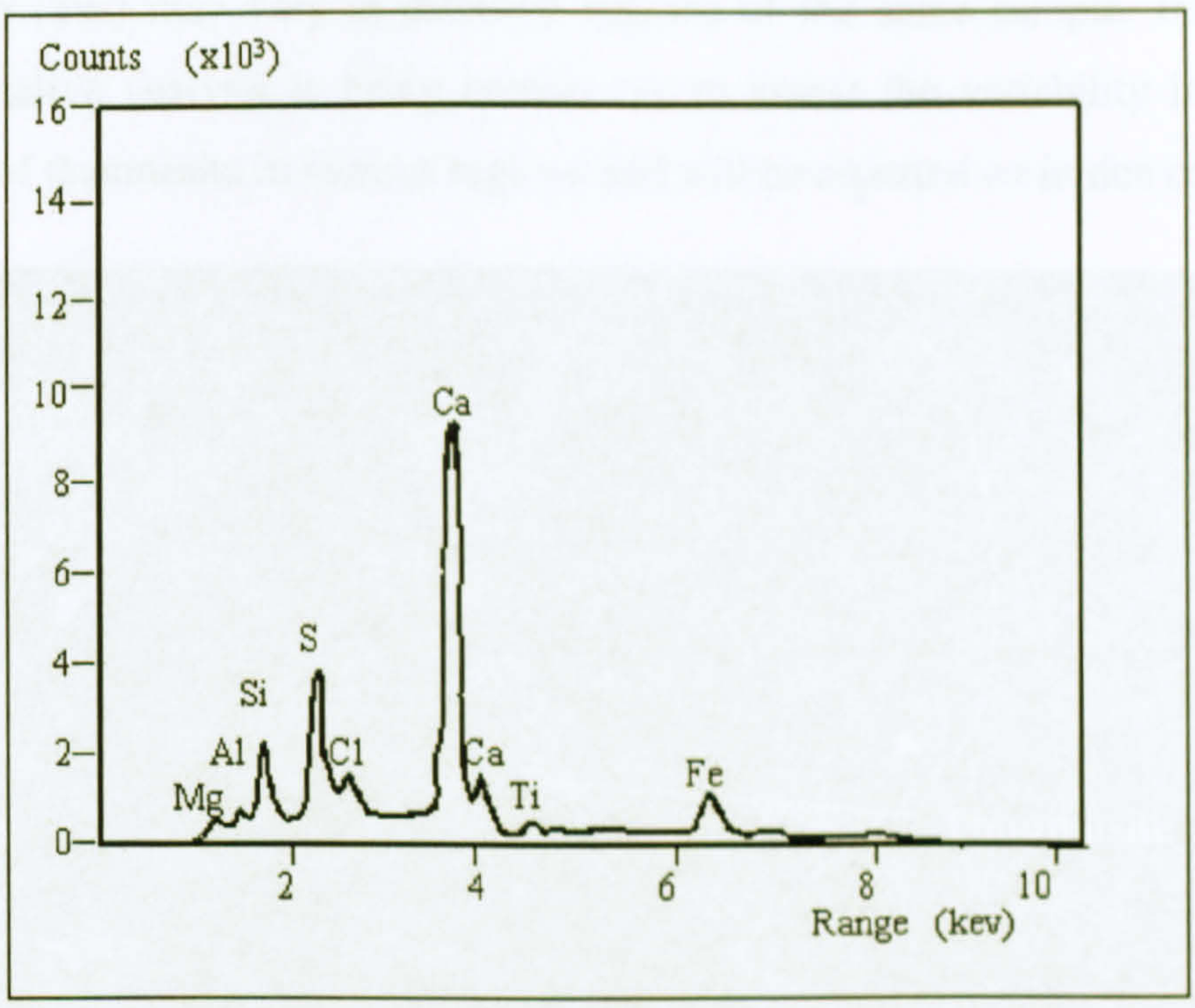

Figure 4.3: EDS of thaumasite in control OPC Figure 4.2.

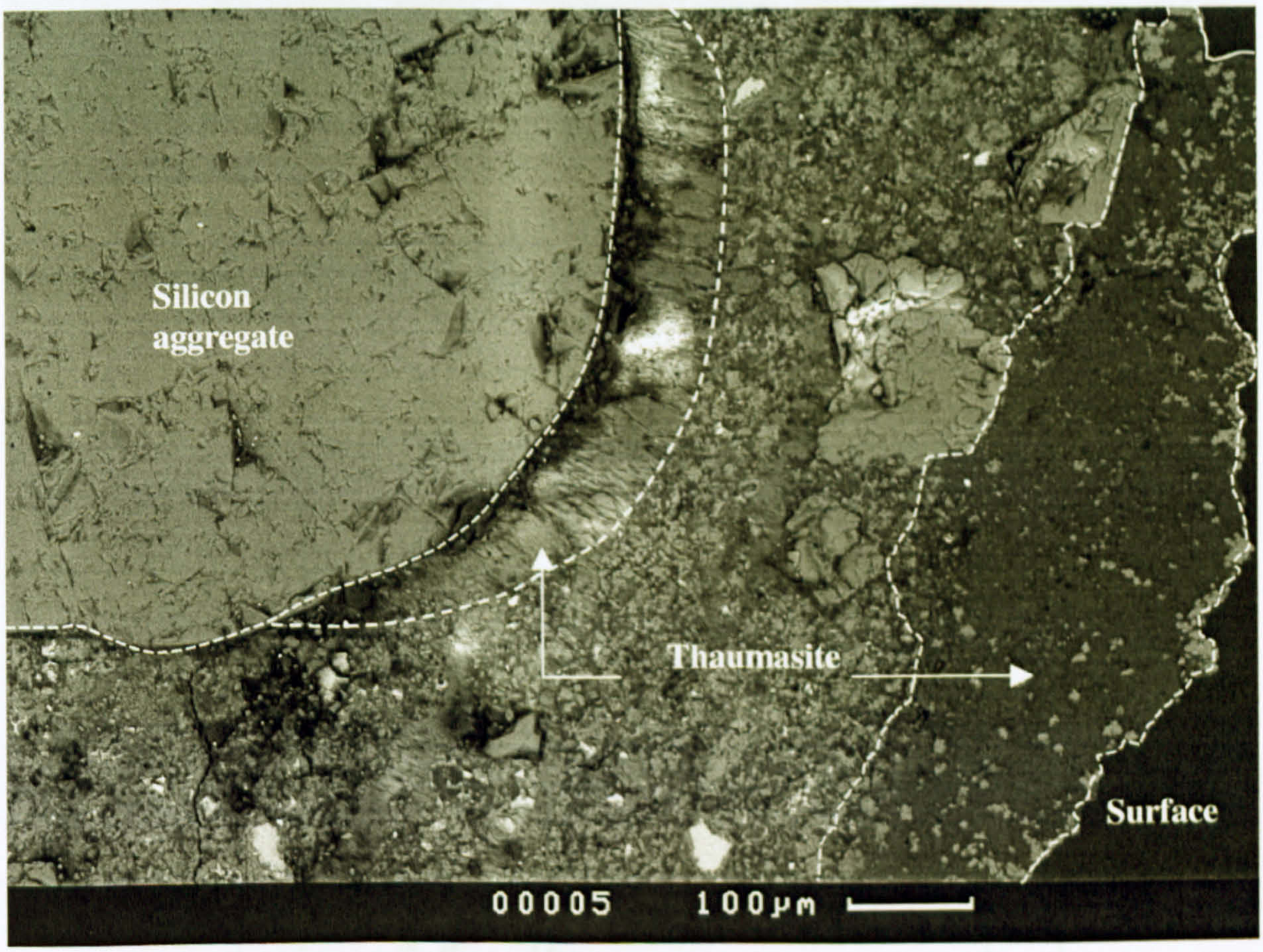

Figure 4.4:Control OPC, detail 2 in Figure 4.1.

Thaumasite texture in a sample seems to vary depending on where it is formed; dark-grey areas were found in the matrix near the surface, whilst needle-like bands were formed at the interface. It seems, therefore, from a comparison of the EDS analyses shown in Figure 4.6 and Figure 4.3, that the chemical composition of the thaumasite

solid solution (Tss) may vary in different regions of the same sample. In a parallel study, quantitative analysis is being carried out to assess the variability in chemical composition of thaumasite in various regions and will be reported on in due course

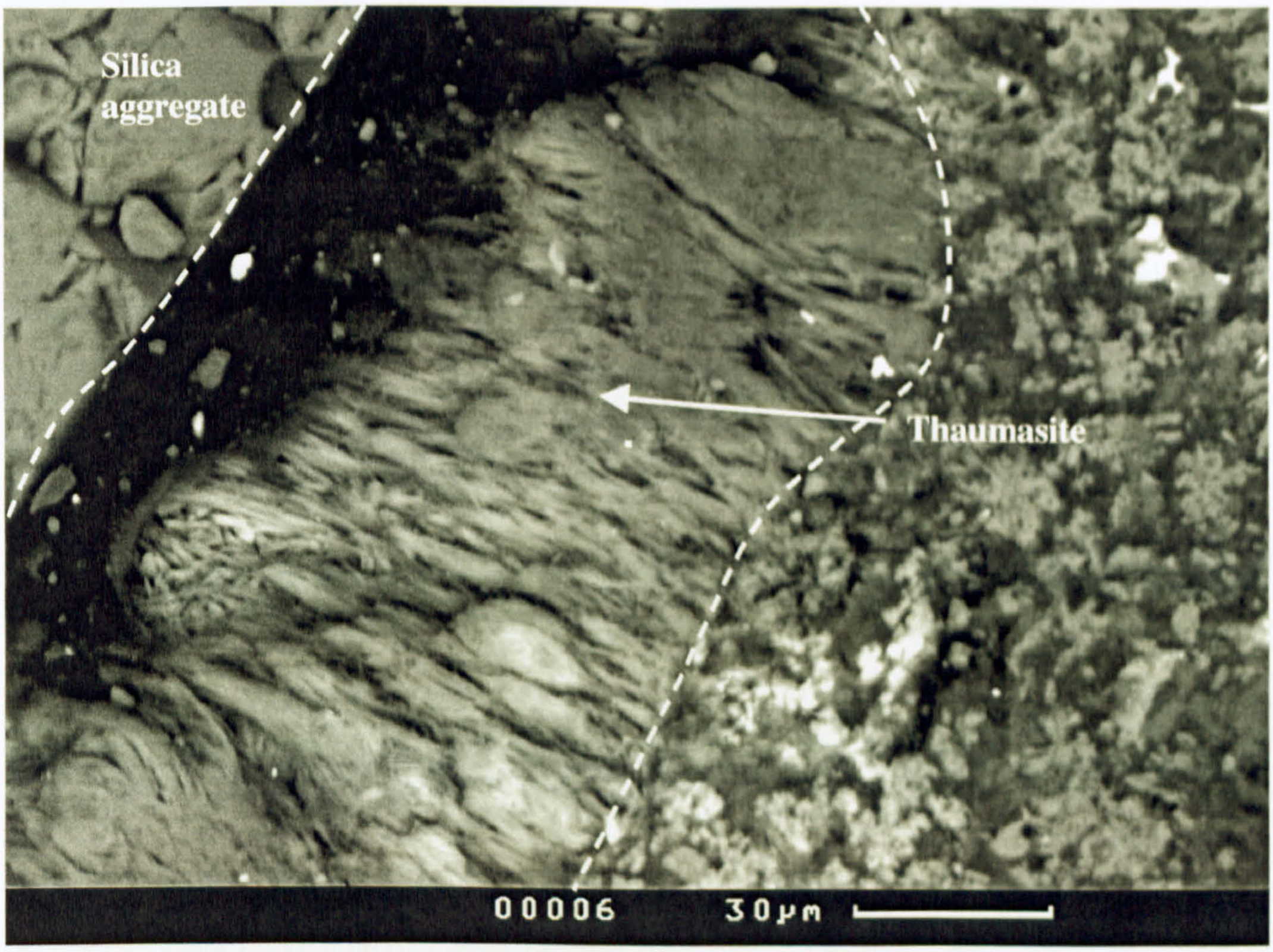

Figure 4.5: Thaumasite surrounding silica grain.

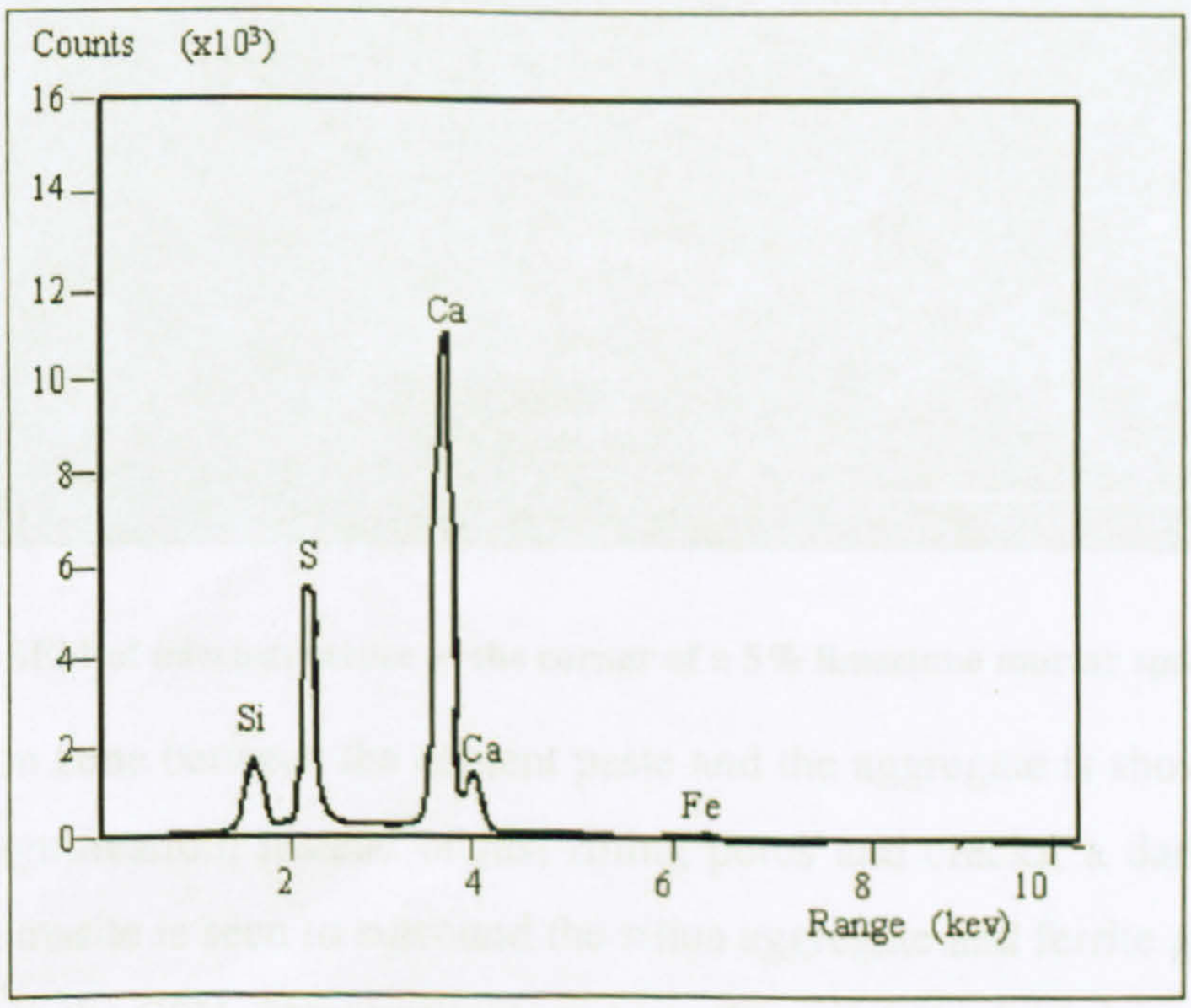

Figure 4.6: EDS of thaumasite in Figure 4.5.

The question arises, how does Tss form in a mortar sample that was made without incorporating any limestone as filler or as aggregate? Inevitably the source of carbonates has to be atmospheric carbon dioxide, as was demonstrated Collett et al. [76].

4.2.2 Mortar with 5% limestone filler

The corner of a sample containing 5% limestone replacement of cement is shown in Figure 4.7 at low magnification. Larger zones of disruption than those observed in the control specimens can be seen in this Figure. Large cracks (dark area inside) are easily detected and the material had started to detach from the bulk sample at about 1000-2000μm away from the corroded edge.

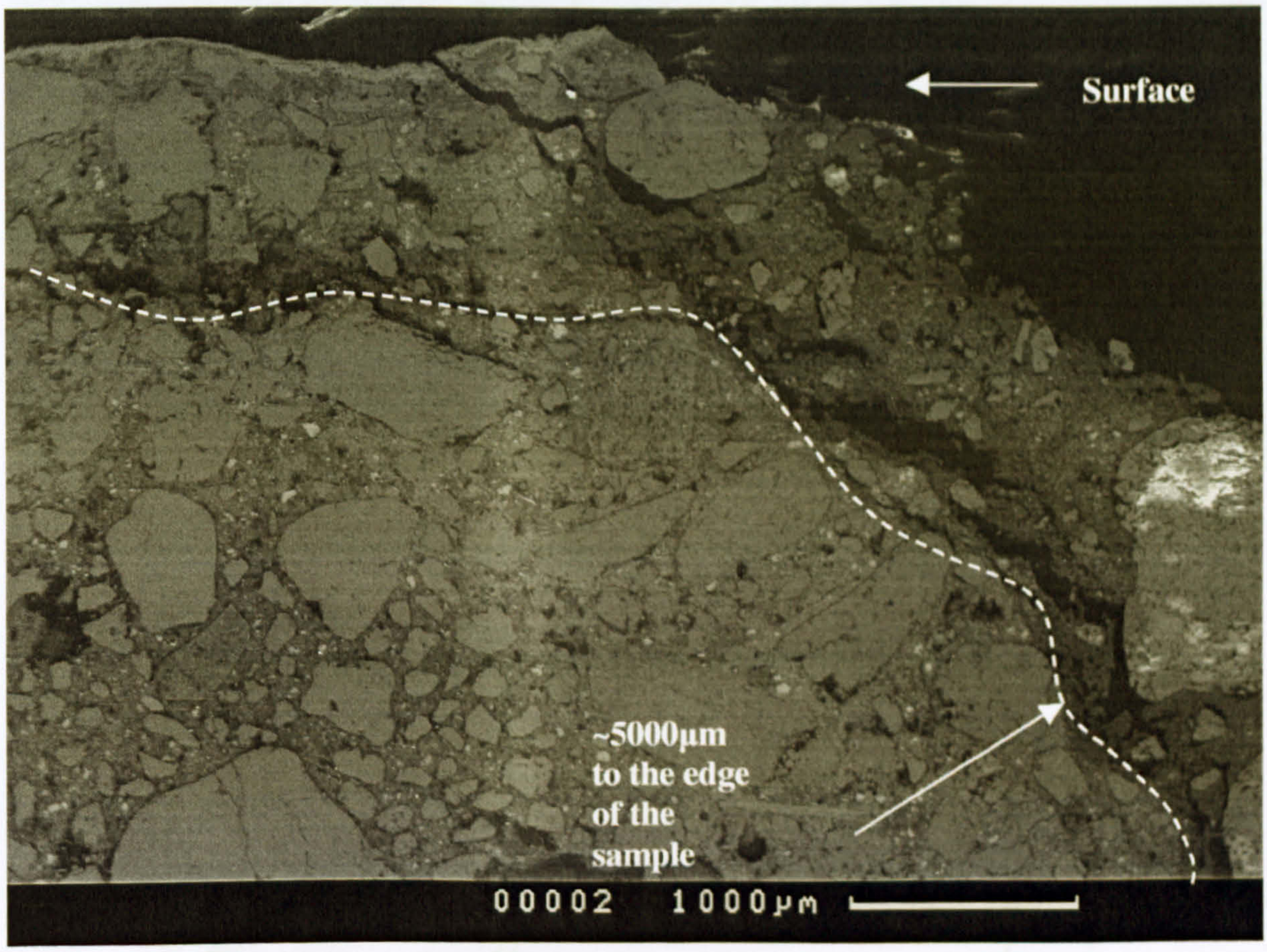

Figure 4.7: SEM of microstructure at the corner of a 5% limestone mortar specimen.

The transition zone between the cement paste and the aggregate is shown in Figure 4.8 at higher magnification. Instead of just filling pores and cracks, a dark-grey layer attributed to thaumasite is seen to surround the silica aggregate and ferrite grains, and is also present within the CSH. The chemical analysis (Figure 4.9) of this layer revealed Š, Si and Ca, which is indicative of thaumasite. Alongside some clinker grains, a mineral containing iron, silicon, potassium and chromium, but not calcium, was also found in

the corroded area as shown in Figure 4.8. This observation indicates that the ferrite phase had been attacked and was decalcified as a result, confirming the findings of Crammond and Halliwell [128], who reported that ferrite could be attacked during thaumasite formation.

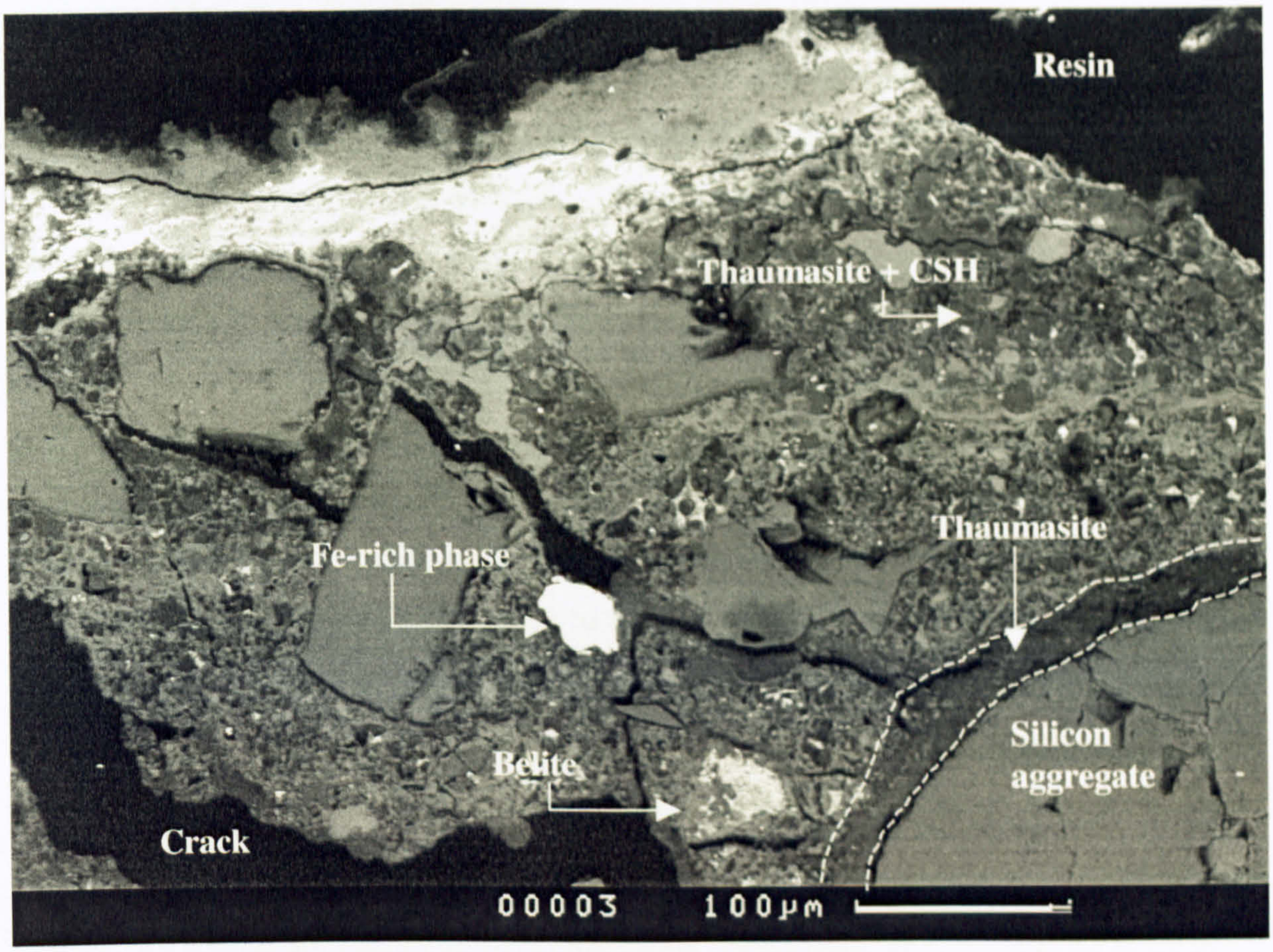

Figure 4.8: SEM of cement matrix of corroded parts of 5% limestone filler mortar.

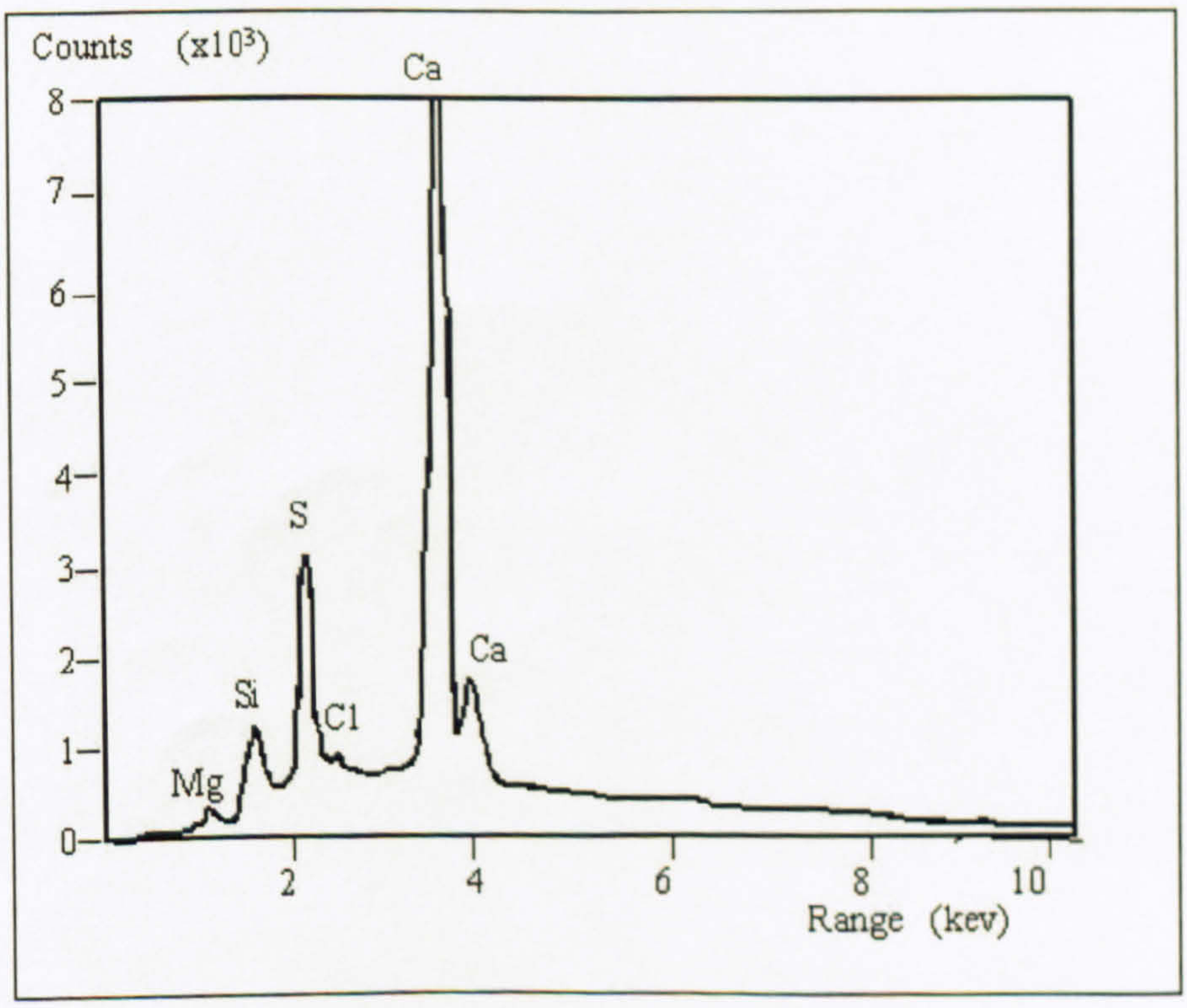

Figure 4.9: EDS of thaumasite around silicon grain in 5% limestone filler sample in Fig 4.8.

4.2.3 Mortar with 15% limestone filler

The micrographs shown in Figure 4.10 and Figure 4.11 indicate that mortar containing 15% limestone filler suffered considerably greater damage when compared to those made with the 5% limestone filler and the control mortars. Although the entire surface was friable, the damage was more severe at the edges and corners, which turned the edges into a rounded shape [13, 18]. The sub-surface parallel cracks extended along the whole surface and they were several times wider than those seen in the 5% limestone mortar. Additionally, the formation of cracks propagated to deeper sites. Thaumasite, as indicated by the EDS analysis shown in Figure 4.12, thus became an all-pervasive phase in the material, as was also observed by Crammond and Halliwell [128]. Although thaumasite has no binding properties, large areas of the cement surface were converted into this phase prior to the total disruption as can be seen in Figure 4.11. This transformation is most likely due to the dry condition to which the samples were finally exposed, since thaumasite becomes mushy in wet concrete. It is noteworthy that thaumasite was more or less homogeneously distributed rather than intermixed with gypsum or CSH, which indicates that the higher the amount of limestone filler distributed in the matrix, the greater its susceptibility to TSA.

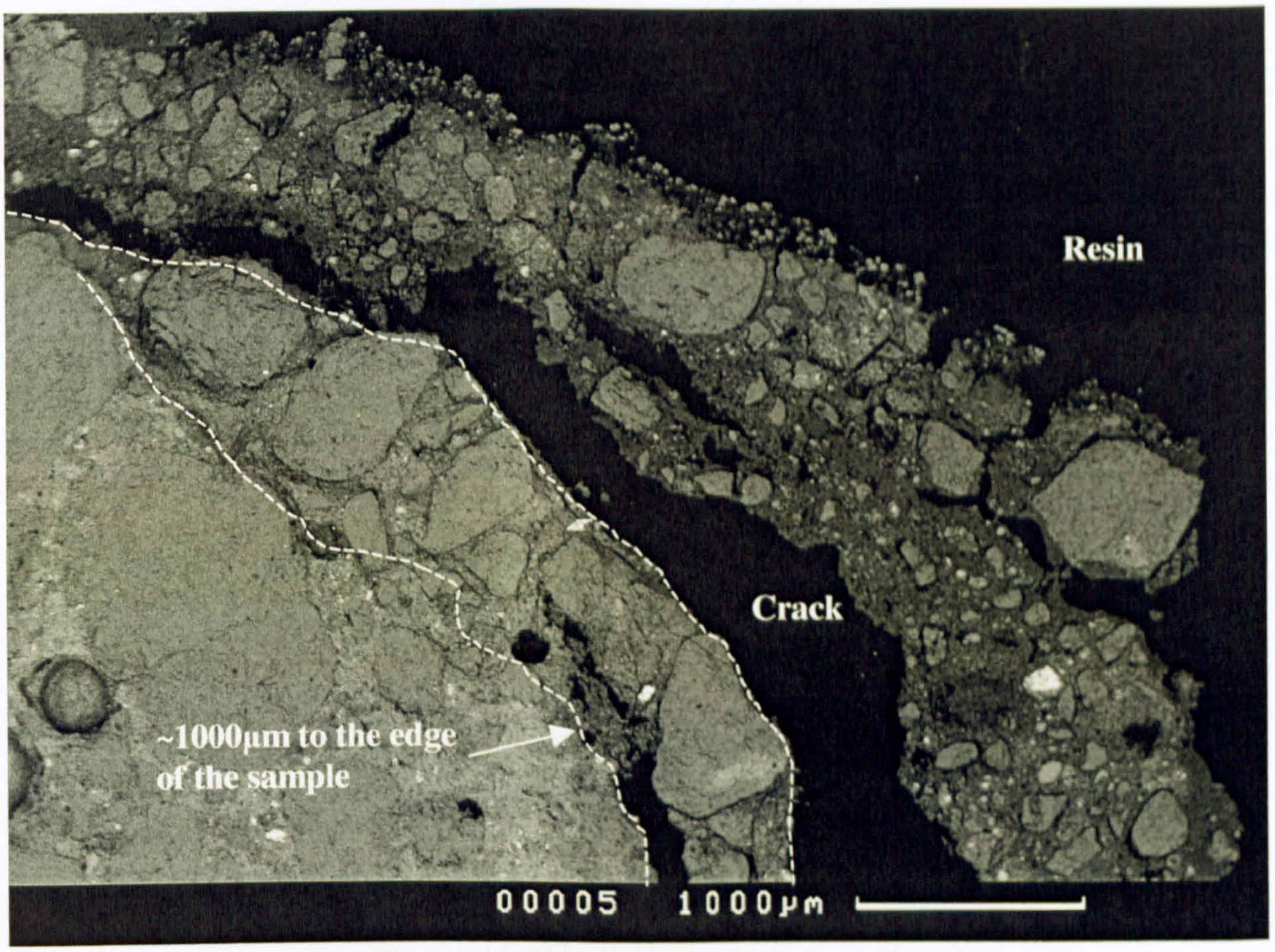

Figure 4.10: SEM of microstructure at the corner of 15% limestone filler mortar specimen.

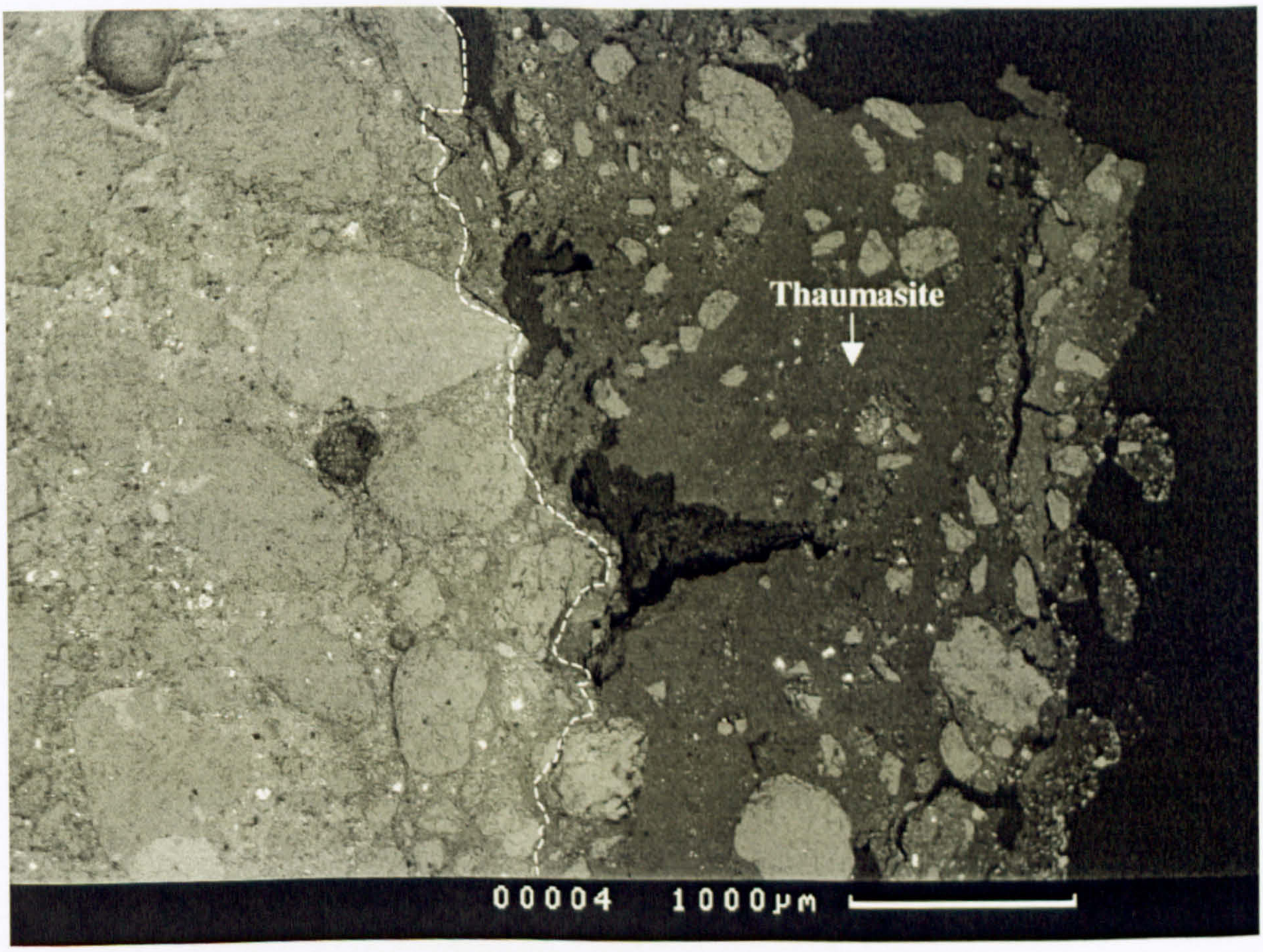

Figure 4.11: SEM of microstructure of the edge of 15% limestone filler mortar specimen.

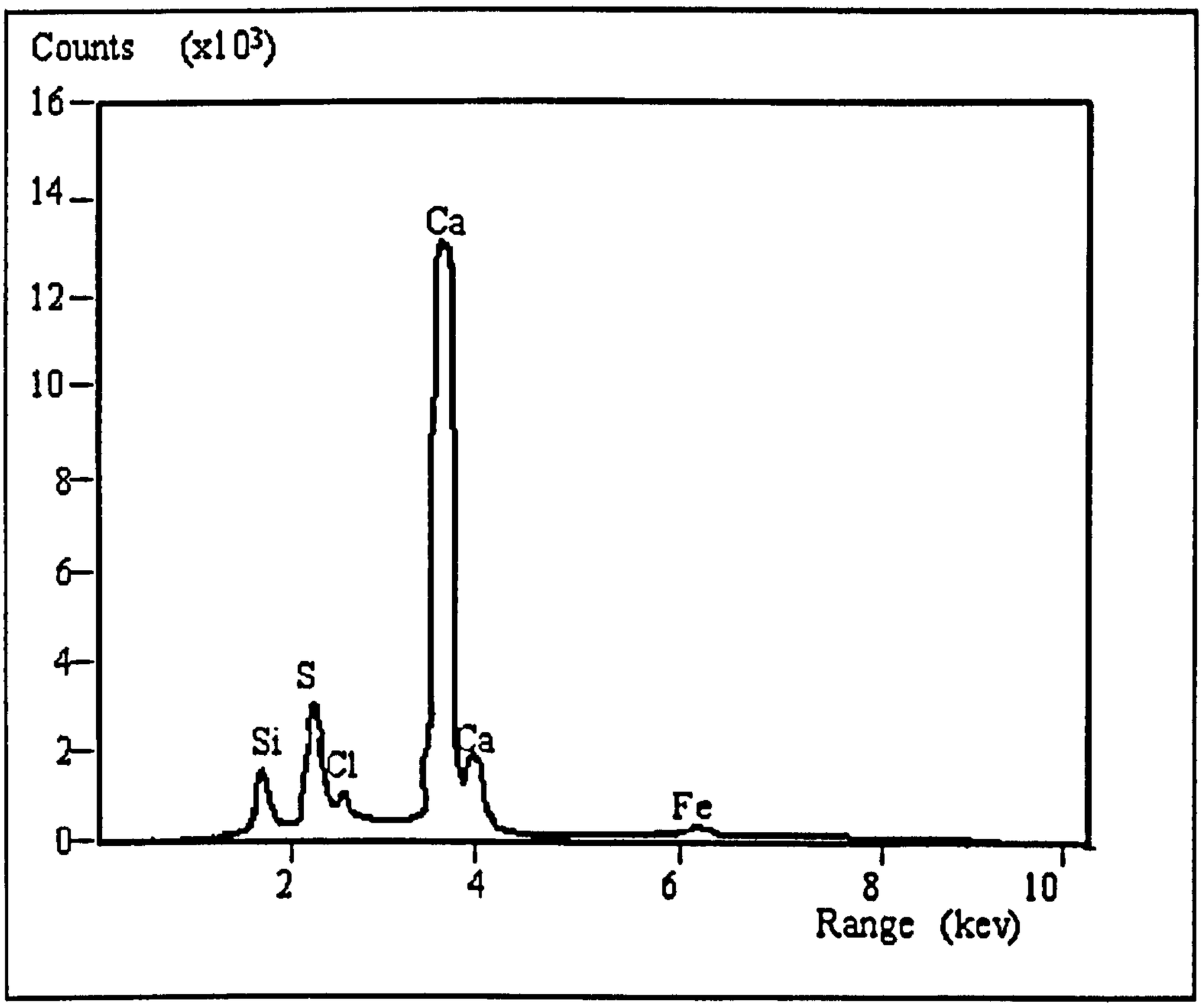

Figure 4.12: EDS of thaumasite in Fig 4.11

Closer investigation reveals a layer of thaumasite surrounding a clinker grain of chemical composition, as shown in Figure 4.14, with clusters of ettringite (or monosulfate) within its original boundaries as can be seen in Figure 4.13. The grain had cracks penetrating inwards from the outside. These cracks either offered sites for the occurrence of ettringite and thaumasite or they were caused by the formation of these reaction products. Interestingly, the chemical composition of such ettringite indicates that it may have contained some silicon, as shown in Figure 4.15. However, the chemical composition of the thaumasite region did not reveal any significant amount of aluminium. The precipitation of ettringite in belite grains has also been reported by Yang and Sharp [80] in samples exposed to an initial heat-curing regime. They concluded that the formation of a more porous inner product in belite allowed deposition of ettringite. Deteriorated clinker grains of similar microstructural features to those presented here was also reported elsewhere Crammond et al. [127].

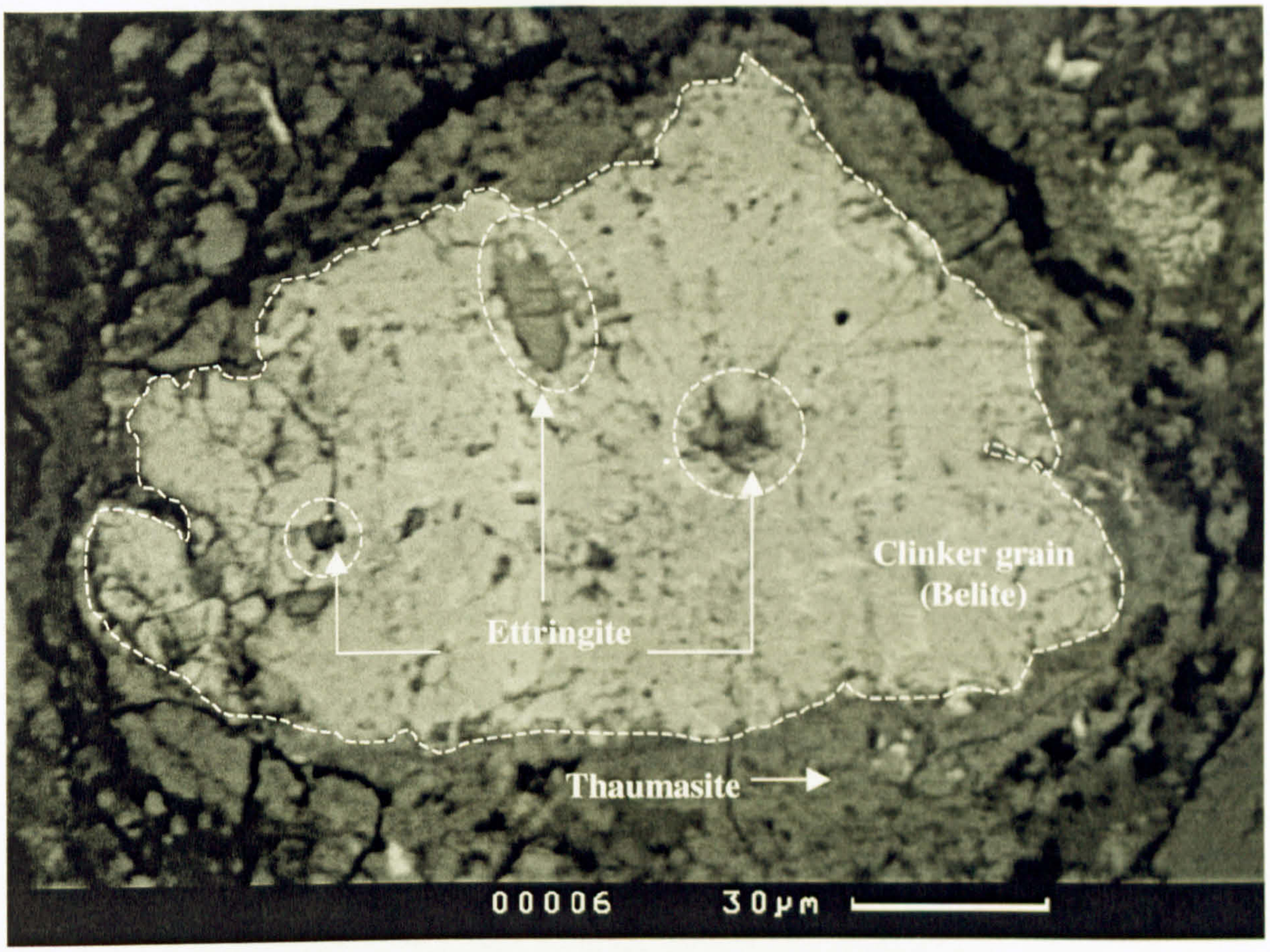

Figure 4.13: SEM of a clinker grain attacked by sulfates to form thaumasite in 15% limestone filler mortar.

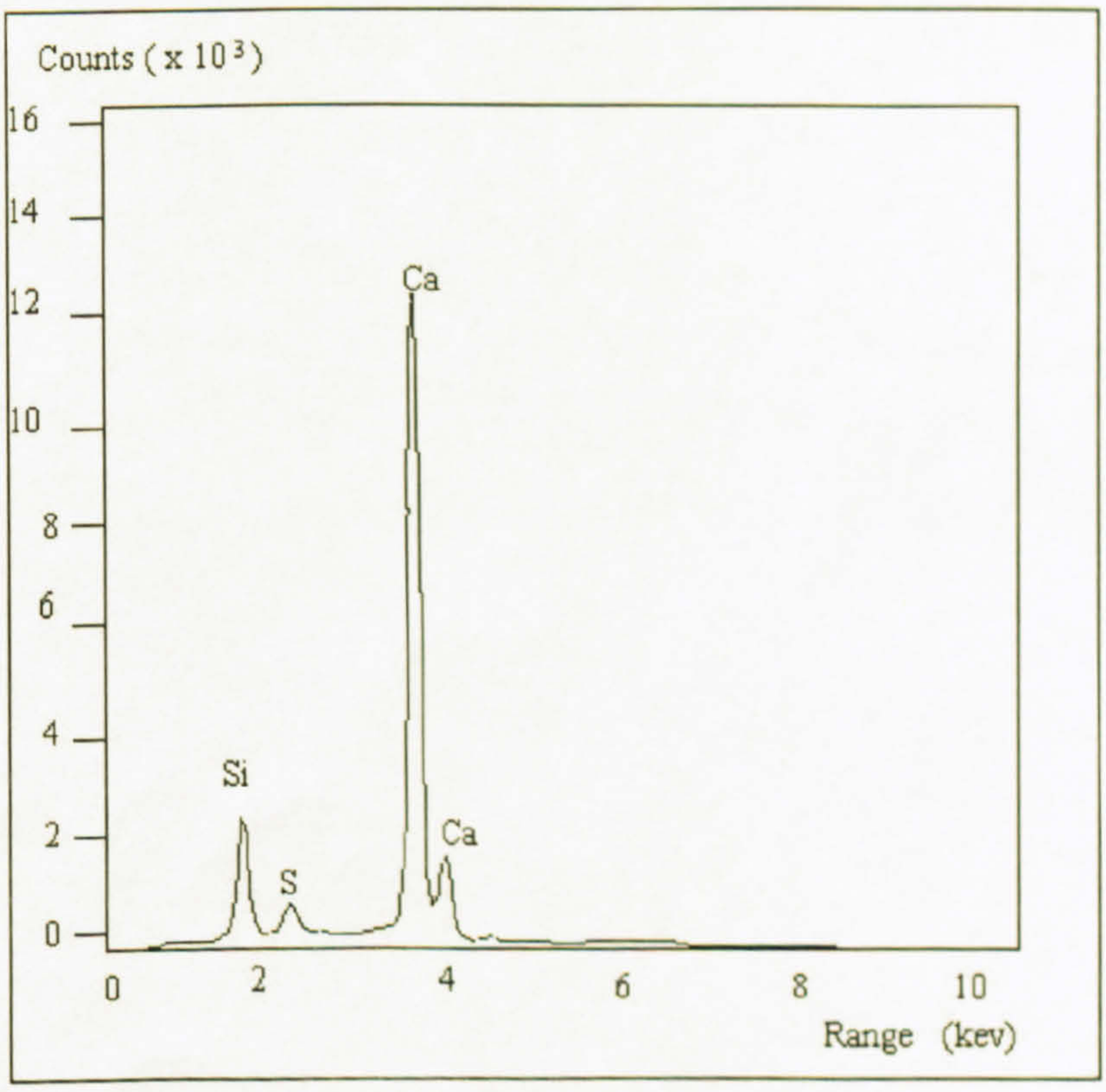

Figure 4.14: EDS of the clinker grain (Belite).

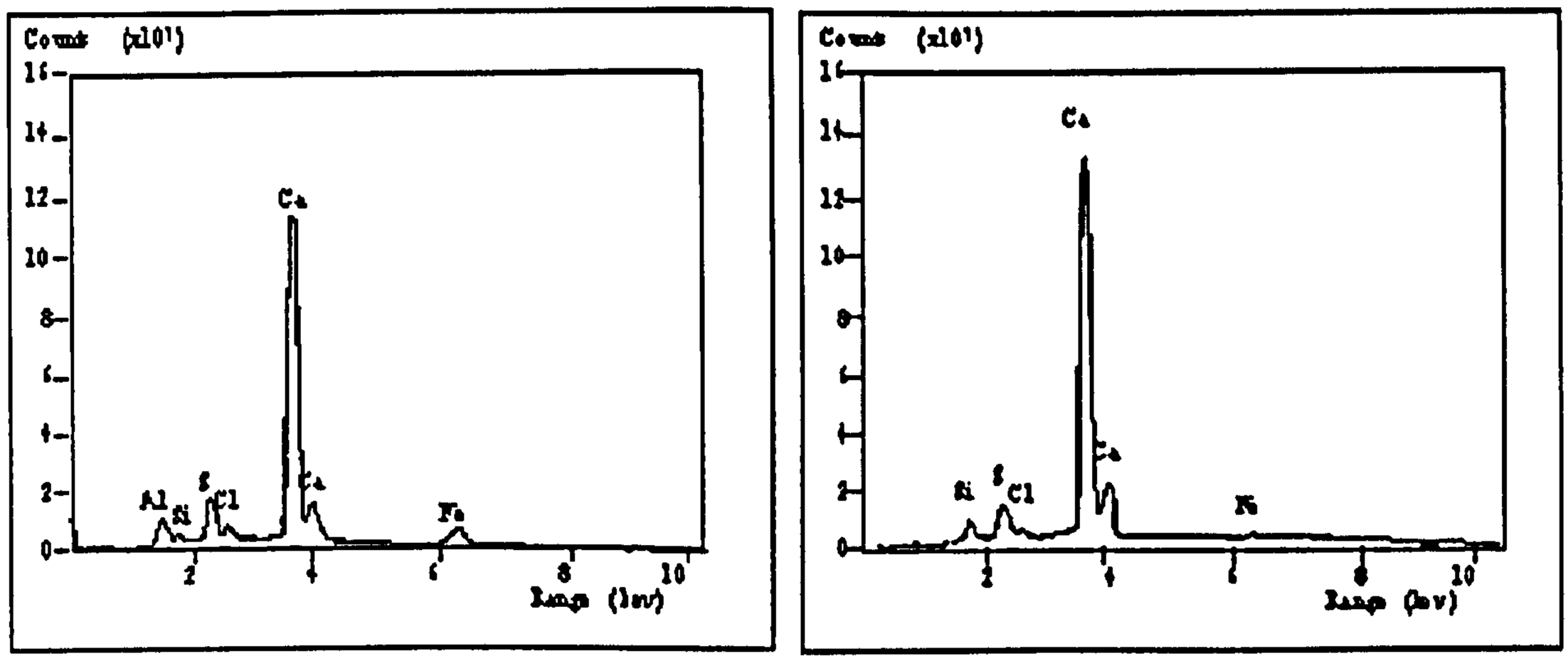

Figure 4.15: EDS of clusters in clinker grain in Fig 4.14: (Left) Ettringite and (Right) thaumasite.

4.2.4 Mortar with 35% limestone filler

Various features of deterioration attributed to TSA in samples containing 35% limestone filler are shown in Figure 4.16. The damage can be seen to be extensive and was in fact more severe than that in samples with lower levels of limestone replacement. Some material had spalled away from the surface leaving the prism smaller than those with lower limestone contents Torres et al. [13]. The cement matrix was totally converted into thaumasite up to about 4000μm depth, rather than intermixed with gypsum as in conventional sulfate attack in the presence of magnesium sulfate solution at room temperature. The pervasive homogeneity of thaumasite distribution was very similar to that observed in the 15% limestone filler mortar samples, but more extensive, as expected since more carbonate was available. It is also important to emphasise that the porosity of this mix must be higher due to dilution of the cement, resulting from the high level of limestone filler present.

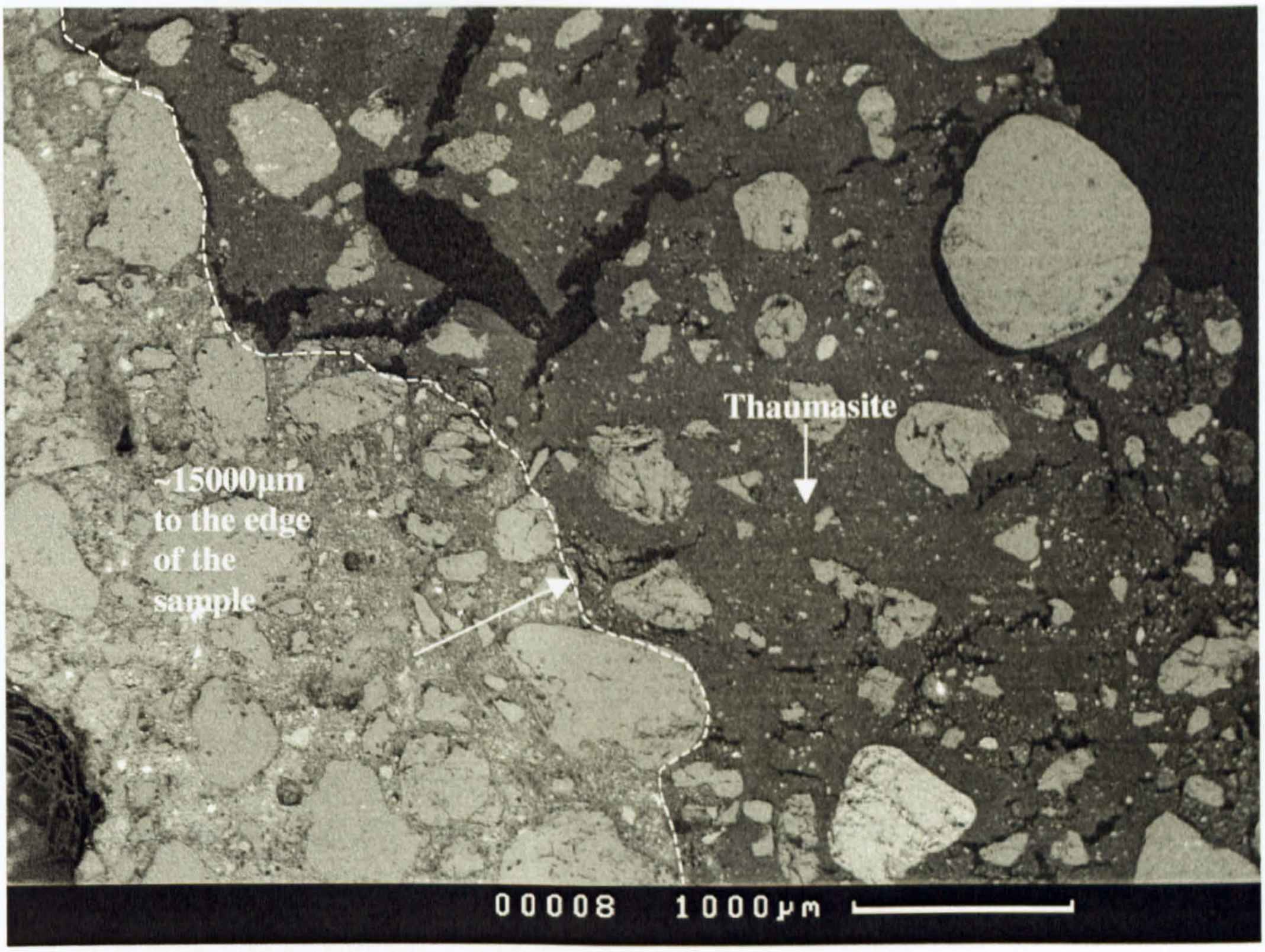

Figure 4.16: SEM of pervasive thaumasite in 35% limestone filler mortar matrix.

Figure 4.17 shows the modifications in the cement matrix arising from the chemical attack, and the following can be identified- the presence of CSH gel with intrusions of sulfate, chloride, iron, potassium and magnesium; CSH+Tss containing some aluminium and titanium; and thaumasite (outer dominant dark area). The thaumasite rich region seems to be progressing inwards replacing CSH in the clinker grain. The chemical composition of the outer thaumasite can be seen in Figure 4.18.

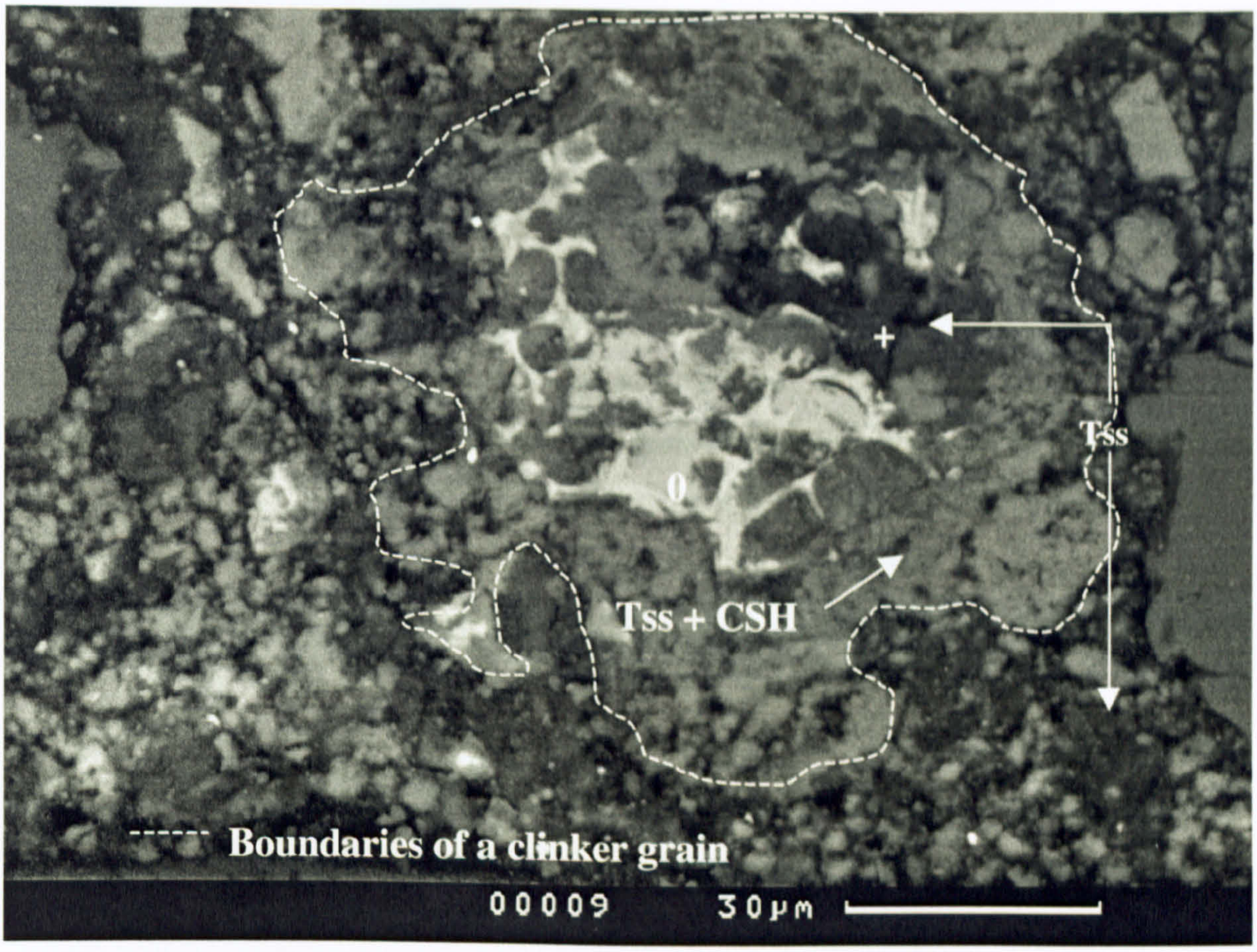

Figure 4.17: SEM of cement matrix in 35% limestone filler: (+) TSS, (o) belite, and attacked CSH.

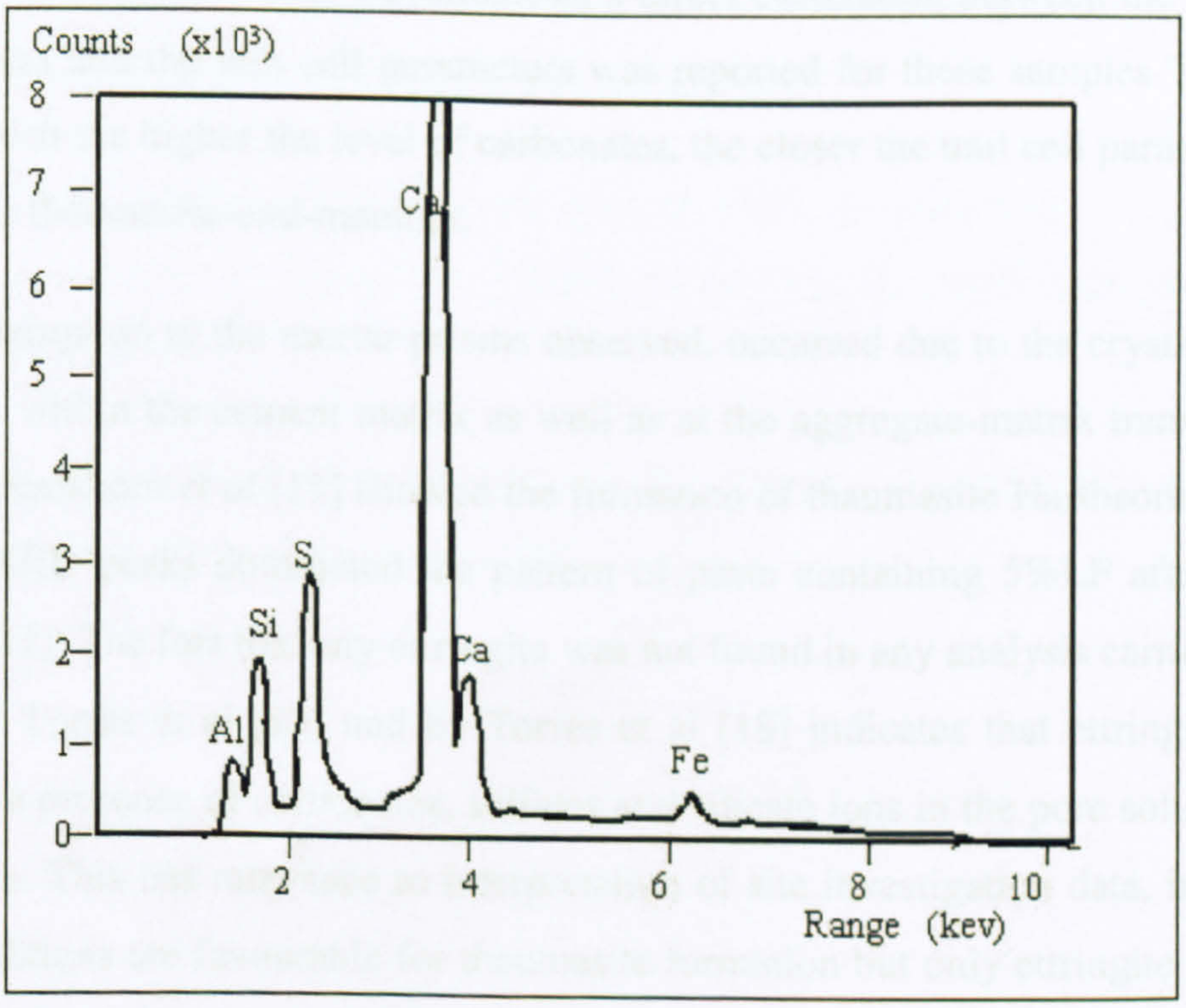

Figure 4.18: EDS of tss in Figure 4.17.

4.2.5 Progress of TSA as a function of limestone content and period of exposure

In comparison with previous papers [11, 31, 47] reporting on the deterioration of the same mortar specimens at an earlier age, the present work reveals that the extent of the deterioration is greater now that the specimens have been exposed to the magnesium sulfate solution for 5 years. Whilst the OPC control sample with no limestone filler exhibited no thaumasite formation at the end of one year exposure Harthsorn [11], now clear evidence of thaumasite is present. The level of deterioration confirmed from microstructural examination using SEM is also greater, the greater the level of limestone. The trend found here between microstructural deterioration and limestone filler content agrees well with the deterioration and general appearance of the bulk samples, as reported by Torres et al [13]. As mentioned earlier, the high level of deterioration found in the 35% limestone filler specimens may have been exacerbated by the dilution of the binding OPC, as the limestone replacement level was increased at a constant water/binder ratio. Nevertheless, a direct correlation between the availability of carbonates and the unit cell parameters was reported for these samples Torres et al. [18], in which the higher the level of carbonates, the closer the unit cell parameter are to those of the thaumasite-end-member.

The disruption to the mortar prisms observed, occurred due to the crystallisation of Tss phases within the cement matrix as well as at the aggregate-matrix transition zone. Although Hartshorn *et al* [11] showed the formation of thaumasite Harthsorn et al. [47], ettringite XRD peaks dominated the pattern of paste containing 5%LF after one year exposure [11]. The fact that any ettringite was not found in any analysis carried out after 4 years by Torres et al [13] and by Torres et al [18] indicates that ettringite is not a stable in the presence of carbonates, sulfates and silicate ions in the pore solution at low temperature. This has relevance to interpretation of site investigation data, in situations where conditions are favourable for thaumasite formation but only ettringite was found, as this should not be interpreted that thaumasite would not develop at a later age.

4.5 Conclusions

The main conclusions derived from this study are summarised below:

- In deteriorated mortar, thaumasite solid solutions of different texture developed in the matrix and at the interface around aggregate grains. The Tss may vary in composition from one region of the sample to another according to the local conditions pertaining at the time of its precipitation

- Thaumasite was observed in the corroded parts of 0, 5, 15 and 35% limestone filler mortars. The extent of deterioration of the mortar prisms was greater as the level of limestone increased. The damage commenced at the surface of the prisms and proceeded inwards. Its extent increased with the period of exposure.

- In OPC prisms, the mode of attack changed with time, from being ettringite based at early age to thaumasite based at later ages. The source of carbonate in the all OPC mortar, where the damage was relatively slight, was most probably due to atmospheric carbon dioxide.

- TSA gradually becomes all pervasive and is potentially very damaging because the consumption of CSH gel destroys the binding properties of the cement matrix.

- Ettringite is not a stable phase in the presence of carbonates, sulfates and silica in the pore solution at 5°C.

Chapter Five

PERFORMANCE OF LIMESTONE FILLER AND METAKAOLIN CONTAINING PORTLAND CEMENT MORTAR UNDER COMBINED CHLORIDE AND SULFATE EXPOSURE

5.1 Abstract

The durability of composite cements containing limestone filler and metakaolin has been investigated after continuous exposure to the combined action of chlorides (0, 0.5, 1.0 and 2.0 % of Cl^- as NaCl) and sulfates (0.6% SO_4^{2-} as $MgSO_4.7H_2O$) at different temperatures (5 and 20°C). The performance of the mortar cubes was assessed by means of visual inspection and the loss of mass. The mineralogy of the deterioration products was determined by x-ray diffraction and infra-red spectroscopy. The change in the pH of the solutions was measured monthly in order to investigate the conditions leading to the damage and mineralogical assemblage of the mortar systems. The effect of chloride and sulfates on the solubility of calcite and gypsum was investigated by means of ion chromatography.

It was found that the effect of chloride concentration on the performance of the mortars in magnesium sulfate solution strongly depends on the temperature and the composition of cement used. On the one hand, chloride ions seem to mitigate sulfate attack in all mixes when the samples were stored at 20°C for one year. On the other hand, chloride presence increased the damage in OPC and limestone filler containing OPC at 5°C, with the damage increasing as the level of limestone filler replacing clinker increased. The mode of attack is attributed to the thaumasite solid solutions, in which both octahedral silicon and aluminium were detected. Mixes with metakaolin did not present any deterioration after 12 months, even with 15% of the OPC cement replaced by limestone filler. However, signs of deterioration started to be detected after 15 months of exposure to sulfate solutions at 5°C, in which gypsum and thaumasite solid solution precipitated within the corroded material.

5.2 Introduction

The presence of chlorides in concrete is basically from natural sources such as seawater (about 2.7-3.0% in solution) and aggregate (0.05% by mass), or from manmade activities such as the use of de-icing salts in pavements and bridges with subsequent leaching into the concrete water table, where concentration will vary according to weather, run-off etc.

Indeed, investigation into thaumasite affected structures revead that chloride was frequently present, particularly when the damage was most severe. However, a review of the literature (Chapter 2) shows that chloride induced corrosion of steel was perceived to be considered the main concern regarding the effect of chloride in thaumasite-affected areas in most reports. Nevertheless, whether or not chloride plays a role in the durability of concretes subjected to TSA is still not known and, hence, is an objective of this investigation.

5.2.1 Evidence to suggest that chloride plays a role in TSA

A. Field cases

It was Erlin and Stark [64] who presented the first report in which concrete structures were damaged by thaumasite. In a later report, Stark [5] detaild the conditions in which such attack developed. In one of the cases, clusters of thaumasite and other carbonate minerals were found in a grout that was in contact with sulfated ground water in the vicinity of a sodium chloride mine, although it is not clear whether chloride was in the underground water.

Novak and Colville [129] analysed the damage of 20-30 years old concrete in southern California and concluded that salt crystallisation pressure and sulfate attack were responsible for the damage. However, no conventional sulfate phases such as ettringite, gypsum and thaumasite were found, but an orthorhombic thaumasite analogue, birunite ($17CaSiO_3.17CaCO_3.2CaSO_4.30H_2O$), was identified. Little is still known about this rare mineral. For instance, it is not known whether it plays any role in sulfate attack and also if any of its silicate ions are in octahedral coordination with

hydroxyl groups as in thaumasite. Indeed, significant amounts of chloride salts were also identified among the damaged material.

In 1994, Bickley et al. [67] reported on the severe damage caused by thaumasite in two-years old concrete in the Canadian Arctic. The concrete was made with limestone and siliceous aggregates as well as sulfate resisting Portland cement (CAN CSA type 50), whose strength reached between 31.9 to 53.9MPa in its sound parts. It was reported that thaumasite and gypsum replaced calcium silicate hydrate and calcium hydroxide phases, which were not identified in the damaged areas. Also, although no chloride binding phases were detected, a high concentration of chloride was found in the thaumasite areas. It was proposed that chloride could have been intermixed within the thaumasite structure.

Brown and Doerr [130], who studied corroded concrete in the same area as Novak and Colville [129], identified a similar phase assemblage, but thaumasite alongside other sulfate, carbonate and chloride phases was also found this time. It was suggested that some kinetically favoured sodium carbonate phases that precipitated would undergo further transformation towards more thermodynamically stable phases such as thaumasite or calcite. The source of carbonates was reported to be via dissolution of atmospheric CO_2. Also, Friedel's salt ($C_3A.CaCl_2.H_{10}$) was not found in areas where sodium carbonate phases were present, suggesting an incompatibility of these phases.

More recently, new cases of TSA have been found in environments subject to some chloride activity. Indeed, Hagelia et al. [3] reported the occurrence of thaumasite in some Norwegian concrete, where it is interesting to note that one of the most advanced stages of TSA was found in a 10-year-old concrete lining a tunnel in which the groundwater contained significant amount of chlorides and sulfates. In another study, Conjeau [99] observed thaumasite in 130-year-old concrete exposed to seawater in France.

Thaumasite also caused extensive deterioration to a cement: lime: sand bedding mortar in the steps of a harbour steps in the UK, as reported by Sibbick et al. [17]. Poor quality materials, high sulfate concentration, wetting and drying, as well as salt crystallisation pressure were also responsible for increasing the damage imposed by TSA, according to the authors. Indeed, the mortar was approximately two years old when signs of significant damage were detected and the older concrete foundations were also affected by thaumasite formation.

The most frequent occurrence of thaumasite so far was found within bridge structures, as reported by Crammond [63]. Indeed, these structures are often subjected to frequent applications of de-icing salts during winter. Indeed, the Thaumasite Expert Group Report [2] (TEG) assessment of the M5 motorway bridges identified that the chloride-induced corrosion risk increased in thaumasite affected areas. Wimpenny and Slater [15] and Slater et al. [16] also ratified this conclusion. They pointed out that lower concentrations of chlorides were found at the surface due to a seasonal washout, in areas where thaumasite was dominant, and also that chloride released by the cement matrix as a result of sulfate attack accumulated at the reinforcement interface, which induced corrosion. These findings slightly differ from the observations of Bickley et al. [67] in the sense that higher concentrations of chloride were found in such attacked areas.

Also in the M5 bridges, Eden [97] reported severe damage caused by TSA in a 29 year-old concrete made with sulfate resisting Portland cement. Because of a higher concentrations of chlorides at increased depth into the concrete, and the precipitation of gypsum in the clay-concrete interface, it was pointed out that chloride might contribute to TSA by increasing the solubility of gypsum in areas containing chloride and sulfate.

B. Laboratory studies

No published laboratory data assessing the role of chloride in the occurrence of TSA could be found. However, a small number of publications reveal that chloride may have another role in the durability of the cement matrix other than inducing corrosion only.

Conjeaud [99] studied Portland cement mortar samples immersed in synthetic seawater at 20°C. It was found that the intensity of the damage was more pronounced in samples in which 'Si-ettringite' (also previously reported as Woodfordite [131]) precipitated after 2 years. This phase is currently considered to belong to a thaumasite-ettringite solid solution [84]. Also, the concentration of chlorides follows a different pattern in those which 'Si-Ettringite precipitated than in the rest of the samples. Rather than at the surface, the highest chloride concentration reached at the core of the samples in which 'woodfordite' precipitated. This trend is similar to that observed in UK thaumasite-affected columns. Walkley and Roy [110] also found 'woodfordite' in grouts immersed in high chloride brine at 38°C, in which carbonates and sulfates were present.

In order to investigate why the destructive effect of $CaCl_2$ salts in concrete is higher at lower temperatures, Chatterji [115] studied carbonated and fresh ground paste immersed in several concentrations of $CaCl_2$ at 5, 20 and 40°C. He found that the precipitation of a complex salt containing $Ca(OH)_2$, $CaCO_3$ and $CaCl_2$, which was not identified, was responsible for damage in concrete. The damage was found to be more pronounced:

(i) At lower temperatures (mainly at 5 °C and also at 20°C but not at 40°C);

(ii) The formation of such a complex salt depended on the presence of calcium hydroxide (lime leached samples neither develop this salt nor damage);

(iii) At high concentrations of calcium chloride.

Microstructural examination revealed that this mineral had biaxial and needle-shaped, as has thaumasite. The XRD diffraction 'lines' were 9.56 and 5.46, but also 3.0 and 2.54 Å in some cases. A comparison between the diffraction lines (d-spacings) of this salt and the XRD standard patterns of thaumasite (powder diffraction file patterns PDF 785-1688 and 70-2438) can be found in Table 5.1.

Table 5-1: XRD pattern of transitory unidentified phase in Chatterji and two thaumasite XRD standard patterns.

d-spacing in ref. [115]	XRD standard d-spacing of Thaumasite (PDF)	
	75-1688	70-2438
9.56	9.55	9.56
5.46	5.51	5.52
3.00	3.04	3.04
2.54	2.56	2.50

Chatterji [115] also reports the occurrence of another mineral, with XRD peaks at 9.65 Å and 5.46 Å for lower concentrations of chlorides, which could possibly be a distortion of the unit cell parameter c=9.56 Å, caused by differences in the CO_3^{2-} to SO_4^{2-} ratio within the crystal structure of thaumasite (This ratio will be discussed in the Chapter 6). In his conclusion, neither the formation of chloroaluminate nor the leaching of calcium hydroxide were responsible for the aggressiveness of calcium chloride at lower temperatures. This was due to the crystallisation of the reported salt.

Bertsson and Chandra [116], who found severe damage in laboratory tested concrete sleepers exposed to chlorides at 5°C, also accredited the damage to the

crystallisation of a 3 micron needle-like salt, which they suggested to be similar to that reported by Chatterji [115].

5.2.2 Summary

From field cases, it can be found that not only was chloride present in several instances of TSA, especially in instances when the formation of thaumasite seemed implausible such as in temperatures higher than 15°C, but also the severity of the attack seems to be increased with its presence. Apart from Bickley et al. [67] and Eden [97], who commented that chloride may play a role in TSA, most of the published literature focuses on the corrosion aspect that is aggravated by the presence of chloride that percolates through a weak and porous thaumasite damaged area. On the other hand, there seems to be evidence from laboratory work to suggest that chloride may also play a significant role in the mechanism of TSA, although such interaction cannot be established in some cases because of lack of clearer data.

The current standard on concrete in conditions prone to develop TSA [14] states that chloride usually mitigates sulfate attack, as it is indicated by many researches in conventional sulfate attack, especially in seawater. However, there is no published work on the effect of chlorides in the thaumasite form of sulfate attack. Therefore, the main thrust of this work is:

(i) To Evaluate whether chloride plays any significant role on TSA.

(ii) To ascertain whether its role is similar to that of chloride in seawater.

(iii) To ascertain whether the high pozzolanicity metakaolin would prevent TSA in high carbonate filler content mortar.

(iv) To investigate the effect of chloride on pH of test solutions and the main mechanisms affecting the durability of the specimens.

(v) To investigate the influence of temperature on the role of chloride, sulfate and carbonate ions in TSA.

5.3 Results

The parameters, materials and methodology used in this chapter are described in Chapter 3. Whenever more detail is necessary, further explanation is given in the course of the following sections.

5.3.1 Visual Assessment

A. Up to 12 weeks

The first signs of deterioration were detected at corners and edges of the specimens after 56 days immersion in salt solutions, there was more evidence of attack in ordinary Portland cement (OPC) samples and in samples containing OPC plus limestone filler (LF) at 5°C than at 20°C. As far as the carbonate content is concerned, mortars made with 15% LF were more damaged than those based on either OPC or OPC plus 5% LF in pure sulfate solution. At this stage, samples immersed in combined chloride and sulfate solutions showed lesser signs of deterioration, with the exception of mortar containing 15% limestone at 5°C in which the damage was similar to that caused in the same mix in sulfate solution at the same temperature.

Figure 5.1 and Figure 5.2 show the visual assessment after 84 days. At this very early age, it is not possible to tell whether chloride plays any role in the attack.

However, the damage to 15%LF samples immersed in magnesium sulfate and 2.0% chlorides (M20) were similar to that of samples in pure magnesium sulfate (M). Also, samples immersed in sulfate and 0.5%Cl^- (M5) presented the least damage of all salt solutions, and sulfate plus 1.0%Cl^- (M10) showed the largest deposit of a white material on the surface of the cubes. The damage was characterised by some spalling and blisters at the edges at 5°C, but not at 20°C. This seems to indicate that the expected mitigation of chloride over sulfate attack may not hold at lower temperature as time progresses.

As for 5%LF, no evident distinction can be made between salt solutions, except that some white deposit formed in all samples but less in M20.

In OPC samples, deterioration occurred at the edges and corners at both temperatures 5°C and 20°C, but this was slightly more intense at the lower temperature.

Metakolin mortars (MK) did not undergo any superficial signs of damage in any solution or temperature.

Immersion in synthetic seawater (SEA), did not promote any deterioration in OPC and 15% LF mixes at both 5°C and 20°C. At this age, 15%LF surface colour was whiter than that of OPC in the same solution.

	W	M	M5	M10	M20	SEA
OPC (0%LF)						
OPC+5%LF						
OPC+15%LF						
OPC+15%LF+MK						

Figure 5.1: Samples after 84 days in different solutions at 5°C.

	W	M	M5	M10	M20	SEA
OPC (0%LF)						
OPC+ 5%LF						
OPC+ 15%LF						
OPC+15%LF+ MK						

Figure 5.2: Samples after 84 days in different solutions at 20°C.

B. After 24 weeks

As time progressed, the different effects of chloride, carbonate and temperature on the damage became more evident, as can be seen in Figures 5.3 and 5.4.

Mixes \ Solutions	W	M	M5	M10	M20	SEA
OPC (0%LF)						
OPC(5%LF)						
OPC(15%LF)						
OPC(15%LF+ 10%MK)						

Figure 5.3: Samples after 168 days in different solutions at 5°C.

Mixes \ Solutions	W	M	M5	M10	M20	SEA
OPC (0%LF)	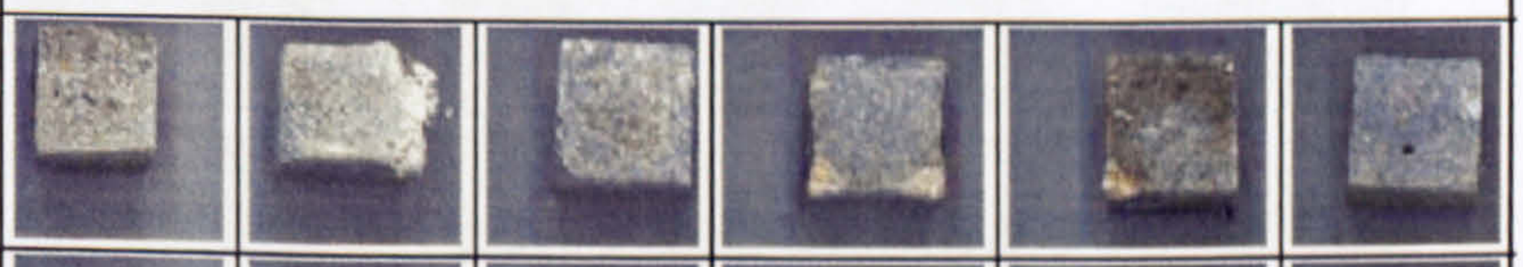					
OPC(5%LF)	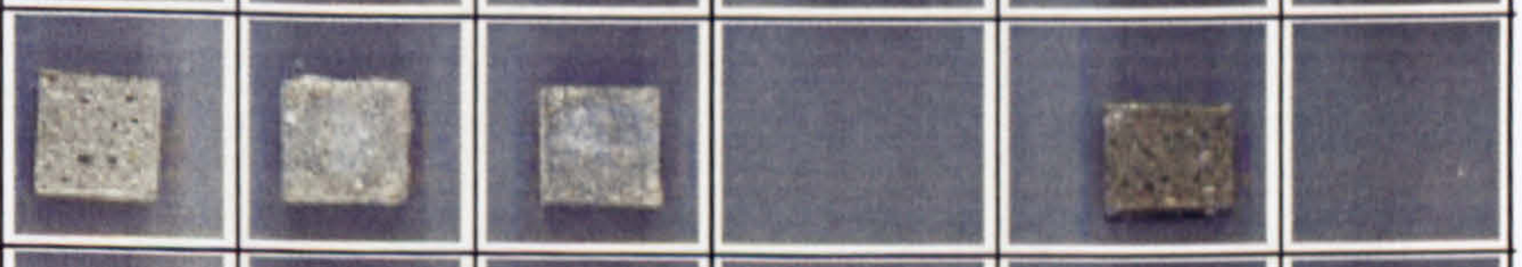					
OPC(15%LF)	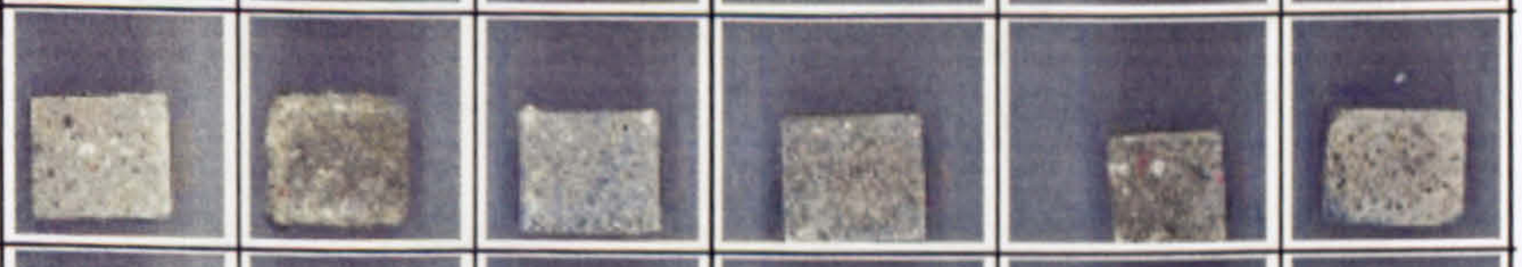					
OPC(15%LF+ 10%MK)						

Figure 5.4: Samples after 168 days in different solutions at 20°C.

Whereas litlle sign of deterioration could be detected for samples stored at 20°C, a white mushy deposit covered the surface of 15% LF cubes in salt solutions at 5°C. 15%LF in M5 was virtually unattacked when compared to the damage of 15%LF in M20, 15%LF in M10 and 15%LF in M, which decreased with the level of chloride in solution.

In 5% LF at 5°C, the combined effect of chloride and sulfate is not clearly seen. There was strong deposition of a white and mushy material over the surface of cubes immersed in M solution, which was more prominent than in OPC in M and M5 but less than in M20. The sequence of damage does not follow the same pattern seen in the 15%LF samples at low temperature, since the damage in samples immersed in M is more intense than those in M5 and M20. Again, no significant damage was detected in any solution at 20°C.

A similar trend as seen for 15%LF samples seems to be happening in OPC (O%LF) mixes, but with lesser intensity. White mushy material formed on the surface, and also at the edges of the cubes. 0%LF samples in M5 seem to be less attacked than the other salt solutions. This also seems to be the case at 20°C, where 0%LF samples immersed in M5 are less damaged than those immersed in pure magnesium sulfate (M).

C. After 44 weeks

Figure 5.5 and shows the appearance of samples immersed in salt solutions at 5°C.

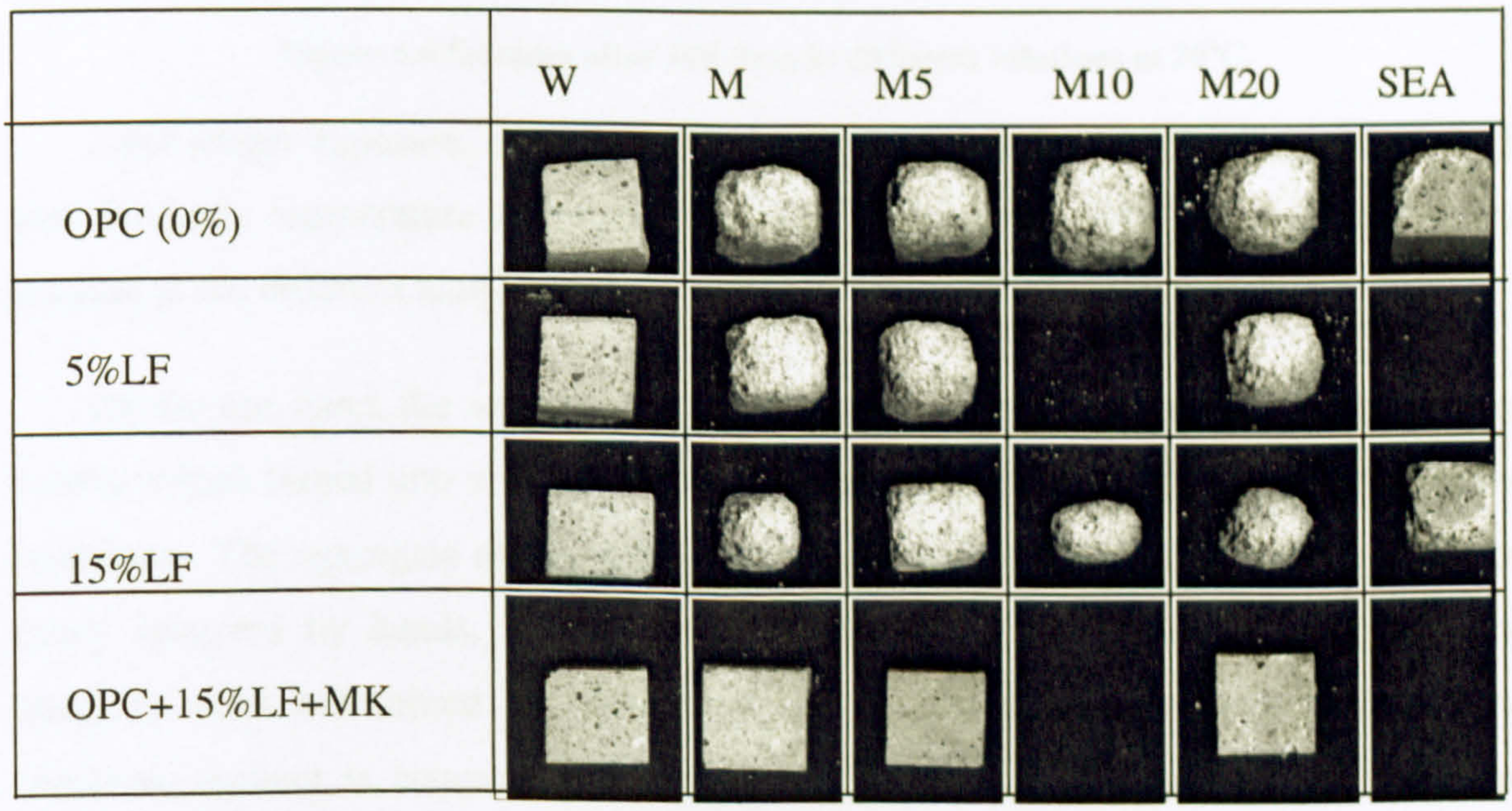

Figure 5.5:Samples after 308 days in different solutions at 5°C.

The peforamance of samples immersed in the test solutions at 20°C is shown in Figure 5.6.

	W	M	M5	M10	M20	SEA
OPC (0%LF)	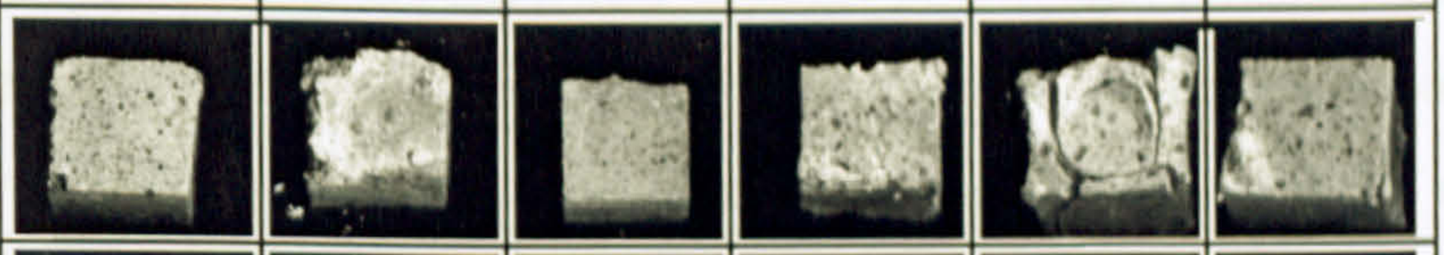					
5%LF	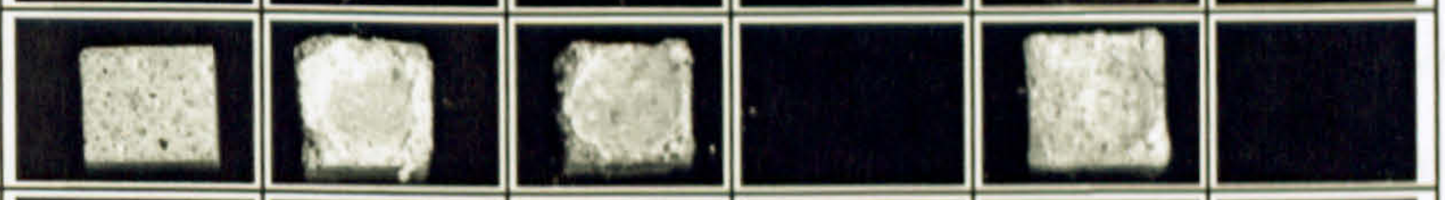					
15%LF	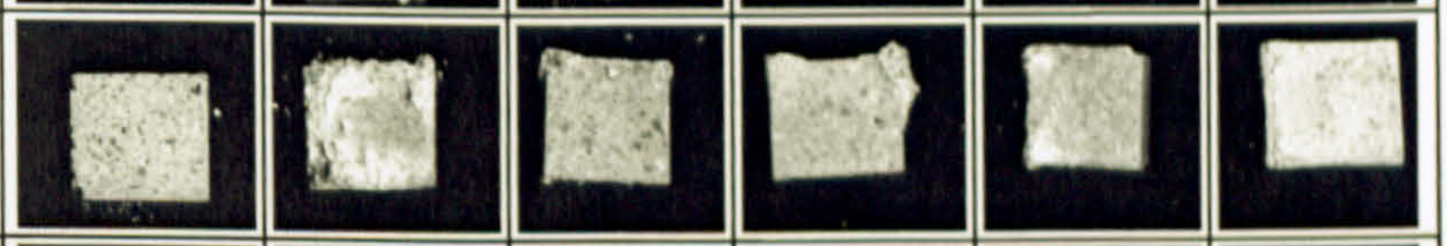					
OPC+15%LF+ MK	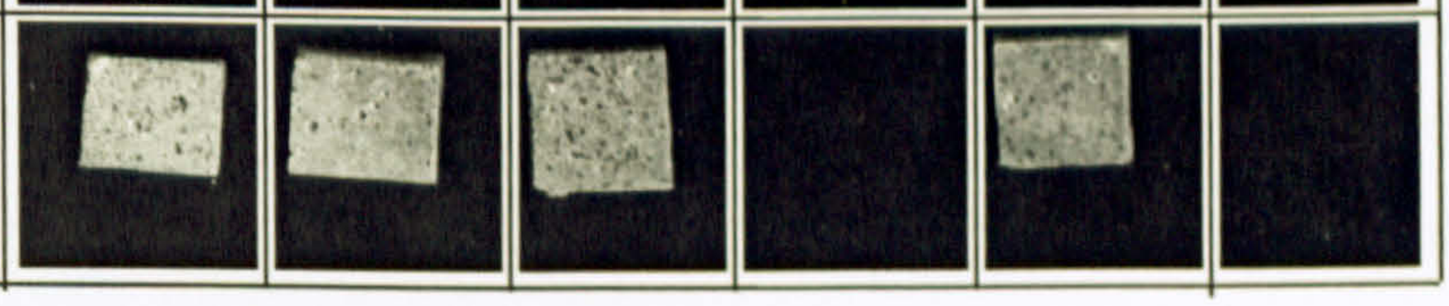					

Figure 5.6:Samples after 308 days in different solutions at 20°C.

After longer exposure, the effect of chloride on the sulfate attack became clearer. It was evidently temperature dependent, as seen by both the form and intensity of the damage at the different temperatures.

On the one hand, the attack at 5°C was marked by an overall failure of the cement matrix, which turned into a white mushy material that precipitated in the bottom of the containers. The aggregate of the remaining cubes was totally exposed, and it could be easily removed by hands. There was no resemblance to the original shape as the attacked cubes had turned into round shapes. In this mode of attack, as far as the carbonate content is concerned, the higher the amount of carbonate filler, the more intense the attack, irrespective of the presence of chlorides in solution at 5°C. Indeed, the 15%LF mortar showed the highest degree of attack.

The intensity also varied with the concentration of chlorides in solution. The worst case occurred in samples immersed in the combined solution of sulfates and 1%Cl^- (M10), followed by 2%Cl^- (M20), pure sulfate (M), 0.5%Cl^- (M5) and seawater (SEA). Mortars with 5% LF showed the second highest degree of damage. Again, the combination of chlorides and sulfates seemed to have worsened the attack, although it can be more evident by looking at the overall view of the samples after one year of

exposure (section D-Figure 5.8). As for OPC without limestone, the attack was less intense than that of 5%LF samples. However, the surface has turned into a white mushy material, which precipitated at the bottom of the containers, as it did not have any binding capacity to remain with the rest of the mortar. Once more, the combined effect of chlorides and sulfate was detrimental, particularly when the preformanceof the samples was looked at after one year (section D-Figure 5.9).

Samples containing metakaolin did not show any damage at this age. Minute white spots were observed in some pores, and at some corners of the cubes, which were more evident in sulfate solution (M). Although this observation cannot be used as an indication of any susceptibility to such chemical attack, these samples were observed for longer periods so that an account of their long-term performance could be given (section D-Figure 5.11).

It is important to emphasize the fact that some white-yellowish layers were either attached to the cubes or precipitated as a whole at the bottom of the containers in all the attacked mixes. These layers were exposed to atmospheric carbonation prior to the immersion period. Therefore, carbonation probably prevented the attack from taking place at the surface, but did not prevent the attack that took place immediately underneath the carbonated surface, resulting in the detachment of the layer from the bulk sample. This finding follows the same trend observed in the long-term samples immersed in salt solutions at 5°C, which were previously exposed to air at both 5°C and 20°C.

On the other hand, samples immersed in salt solutions at 20°C showed only superficial damage, marked by some attack at corners and edges. Also, extensive cracks and delamination of the corroded surface developed in OPC in M20, and to a slight extent in both 5%LF and 15%LF in the same solution. The cubes still resembled their original shape, and the intensity of the attack was much less when compared to that at 5°C. Although the corroded material could be removed by hand, the cores still retained some strength. The overall appearance of the corroded material was of flake-like fragments rather than the mush, white was observed at 5°C.

Although the mitigation effect of seawater on the sulfate attack was identified in both mixes 15%LF and OPC at both 20°C and 5°C, more damage was detected in samples immersed at lower temperature, and also with 15% replacement of carbonate filler.

D. After 53 weeks

To give an idea of the uniformity of the attack throughout the samples, Figure 5.7 to Figure 5.9 show the general features of OPC and OPC plus limestone filler samples after 53 weeks of immersion in salt solutions at different temperatures.

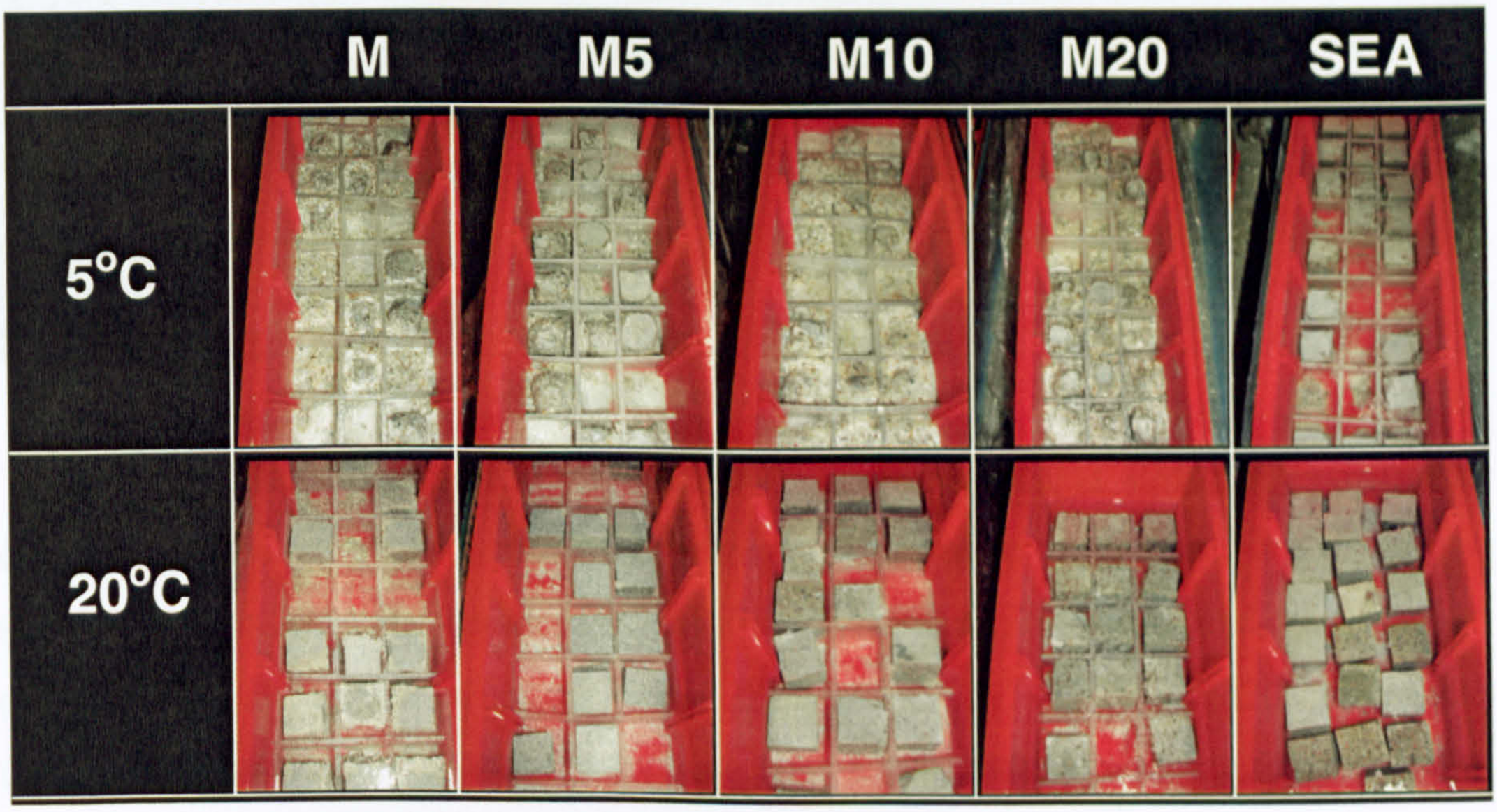

Figure 5.7:General view of 15%LF samples after 53 weeks

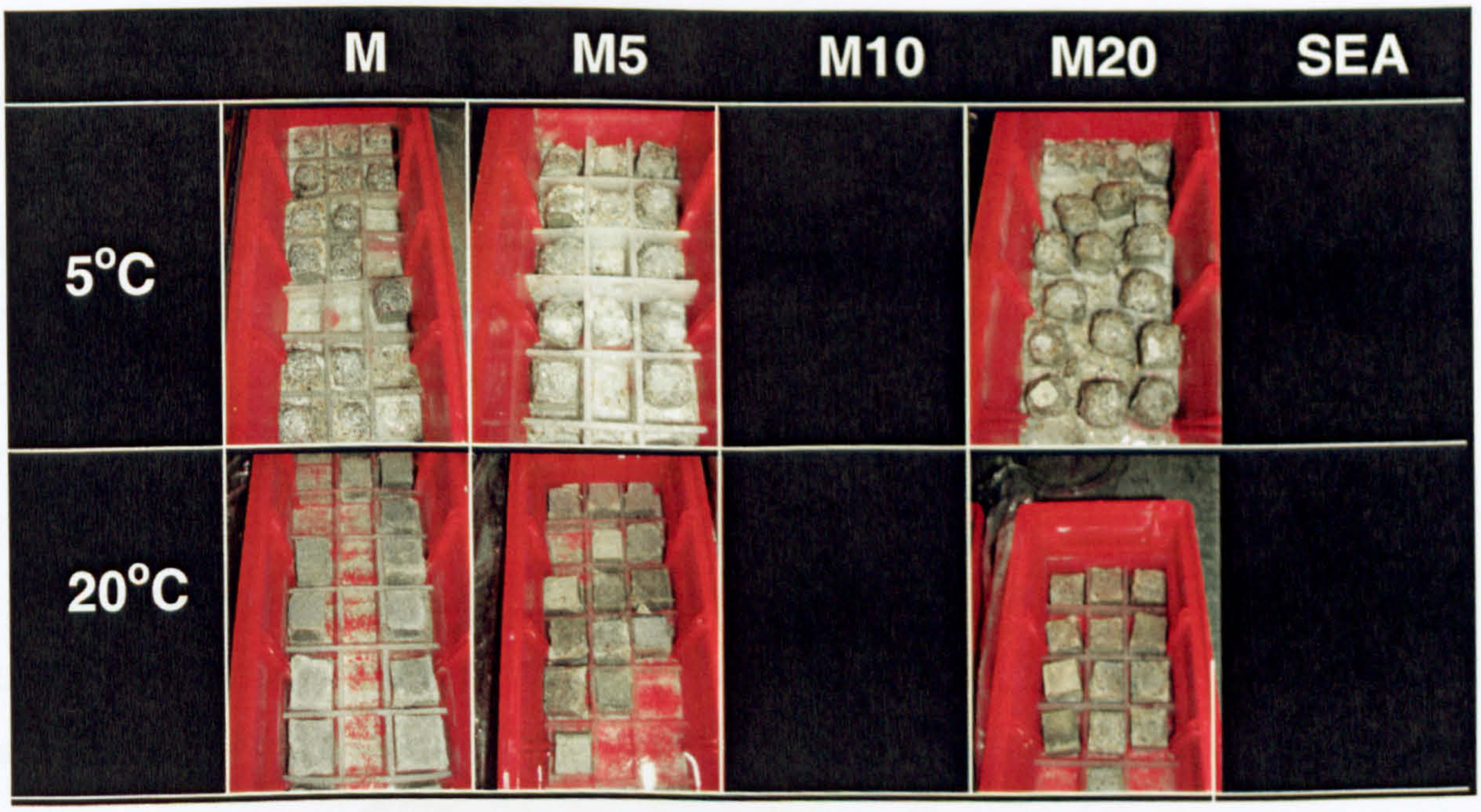

Figure 5.8: General view of 5%LF samples after 53 weeks.

Figure 5.9:General view of OPC samples after 53 weeks

It can be seen that the role of chloride in sulfate attack is strongly temperature dependent, in which it seems either to mitigate or to catalyse the mechanisms of sulfate attack. Thus, at 20°C, the presence of chloride in sulfate solution reduced the intensity of attack in all mixes, with the only exception being OPC in M20, in which delamination of the surface and cracks have been a markedly dominating feature of the attack.

At 5°C, however, all the OPC mixes with and without limestone filler suffered extensive damage and almost totally disintegrated after 53 weeks. The apparent trend being the higher the carbonate content, the greater the intensity of the attack. At this stage, the corroded material that precipitated at the bottom of the containers was totally mushy. It is still possible to identify the carbonated surfaces that were not attacked in all mixes, although it did not pose any protection to the core but could easily be detached from the bulk sample by hand. These carbonated surfaces were very often broken in flake-like pieces in advanced stages of deterioration. In most cases, these surfaces were confined between precipitated mushy material and directly in contact with the wall of the container. Such cubes were turned upside down in the Figures 5.7 to 5.9 for a better appreciation of this description at the time when those photographs were taken.

Samples containing metakaolin were in good condition up to 53 weeks in all solutions and temperatures, as shown in Figure 5.10.

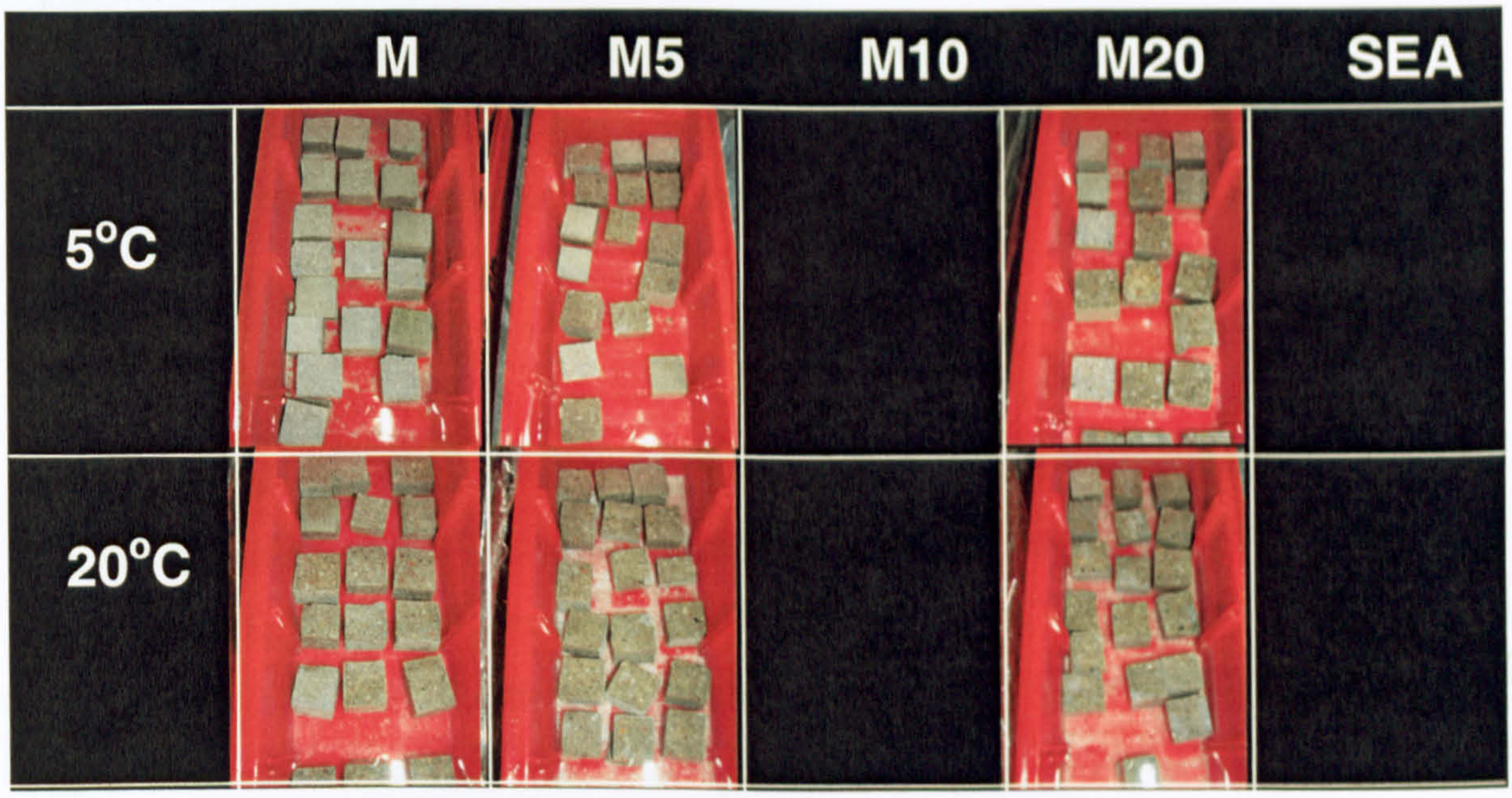

Figure 5.10: General view of MK samples after 53 weeks

However, they were monitored for a longer period of time for reasons already reported. As they reached the age of 60 weeks, the amount of white deposit greatly increased at the corners and flaws were noticed in samples immersed in M at 5°C, and to a lesser extent in the other solutions.

Figure 5.11 clearly shows that this mix was only attacked in pure sulfate solution at 5°C after 72 weeks, but not in other salt solutions.

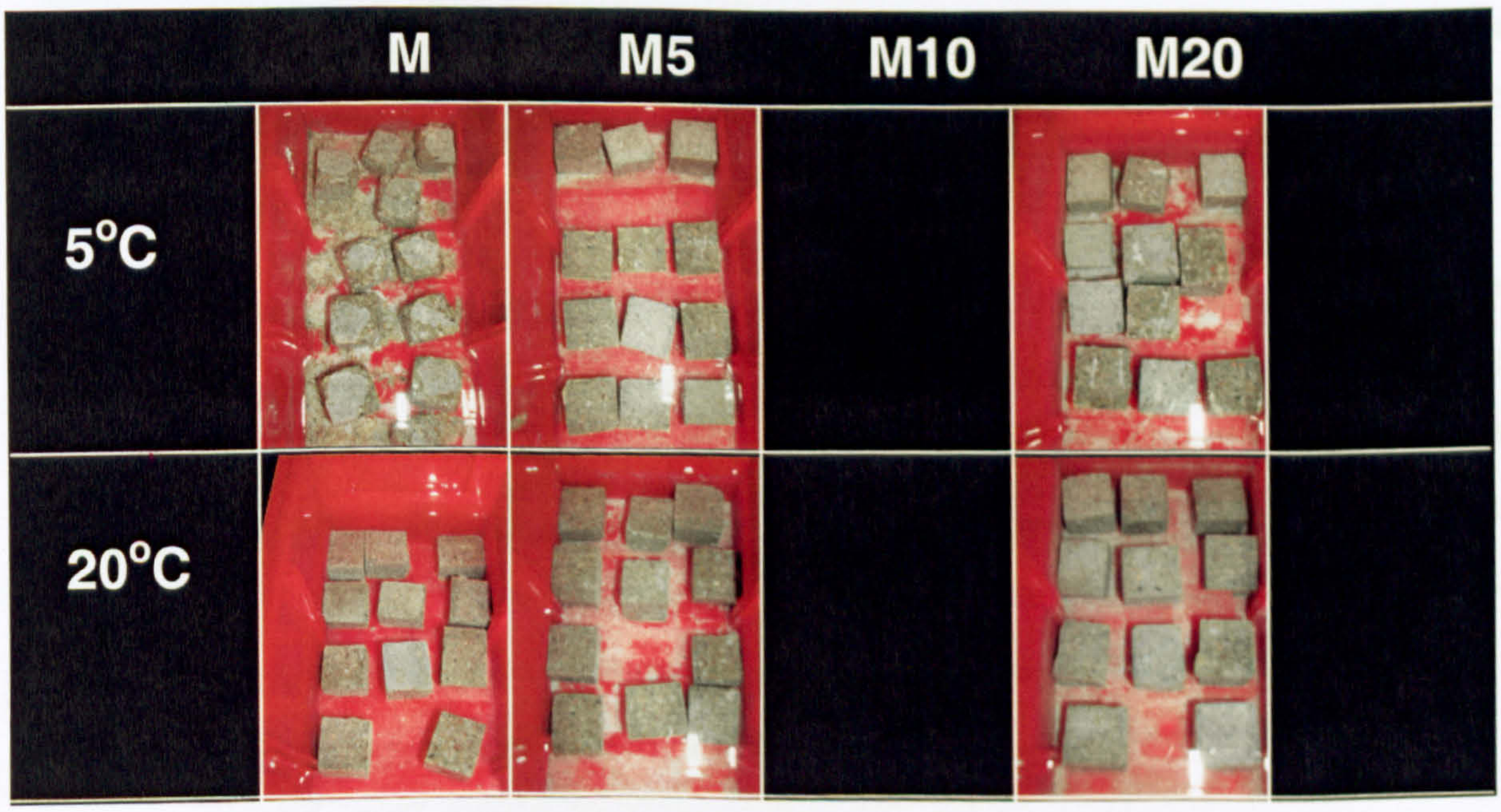

Figure 5.11: General view of MK samples after 72 weeks

Nevertheless, the mode of attack was not characterised by the formation of white mushy material but rather of a flake-like material, which crumbled to the bottom of the container. However, the intensity of the attack was significant so that most of the original shape had been lost as the attack predominantly occurred at corners and edges. As it can be noticed, the rate of attack was remarkably sudden, when compared with the appearance of these samples after 53 weeks. As described earlier, carbonated layers have also been progressively delaminated in this solution.

E Seawater

For samples immersed in seawater, the damage was not only remarkably less than in other salt solutions but it also depended on both carbonate content and temperature. At 20°C, OPC performed worse than 15%LF, which did not present any significant damage after 53 weeks. The mode of attack was marked by expansion at the corners and edges. The carbonated coat was detached from the bulk samples in the same way as described previously for carbonated surfaces. The surfaces that were not exposed to atmospheric CO_2 did not show signs of cracking but the aggregate became more exposed, as part of the cement matrix had been attacked. At 5°C, the intensity of the attack in the sample containing 15%LF was greater than that of OPC, which is the inverse of what occurred at 20°C. A possible explanation for this observation can be found in the role of carbonates in the main mechanisms of sulfate attack at different temperatures. On the one hand, the replacement of Portland cement by the limestone filler reduces the amount of hydrated products susceptible to both magnesium and sulfate ions at higher temperatures, in which conventional sulfate attack is expected to occur and the carbonate species tend to precipitate as aragonite [47]. On the other hand, especially at the lower temperature, carbonate ions participate in thaumasite formation [11], hence accelerating the TSA observed at this temperature.

The overall trend of attack involving chlorides, sulfates, carbonates and Portland cement hydrates indicates a strong dependence on the storage temperature. These visual observations point to the understanding that chlorides play different roles in sulfate attack, where different mechanisms seem to be involved as carbonate concentration and temperature changes. Therefore, the hypothesis that the presence of chloride would mitigate TSA [14], based on seawater experience, does not seem to hold under all conditions and needs further investigation.

F. Long term specimens

In order to address the effect of carbonation on TSA, some samples that have been exposed in air for 5 years were also immersed in salt solution at different temperatures. The original 40x40x160mm prisms were cut in small 20mm cubes, and the cross-section can be seen in Figure 5.12. The pink region indicates high pH and the presence of portlandite ($Ca(OH)_2$), whereas the grey region indicates lower pH where portlandite has reacted with atmospheric CO_2 to form calcite. It can be seen that the carbonation depth, assessed by the phenolphthalein test [30], reached about 13 and 5mm, and was higher in samples exposed to air at 20°C (15LT20) than at 5°C (15LT5). Dry conditions, as inside the fridge, do not favour carbonation, which happens faster in humid conditions, such as in the laboratory atmosphere [30].

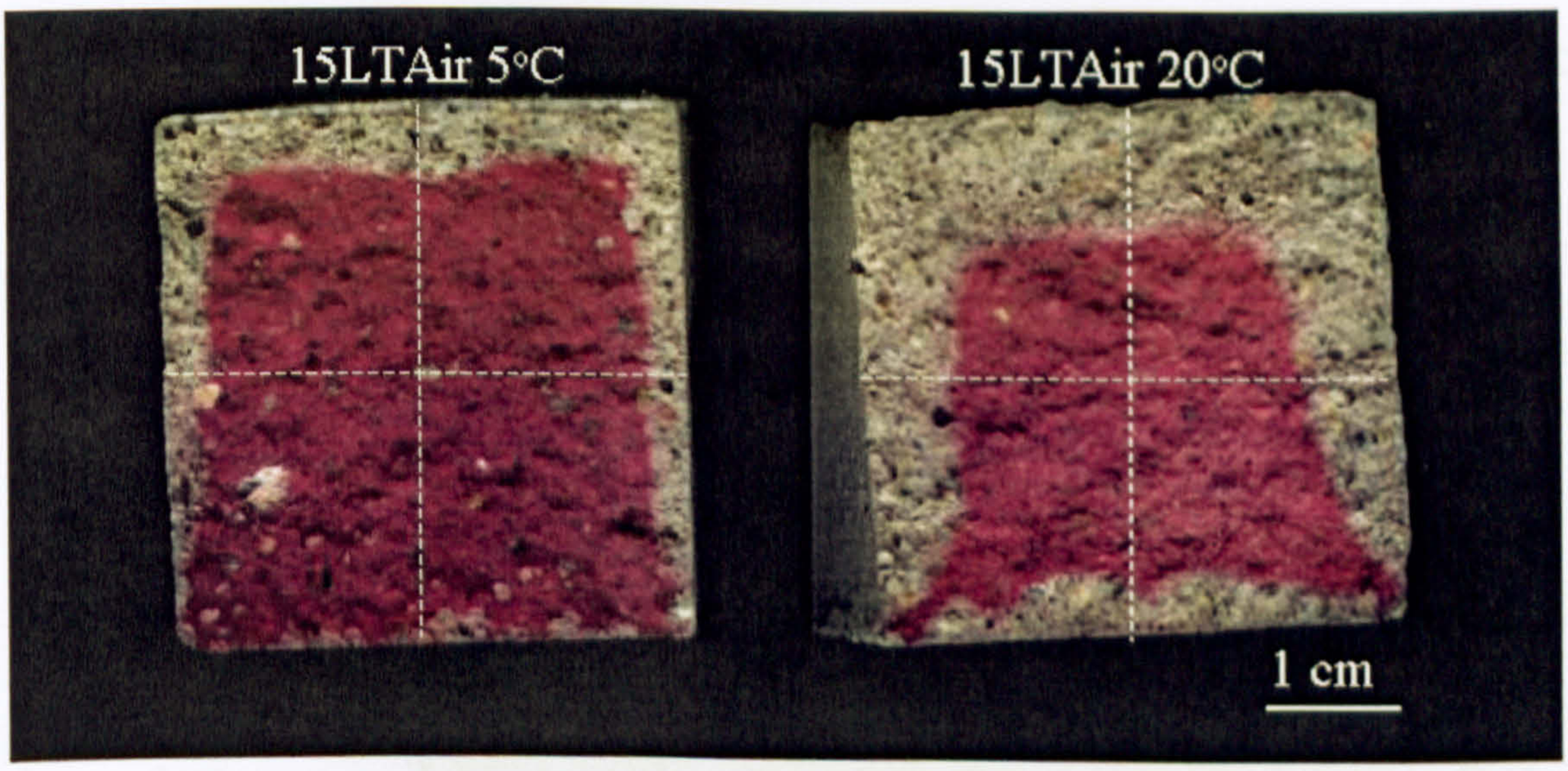

Figure 5.12: Carbonation in long term specimens exposed to air for 5 years prior to the immersion in salt solutions: (left) 15LT5 at 5°C; (right): 15LT20 at 20°C; (dotted line): where sub-samples were cut.

After immersion in salt solutions for 6 months, some blisters could be identified in samples immersed at 5°C but not at 20°C, as can be seen in Figure 5.13 and Figure 5.14. Indeed, more damage could be detected in both 15LT5 and 15LT20 samples immersed in M5 (0.5%Cl^- + 0.6% SO_4^{2-}) than in either pure magnesium sulfate (M) or combined sulfate and 2.0% Cl^- (M20). The carbonated zone, which became yellowish, was not attacked in any case.

TEMP	M	M5	M20
20°C	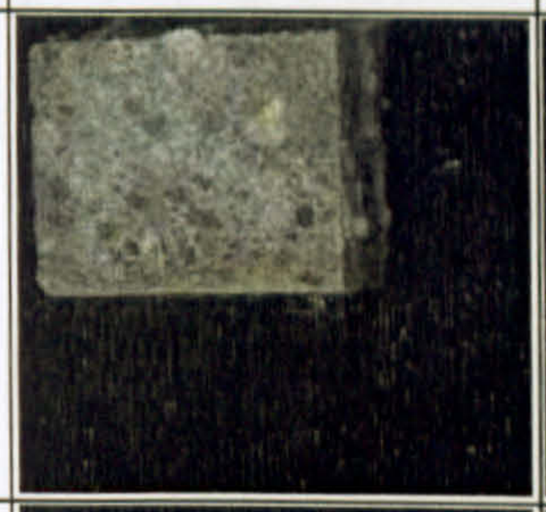	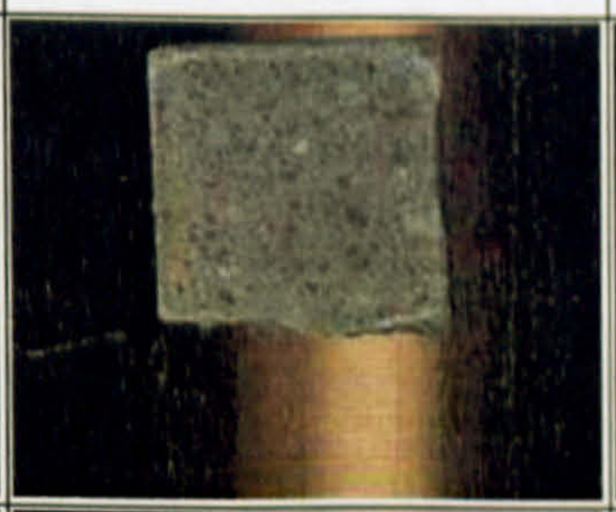	
5°C		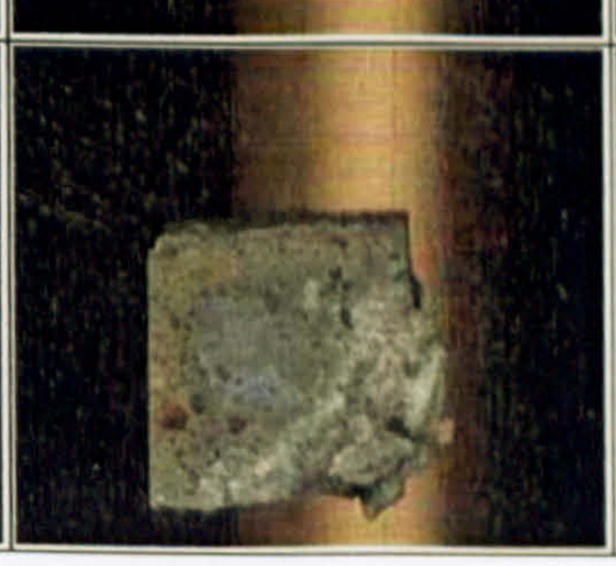	

Figure 5.13: Long-term specimens (15LT5) immersed in salt solutions after 6 months at (top): 20°C; (bottom): and 5°C .

TEMP	M	M5	M20
20°C		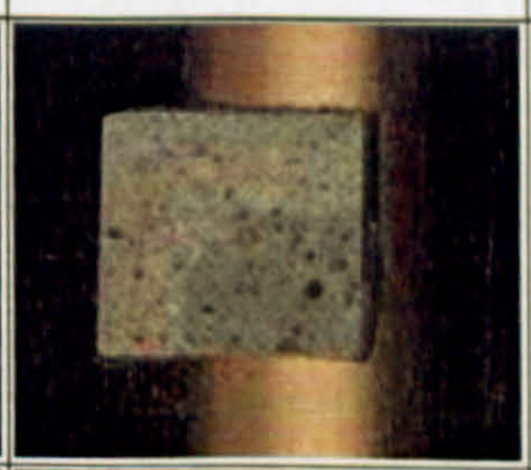	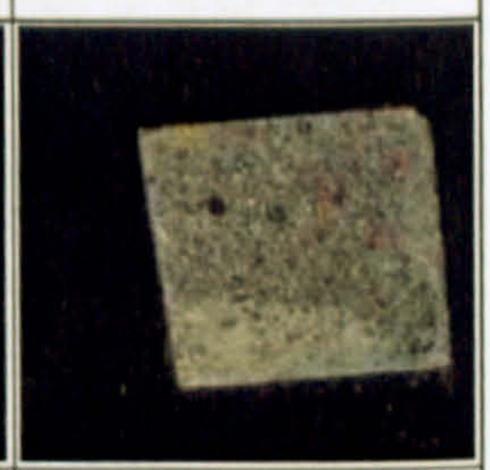
5°C			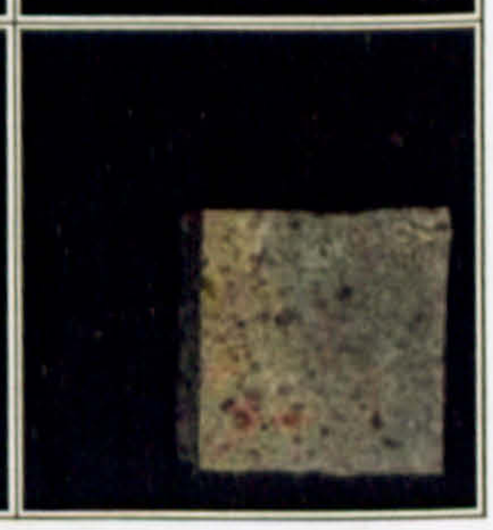

Figure 5.14: Long-term specimens (15LT20) immersed in salt solutions after 6 months: (top): 20°C; (bottom): 5°C.

After 12 months, extensive damage developed in all samples immersed in salt solutions at 5°C, which was characterised by the formation of a white-yellow mushy material that detached from the samples. These features can be seen in Figure 5.15 and Figure 5.16. At 20°C, no signs of attack were observed in either 15LT5 or 15LT20 samples, except when immersed in 0.5%Cl and 0.60% SO_4 (M5), in which swelling, cracking and the deposition of a yellowish material occurred at the corners of both samples, being more intense in 15LT5.

TEMP	M	M5	M20
20°C	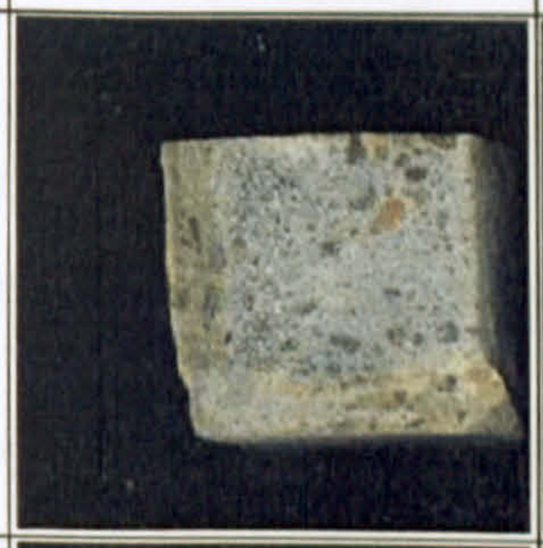		
5°C			

Figure 5.15: Long-term specimens (15LT5) immersed in salt solutions after 12 months: (top): 20°C; (bottom): 5°C.

TEMP	M	M5	M20
20°C			
5°C			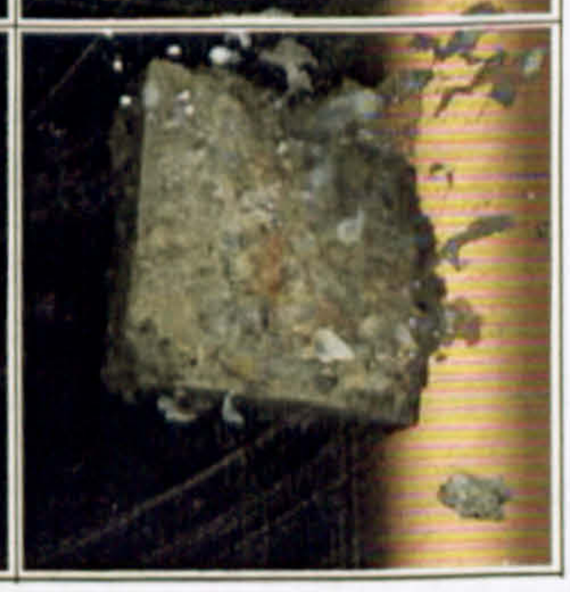

Figure 5.16: Long-term specimens (15LT20) immersed in salt solutions after 12 months: (top): 20°C; (bottom): 5°C.

As far as the carbonated zone is concerned, the white-yellow mushy material detached from these zones, but immediately underneath. Also, the thicker carbonated zone of 15L20 samples developed cracks at 5°C, but not at 20°C. Less carbonated samples (15LT5) developed the greatest damage, when compared to that with highly carbonated samples (15LT20).

5.3.2 Mass loss of new specimens in salt solutions

Because the extent of damage was not as visually clear in low and no carbonate filler samples as it was in 15%LF samples, an attempt was made to quantify the trends observed by the visual assessments, described in the previous section. This was achieved by measuring the mass change in some selected cubes.

Figure 5.17 shows the plot of mass (mean of six separate determinations) against solution type after 1 year of immersion at 5°C.

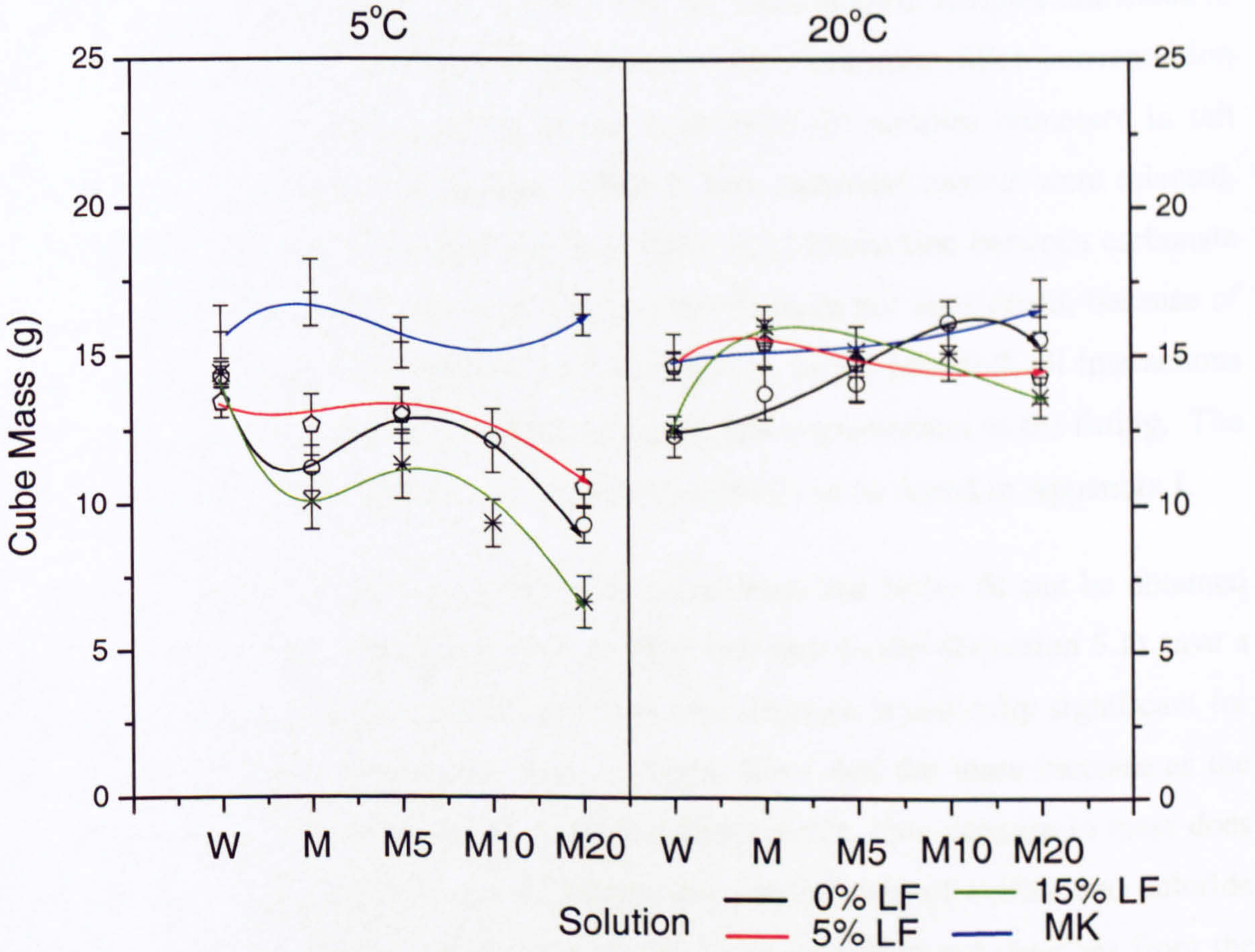

Figure 5.17: Mass profile in cubes immersed in salt solution after 1 year.

It can be seen that whereas little difference in the mass loss can be identified between the mixes at 20°C, significant differences were detected at 5°C, when compared to the mass of the samples immersed in water. Metakaolin containing samples did not present significant mass variation after 1 year at both temperatures. The higher the carbonate content, the greater the mass loss due to the chemical attack. The mass of all samples immersed in 0.5% Cl^- (M5) was somewhat higher than in the other salt solutions. This observation appears to agree with what was observed in Figure 5.5 in which samples immersed in chloride concentrations above 1.0% Cl^- (M10) developed greater damage than samples immersed in pure sulfate solution (M). This effect was more evident in 15%LF samples. It is possible to identify that 15%LF and 0%LF

showed a similar trend, but higher mass loss was shown in the former as expected in high limestone filler containing mortars not only in cold sulfate solution, but also in chloride solutions. This is in contrast with the damage mitigation which seems to have happened at higher temperature.

Since this observation indicates some correlation between carbonate content, chloride concentration and mass loss, several attempts were made to estimate the extent of such correlation. The experimental data (*) shown in Figure 5.17 has been analysed by means of multivariate statistics. The relative mass loss (m_i / m_{0w20^oC}) refers to the ratio of the mass of a particular sample (m_i) over the mass of OPC samples immersed in water at 20°C (m_{0w20^oC}). The chosen parameters were limestone filler concentration (Cc), chloride concentration (Cl), and temperature (blue for samples immersed in salt solutions at 5°C, and black for samples at 20°C). Two statistical models were selected. In the Model 1, the linear carbonate content factor (Cc) interaction between carbonate content and chloride concentration (CcCl) in solution were not considered, because of the poor significance in the t-student test (Appendix I). In the Model 2, all interactions were included, however it did not introduce significant improvement to the fitting. The statistical analyses and Analyses of Variance (ANOVA) can be found in Appendix I.

Whereas poor fit was found at 20°C, it can be seen that better fit can be obtained when all the factors are included at 5°C. At 20°C, the best model (Equation 5.1) gave a poor multivariate regression coefficient (R^2=0.64), although statistically significant for 73% confidence limit. The relative mass contours show that the mass increase as the level of both carbonate and chloride increase (Figure 5.18). This increase in mass does not mean any improvement of the mortars as the precipitation of sulfate and chloride bearing phases can increase the mass if the attacked zone does not detaches from the sample.

$$Rmass20 = \underset{\pm 0.04}{1.13} + \underset{\pm 0.009}{0.008}\,Cl - \underset{\pm 0.00038}{0.00018}\,Cl^2 - \underset{\pm 0.00033}{0.0007}\,Cc.Cl + \underset{\pm 0.00033}{0.0227}\,.Cc - \underset{\pm 0.0007}{0.00123}\,Cc^2 \quad \textbf{(5-1)}$$

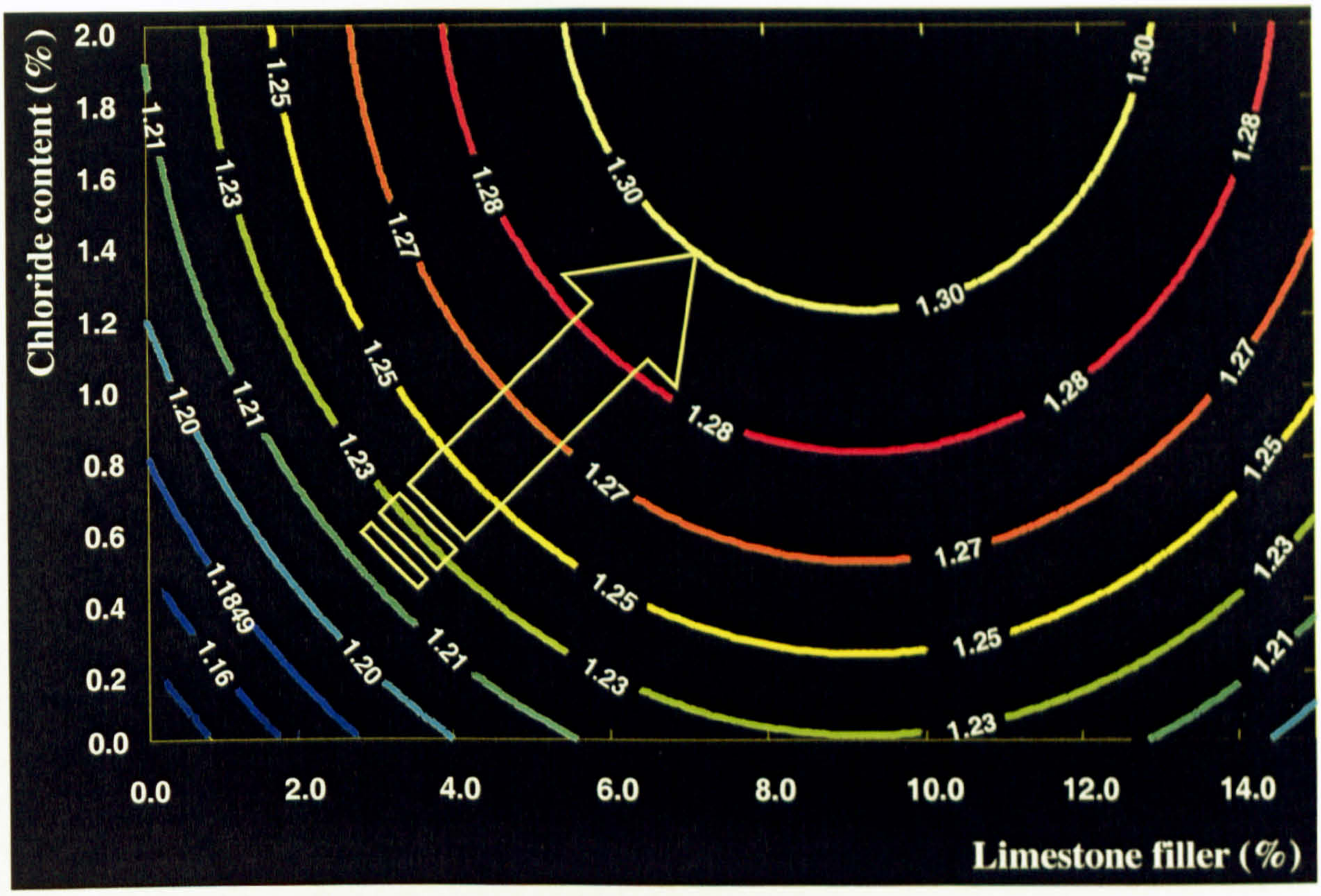

Figure 5.18: Iso-relative mass contours at 20°C.

At 5°C, the relative mass decreased as the level of limestone increased, but chloride in solution also played a strong role on the chemical attack responsible for the damage (Figure 5.18). As far as prediction is concerned (99.97% confidence limit), the Model 1 (Equation 5.2), the linear factor carbonate content (Cc) and its interaction with chloride (CcCl) independent variables were excluded, because the t-test indicates they have 50% and 98% chances, respectively, of being actually zero as seen (Prob>T). The multivariate regression coefficient is 0.957. These figures indicate that, alongside carbonates, chloride is also a strong factor affecting the relative mass losses, thus, negatively affecting the chemical attack observed (Figure 5.5), as material detached from the bulk of the samples and precipitated at the bottom of the containers.

$$Rmass = \underset{\pm 0.02}{0.907} + \underset{\pm 0.015}{0.071}Cl - \underset{\pm 0.002}{0.01}Cl^2 + \underset{\pm 0.00008}{0.00031}Cl^3 - \underset{\pm 0.0001}{0.0009}Cc^2 \qquad (5.2)$$

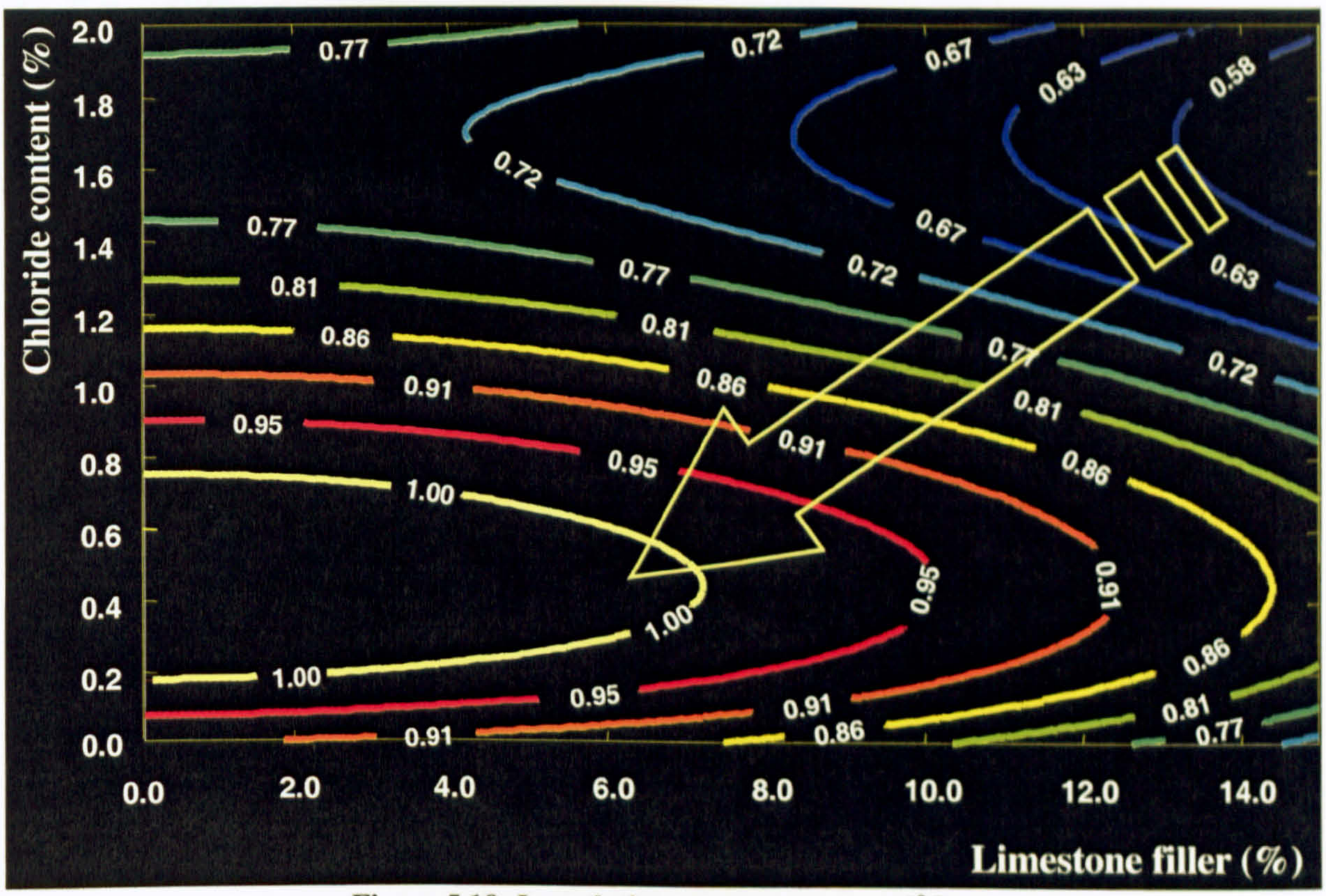

Figure 5.19: Iso-relative mass contours at 5°C.

At 5°C, this model predicts that an increase in carbonate content at the Cl^- concentration of about 1.1% would result in a greater mass loss rate. This maximum can possibly be confirmed by the profile found at 1.0% Cl^-, in which greater damage was also associated with 15%LF (Figure 5.5). This model also predicts that an increase in carboante content would develop a minimum variation of the relative mass at the chloride concentration of 0.50%, indicating certain mitigation of the attack. It is important to bear in mind that although the difficulty of removing all damaged material from the specimens reduces the accuracy of this approach, it is possible to detect that the use of chloride as a factor affecting the attack greately improved the fitting. Indeed, the effect of chloride on the attack of the samples strongly reduced with increase in temperature. The damage of the specimens that reflected in a loss of mass was associated to both the concentration of chloride ions and the amount of carbonate replacement at 5°C. It is therefore, important to identify the principal mechanism of attack, so that the role of chlorides can be investigated.

5.3.3 Mineralogy of products of deterioration

In order to clarify the findings observed in the visual inspections reported in the previous section, the mineralogy of deteriorated products was identified by means of X-Ray Diffraction (XRD) and infrared Spectroscopy (IRS). Also, attempt was made to correlate the formation and stability of such products with the mode of attack by using pH measurements in the salt solutions investigated.

A. X Ray Diffraction (XRD)

Although already described in the methodology chapter of this thesis, it is important to re-state that all XRD patterns were corrected for two-theta shift by means of a least-square procedure, as explained in Chapter 3 (Section 3.9.1). This is an indispensable procedure for successful distinctions between thaumasite and ettringite, which can produce a series of solid solutions. Indeed, instrumental factors associated with the geometry of the diffractometer can lead to undesirable errors, which can create difficulties for such differentiation.

The key for sample identification is described as follows:

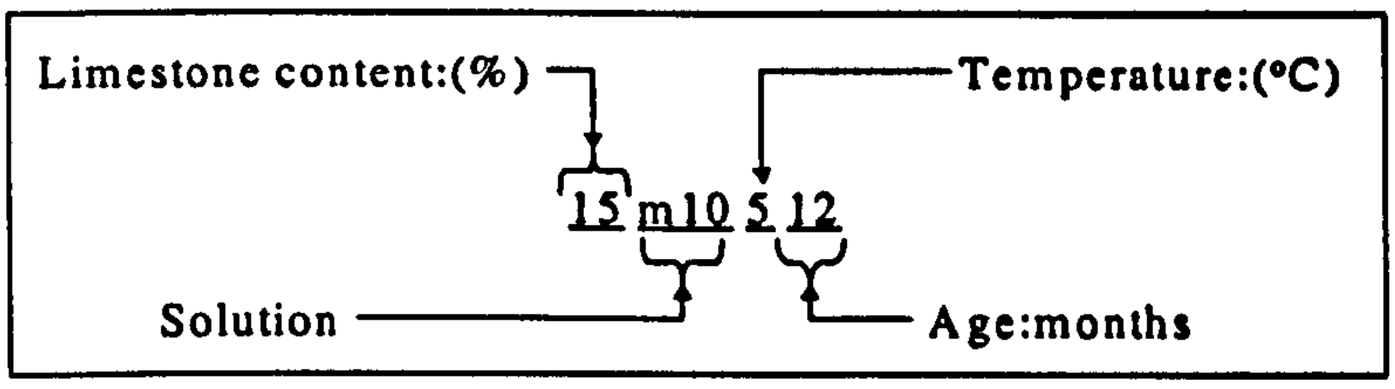

For instance, a sample containing 5% limestone filler immersed in 0.5%Cl^- and 0.60% SO_4^{2-} at 20°C after 12 months would read: 5M52012. Another example, a sample with 15% limestone filler and 10% metakaolin immersed in 2.0% Cl^- at 5°C after 12 months would read: MKM20512.

A.1 OPC samples containing 15% limestone filler

Corroded material

Not surprisingly, sulfate phases were dominated by thaumasite in 15%LF samples in all salt solutions at 5°C after 12 months, as can be seen in Figure 5.20 (red lines). Because of the degree of overlapping between thaumasite and ettringite, the presence of thaumasite is best accessed at higher angles (16.01, 26.01, 32.83, 35.73 and 41.66 *2theta*). Even though it appears to be absent, the occurrence of little amounts of ettringite (black lines) cannot be ruled out since the broadening of some peaks was detected (see 9.096, 15.79, 17.83 and 25.59 *2theta*). Traces of gypsum (11.59, 20.72, 31.10 and 33.34 *2theta*) can also be observed in all solutions, but more evidently in samples immersed in 0.5%Cl^- solution (pattern B) (see peaks 20.36 and 31.11 *2theta*). No Friedel's salt was detected among the corroded material in any solution (stronger peaks at 11.16 and 31.03 *2theta*). Traces of brucite were found in all sulfate solutions (see peaks 18.52 and 37.98 2 theta), and it appears slightly more pronounced in M5 (pattern B) and M10 (pattern C). At this temperature, the main carbonate phases detected were thaumasite and calcite (peaks at 23.05, 29.40, 35.97, 39.40, 43.16, 56.56,

57.40 and 58.08 *2theta*) but not aragonite (peaks at 26.21, 27.22, 33.13, 36.18, 37.26, 37.88 and 45.85 *2theta*). Because of the use of Philips aluminium back filling holders, the presence of aluminium peaks (38.47 and 44.74 *2theta*) can be identified in samples where the powder did not cover the whole illuminated area of the Siemens diffractometer.

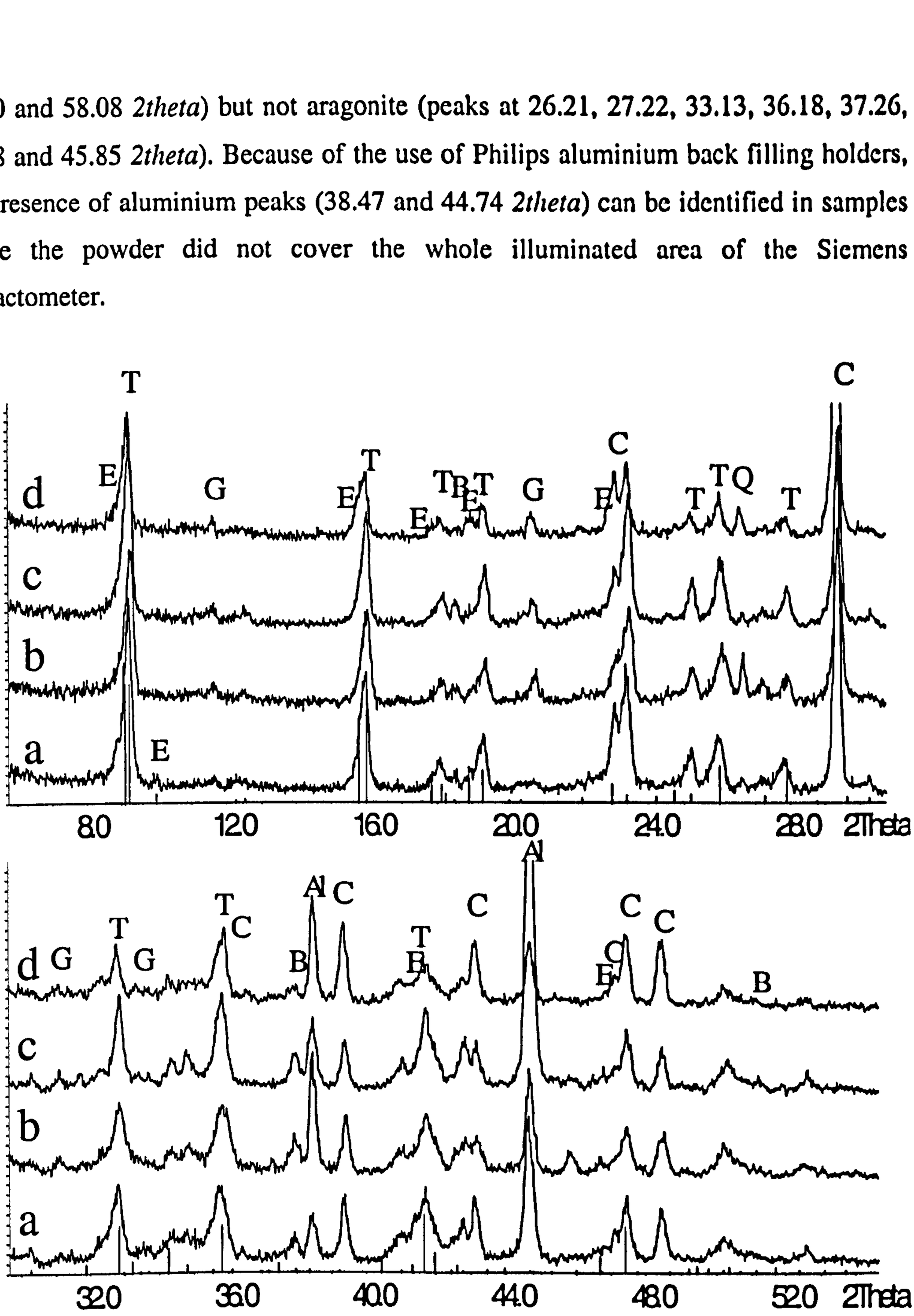

Figure 5.20: XRD of corroded materials in 15%LF mortar after 1 year in different solutions at 5°C. (a): 15M512; (b): 15M5512; (c): 15M10512; (d):15M20512; (black line): ettringite; (red line): thaumasite; (G): gypsum; (C): calcite; (Q): quartz; (Al): aluminium from the powder holders; (B): brucite.

As for 15%LF at 20°C, conventional sulfate attack phases developed in all sulfate solutions, which was dominated by the presence of ettringite (see 9.096, 15.79, 17.83 and 25.59 *2theta*) and gypsum (11.59, 20.72, 31.10 and 33.34 *2theta*). As can be seen in Figure 5.21, a greater amount of ettringite and gypsum was found in pure sulfate solution, whereas gypsum was predominant in sulfate solution containing 1.0%Cl^-. As the level of chloride increased to 2.0% in sulfate solution, less ettringite and gypsum deposited within the corroded material.

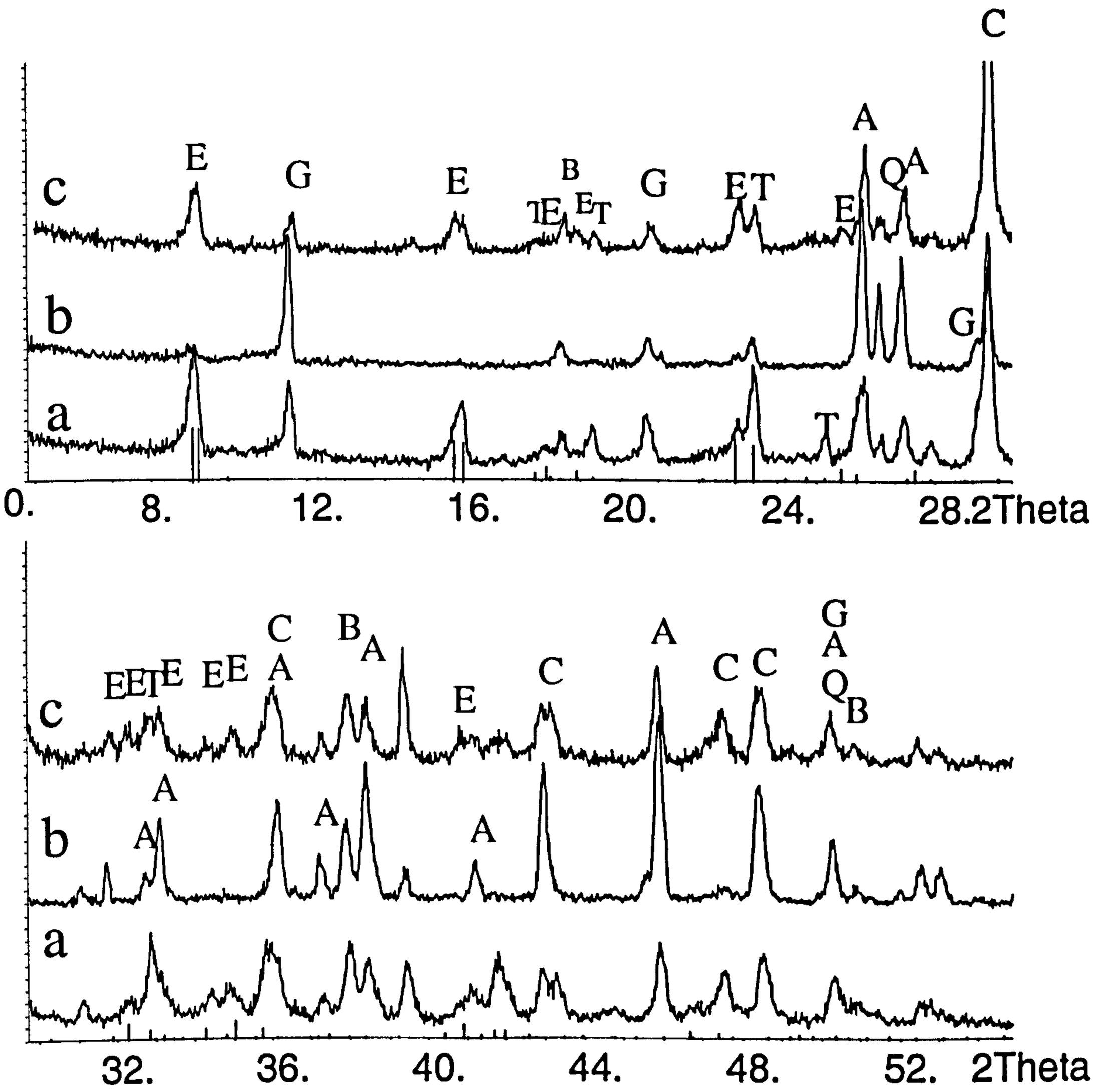

Figure 5.21: XRD of corroded materials in 15%LF mortar after 1 year in different solutions at 20°C. (a): 15M2012; (b): 15M102012; (c): 15M202012; (black line): ettringite; (red line): thaumasite; (G): gypsum; (C): calcite; (Q): quartz; (A) aragonite; (B): brucite.

With regards to the carbonate phases, both calcite and aragonite (peaks at 26.21, 27.22, 33.13, 36.18, 37.26, 37.88 and 45.85 *2theta*) were detected. Consistent amounts of calcite were always identified in all salt solutions, which can be expected due to this level of cement replacement by limestone. The precipitation of aragonite in samples immersed in M5 will deserve further discussion.

The precipitation of brucite within the corroded material seemed to reduce as the chloride content increased in the solution. The intensity of brucite peaks was higher at 20°C than at 5°C (see peaks 18.52, 37.98 and 50.79 *2 theta*).

It is important to point out that, in some peaks assigned as ettringite, a slight two-theta shift towards higher angle can also be found at this temperature, more prominently in solution M. This is an indication that ettringite has suffered some alteration in its structure, possibly towards thaumasite solid solution type of phase, in these high limestone filler samples (15%LF).

Bulk samples

Figure 5.22 shows the XRD pattern of the bulk samples after removing the superficial corroded material, which was subject of previous discussion (section 3.9.1). Each phase detected will be discussed separately.

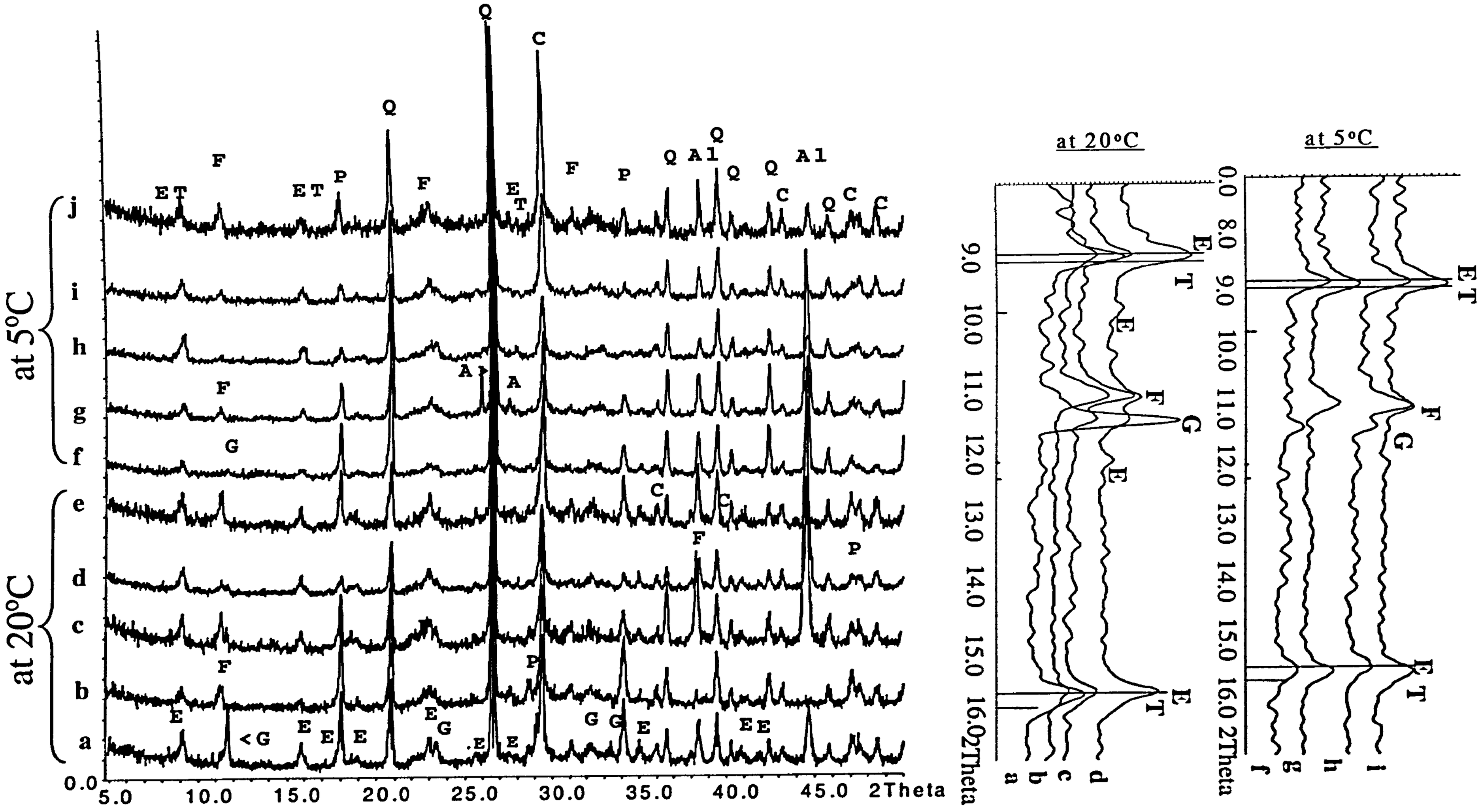

Figure 5.22: XRD of 15%LF bulk sample after 1 year. (left): pattern up to 50° 2theta; (right): pattern up to 17° 2theta; (a): M20; (b): M520; (c): M1020; (d): M2020; (e) SEA20; (f) M5; (g): M55; (h): M105; (i): M205; (j): SEA5; (black line and E): ettringite; (red line and T): thaumasite; (F): Friedel's salt; (G): gypsum.

Portlandite (P): Unlike the XRD pattern of samples at the surface, portlandite was identified in the bulk of all samples. The intensity of portlandite peaks was more intense at higher temperatures and at lower concentrations of chlorides. The highest intensity occurred in pure magnesium sulfate solution (patterns a and f), followed by 0.5%Cl^- and seawater (patterns b, g, e and j). The presence of portlandite indicates that further reaction can be expected in this system, as it is not stable in the presence of sulfate ions. As the chloride concentration increased, the less portlandite was found, which was more evident at 5°C (patterns d, h and I). This dependence between portlandite, temperature and chloride can possibly be explained by:

(i) Higher solubility at lower temperatures increases the chances of the dissolution of portlandite [12] that promptly reacts with sulfate ions to form gypsum and brucite in presence of magnesium [12, 48];

(ii) Leaching of portlandite can occur in the presence of chlorides due to the osmotic pressure [99, 115];

(iii) Possible reaction between chlorides to form calcium chloride aluminate hydroxide hydrate (Friedel's salt).

Gypsum (G): The precipitation of gypsum was scarcely observed in samples at 5°C. As for samples at 20°C, significant amount of gypsum was only detected in magnesium sulfate solution and seawater (patterns a and e), but was not observed in any other sodium chloride solution (patterns b to d). At the lower temperature, it is possible that the sulfate ions were more engaged in the formation of thaumasite. At the higher temperature, the reduced amount of portlandite that may have reacted with chloride to form Friedel's salt (commonly observed at this temperature) reduced the chances of the precipitation of gypsum. In addition, the presence of chloride may have leached out portlandite as reported by other researchers [99, 115], which also reduced the availability of lime inside the sample to participate in gypsum formation. This hypothesis is discussed in further sections, with the analyses of the solution pH (section 5.3.4) and the solubility of gypsum in the presence of carbonate, chloride and magnesium sulfate (Appendix II).

Friedel's salt (F): Although Friedel's salt readily precipitates in the presence of chlorides due to reaction with the aluminate phases of the cement, the amount of Friedel's salt detected was not so prominent in the bulk sample, and it was absent in the surface. The temperature also affected the intensity of Friedel's salt peaks (11.16 and 31.03 *2theta*), which were higher at the higher temperature. This can be indicative of a low chloride binding capacity due to:

(i) The dilution effect of 15% limestone filler replacement,

(ii) The aluminate content of the original Portland cement was combained with sulfate ions to form ettringite, which can be stable even in the presence of Friedel's salt [132].

(iii) The presence of carbonates inhibits the formation of monosulfate [32, 133], whose absence reduces the chances of Friedel's salt formation [132, 133].

(iv) Friedel's salt is also unstable in pH below 10, which is the sort of value achieved when insoluble brucite precipitates at the surface or in carbonated zones of the mortar, especially at 20°C [106, 107].

(v) The dissolution of Friedel's salt in the presence of calcium carbonate causes the precipitation of calcium carbonate, hydrogarnet and ultimately AH_3, with the release of Ca^{2+} and Cl^- into solution [105, 106]. The effect of pH on the stability of F in the presence of carbonate and sulfate ions at 5°C will be discussed in further sections.

(vi) Thaumasite and Friedel's salt might not be thermodynamically compatible, which might affect the chloride binding capacity of the cement matrix (to be discussed in Chapter 6).

Ettringite/Thaumasite (ET): At 20°C, XRD peaks 9.096 and 15.79 (patterns a to d-Figure 5.22: right) matched those of ettringite. As the temperature decreased, it can be seen that there was a shift of these peaks assigned to ettringite towards those of thaumasite d-spacing (red line in Figure 5.22: right). Similar shifts were observed by Torres et al. [13, 18] who concluded they correlate with the thaumasite-ettringite solid-solution and the amount of limestone filler in mortar. The extent of the thaumasite-ettringite solid solution is a subject of further investigation, with determination of the lattice parameters and the chemical composition of the thaumasite formed (Chapter 6).

Aragonite (A): It is important to note that aragonite was only detected at 5°C in M5 (pattern g), in which less damage was also detected (Figure 5.5), but it precipitated more abundantly at 20°C in all solutions, especially those with higher levels of chlorides in solution. Aragonite is a metastable form of $CaCO_3$ compared with calcite, which is thermodynamically more stable. However, aragonite is reported to be kinetically more favourable to precipitate than calcite in the presence of magnesium species [82].

A.2 OPC with and without 5% limestone filler and metakaolin

The main phases identified in OPC mixes with and without 5% limestone filler, as well as OPC with 15% limestone filler and 10% metakaolin, are tabulated in Table 5.2. The data refers to analyses carried out after 12 months in the test solutions. Each mineral is considered in turn in the subsequent paragraphs.

OPC and OPC with 5% limestone filler

In general, the phase assemblage follows a similar trend as found in OPC with 15% limestone filler samples.

Gypsum (*G*): At 20°C, gypsum was commonly found in both the bulk sample and the corroded material. At 5°C, gypsum was mostly observed within the corroded material, and it was only found in the bulk sample of 5%LF immersed in M, at this temperature.

Portlandite (*P*): Portlandite was only observed in the bulk of the samples, in all mixes, solutions and temperatures. The presence of portlandite in the metakaolin mixes indicates that the pozzolanic reaction was not complete, possibly because of the amount used (10%). Even so, there was not much gypsum precipitation because of the duffusion of the sulfate ions in the samples.

Brucite (*B*): Possibly because of it low solubility [48], brucite was preferably observed within the corroded material but not in the bulk of the samples. The intensity of XRD peaks appeared to decrease as the temperature decreased.

Friedel's salt (*F*): Whereas Friedel's salt was commonly found in the bulk of the samples, especially at 20°C, it did not precipitate within the corroded material, except in OPC without limestone replacement. The metakaolin samples developed the highest amount of Friedel's salt and the intensity of its XRD peaks increased with the chloride concentration and the temperature. Friedel's salt did not form when thaumasite formed.

Table 5-2: Phase assemblage in OPC samples with and without 5% limestone filler and metakaolin (MK).

Sample				Main phases						
Filler (%)	Temperature (oC)	Solution	Type	Ettringite	Thaumasite	Friedel's salt	Gypsum	Portlandite	Brucite	Aragonite
0	5	M	Bulk	**	nd	-	-	*****	-	-
			CMat	*	****	-	*	-	**	*
		M5	Bulk	**	nd	**	-	***	-	-
			CMat	*	***	-	*	-	*	*
		M10	Bulk	**	nd	**	-	**	-	-
			CMat	*	*****	-	*	-	**	-
		M20	Bulk	**	nd	***	-	**	-	-
			CMat	*	****	-	*	-	*	*
	20	M	Bulk	***	-	-	****	****	-	-
			CMat	***	-	-	*	-	***	*
		M5	Bulk	**	-	***	*	****	-	-
			CMat	nd	nd	nd	nd	nd	nd	nd
		M10	Bulk	***	-	**	****	**	-	-
			CMat	*	-	*	****	-	**	*****
		M20	Bulk	**	-	*	***	*	-	-
			CMat	****	-	*	****	-	***	***
5	5	M	Bulk	-	**	-	*	**	*	-
			CMat	-	****	-	*	-	*	-
		M5	Bulk	***	*	**	-	****	-	-
			CMat	*	*****	-	**	-	*	*
		M20	Bulk	****	*	***	-	****	-	-
			CMat	*	*****	-	**	-	*	-
	20	M	Bulk	**	-	-	****	****	-	-
			CMat	***	nd	-	****	-	***	*****
		M5	Bulk	***	-	*	****	*	-	-
			CMat	****	nd	-	*	-	*	**
		M20	Bulk	***	-	**	*****	*	-	-
			CMat	*	nd	-	*****	-	*	****
MK	5	M	Bulk	*	-	-	**	****	-	-
		M5		*	-	*	**	****	-	-
		M20		*	-	***	-	****	-	-
	20	M	Bulk	*	-	-	***	****	-	-
		M5		*	-	***	-	**	-	-
		M20		**	-	****	-	*	-	-

(Bulk): bulk sample; (CMat): corroded material; (*): relative intensity; (-): not found; (nd): not determined because of lack of material or weak XRD intensity.

Ettringite (*E*): The precipitation of ettringite appears to be favourable at high temperatures (20°C), where it was identified in both the bulk of the sample and the corroded material in all mixes and solutions, whereas at 5°C, ettringite was mostly found in the bulk of the samples in all mixes and solutions. At the latter temperature, the

corroded material was dominated instead by thaumasite. The stability of ettringite appears to be affected by the presence of carbonates, but no clear trend could be observed with respect to chloride concentration at any temperature.

Thaumasite (*T*): The higher the carbonate content, the higher the deposition of thaumasite, as expected. However, even OPC without limestone developed thaumasite. In the case of OPC without limestone, the source of carbonates was the atmospheric carbonation of lime containing phases of the cement, with the exposure to air for 21 days prior to the immersion in the selected solutions. Another source of carbonates in O%LF mix was the formation of bicarbonates due to the dissolution of atmospheric CO_2, which was always present through out the experiment. There was no cross contamination between solutions because each mix was placed in a different container (see section 3.3-Chapter 3). The presence of chloride somehow increased the precipitation of thaumasite in most samples, but thaumasite did not form in metakaolin containing mix in any solution or at any temperature. In the highly carbonated samples, however, some XRD peaks associated with thaumasite can be detected. Thaumasite was much more common within the corroded material than in the bulk of the sample, where XRD peaks associated with ettringite-thaumasite solid solution were more prominent.

Aragonite (*A*): The precipitation of aragonite seemed to increase as the temperature increased and it was never a major component at 5°C. Also abundant deposition of aragonite occurred most favourably within the corroded material rather than in the bulk of the sample. No clear trend could be found between the precipitation of aragonite and increase in the concentration of chloride in solution in these mixes. The most intense XRD peaks of aragonite were observed in 0%LF mixes immersed in M10 at 20°C.

This observation indicates that greater damage was associated with the precipitation of thaumasite than with the precipitation of aragonite. Since CO_3^{2-} ions are shared by both minerals, the precipitation of aragonite would result in the precipitation of less thaumasite (Figs 5.5, 5.20 and 5.21);

The fact that aragonite was detected at all chloride concentrations at 20°C but scarcely at 5°C appears to indicate that the solubility of calcium carbonate is affected by the presence of chlorides, and that temperature also plays a strong role. This is subject of further discussion (see Appendix II).

Metakaolin

In metakaolin mixes, despite the presence of 15% limestone filler, no thaumasite formed after one year of exposure in the selected salt solutions, but the formation of ettringite and gypsum, did form without expansion or visual signs of damage did occur (Figure 5.6 and 5.10).

After 73 weeks though, samples immersed in magnesium sulfate alone developed significant damage (Figure 5.11). XRD analyses of these samples (Figure 5.23) shows that prodominatly gypsum and also an ettringite solid solution were responsible for the attack. Some peaks can be assigned to both ettringite (black lines) and thaumasite (red lines), which suggests the possibility that these phases precipitated together. However, there are other peaks that can also be assigned to an orthorhombic polymorph of thaumasite (brown lines and PDF 44-1413). This mineral has not yet been reported as a product of sulfate attack. Further examination with infrared spectroscopy will address these possibilities (section 5.2.5B). The hump between 13 and 14°2θ could not be identified.

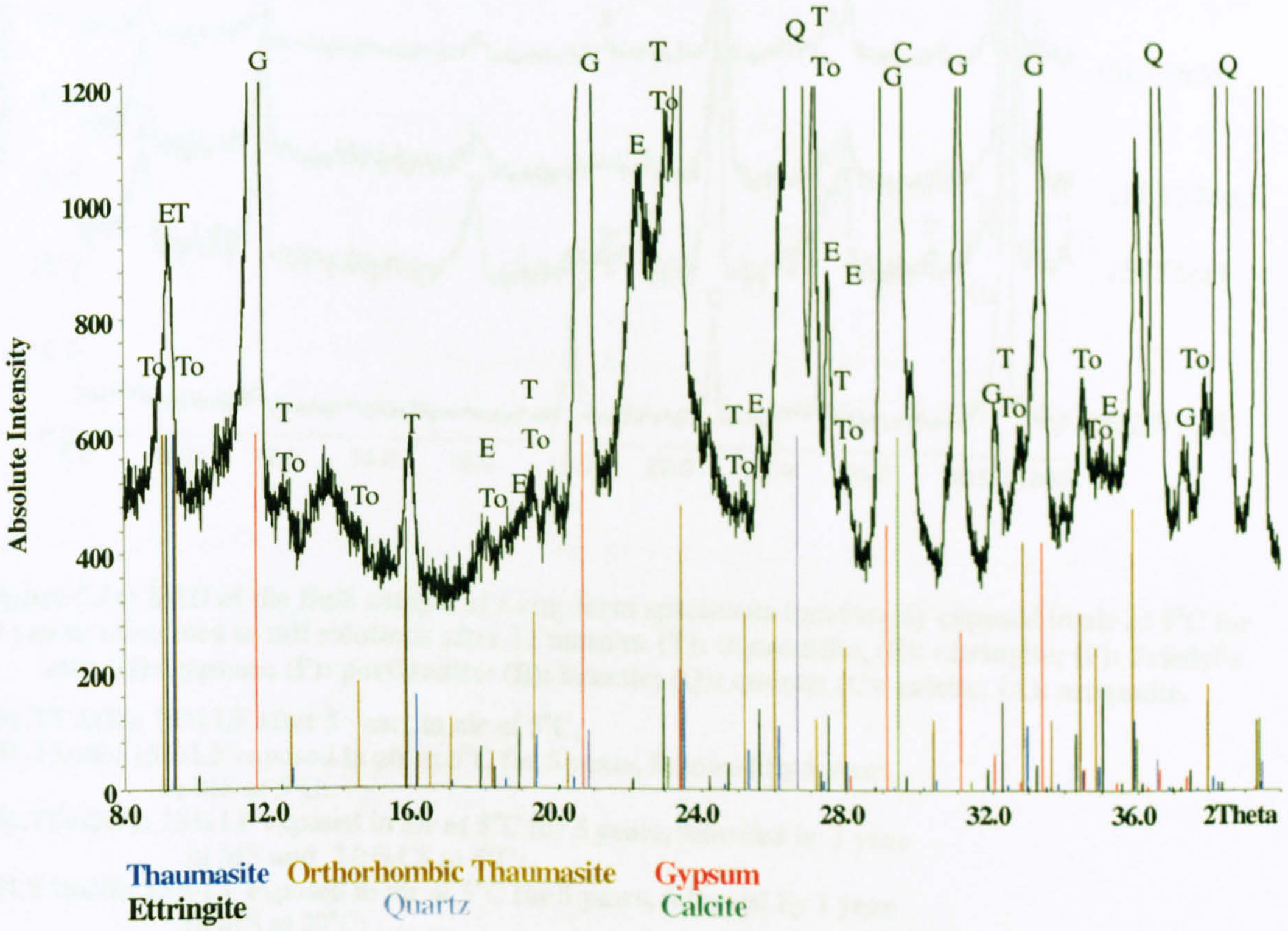

Figure 5.23: MK after 73 weeks in magnesium sulfate at 5°C: (To): orthorhombic thaumasite, (T) thaumasite, (E) ettringite, (G) gypsum; (Q) quartz and (C) calcite.

A.3 Long term specimens

Figure 5.24 shows the XRD pattern of 15LT5 samples immersed in salt solutions at 5°C for 1 year. At 5°C, no chloride-bearing phase was identified. However, extensive deposition of gypsum and thaumasite were detected, more intensely in the less carbonated samples. It can be seen that portlandite was consumed in the formation of gypsum, and this was more pronounced at 5°C. Where Friedel's salt precipitated, the intensity of the gypsum peaks wwas reduced. Aragonite was observed at 20°C, but not easily detected at 5°C. Traces of brucite was also observed, more clearly in chloride free solutions at both temperatures.

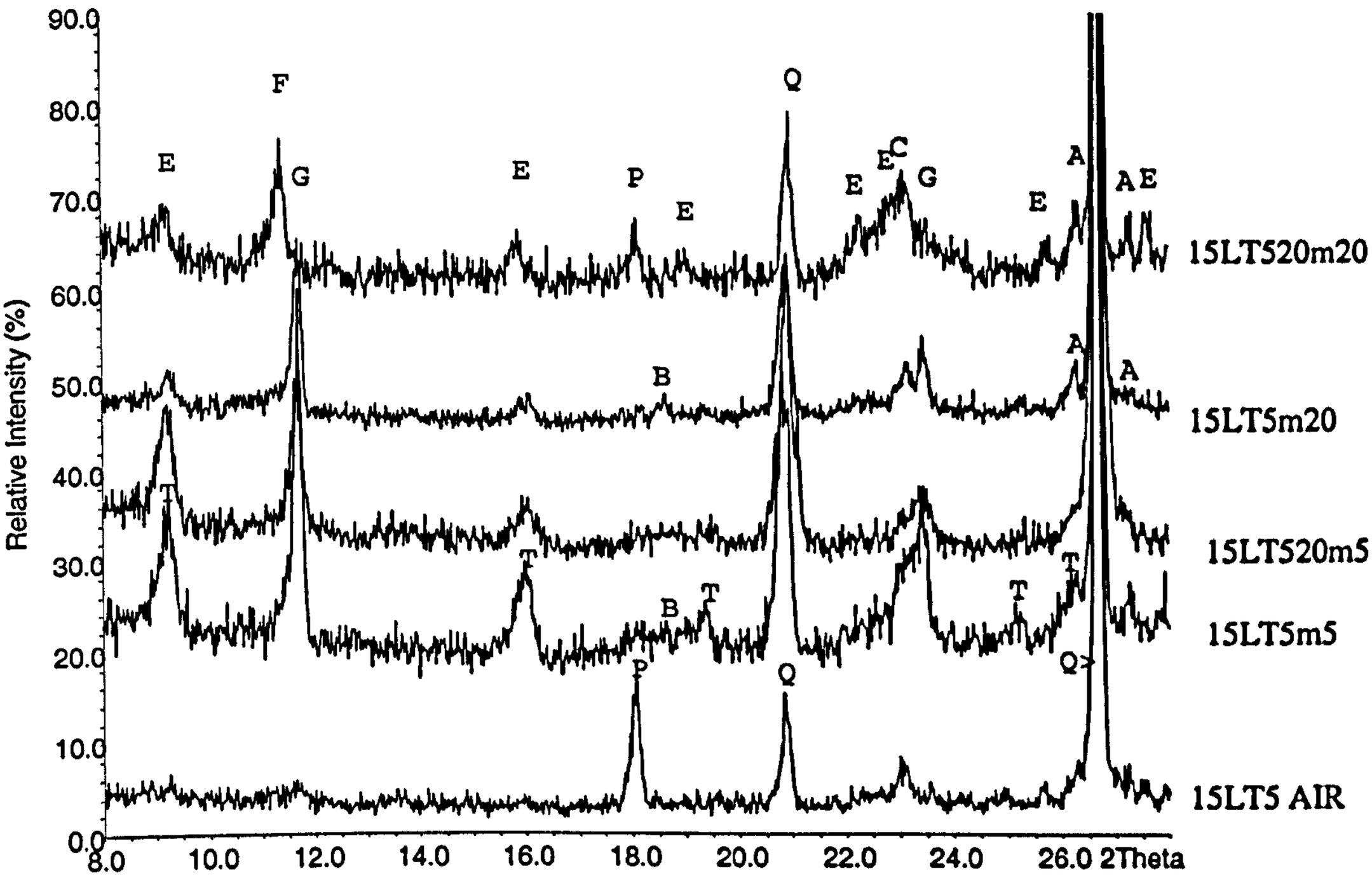

Figure 5.24: XRD of the Bulk sample of Long-term specimens (previously exposed in air at 5°C for 5 years) immersed in salt solutions after 12 months. (T): thaumasite, (E): ettringite; (F): Friedel's salt; (G): gypsum; (P): portlandite; (B): brucite; (Q): quartz; (C): calcite; (A): aragonite.

(15LT5 AIR): 15%LF after 5 years in air at 5°C;
(15LT5m5): 15%LF exposed in air at 5°C for 5 years, followed by 1 year in MS at 5°C;
(15LT5m205): 15%LF exposed in air at 5°C for 5 years, followed by 1 year in MS and 2.0%Cl^- at 5°C;
(15LT5m20): 15%LF exposed in air at 5°C for 5 years, followed by 1 year in MS at 20°C;
(15LT5m2020): 15%LF exposed in air at 5°C for 5 years, followed by 1 year in MS and 2.0%Cl^- at 20°C;

Figure 5.25 shows the XRD pattern of 15LT20 samples immersed in salt solutions for 1 year. Indeed, where no visual damage was detected, Friedel's salt, ettringite and traces of gypsum were the only phases identified in samples immersed in magnesium sulfate (MS) and combined sulfate and sodium chloride at 20°C. The intensity of portlandite peaks was much more pronounced at 20°C than at 5°C, except in chloride containing solutions where it was significantly reduced. Although thaumasite appears to have precipitated, its presence cannot be entirely confirmed due to a low intensity compared with the background noise. Aragonite was observed in chloride containing solutions, especially at 20°C and possibly traces at 5°C.

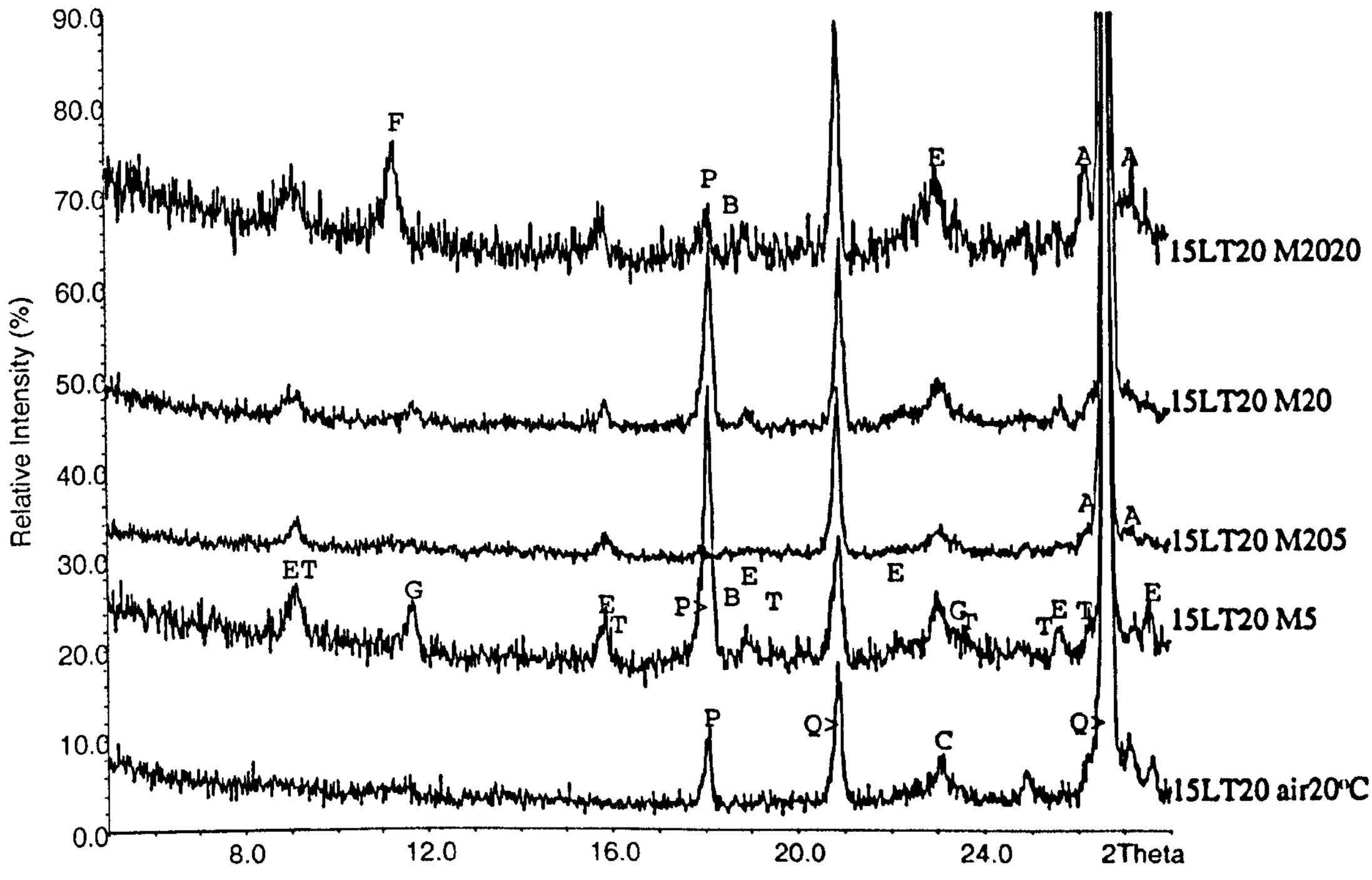

Figure 5.25: Bulk sample XRD of Long term specimen (previously exposed in air at 20°C for 5 years) immersed in salt solutions after 12 months (LT20). (T): thaumasite, (E): ettringite; (F): Friedel's salt; (G): gypsum; (P): portlandite; (B): brucite; (Q): quartz; (C): calcite; (A): aragonite.
(15LT20 AIR): 15%LF after 5 years in air at 20°C;
(15LT20m5): 15%LF exposed in air at 20°C for 5 years, followed by 1 year in MS at 5°C;
(15LT20m205): 15%LF exposed in air at 20°C for 5 years, followed by 1 year in MS and 2.0% Cl^- at 5°C;
(15LT20m20): 15%LF exposed in air at 20°C for 5 years, followed by 1 year in MS at 20°C;
(15LT20m2020): 15%LF exposed in air at 20°C for 5 years, followed by 1 year in MS and 2.0% Cl^- at 20°C;

B. IR Spectra

The importance of infrared spectroscopy in differentiating between ettringite and thaumasite is widely accepted. This is because of the unique vibration of octahedral silicon at 500 reciprocal centimetres, which indicates whether the cement matrix has undergone any transition towards thaumasite formation.

B.1. 15% Limestone filler

Figure 5.26 shows IR spectra of 15% LF mixes exposed to salt solutions at 5°C, which clearly confirm the findings identified by XRD that thaumasite was responsible for the attack in all salt solutions.

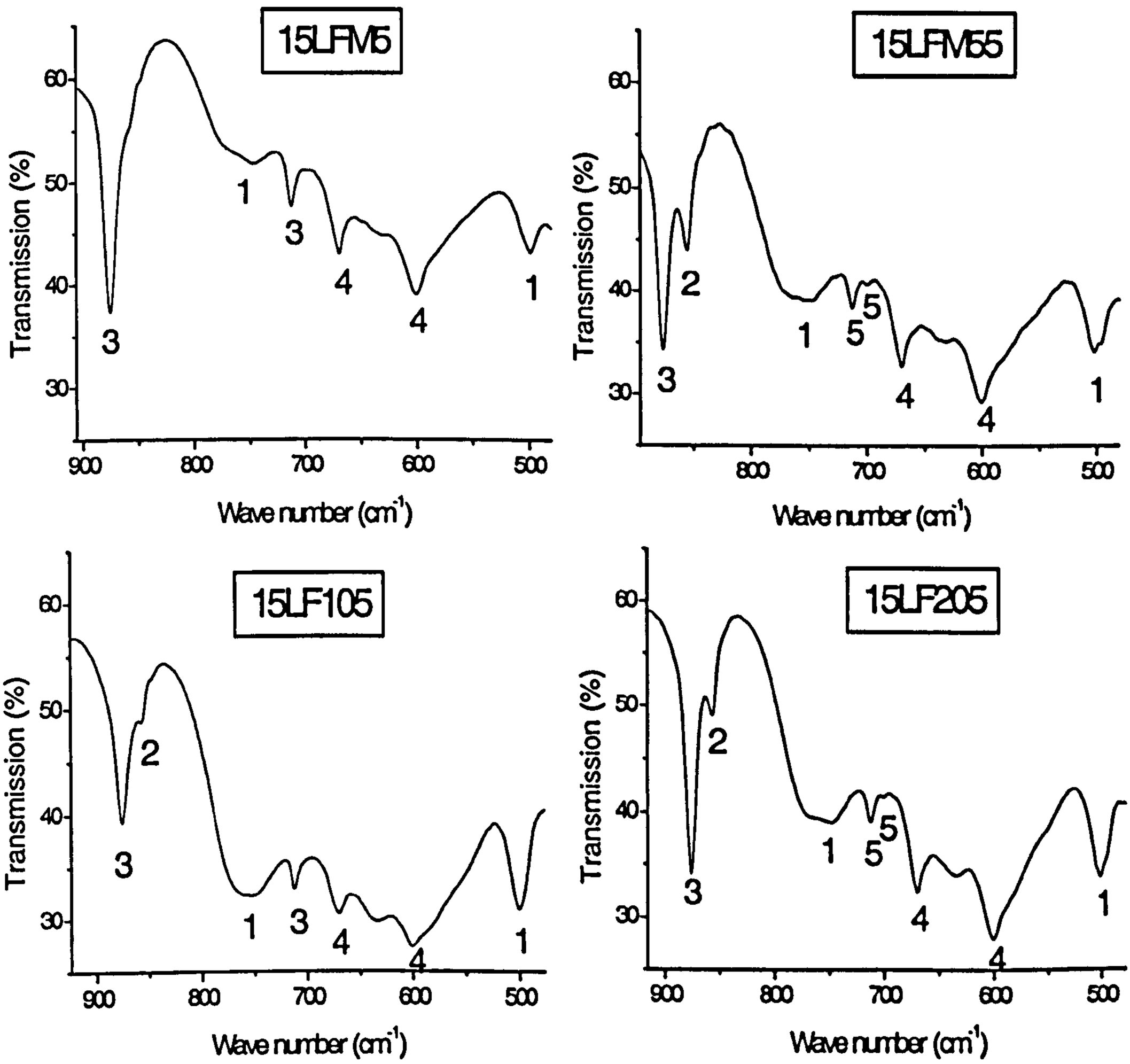

Figure 5.26: Infrared spectra of the corroded material in 15%LF after 12 months at 5°C. (1): $Si(OH)_6$; (2): $Al(OH)_6$; (3): CO_3^{2-}; (4): SO_4^{2-}; (5): v4-aragonite.

Indeed, the sharp 500 cm^{-1} and the broad 755 cm^{-1} peaks, which are assigned to the $Si(OH)_6^{2-}$ group, indicate that thaumasite was present in all salt solutions [134]. However, the presence of the peak at 855 cm^{-1}, which is attributed to the $Al(OH)_6^{3-}$ group, can be an indication that thaumasite was not present as the end member of the solid solution [135]. Further consideration will be given to this observation in the Chapter 6, where the composition of the thaumasite will be discussed. Peaks at 603 cm^{-1} and 675 cm^{-1} are assigned to SO_4^{2-} group, which belong to sulfate phases such as thaumasite, ettringite and gypsum, simultaneously. Peaks 725cm^{-1} and 875 cm^{-1} are assigned to CO_3^{2-} groups that belongs to thaumasite and calcite [136]. It appears that traces of aragonite have also deposited in the 0.5%Cl^- and also at 2.0%Cl^- samples (peaks 5 in Figure 5.26), as indicated by the doublet peaks around 700 cm^{-1}.

The IR spectra at 20°C are shown in Figure 5.27.

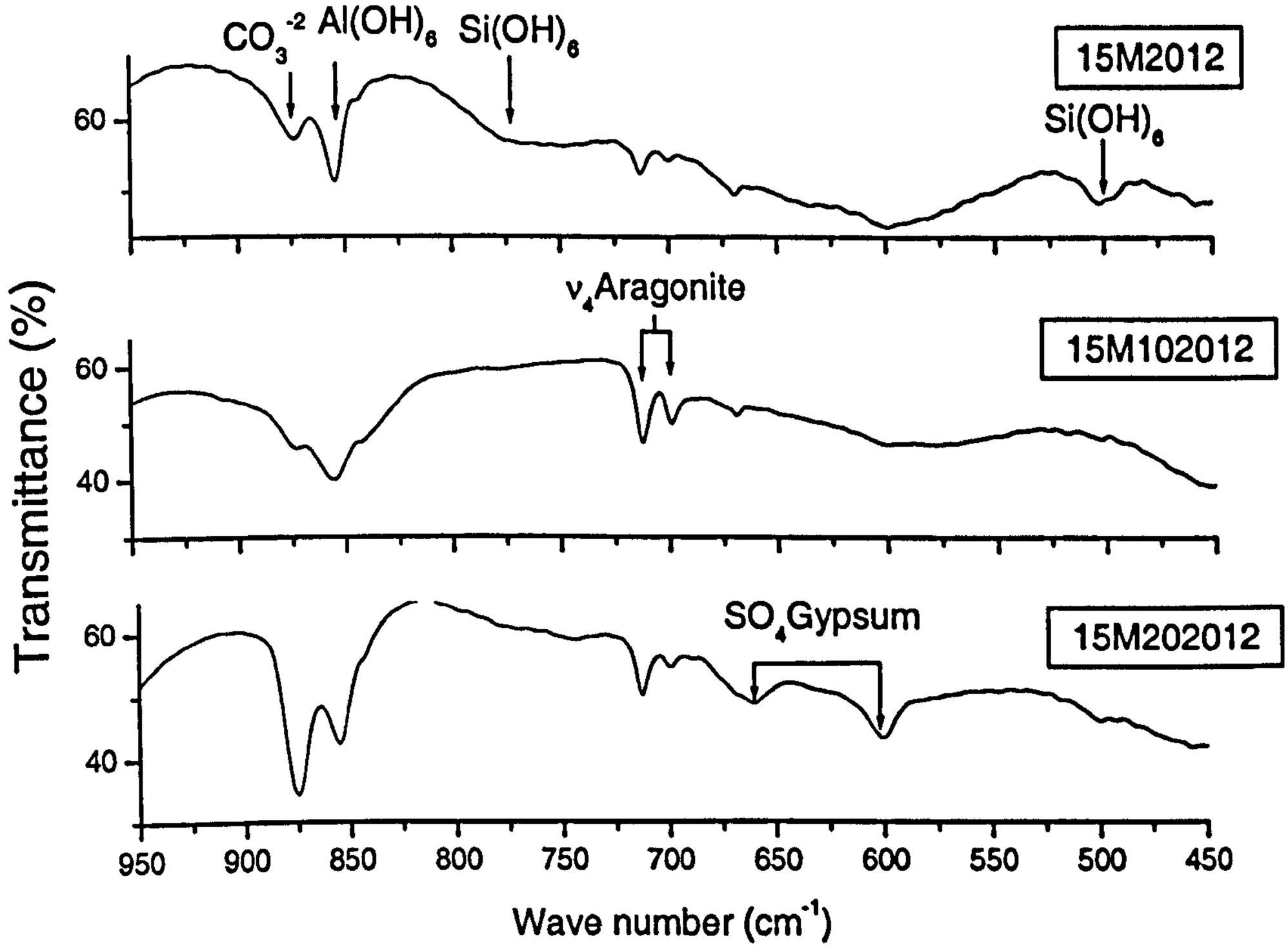

Figure 5.27: Infrared spectra of the corroded material in 15%LF after 12 months at 20°C.

It was found that the $Al(OH)_6^{3-}$ and the SO_4^{2-} groups, which are associated with ettringite and gypsum, are present in all cases. Peaks associated with CO_3^{2-} group are also in good agreement with the description given in XRD, which registered the

significant deposits of aragonite that occurred in M10 and to a lesser extent in other solutions. The carbonate peak 875 cm^{-1} is associated with calcite, which was more predominant due to the level of 15% limestone filler replacing the cement. The identification of aragonite and not thaumasite indicates that this mineral precipitated as a calcium and carbonate ions entered in solution.

It is worthy to point out that $Si(OH)_6^{2-}$ peaks were also identified in the M and M20 solutions, and possible traces in the M10 solution. This finding indicates that some silicon was either taken up by the ettringite or thaumasite formed in these systems, as suspected by the XRD patterns (Fig 5.21).

B.2. 5% Limestone Filler

Figure 5.28 shows the IR spectra of OPC containing 5%LF in salt solutions at 5°C.

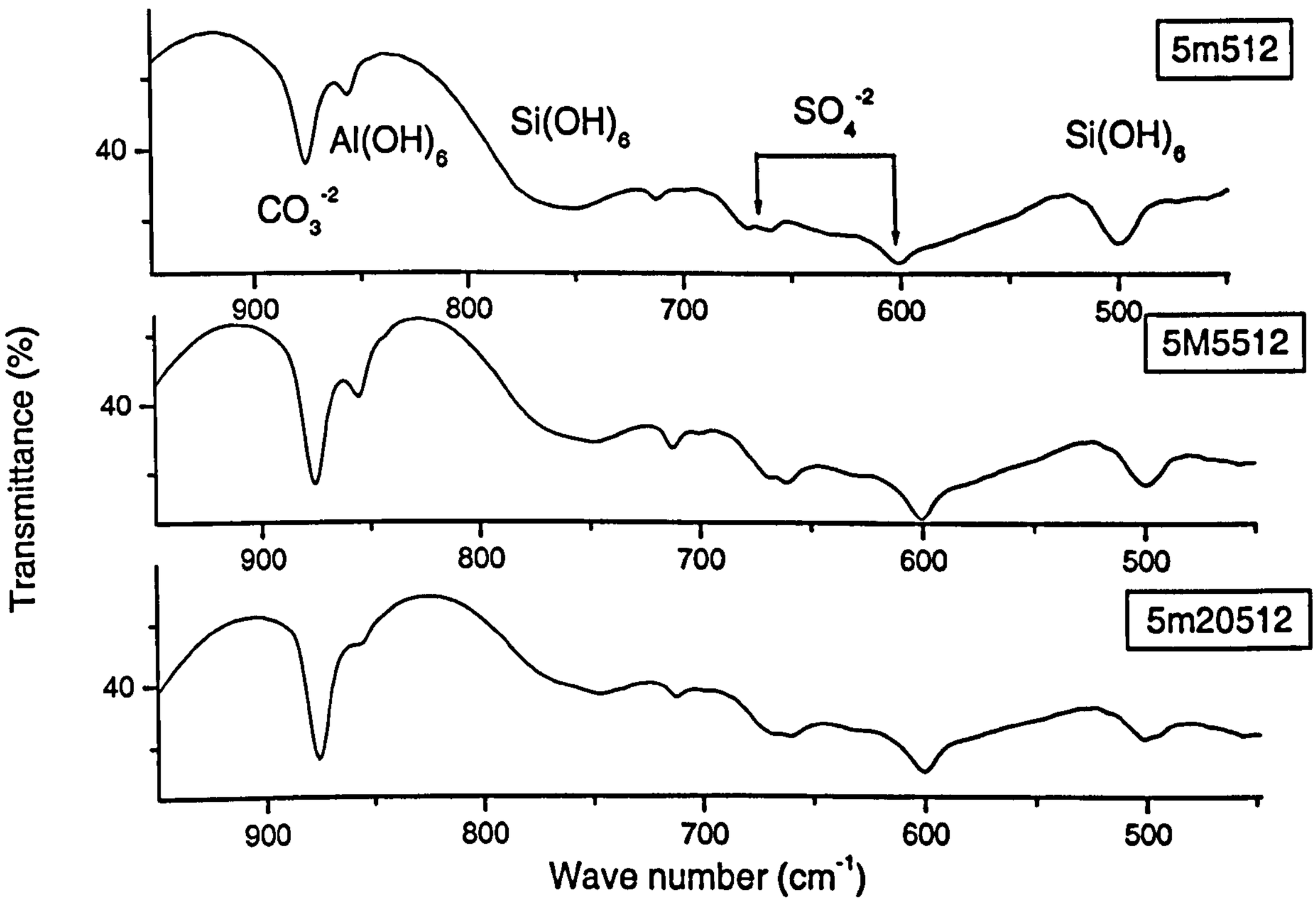

Figure 5.28: Infrared spectra of the corroded material in 5%LF after 12 months at 5°C

Once again, it is evident that the damage identified at 5°C in 5%LF samples was definitely caused by TSA, as can be seen by the presence of the 500 cm^{-1} and 755cm^{-1} peaks, indicating Si in octahedral coordination. The presence of a solid solution was clear by the identification of the peak 855 cm^{-1}, attributed to $Al(OH)_6$. Vibration bands for sulfate were also identified, which were assigned to gypsum and ettringite/thaumasite solid solution. The carbonate group belongs mainly to calcite and

thaumasite, but traces of aragonite can also be identified in the 0.5%Cl^- solution (doublet peaks around 700cm^{-1}). The presence of aragonite was also detected in samples containing 15% LF in this solution. Indeed, this observation seems to correlate with the fact that less damage was found in this solution, more clearly observed in the visual inspection of 15%LF mix (Fig 5.5) and the mass loss profile (Fig. 5.17 and 5.19).

As can be seen in Figure 5.29, vibration bands of octahedral silicon were virtually absent at 20°C, despite some small shoulders at 500 cm^{-1}, which can be an indication of the ettringite solid solution or the precipitation of both thaumasite and ettringite.

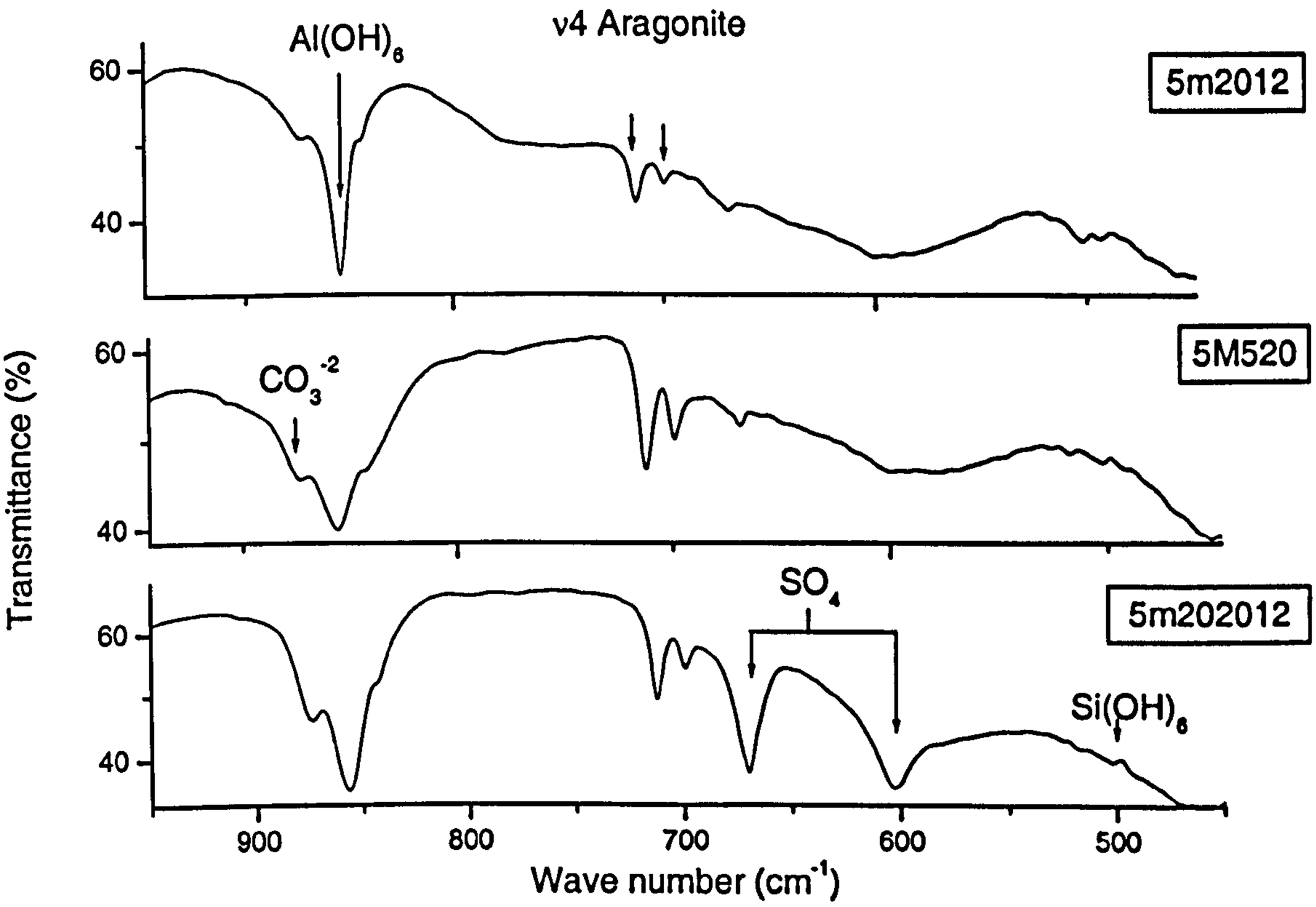

Figure 5.29:Infrared spectra of the corroded material in 5%LF after 12 months at 20°C

The presence of the octahedral aluminium peak at 855 cm^{-1}, and sulfate bands at 603 cm^{-1} and 675 cm^{-1} associated with ettringite and gypsum, respectively, characterises conventional sulfate attack, as previously confirmed by XRD as being responsible for the damage in such samples. Carbonate bands can also be identified and assigned to both calcite and aragonite, and their intensities reflect the profiles found by XRD analyses.

B.3. OPC

Features of the IR spectra observed in OPC samples at both temperatures support the XRD findings that TSA attacked OPC mortars at 5°C and 20°C, as seen in Figure 5.30 and 5.31.

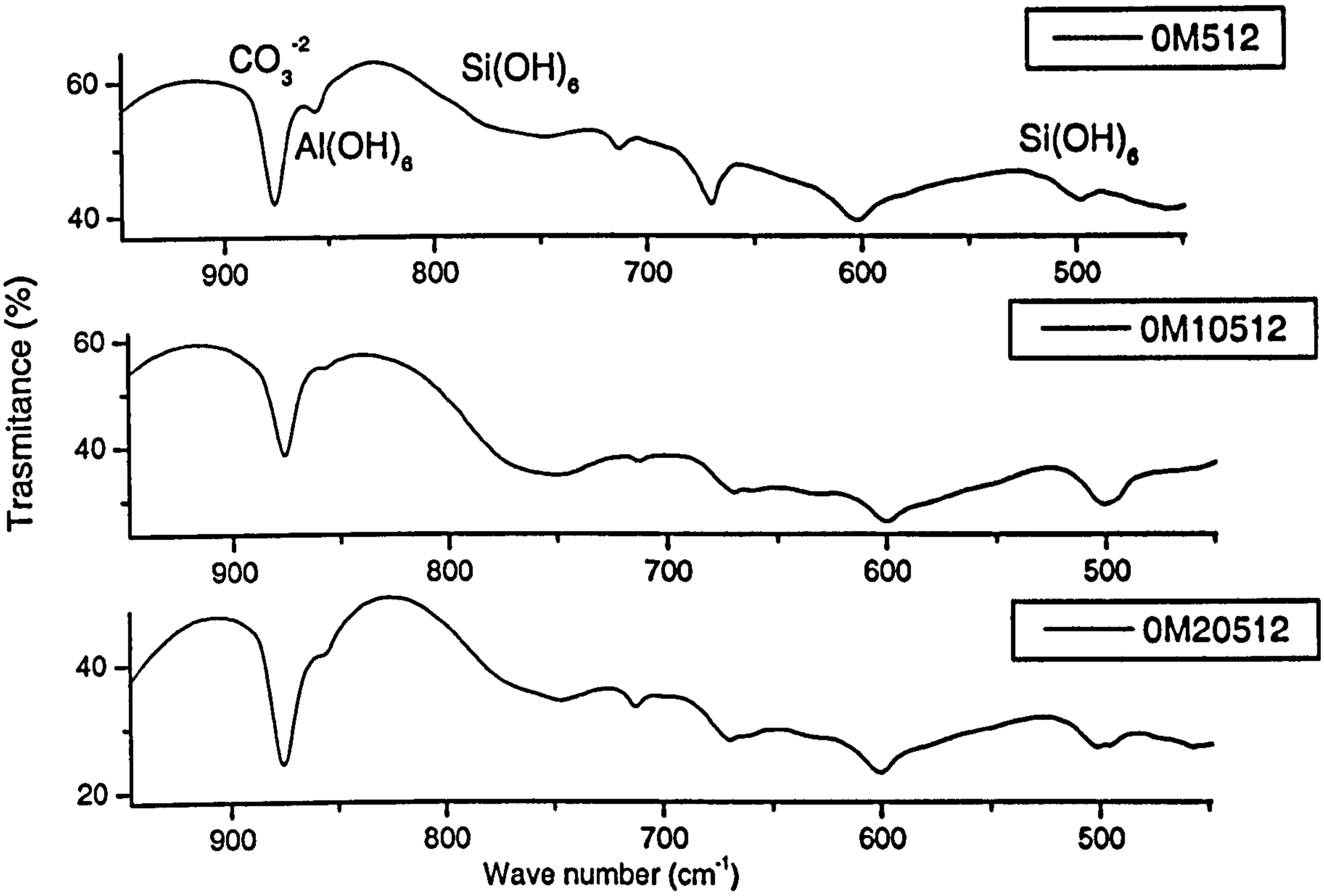

Figure 5.30: Infrared spectra of the corroded material in OPC mixes after 12 months at 5°C

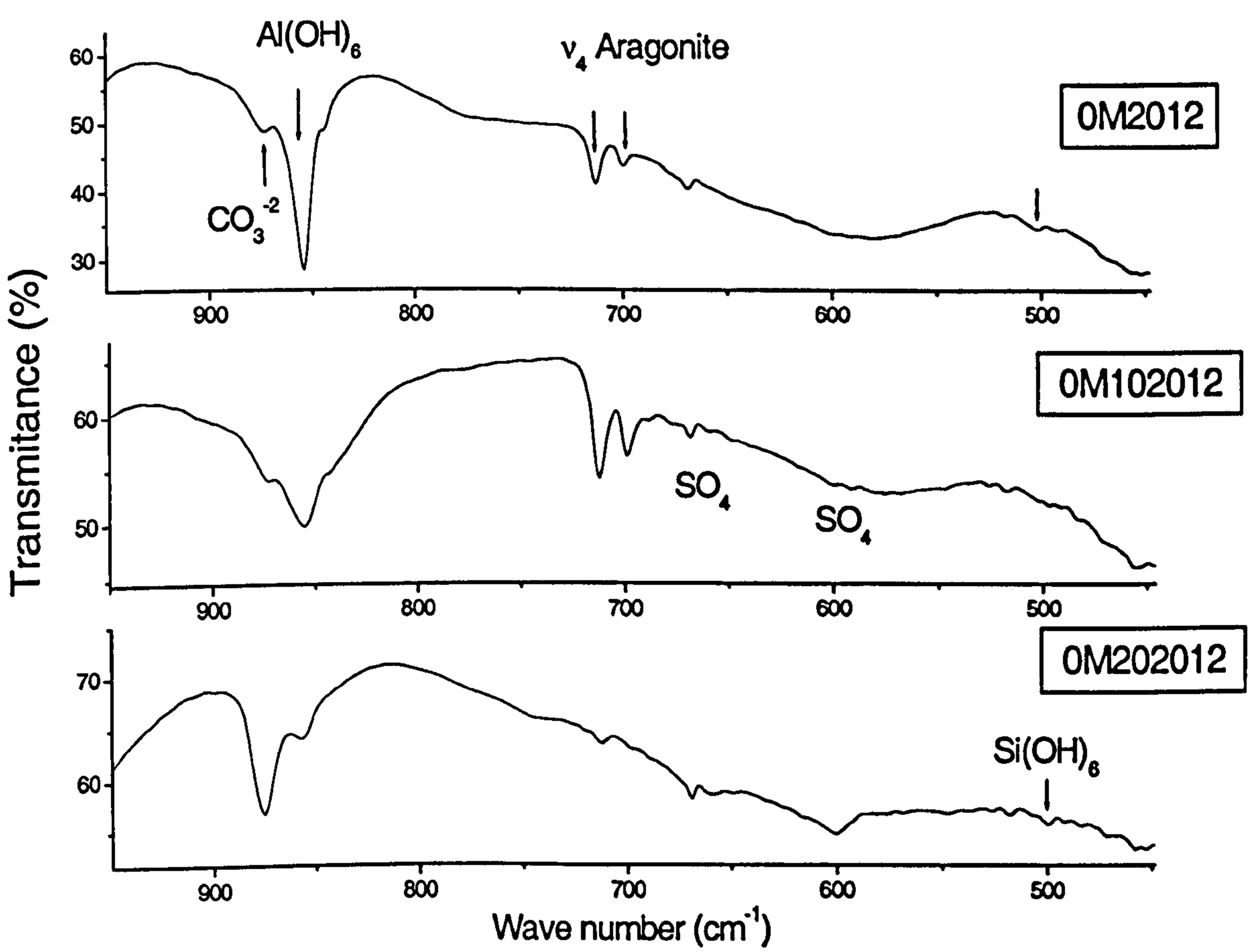

Figure 5.31: Infrared spectra of the corroded material in OPC mixes after 12 months at 20°C

The patterns are remarkably different. At 20°C, the peaks assigned to $Al(OH)_6$ (855 cm^{-1}) and SO_4^{2-} (603 cm^{-1} and 675 cm^{-1}) indicates that conventional sulfate attack phases ettringite and gypsum occurred at the higher temperature, whereas the peaks assigned to $Si(OH)_6$ indicates that thaumasite sulfate attack was responsible for the damage observed at 5°C in Figure 5.5. Carbonate bands associated with both calcite and aragonite were identified at both temperatures, nevertheless, aragonite bands were much more pronounced at 20°C, especially in solutions M and M10. Yet again, in this mix, the sources of carbonate ions were the atmospheric carbonation during the first 21 days in air and dissolution of atmospheric CO_2 in salt solution during the period of exposure.

B.4. OPC containing 15% limestone filler and 10% metakaolin

Figure 5.32 shows the infrared pattern of mortar samples containing metakaolin and limestone after 53 weeks of immersion in different salt solutions at 5°C and 20°C, respectively. It can be seen that parts of either raw metakaolin or an aluminium silicate hydrate, which were not found by XRD because they are amorphous, have been detected as shown by peaks 1 to 3, alongside carbonates (peak 4) and traces of octahedral aluminium at 855cm^{-1}. Sulfate bands at 603 and 675 cm^{-1} could not be detected, except for traces of the 675 cm^{-1} peak in some instances.

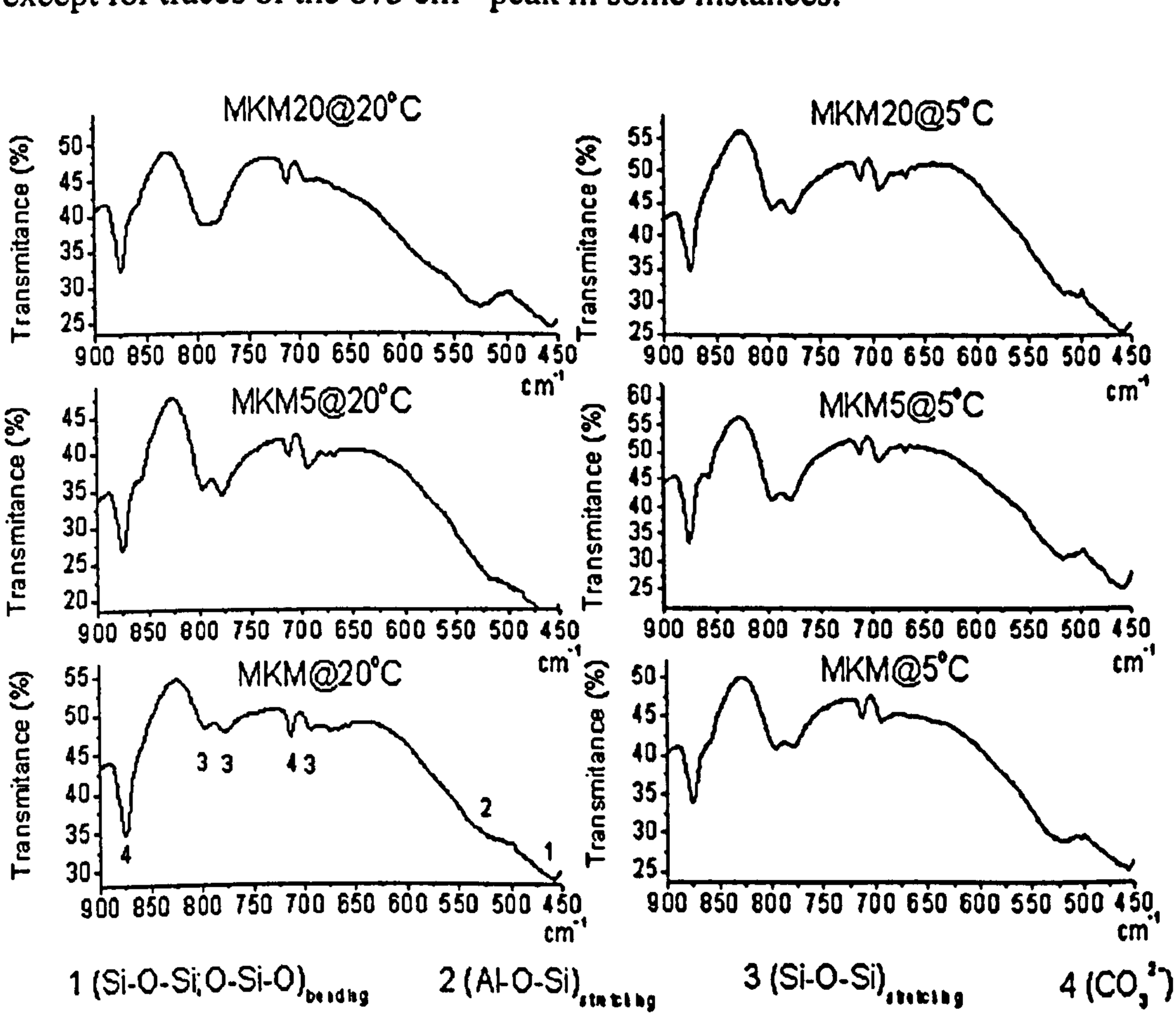

Figure 5.32: Infrared spectra of MK mix in salt solutions after 53 weeks

PAGE NUMBERING AS ORIGINAL

existence of a different symmetry in this series is not known. However, samples with higher lattice parameter *c* have been identified, in which could be due to a low carbonate to sulfate ratio [18]. Indeed, in the case of the thaumasite orthorhombic polymorph (PDF #44-1423), its formula does not contain carbonates ($Ca_3Si(OH)_6.(SO4)_2.9H_2O$). Yet, although the chemical formula suggests that Si is octahedrally coordinated with hydroxyls, no published research was found corroborate this.

B.5 Long term specimens

Investigation of long-term samples confirmed the presence of thaumasite in all samples immersed at 5°C. It appears that more thaumasite precipitated in the less carbonated samples (15LT5) than in the highly carbonated samples (15LT20), as can be seen by the intensity of the peaks associated with octahedral silicon and sulfates and carbonates, as shown in Figure 5.34 and Figure 5.35. The presence of aluminates can be an indication that thaumasite did not crystallize as the end member, but as a solid solution. This observation confirms the findings obtained by XRD (section 5.2.5A3) in which thaumasite and ettringite were suspected to have precipitated at 5°C.

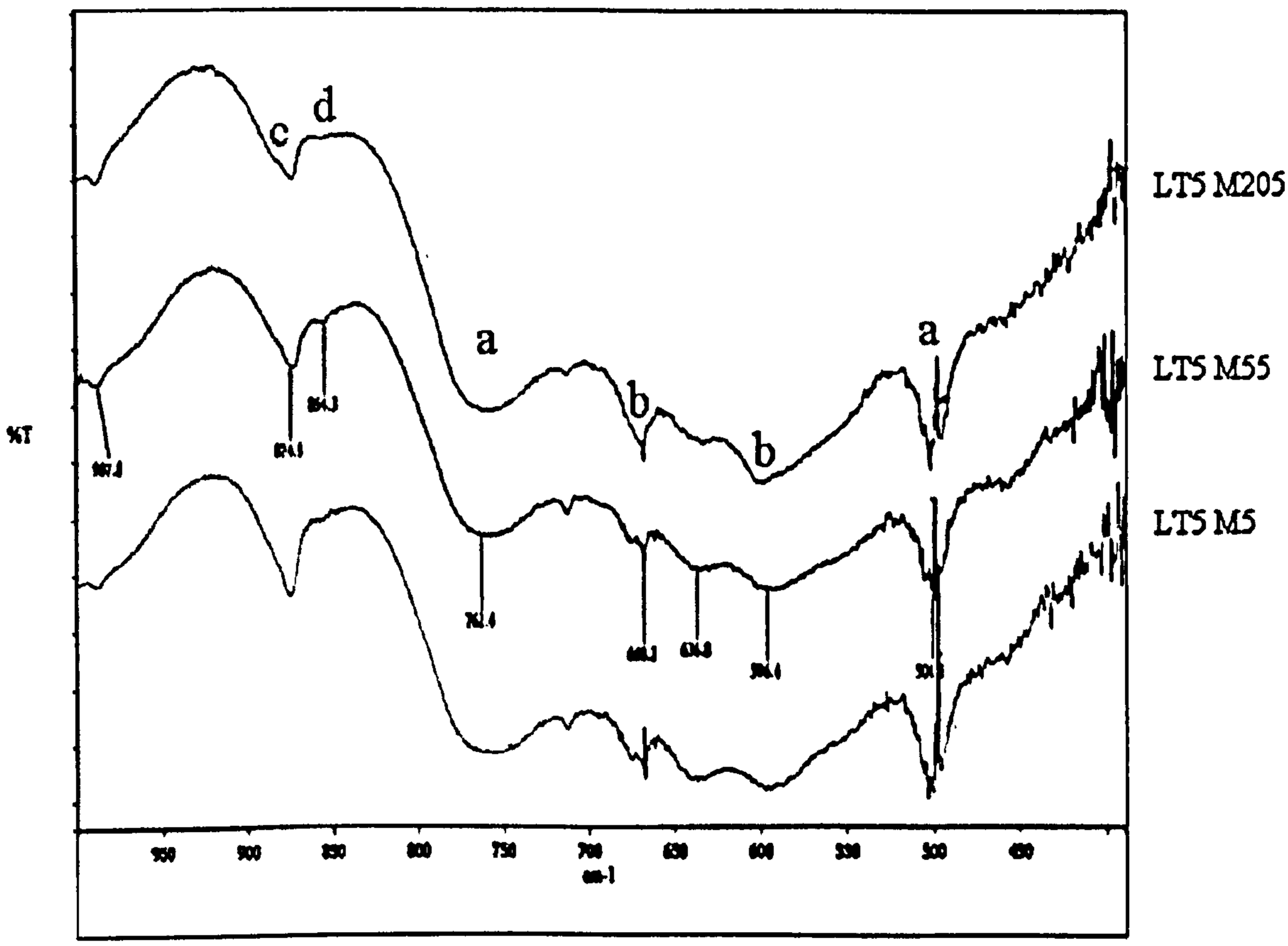

Figure 5.34: IR spectra of the bulk sample of long-term specimens (previously exposed in air at 5°C for 5 years) immersed in Cl^- + SO_4^{2-} at 5°C after 12 months (15LT5).
(a) $Si(OH)_6^{2-}$; (b) SO_4^{2-} ; (c) CO_3^{2-} ; (d) $Al(OH)_6^{3-}$.

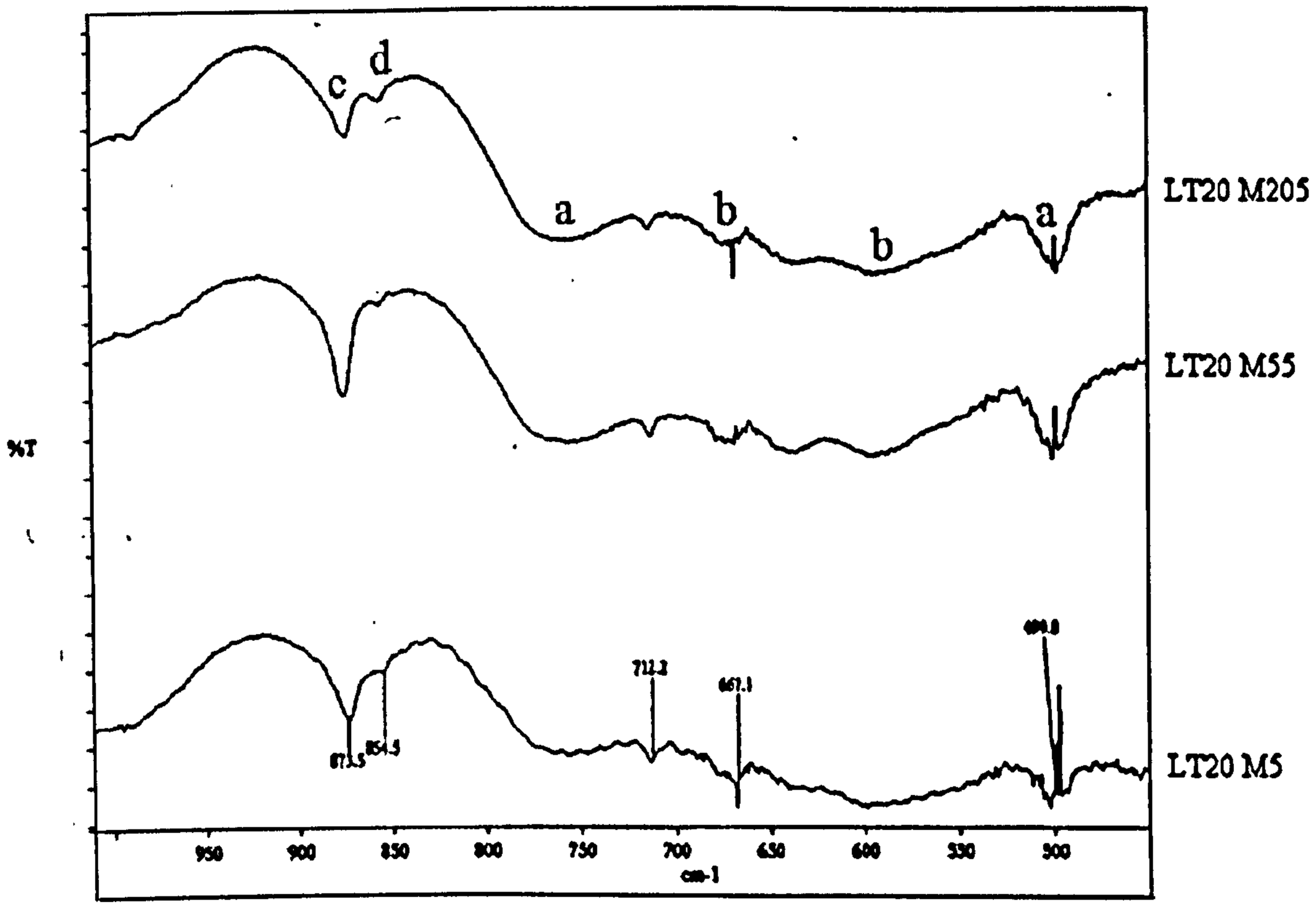

Figure 5.35: IR spectra of bulk sample of long-term specimens (previously exposed in air at 20°C for 5 years) immersed in $Cl^- + SO_4^{2-}$ at 20°C after 12 months (LT5).

(a) $Si(OH)_6^{2-}$; (b) SO_4^{2-} ; (c) CO_3^{2-} ; (d) $Al(OH)_6^{3-}$.

5.3.4 Effect of combined chloride and sulfate on the pH

As far as thaumasite is concerned, Gaze and Crammond [70] reported that it only forms in alkaline environments, higher than pH of 10.5. Also, they pointed out that thaumasite would form in conditions where ettringite is stable (pH>10.7 [12]). In further studies, this threshold was later explained as the pH (10.33 at 5°C) at which the species CO_3^{2-} and HCO_3^{1-}, which take part in the thaumasite formation, are in equilibrium [76].

In normal conditions, the pore solution in Portland cement matrix is alkaline, mostly because the dissolution of alkalis present in the cement, especially Na_2O and K_2O, elevates the pH to levels higher than 12.9 [137]. On the one hand, however the cement pore solution is mostly affected by the equilibrium of these dominant reactions, the pH at equilibrium can be buffered at lower values by the interaction with other ionic species such as magnesium. In this latter case, the precipitation of very insoluble phases such as brucite buffers the pH at 10.50. Table 5.3 shows some examples of typical reactions that occur when mortar samples are immersed in water and magnesium sulfate solution, and their respective pH at equilibrium.

Table 5-3: Reaction paths and the respective pH at equilibrium at saturation levels

Phase		Reaction	pH	Ref.
Dissolution of alkalis from the cement	1	$Na_2O + H_2O \rightarrow 2NaOH$ (0.1M) (1.0M)	12.90 14.00	[138]
Strong dissolution of lime that occurred immediately after immersion in neutral solution	2	$Ca(OH)_2 \leftrightarrow Ca^{2+} + 2OH^-$	12.40	[138]
Formation of brucite in magnesium sulfate solution	3	$Ca(OH)_2+MgSO_4.7H_2O \rightarrow Mg(OH)_2+CaSO_4.2H_2O +5H_2O$	10.50	
Carbonation of portlandite via bicarbonates and dissolution of calcite	4a	$Ca^{2+} + 2OH^- + CO_2 \leftrightarrow CaCO_3 + H_2O$	$10.33^{(1)}$	[82]
	4b	$2CaCO_3 + H_2O \leftrightarrow 2Ca^{2+} + CO_3^{2-} + HCO_3^{1-} + OH^-$		
	4c	$CaCO_3 + H_2O \leftrightarrow Ca^{2+} + HCO_3^{1-} + OH^-$	$8.48^{(2)}$	
Dissolution of CO_2	5a	$CO_2+H_2O \leftrightarrow H_2CO_3$ $H_2CO_3 \leftrightarrow H^+ + HCO_3^{1-}$	6.40	
At pH>10.33	5b	$HCO_3^{1-} \leftrightarrow H^+ + CO_3^{2-}$	10.33	
Calcite: (1) in the absence of atmospheric CO_2; (2) at normal pressure of atmospheric CO_2 (0.03%vol).				

More leaching of calcium hydroxide will favour reaction 2, and the pH will further rise. As cracks and attacked surfaces expose hydrated cement to more sulfate, reaction 3 will keep the pH at around 10.50. In the case where magnesium ions become depleted, reaction 4b and/or 4c proceed, depending on the presence of atmospheric CO_2.

All solutions were kept unchanged for 197 days to study pH variation due to the governing mechanisms and whether this could be correlated to sample deterioration observed during this period.

A. 15% Limestone Filler

Figures 5.36 and 5.37 show pH variation in 15%LF samples immersed in water and salt solutions at 5°C and 20°C respectively. The black columns are the pH after the first day of immersion of the samples in the test solutions and at the time of the replenishments after 192 and 292 days. The red marks indicate pH higher than 10.5 throughout the experiment. In order to investigate the conditions in which thaumasite is more prone to occur, the pH threshold of 10.5 was taken and pH levels higher than this were then highlighted.

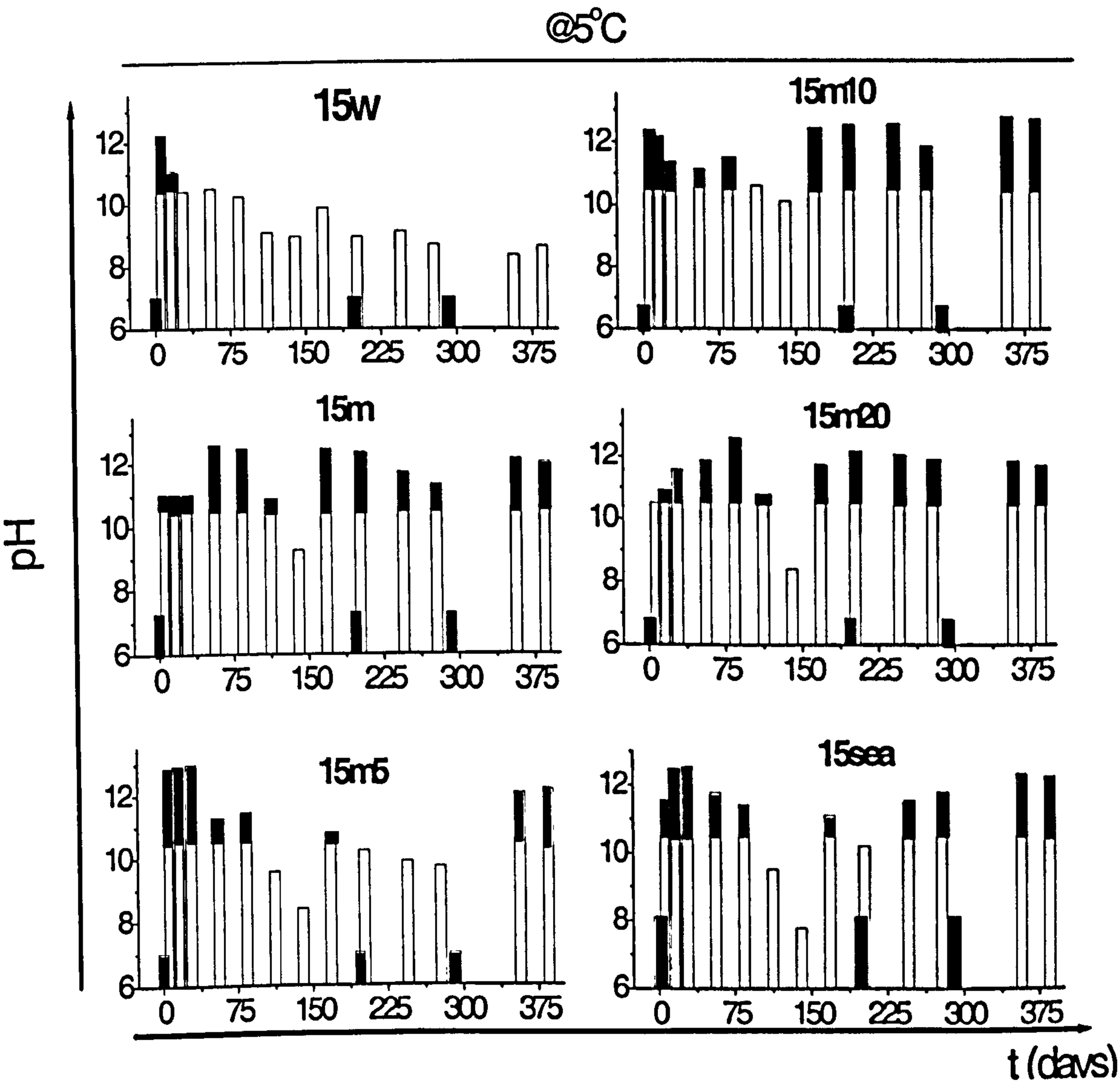

Figure 5.36: pH variation in 15%LF at 5°C. Solutions replenished at 197 and 292 days (full black columns) and pH higher than 10.5 (red and black marks). Initial pH of all solutions were around 7, and seawater pH was 8.12 (Table 3.11).

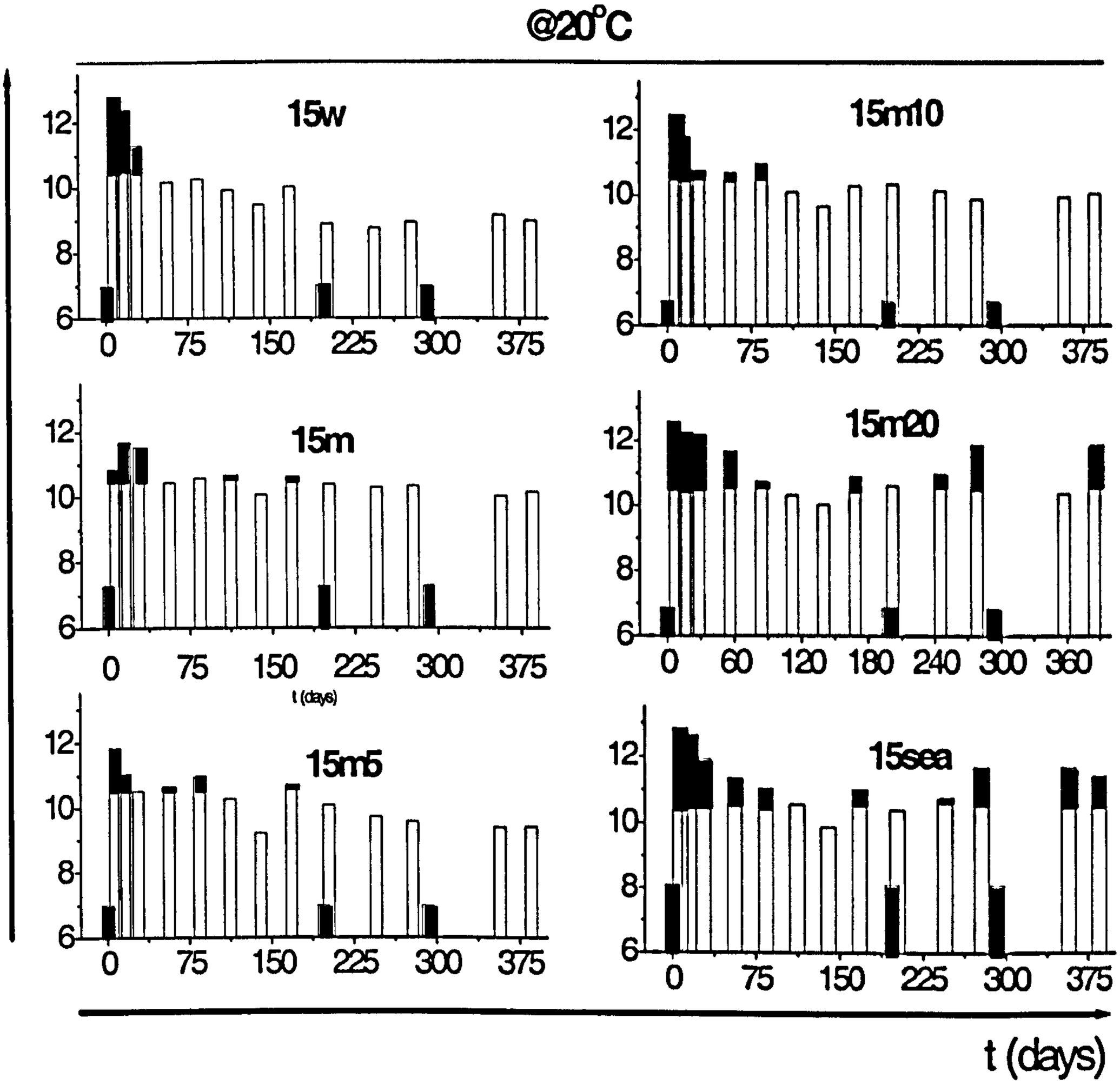

Figure 5.37: pH variation in 15%LF at 20°C: Solutions replenished at 197 and 292 days (full black columns) and pH higher than 10.5 (red and black marks). Initial pH of all solutions were around 7, and seawater pH was 8.12 (Table 3.11).

Water: the pH value rapidly reached its maximum (about 12.3) and gradually decreased towards 8.5~9.0 throughout the time of the experiment at both temperatures. Some increase in pH was also detected when water was replenished after 197 days and 292 days in both temperatures, but it gradually stabilised around 8.5 to 9 after both the first and the second replenishing time respectively. Because the pH tended to stabilise at 8.5 to 9.0, it appears that the initial dissolution of portlandite (reaction 2-Table 5.3) was followed by the precipitation of calcium carbonate, with pH of 8.48 (reaction 4b-Table 5.3).

Salt solutions: The combined effect of chloride and sulfate on pH changed with temperature. It can be seen that the pH of the systems immersed at 5°C were mostly higher than 10.5. At later ages, all salt solutions were alkaline (pH>12.0). As far as pH higher than 10.5 is concerned, M5 (0.5%Cl^-), in which mortar samples were less damaged than in other solutions (Fig. 5.3, 5.5 and 5.18), also maintained pH below this threshold during most of the exposure time.

Nevertheless, chloride-containing solutions at 20°C had their pH below 10.5 after about 75 days, especially at later ages. Exception is made to samples immersed in 2.0%Cl^- (M20) and seawater, in which the pH increased towards values higher than 11.5, possibly due to the dissolution of portlandite that would shift the pH at higher values(reaction 2-table 5.3). However, no signs of deterioration were found at this stage (Fig. 5.6). In M5 solutions, pH reached its lower values around 8.5 ~9.0 for most solutions at later stages, possibly because of the effect of calcium carbonate equilibrium pH in the presence of atmospheric CO_2 (reaction 4-table 5.3). As for M (0%Cl^-) and M10 (1%Cl^-), pH stayed stabilised at around 10.0, which indicates that brucite formation was controlling the alkalinity (reaction 3-Table 5.3).

After the first and second replenishment of the solutions, the pH broadly increased to 12.0 in all solutions at 5°C, which was clearly higher than those at 20°C. Such an increase can be related to alterations at the surface of the samples either by propagation of cracks or surface deterioration, or both, observed at low temperature but not at high temperature at this age. These exposed unattached inner parts of the samples were exposed to lower pH salty solution and therefore more lime was released to stabilise the equilibrium between the cement paste and solution.

In order to evaluate whether the rate of pH variation with time can be associated with the damage observed in visual inspection, the first derivative of pH against time at 5°C ad 20°C is plotted in Figure 5.38. This approach was used because the pH sharply increased after the first replenishment of solutions in all mixes, but it appeared to be correlated with the intensity of the attack observed during the visual inspection (Fig 5.5) and mass loss (Fig 5.18) caused by the attack.

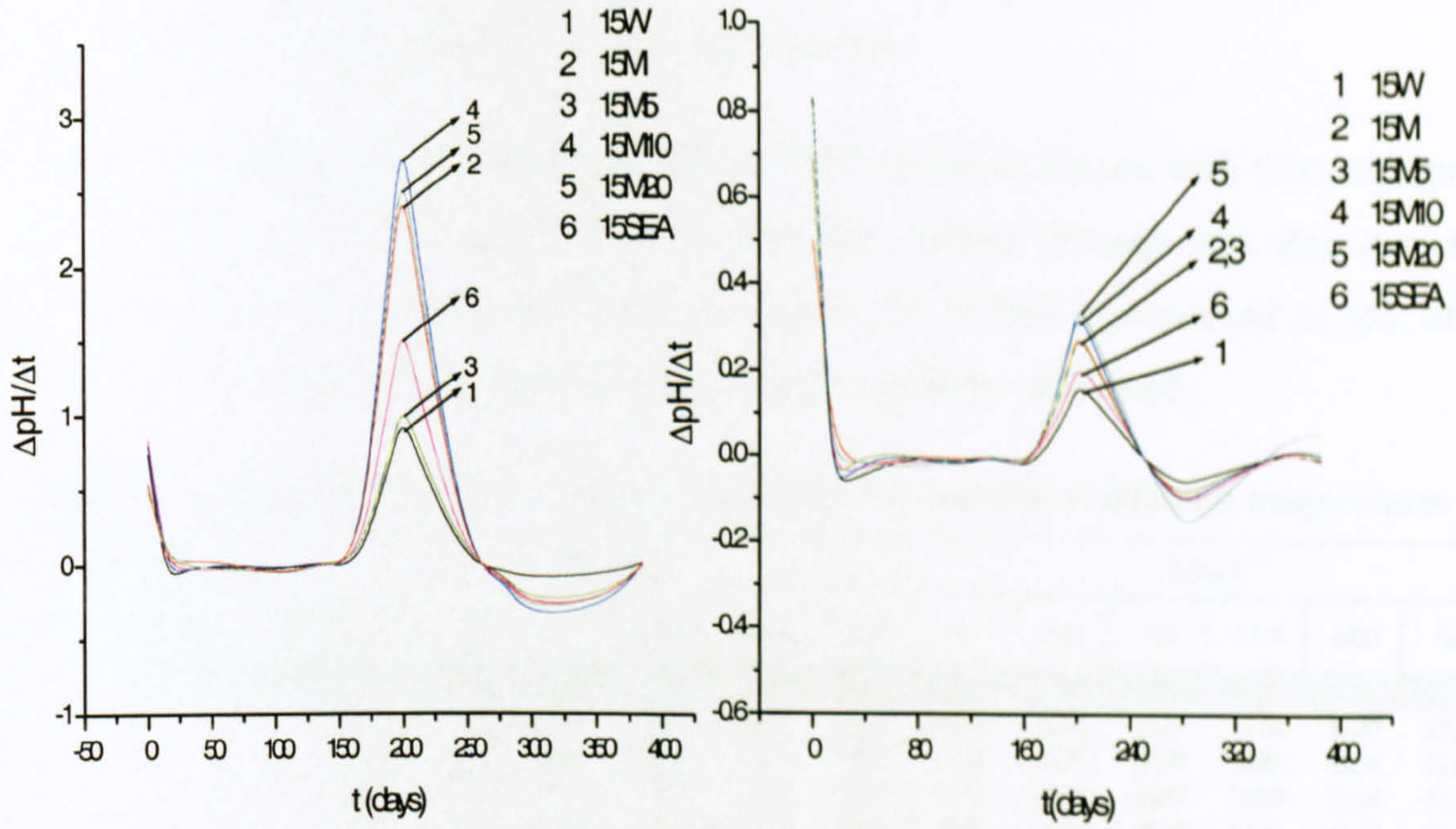

Figure 5.38: pH variation gradient with time in 15%LF, at: at 5°C (left) and at 20°C (right).

It can be seen that the intensity of the pH gradient can be associated with the level of damage detected previously (Figure 5.5, 5.17 and 5.19), where the order of aggressiveness of the damage at 5°C was M10, M20, M, M5 and seawater. However, at 20°C, a closer inspection reveals that the effect of chloride seems also to promote the release of hydroxyls in a similar fashion as it does at 5°C (M10>M20>M> Sea>M5) but at a far lower intensity (note the change of y-axis in Fig. 5.38).

The variation of pH in solutions containing OPC samples (with and without 5% limestone filler) and metakaolin is shown in Table 5.4. As a whole, a similar trend was also observed in these mixes as in 15%LF, in which:

(i) pH tended to increase with time as the chloride level increased in solution, especially at lower temperature;

(ii) In water, the pH tended to be stabilised at around 9.0 in all mixes, possibly due to the buffering effect of the equilibrium of calcium carbonate with atmospheric CO_2.

(iii) At lower temperatures, the pH was mostly kept higher than 10.5 throughout the exposure time in both 0%LF and 5%LF, whose pH profile was broadly similar to 15%LF mix.

(iv) However, the pH tended to stabilise below 10.0 in the MK samples, especially at later age. This trend can be associated with the pozzolanic

activity of metakaolin, which consumes soluble lime and also improves the pore system making it more impermeable.

(v) At 20°C, the pH decreased below 10.0 in most solutions with time, except in 0%LF in M20 (2.0%Cl^-) and seawater, where damage was also detected (Fig 5.6). Also, the pH was around 11.04 in 5%LF immersed in M5, after 385 days, but no signs of deterioration could be identified.

Table 5-4: pH variation in OPC (with and without 5%LF) and MK at different temperatures

Temperature		20 deg C						5 deg C					
Mix	Days \ Sol	W	M	M5	M10	M20	Sea	W	M	M5	M10	M20	Sea
0%LF	0	7.00	7.28	7.01	6.78	6.85	8.12	7.00	7.28	7.01	6.78	6.85	8.12
	7	12.76	10.72	12.12	12.55	12.55	12.65	12.96	10.85	12.67	11.04	12.67	12.64
	15	12.00	11.60	10.69	12.03	12.17	12.06	11.28	10.87	12.70	12.83	12.56	11.80
	28	10.05	10.46	10.28	10.95	11.45	11.90	10.23	11.15	12.87	12.90	11.94	11.37
	56	10.27	10.68	10.81	10.72	10.84	10.98	10.44	11.19	11.48	13.61	11.54	11.16
	84	9.76	9.99	10.08	10.38	10.14	10.21	9.81	10.33	10.68	12.32	10.80	10.14
	112	9.90	10.26	9.94	10.05	10.28	10.22	9.35	9.88	9.70	10.31	10.21	9.22
	140	9.52	9.18	9.12	9.15	9.78	9.69	9.42	10.14	10.80	10.19	9.86	8.93
	168	10.31	10.42	10.33	10.59	10.86	10.38	9.97	11.25	12.69	12.99	11.99	10.39
	197	7.00	7.28	7.01	6.78	6.85	8.12	7.00	7.28	7.01	6.78	6.85	8.12
	202	9.35	10.35	10.20	10.35	10.22	10.48	9.51	11.59	11.59	11.94	11.85	10.74
	245	9.03	10.35	9.70	10.11	10.29	11.67	9.33	12.54	10.51	12.78	12.03	11.43
	278	9.11	10.40	9.69	10.07	12.03	12.05	9.20	12.62	10.24	12.84	11.81	11.99
	292	7.00	7.28	7.01	6.78	6.85	8.12	7.00	7.28	7.01	6.78	6.85	8.12
	357	9.22	10.04	10.05	10.03	11.42	12.01	9.14	12.36	12.30	12.90	11.98	12.35
	385	9.23	10.15	9.97	10.10	11.87	11.98	9.00	12.41	12.56	12.52	12.39	11.92
5%LF	0	7	7.28	7.01	-	6.85	-	7	7.28	7.01	-	6.85	-
	7	12.84	12.57	12.29	-	10.75	-	13.11	12.53	12.7	-	11.07	-
	15	12.07	11.56	12.08	-	11.22	-	11.21	12.59	11.94	-	12.71	-
	28	11.1	11.07	10.82	-	11.03	-	11	12.48	12.33	-	12.77	-
	56	10.27	10.48	10.86	-	11.11	-	10.28	11.06	11.2	-	13.6	-
	84	9.84	9.88	10.2	-	10.43	-	9.59	10.42	10.29	-	12.41	-
	112	9.78	10.01	10.34	-	10.62	-	9.29	10.33	9.83	-	10.69	-
	140	9.29	9.93	9.74	-	10.19	-	9.34	10.71	8.84	-	9.33	-
	168	10.02	10.51	10.68	-	11.45	-	9.92	13.19	10.6	-	10.9	-
	197	7	7.28	7.01	-	6.85	-	7	7.28	7.01	-	6.85	-
	202	9.46	10.29	10.27	-	10	-	10.18	11.84	10.17	-	11.06	-
	245	9.53	10.37	10.6	-	10.12	-	9.23	12.87	10.14	-	12.08	-
	278	9.39	10.42	10.16	-	11.21	-	9.23	12.92	10.01	-	11.95	-
	292	7	7.28	7.01	-	6.85	-	7	7.28	7.01	-	6.85	-
	357	9.27	10	10.1	-	9.95	-	9.05	12.63	12.12	-	12.18	-
	385	9.27	10	11.04	-	10	-	9.32	12.22	12.48	-	12.1	-
MK	0	7	7.28	7.01	-	6.85	-	7	7.28	7.01	-	6.85	-
	7	12.27	10.2	10.46	-	10.67	-	12.2	10.71	10.8	-	10.8	-
	15	11.81	10.17	10.52	-	10.93	-	11.65	10.78	11.03	-	11.24	-
	28	11.02	9.95	10.3	-	10.8	-	11.73	10.6	10.86	-	11.71	-
	56	10.14	10.16	10.55	-	10.81	-	10.36	10.75	10.92	-	11.98	-
	84	9.98	10.17	10.68	-	10.72	-	9.9	10.72	10.83	-	11.07	-
	112	9.52	9.58	10.07	-	10.25	-	8.84	9.47	9.17	-	9.7	-
	140	9.02	9.01	9.85	-	9.4	-	8.88	9.56	9.38	-	9.65	-
	168	9.73	9.83	10.38	-	10.86	-	9.26	10.24	10.53	-	10.72	-
	197	7	7.28	7.01	-	6.85	-	7	7.28	7.01	-	6.85	-
	202	9.2	9.94	9.9	-	10.32	-	8.95	9.91	10.44	-	10.62	-
	245	9.1	9.59	9.59	-	10.24	-	9.24	9.63	9.86	-	10.21	-
	278	9.19	9.4	9.5	-	10.12	-	9.46	8.75	9.95	-	9.68	-
	292	7	7.28	7.01	-	6.85	-	7	7.28	7.01	-	6.85	-
	357	9	9.44	9.63	-	10.09	-	9.2	9.7	9.67	-	10.2	-
	385	9.18	9.35	9.5	-	9.93	-	9.3	8.95	9.79	-	9.88	-

The gradient of pH change in 0%LF, 5%LF and MK mixes can be seen in Figures 5.39 to 5.41.

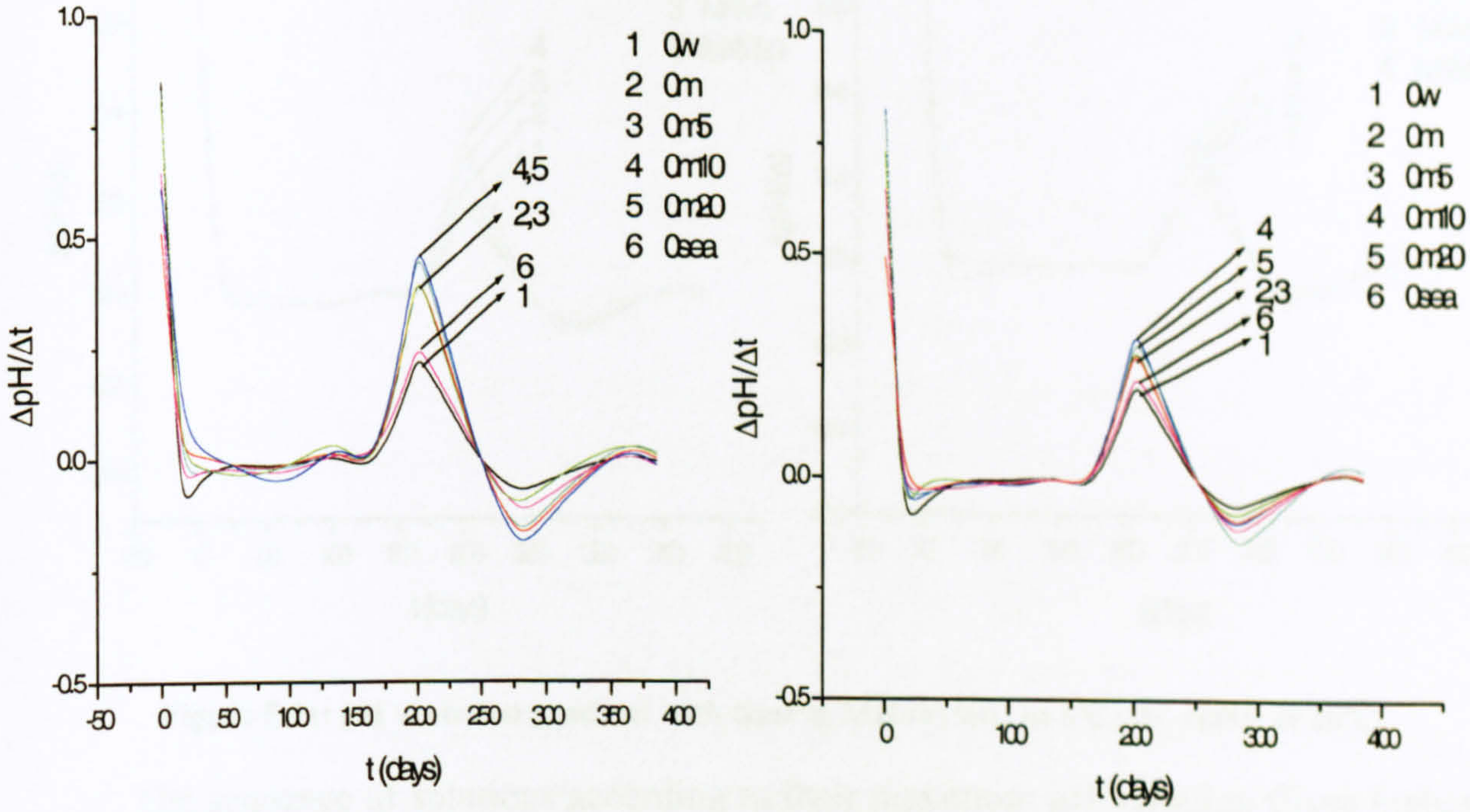

Figure 5.39: pH variation gradient with time in OPC.: at 5°C(left) and at 20°C(right).

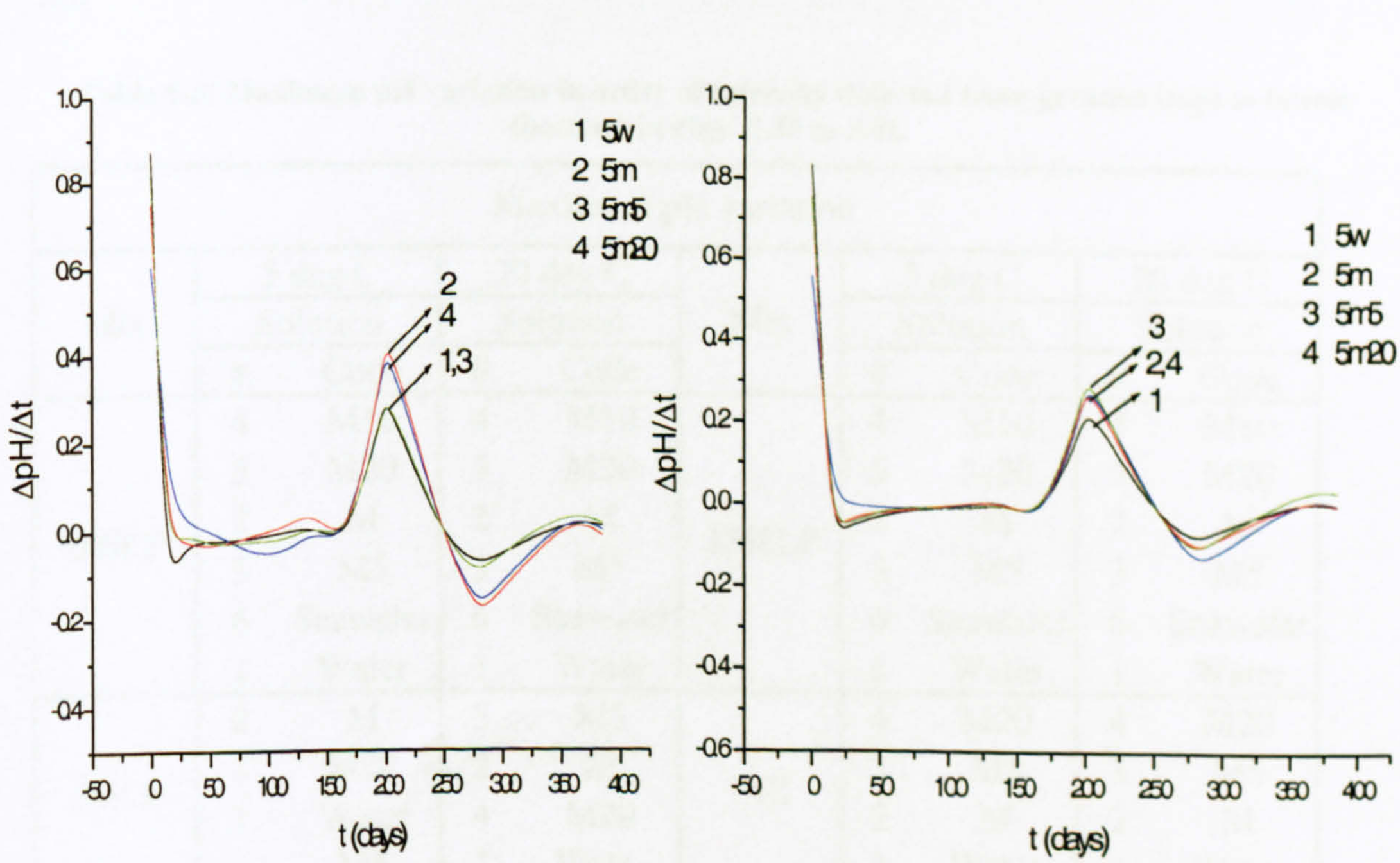

Figure 5.40: pH variation gradient with time in 5%LF.(a) left: at 5°C; (b) right: at 20°C.

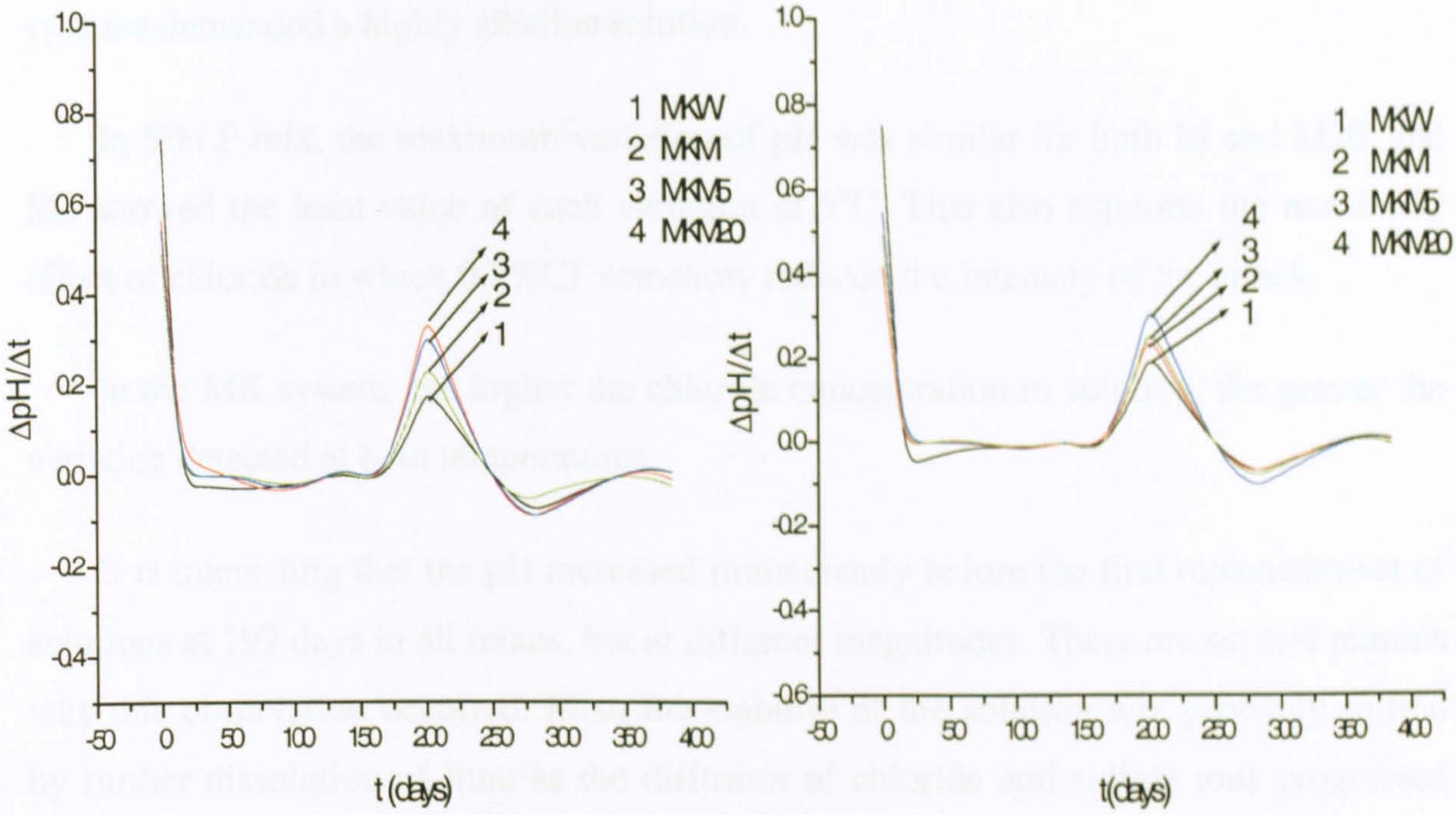

Figure 5.41: pH variation gradient with time in MK.(a) left: at 5°C; (b) right: at 20°C.

The sequence of solutions according to their maximum pH variation (from highest to the lowest variations) detected in Figs. 5.38 to 5.41 is summarised as shown in Table 5.5.

Table 5-5: Maximum pH variation in order of intensity detected from greatest (top) to lowest (bottom) in Figs. 5.38 to 5.41.

Maximum pH variation								
Mix	5 deg C Solution		20 deg C Solution		Mix	5 deg C Solution		20 deg C Solution	
	#	Code	#	Code		#	Code	#	Code
0%LF	4	M10	4	M10	15%LF	4	M10	4	M10
	5	M20	5	M20		5	M20	5	M20
	2	M	2	M		2	M	2	M
	3	M5	3	M5		3	M5	3	M5
	6	Seawater	6	Seawater		6	Seawater	6	Seawater
	1	Water	1	Water		1	Water	1	Water
5%LF	2	M	3	M5	MK	4	M20	4	M20
	4	M20	2	M		3	M5	3	M5
	1	Water	4	M20		2	M	2	M
	3	M5	1	Water		1	Water	1	Water
(#) Code number given in Figs. 5.38 to 5.41.									

It can be seen that the presence of chloride appears to have affected the leaching of hydroxyls in a similar way for 0%LF and 15%LF, at both temperatures, and also, in the MK system. In these solutions, the higher the chloride concentration, the higher the variation. M10 and M20 presented similar values but M10 was higher in 15%LF, which trend is clearer at 5°C (Fig 5.38). The maximum variation in M5 was less than in M, in

which also less damage was detected. It appears that the mechanism of attack in these systems demanded a highly alkaline solution.

In 5%LF mix, the maximum variation of pH was similar for both M and M20, and M5 showed the least value of such variation at 5°C. This also supports the non-linear effect of chloride in which 0.5%Cl^- somehow reduced the intensity of the attack.

In the MK system, the higher the chloride concentration in solution, the greater the variation detected at both temperatures.

It is interesting that the pH increased immediately before the first replenishment of solutions at 197 days in all mixes, but at different magnitudes. There are several reasons why this observation occurred. First, the stability of the solution was probably shifted by further dissolution of lime as the diffusion of chloride and sulfate ions progressed inside the samples, which can also induce cracks and increase the openness of the system. Another aspect that can be considered is that the mechanism of attack demanded a more alkaline solution. In the case of brucite, the pH would be around 10.5. In the case of thaumasite, which was detected as responsible for the attack in samples immersed in cold solution, it has been postulated that the pH should be higher than 10.5 [70].

In an attempt to study this increase in pH of solutions and the damage to samples detected in previous sections, the correlation between both factors, the relative mass of samples (Fig 5.18) and the magnitude of these increases in pH was then calculated, as shown in Figure 5.42.

Despite a poor correlation coefficient (R^2=0.30), it appears that the higher the relative mass loss, the higher the pH. Because the starting pH of solutions was mostly 7.0, the first pH variation (after approximately six months without the replenishment of the solutions) was raised by between 1 and 3 units. This value represents a pH of about 8 to 10.0. Once more, the pH at the stability of calcite and brucite formation is 8.48 and 10.5, respectively.

Yet again, a poor correlation was also observed between these two factors one month after the first replenishment, but this time with a slightly better correlation factor (R^2=0.37), although a similar trend was also observed. Nevertheless, the maximum variation points fell between the pH of 10 and 13. After 357 days, despite a very poor

correlation between relative mass and alkalinity, nearly all points fell above the pH of 12.0, at which greater damage was also detected visually.

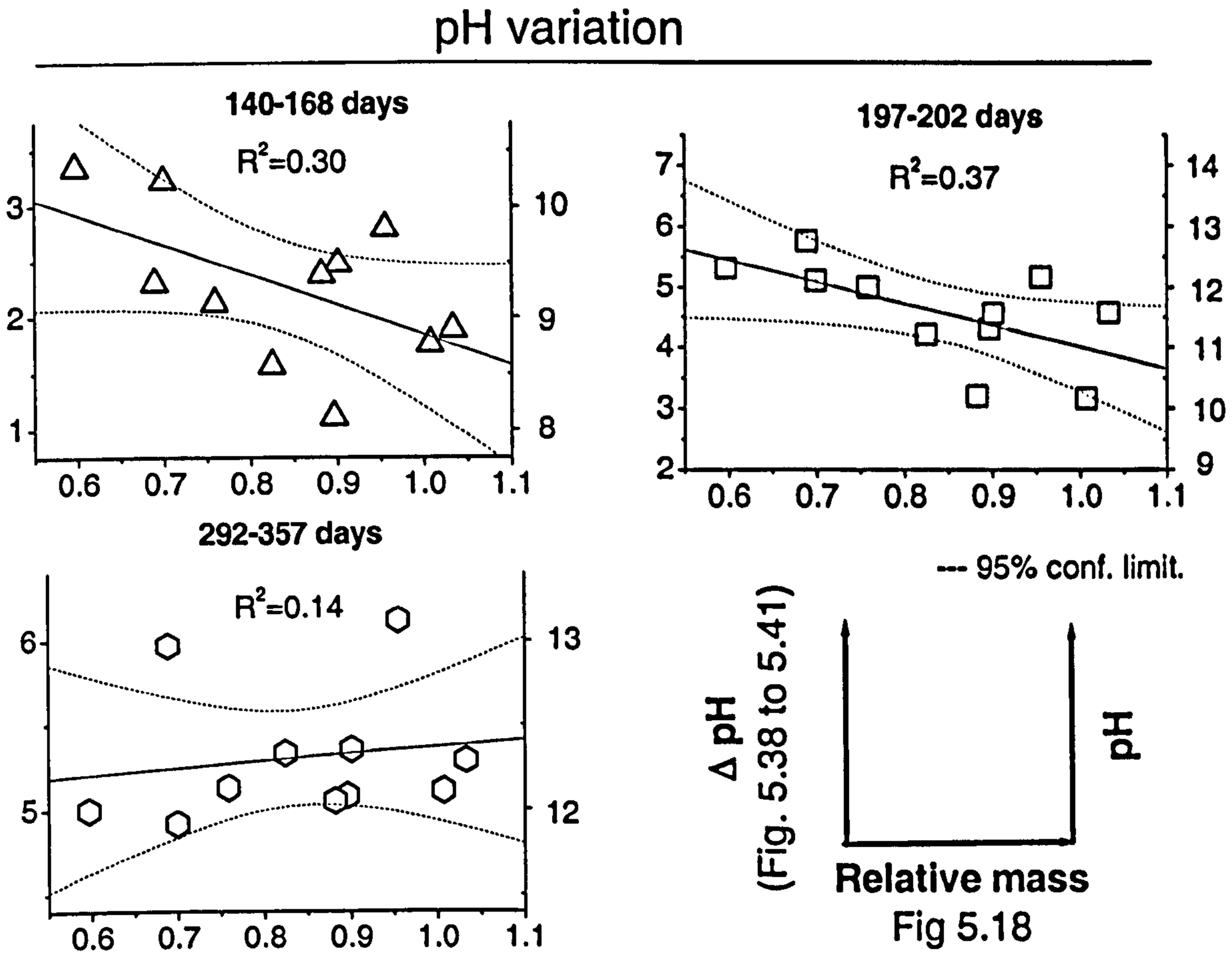

Fig 5.18

Figure 5.42: Correlation between pH variations and relative mass loss at different ages in samples immersed in salt solutions at 5°C.

The poor correlation between pH variations and mass loss due to chemical attack indicates the complexity of the attack. Indeed, although TSA demands a highly alkaline environment, the presence of other species such as chloride, magnesium, sodium, carbonates and atmospheric CO_2, are competing to achieve the equilibrium of the system.

In general, the data suggest that pH is a controlling factor on the thaumasite form of sulfate attack, which demands alkaline solution, perhaps via the dissolution of portlandite (reaction 2-Table 5.3). Indeed, this mineral was not identified in any corroded material, particularly at 5°C where thaumasite precipitated. Another possible source of hydroxyls into solution is from the decalcification of the CSH, which promotes loss of integrity of the matrix, especially in the presence of thaumasite that eventually becomes all pervasive and destroys the cement matrix (Chapter 4). Also, pH values that tended to stabilise between 8.5 and 10.0 at later ages, especially at 20°C,

seem to agree with the findings by XRD and IRS in which aragonite and brucite were both detected (Figures 5.21, 5.27, 5.29, 5.31 and Table 5.2).

5.4 Discussion

In this study, Portland cement mortar cubes containing different levels of limestone filler were immersed in water, sulfate solution, combined chloride and sulfate solution, and seawater at 5°C and 20°C for 1 year, with the objective to:

(i) To evaluate whether chloride plays any significant role in TSA;

(ii) Determine whether its role is similar to that of chloride in seawater;

(iii) Ascertain whether the high pozzolanicity of metakaolin would prevent TSA in high carbonate filler content mortar;

(iv) Determine the effect of chloride on the pH and the main mechanisms.

5.4.1 Evidence suggesting a detrimental role for chloride in thaumasite formation

An overall view of the samples evidently shows that the role of chloride in sulfate attack primarily varies with temperature, chloride concentration and also carbonate content.

At 20°C, the presence of chloride seemed to mitigate against sulfate attack, with the only exception being OPC specimens immersed in 0.60% SO_4^{2-} and 2.0% Cl^-, where extensive cracking and expansions of corners and edges were observed. The presence of calcium carbonate filler seemed beneficial in reducing the damage during the period of this research. Probably, the dilution caused by the replacement of the cement clinker by limestone filler, which reduced the amount of hydrates susceptible to sulfate attack, and also the filler effect itself, which fills the pores and helps hydration by offering sites for nucleation of hydrated products, were sufficient to hinder the attack. At this temperature, chlorides that diffuse rapidly:

(i) Reacted with aluminate phases and formed Friedel's salt, which reduces the chances of sulfate ions to generate ettringite, as secondary ettringite depends on the availability of monosulfate [139] .

(ii) Due to an increase in the solubility of $CaCO_3$ by the presence of chlorides (Appendix II, [82]), chloride ions in solution induce the precipitation of

aragonite at the surface (Figures 5.21, 5.27, 5.29, 5.31 and Table 5.2). The precipitation of aragonite, therefore, indicates that a counter diffusion of CO_3^{2-} was perhaps established in order to compensate the charge imbalance generated by the binding of chlorides in the CSH and in the formation of Friedel's salt [140], hence, reducing the attack due to thaumasite formation.

(iii) However, the remaining sulfate reacted with portlandite, and conventional sulfate attack predominated, accompanied by gypsum and ettringite formation.

At 5°C, however, a higher concentration of chlorides led to a greater extent of attack, especially when additional carbonates were present (Figure 5.5, 5.7, 5.9, 5.17 and 5.18). In these samples, extensive damage was detected, with morphology that was remarkably different from the attack observed at 20°C (Figure 5.6). Rather than cracks and expansion at corners and edges, these samples presented a white mushy non-cohesive deposit over the surface that also precipitated at the bottom of the containers, exposing the aggregate. At this temperature, little or no aragonite was detected, which indicated that the carbonates were actually engaged in the precipitation of thaumasite, as already known (Figures 5.20, 5.26, 5.28, 5.30 and Table 5.2).

Greater damage was detected at higher chloride concentrations, more evidently in high limestone containing mortars. However, all mixes tended to lose mass in a similar fashion, a statistical model suggests that chloride concentration was a strong factor affecting the mass profile alongside carbonate content. Statistical analysis of the data indicates that the use of chloride concentration in solution improved the quality of fit that correlates relative mass with carbonates and chloride concentrations. This model also suggests that there should be an optimum chloride concentration in which the attack generates the higher rate of loss in mass at around 1.1%Cl^-, which is in agreement with the visual observation of the specimens (Figure 5.5, 5.17 and 5.19).

Although poor correlation was found between the sudden increase in pH at certain ages (after 167 days, first and second solution replenishment), the higher mass loss was usually associated with higher pH (Figures 5.38 to 5.42 and Tables 5.4 and 5.5). The pH of those specimens that developed greater damage tended to be very alkaline (pH> 12.0).

The mode of the attack varied with temperature, which was a key factor affecting the mechanisms of the attack. At 20°C, the convetnional sulfate attack phases gypsum

and ettringite were detected among the deteriorated products in all samples with and without limestone filler. This finding is expected since either phases can coexist in the presence of chlorides [132]. However, because ettringite destabilises at pH below 10.7, a reduction in pH below 10.5 due to both brucite formation or at the equilibrium in the calcium carbonate system in the presence of atmospheric CO_2 (pH at 8.48), or both, led to more gypsum precipitating in some systems where the pH was mostly below 10.0 (Tables 5.2 and 5.3). At 5°C, the dominant mechanism of attack was TSA, where no Friedel's salt was detected in the corroded material in any OPC (with and without limestone filler) immersed in chloride containing solutions (Figure 5.20 and Table 5.2). Friedel's salt was detected within the bulk of the sample, which indicates that it is not stable in the presence of carbonates [105, 106], or perhaps in the presence of thaumasite. Chloride ions were likely to be in solution, since no chloride bearing phases where detected.

Since the sources of carbonate were both dissolution of calcite and atmospheric CO_2, it was not possible to determine which source was most affected by chloride (Appendix II). However, the precipitation of aragonite, which is a meta-stable $CaCO_3$ polymorph, indicates that carbonate and bicarbonate species in solution reacted with calcium from highly soluble portlandite. Although aragonite is less thermodynamically stable than calcite, its precipitation is favoured by kinetic factors in the presence of Mg^+ ions, as in seawater. Indeed, it has been shown that the intrusion of these ions reduces the crystal growth rate of calcite rather than aragonite [82].

At high concentrations of limestone filler, bicarbonates would still be in solution for longer period of times. This can favour the incorporation of carbonates in ettringite, and facilitated the formation of ettringite solid solution [84]. Because the crystal growth rate of thaumasite formation is far slower at high than at low temperatures (Tables 2.1 and 2.2), and also the incorporation of carbonates seems to be necessary to facilitate the uptake of octahedral silicon [10, 84], a significant amount of soluble silicate, carbonate and sulfate is needed to form thaumasite at the higher temperature.

By analogy to the formation of aragonite in preference to calcite in Mg^{2+} rich solutions, it appears that the effect of the increased carbonate ions in solution as a result of chloride on the precipitation of thaumasite at high temperatures is also controlled by kinetic considerations. This appears to be the reason why aragonite was observed abundantly in samples immersed in 1.0%Cl at 20°C, but thaumasite was abundant in the same mix and solution at 5°C (Figures 5.20, 5.21, Table 5.2, Figures 5.26 to 5.31).

5.4.2 The effect of carbonation on TSA

Long-term specimens developed signs of deterioration earlier when immersed in combined chloride and sulfate solution than in pure sulfate solution at 5°C, although the extent of damage was similar after 1 year. As far as carbonation is concerned, the carbonated area (Figure 5.12) did not develop any mushy material at the surface, but the core that was not exposed to atmospheric CO_2 prior to the immersion was destroyed after being immersed in salt solution. Indeed, it has been observed that some carbonated layers were also delaminated from the bulk of the sample, which suggests that the reaction occurred underneath the superficial carbonated zone. At 20°C, no significant attack has been observed, in any solution or degree of carbonation (Figures 5.13 to 5.16).

5.4.3 The effect of chloride in the thaumasite form of sulfate attack in seawater

In seawater, both samples with and without limestone filler behave in a similar manner. Because the amount of corroded material was insufficient to perform XRD, the analysis was performed on the bulk sample. Indeed, both samples developed similar phases: calcium aluminium chloride hydrate (Friedel's salt), ettringite (at 20°C) and ettringite/thaumasite solid solution of some sort (at 5°C), which was difficult to evaluate due to the low intensity of the XRD peaks (Figure 5.22). It can be concluded that the greater the amount of cement replacement, the lesser the amount of Portlandite. Also, the presence of portlandite indicates that both systems are not in their stable condition, since portlandite is highly soluble and reactive with respect to sulfate to form gypsum. The extent of damage was possibly lessened by several factors:

(i) Sea water contains 50% less sulfates than the amount that was administrated in sulfate solutions;

(ii) A Significant amount of potassium carbonate was present, which may reduce the solubility of calcium as does sodium carbonate [82];

(iii) Seawater contains 12% more magnesium, which increases the chances of brucite precipitation at the surface. Also, these magnesium ions would favour the precipitation of aragonite, which alongside brucite forms a double layer that reduces diffusion of ions inside the concrete [50];

(iv) The pH of seawater is buffered at about 8.5, possibly too low for thaumasite formation [70]

Therefore, the factors that mitigate sulfate attack in seawater solution did not mitigate TSA in samples immersed in combined magnesium sulfate and sodium chloride at 5°C.

5.4.4 The use of metakaolin to prevent TSA

It has been observed that metakaolin containing mortars developed a certain degree of damage after 73 weeks in magnesium sulfate solution at 5°C, but not at 20°C (Figure 5.11). The XRD and IRS peaks show that the attack was caused by gypsum and an ettringite solid solution (Figures 5.23 and 5.33). However, some peaks also seem to fit that of an orthorhombic type of thaumasite (PDF 44-1423), in which much less carbonate seems to be present. It has not been reported whether the silicon in this orthorhombic thaumasite is in octahedral coordination with hydroxyl groups.

However eventhough this pozzolan hindered thaumasite formation up to 18 months, it is not possible to establish whether this pozzolan is suitable for preventing this type of attack in the long-term. The amount applied (10% replacement of the cement) is a reasonable amount to be recommended. Indeed, the optimum metakaolin content has been reported to be either:

(i) Between 10 to 15% by the mass of cement without superplasticizers, which gives good workability and reduced diffusion rates for both chlorides and sulfates [141],

(ii) Up to 20% if superplasticizer is to be used as reported by Wild et al. [142],

The replacement of Portland cement by metakaolin has been successfully tested in laboratory conditions susceptible to TSA. Smallwood et al [122] reported that OPC replaced by 7% metakaolin did improve the general performance of concretes to TSA, although signs of exfoliation and the formatio of a white deposit at the surface were also reported. Also, Tsivilis et al [73] investigated the effect of 10% MK to prevent TSA in concrete containing 15% LF. It was found that the use of this pozzolan improved the concrete resistance after 12 months of exposure to a high concentration of magnesium sulfate at 5°C.

Indeed, a thorough investigation is needed to evaluate:

(i) Whether the presence of the remaining portlandite alone was enough to pose such a susceptibility to disruption, as can be thought due to significant gypsum formation, in which case more metakaolin would eventually mitigate the attack as the pozzolanic reaction consumes lime;

(ii) Whether the formation of the ettringite (or thaumasite) solid solution was the predominant factor determining the damage in which the nature of the CSH produced by such an aluminium rich pozzolan, is also responsible for the damage observed.

In fact, it is expected that the improvement brought about by the use of pozzolanic materials reduces the diffusion of foreign ions such as sulfates and chlorides. The reason why damage was detected after just 18 months was that enough sulfate ions were still available in solution to impose significant damage to the sample.

5.4.5 Effect of chloride on the pH profile in the presence of carbonates and sulfates

In general, the profile of pH variation with time was determined by at least four major reactions:

(i) The prompt release of lime immediately after immersion in neutral pH solution so that the pH went up to 12.40;

(ii) In water, calcium and hydroxyl ions react with atmospheric CO_2, which buffers the pH stabilising at around 8.48 or around 10.23 in CO_2-free solutions;

(iii) As samples came into contact with salt solution, a counter diffusion of hydroxyls, sulfates and chlorides is established and the pH is controlled by brucite precipitation at the surface of the samples. The pH buffers at around 10.50;

(iv) As damage is produced in the cement matrix by sulfate attack, lime-rich fresh parts of the samples are exposed to salt solution and a new release of lime raises the pH. Providing more salt is available, especially containing magnesium sulfate, the pH will be buffered according to stage III. This can also happen when samples come into contact with fresh solutions according to reactions I, II and III.

The role of chloride in affecting the pH was much more pronounced at 5°C than at 20°C. The presence of chlorides promoted an increase in pH, but more significantly at lower temperatures, and likewise for carbonate filled samples. Indeed, samples immersed in salt solutions were in contact with cold solutions with pH higher than 10.5for most of the time reported in this research (Figure 5.36 and Table 5.4). As for 20°C, the pH was gradually stabilised at around 10.0 (Figure 5.37 and Table 5.4). Whenever signs of damage were detected by visual inspection, namely OPC and 15%LF in both 2.0%Cl and seawater, the pH increased towards 12. At 5°C, although poor correlation between damage and a sudden increase in pH after 168 days and after the first replenishment, the higher the increase of pH, the lower the relative mass of the specimens (Figure 5.42). After the second replenishment (292 days), the pH rose above 12 in most solutions at low temperature. No consistent trend could be established at 20°C since most of the samples developed only very superficial damage. These observations indicate that thaumasite demands an alkaline environment to precipitate.

There are at least three factors that could explain the need for high pH in thaumasite formation, and the contribution of chloride to such alkalinity:

(i) Because carbonates enter into the thaumasite structure as CO_3^{2-}, the lowest pH in which significant activity of carbonate (CO_3^{2-}) species in solution is 10.33 at 25°C and 10.55 at 5°C. At lower pH, bicarbonate (HCO_3^-) activity is much higher than that of carbonate until it reaches the stability of calcite at the pH of 8.35 at 5°C (in atmospheric CO_2), below which more CO_2 is dissolved and the equilibrium returns to 8.35 via the dissolution and precipitation of calcite in the system [82];

(ii) Silicate solubility is extremely low at pH of 10 (0.0001 moles/l). However, the amount of dissolved silica sharply increases 10, 100 and 1000 times if the pH increases to approximately 10.85, 11.7 and 12.4, respectively. These figures are given for a temperature of 25°C (Figure 5.43) [82].

(iii) If thaumasite precipitation occurs when ettringite is stable [70], the pH would need to be above 10.7 [143]. The presence of chloride can increase the stability of ettringite at a pH as low as 9.47 [132], which might increase the chances of thaumasite formation via the 'woodfordite' route [84].

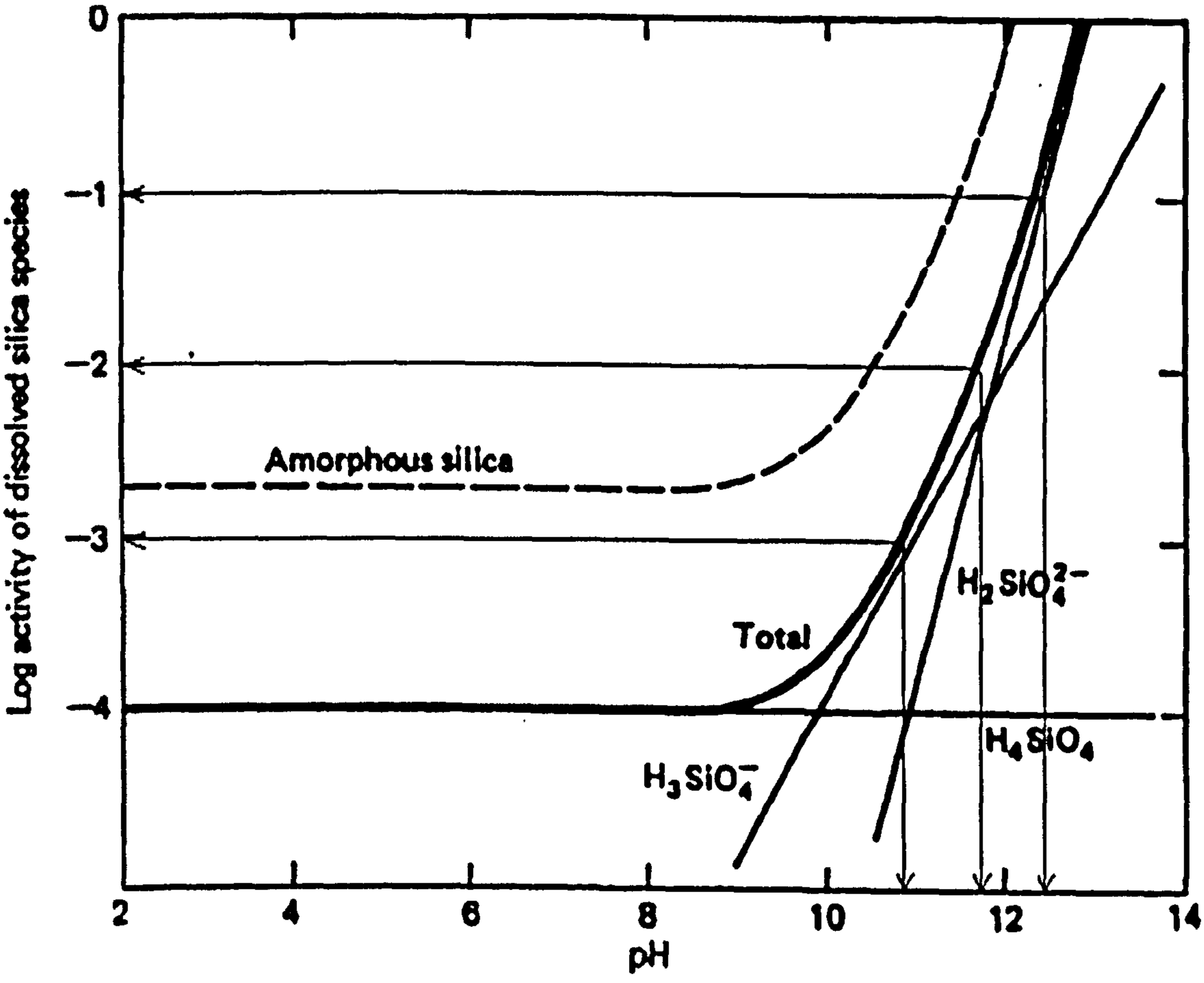

Figure 5.43: Dissolution of silica species (as shown in [82])

5.4.6 Mechanism by which chlorides affect TSA

From the observations above, the combination of chloride ions and the primary risk factors of TSA that are expected to enhance the potential damage associated with the thaumasite form of sulfate attack, namely:

(i) Low temperature;

(ii) Source of carbonate ions;

(iii) Source of sulfates;

(iv) Moist environment

Indeed, the detrimental effect of chloride was more prominent when a higher concentration of carbonates was present, mainly limestone filler but also atmospheric CO_2. However, longer exposure to CO_2 created a thicker carbonated zone, which had a relatively low pH and hence prevented the deposition of thaumasite at the surface, but thaumasite formed immediately underneath this layer in the core of the samples.

The dilution of clinker by limestone affects the microstructure of samples in many ways, which also have an adverse effect on the cement with respect to sulfate attack:

- Limestone filler increases the tortuosity of cement matrix by filling the pores and offering nucleation of sites for hydration products [39];

- These particles offer sites for nucleation of hydration products, especially portlandite, which can interfere: (i) positively, by helping hydration of both silicate and aluminate phases of the cement [32, 36], or (ii) negatively, by increasing more porous transition zone. Probably increasing the susceptibility to gypsum formation at the limestone-cement interface in the case of sulfate attack, as portlandite tends to precipitate at the limestone-paste interface [144];

- The higher the dilution, the higher the water to cement ratio, which is the chief factor in promoting higher permeability and lower strength in concretes [30], therefore reducing the performance of the cement matrix.

- Carbonate solubility increases mainly at low temperatures, and also in the presence of chlorides and atmospheric CO_2 (Appendix II), which undoubtedly increases the chance of TSA.

Figure 5.44 proposes a phenomenological model for the interaction of thaumasite and chlorides.

In this model, thick arrows indicate higher concentration of ionic species. The blue colour tone indicates variation of the pH of the solution at the cement pores (left half of the diagram) and at the interface concrete-solution (right half of the diagram), which varies from alkaline (dark blue) to near neutral (light blue). Interactions at higher temperatures (ca. 20°C) are represented at the top of the diagram and lower temperatures (ca. 5°C) at the bottom.

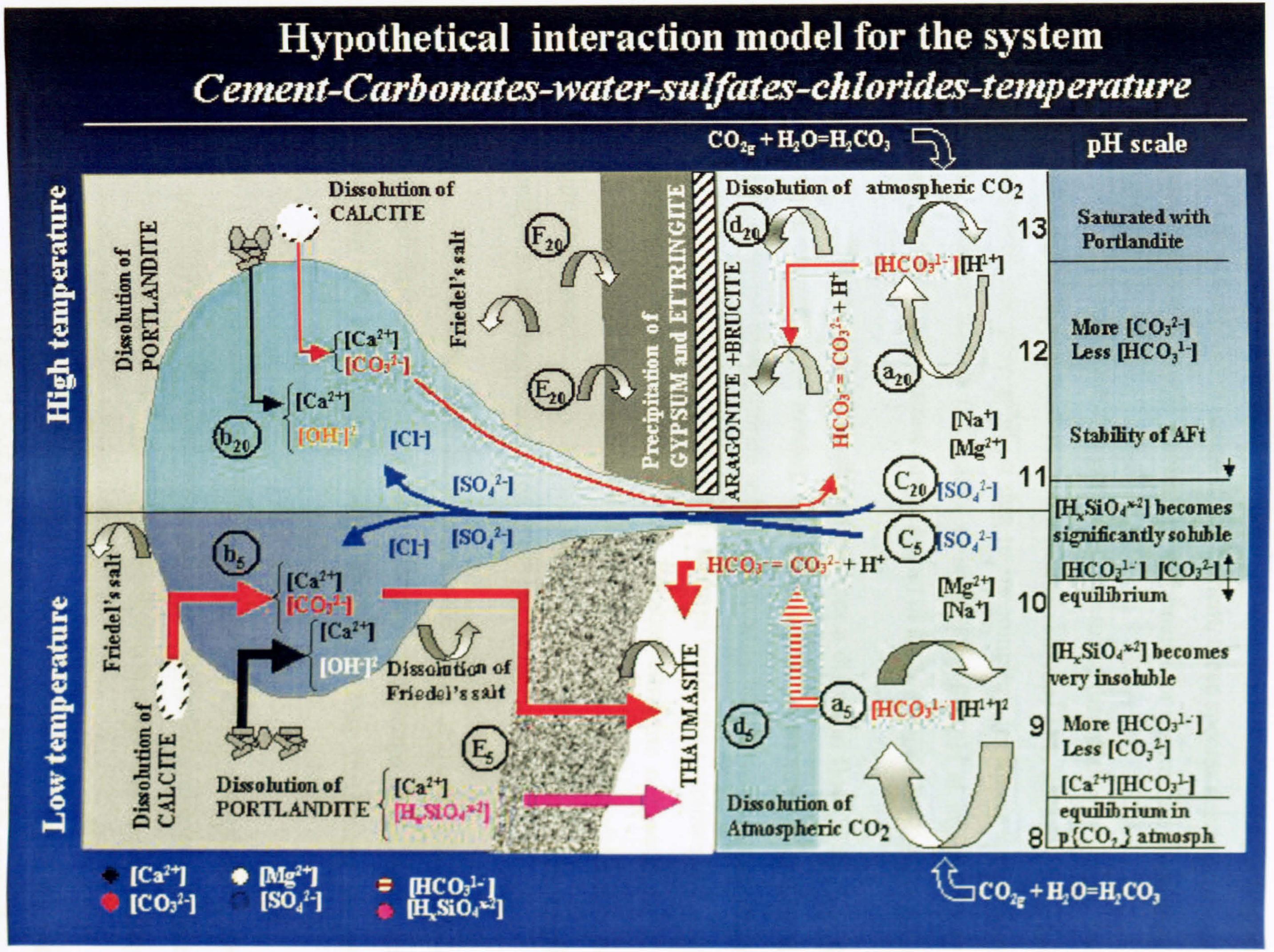

Figure 5.44 : Phenomenological Thaumasite-Chloride Interaction Model.

<u>At 20°C:</u>

a_{20} Atmospheric CO_2 dissolves in water, which produces bicarbonate ions [82]. It appears that this process is increased by the presence of chlorides (Appendix II). In the case when calcite is not added to the cement, these species need to diffuse into the cement pore structure to supply a source of carbonates for thaumasite formation;

b_{20} Carbonates are also generated due to the dissolution of calcite that can be added as a cement replacement material (*red arrow top)* [14, 82]. Calcium hydroxide readily dissolves into pore solution due to its solubility in water, which initiates an immediate diffusion outside the matrix to equilibrate the pH at around 12.48 *(Black arrow top)* [12]. Both dissolutions are increased in the presence of chlorides [82, 115] .

c_{20} The movement of sulfates initiates a diffusion flow in through the pore structure of the cement (*blue arrow*), which immediately generates a counter diffusion of hydroxyls (*orange*) to equilibrate solution neutrality [48]. Gypsum precipitates at the expense of portlandite (E_{20}). Chloride also diffuses inside the specimen and reacts with AFm phases to form Friedel's salt [145]. Because ettringite originated from sulfate attack is formed through monosulfate [12], the precipitation of Friedel's salt seems to reduce ettringite formation (F_{20}). Hence, the presence of chlorides mitigates against the conventional form of sulfate attack at ca. 20°C [94, 100].

d_{20} Whereas insoluble magnesium precipitates at the surface as brucite by combining with hydroxyl ions, carbonate precipitates as aragonite in the presence of Mg^{2+} ions [82], which is more kinetically favourable than thaumasite precipitation. Because:

(i) The presence of chlorides that appear to increase carbonates and lime counter diffusion, due to increase in solubility of calcite (Appendix II and [82]) and possibly increase the leaching out of portlandite [114, 115];

(ii) The nucleation rate of $CaCO_3$ is much faster than that of thaumasite at 20°C (Figure 5.20, 5.21, 5.26 and 5.27). If the pH is controlled by the equilibrium of calcium carbonate, it stabilises at around 8.48 in the presence of atmospheric CO_2 [82];

(iii) The pH in pore solution equilibrates with the pH buffered by brucite at around 10.5 (*marked by light blue colour gradient)*[48];

(iv) Both aragonite and brucite that precipitates at the surface create a double layer that can reduce the diffusion of ions, hence offering some protection to the concrete, as in seawater [48, 50, 99].

<u>At 5°C:</u>

a_5 The amount of dissolution of atmospheric CO_2 increases as the temperature decreases [82]. This also seems to be accelerated in the presence of chloride and sulfate species (Appendix II). Again, these species need to diffuse into the concrete (d_5), in the case when calcite is not added as filler.

b_5 Both lime and calcite solubility increase at lower temperature, mainly in the presence of chlorides, which generates a higher concentration of carbonate, calcium and hydroxyl ions in the pore solution than at 20°C [12, 82, 115].

c_5 As sulfate diffuses, counter diffusion also occurs, as at 20°C, in which hydroxyl concentration increases, with increase in pH [48].

The higher concentration of carbonates in the pore solution shifts the equilibrium towards thaumasite formation. Its rate of nucleation is much faster at low temperatures. Therefore, the counter diffusion is dominated by hydroxyl species since carbonate and calcium ions are needed for thaumasite formation.

d_5 At high pH values (above 10.55), inside the pores of the cement and at the interface concrete-solution, the activity of carbonate, $[CO_3^{2-}]$, becomes higher than that of bicarbonate, $[HCO_3^{1-}]$ [82];

E_5 If the dissolution rate of portlandite is higher than the rate of precipitation of brucite, the solubility of amorphous silica can increase by about 10 to 1000 times in highly alkaline solution (pH approximately 10.85 and 12.4, respectively) (Figure 5.43 from [82]). The precipitation of thaumasite instead of calcite or aragonite is then highly favoured, because of the presence of:

(i) Alkaline solution;

(ii) Significant concentration of carbonates CO_3^{2-};

(iii) Sulfate ions;

(iv) Silicate and calcium ions, from the decalcification and dissolution of the CSH.

5.5 Conclusions

A review of the literature identified that chloride was present in many field cases involving TSA, in which the severity of the attack has been understood to increase by the action of these ions, because they promoted ionic induced corrosion of the steel reinforcement. However, no systematic study was found in the published scientific literature on the investigation of the role of chloride on TSA. It is believed that the lack of research on this topic can be attributed to the fact that little or no chloride has been found within thaumasite affected areas, which may lead to the conclusion that the sole and most detrimental role of Cl^- ions resides in chloride-induced corrosion.

Hence, a systematic research programme has been designed to investigate the influence of chloride on the thaumasite form of sulfate attack in the presence of the main primary risk factors promoting this type of attack.

Based upon the conditions of this current research, it is possible to conclude that:

- Chloride does play a significant detrimental role in TSA, which strongly depends on temperature, carbonate content and chloride concentration. Whereas at high temperature the presence of chloride mitigates against conventional sulfate attack, it deleteriously increases TSA at lower temperature.

- At 5°C, the damage of the specimens assessed by a loss of material from the bulk of attacked samples indicates that chloride played a role in such attack. This observation was confirmed by a better fit of a statistical model that was obtained when chloride was included as a parameter alongside carbonates.

- At 5°C, thaumasite was the main phase responsible for causing deterioration of all mixes containing calcium carbonate, except in the system containing 15% limestone filler and 10% metakaolin. Also, despite the concentration of chloride, Friedel's salt was not identified in any corroded material, but only in the unattacked core of the samples alongside gypsum and ettringite.

- At 20°C, gypsum and ettringite were the main sulfate phases, and aragonite and calcite were the main carbonate phases. Significant amounts of Friedel's salt were identified, and the intensity of its XRD peaks increased as the concentration of chloride increased, especially in metakaolin samples.

- As far as carbonation is concerned, the initial 21 days air exposure contributed to the formation of thaumasite in OPC control samples held at 5°C.

- Extensive carbonation, as in 5 years specimens exposed to air, appears to delay the TSA phenomenon as no thaumasite could precipitate within the carbonated zone at the surface, but gypsum and thaumasite precipitated at the interface between the carbonated zone and the core in mortars immersed in salt solution at 5°C.

- It seems that the ionic species should diffuse through the low pH carbonated zone in order to find suitable conditions for thaumasite deposition at the carbonated zone-core interface.

- The mechanism of sulfate attack in sodium chloride and magnesium sulfate solution differs from that in seawater at lower temperatures such that thaumasite more readily forms in the former case.

- Seawater has a high concentration of potassium carbonate and a higher Mg/SO_4 ratio (almost twice as much) than the tested solution. Important factors to note are:

  (i) Seawater seems to be already saturated with respect to caliucm and potassium carbonates, which facilitate the precipitation of aragonite that can hinder the counter diffusion of other species into the concrete;

  (ii) The high Mg/SO_4 ratio increases the precipitation of brucite;

  (iii) The precipitation of both brucite and aragonite appears to have a blocking effect at the surface of the specimens, and also buffers the pH at lower levels (ca. 8.5).

- The use of metakaolin did lead to excellent performances after 1 year. No thaumasite was detected after 73 weeks exposure to combined sulfate and chloride solutions at 5°C, despite the cement containing 15% limestone filler.

- After 73 weeks, some deterioration was found in the metakaolin mix in pure sulfate solution at 5°C, but not in any other salt solution. The precipitation of both gypsum and ettringite was responsible for the attack.

- Although the absence of octahedral silicon confirms the presence of ettringite, some XRD peaks indicate the presence of thaumasite (possibly of orthorhombic symmetry).

- It is also not clear whether there is a more complex interaction between the alkali aluminate silicate gel and the formation of such thaumasite.

- Thaumasite formation needs an alkaline solution, possibly with pH greater than 10.55.

- Although a poor correlation coefficient was found, it was observed that the rate of a sudden increase in pH, between 140 and 168 days (prior to the first replenishment of the solutions) and between 197 and 202 days (first replenishment of the solutions) could be associated with the relative mass after 12 months of the specimens that were attacked by thaumasite.

- The alkalinity of the solutions increased in the presence of chloride ions. Also, in high carbonate content systems, samples immersed in concentrations higher than 0.5% Cl^- were most severely attacked.

- It is still not clear why 0.5%Cl^- solutions developed the least damage of all salt solutions. This trend persisted throughout all analyses in this research. Further discussion will be given to this issue in the following chapters.

- Whether chloride affects the composition of thaumasite or its effect is primarily catalytic could not be established so far. Also, it could not be established whether the chloride binding capacity of the cement matrix is reduced since Friedel's salt was absent within the corroded material where thaumasite was abundant.

Chapter Six

EFFECT OF COMBINED CHLORIDE AND SULFATE ON TSA: MICROSTRUCTURE AND MICRO-ANALYTICAL RESULTS

6.1 Abstract

Portland cement containing limestone filler (>98%$CaCO_3$) has been immersed in combined chloride (0, 0.5, 1.0 and 2.0% Cl^- as NaCl) and sulfate (0.6% SO_4^{-2} as $MgSO_4.7H_2O$) at 5°C and 20°C for 1 year.

The results indicate that the effect of chloride on magnesium sulfate attack depends on the temperature. At higher temperature, the presence of chlorides seems to mitigate the attack after 1 year of exposure. However, the combined action of chloride and sulfate ions accelerated the damage of mortars containing Portland cement with and without limestone filler at 5°C. The damage was caused by the thaumasite form of sulfate attack (TSA) in all cases, which also increased as the level of limestone increased. Also, higher concentrations of chlorides were detected in the core rather than at the surface in all concentrations of chlorides, which is attributed to a lower Cl^- binding capacity of C-S-H gel at the surface due to chemical alteration caused by TSA at 5°C.

Several clinker silicate grains were attacked by sulfate, which resulted in the precipitation of an ettringite-type solid solution inside the grain, and thaumasite in the surrounding areas. This pattern has been found both in samples immersed in pure sulfate and combined chlorides and sulfate species.

As far as the intensity of attack is concerned, the effect of chloride concentration seems to be non-linear, which can possibly be explained by a combination of a change in the solubility of some phases, counter diffusion of carbonates, and the kinetics of precipitation of some sulfate phases. Considerations will be given whether chloride acts as a catalyst for thaumasite formation or if it interacts within the thaumasite crystal structure hence affecting the composition of the thaumasite.

6.2 Introduction

In the previous chapter, it was observed that a higher degree of damage was often associated with samples immersed in combined chloride and sulfates at 5°C, in which thaumasite was responsible for the attack. Also, a pilot study revealed that dissolved chloride affects the solubility of some minerals such as carbonates and gypsum, which are key ingredients in thaumasite formation (Appendix II).

A literature survey indicates that there is no published data concerning possible interaction between chloride and thaumasite. Yet, the main cases of TSA have been reported to happen in places where chloride salts were present, mainly due to the use of de-icers in bridges, in which the induced corrosion of the steel reinforcement is promoted by chloride ions.

As far as the chloride profile is concerned, it has been reported [16] that thaumasite affected areas offered little resistance to chloride diffusion, due to the damage inflicted in the matrix that open cracks and flaws. Also, it has been reported that the concentration of chlorides was reduced at the surface and increased at the reinforcement-matrix interface [97]. Wimpeny and Slater [15] proposed some interactions of chlorides in different stages of the attack. They identified that not only should there be a reduction of chloride concentration in attacked zones at the surface due to sulfate attack of the matrix, but also that an increased risk of chloride induced corrosion can be lead by higher concentrations at the depth of the reinforcement. Indeed, possible chemical interaction between chlorides and thaumasite has not been considered, most likely because chloride bearing minerals are not often found within attacked areas, which are commonly dominated by thaumasite in advanced stages. However, Friedel's salt was reported to coexist with ettringite solid solution, previously reported as 'Woodfordite', which can be seen as an ettringite type solid solution [65, 99, 110].

In the view point that thaumasite has insignificant aluminium binding capacity, as reported by Barnett et al. [62], the question that arises is whether chlorides play a catalytic role or interact within the thaumasite structure. The implication of this question resides in that chloride-binding capacity of cements is a positive property towards the protection of the reinforcement. Therefore, the structural integrity of the concrete can be negatively affected, as the front of a possible non-chloride binder thaumasite penetrates into the concrete. Indeed, it was observed that chloroaluminates, such as Friedel's salt,

were often found in the core but not at the surface of the samples, which suggests that these minerals are unstable in the presence of thaumasite (*see* section 5.5.3-Chapter 5). Indeed, their structural breakdown would also increase the concentration of chlorides in solution, which eventually would accumulate at the reinforcement-cement interface with severe consequences to the reinforcement [15, 16]. It has been pointed out that because water soluble chlorides can be leached out after snow run-offs through the water table, the concentration of chlorides are often higher underneath TSA affected areas [96, 97]. In an attempt to isolate this aspect, samples in this present research were constantly immersed in salt solution throughout the experiment, until due for testing, so that the bound chloride profile could be evaluated.

Another implication of a non-binding capacity of thaumasite is that chemisorbed chloride in C-S-H, which is affected by the Ca/Si ratio [146], would be released into the pore solution, since C-S-H takes part in the formation of thaumasite. This would result in an increase of Cl/OH ratio hence increasing the risk of corrosion.

An additional aspect of the presence of chlorides is that it affects the pH of cement pore solution. Indeed, it has been reported that chlorides, which chemically bind within the cement matrix, release hydroxyls to equilibrate the solution neutrality [147], therefore, increasing the pH of the pore solution [140]. It is possible, though, that such an increase in pH would also promote TSA. Indeed, an increase in pH was observed in all samples that suffered from TSA (see section 5.3.4). This observation supports the view of Gaze and Crammond [70] and, also, Collett et al. [76] who pointed out that high pH (>10.5) is necessary for thaumasite formation, because:

(i) Thaumasite would not form when ettringite is unstable;

(ii) Calcium bicarbonate, which is required to produce thaumasite, is in equilibrium with calcium carbonate at the pH of 10.33 at 25°C.

Also, in the previous Chapter 5, it was identified that three other factors can corroborate with the need for such a pH threshold:

(i) Ettringite stability is increased in the sense that it can be stable in a pH as low as 9.5, in the presence of chloride [132];

(ii) At 5°C, bicarbonate is in equilibrium with carbonates at the pH of 10.55 [82], and its concentration in solution appears to increased in the presence of Cl^- (*see* Annexe II);

(iii) The solubility of ionic hydrous silica and amorphous Si, which are significantly important in thaumasite formation, dramatically increases in alkaline media but also decreases dramatically in pHs below 10 [82]. This could also be affected by the presence of Cl^- that increases pore solution pH. Indeed, calcium, carbonate and silicon of the CSH are engaged in thaumasite formation according to equation 6.1 [11], which is probably the main route for TSA [63]. In fact, it is the disruption of CSH that makes TSA so detrimental to the concrete, since the former silicate is responsible for the binding properties of the cement matrix.

$$C_3S_2H_3 + CH + 2C\bar{C} + 2MS + 28H \rightarrow 2C_3S\bar{C}\,\bar{S}\,H_{15} + 2MH \qquad (6\text{-}1)$$

This equation differs from the classical magnesium sulfate attack, which turns the calcium silicate hydrate into MSH according to Equation 6.2, after calcium hydroxide is depleted by precipitation of brucite. This reaction is also very detrimental to the concrete due to the low solubility of brucite that buffers the pH below the stability of C-S-H, which releases its lime and ultimately reacts with low soluble magnesium at the surface. Because magnesium silicate hydrate has no binding capacity, its formation at the surface delaminates concrete as a result. One could see the detrimental role of magnesium ions as masking the effective actual role of TSA on damaging concrete.

$$C_3S_2H_3 + 3M\bar{S} + 6H \rightarrow 3C\bar{S}H_2 + 2MSH + MH \qquad (6\text{-}2)$$

However, there are some instances in which a high magnesium concentration may impede the diffusion of sulfates into test cements by the formation of brucite at the surface. Indeed, Bonen and Cohen [48] studied the microstructure of OPC cement paste (w/c=0.4) after 1 year of immersion in strong magnesium sulfate (2.1 and 4.2%) at 20°C. Not only was strong decalcification at the surface (Ca/Si ~1.2) identified, but also the strong magnesium solution promoted rather higher values (Ca/Si ~2.1) below 500μm from the surface than lower concentrations of magnesium. This was attributed to a strong deposition of brucite at the surface. Typical Ca/Si values for CSH are around 1.6~2.1 [12]. As for the concentration of magnesium, Gollop and Taylor [104] reported that its concentration (Mg/Ca) was found to be below 0.09 at the surface and 0.04 within the unattacked core in cement paste immersed in 2.4% magnesium sulfate, which indicates, according to the authors, the very low solubility of Mg ions in cement paste.

Perhaps one of the most striking features of the interaction of chlorides in thaumasite prone systems is the observation that it dramatically increases the solubility of carbonates at low temperatures (*see* Appendix II). It is possible to think that the extra availability of carbonate ions induced by the presence of chloride would:

(i) Reduce the time for the on-set of thaumasite formation, and

(ii) Increase the potential damage expected in the same period of time when compared to systems without chlorides (*see* Figures 5.5,5.6 and 5.18-chapter 5).

At the present, whether it could be regarded as a pure catalytic role is not known. As for a possible interstitial or substitutional interaction of chloride ions in the thaumasite crystal structure, there have not been any studies on whether such an increase in the solubility of carbonates would eventually promote thaumasite to exchange its carbonates by chlorides. If this is so, less carbonate would be necessary to promote the precipitation of a thaumasite-chloride analogue that could also promote damage by containing octahedral silicon. This could possibly be associated with the precipitation of the 'unidentified' salt that caused damage in concrete as reported by Chatterji [115], whose XRD peaks closely resembled those of thaumasite (see Table 5.1-Chapter 5).

The objectives of this chapter are:

- To Identify the main changes in the microstructure of samples containing 15% limestone filler at 5°C in several concentrations of chloride after 1 year;
- To Investigate whether the chloride effect on TSA is primarily catalytic or if it takes part in the reaction of thaumasite formation by assessing the composition of thaumasite in several chloride concentrations;
- To Evaluate how the damage identified in *Chapter 5* corresponds to alterations in the cement matrix composition;
- To Identify chloride and magnesium ion profiles across tested mortar containing limestone filler.

6.3 Results

6.3.1 Microstructure of TSA in 15%LF samples in salt solutions at 5°C

A. 15% limestone filler in 0.60% SO_4 at 5°C

Fig 6.1 shows the damage inflicted in samples containing 15% limestone after 1 year immersed in magnesium sulfate solution at 5°C. The intensity of the attack can be estimated in that the sample lost approximately 50% of its section, which was originally 20mm. In the first 1000μm, a non-cohesive band has developed around the aggregate particles from outside inwards. The cement matrix has suffered strong chemical alteration at the surface as evidenced by the formation of a dark grey band of thaumasite that dominated the corroded area (Fig 6.1).

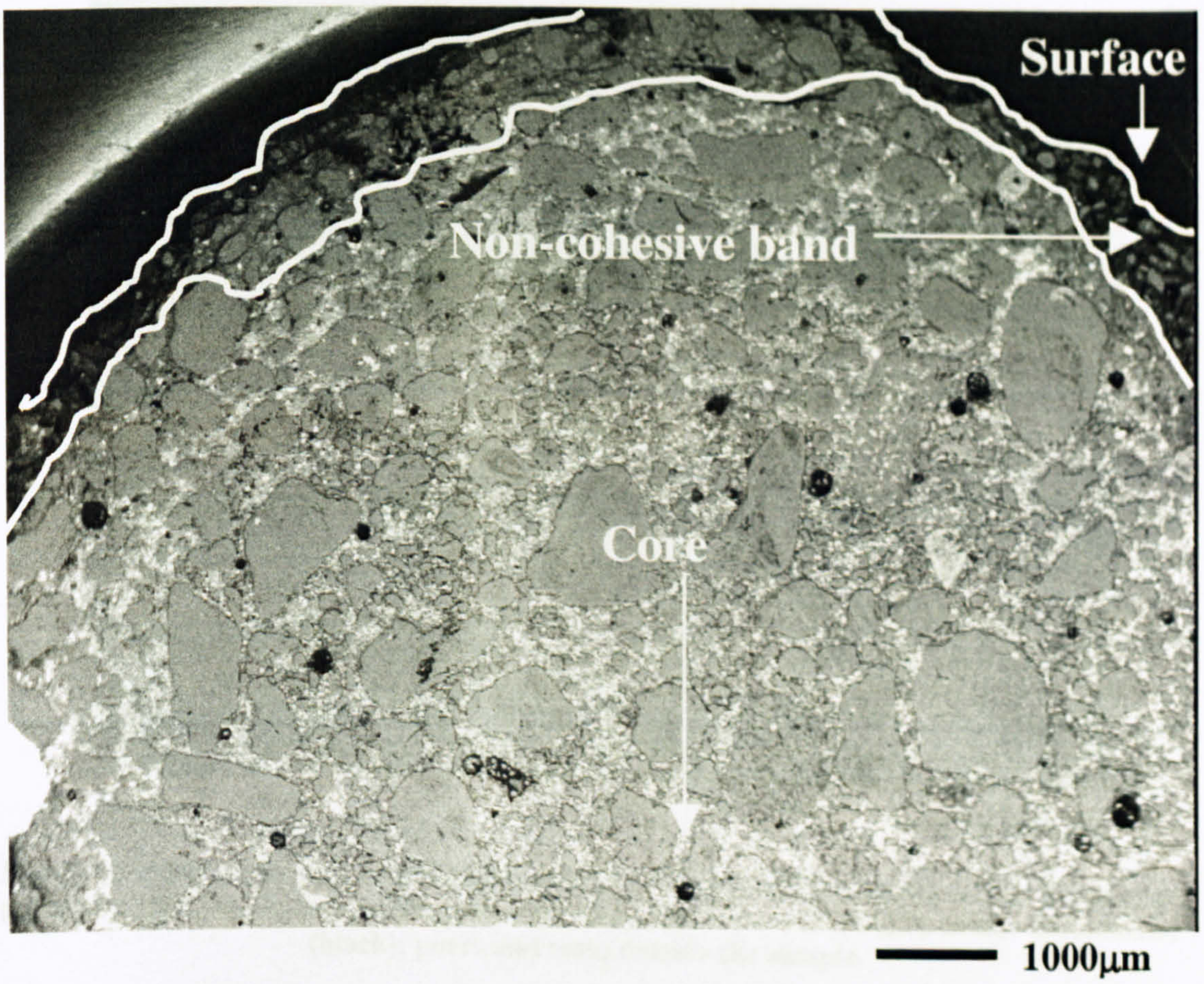

Figure 6.1: 15% LF in magnesium sulfate at 5°C-surface. (large grey particles): silica aggregate; (bright grey area): cement matrix; (dark grey area): thaumasite; (black): pores and resin outside the sample.

Also, sub-parallel cracks developed at the cement matrix- aggregate interfaces, and through the matrix itself, as shown in Fig 6.2 taken at higher magnification. The light grey phases are composed of the residual clinker grains of the cement. It is also possible to see some of these grains, mostly the calcium silicate phases alite (C_2S) and belite

(C_3S), were attacked by sulfate by developing both intermixed CSH + thaumasite- around the cement grain and clusters of ettringite-solid solution, as seen in Fig 6.3 and Fig 6.4. This observation was already reported in previous chapters, in which ettringite solid solution precipitated in belite grains (Figures 4.13 to 5.15 Chapter 4). The identification of these phases was based on the quantitative X-ray microanalysis and the atomic compositions will be discussed in further sections.

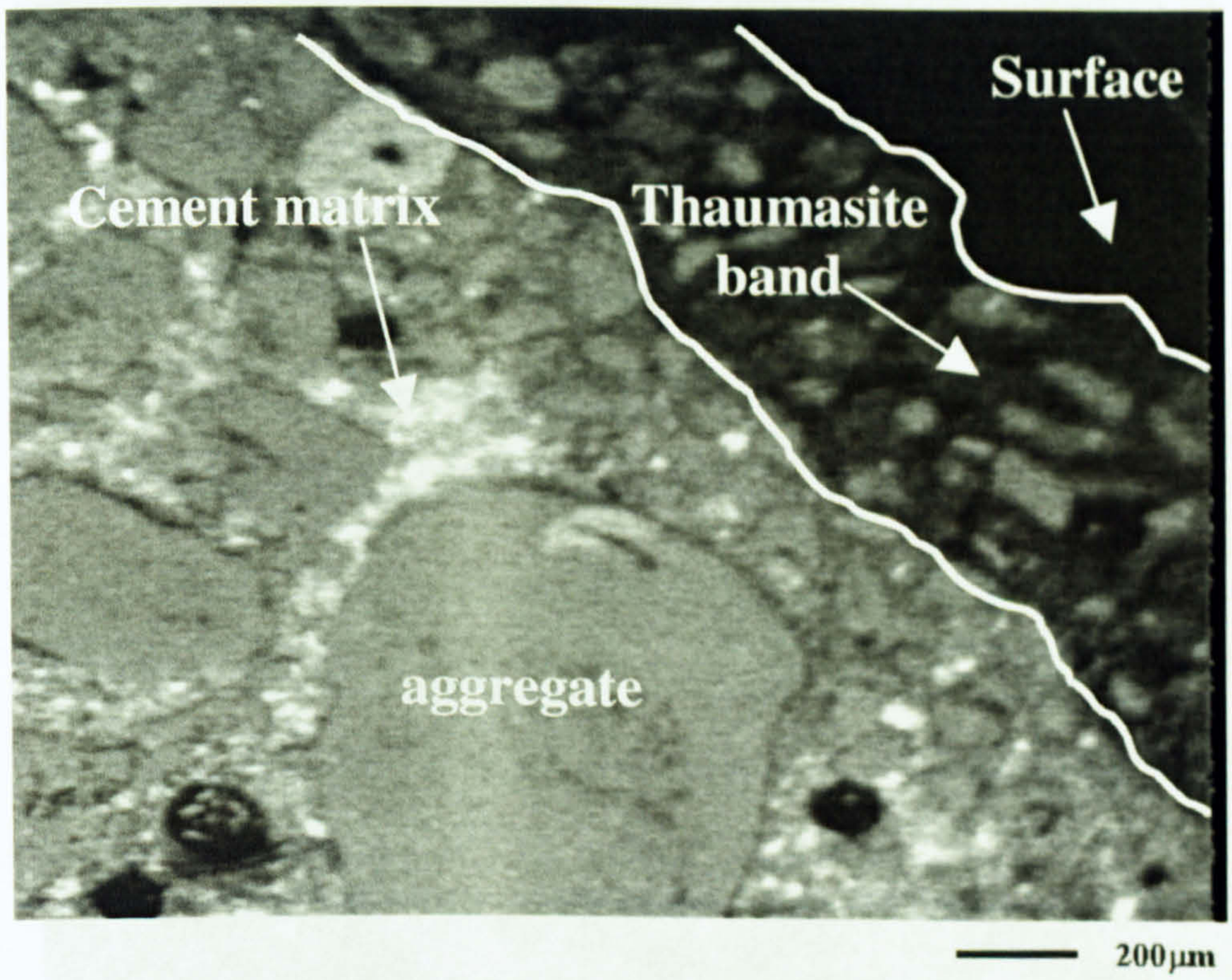

Figure 6.2: 15% LF in magnesium sulfate at 5°C-surface (Higher magnification). (large grey particles): silica aggregate; (bright grey area): cement matrix; (dark grey area): thaumasite; (black): pores and resin outside the sample.

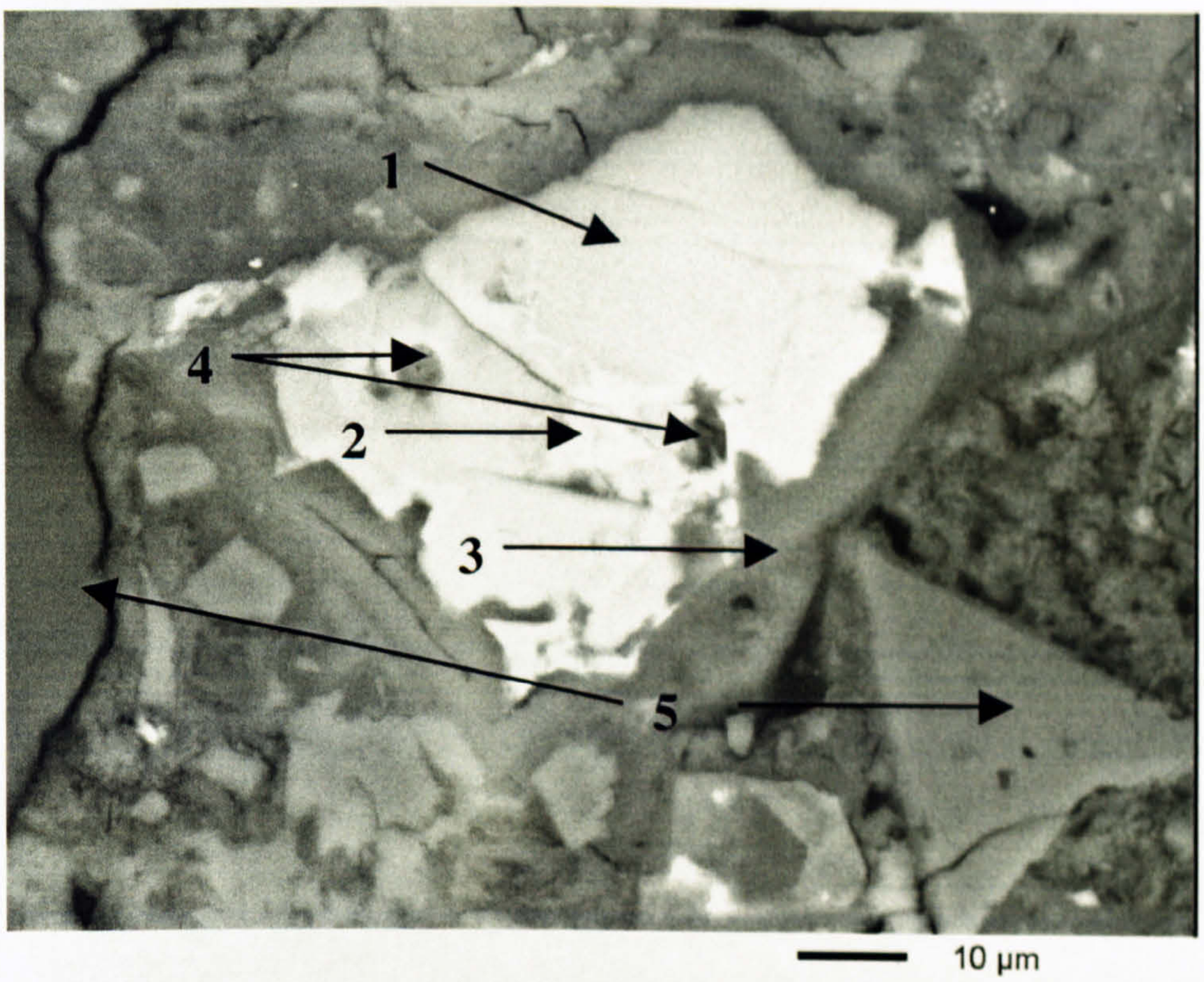

Figure 6.3: Unhydrated clinker grain. (1) belite; (2) Alite; (3) thaumasite + CSH; (4) ettringite solid solution; (5) aggregate particles.

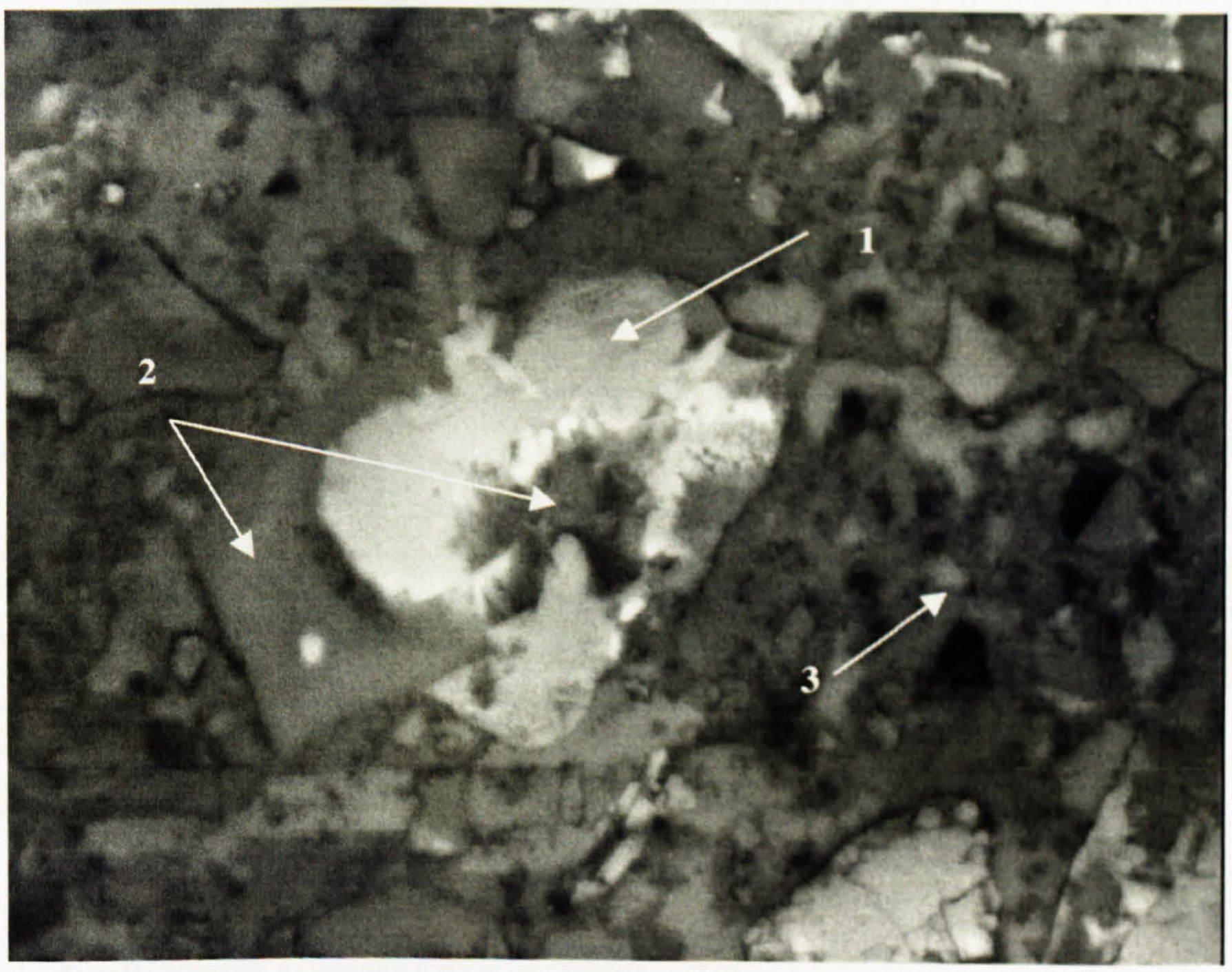

Figure 6.4: Another residual clinker grain. (1) belite; (2) thaumasite/ettringite solid solution; (3) hydrated cement matrix.

B. 15% limestone filler in 0.60% SO_4 and 0.50 %Cl^- at 5°C

Fig. 6.5 and Fig. 6.6 show the attack in samples immersed in combined chloride (0.50%Cl^-) and sulfate (0.6%SO_4^{2-}) after 1 year at 5°C. Compared with samples immersed in pure sulfate solution, the intensity of the attack was somewhat lessened in that approximately 70% of the cross section was retained. The thickness of the external dark grey band attributed to thaumasite was c.a. 1000 μm in sample immersed in pure magnesium sulfate solution (Figure 6.2). However, similar features can be identified such as thaumasite dark bands around cement matrix-aggregate interfaces, as well as intense sub parallel cracking within the matrix. Again, residual cement grains can be detected at the surface. It can be seen that the bonding between the silica aggregate particles and the cement matrix was lost, which demonstrates that the CSH has lost its binding capacity as it turned into thaumasite.

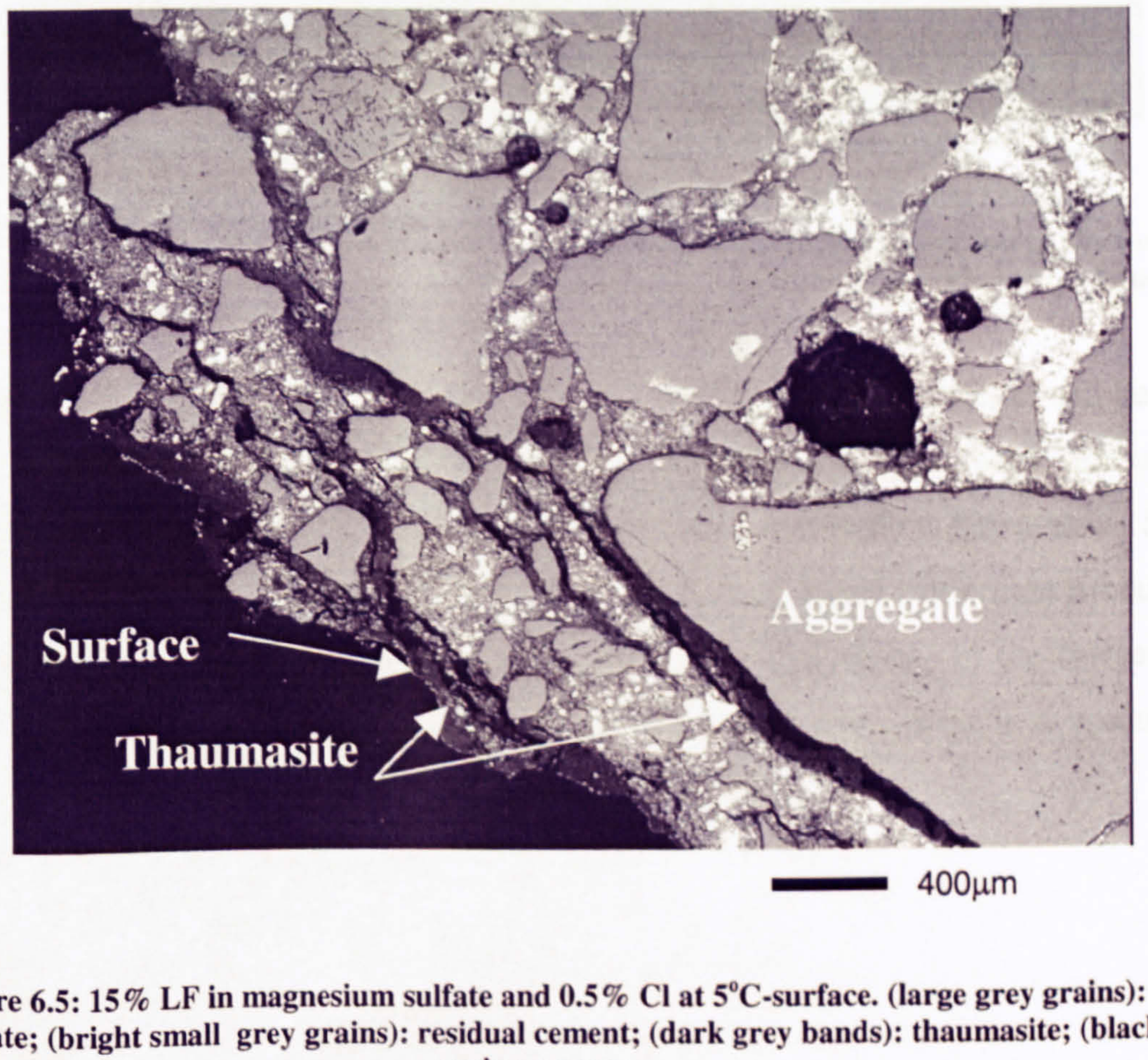

Figure 6.5: 15% LF in magnesium sulfate and 0.5% Cl at 5°C-surface. (large grey grains): aggregate; (bright small grey grains): residual cement; (dark grey bands): thaumasite; (black): resin or pores.

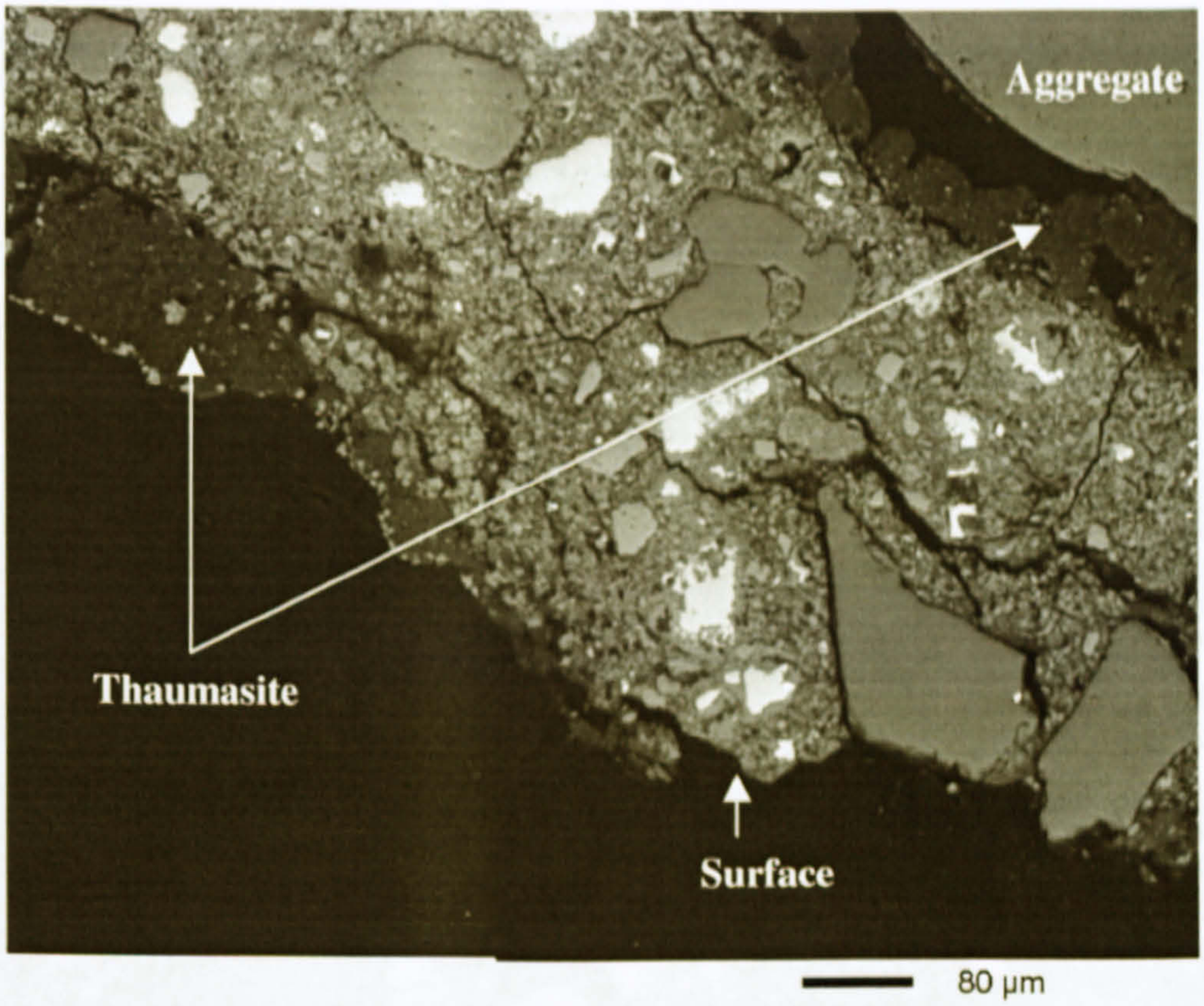

Figure 6.6: 15% LF in magnesium sulfate and 0.5% Cl at 5°C-surface (higher magnification). (large grey grains): aggregate; (bright small grey grains): residual cement; (dark grey band): thaumasite; (black): resin or pores.

Higher magnification shows the matrix at the surface of the sample, as can be seen in Fig 6.7. The CSH developed a network of cracks and became very porous, as thaumasite deposited both around aggregate particles and within the matrix. Some residual clinker grains can also be identified. The inner (ip) and outer (op) product of hydration are differentiated by their texture and type of hydration. In the former, the hydration of clinker occurs within the grain itself, whereas the latter is a product of clinker hydration within the water filled spaces in the matrix [12].

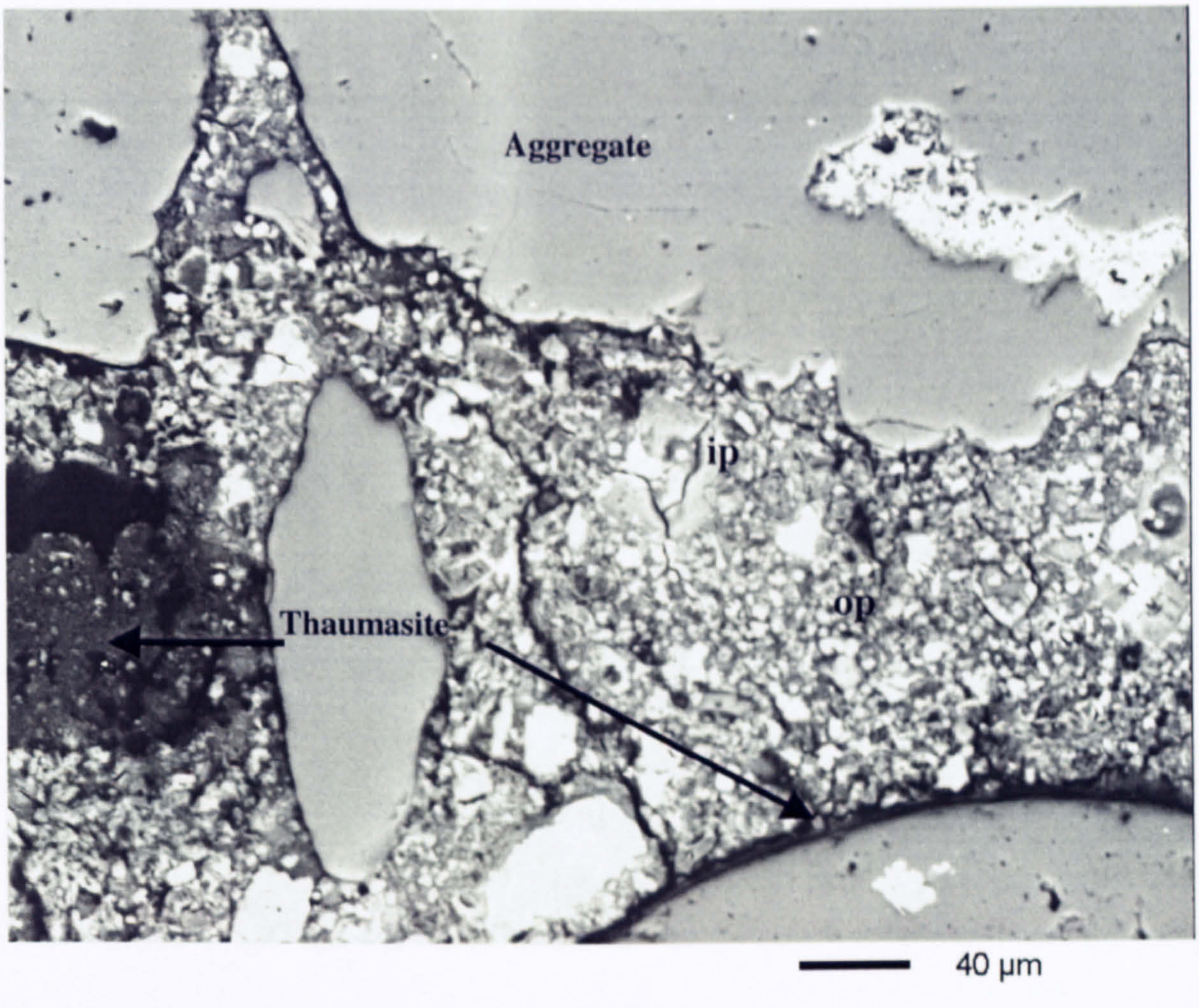

Figure 6.7: 15% LF in magnesium sulfate and 0.50% Cl at 5°C- Matrix at the surface. (higher magnification). (large grey grains): aggregate; (bright grey grains): residual cement; (dark grey): thaumasite; (black): resin or pores; (ip): inner product of hydration; (op): outer product of hydration.

At the core, the sample shows common features of hydrated cement mortar, as can be seen in Figure 6.8. Alongside the aggregate particles, the cement matrix contains CH, outer and inner products of hydration, and pores.

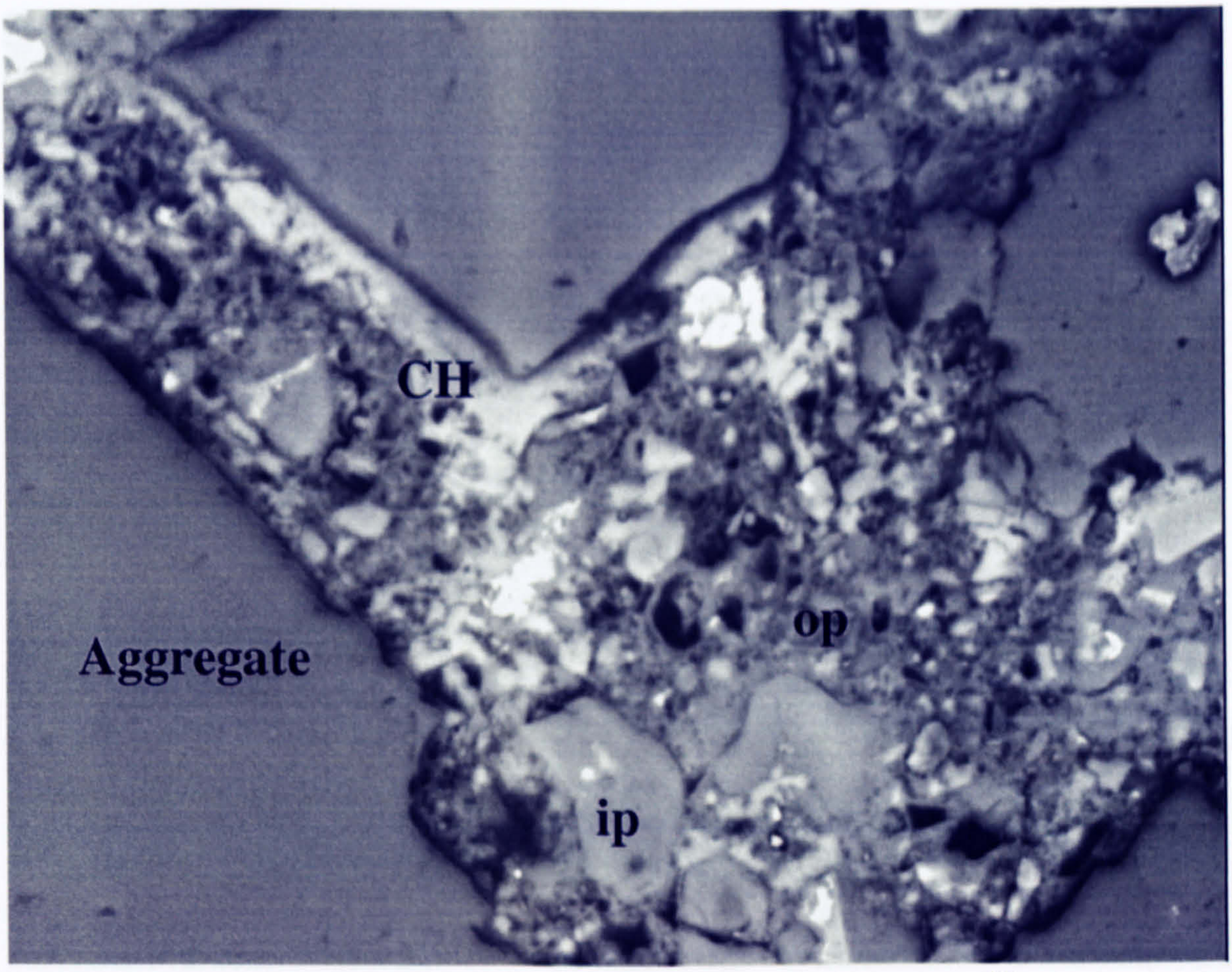

Figure 6.8: 15% LF in magnesium sulfate and 0.50% Cl at 5°C-Matrix at the core. (higher magnification). (large grey grains): aggregate; (bright grey grains): residual cement; (black): resin or pores; (CH): calcium hydroxide; (ip): inner product of hydration; (op): outer product of hydration.

C. 15% limestone filler in 0.60% SO_4^{2-} and 1.0% Cl at 5°C

Once again, the formation of dark grey bands of thaumasite around aggregates and also within the matrix was responsible for massive formation of cracks throughout the sample and at the surface in samples containing 15% LF immersed in 1.0% Cl^- and 0.60% SO_4^{2-} at 5°C after 1 year, as can be seen in Fig 6.9. In severely attacked zones, only thaumasite and aggregate can be identified, which marks the massive alteration of the cement matrix. Nevertheless, residual cement particles alongside hydrated products were engulfed by a sub-parallel crack formation of thaumasite beneath the surface, which indicates that severe damage occurred even where the matrix has not been entirely converted into thaumasite.

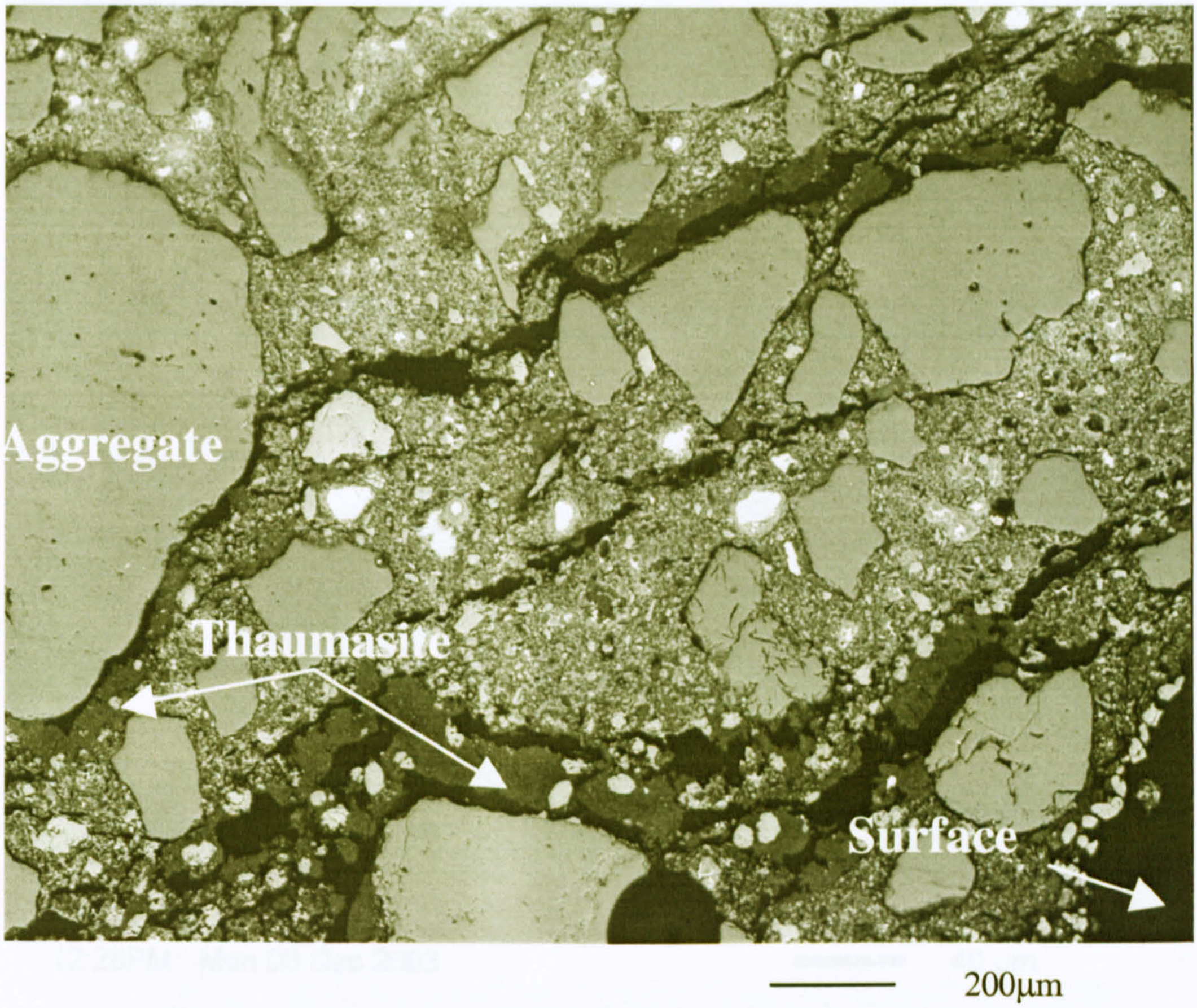

Figure 6.9: 15% LF in magnesium sulfate and 1.0% Cl at 5°C-surface. (lower magnification). (large grey grains): aggregate; (dark grey): thaumasite ; (bright grey grains): residual cement; (black): resin or pores.

In the core, normal features of hydrated cement can be seen in Fig 6.10, in which aggregate, residual clinker, inner and outer products of hydration can be detected. No thaumasite formation could be detected at this magnification.

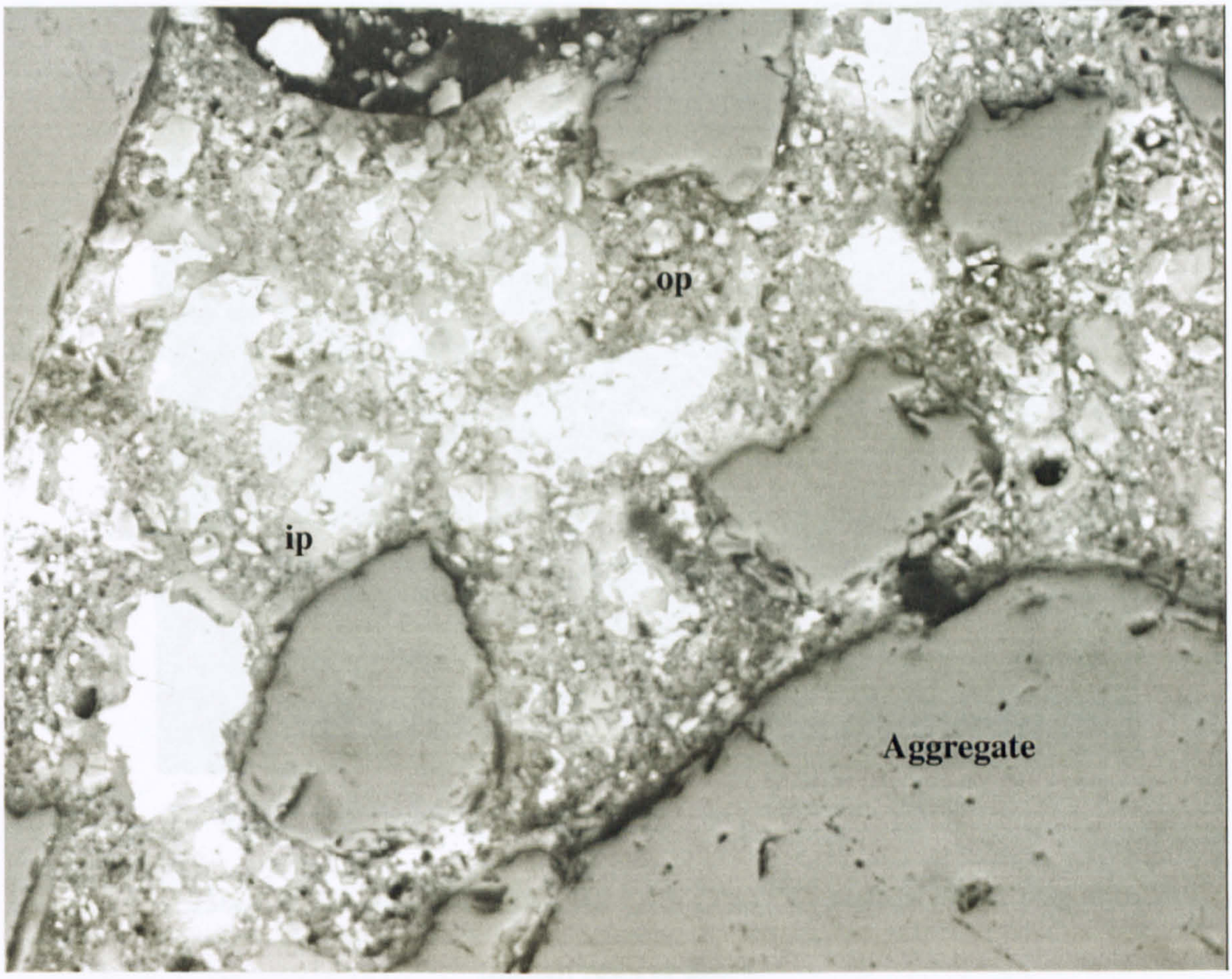

Figure 6.10: 15% LF in magnesium sulfate and 1.0% Cl at 5°C- Matrix at the core. LF in magnesium sulfate and 1.0% Cl at 5°C-surface. (higher magnification). (large grey grains): aggregate; (bright grey grains): residual cement; (black): resin or pores.

D. 15% limestone filler in 0.60% SO_4^{2-} and 2.0% Cl^- at 5°C

As for samples immersed in 2.0% Cl^- plus sulfate, dark grey thaumasite bands advanced inward, parallel to the surface of the sample. It can be seen in Fig 6.11 that the surface layer of about 500µm was detached from the bulk sample by a 40µm crack surrounded by thaumasite. Also, sub parallel cracks developed within the cement matrix. Some residual clinker grains can still be found at both the surface and core of the sample. Fig 6.12 shows silica aggregate; anhydrous clinker as well as inner and outer products.

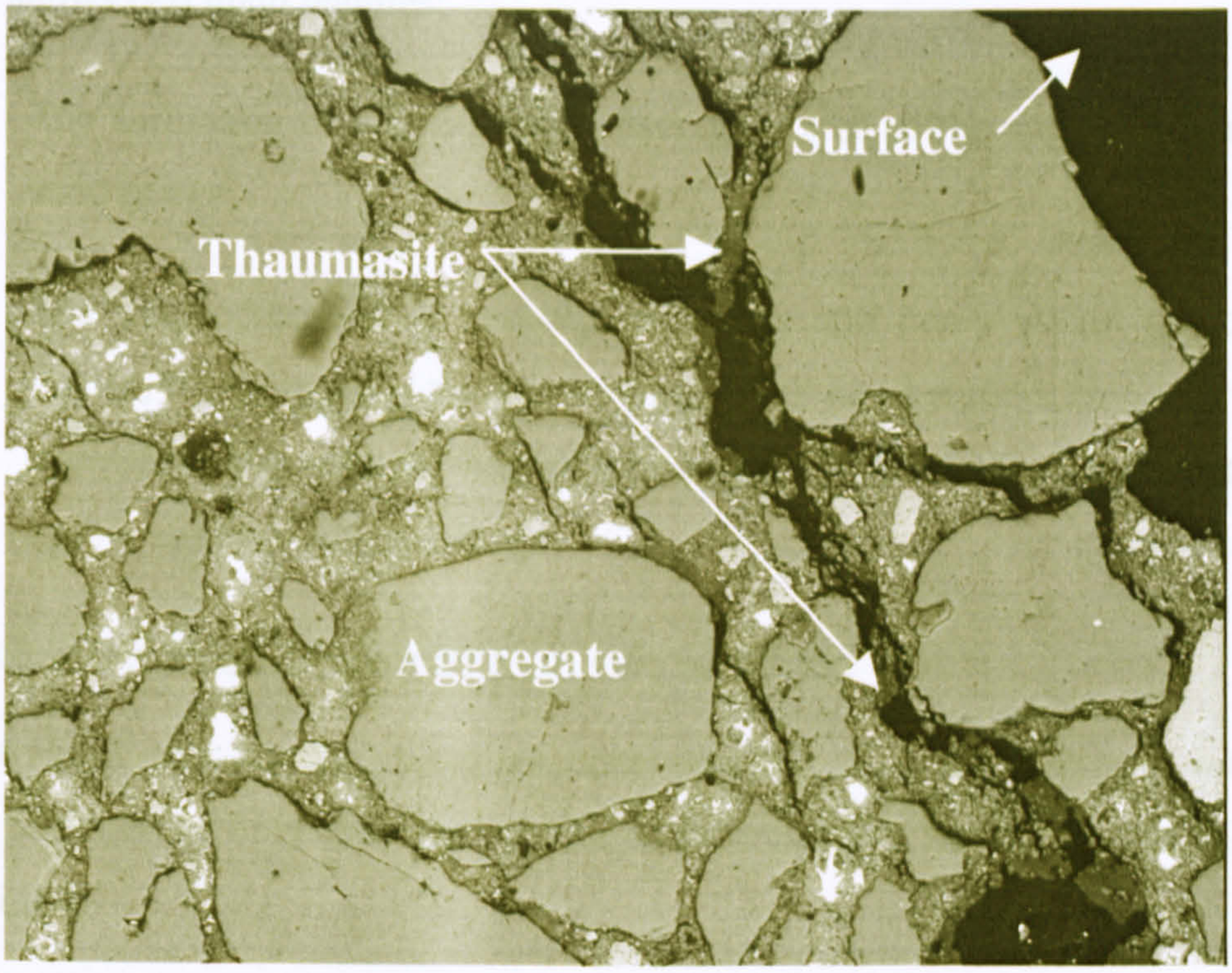

Figure 6.11: 15% LF in magnesium sulfate and 2.0% Cl^- at 5°C- surface. (lower magnification). (large grey grains): aggregate; (dark grey): thaumasite ; (bright grey grains): residual cement; (black): resin or pores.

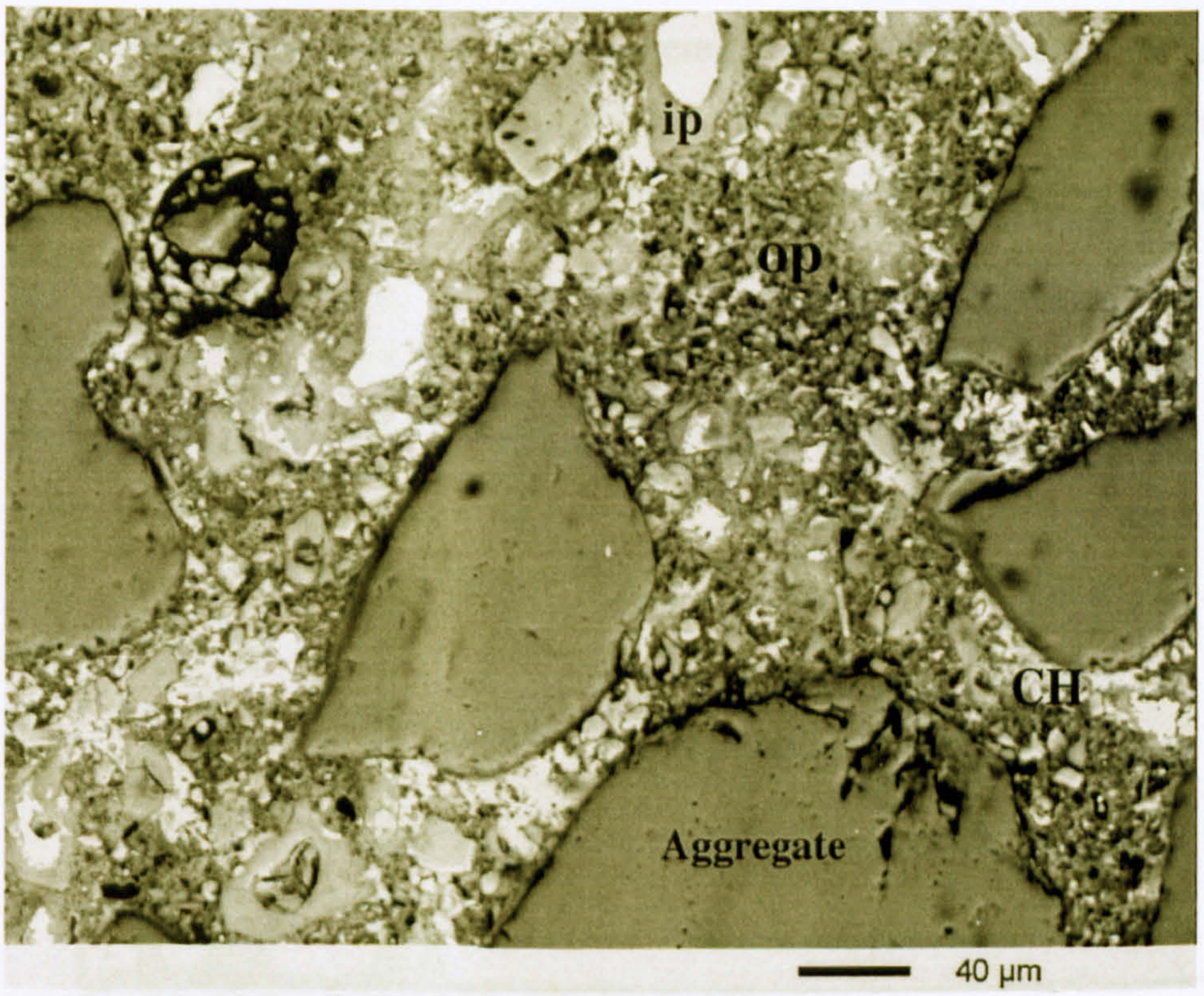

Figure 6.12: 15% LF in magnesium sulfate and 2.0% Cl^- at 5°C- Matrix at the core. (higher magnification). (large grey grains): aggregate; (bright grey grains): residual cement; (CH): calcium hydroxide; (black): resin or pores.

Despite chloride concentration, the microstructure of thaumasite-attacked areas of the mortar shows two main features:

(i) The formation of a non-binding dark grey area at the surface and around sand grains;

(ii) The development of a network of cracks and pores within the cement matrix, where residual clinker grains can still be identified. Hence, it is still necessary to investigate how chlorides affect the chemical composition of both features of the attack.

6.3.2 Characteristics of thaumasite in salt solutions

The objective of this section is to evaluate whether chloride interacts with the thaumasite structure or only acts as a catalyst in thaumasite formation by investigating its composition.

A. Energy Dispersive X-ray Analysis

A1. 15%LF in 0.50%Cl^- +0.60%SO_4^{2-}

For the sample immersed in 0.50%Cl^- and 0.60% SO_4^{2-}, the main elements detected in the dark grey area at the surface (*see* Fig 6.6) were Ca, S, Si, with smaller amounts of Al^{3+} and Cl^-, but no Fe^{3+}, as can be seen in Fig 6.13 and 6.14. In both EDXs, the low intensity of the chloride peak suggests little uptake of this ion by the thaumasite formed at different parts of the surface.

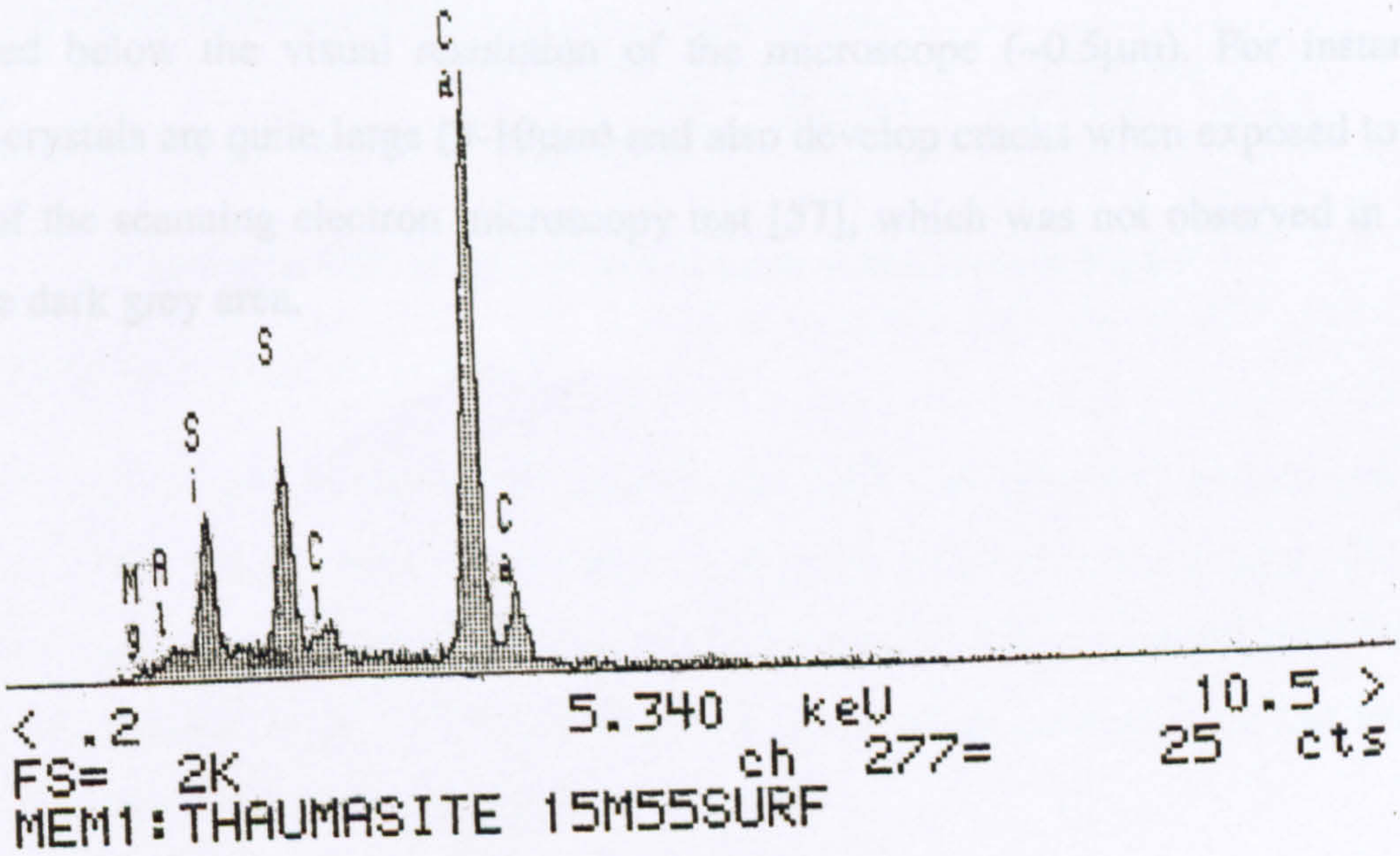

Figure 6.13: EDX of the dark band area in Fig 6.6.

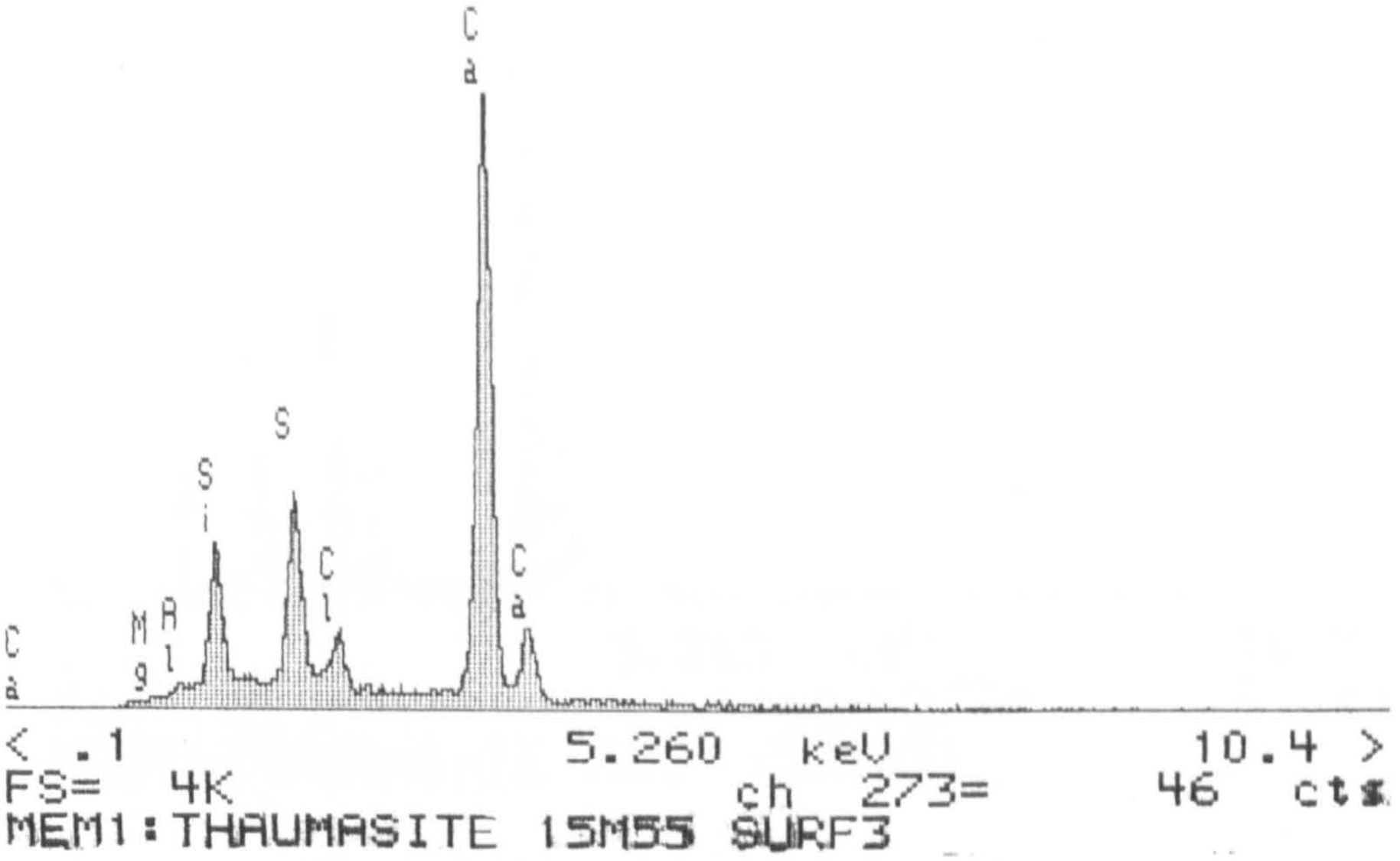

Figure 6.14: EDX of another part of the dark band area in Fig 6.6.

A2. 15%LF in 1.00%Cl^- +0.60% SO_4^{2-}

As the concentration of chloride was increased to 1.0%, the intensity of the Cl^- peak did not significantly change in the thaumasite band at different points of the surface (*see* Fig 6.9), as can be seen in Fig 6.15. Fig 6.16 also shows that some thaumasite-ettringite solid solution precipitated within the external corroded material, as indicated by the higher intensity of the Al peak. Obviously, some aluminate phases such as AFt, AFm and Friedel's salt could well be intermixed. In the case of a mixture of ettringite or monosulfate and thaumasite, it is important to envisage the homogeneity of the dark grey area, which should not be expected to be a mixture of phases unless they precipitated below the visual resolution of the microscope (~0.5μm). For instance, ettringite crystals are quite large (3-10μm) and also develop cracks when exposed to the vacuum of the scanning electron microscopy test [57], which was not observed in any part of the dark grey area.

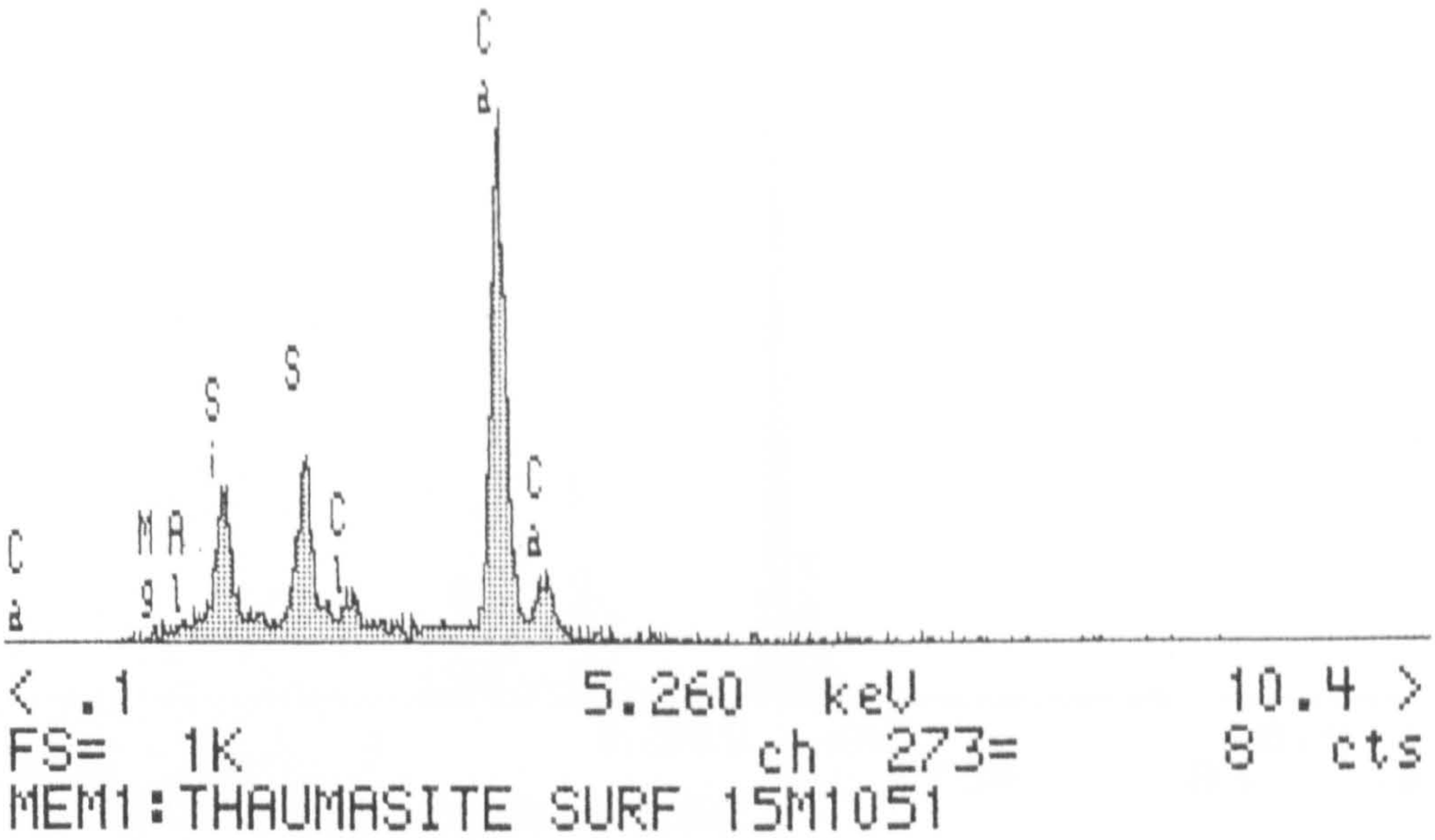

Figure 6.15: EDX of the dark band area in Fig 6.9

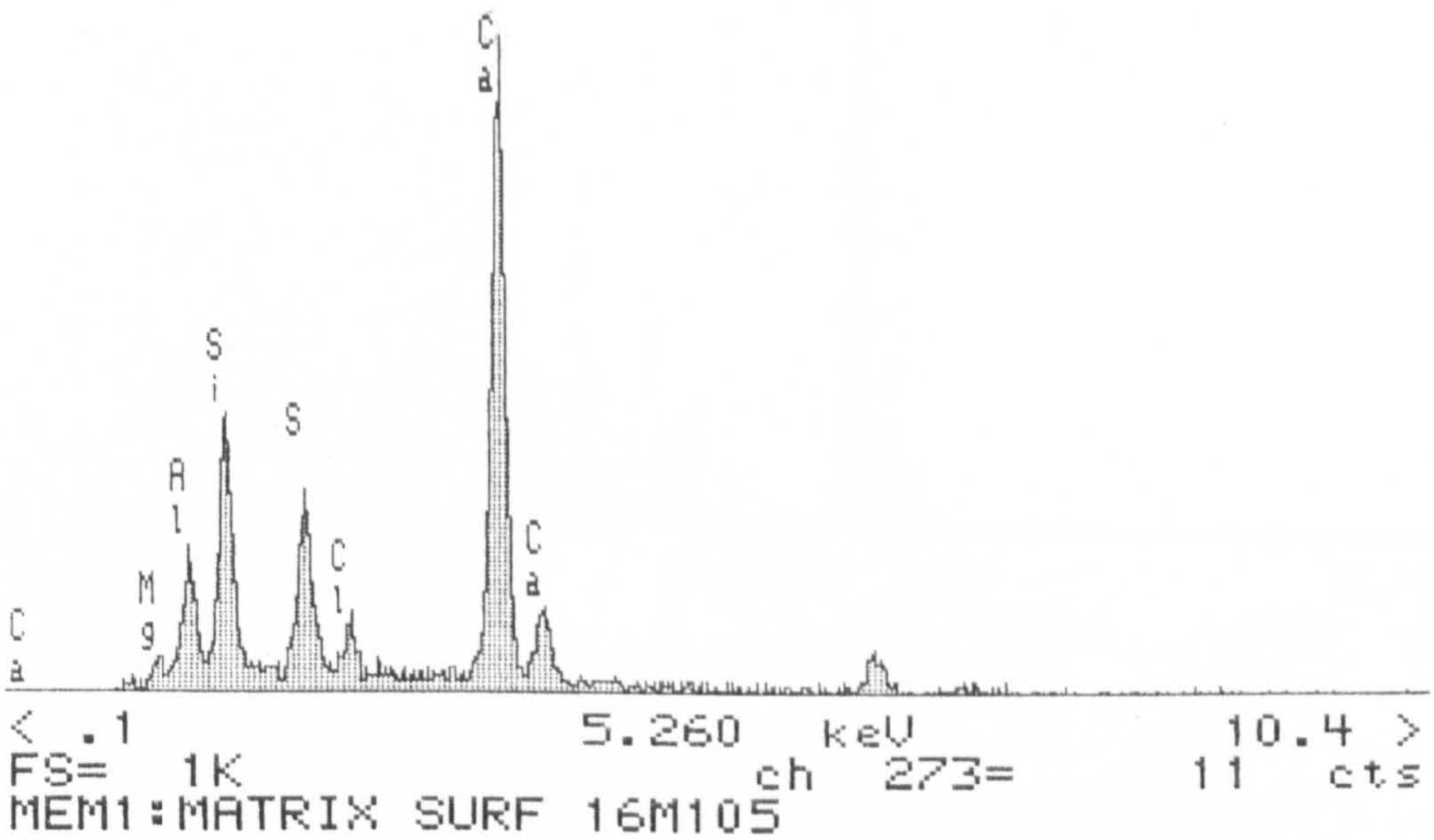

Figure 6.16: EDX of another part of the dark band area in Fig 6.9

A3. 15%LF in 2.0%Cl^- +0.60% SO_4^{2-}

At the highest concentration of chloride (2.0%Cl^-) investigated in this project, thaumasite, which the presence of Al indicates to be in its solid solution state, did not take up any significant amount of chloride as can be seen by the low intensity of the Cl^- peak in both patterns in Fig 6.17 and Fig 6.18, even when compared to the lowest concentration (*see* Fig 6.13 and 6.14).

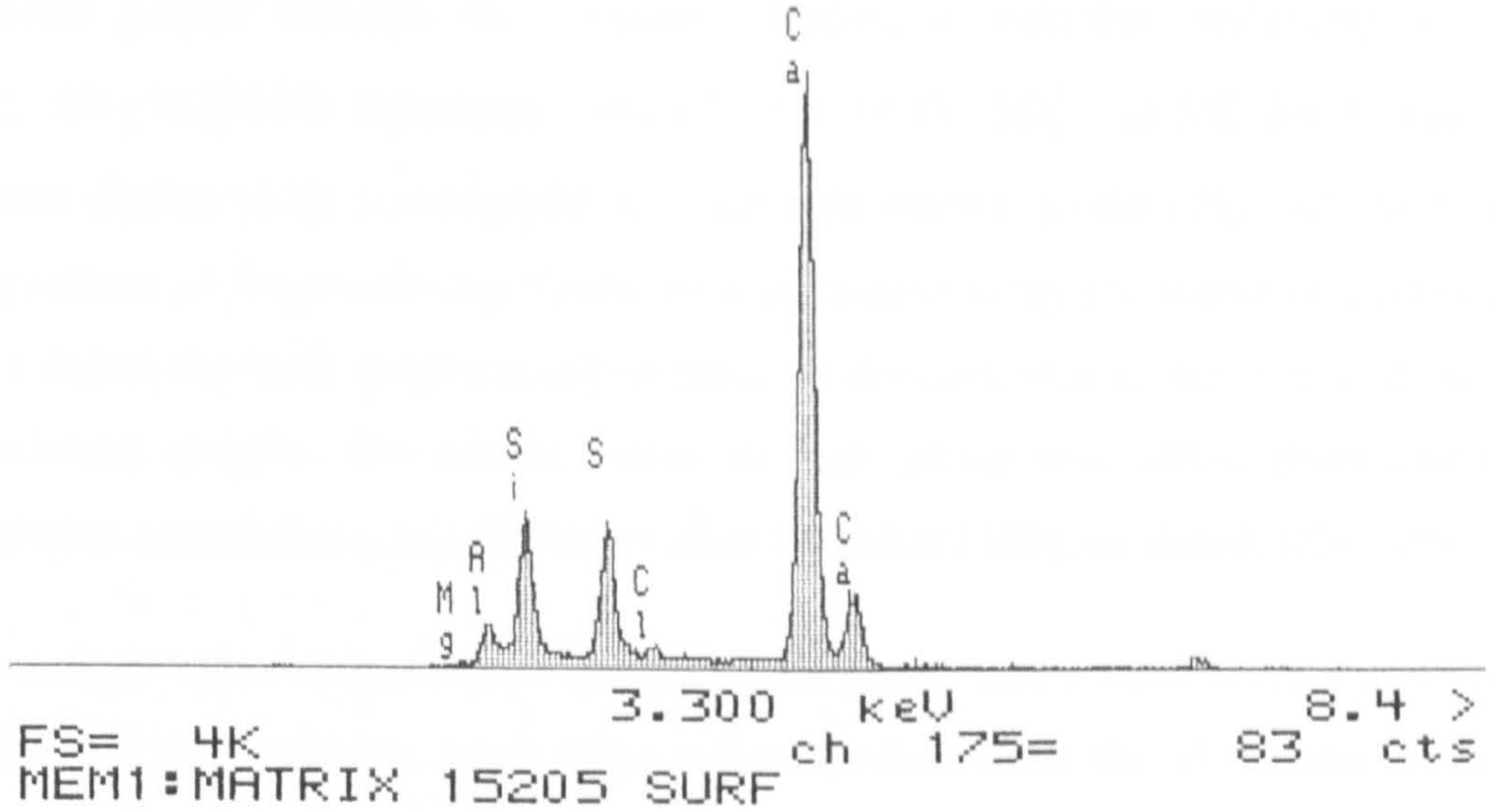

Figure 6.17: EDX of the dark band area in Fig 6.11.

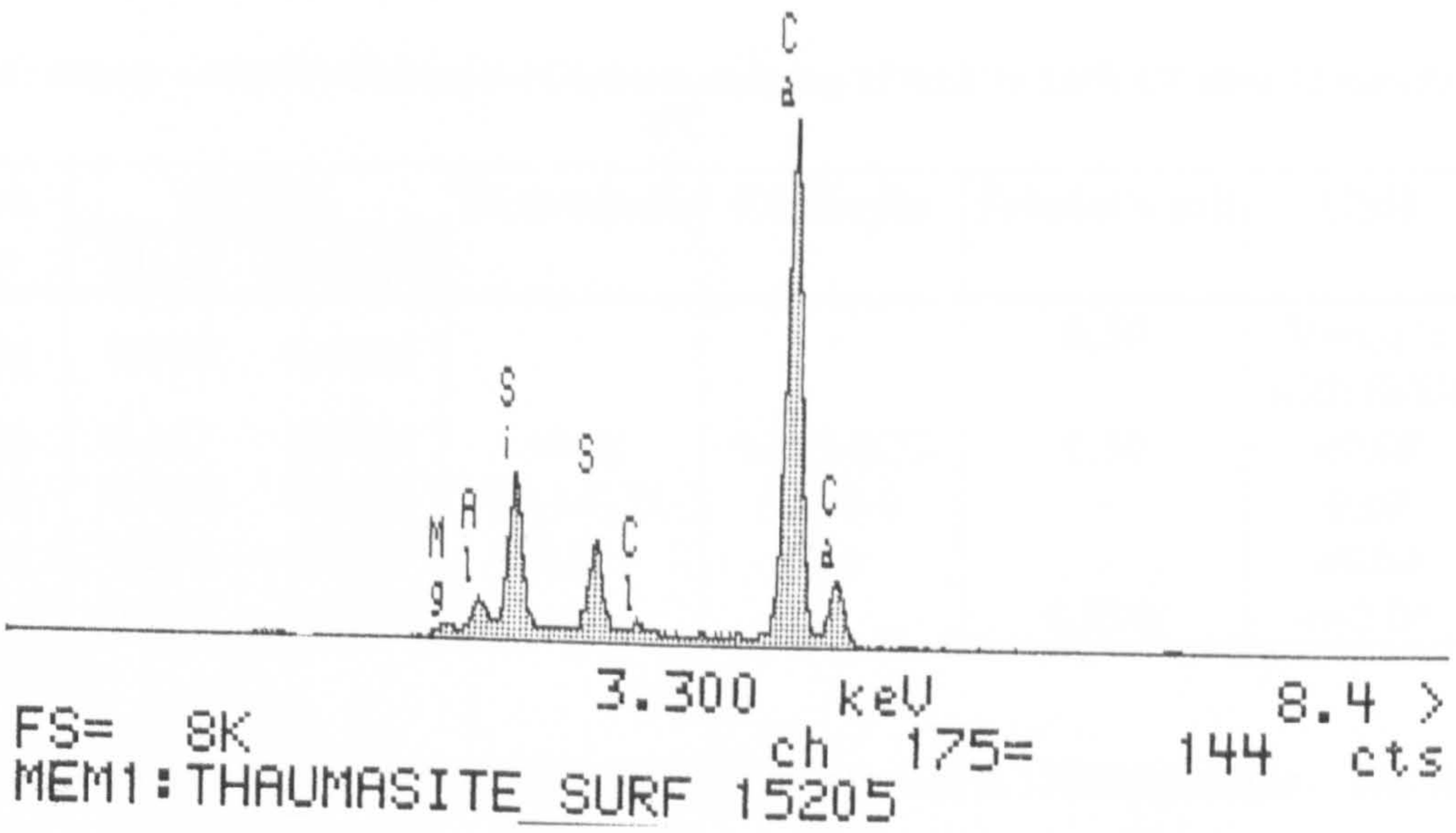

Figure 6.18: EDX of another part of the dark band area in Fig 6.11.

The EDX analyses indicate that the absence of higher chloride peaks in the dark grey area of samples immersed in all salt solutions is in agreement with the XRD analyses (see section 5.3.3-Chapter 5), in which no Friedel's salt was detected in any of the corroded material of these samples. Such lower levels of chloride appear to indicate a very low or non-existent chloride binding capacity for thaumasite.

B. Quantitative X-ray microanalysis

Because greater damage was visually detected in samples containing 15% of limestone filler (15M10) immersed 1.0% Cl^- and 0.60% SO_4^{2-}, at 5°C for 1 year, this sample was chosen to be investigated in depth with respect to the effect of chloride in the composition of thaumasite by means of quantitative x-ray microanalysis (QXMA). Table 6.1 shows the bulk chemical composition of the dark area at the corroded surface of the selected sample. The atomic ratios of each phase was either determined by stoicheometric calculations, as tabulated values by Odler [148], or stated, otherwise.

The atomic ratio composition of the grey area shows that it consists of a mixture of thaumasite and other phases, since these values deviate from the ideal stoichiometric composition of such a mineral. Indeed, closer investigation at the S/Ca and Si/Ca plots (Fig 6.19) reveals that although thaumasite solid solution is dominant, this area also contains CSH gel, and possibly gypsum.

Table 6-1: Atomic ratio distribution in samples containing 15%LF in 1.0% Cl^- after 12 months at 5°C.

Atomic ratio	QXMA		Thaumasite	Ettringite	Friedel's salt	CSH
	Mean	Sd Error				
Cl/Ca	0.045	0.0058	-	-	0.50	Variable with Si/Ca
Al/Ca	0.157	0.0051	<0.02	0.165-0.33	0.50	<0.08
Si/Ca	0.402	0.0052	0.31-0.33	0.165-0	-	0.60
S/Ca	0.212	0.0213	0.33	0.5	-	<0.03
Cl (%)	0.741	0.1382	-	-	4.55%	<~2.0*

* ref. [146].

Figure 6.19 shows the plot of S/Ca and Si/Ca ratios of a 15M10 sample. The S/Ca and Si/Ca atomic ratios lead to the conclusion that the dark grey band area mostly consisted of a mixture of thaumasite solid solution and CSH. However, some points suggest that this band can also contain a mixture of CSH, gypsum and AFm, below the resolution of the microscope. Because of the homogeneity of such a band, it is also possible that this variation of the atomic ratios could be caused by differences in the composition of the thaumasite-ettringite solid solution.

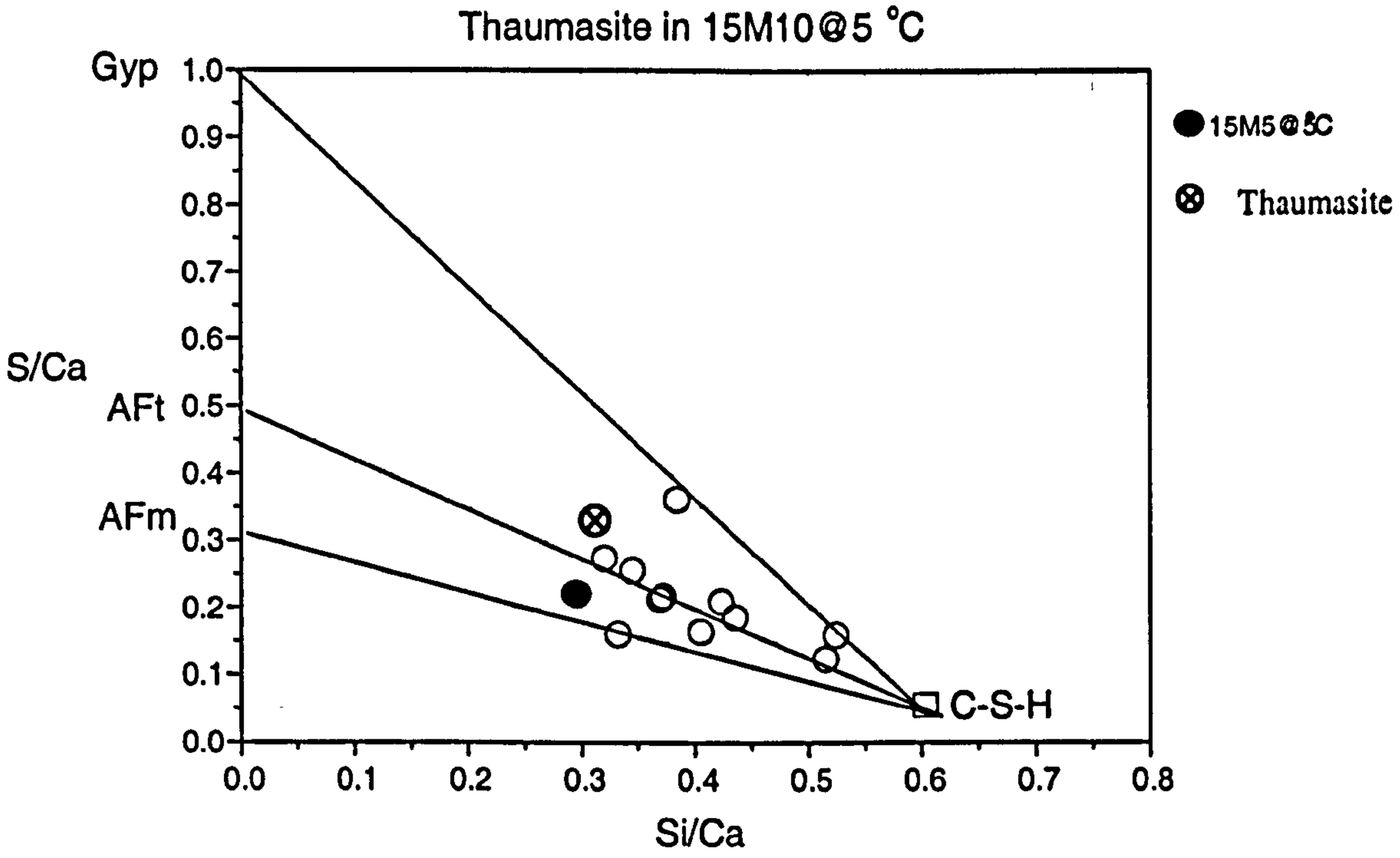

Figure 6.19: Plot of S/Ca and Si/Ca atomic ratios for thaumasite at the surface of samples containing 15%LF in 0.5 and 1.0%Cl^- after 12 months at 5°C

As far as chloride is concerned, Fig 6.20 shows that although there is no obvious trend for chloride binding and aluminates, it appears that chloride has been distributed according to the combined binding capacity of: (i) aluminate bearing phases, AFm distributed within the CSH gel; and (ii) in a mixture of CSH gel and Friedel's salt.

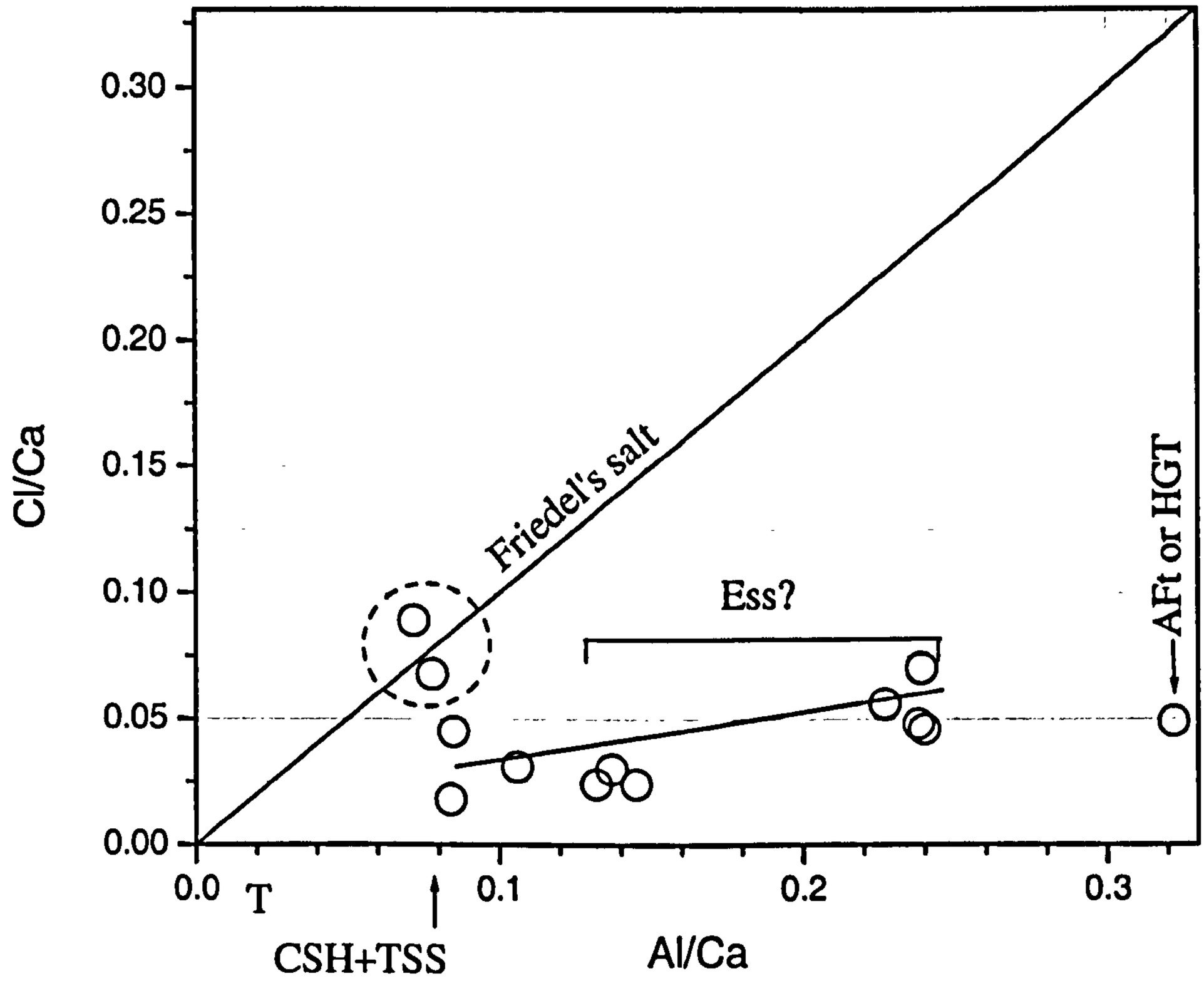

Figure 6.20: : Plot of Cl/Ca and Al/Ca atomic ratios for thaumasite at the surface of samples containing 15%LF in 0.5 and 1.0%Cl^- after 12 months at 5°C. (ESS): ettringite solid solution; (T): thaumasite; (Aft): ettringite; (HGT): hydrogarnet.

Because thaumasite seems to tolerate a small amount of Al^{3+}, according to Barnett et al. [62], EDX and x-ray microanalyses data also seem to suggest that thaumasite may tolerate small amounts of chloride as well.

However, the determination of bound chloride by x-ray microanalysis has its limitations. For instance, the use of higher voltage can lead to higher values of chloride in very corroded areas of bulk samples since its interaction volume would be also filled with pores impregnated with other salts such as NaCl and even resin, which also contain chlorine. Therefore, a precise distinction of which phase is contributing to the chlorine signal is rather complicated. For instance, the primary electron range drops from ~5 μm to 2μm when the voltage drops from 25kV to 15kV. On the other hand, although the spot analysis resolution using 15kV would increase with respect to minerals of that order of size, such as thaumasite, it would not be sufficiently representative as far as the analysis of the composition of the matrix is concerned. Also, Beaudoin et al. [146] and Jensen et al. [149] have pointed out that although electron probe micro-analysis is very useful and with excellent resolution (few μm compared to mm in titration methods) for the assessment of chloride profiles in cement based materials, the results are affected by the spatial distribution of chlorides.

C. Unit cell parameters

EDX and x-ray microanalyses appear to indicate that thaumasite has only a limited or non-existent ability to bind chloride, which was mostly bound within the mixture of Friedel's salt, CSH and AFm distributed within the cracks and flaws underneath, rather than in the dark grey area. However, it is still necessary to consider the possibility that thaumasite can accommodate some chloride in its crystal structure, with a Cl/Ca ratio of up to ca. 0.045 ± 0.006 (95% confidence limit). In order for Cl^- to enter the crystal structure of thaumasite, it is important to consider that:

(i) Charge balance must be equilibrated, in which $2Cl^-$ would replace $1CO_3^{2-}$, or $1Cl^-$ and either Na^+ or H^+ would enter into the structure without replacing carbonates, for instance; and

(ii) There can possibly be a change in symmetry, given relatively large size of Cl^- ionic radii (1.81Å), which bond length can require up to 3.0 Å.

Hence, the determination of the lattice parameter of the corroded material can detect differences caused by the intrusion of ionic species such as Cl^-, particularly if a change in symmetry is detected. This resolution makes lattice parameter determinations via XRD one of the most accurate techniques to investigate solid solutions in minerals such as ettringite and thaumasite [62].

Beaudoin [146] reported that increase in *c*-spacing occurred in hexagonal aluminates hydrates as a result of intrusion of Cl^- into their crystal structures, which lead to the hypothesis that chloride would also adsorb within the CSH interlayer (No data or reference were presented). Therefore, it has been attempted to detect possible alterations in the thaumasite structure by means of changes in the lattice parameters.

Fig 6.21 shows XRD patterns of samples containing 15% LF immersed in the four salt solution reported in this chapter (0, 0.5, 1.0 and 2.0%Cl^-), at 5°C for 1 year. The most intense XRD peaks assigned to thaumasite (full line) can be clearly identified at 9.206°, 16.028° and 25.978° 2θ, corresponding to the Miller indices 100, 110 and 211, respectively (PDF 46-1360). Although it is not obviously evident, traces of ettringite (dashed line) also seem to be present in all solutions, but more markedly in the samples immersed in 2.0%Cl^-, as can be seen by a broadening of the referred peaks toward lower

angles and the presence of some spikes. Indeed, it has been observed that the detached material contained thaumasite as well as other phases in all mixes (*see* Figs 6.2, 6.6, 6.9 and 6.11).

Although the presence of ettringite and/or ettringite solid-solution simultaneously causes some difficulties in the precise determination of unit cell parameters, the study of thaumasite-ettringite solid solutions is not necessarily invalidated as far as the dominant phases are concerned. Indeed, it is possible to evaluate lattice parameters since the determination of unit cell parameters requires a precise peak position rather than peak shape as required by other methods such as the Rietveld refinement, which can be powerfully used for more advanced studies such as structure refinement. Indeed, the use of the Rietveld method in multiphase systems requires a model for each phase, which can be impractical in systems with various phases of uncertain composition such as in this study [150].

Therefore, the use of internal standards, such as quartz and calcite, was necessary to acquire the zero shift correction, on the basis of least square refinement, so that a precise location of the peaks can be achieved, as reported by Torres et al [18]. The software *Stoe-WinXpow* supplies both programmes *Calibrate* and *Index* that enables (i) zero shift correction and (ii) unit cell parameters determination, respectively, which not only takes into account the main peaks but the full pattern. It is estimated that the lattice refinement significance interval on the basis of 95% confidence limit is ca d ±0.005Å using this technique (*see* section 3.9.1-Chapter 3).

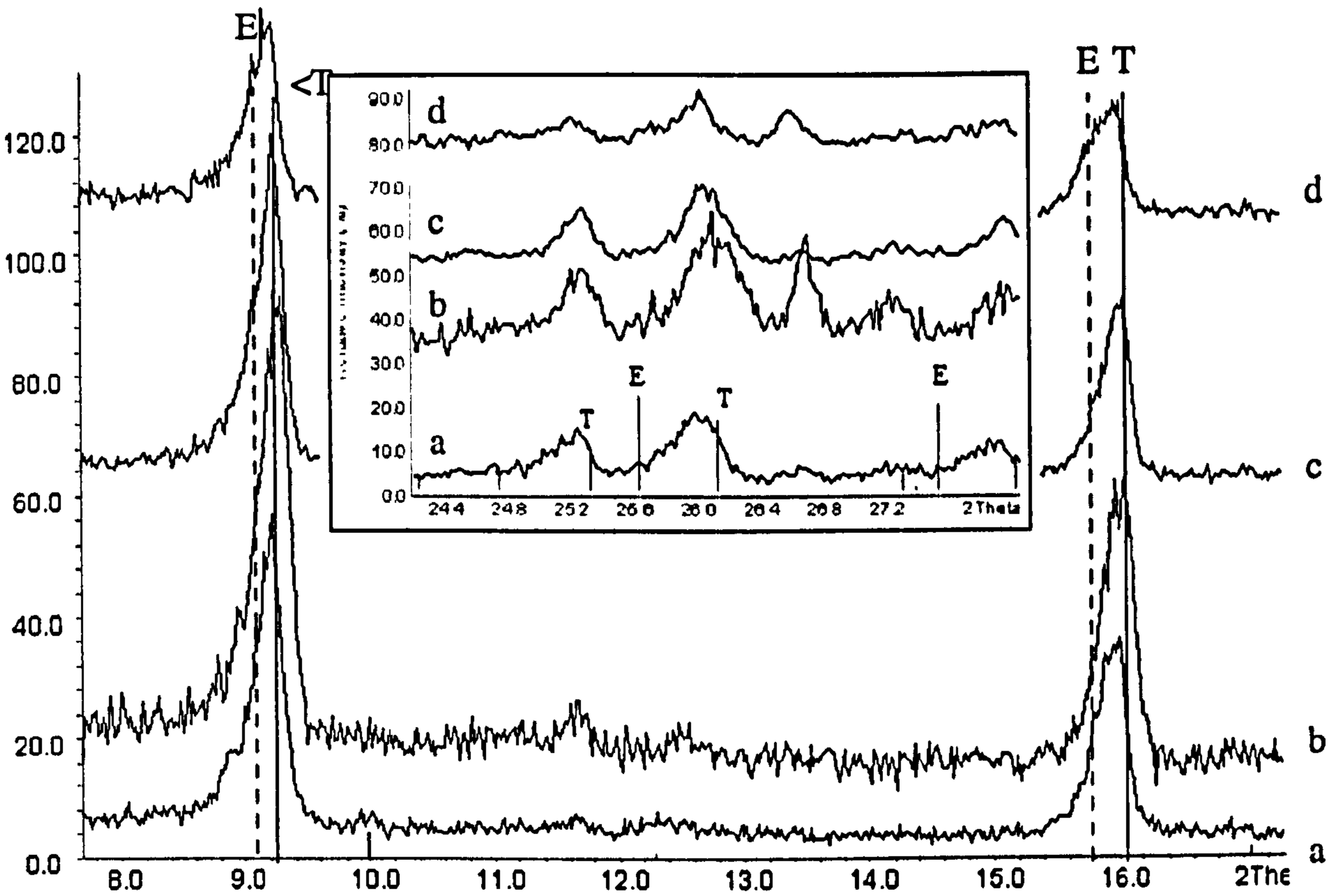

Figure 6.21:XRD of corroded material in 15%LF samples immersed in salt solution at 5°C. (a): 0.6% SO_4^{2-} ; (b): 0.6% SO_4^{2-} + 0.5%Cl; (c): 0.6% SO_4^{2-} + 1.0%Cl; (d): 0.6% SO_4^{2-} + 2.0%Cl;(E): ettringite; (T): thaumsite.

Three distinguished d-spacings for thaumasite and ettringite, their respective Miller indices and also the unit cell parameters calculated in samples with various amounts of limestone filler in salt solutions after 1 year at both 5°C, as listed in Tables 6.2.

Table 6-2: Unit cell determination of mortar samples at 5°C in salt solutions after 1 year.

Temperature (°C)	Limestone content (%)	Chloride content (%)	d-spacing (Å)		Miller Indices			Lattice parameter (Å)	
			obs	Calc Win Xpoe Stoe	h	k	l	a	c
5	15	0.0	9.599	9.582	1	0	0	11.064	10.449
			5.525	5.532	1	1	0		
			3.427	3.422	2	1	1		
		0.5	9.506	9.570	1	0	0	11.051	10.437
			5.527	5.526	1	1	0		
			3.414	3.418	2	1	1		
		1.0	9.565	9.579	1	0	0	11.061	10.435
			5.529	5.531	1	1	0		
			3.419	3.421	2	1	1		
		2.0	9.630	9.583	1	0	0	11.065	10.459
			5.550	5.533	1	1	0		
			3.423	3.422	2	1	1		
	5	0.0	9.515	9.568	1	0	0	11.048	10.399
			5.528	5.524	1	1	0		
			3.413	3.136	2	1	1		
		0.5	9.584	9.573	1	0	0	11.054	10.398
			5.548	5.527	1	1	0		
			3.411	3.417	2	1	1		
		2.0	9.558	9.568	1	0	0	11.048	10.412
			5.539	5.524	1	1	0		
			3.417	3.416	2	1	1		
	0	0.0	9.547	9.576	1	0	0	11.064	10.449
			5.542	5.529	1	1	0		
			3.437	3.419	2	1	1		
		0.5	9.560	9.578	1	0	0	11.051	10.437
			5.545	5.530	1	1	0		
			3.406	3.419	2	1	1		
		1.0	9.530	9.570	1	0	0	11.061	10.435
			5.534	5.526	1	1	0		
			3.412	3.416	2	1	1		
		2.0	9.558	9.587	1	0	0	11.065	10.459
			5.539	5.535	1	1	0		
			3.417	3.422	2	1	1		

The data show that all the cell parameters of the corroded products developed within OPC and carbonated filler samples were found to conform within the limits of the thaumasite type of phase, say a<11.11 Å and c<10.475 Å [151, 152]. As can be seen in Fig 6.22, within the experimental error, most lattice parameters lie within a<11.055 Å and c<10.410 Å, which are reported as for the mineral thaumasite by Edge and Taylor [134], and sometimes even slightly smaller. An exception is made for 15% limestone filler samples in which c parameters were greater, despite chloride concentration.

Although thaumasite solid solution precipitated in some samples immersed in pure sulfate solutions at 20°C, ettringite solid solution was the dominant phase at this higher temperature. Because of the low intensity of the thaumasite peaks at 20°C, the determination of unit cell parameters, which would be restricted to one peak only, is not reported for this particular temperature.

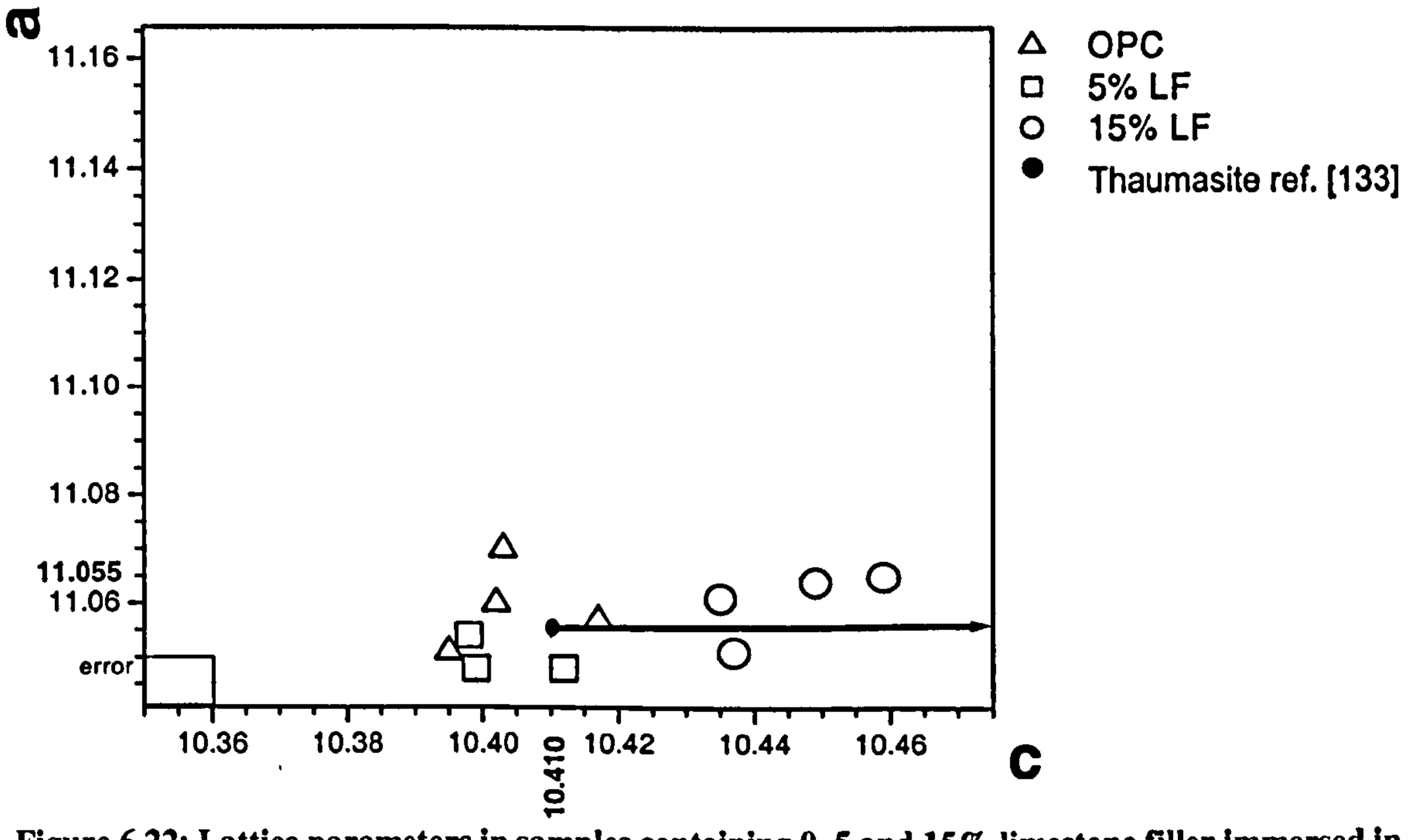

Figure 6.22: Lattice parameters in samples containing 0, 5 and 15% limestone filler immersed in salt solutions at 5°C after 1 year.

Closer investigation shows that a is less affected than c by the concentration of chloride, as can be seen because most points in Fig 6.23 fell within the band that corresponds to the expected a value for thaumasite, as described by Edge and Taylor [134]. Also, as far as c unit is concerned, it is interesting to point out that there seems to be a minimum in the c dimension in both samples with 15%LF and 0%LF immersed in 10g/l Cl^- (1.0%) plus sulfate (0.6%). Samples immersed in such concentration also appeared to have developed the worst damage, which was more evident in high filler

content samples. Also, the fact that *c* increased, as the level of chloride further increased, seems to agree to features of the attack observed in the chapter 5 in which a higher concentration of chloride leads to a slightly lesser intensity of attack, more evident in samples containing 15% limestone filler (*see* Figs 5.5, 5.17 and 5.19-Chapter 5).

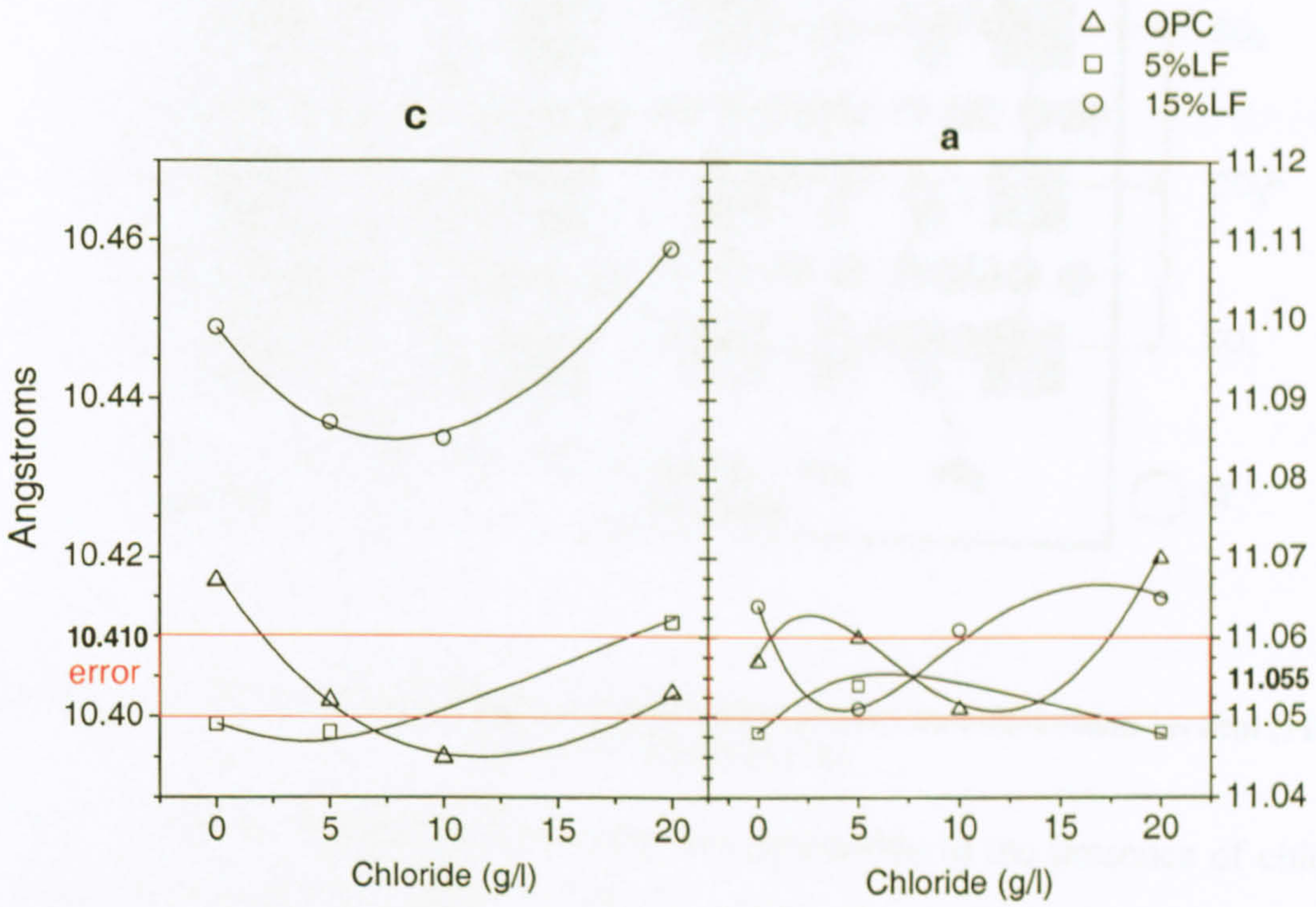

Figure 6.23: Unit cell parameters versus chloride concentration in samples containing 0, 5 and 15% limestone filler immersed in salt solutions at 5°C after 1 year.

Higher *c*, without significant change in *a*, indicates less carbonate, or more sulfate, in the unit cell since carbonate affects *c* more than *a*, as observed by Torres et al [18]. When considering the crystal structure of thaumasite and ettringite, the replacement of sulfate by carbonate strongly affects *c* by increasing the symmetry of the unit cell which makes the *c* dimension of thaumasite to be a half of that of ettringite, as seen in Fig 6.25. In ettringite, tetrahedral sulfate ions, which occupy space along both *a* and *c*, are subsequently stacked within the channels parallel to the $Ca_3[Al(OH)_6.12H_2O]^{3+}$ columns, whereas they alternate positions with planar carbonate ions, which occupy more space along the *a* dimension but not the *c* dimension, in thaumasite.

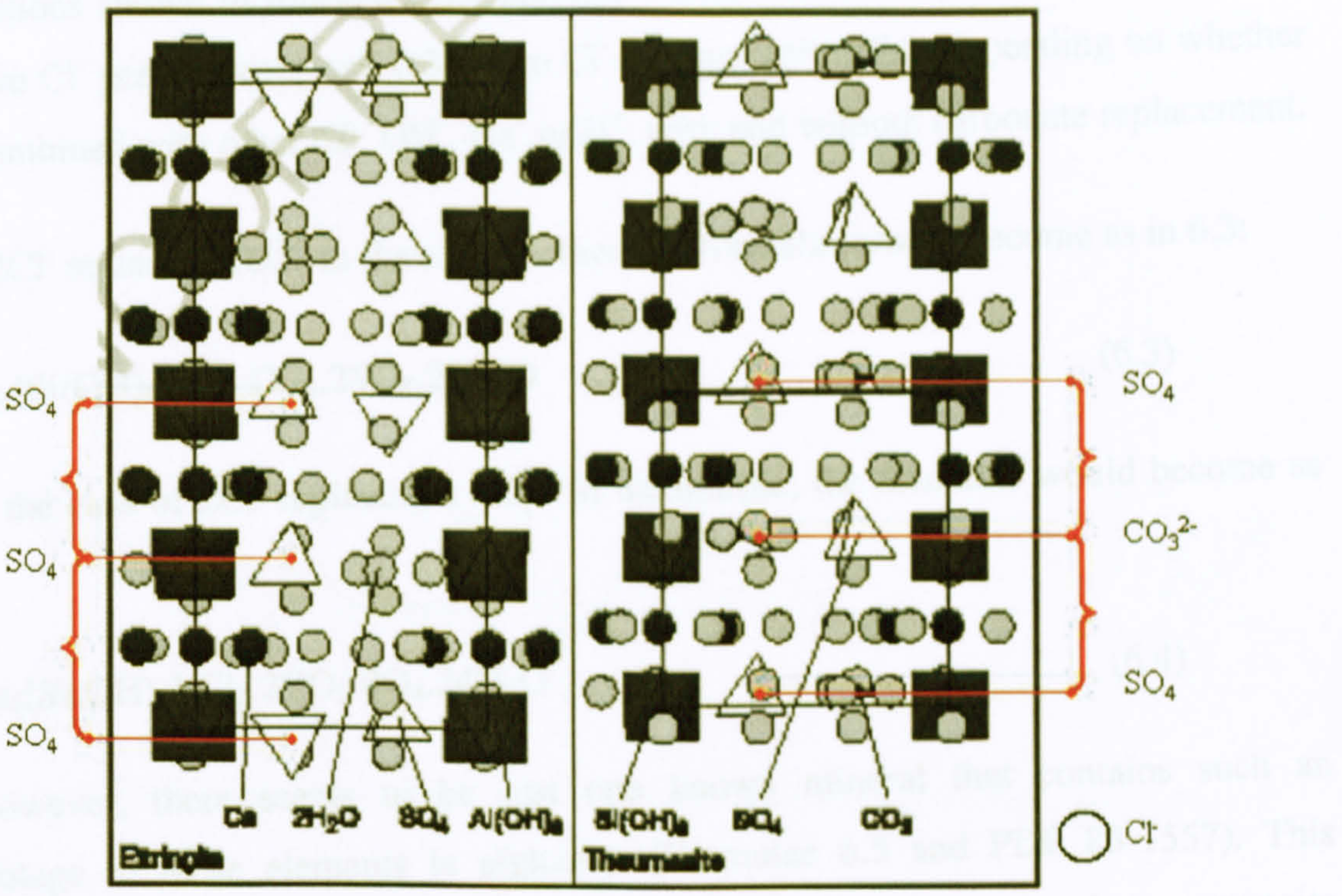

Figure 6.24: Crystal structure of ettringite and thaumasite projection c-dimension vertical [110], as shown in Torres et al. [18].

Hence, it appears that purer thaumasite was favourable to the presence of chloride at a certain concentration, namely 1.0%Cl^-, which also caused greater damage, as visually detected. This seems to agree with the hypothesis that higher availability of carbonates in this concentration enhanced the chances of thaumasite formation. However, it is not clear whether the increase in *c*-dimension in higher chloride concentration was caused either by an increase in carbonate counter diffusion, as proposed in Chapter 5, or by some sort of chloride interaction.

Suppose that there is a possibility for Cl^- to enter into solid-solution in the thaumasite structure within one unit cell, and that it is responsible for the observed increase in *c*-dimension, as pointed out for aluminate phases by Beaudoin et al. [146]. It is important to consider that:

(i) Charge balance must be equilibrated within the mineral;

(ii) There can possibly be a change in symmetry, given the relative large ionic radii of Cl^- (1.81 Å), whose bond length can require up to 3.0 Å, as in $CaCl_2$.

Hence, the hypothetical chloride containing thaumasite, with the tentative chemical compositions shown in formulae 6.3 and 6.4, would theoretically have Cl/Ca between 0.66 (two Cl^- per unit cell) and 0.33 (two Cl^- per two unit cells), depending on whether Cl^- is combined with other Cl^-, OH^-, Na^+ or H^+, with and without carbonate replacement.

If $2Cl^-$ replace 1 CO_3^{2-} in thaumasite, then the formulae would become as in 6.3:

$$Ca_6[Si(OH)_6]_2Cl_2.CO_3.2SO_4.24H_2O \qquad (6.3)$$

In the case of $2Cl^-$ replacing 1 SO_4^{2-} in thaumasite, the formulae would become as in 6.4:

$$Ca_6[Si(OH)_6]_2Cl_2.2CO_3.SO_4.24H_2O \qquad (6.4)$$

However, there seems to be just one known mineral that contains such an assemblage of these elements is afghanite (Formulae 6.5 and PDF 85-1557). This mineral is found to be hexagonal but its symmetry has been reported as being ettringite type (P31c) or thaumasite type (P63mc), by Ballirano et al. [153] and Rastsvetaeva et al. [154], depending on the concentration of those elements. Although its lattice parameters are a=12.80 Å and c=21.41Å, which is close to that of c for ettringite (21.415 Å), its composition greatly differs from that of thaumasite, ettringite or Friedel's salt.

$$(Na,Ca,K)_8\,(Si,Al)_{12}.O_{24}.(\,SO_4\,,\,Cl\,,\,CO_3\,)_3\;1H_2O \qquad (6\text{-}5)$$

Although some peaks in 15%LF immersed in 2.0%Cl^- after 1 year could possibly be assigned to afghanite, as shown in Figure 6.25, the precise identification of such a phase can be very problematic, for it contains several overlapping peaks with a number of phases including ettringite, thaumasite, calcite and particularly Epsom salt, which was used as the source of sulfate in this research.

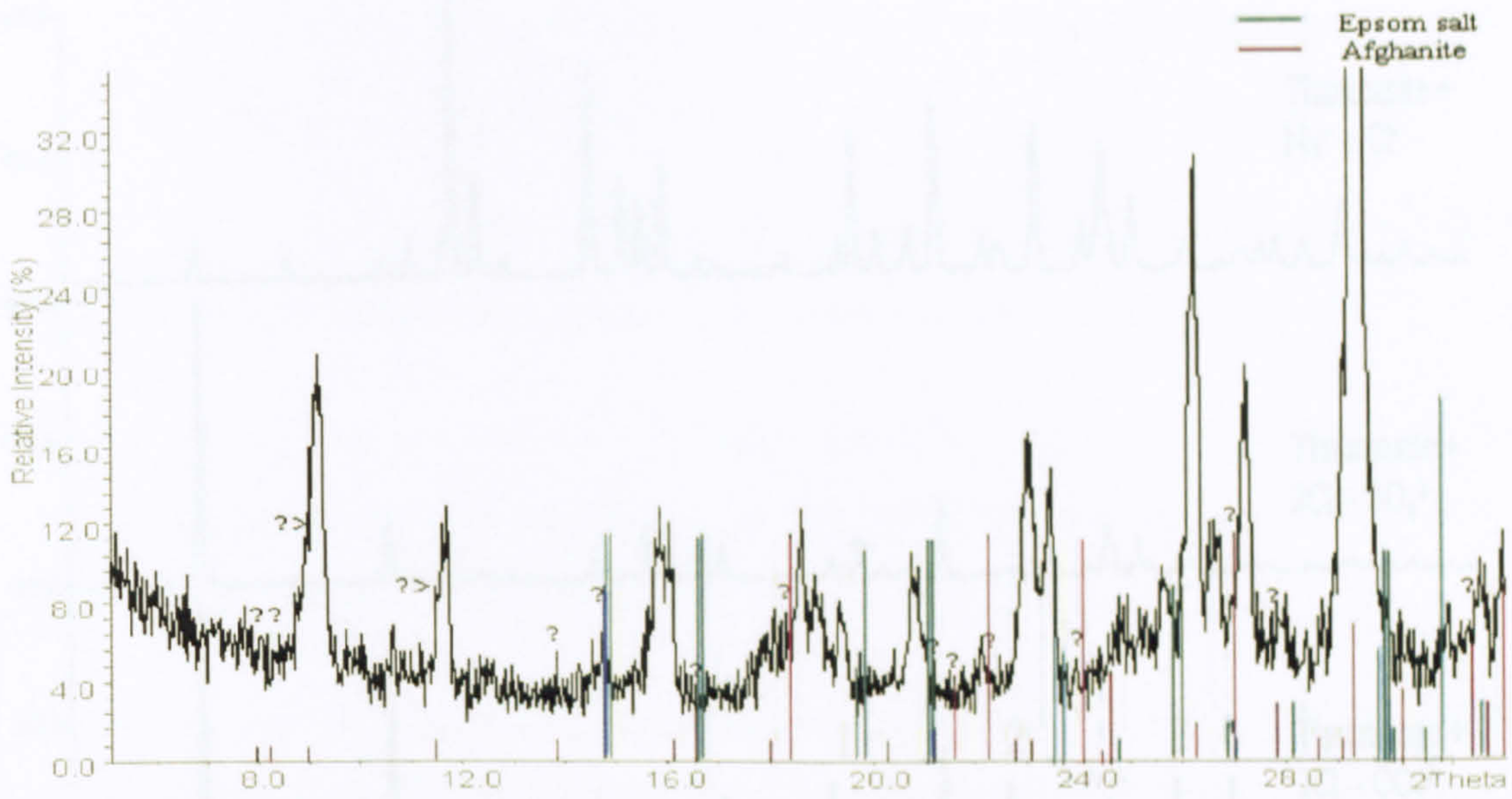

Figure 6.25:XRD of 15%LF in 2.0%Cl^- after 1 year at 5°C. Featuring Afghanite and Epsom salt patterns.

When considering the large ionic radii of chloride ions and the existence of afghanite, it appears that any chloride solid solution would cause strong alteration in the crystal structure of thaumasite.

C1. Theoretical pattern of chloride containing thaumasite

In an attempt to evaluate whether the intrusion of chloride in the thaumasite structure would cause severe changes in the XRD pattern, a simulation was carried out using the software suite *WinXpoe-Theo*. The XRD pattern of the thaumasite in (a) 15%LF immersed in 2%Cl^- after 1 year at 5°C was compared to (b) the starting model taken from Barnett et al. 1999, from which (c) $2Cl^-$ replaced $1CO_3^{2-}$, (d) $2Cl^-$ replaced $1SO_4^{2-}$and (e) $1Cl^-$ and $1Na^+$ entered the unit cell within the interstitial space along *c*, as shown in Fig 6.27. The Ca-Cl bond length was taken from Busin [155] for $CaCl_2$ (2.71Å).

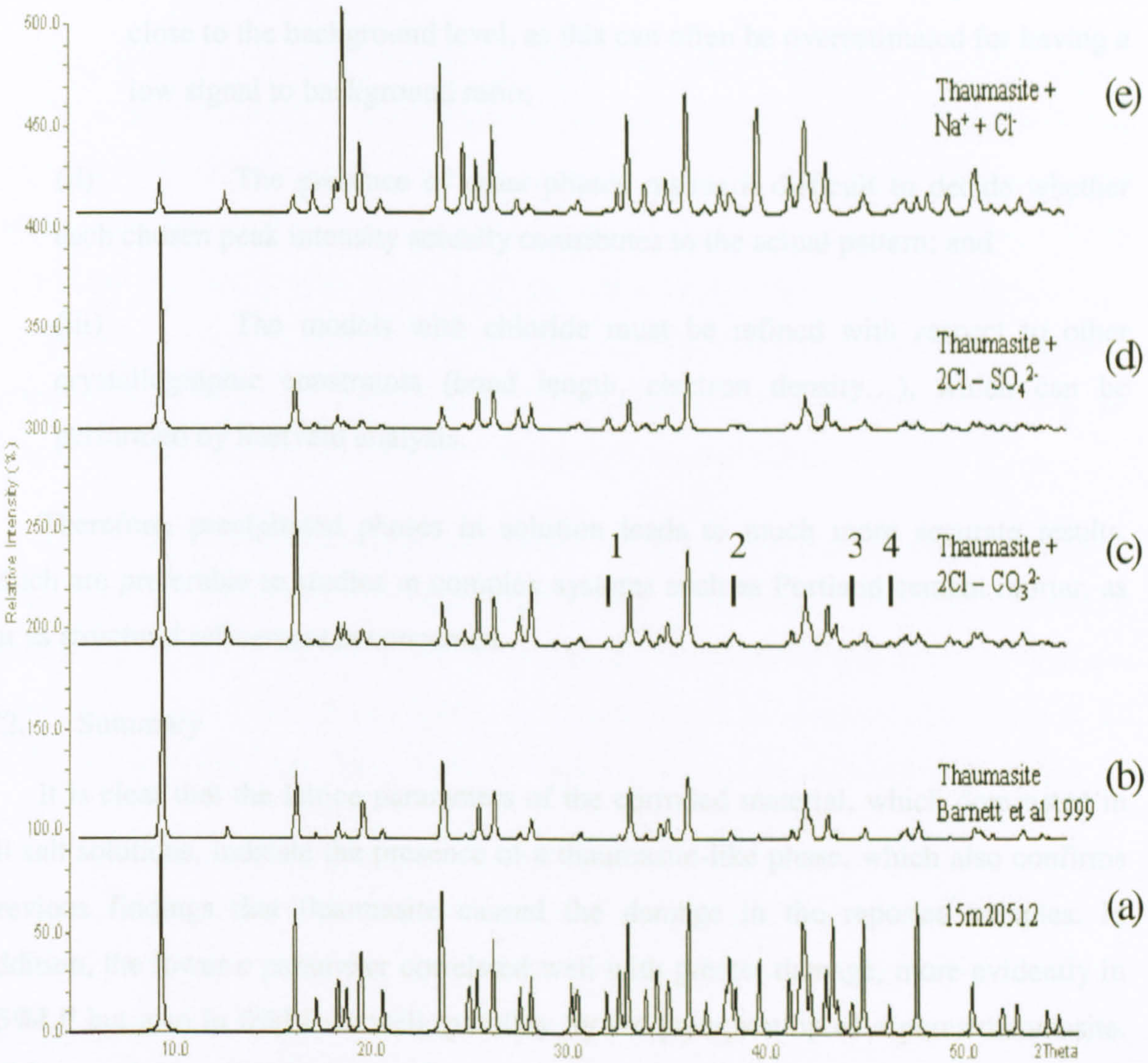

Figure 6.26: Comparison between 15%LF in 2.0%Cl^- and some theoretical patterns

It can be seen that the XRD pattern of the sample shown in Figure 6.26 (a) has similarities to the theoretical pattern (curve b) proposed by Barnett et al. [65]. The region around 31.8° (c1), 36.8° (c2), 44.16 ° (c3) and 46° (c4) 2theta, may suggest possible similarities between the sample and the pattern where Cl^- replaced carbonates (curve c) or sulfate (curve d), at a lesser extent. The hypothesis that sodium and chloride enter into the thaumasite structure (curve e) seems unlikely, since the pattern would be severely distorted, possibly because the presence of sodium would affect the stability of the column by the replacement of calcium by Na^+.

Nonetheless, it was not possible to obtain a precise analysis of intensities and, therefore, an accurate distinction of such hypothetical replacements, since:

(i) It is difficult to estimate the actual intensities of weak peaks that are close to the background level, as this can often be overestimated for having a low signal to background ratio;

(ii) The presence of other phases makes it difficult to decide whether each chosen peak intensity actually contributes to the actual pattern; and

(iii) The models with chloride must be refined with respect to other crystallographic constraints (bond length, electron density...), which can be performed by Rietveld analysis.

Therefore, precipitated phases in solution leads to much more accurate results, which are preferable to studies in complex systems such as Portland cement mortar, as far as structural refinement is concerned.

C2. Summary

It is clear that the lattice parameters of the corroded material, which dominated in all salt solutions, indicate the presence of a thaumasite-like phase, which also confirms previous findings that thaumasite caused the damage in the reported samples. In addition, the lower *c* parameter correlated well with greater damage, more evidently in 15%LF but also in 0%LF as well, possibly by the precipitation of a purer thaumasite. With regards to chloride interacting within thaumasite crystal structure, Cl/Ca ratios were very low (< 0.089), and ratios around 0.33 were not observed in any x-ray analysis of any sample. However, it is important to underline that x-ray microanalysis resolution cannot resolve features smaller than 5μm with the set up used in these analyses. Once more, the simulation of the diffraction pattern also seems to support the view that chloride possibly does not enter into solid solution with thaumasite, but very small amounts of replacement cannot be totally ruled out at this stage.

D. Infrared Spectroscopy (IRS)

Evidently, it is not the uptake of carbonates but the decalcification and the release of Si^{4+} from CSH, which is responsible for most of the structural properties of concrete that makes thaumasite so detrimental to Portland cement concretes. However, the presence of carbonates in the crystal structure of thaumasite facilitates the increase in the coordination of Si from 4 to 6, as postulated by the charge dislocation theory in Bensted [84], in which carbonates can spread the charges on the hydroxyl groups to accommodate the higher coordination of Si. Therefore, it is important to assess the amount of silicon and its correlation with chloride concentration.

It is widely accepted that the contribution to the IRS wave band $500cm^{-1}$, which is exclusively due to octahedral Si, is an excellent way to differentiate between thaumasite and ettringite [10]. Moreover, it can be also used to evaluate the degree of purity of the thaumasite composition, which seems to tolerate small amounts of aluminium in its crystal structure [62], and also to estimate the level of solid solution in both minerals.

Studies in Cl^- bearing phases are usually performed using far infrared spectroscopy (IRS) technique, since most chloride vibrational bands occur below $200\ cm^{-1}$, which is the reason why NaCl discs are also used as transparent material when using the Nujol technique in MID IRS (Perkin-Elmer Manual). However, it has been reported that molecules such as ClO_4^-, hydrotalcite and $AlCl_3$ show peaks around $594\text{-}635cm^{-1}$ [156]. Therefore, although it is not possible to identify whether Cl^- enters into thaumasite using IRS, an attempt was made to evaluate whether the presence of Cl^- affects the composition of thaumasite with respect to both the net Si peak intensity and calculated moles of Si.

1 Net intensity of $Si(OH)_6$ peak($^{Net}Si_{500}$):

The maximum intensity was calculated automatically by the built in software of IRS system (*Spectrum*), which consists of the vertical height between the lowest point of the peak and the tangent line connecting the offsets of the peak $855cm^{-1}$ and $500cm^{-1}$ for Al-O-H and Si-O-H, respectively as shown in Figures 6.27 to 6.32.

2 Moles of $Si(OH)_6$

It is reported that the ettringite-thaumasite solid-solution tolerates at maximum 2 moles of either Si or Al, as in formulae 6.6 [62].

$$Ca_6[(Si,Al).(OH)_6]_2.(CO_3)_2.(SO_4)_2.24H_2O \qquad (6.6)$$

Hence, the number of moles of Si can be estimated based on the Equation 6.7, where Si_{500} and Al_{855} correspond to the net intensity of the referred atom and wave band, respectively, as tabulated in table 6.3.

$$\begin{cases} \text{Si} + \text{Al} = 2 \quad \text{(i)} \\ \dfrac{Si}{Al} = X \qquad \text{(ii)} \Rightarrow \text{Al} = \dfrac{Si}{X} \text{ in (i): } \text{Si} + \dfrac{Si}{X} = 2 \Rightarrow \text{XSi} + \text{Si} = 2\text{X} \Rightarrow \text{Si} = \dfrac{2X}{1+X} \end{cases}$$

$$Si_{moles} = \frac{2(Si_{500}/Al_{855})}{1+(Si_{500}/Al_{855})} \text{ ; and } \text{Al}_{moles} = \text{Si}_{moles} - 2 \qquad (6.7)$$

The reason for the use of both approaches is because the assumption that the number of moles of Si and Al will not exceed two within the corroded material may not be true in complex systems such as those studied in this research, because the Al-O-H vibrational wave band can also be shared by other possible coexisting phases such as ettringite, Friedel's salt and hydrogarnet, in which case the value of Si_{molcs} would be underestimated.

Fig. 6.33 and 6.34 show the profile for octahedron Si as net intensity and moles at 5°C, respectively, whose values were taken from Table 6.5.

$Si(OH)_6$

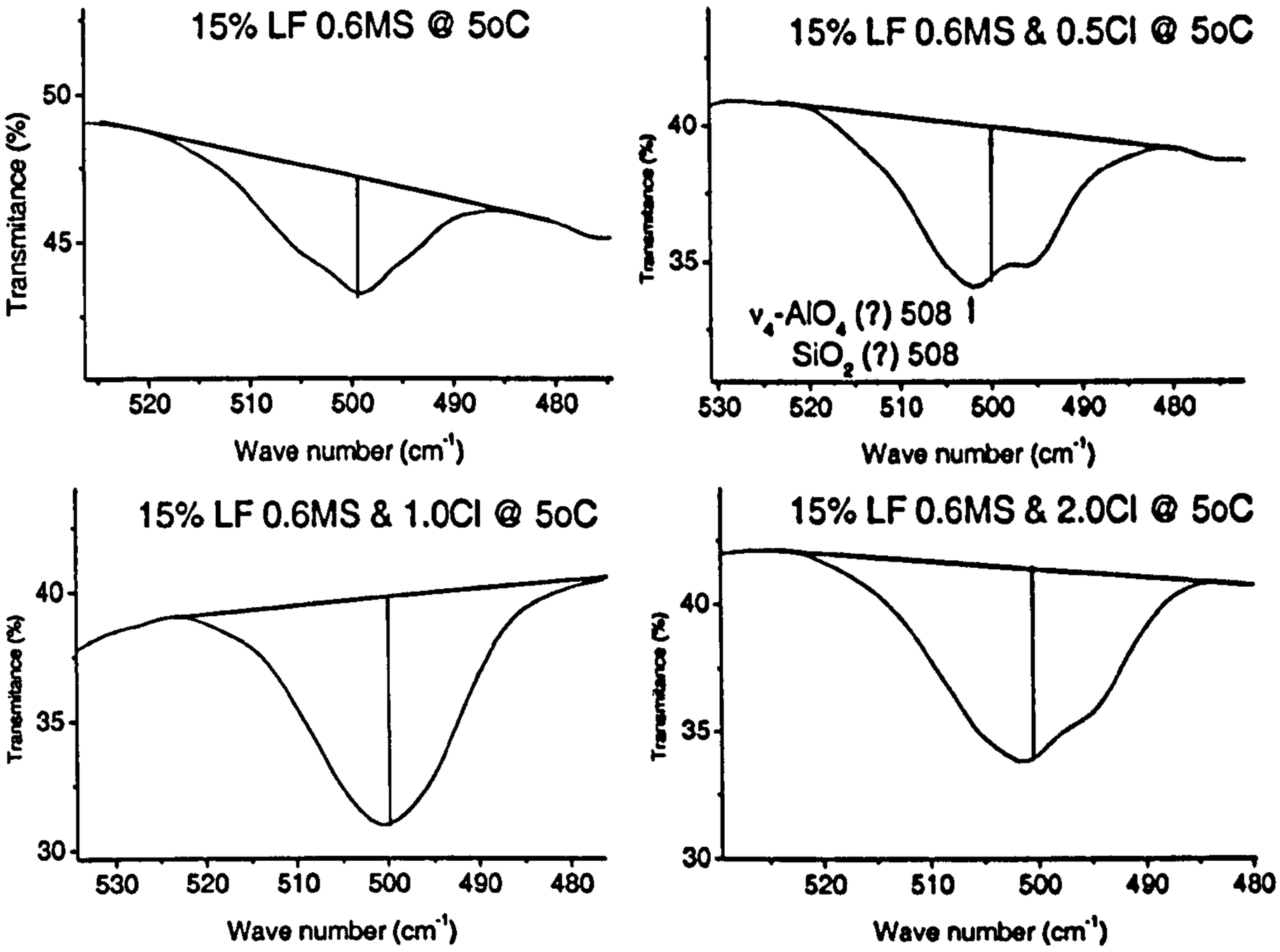

Figure 6.27: IR wave band of 6-coordinated Si in 15%LF after 12 months at 5°C

$Al(OH)_6$

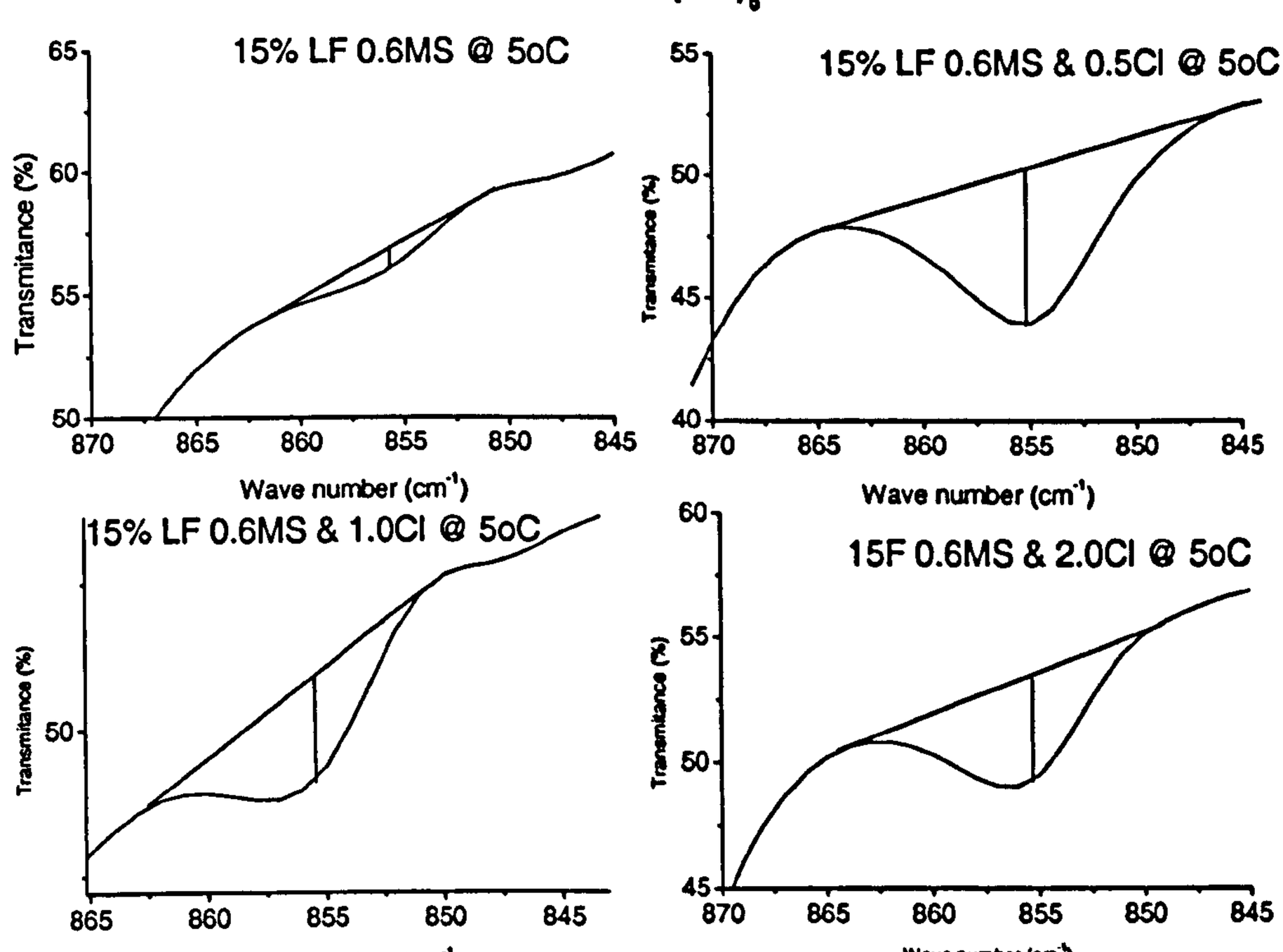

Figure 6.28: IR wave band of 6-coordinated Aluminium in 15% LF after 12 months at 5°C

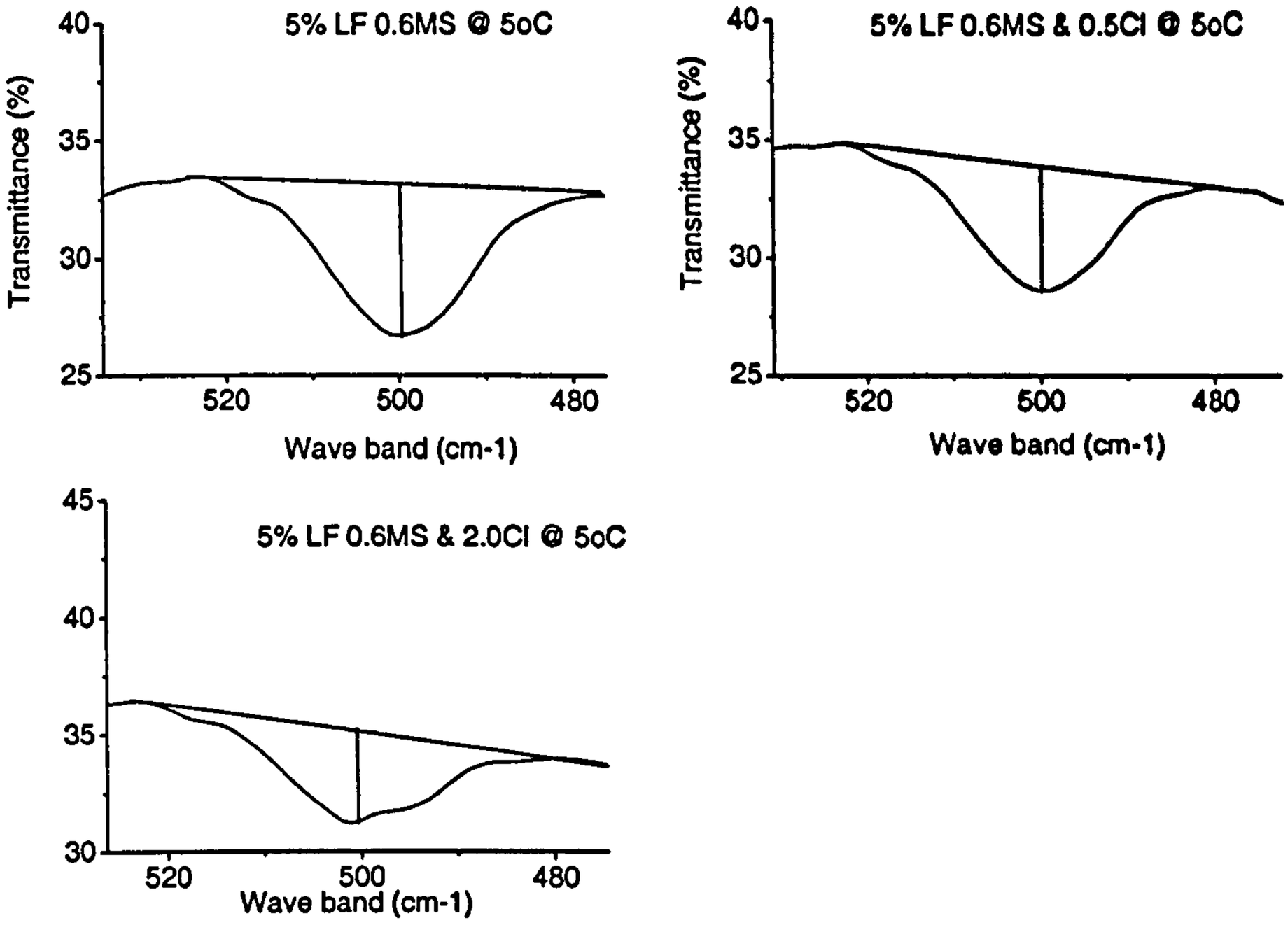

Figure 6.29: IR wave band of 6-coordinated Si in 5%LF after 12 months at 5°C

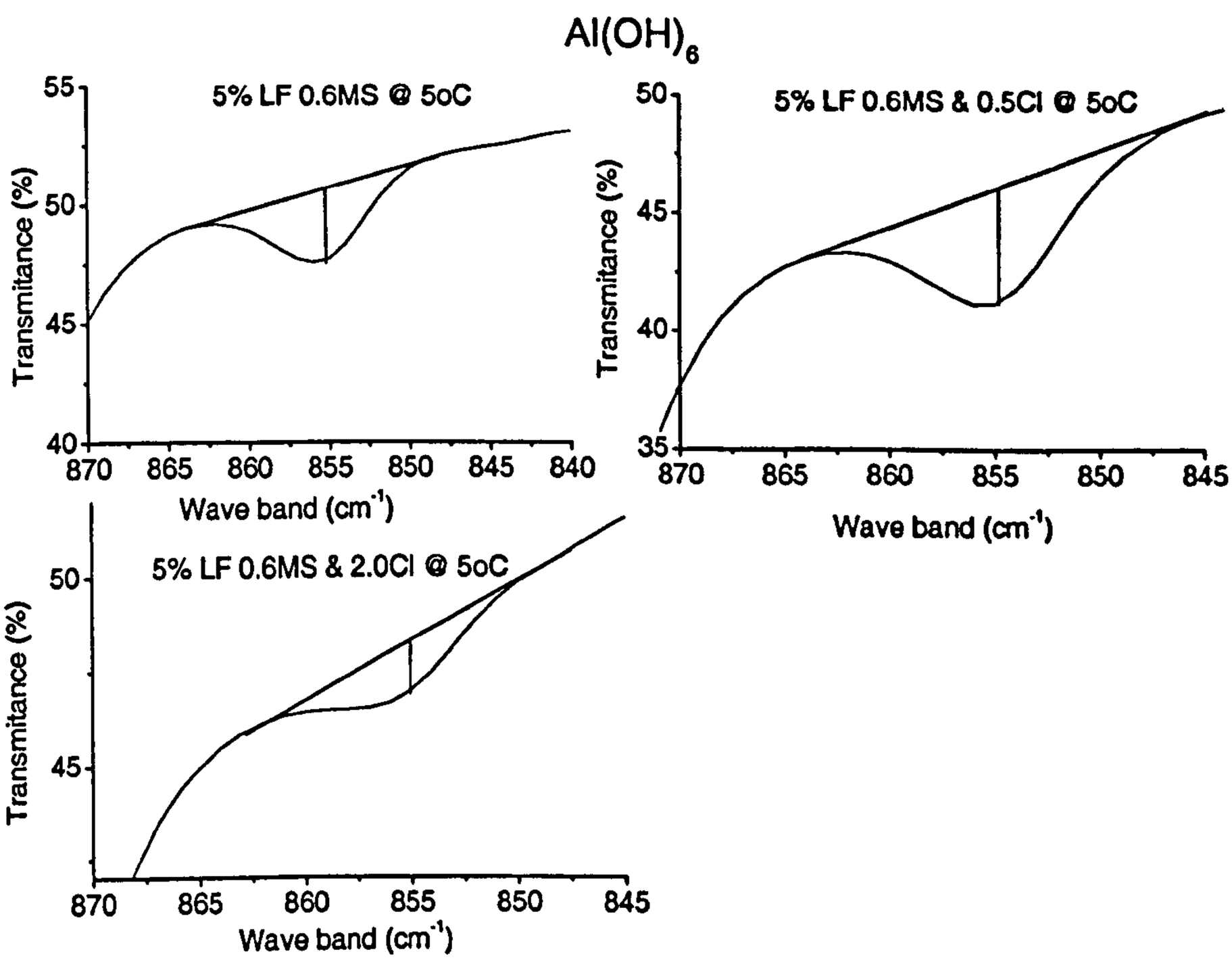

Figure 6.30: IR wave band of 6-coordinated Aluminium in 5% LF after 12 months at 5°C

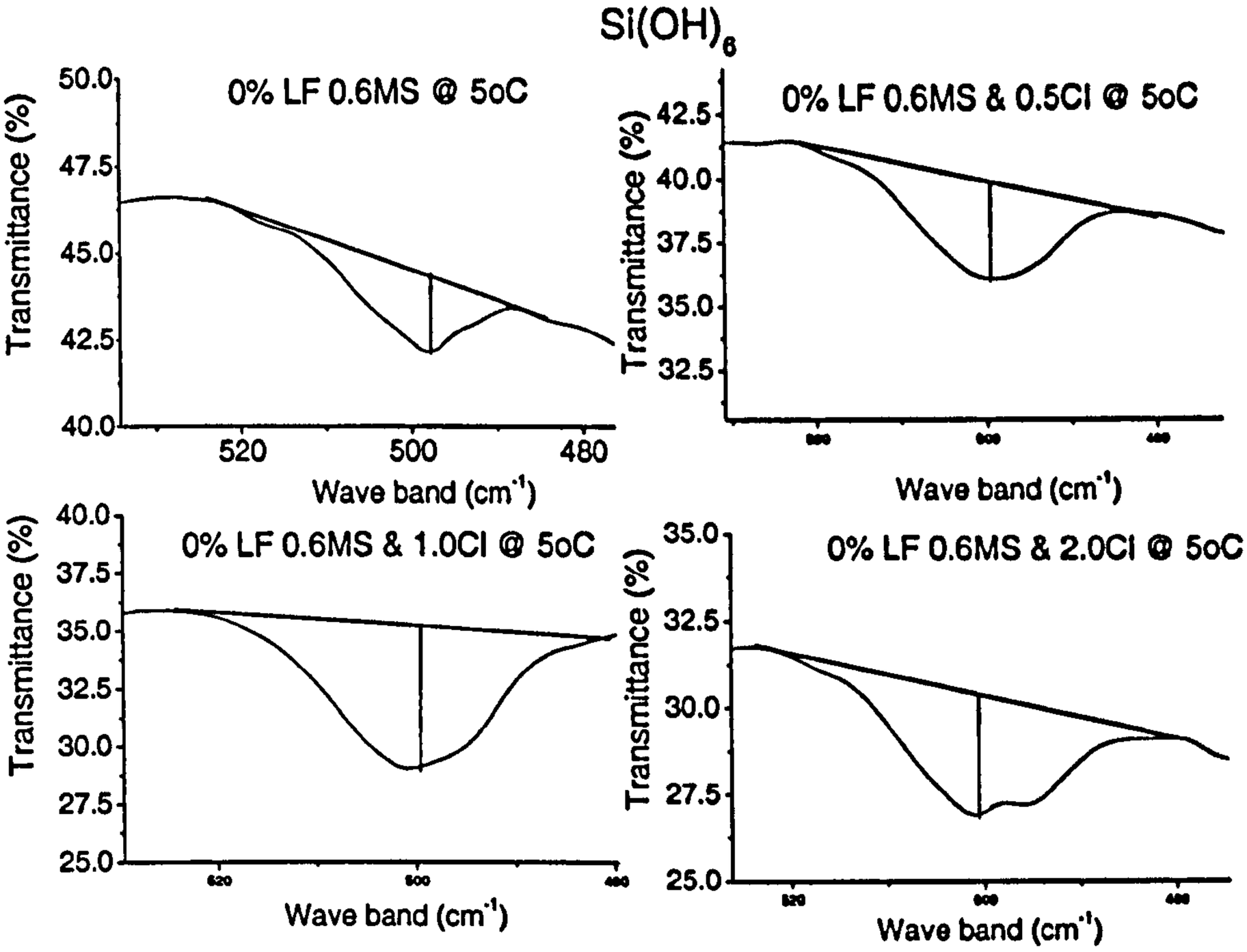

Figure 6.31: IR wave band of 6-coordinated Si in 0%LF after 12 months at 5°C

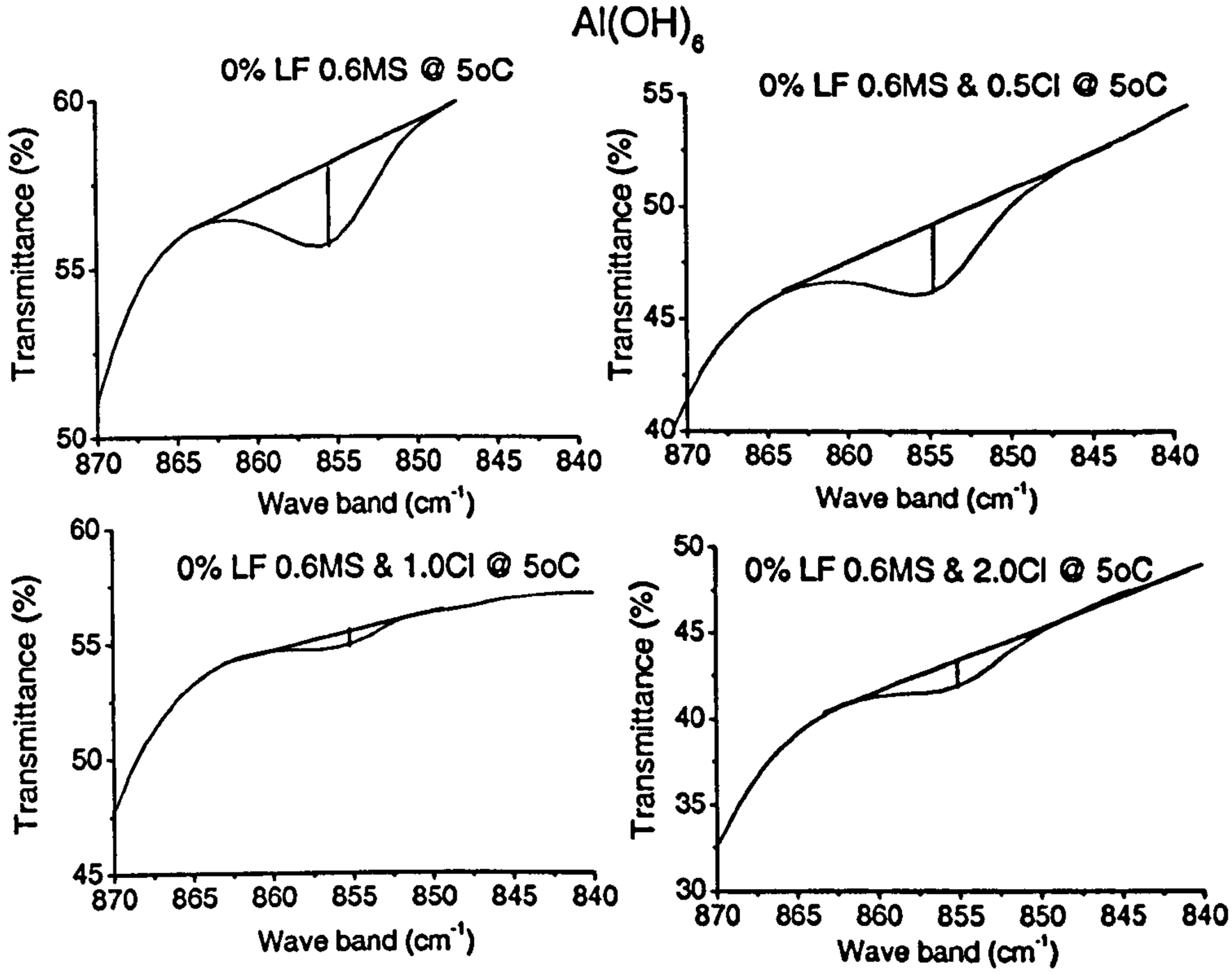

Figure 6.32: IR wave band of 6-coordinated Aluminium in 0% LF after 12 months at 5°C

Table 6-3: Net intensities and calculated moles of Si and Al in samples with and without limestone filler after 12 months at 5°C

	Age (Months)	Temp. (oC)	Cc (%)	Cl (%)	Si_{500} (%)	Al_{855} (%)	Al (moles)	Si (moles)
0m5	12	5	0	0.0	1.97	2.42	1.10	0.90
0m55	12	5	0	0.5	3.43	2.90	0.92	1.08
0m105	12	5	0	1.0	6.30	0.64	0.18	1.82
0m205	12	5	0	2.0	3.25	1.55	0.65	1.35
5m5	12	5	5	0.0	6.30	3.00	0.65	1.35
5m55	12	5	5	0.5	5.19	4.63	0.94	1.06
5m205	12	5	5	2.0	3.78	1.38	0.53	1.47
15m5	12	5	15	0.0	8.79	1.75	0.33	1.67
15m55	12	5	15	0.5	5.73	6.17	1.04	0.96
15m105	12	5	15	1.0	7.47	3.42	0.63	1.37
15m205	12	5	15	2.0	3.90	0.67	0.29	1.71

As far as carbonate content is concerned, the intensity of Si_{500} tend to increase as carbonate content increased in both systems with and without chloride, but higher intensity has been observed in the later case. A similar trend was also observed when considering Si_{moles}, but the amounts were less than in the former method and also somewhat inconsistent with respect to 0.5%Cl^- in which silica moles decreased with increasing carbonate content.

With regards to the concentration of chlorides, Si_{500} intensity presented two different patterns, which depended on the presence of carbonate filler and the interval of Cl^- concentration. For 0%LF, increase in Cl^- concentration resulted in an increase in Si_{500} intensity, but samples immersed in 1.0% Cl^- showed the highest value. In carbonate filled samples, Si_{500} decreased as the level of chloride increased, except for 15%LF in 1.0%Cl, in which it was higher than both 0.5 and 2.0%Cl^-.

When considering Si_{moles}, increase in Cl^- concentration was not linear in carbonate filled mixes so that there was a minimum around 0.5%Cl^-, followed by an increase at 2.0%Cl^-, which presented a slightly higher value than pure sulfate solution in both 5 and 15%LF. As for 0%LF, Si_{mole} increased with Cl^- concentration, particularly for 1.0%Cl^-. The values of Si_{moles} at 5°C were always greater than 0.9.

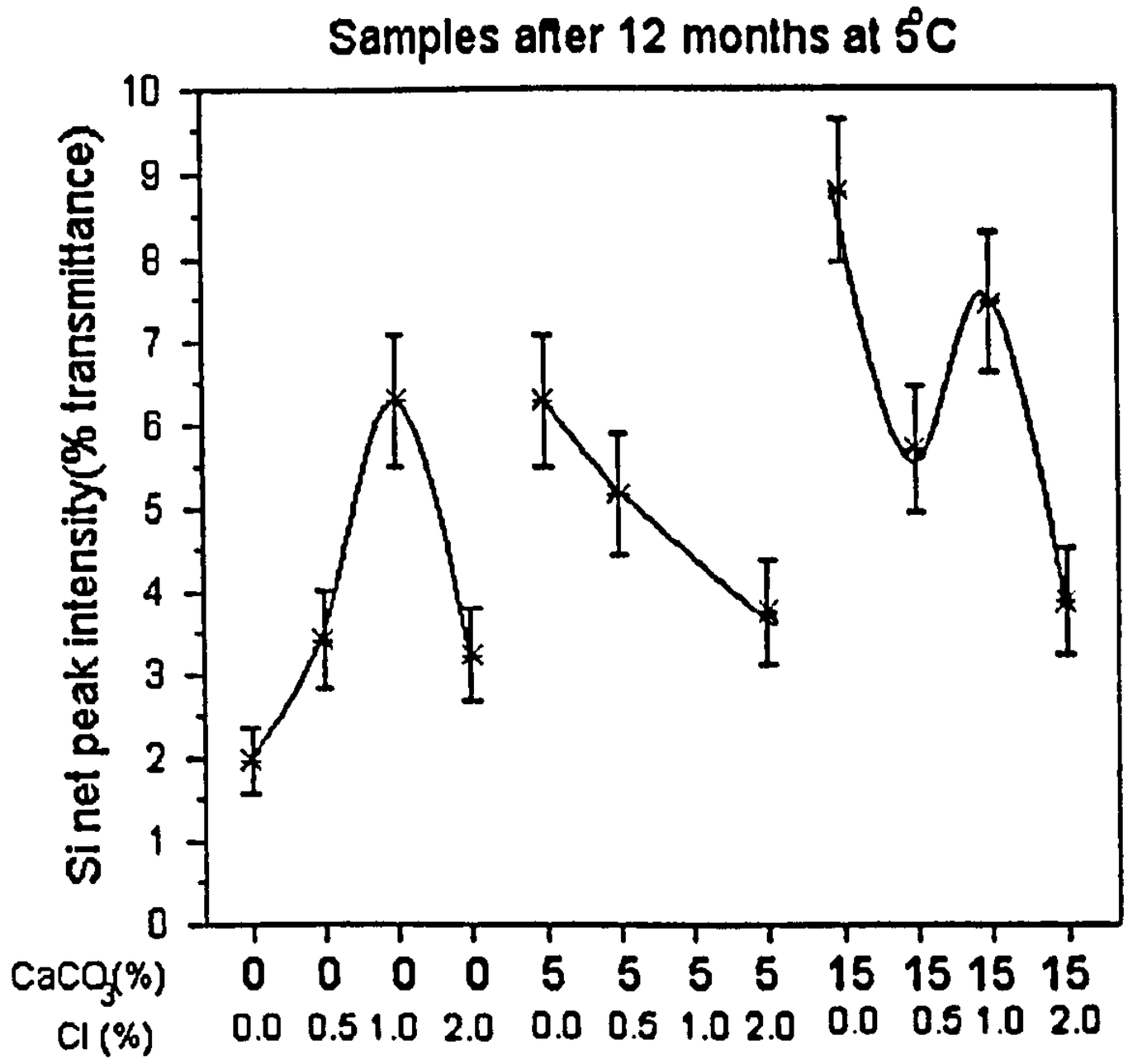

Figure 6.33: IR net intensity of $Si(OH)_6$ in samples with and without limestone filler after 1 year at 5°C.

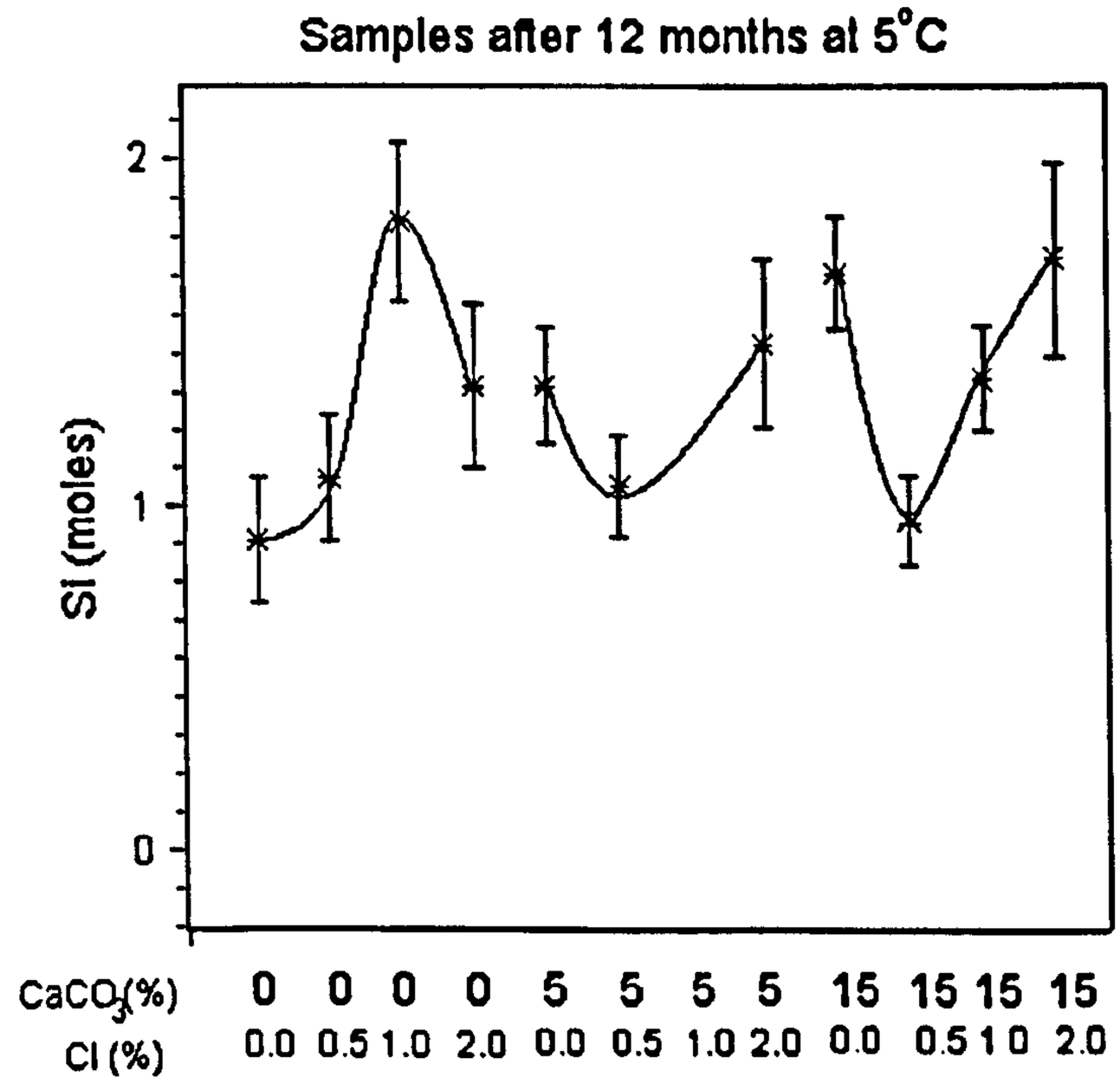

Figure 6.34: Moles of $Si(OH)_6$ in samples with and without limestone filler after 1 year at 5°C.

Although the magnitude of the errors in both approaches do not allow a precise quantification of the role of chloride in the composition of thaumasite, it is observed that the non-linearity of the trends with respect to chloride, carbonate concentrations and Si (specially in Si_{moles}) correlate to some extent (R^2=0.79) with the pattern observed in mass change of the cubes in chapter 5 (see Figure 6.35 and compare with Fig 5.18). It can be seen that higher content of octahedral Si moles indicates that the system suffered greater attack of the matrix by thaumasite, hence, suffering greater damage that

is confirmed by greater mass loss. It is still not very clear why the net intensity of Si peak gave very poor correlation (R^2~0.27).

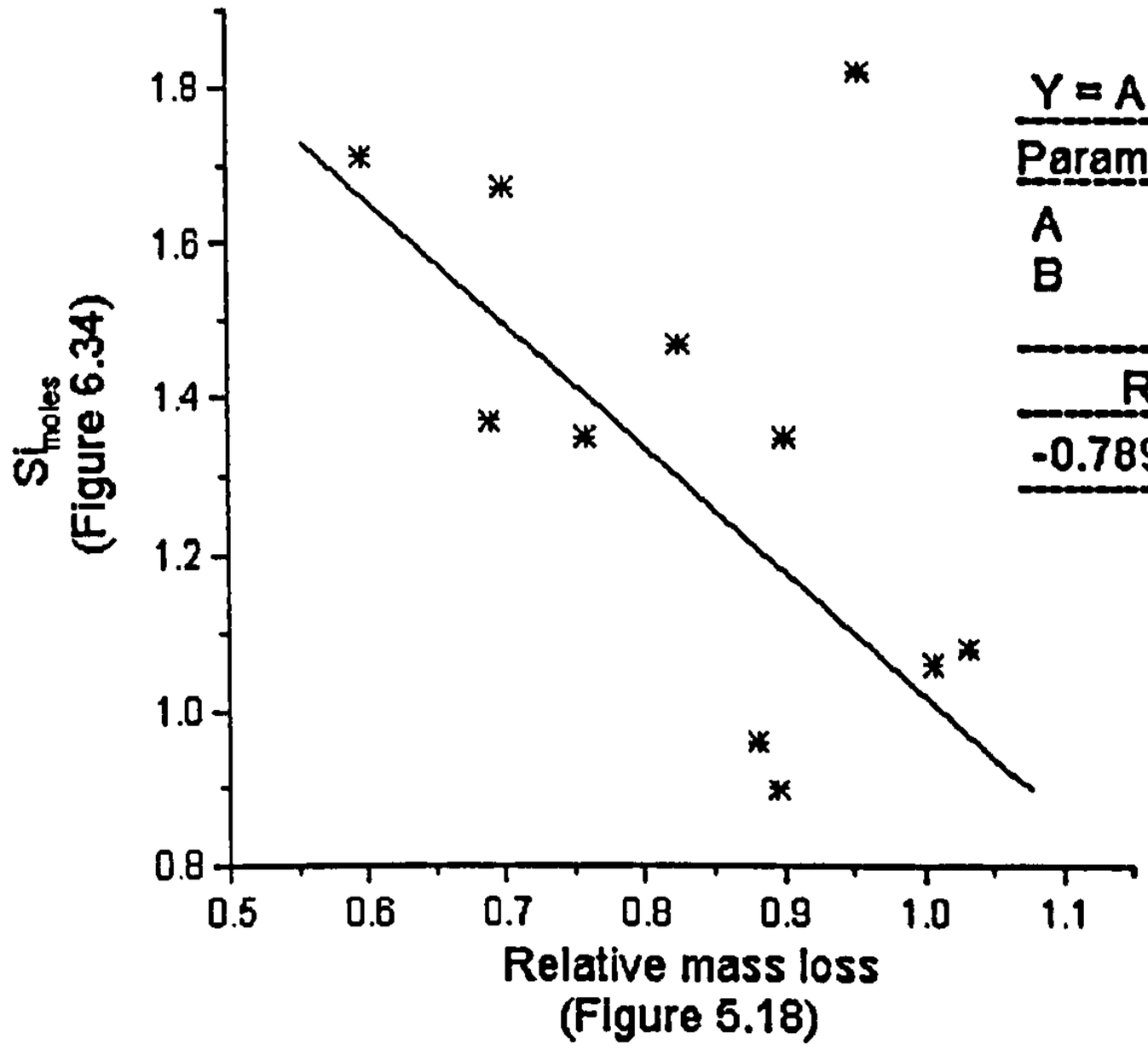

Y = A + B * X

Parameter	Value	Error
A	2.60211	0.36425
B	-1.58058	0.43377

R	SD	N	P
-0.78994	0.18456	10	0.00655

Figure 6.35: Linear regression of octahedral Si moles and relative mass loss.

It is important to underline that octahedral silicon has also been identified in several mixes and solutions at 20°C, especially in 0% and 15%LF immersed in pure magnesium and combined with 2.0%Cl^-. However, the low intensity of Si_{500} and the coexistence of AFt, AFm and thaumasite solid solution did not allow a precise interpretation of the data. However, a high intensity of Si^{4+} associated in an octahedral coordination with hydroxyls also correlated well with the damage detected in 0%LF immersed in 2.0%Cl^- (see Fig 5.6 and Fig. 5.9-Chapter 5).

E. Summary

The effect of chlorides on the composition of thaumasite has been investigated by means of EDX, x-ray microanalysis, lattice parameters and infrared spectroscopy. Although the data suggest that Cl^- affected the composition of thaumasite, it appears that it does not interact within the crystal structure, since:

(i) No significant amount of chloride was detected by EDX;

(ii) X-ray microanalysis showed significantly low Cl/Ca ratio, definitely below 0.33 value expected for 1 Cl^- entering the unit cell;

(iii) Since a chloride ionic radius is large, the fact that all unit cell parameters comfortably fell within the thaumasite group indicates that chloride does not appear to enter into the thaumasite crystal structure. This has also been suggested by the smaller *c* unit cell parameter and the modelled XRD pattern of 15% limestone containing mortar sample; and

(iv) Despite the inability of mid IRS to detect chloride peaks, both net octahedral and moles of silicon data indicate that chloride affects the composition of thaumasite, in which the amount of octahedral Si moles appears to increase with chloride concentration, hence, increasing the purity of the thaumasite solid solution and ultimately inflicting greater damage to the samples (see Fig 6.35).

Therefore, chloride seems to play a catalytic role in where the higher solubility of carbonates increase the chances of thaumasite formation in a purer type of solid solution. This suggests that the chloride binding capacity of the cement is altered as the TSA affects the matrix.

6.3.3 Chloride binding capacity of Portland cement mortar containing limestone filler in salt solutions

The chloride binding capacity of 15% limestone containing cement mortar has been investigated by quantitative x-ray microanalysis, in which 16 spot analysis were carried out in the core as well as at the surface. In order to determine the Al/Ca and Si/Ca atomic ratios and the binding capacity of the cement matrix, as well as the distribution of other species such as magnesium and sodium, areas that contained remaining cement grains, silicon aggregate particles, large hydrated phases and the dark grey bands of thaumasite were avoided.

A. 15% limestone filler in 0.60% SO_4^{2-} at 5°C

Fig. 6.36 shows the chemical composition of the CSH at the surface and core. It can be seen that whereas the matrix of a mixture of calcium hydroxide, CSH gel and ettringite at the core, as expected in a conventional sulfate attack. The composition of few points shifted towards a line parallel with the ettringite-thaumasite solid solution line. The composition of the matrix at the surface showed a rather different profile. Indeed, instead of an expected decalcification as in classical magnesium sulfate attack, the CSH gel composition fell in a line parallel to the ettringite-thaumasite solid solution

line, and also parallel to the CSH-thaumasite line (c). Because both calcium and silicon participates in the formation of thaumasite, this observation indicates that not only does CSH gel release both ions, line (a), but also that some aluminium derived from a possible dissolution of ettringite precipitated within the gel (b). The highest Al/Ca point possibly indicates that hydrogarnet was also mixed within the matrix.

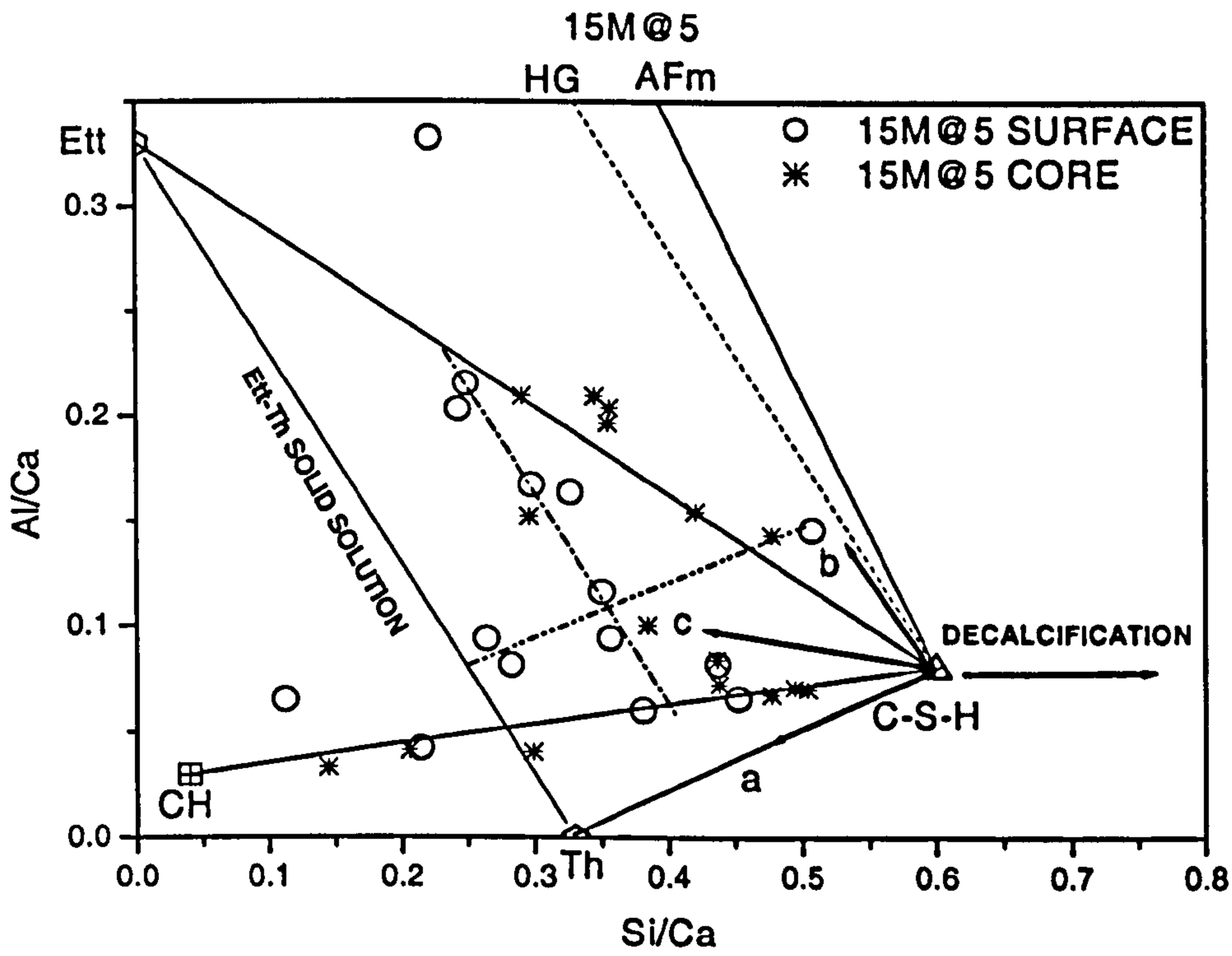

Figure 6.36: Al and Si atomic ratio plot of cement matrix in 15%LF in $MgSO_4$ at 5°C after 1 year.

It can be seen in Fig 6.37 that the matrix composition in the core fell along the CSH-AFm line. However, it appears that some sulfate was more distributed within CSH gel and some points fell below AFm-origin line, which could possibly indicate that some of the aluminates have precipitated as a result of the conversion of ettringite into hydrogarnet, $Ca_3[Al(OH)_6]_2$, which also seems to confirm that ettringites role in thaumasite formation is more likely to occur via a through solution mechanism [63][11]. At the surface, the matrix composition is, however, different from that at the core, as expected in sulfate-attacked areas, in a sense that the distribution of sulfates is rather scattered within AFt-AFm lines. Indeed, AFm converts into AFt in the presence of sulfates. Nevertheless, it is possible to identify that sulfates agglomerated within three main groups:

(i) Low Al/Ca<0.1, which is also possibly attributed to combined thaumasite and CSH;

(ii) Around 0.15<Al/Ca<0.22, that could be assigned to some sort of ettringite solid solution; and

(iii) Perhaps hydrogarnet (HG), as a result of the disruption of ettringite, as discussed earlier.

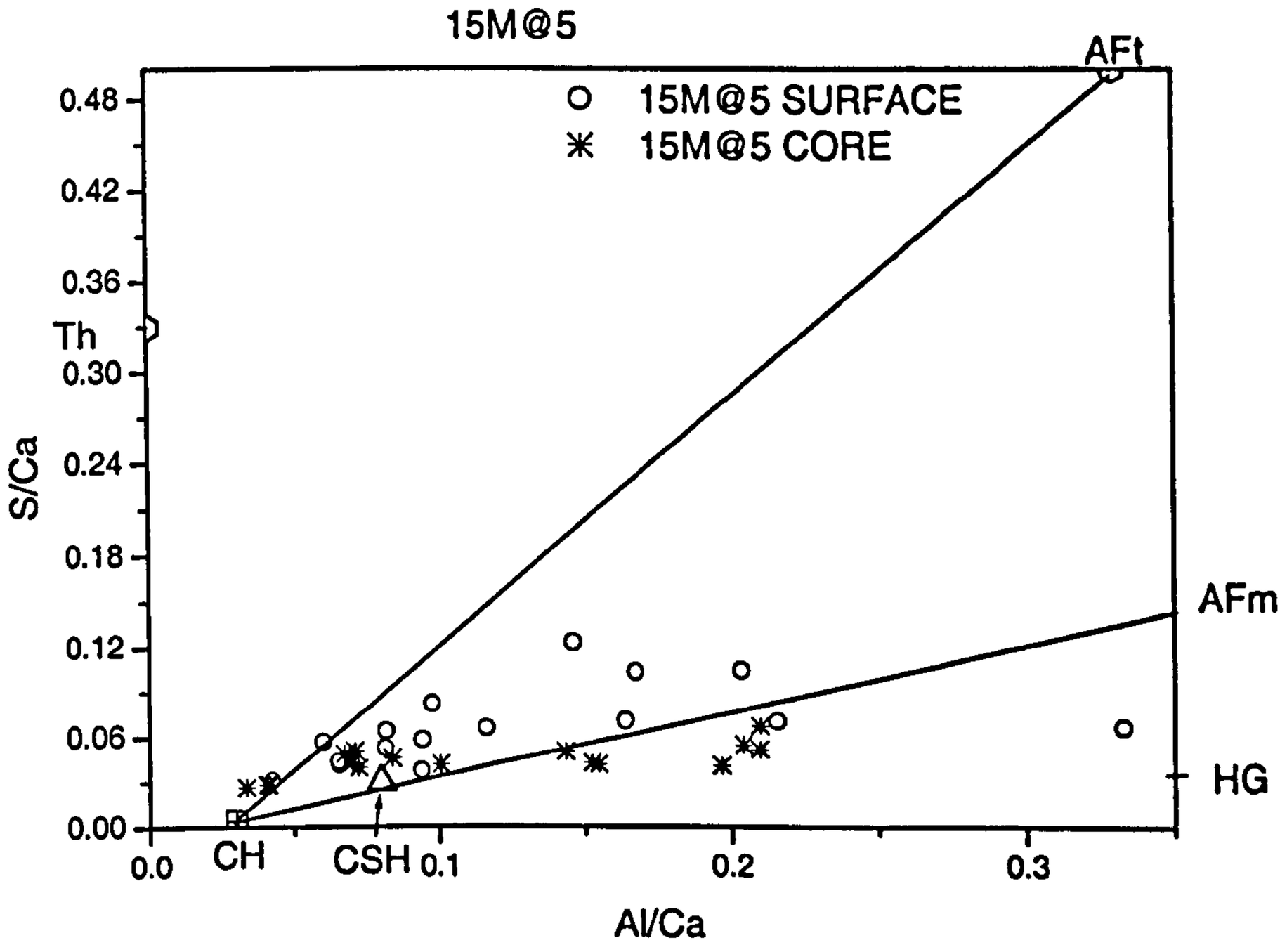

Figure 6.37: : S and Al atomic ratio plot of cement matrix in 15%LF in $MgSO_4$ at 5°C after 1 year

B. 15% limestone filler in 0.6% SO_4 and 0.5 %Cl^- at 5°C

The chemical composition of the matrix 15%LF immersed in combined sulfate and 0.5%Cl^- at 5°C after 1 year can be seen in Fig 6.38. Although thaumasite has been found at the surface in similar fashion as in samples in pure sulfate solutions, the composition of the matrix at the surface fell within the CH-CSH line, except in few instances where it seemed to fall parallel to the ettringite-thaumasite and thaumasite-CSH lines. Even though, the cement matrix was less altered than in samples immersed in sulfate solution without added chloride. This is in agreement with less damage which was observed in 0.5% Cl^- (see Fig 5.5 and Fig 5.7-Chapter 5). Indeed, thaumasite was responsible for weakening the aggregate-cement interface that separated from the bulk sample. It is important to underline that although these analyses were taken in damaged areas,

exclusively in the matrix, the main corroded material had detached from the bulk sample and precipitated at the bottom of the container. Analyses of this material by XRD and IRS showed that the main crystalline material was thaumasite.

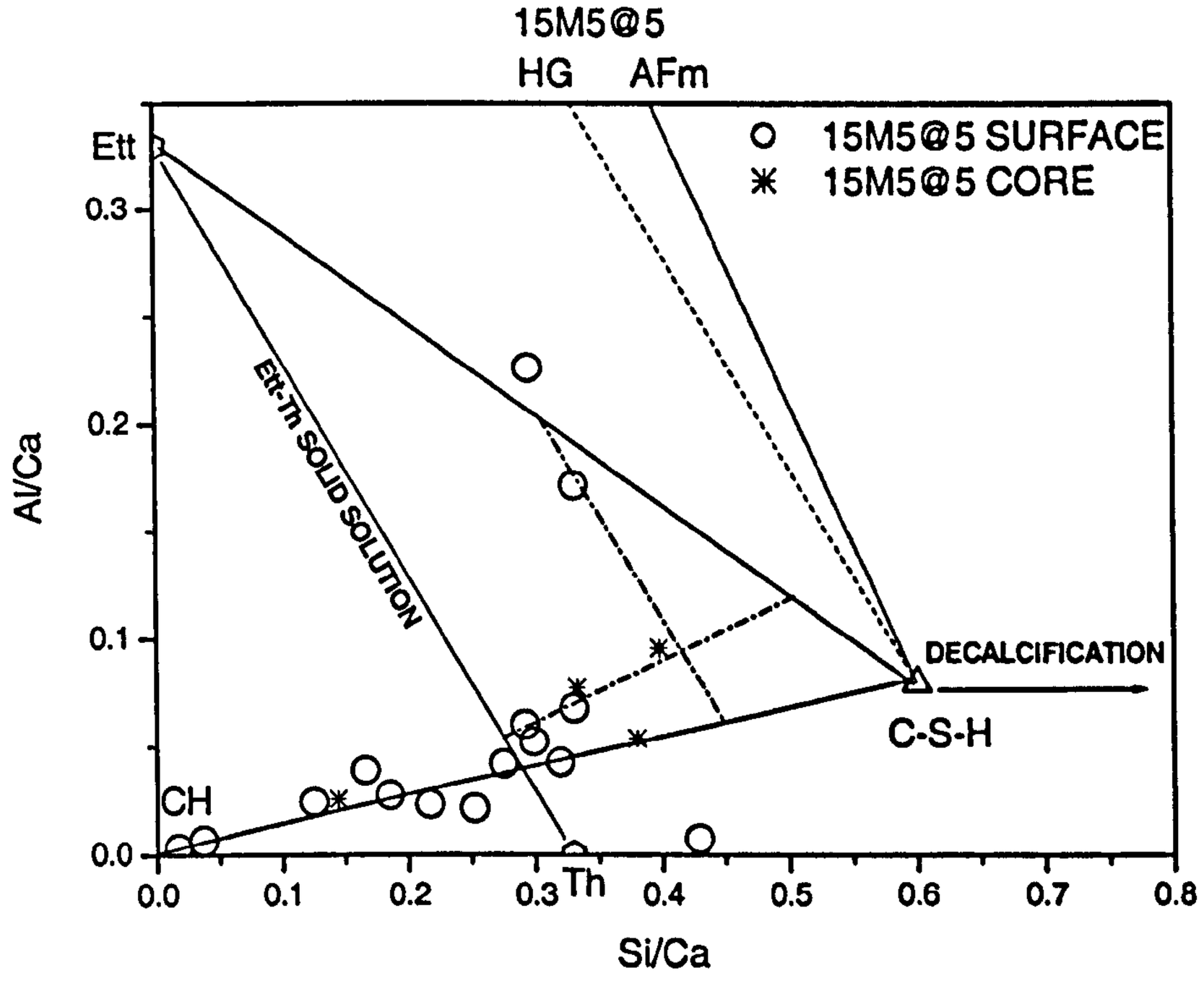

Figure 6.38: Al and Si atomic ratio plot of cement matrix in 15%LF in $MgSO_4$ and 0.5% Cl at 5°C after 1 year.

The sulfate and aluminium atomic plot is shown in Fig 6.39. In the core, the chemical composition points fall close to the CH-CSH-AFm line, as expected for a mixture of conventional hydrate products. Nevertheless, the composition of the corroded material in the surface layer seems more defined than that of samples immersed in pure sulfate solution, because most points fell close to the AFt-origin line, except for two isolated points, which fell between the AFm-AFt lines. When considering that thaumasite is far more aggressive than ettringite, this observation appears to be in agreement with:

(i) Less damage was detected in samples immersed in this solution (*see* Fig 5.5), and

(ii) Less octahedral silicon was detected within the sulfate phase (see Fig 6.33 and Fig 6.34), and

(iii) Less calcium sulfate-bearing phases have been detected by XRD in the bulk sample immersed in this Cl^- concentration, whose peaks could not be positively assigned to either ettringite or thaumasite due to the low intensity to background ratio, and also extreme peak broadening (*see* Fig 5.22).

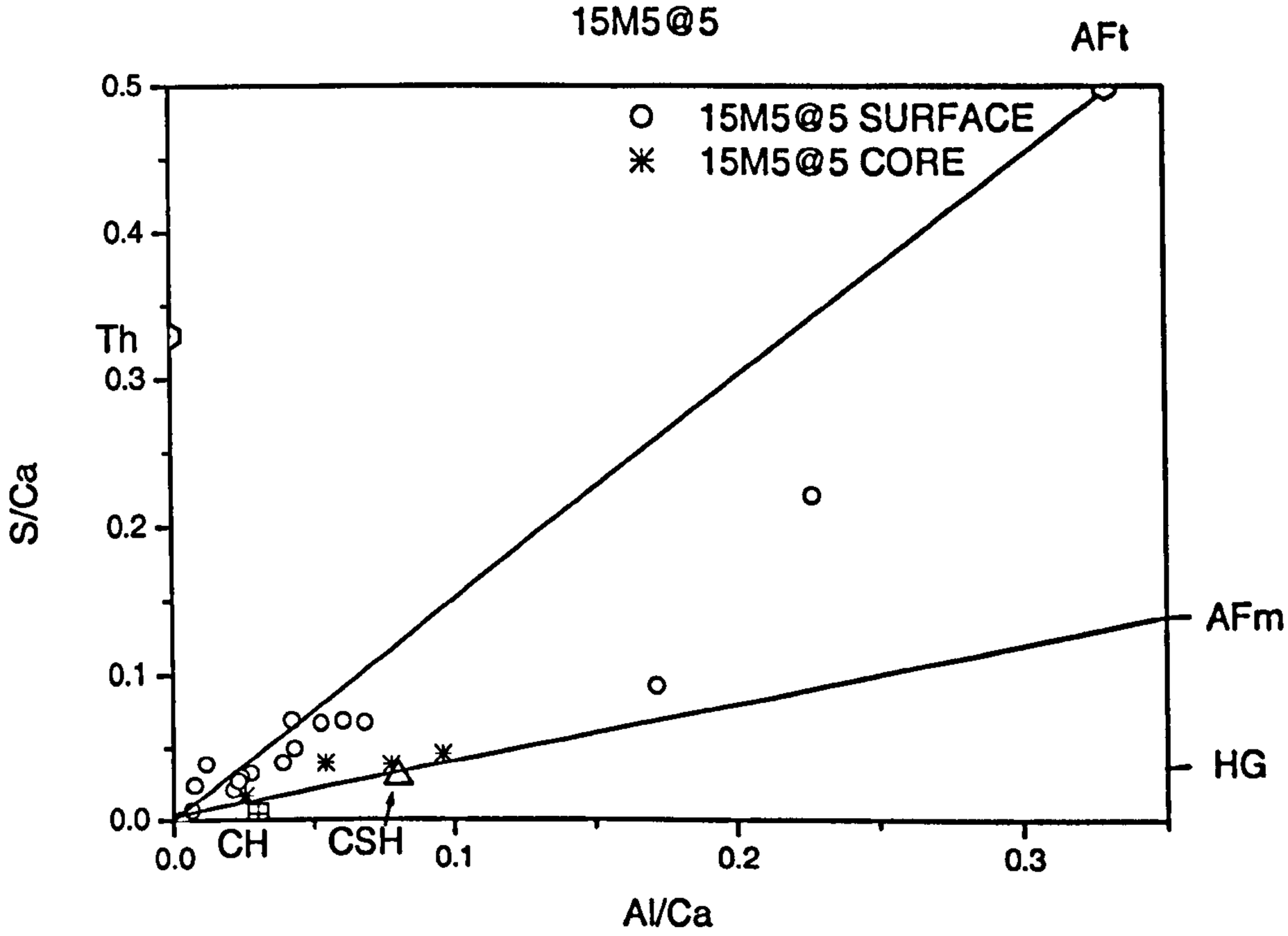

Figure 6.39: S and Al atomic ratio plot of cement matrix in 15%LF in $MgSO_4$ and 0.5% Cl at 5°C after 1 year.

C. 15% limestone filler in 0.60% SO_4 and 1.0% Cl^- at 5°C

Figure 6.40 shows the x-ray microanalysis of the surface and core of 15%LF immersed in sulfate plus 1.0%Cl^- at 5°C after 1 year. It can be seen that both surface and core matrix compositions lay in a more scattered fashion around Si/Ca and Al/Ca ratios of 0.4 and 0.1, respectively. Although no correlation can be precisely drawn due to the intense variation in its composition, it seems that the CSH gel released both calcium and silicon to contribute to thaumasite formation within the gel. Also, aluminium precipitated as an ettringite-solid solution, and two points fell in a line parallel to the hydrogarnet-CSH line, possibly due to the disruption of ettringite, at the surface. Hence, both the core and surface regions suffered more alteration than samples immersed in pure sulfate or combined sulfate with 0.5% Cl^-, which is in agreement with the

observations reported with respect to the visual assessment of the samples as described in the previous chapter in which:

(i) Greater damage was also identified (*see* Fig 5.5);

(ii) A lower lattice parameter of 15%LF samples (*see* Fig 6.24), which is indicative of a purer thaumasite crystal structure, and

(iii) High values of Si have been detected (*see* Fig 6.33 and 6.34).

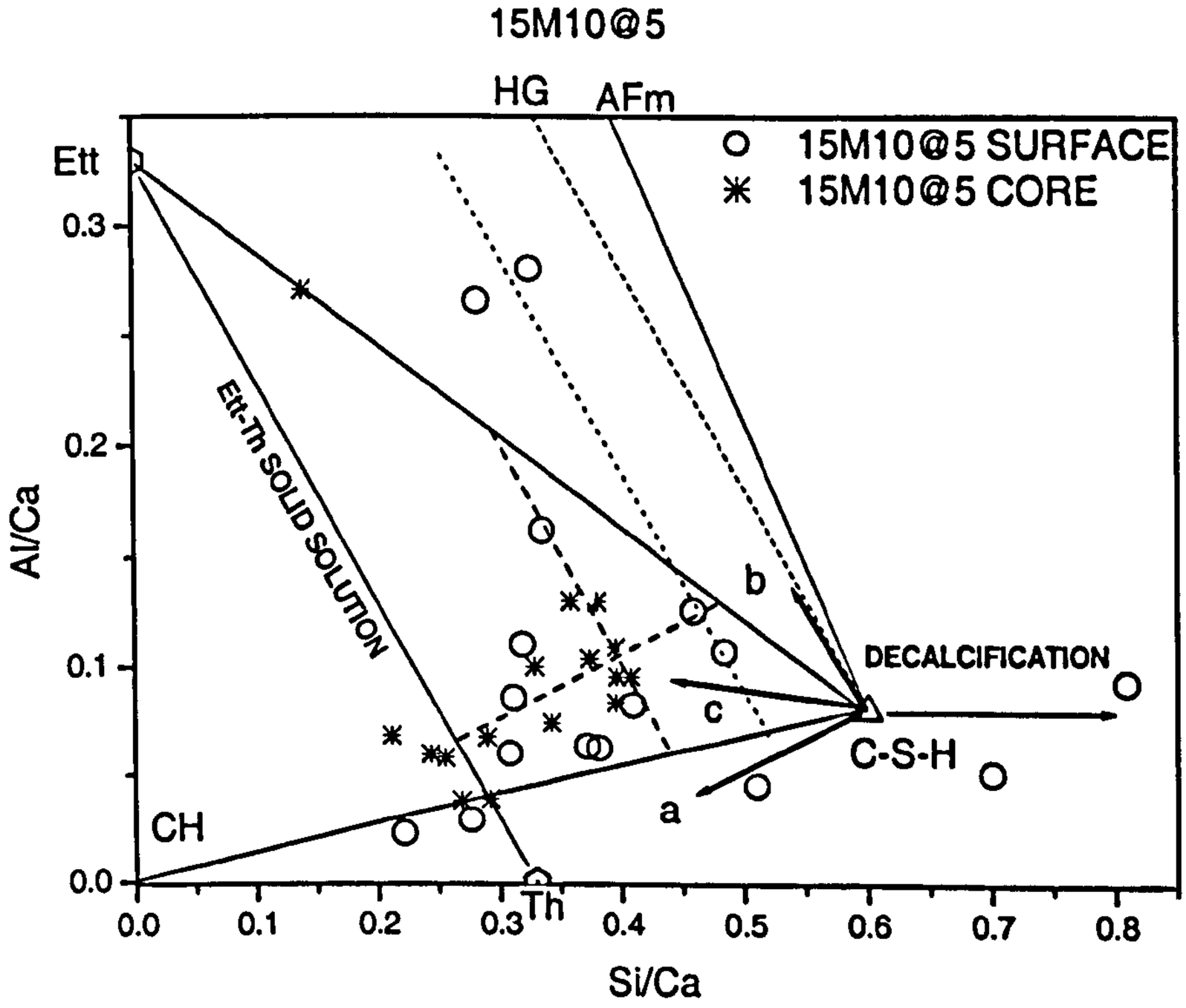

Figure 6.40: Al and Si atomic ratio plot of cement matrix in 15%LF in $MgSO_4$ and 1.0% Cl^- at 5°C after 1 year.

Although the sulfate profile of the matrix in the core seems typical of normal hydration of Portland cement, characterised by a mixture of CH and CSH along the AFm-origin line (however CSH gel suffered alteration in its Si/Ca ratio), the sulfate profile at the surface is much more scattered than in the 15%LF samples immersed in pure sulfate and combined sulfate and chloride solutions at the surface, as can be seen in Fig 6.41. One point fell along the thaumasite-ettringite line. In some instances, the matrix composition appears to be along the hydrogarnet-CSH line, which favours the hypothesis that ettringite has decomposed into hydrogarnet or into thaumasite, as a result of sulfate being released into solution.

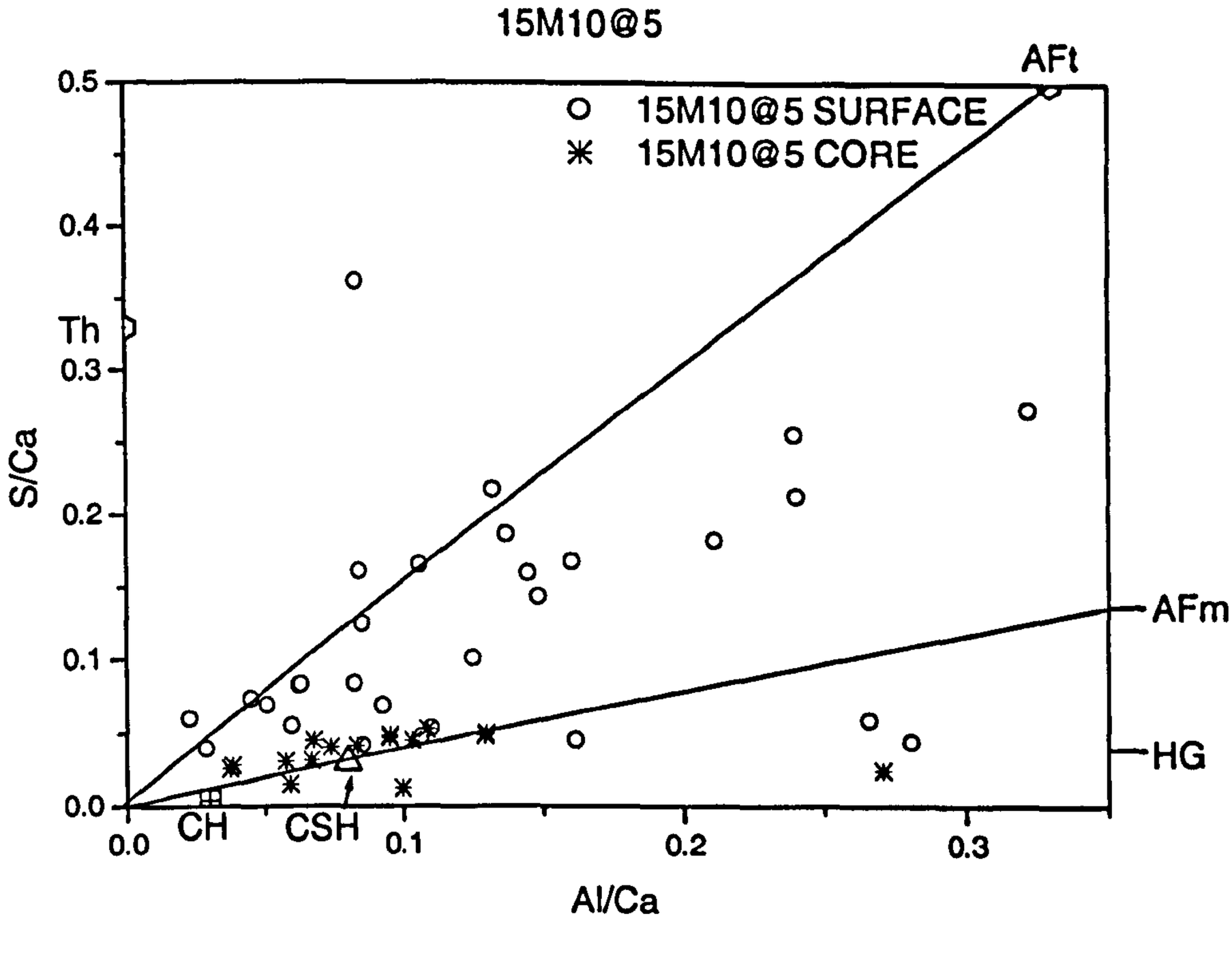

Figure 6.41: S and Al atomic ratio plot of cement matrix in 15LF in $MgSO_4$ and 1.0% Cl^- at 5°C after 1 year.

D. 15% limestone filler in 0.60% SO_4 and 2.0% Cl at 5°C

The Al/Si plot of 15%LF immersed in combined sulfate and 2.0%Cl^- is shown in Fig 6.42. As for samples immersed in 1.0%Cl^-, the matrix composition is scattered around the centre of the plot (Al/Ca~0.1 and Si/Ca~0.4).

At the surface, the matrix composition fell around the line parallel to the ettringite-thaumasite line, and also seems to consist of a mixture of CH, ettringite and CSH gel. An isolated point towards a mixture of CSH and hydrogarnet type of phase was also detected.

In the core, there seems to be a mixture of CH, ettringite, CSH gel, and possibly a mixture of thaumasite or even unhydrated belite. Also, some scattered points within the centre of the plot seem to be along an axis parallel to the ettringite-thaumasite solid

solution line. Considering that simultaneous Si and Ca were removed from CSH, a possible reason why its composition moved towards the centre of ettringite-thaumasite-CSH, the matrix suffered more intense alteration at the surface than at the core, but somewhat less than that observed in samples immersed in combined sulfate and 1.0% Cl^-. Nevertheless, the core also suffered significant alteration when compared to those samples immersed in combined sulfate and 0.5%Cl^- and sulfate alone, respectively.

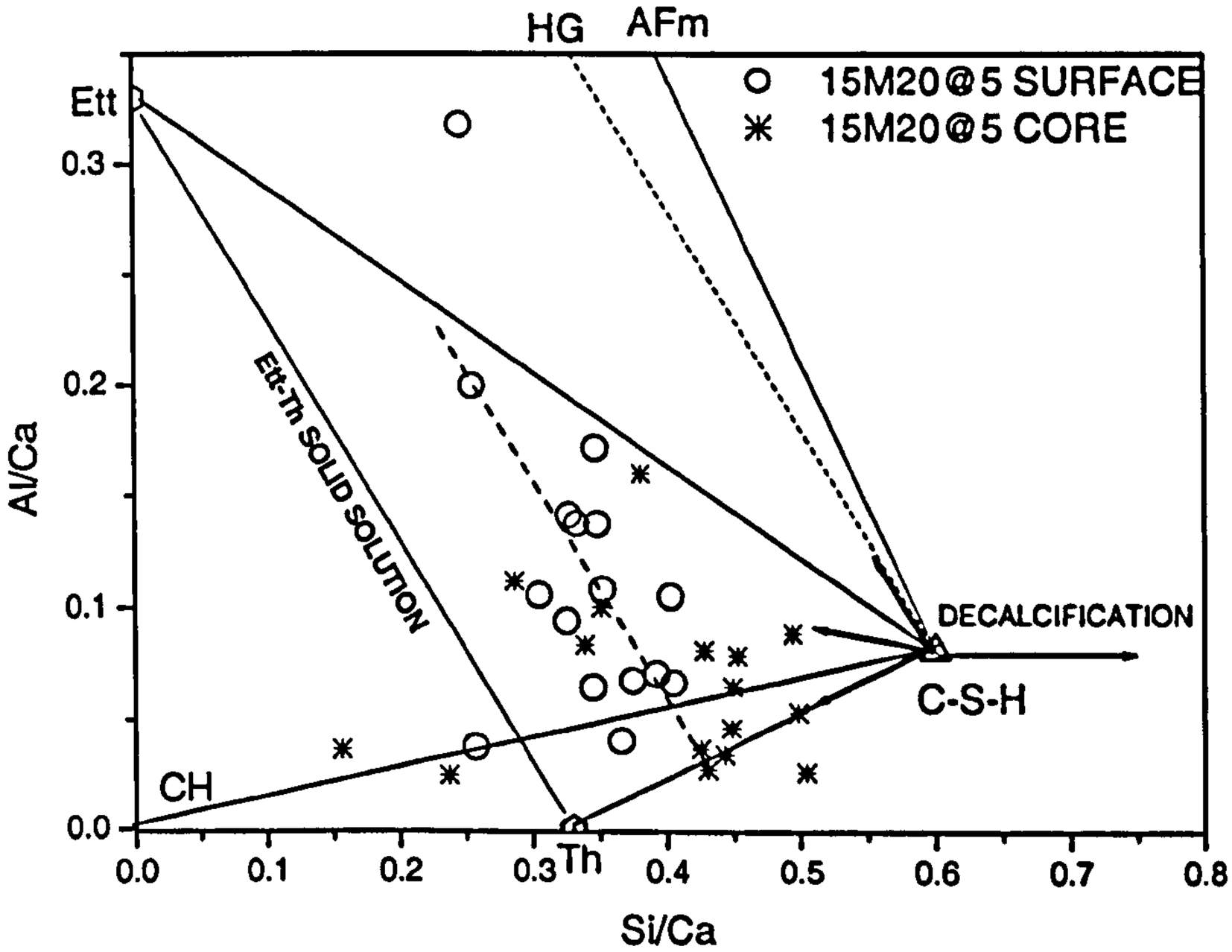

Figure 6.42: Al and Si atomic ratio plot of cement matrix in 15%LF in $MgSO_4$ and 2.0% Cl^- at 5°C after 1 year.

The sulfate profile is shown in Fig 6.43. Although some of the points fell along the AFm-origin line, the points were mostly distributed between the AFm and AFt lines, and mostly concentrated within S/Ca<0.1. This observation can possibly be attributed to the precipitation of a thaumasite-containing aluminium phase within the C-S-H. Also, there was not much distinction between the core and the surface regions, indicating that there was an overall chemical change due to the attack across the sample. In this sense, 2%Cl posed a higher degree of chemical change at the core than 1%Cl^-. Therefore, because TSA propagates from the surface inwards, the higher concentration of Cl^- seems to have given the conditions to develop a solid solution at greater depths than in the solutions with lower concentration or absence of Cl^-. Once more, a few points fell close to the hydrogarnet-CSH line, which is consistent with previous observations in

which it is suspected that the ettringite would have decomposed due to its instability in thaumasite prone systems.

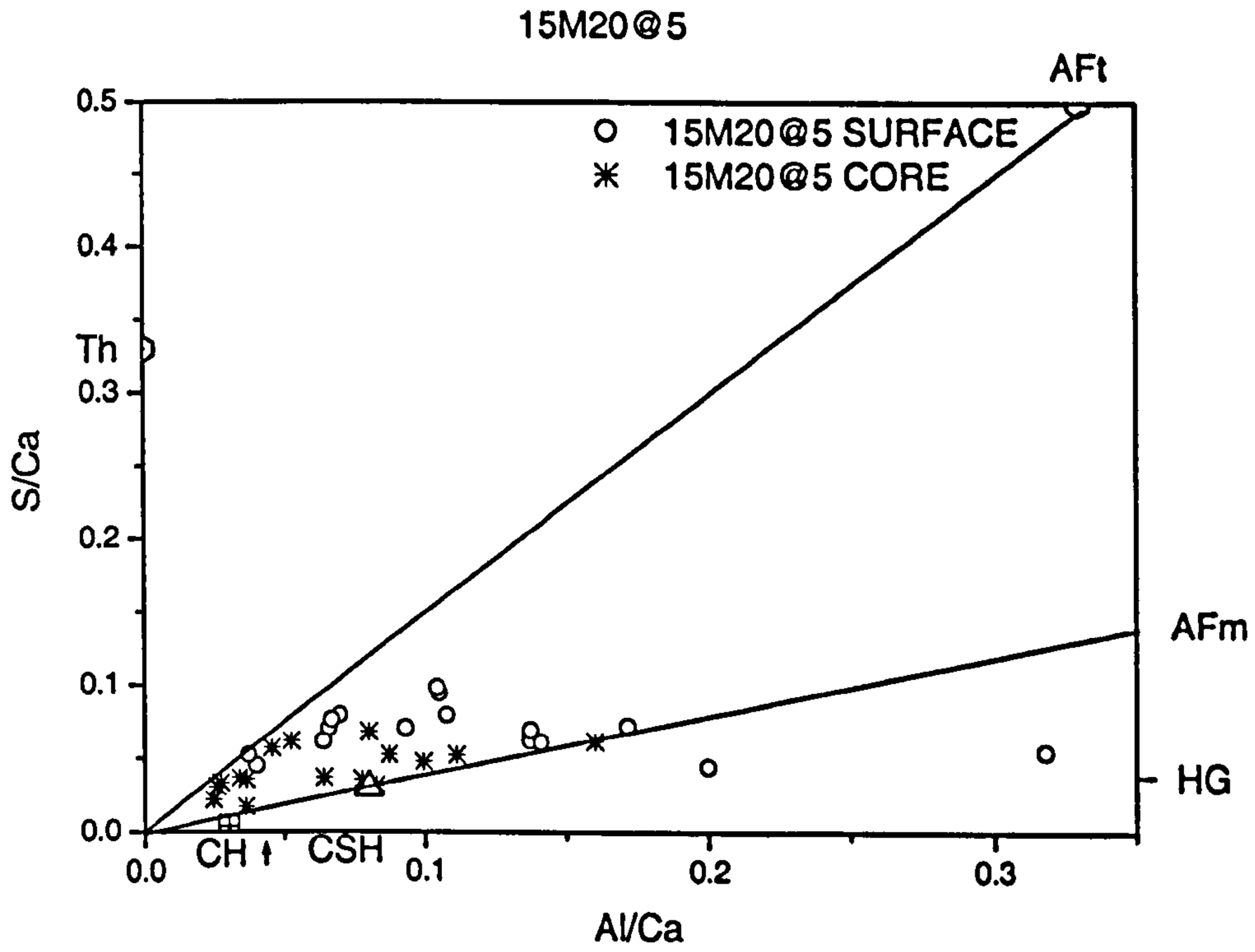

Figure 6.43: Al and Si atomic ratio plot of cement matrix in 15%LF in $MgSO_4$ and 2.0% Cl^- at 5°C after 1 year.

It is still important to access the profile of both chloride and magnesium in order to assess the chloride binding capacity of damaged areas, and also, whether or not magnesium played any role in the disruption of the matrix, hence, aggravating the scenario with respect to TSA.

6.3.4 Chloride and magnesium profiles in 15%LF samples in salt solution at 5°C

A. 15% limestone filler in 0.60% SO_4^{2-} at 5°C

The presence of chlorine in samples immersed in magnesium sulfate without added chloride indicates that x-ray microanalysis is sensitive to the chlorine found in the resin, as can be seen in Figure 6.44. Rather than being almost constantly distributed as in the core, the Cl/Ca ratio was more scattered at the surface, as can be expected since more flaws and micro porosity, which can be filled with the low viscous resin during sample preparation, is found at the surface due to the attack. Indeed, salt solutions were prepared using deionised and demineralised water with no Cl^-. Another source of Cl is Portland cement itself, which can contain about 0.02% by mass of cement [12]. Also, no correlation was found between Cl^- and Al^{3+}, in spite of Al^{3+} bearing phases being more prone to binding chlorides, as shown in Figure 6.45.

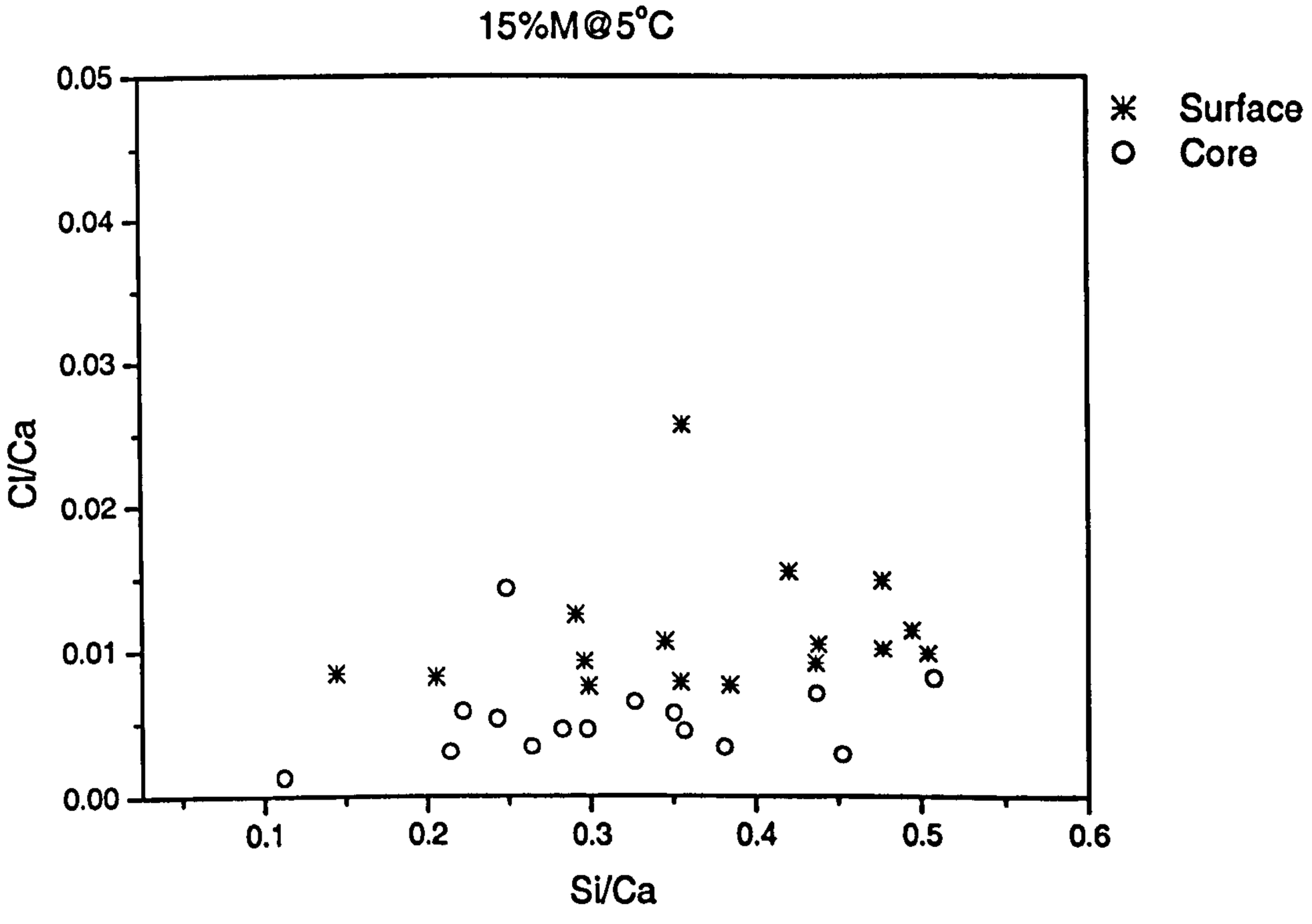

Figure 6.44: Cl and Si atomic plot in 15%LF samples immersed in 0.6% SO_4^{2-} after 1 year at 5°C

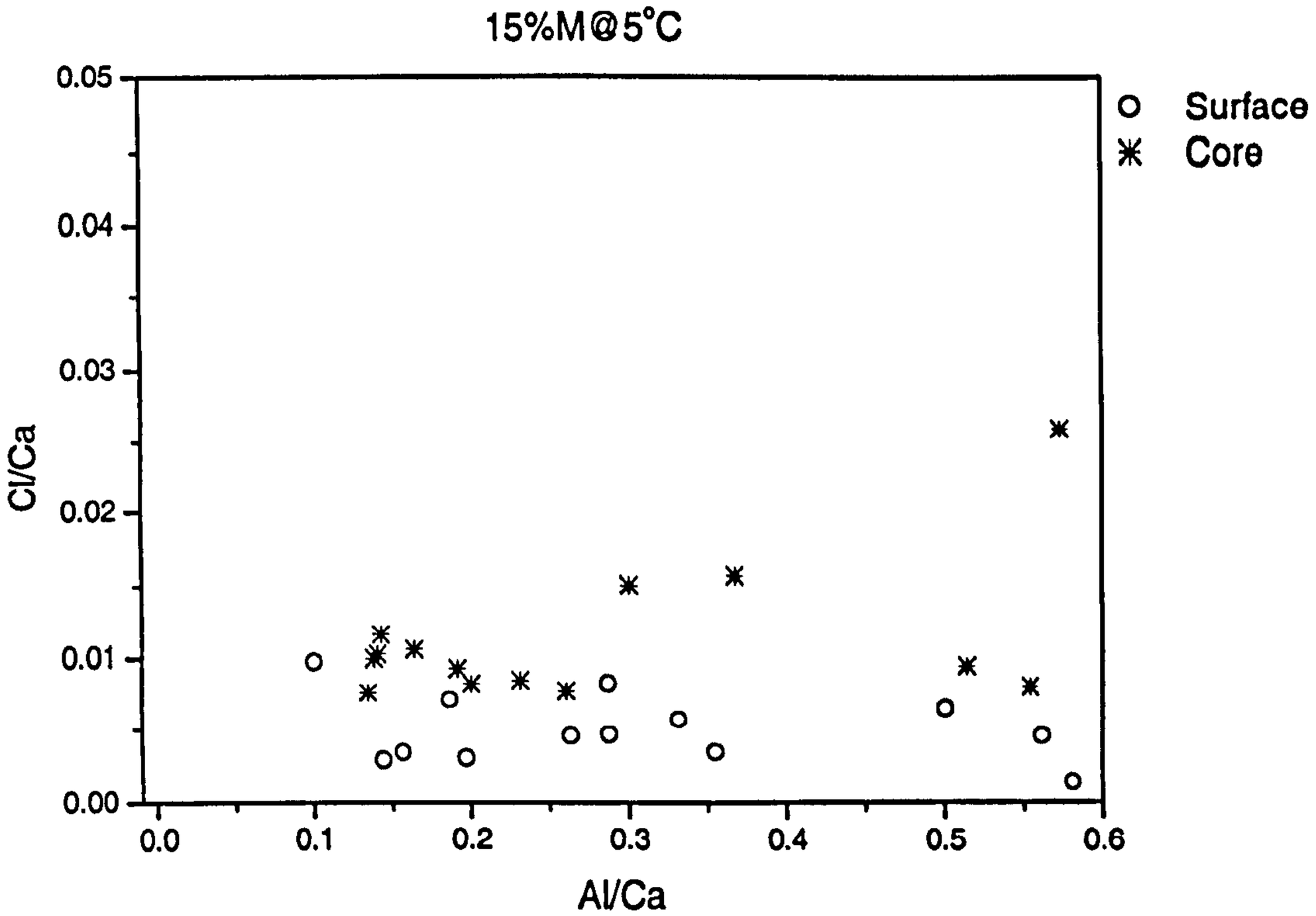

Figure 6.45: Cl and Al atomic plot in 15%LF samples immersed in 0.6% SO_4^{2-} after 1 year at 5°C.

As for the magnesium distribution, Fig 6.46 shows that low concentrations of this ion can be found in both the core and, particularly, at the surface. Almost all the Mg/Ca ratios were below those reported by Gollop and Taylor [104], which shows values around 0.05 for sound parts of OPC immersed in magnesium sulfate and sodium sulfate after 6 months at 20°C. Also, no correlation could be found between Mg and Si, which suggests that magnesium did not abnormally interact with CSH to form MSH, particularly within the surface, where higher damage can be identified. As magnesium replaces calcium in C-S-H, it would be expected that the Mg/Ca ratio would be much greater than that observed.

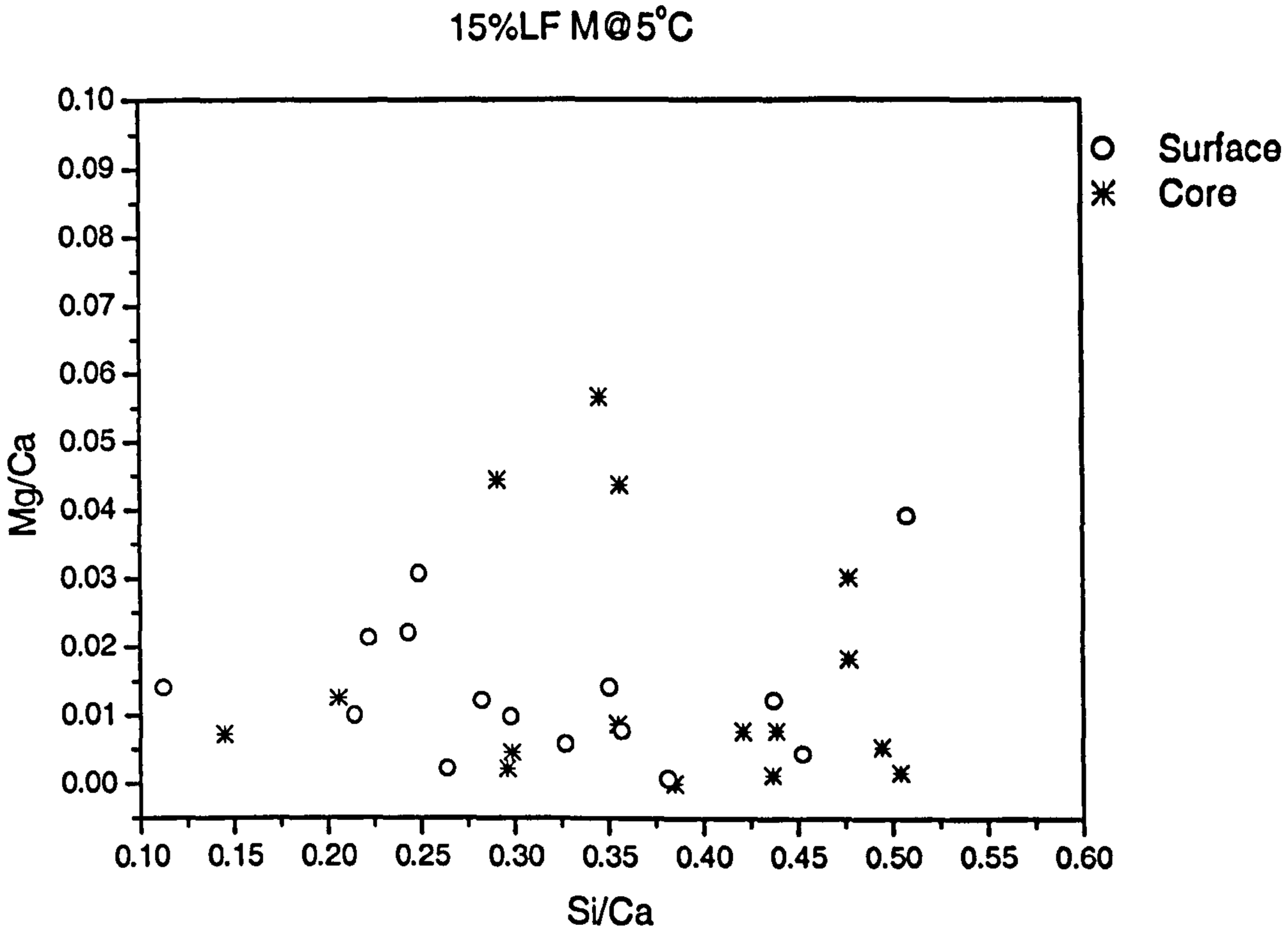

Figure 6.46: Mg and Si atomic plot in 15%LF samples immersed in 0.6% SO_4^{2-} after 1 year at 5°C.

B. 15% limestone filler in 0.60% SO_4^{2-} and 0.5 %Cl^- at 5°C

Fig 6.47 and 6.48 show Cl/Si and Cl/Al atomic ratios of 15%LF samples immersed in 0.5%Cl^- and sulfate solution after 1 year at 5°C. It can be seen that chloride binding correlated more with Al than with Si, as expected since aluminate phases are prone to bind chloride and form Friedel's salt [139, 147]. Indeed, the points in the core fell along parallel to the Friedel's salt line, whose coefficient of regression was 0.99. Poorer correlation at the surface confirms that the attack reduced the chloride binding capacity, as also evidenced by the absence of Friedel's salt in XRD analyses of the corroded material.

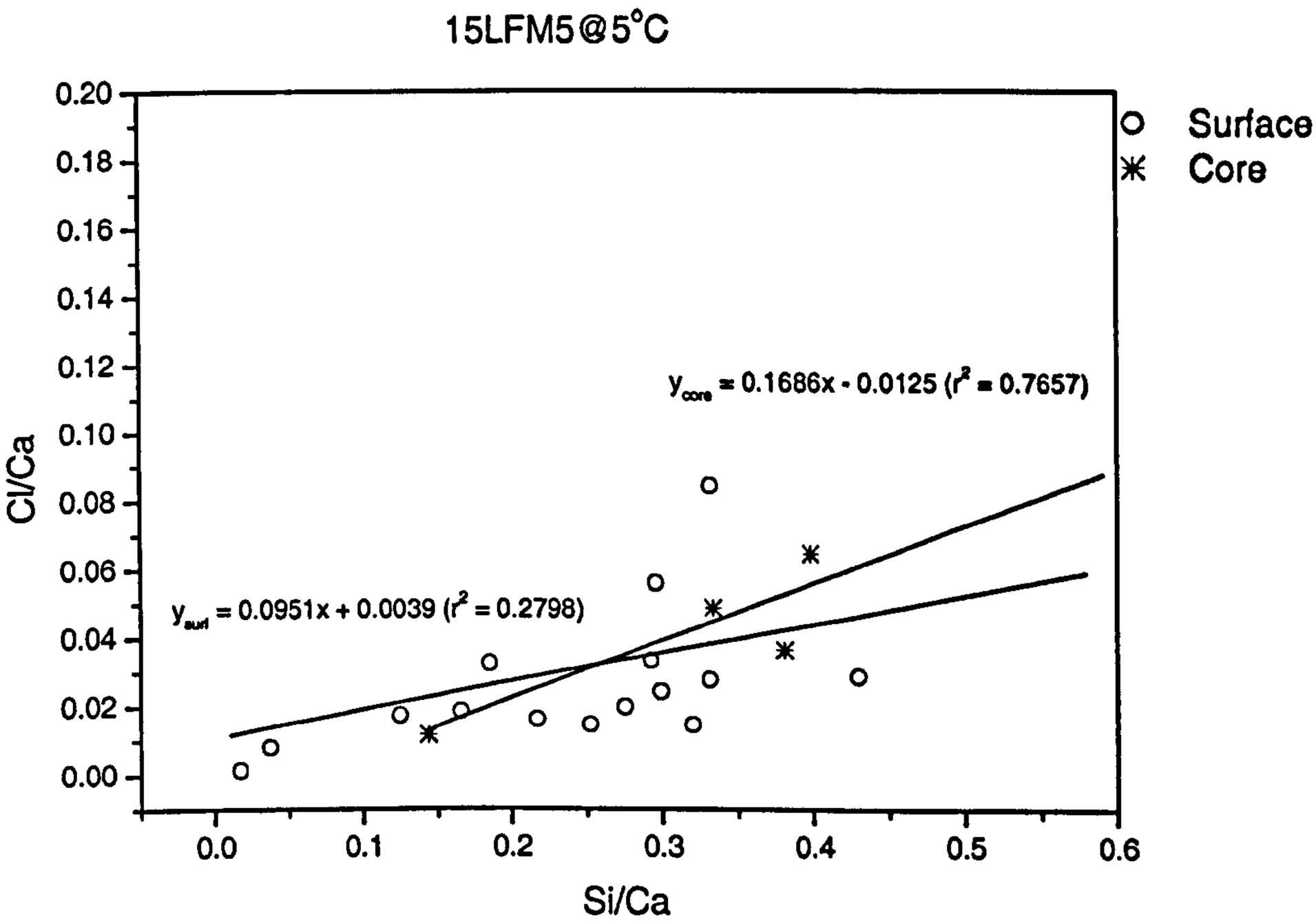

Figure 6.47: Cl and Si atomic plot in 15%LF samples immersed in 0.5%Cl⁻ and 0.6% SO_4^{2-} after 1 year at 5°C.

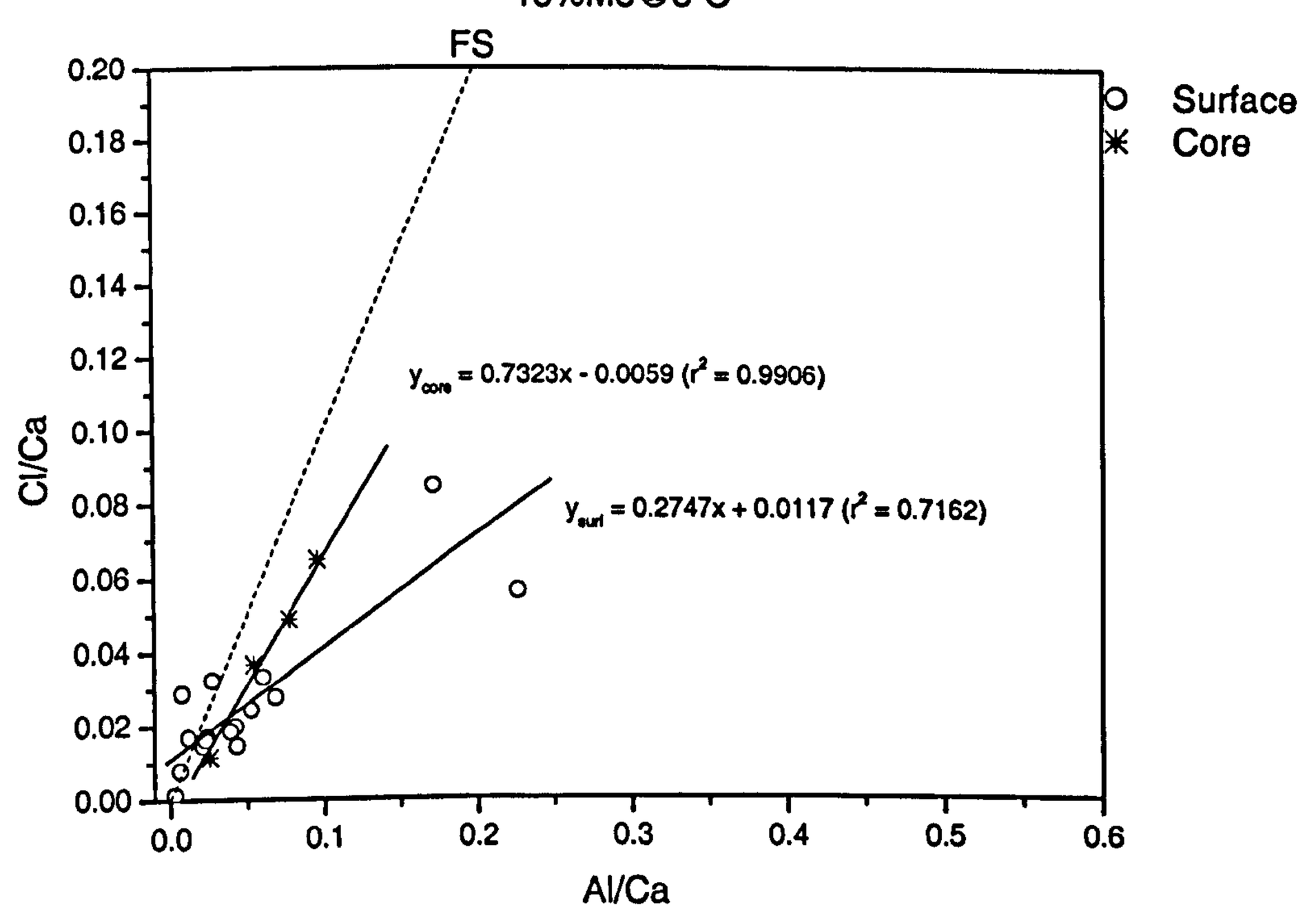

Figure 6.48: Cl and Al atomic plot in 15%LF samples immersed in 0.5%Cl⁻ and 0.6% SO_4^{2-} after 1 year at 5°C.

The correlations of the regressions indicate that chloride prefer to bind within the aluminate phases rather than the silicate phases of the cement matrix, most likely in the form of Friedel's salt, as confirmed by XRD. Also, the attack at the surface reduced the

capacity of the cement to bind chloride, as confirmed by comparison of the poor correlation at the surface with a better correlation in the core.

Indeed, the chloride binding was higher in the core than at the surface, which confirms the findings of analyses in the thaumasite areas of the samples, in which chloride was found to bind in two groups: (i) by the AFm phases in the form of Friedel's salt and (ii) within the CSH (*see* Fig 6.20), but less favourable in thaumasite. In addition, the Cl/Ca ratio decreased when Si/Ca decreased. This finding is apparently contradictory with that of Beaudoin [146], in which Cl binding capacity increased with Ca/Si ratio. However, it can be seen that calcium silicate hydrate in this sample differs from a typical CSH in that it had suffered chemical alteration due to TSA, hence, it contained a lower ratio of Si/Ca.

As far as magnesium is concerned, it can be seen from Figure 6.49 that the Mg/Ca ratios were very low, when compared to values for the sound cement matrix as discussed earlier. Such a range not only confirms as expected the low diffusivity of magnesium in Portland cement, but also indicates that it did not form M-S-H, and hence a strong role of this ion in promoting the damage observed by visual inspection.

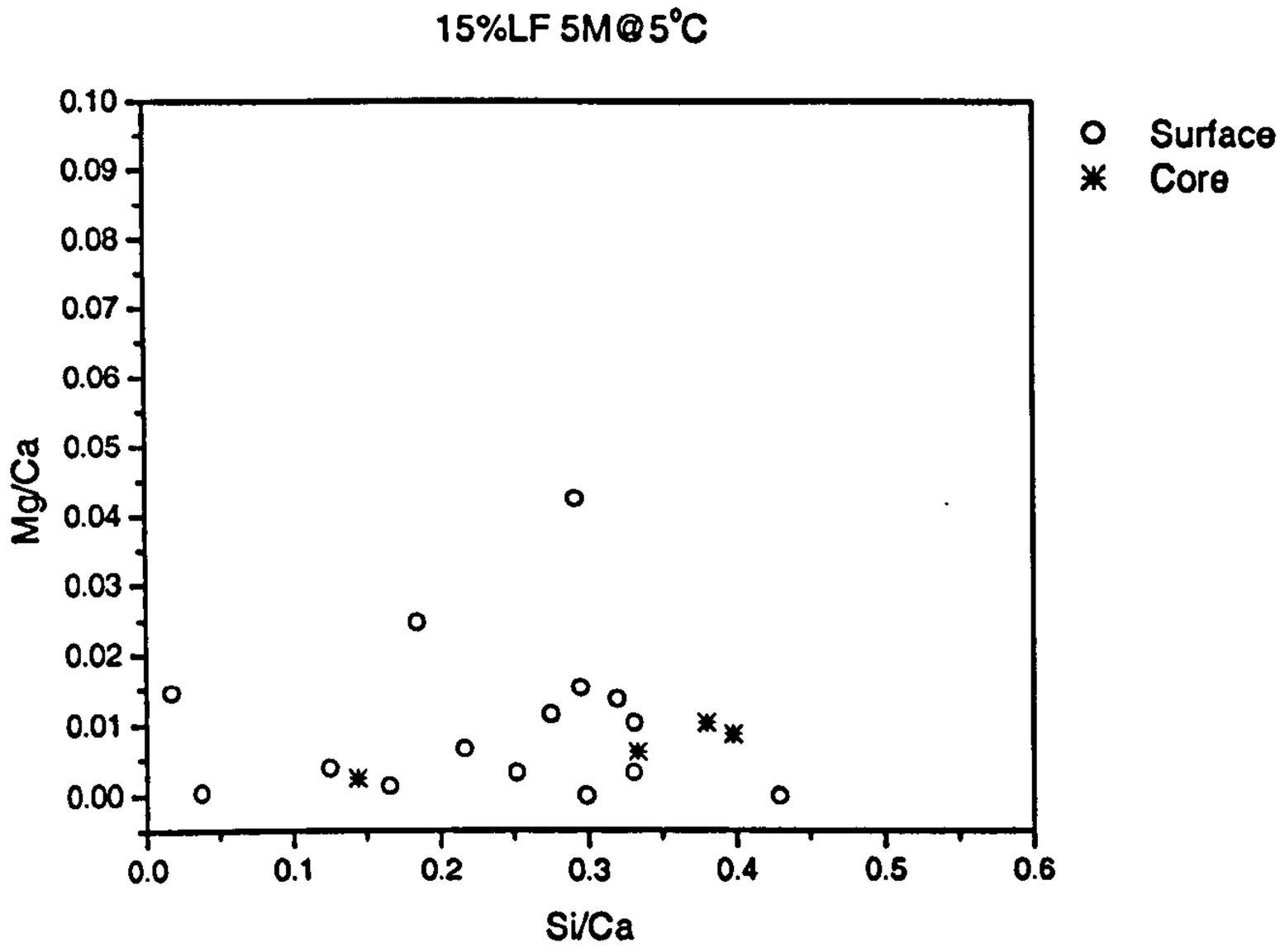

Figure 6.49: Mg and Si atomic plot in 15%LF samples immersed in 0.5%Cl^- and 0.6% SO_4^{2-} after 1 year at 5°C.

C. 15% limestone filler in 0.60% SO_4^{2-} and 1.0% Cl^- at 5°C

In this system, as can be seen from Fig 6.50, the chloride profile appears scattered at the surface, although some sort of correlation seems to be occurring with silicates in which chloride binding capacity in the core region reduced as the Si/Ca decreased. It may be that this unexpected behaviour is associated with the nature of TSA in which both silicon and calcium are released from the CSH, since the chloride binding capacity of the CSH depends on the ratio of these elements [146].

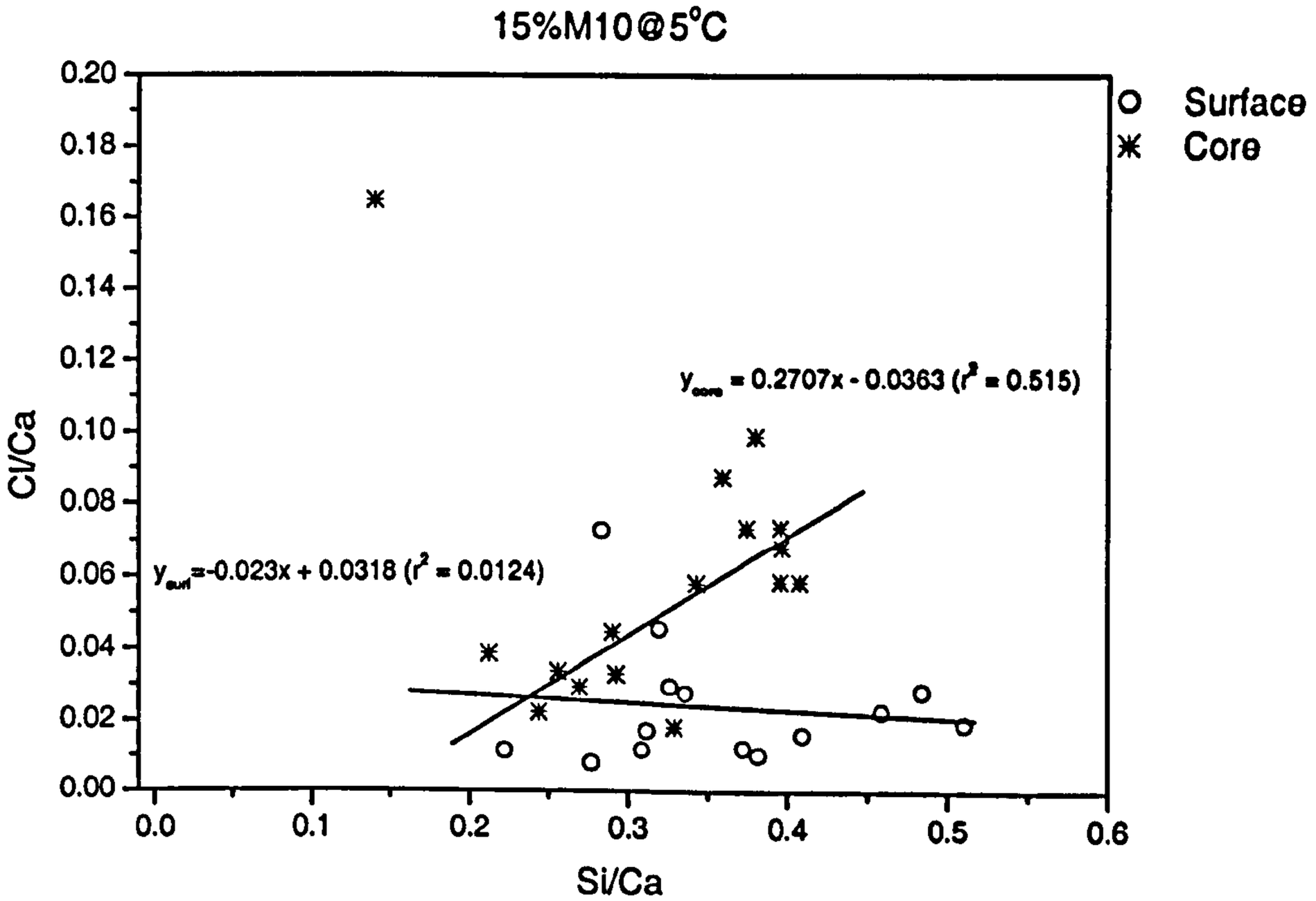

Figure 6.50: Cl and Si atomic plot in 15%LF samples immersed in 1.0%Cl^- and 0.6% SO_4^{2-} after 1 year at 5°C

The correlation with aluminates is reasonably clearer, as shown in Figure 6.51. The higher the Al/Ca, the higher the Cl/Ca ratio, particularly at the core. The points in the core region fell almost parallel to the Friedel's salt line. This is indicative of the higher chloride binding capacity of aluminate phases. As expected, higher chloride concentration in solution leads to higher Cl/Ca ratio in the surface regions in this sample than that of samples immersed in 0.5%Cl^- (see Fig 6.48). However, when the data from the core regions of both solutions containing 1.0%Cl^- and 0.5%Cl^- (Figures 6.51 and 6.48) are compared, the Cl^- concentration of the former appears slightly similar to the latter. This unexpected behaviour could possibly be explained by more damage being inflicted by TSA in the matrix of samples immersed in the former concentration than in the latter.

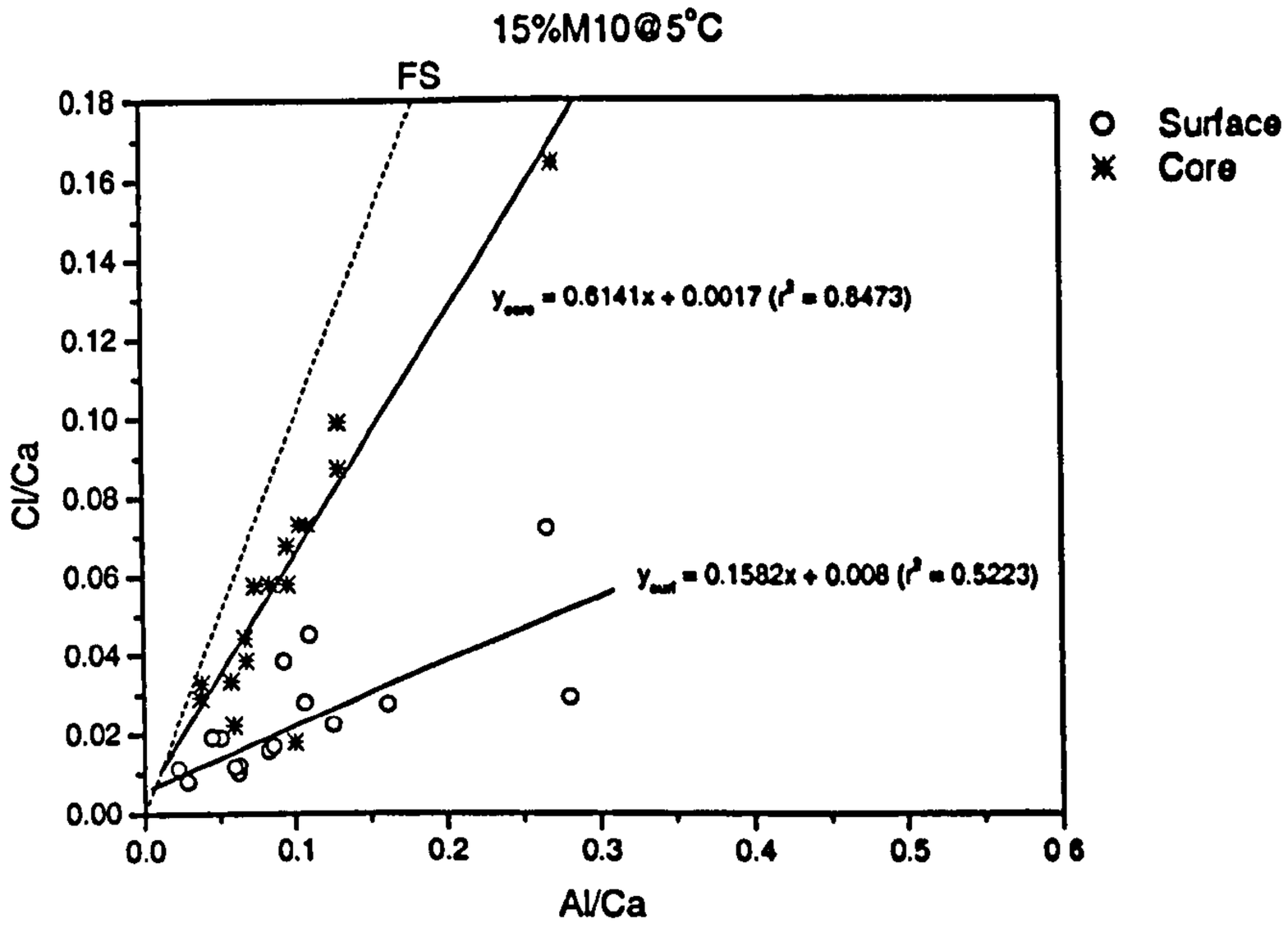

Figure 6.51: Cl and Al atomic plot in 15%LF samples immersed in 1.0%Cl^- and 0.6%SO_4^{2-} after 1 year at 5°C.

Once more, Fig 6.52 shows that Mg/Ca ratio was low and fell below 0.04, except for two points at the surface. Again, poor correlation was observed between Mg and Si, which corroborates to that thaumasite formation was predominately responsible for the damage rather than the typical conversion of CSH into the non-binder magnesium silicate hydrate as in conventional magnesium sulfate attack.

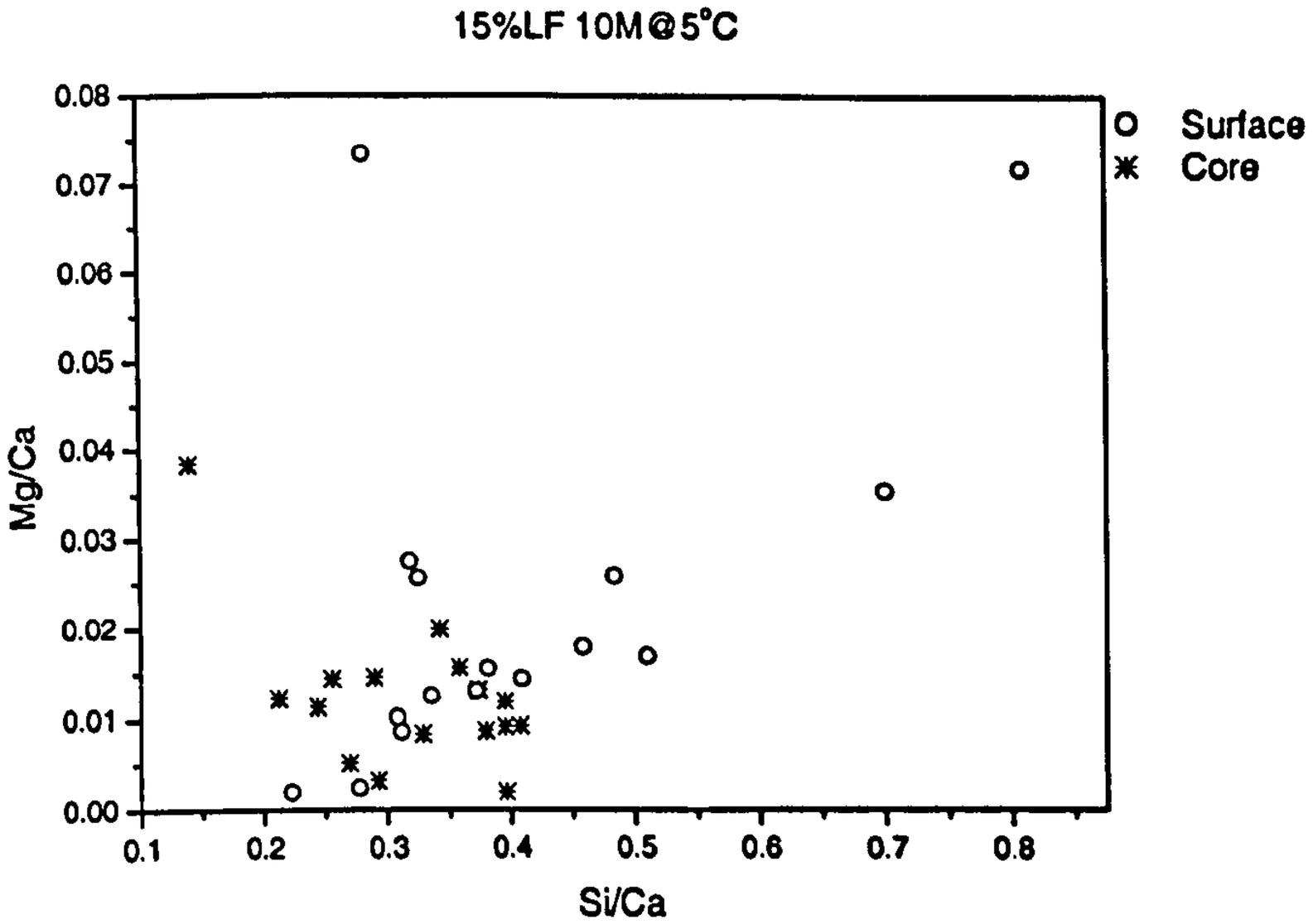

Figure 6.52: Mg and Si atomic plot in 15%LF samples immersed in 1.0%Cl^- and 0.6%SO_4^{2-} after 1 year at 5°C.

D. 15% limestone filler in 0.60% SO_4^{2-} and 2.0% Cl^- at 5°C

In 15%LF immersed in 2.0%Cl^- and sulfate solution after 1 year at 5°C, chlorides were favourably bound with aluminates rather than with silicates, in a similar fashion as happened in samples with lower concentrations of Cl^-, as can be seen in Figure 6.53 and

6.54. Whereas the correlation between Cl and Si is poor in both surface and core regions, as happened at all Cl^- concentrations, the chloride binding capacity here is slightly higher than in 0.5% and 1.0%Cl^- respectively. Indeed, whereas the chloride binding capacity appears to be determined by the aluminate composition of the cement in the core, which indicates that the matrix has been less attacked in this area, it was significantly reduced at the surface, but somewhat less than at the other concentrations of chlorides in solution.

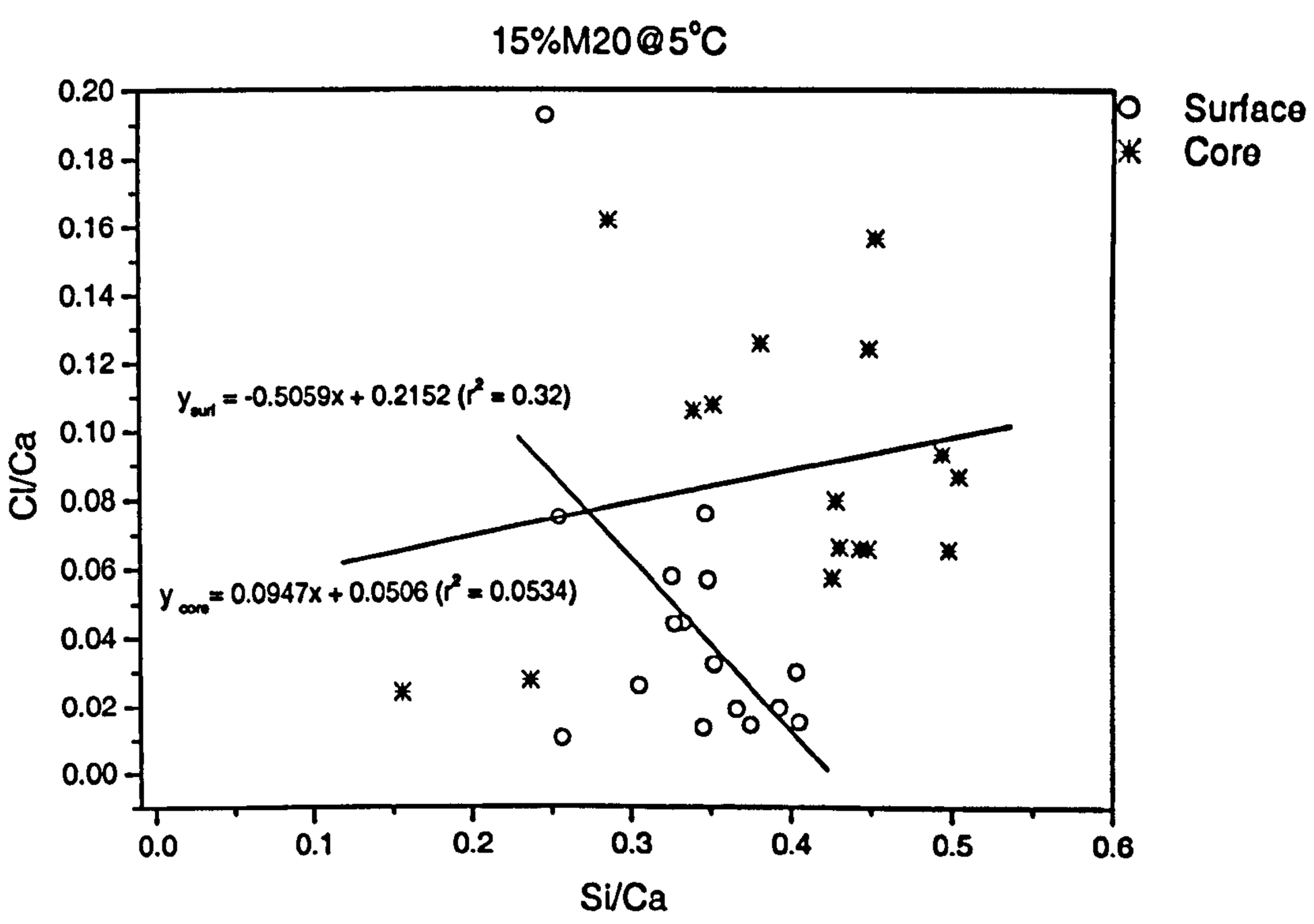

Figure 6.53: Cl and Si atomic plot in 15%LF samples immersed in 2.0%Cl^- and 0.6%SO_4^{2-} after 1 year at 5°C

The Cl/Ca and Al/Ca plot is shown in Fig 6.54. It can be seen that Not only the C/Ca ratio was greater at this concentration, but both the surface and core regions composition fell almost parallel to the Friedel's salt-origin line. This observation appears to confirm that chloride ions preferably binds with the aluminate phases to form Friedel's salt but not with silicate phases such as thaumasite. Indeed, Friedel's salt was not identified in any corroded material in any chloride concentration, as also shown by the XRD analyses.

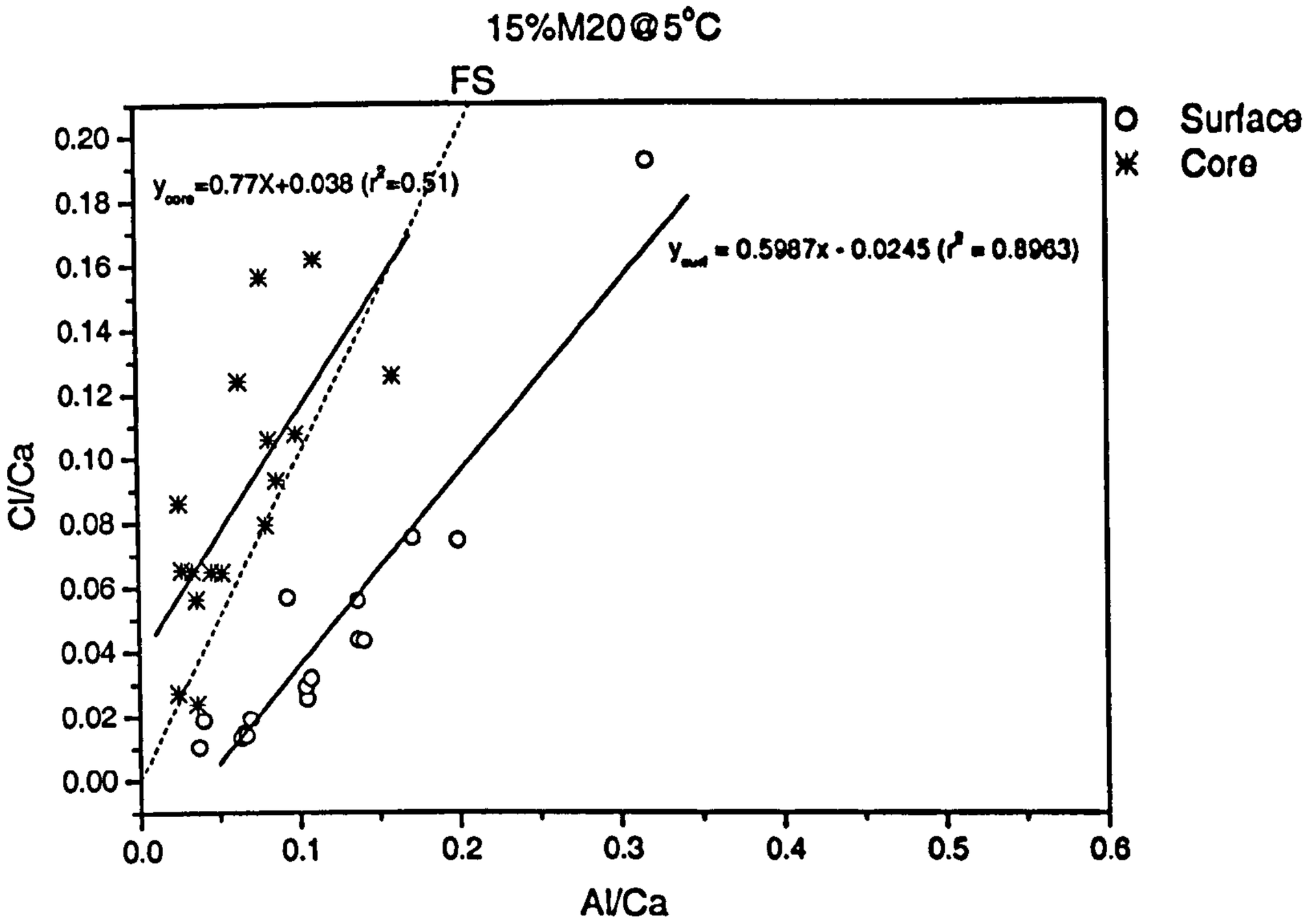

Figure 6.54: Cl and Al atomic plot in 15%LF samples immersed in 2.0%Cl^- and 0.6%SO_4^{2-} after 1 year at 5°C.

Fig 6.55 shows the magnesium to silicon profile. It can be seen that Mg/Ca ratio was below 0.04 in all cases in both core and surface, except for one point. Yet again, no correlation can be drawn between Mg and Si, which confirms previous observations that the role of magnesium was not predominant compared with the attack imposed by thaumasite formation.

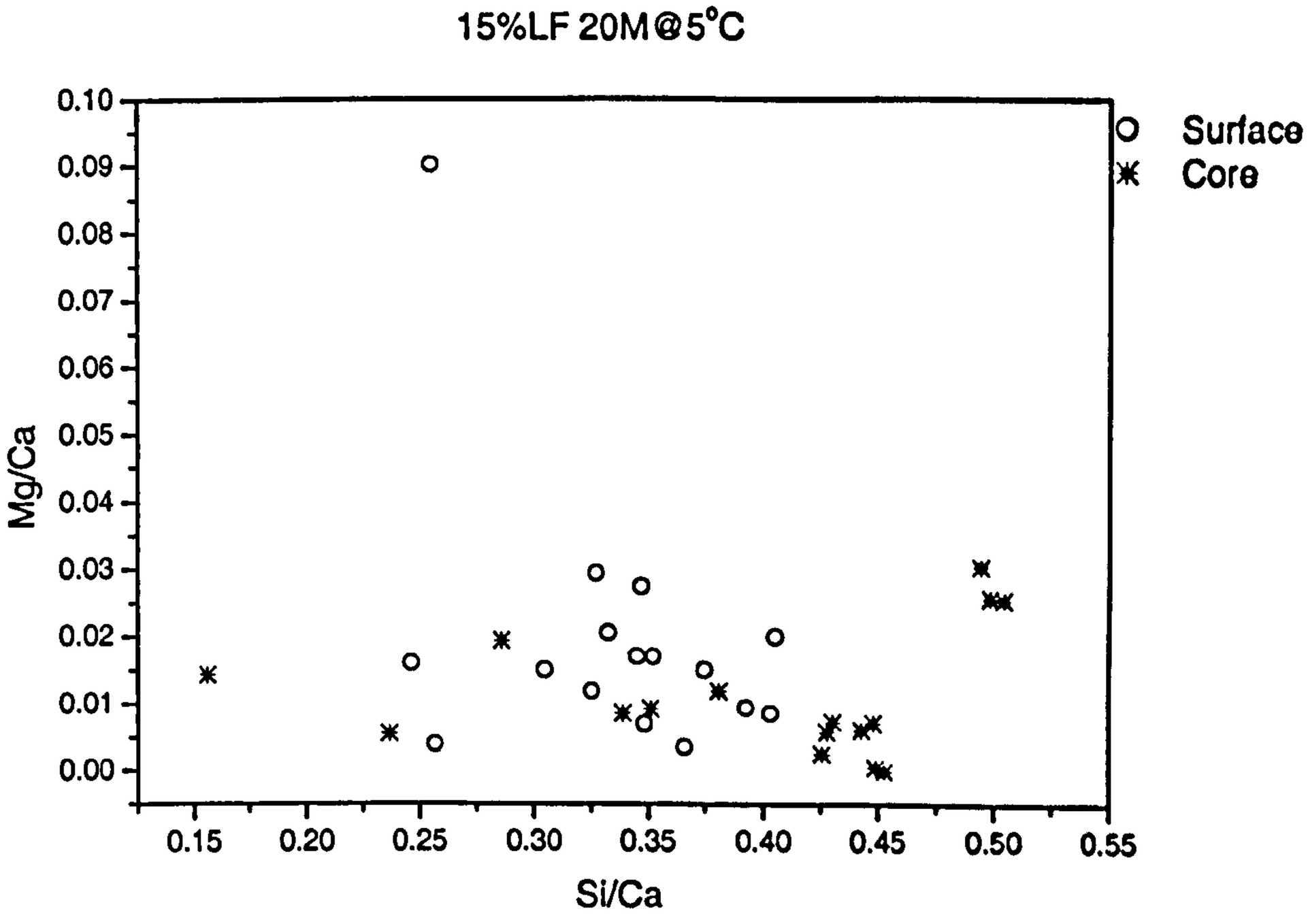

Figure 6.55: Mg and Si atomic plot in 15%LF samples immersed in 2.0% Cl^- and 0.6% SO_4^{2-} after 1 year at 5°C.

6.4 Discussion

6.4.1. Microstructural features of TSA in mortars containing limestone filler immersed in combined sulfate chloride solutions at 5°C

Overall, it was not possible to distinguish the effect of chloride on the characteristics of the damage. Indeed, the microstructural feature of the attack in samples immersed in sulfate and combined chloride and sulfate looked very similar, except perhaps in terms of the section size of the remaining bulk sample. Details can be found in section 5.3.1 of the previous chapter.

Generally, the attack was markedly greater at the surface. In very severe zones of attack, all samples developed a dominant dark grey band, in which no classic features of hydrated Portland cement paste could be identified, but only quartz aggregate particles embedded in a mass of thaumasite. Rather than a mixture of phases, the occurrence of these distinct bands indicates that carbonates were primarily engaged in thaumasite formation, rather than precipitating as calcium carbonates, since no popcorn calcite was identified [17], with the exception of a few white points at the very edge of some samples (as in Fig 6.6), which could not be analysed because of its weak signal in EDX.

Another feature of these bands is the absence of cracks inside these dark grey areas. This observation is indicative of typical features of thaumasite, since it seems to be more stable than ettringite under high vacuum, as was also observed in chapter 4 (Figures 4.11 and 4.16), in which the massive grey band, with no detectable internal cracks, dominated the whole damaged area in carbonate filled mortar after 5 years in sulfate solution. However, Yang and Buenfeld [57] pointed out that both thaumasite and ettringite develop extensive cracks when submitted to the vacuum used in backscattered electron image (BEI), but thaumasite developed fewer cracks than ettringite at low vacuum. That thaumasite suffers less damage in high vacuum was also reported by Lachowski et al. [58], who were able to successfully perform electron diffraction in thaumasite but not in ettringite, which suffered severe damage to its structure due to dehydration under the high vacuum of the transmission electron microscope (TEM).

A network of cracks developed throughout the cement matrix. It was also possible to see that the binding capacity of the matrix appeared to have been destroyed by the presence of these dark grey zones in a way that material found within these bands had been detached from the bulk sample, even before the matrix had been entirely converted into thaumasite.

Higher magnification of the cement matrix showed that whereas classic features of hydrated cement were identified at the core (Figures 6.8, 6.10, 6.12), suggesting that little or no attack occurred in this region, the surface had been severely attacked (as in Figures 6.7, 6.9, 6.11). Indeed, high porosity and cracked zones were identified in the surface regions as well as some clinker grains that had been attacked, developing a mixture of thaumasite and ettringite solid solutions intermixed with the CSH (as in Figure 4.11,4.16, 6.3 and 6.4).

6.4.2 Effect of chloride on the composition of thaumasite

A. EDX/ X-ray microanalysis

EDX analyses of the dark grey material that dominates the attacked surface areas has shown a distinctive composition of a thaumasite type of phase (Figures 6.13-6.18), as expected in high carbonate cements at low temperatures in sulfate environments, and, also, confirming what had been found in the features of the dark grey material in BEI.

As far as chloride is concerned, EDX spot analysis showed that small amounts of chlorine were detected in the dark areas, independently of chloride concentration of the

solution. Further investigation using x-ray microanalyses, however, could not unambiguously determine in which phase the chloride was bound, but it seemed it was bound by the combined action of the aluminate phases (as in Friedel's salt), and within the C-S-H, but also due to resin impregnation. Nonetheless, the results indicated that this value fell within what has been found in field cases, around Cl^- 0.75% [96, 97]. In addition, the Cl/Ca ratio of thaumasite would be up to a maximum value of ca. 0.045 ±0.006, which is below that ratio for the theoretical thaumasite-chloride analogue of Cl/Ca=0.33.

B. Unit cell parameters

As far as the thaumasite crystal structure is concerned, it has been observed that its lattice parameters fell comfortably within what is expected for a thaumasite solid solution, sometimes reaching values below that reported for pure thaumasite (Figure 6.22) [134]. Also, the chloride concentration was found to affect the *c* dimension more than *a*, which indicates that chloride appears to affect the composition of thaumasite by increasing the availability of carbonates in solution. It can be seen from Figure 6.23 that this trend was observed in all mixes with and without limestone filler.

In order to evaluate the effect of calcium carbonate (Cc) filler content, concentration of chloride in solution (Cl), and the interaction between both factors (CcCl) in the variation of the unit cell parameter, statistical analysis was performed using multivariate polynomial curve fitting. Figure 6.56 shows that the experimental data (*) is well explained by the statistical model (o) shown in Tables 6.4 and 6.5. It can be seen that not only *c* dimension of the unit cell is affected by carbonate, but also by chloride concentration and the interaction between both factors. The goodness of fit is confirmed by the multivariate correlation factor of 0.9727 (Table 6.4 and 6.5). Indeed, all parameters were statistically significant, with a confidence limit higher than 91.3%, as shown by the t-test coefficient (Prop>$|t|$).

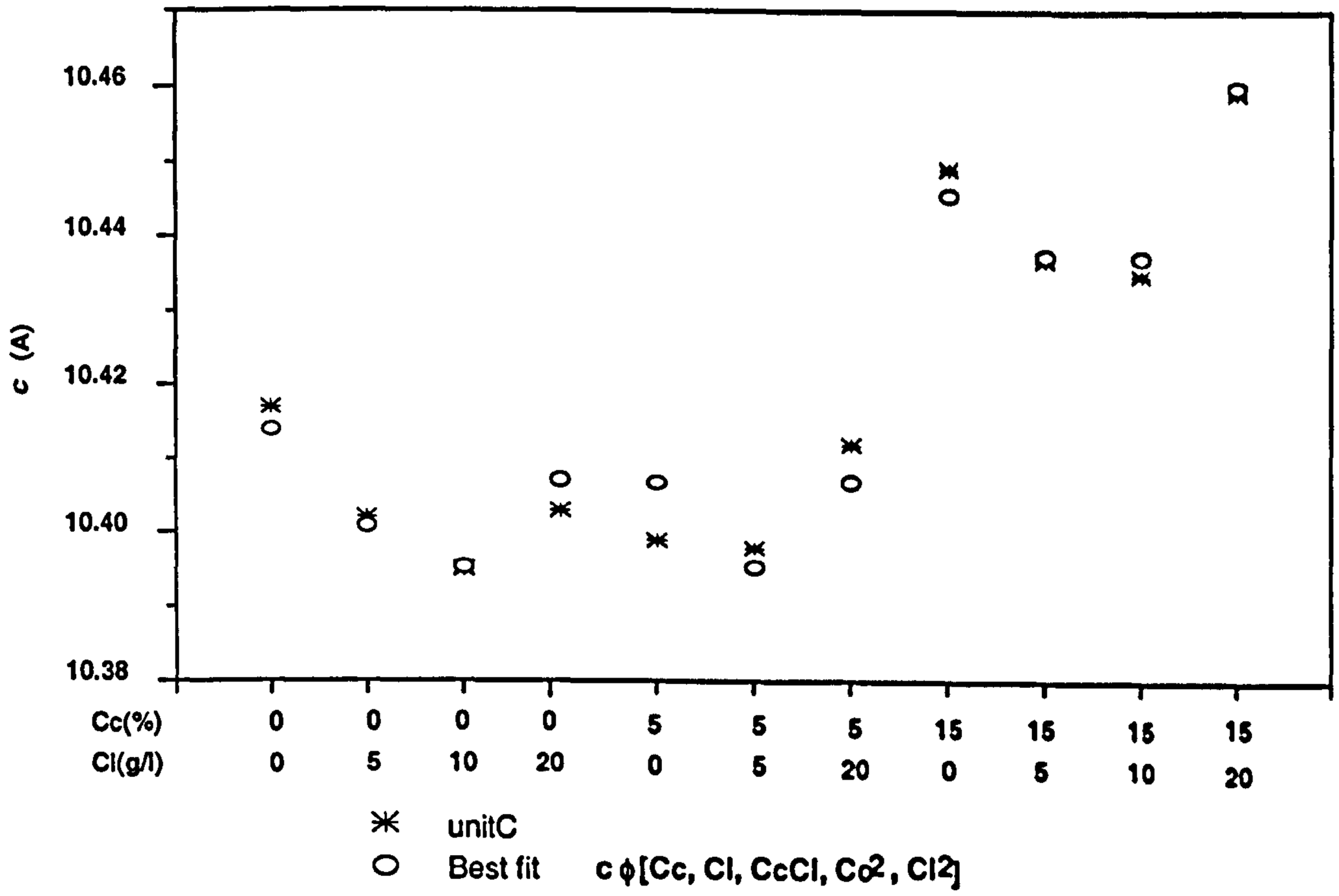

Figure 6.56: Unit cell parameter c as a function of carbonate content and chloride concentration in samples immersed in salt solutions for 1year at 5°C.

Table 6-4: Multiple Regression of unitC-Cc-Cl model on 15%LF in salt solutions at 5°C

Independent: Column(Cc) -> Column(Ccsquare)
Dependent: Column(unitC)

Parameter	Value	Error	t-Value	Prob>|t|
Y-Intercept	10.41396	0.00422	2468.58278	<0.0001
Cc	-0.00321	0.00121	-2.64122	0.04591
Cl	-0.0034	8.51024E-4	-4.00013	0.01032
Clsquare	1.52937E-4	3.80692E-5	4.01733	0.01015
CcCl	7.01601E-5	3.30271E-5	2.12432	0.08703
Ccsquare	3.53974E-4	7.3971E-5	4.7853	0.00495

R-Square(COD)	Adj. R-Square	Root-MSE(SD)
0.97268	0.94537	0.00528

Table 6-5: ANOVA Table of Cunit-Si-Cc model on 15%LF in salt solutions at 5°C.

Item	Degrees of Freedom	Sum of Squares	Mean Square	F Statistic
Model	5	0.00496	9.91006E-4	35.60925
Error	5	1.3915E-4	2.783E-5	
Total	10	0.00509		

Prob>F
6.50416E-4

Indeed, it appears that the concentration of chloride corresponding to the formation of thaumasite with the smallest *c* unit (therefore purer) decreases as the level of carbonate increases, in a linear fashion, as can be seen in (a) and (b) of Fig. 5.57.

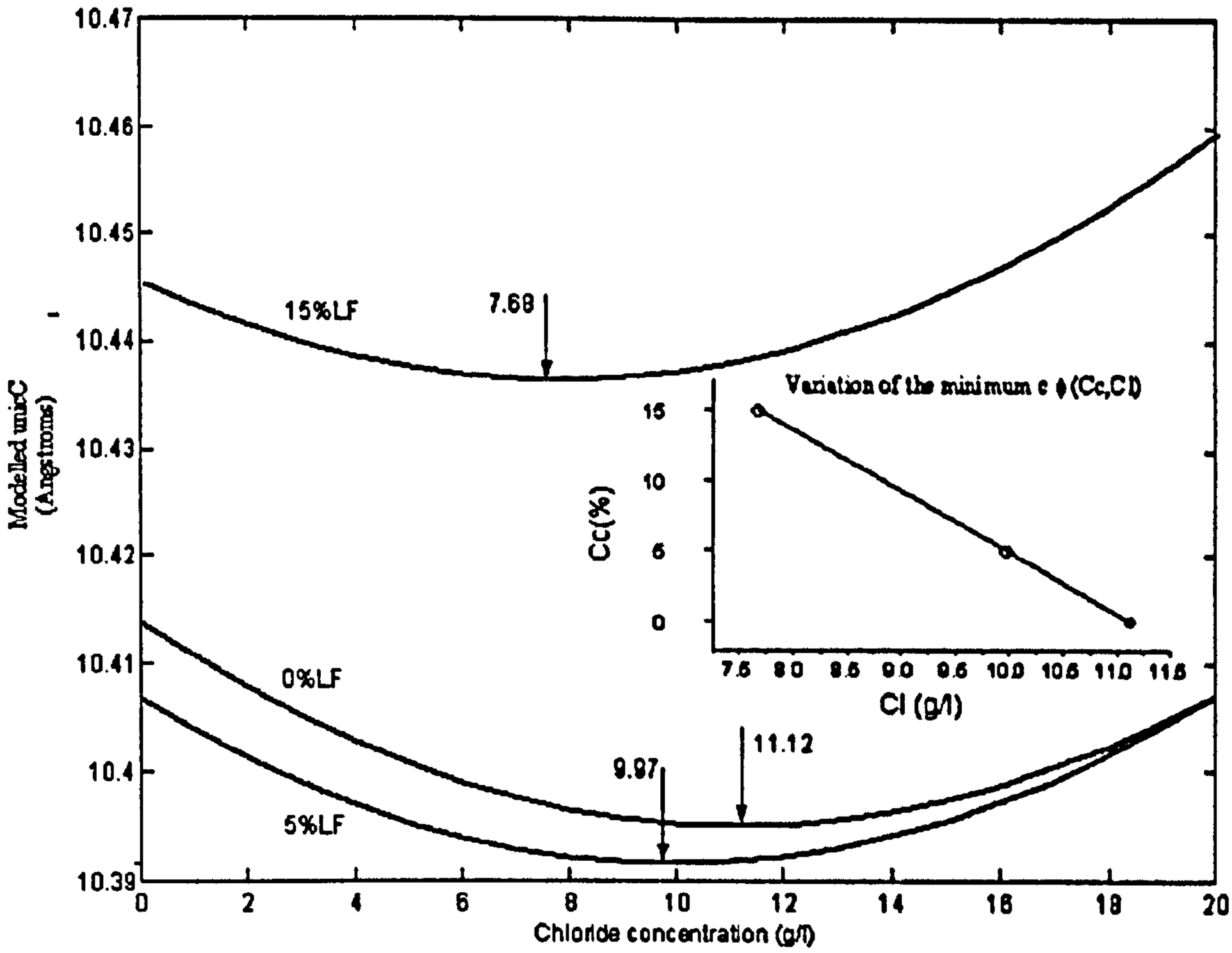

Figure 6.57 : (a) main graph: Modelled unit c parameter versus chloride concentration ; (b) insert graph: variation of the minimum unit cell *c* versus carbonate content and chloride concentration.

Indeed, the maximum predicted rate of mass loss with increase in carbonate content, which was identified to occur in chloride concentrations around 11.11g/l (Figure 5.19), is in good agreement with the chloride concentration predicted to produce purer thaumasite at around 11.12g/l in OPC, but slightly higher than that in 5% and 15%LF samples, at 9.97 and 7.68%, respectively. Hence, these correlations between greater damage, minimum *c* unit cell values, carbonate and chloride concentration seem to corroborate with the hypothesis that higher concentrations of chloride induced a strong carbonate counter diffusion that (i) promoted the deposition of calcium carbonate (calcite or aragonite, in the case of Epsom salt solution) and (ii) calcium carbonate predominated over the precipitation of thaumasite, which is kinetically slower. Therefore, less damage would be observed as chloride levels further increased.

However, the existence of afghanite, which contains all the elements also present in thaumasite, and also has a similar symmetry and similar *c* dimension to ettringite, can

lead to the hypothesis that there could be a possible interaction between chlorides and thaumasite within its unit cell. This possibility, although very remote due to the size of Cl^- radii and bond length, would lead to a distortion of the cell parameters. For that reason, simulated XRD patterns were calculated in which Cl^- would replace carbonates at the same location. Comparing the modelled XRD pattern with that of a sample obtained at the highest concentration of chlorides in solution, bearing in mind the limitations of crystal structure analysis in multiphase samples, indicated that this substitution did not seem to have occurred. Also, higher Cl/Ca ratio would also be expected if any chloride thaumasite analogue had precipitated (Cl/Ca ~ 0.33), which was not identified in any spot analyses (Cl/Ca ~0.04).

Hence, the analysis of lattice parameters indicates that the role of chloride in thaumasite formation seems to be primarily catalytic, as it seems not to have entered into solid solution with thaumasite. Therefore, it is more likely that the presence of chlorides affected the thaumasite structure by making more carbonates was available in solution. It is also believed that excessive carbonates counter diffusion, which was generated by the interaction between high chloride concentration and aluminate phases, and even C-S-H gel, can explain why the *c*-dimension was mostly affected.

C. IRS

Considering the unambiguous identification of 6-coordinated Si as belonging to thaumasite type phases, IRS data show that the estimated amount of silicon increased more with an increase in carbonate level in the cement than with an increase of chloride concentration in solution for all levels of carbonate replacement (Figure 6.34). In OPC, the presence of chloride increased the precipitation of $Si(OH)_6$ within the corroded material, particularly when the Cl^- concentration was 1.0%. A reasonable correlation between the amount of Si moles and the relative mass loss (Figure 6.35) confirms that the damage inflicted in the samples was due to the precipitation of thaumasite.

It is believed that the damage caused in the present systems was better reflected by net intensity of $Si(OH)_6$ than the calculated moles, as indicated by the fact that the amount of Si moles correlated reasonably well with the relative mass loss (Figure 6.35). The number of moles of silicon was always higher or equal to 1 in all solutions at 5°C, but below 0.5 at 20°C, which reflects what has been identified previously by other techniques that thaumasite and ettringite solid solutions were responsible for the attack at 5°C and at 20°C, respectively.

6.4.3. Effect of chloride on the chemical alterations of cement matrix due to TSA

In general, the cement matrix containing 15% limestone filler suffered greater attack in combined chloride and sulfate solution than in pure sulfate solution, except for that immersed in 0.5%Cl^-. Indeed, typical profiles of hydrated Portland cement were detected in the core of samples immersed in pure sulfate and combined 0.5%Cl^- and sulfate, in which most points fell adjacent to the CH-CSH and CSH-ettringite lines. On the other hand, the matrix in the core of samples immersed in 1.0% and 2.0%Cl^- suffered a rather different chemical alteration than the traditional decalcification as expected for conventional attack, in which their CSH appeared to have lost its calcium as well as its silicon. This observation is confirmed by the fact that most points fell within CSH-ettringite, CSH-thaumasite and thaumasite-ettringite parallel lines, almost converging to the central point of this theoretical triangle.

Similar features of points falling within the boundaries of ettringite-thaumasite-CSH lines have also been identified at the surface of all samples that have been severely attacked, except for that immersed in 0.5%Cl^- in which composition predominantly fell adjacent to CH and C-S-H line, yet again, where less damage had been observed (discussed in previous chapter) and also retained less octahedron Si.

Sulfate aluminate profiles at the core showed that most of the points fell along the CH-AFm line, which is considerably common for normally hydrated Portland cement, except, perhaps, for samples immersed in pure sulfate and 1.0%Cl^-, in which some points fell along CH-hydrogarnet line.

The average atomic plot of the cement matrix of 15%LF in sulfate and combined sulfate and chloride solution after 1 year at 5°C can be seen Table 6-6. The analyses of each atomic ratio will be discussed in the sections below.

Table 6-6: Mean atomic ratio composition of the matrix in 15%LF samples immersed in salt solutions afer 1 year at 5°C.

Sample	Atomic ratio	Surface		Core		Typical Values for CSH
		Mean	Sd_{Error}	Mean	Sd_{Error}	
15M5	Si/Ca	0.299	0.025	0.370	0.026	0.600
	Al/Ca	0.127	0.022	0.116	0.016	0.080
	S/Ca	0.062	0.006	0.044	0.003	0.030
15M55	Si/Ca	0.238	0.029	0.314	0.058	0.600
	Al/Ca	0.054	0.016	0.063	0.015	0.080
	S/Ca	0.062	0.006	0.044	0.003	0.030
15M105	Si/Ca	0.407	0.039	0.318	0.020	0.600
	Al/Ca	0.103	0.019	0.095	0.014	0.080
	S/Ca	0.063	0.005	0.036	0.003	0.030
15M205	Si/Ca	0.336	0.013	0.395	0.025	0.600
	Al/Ca	0.116	0.018	0.065	0.009	0.080
	S/Ca	0.068	0.004	0.042	0.004	0.030

A. Silicon profile

As far as chloride is concerned, the average Si/Ca at the surface appears to have varied accordingly to what has been assessed by visual inspection, lattice parameter determinations and also the amount of octahedron silica in the system, in which higher damage was detected in 15%LF immersed in 1%Cl^-, as can be seen in Figure 6.58.

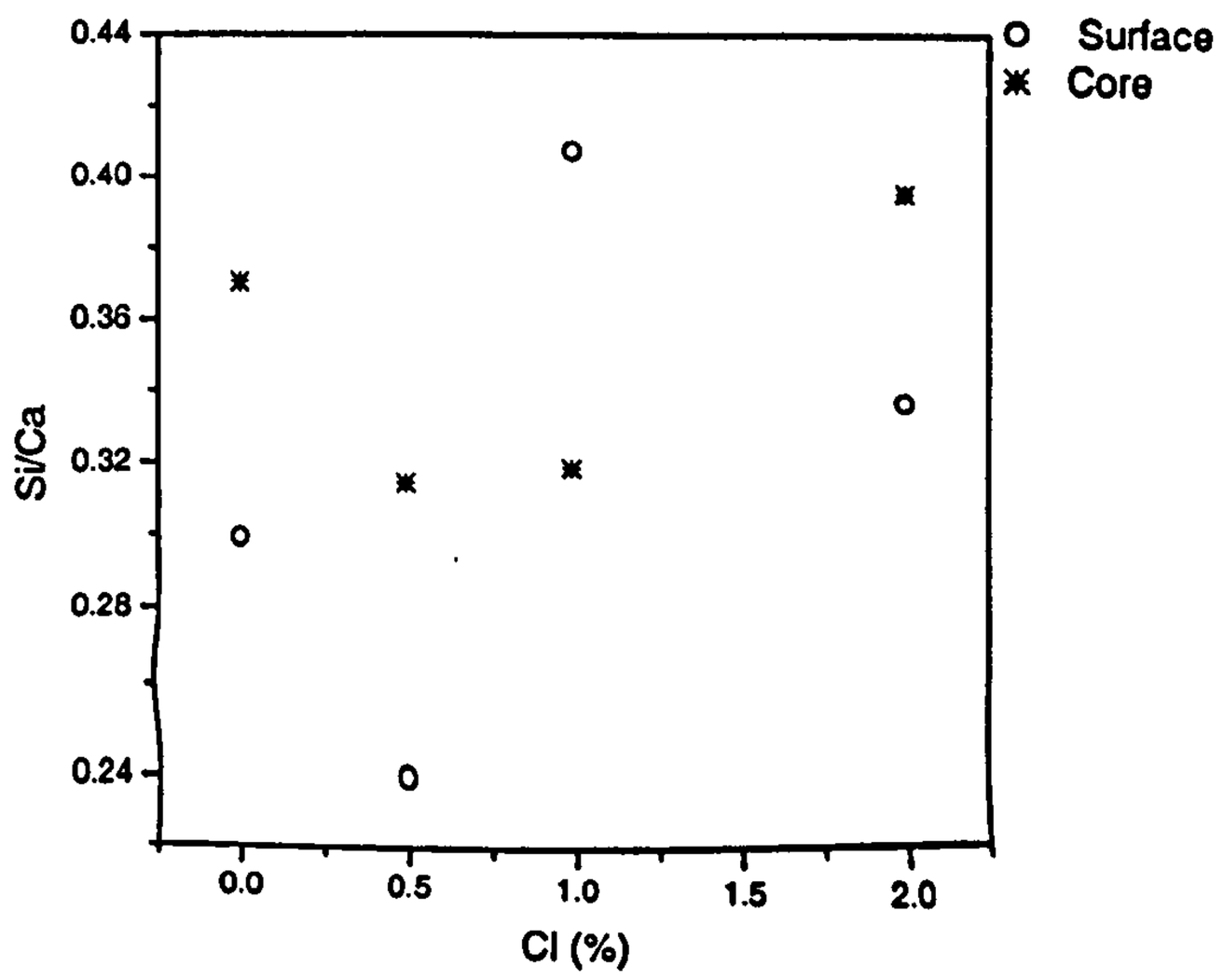

Figure 6.58: Mean Si/Ca atomic ratio in 15%LF after 1 year in salt solution at 5°C

Although quantitative x-ray microanalysis (QXMA) cannot detect the coordination of silicon, which can make it difficult to correlate the damage observed in Chapter 5

(see Figure 5.5) with respect to Si/Ca values alone, some sort of correlation can be found between Si/Ca values from QXMA and the net intensity of Si peaks in IRS, as can be seen Figure 6.59. In this plot, each value (i) has been normalised to the minimum value observed for both Si/Ca (Si/Ca min) and the intensity of the peak at 500cm^{-1} ($^{Net}Si_{500}$min).

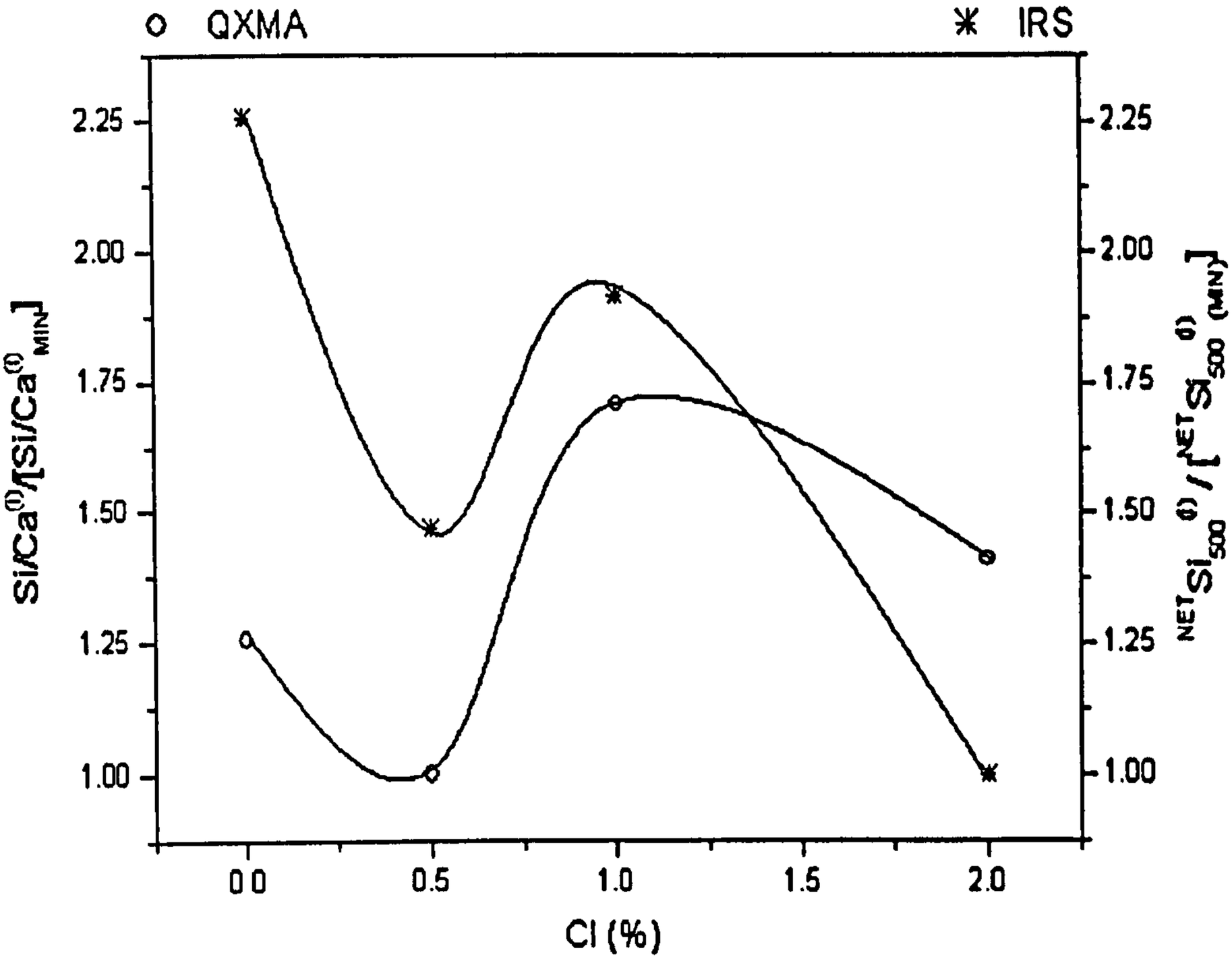

Figure 6.59 Si/Ca plot and net Si intensity in IRS as a function of chloride concentration.

Further analysis reveals however that poor linear correlation was found in Figure 6.60 between these two parameters (Si/Ca and $^{Net}Si_{500}$). However, there was a good correlation when another parameter (chloride) was included, as shown in Figure 6.61.

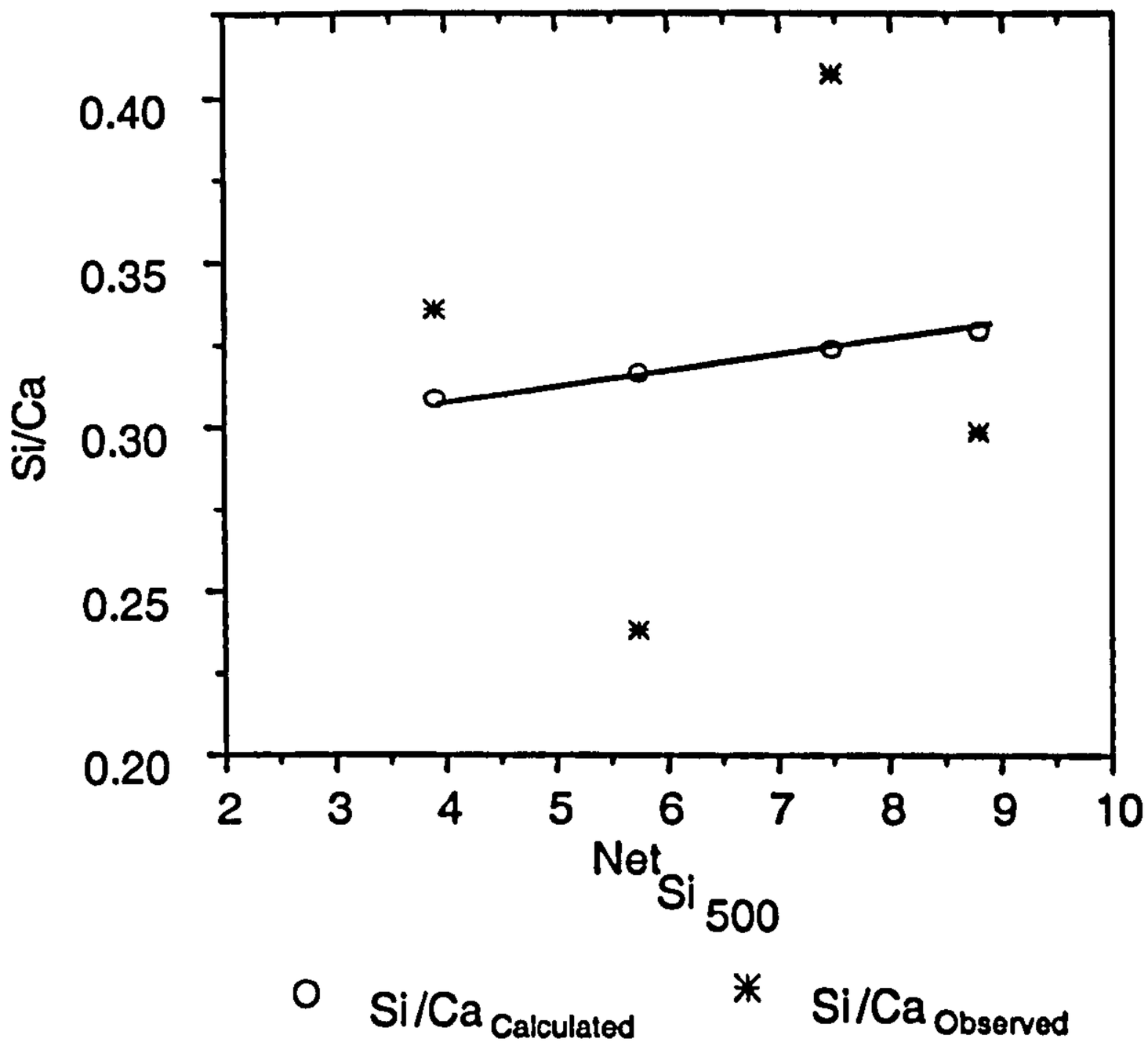

Figure 6.60 Linear correlation between Si/Ca and $^{Net}Si_{500}$.

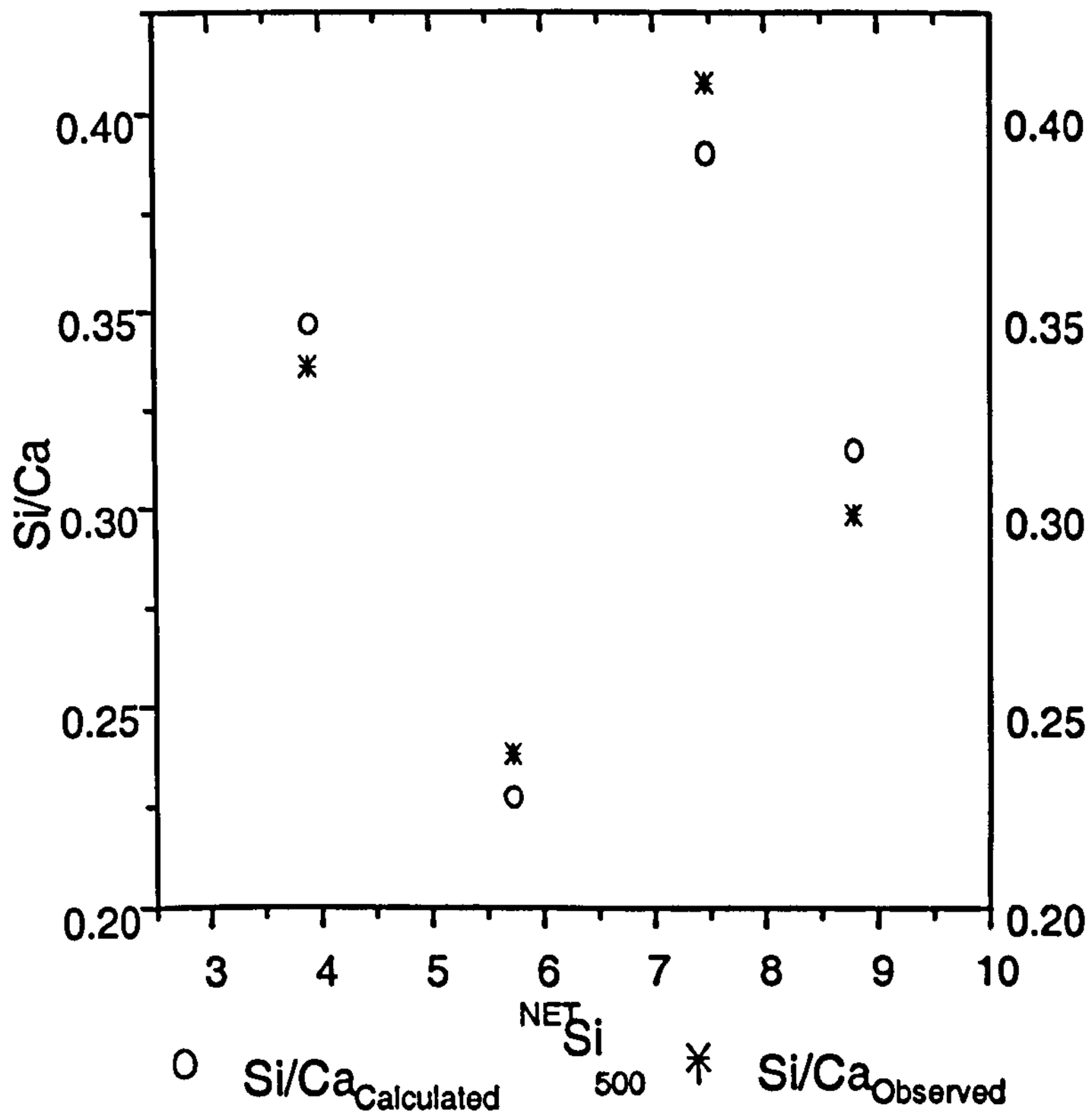

Figure 6.61:Correlation between Si/Ca and $^{Net}Si_{500}$ including the factor Cl.

This observation suggests that some of the silicon detected within the CSH is 6-coordinated by hydroxyl ions, which supports the previous identification of a mixture of thaumasite solid solution and CSH, being present in these corroded mortars.

This approach helps to clarify one of the main features of the chemical alteration suffered by CSH, which was marked by the presence of octahedral silica in all

solutions, but most intensely in samples immersed in 1.0%Cl^-. Indeed, it becomes apparent that the analysis of Si/Ca alone can underestimate the degree of damage caused by thaumasite. In fact, TSA brings different features to the microanalysis of cement matrix, for its Si/Ca raio is 0.33, which is also similar to that of anhydrous clinker grains (alite). Also, its low aluminium binding capacity makes it even more difficult to assess the actual composition or alteration of the CSH gel, as this gel also tolerates low aluminium in Portland cement (Al/Ca~0.08). Conventional sulfate attack decalcification, as reported by Bonen and Cohen [48], would have lead to Si/Ca ratios higher than the typical 0.6. When affected by magnesium sulfate, Bonen and Cohen reported Si/Ca values in Type I Portland cement paste immersed for 1 year in 4.1%$MgSO_4$ at 20°C around 1 to 0.43, in the surface (damaged) and core (sound), respectively. In the case of thaumasite, as pointed out earlier, it seems that CSH not only decalcified but also lost hydrosilica, since thaumasite would demand both ions alongside sulfate and carbonate. CSH seems to dissociate incongruently in thaumasite prone areas at a preliminary stage of the attack, as appears to have happened since typical outer product features could still be distinctively seen in the damaged cement paste matrix between the thaumasite dark grey areas. Suppose, also, that it releases more of its silicon as $[H_xSiO_4^{-(4-x)}]$ than its lime as $[Ca^{2+}].[OH^-]$. The remaining product would have a lower Si/Ca ratio than a sound or decalcified calcium silicate hydrate. Incongruent dissolution was reported by Harris et al. [157], in which CSH is proposed to dissolve at the initial stages as in equation 6.3:

$$(xCaO.SiO_2.yH_2O)_{solid} \rightarrow \{(x-a)CaO.(1-b)SiO_2.yH_2O\}_{solid} + a\,Ca(OH)_{2aq} + b\,SiO_{2aq} \qquad (6\text{-}3)$$

Where, $Ca(OH)_{2aq}$ and SiO_{2aq} represent the possible ionic species in solution.

B. Aluminium profile

Figure 6.62 shows the mean Al/Ca ratio plotted against chloride concentration in solution. It can be seen that the values at the core were approximately similar to typical values for CSH gel. In pure sulfate and 1.0%Cl^-, though, where greater damage was also detected by visual inspection, this ratio was slightly higher. At the surface, however, Al/Ca were exceedingly higher, at least in the order of 30% or more. This trend was not observed in samples immersed in 0.5%Cl^-, in which Al/Ca was less than that expected for a CSH gel, and where the lowest damage had also been observed by visual assessment for 15%LF containing samples (Figure 5.5).

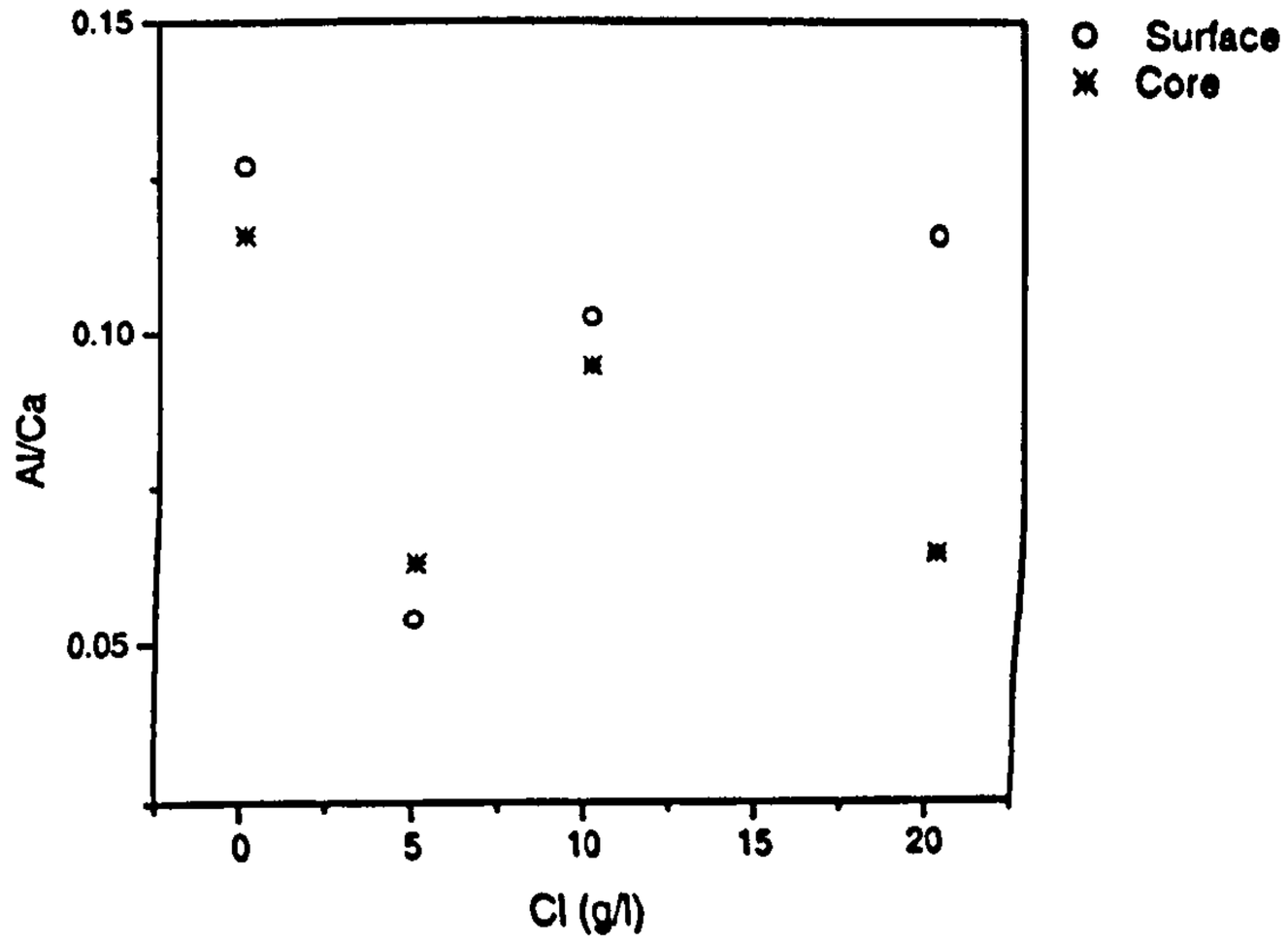

Figure 6.62: Mean Al/Ca atomic ratio in 15%LF after 1 year in salt solution at 5°C

C. Sulfate profile

Perhaps the clearest difference between the characteristics of the core and surface regions can be identified by the S/Ca ratio, as shown in Figure 6.63. Indeed, whereas these ratios in the core were slightly higher than for a typical value for CSH gel, they practically doubled at the surface in all solutions. However, they were still far away from the calculated values for thaumasite or ettringite, S/Ca ratios of 0.33 and 0.5, respectively, possibly because these phases were intermixed within the CSH gel at a sub-micron level and could not be resolved by BEI-EDX of the microscope.

The increase in chloride concentration promoted an increase in the uptake of sulfates within the matrix. However, it was not possible to establish any consistent trend between the apparent damage assessed previously and the sulfate profile, since damage caused by TSA is more predominantly marked by the disruption of the matrix and by the dissolution of CSH than by the sole uptake of sulfates by the cement matrix. This uptake can also result in the precipitation of other less aggressive calcium sulfate hydrate phases such as gypsum and ettringite.

Nonetheless, a closer investigation of the sulfate profile at the surface indicates a similar trend to that observed in the correlation between the *c* dimension and the chloride content (Figure 6.23), in which *c* increased as Cl^- concentration increased from 1.0% to 2.0%. As pointed out earlier, the higher the value of *c*, the more tetrahedral sulfates within the spaces parallel to the calcium aluminate columns. The lattice parameters had been determined using the corroded material that precipitated at the

bottom of the containers rather than bulk samples, as in EDX. Any correlation between the matrix at the surface and the corroded material precipitated in the bottom of the containers can be possible because the solid solution that precipitated in the bottom can also be present within the gel, hence, the similarity of trends.

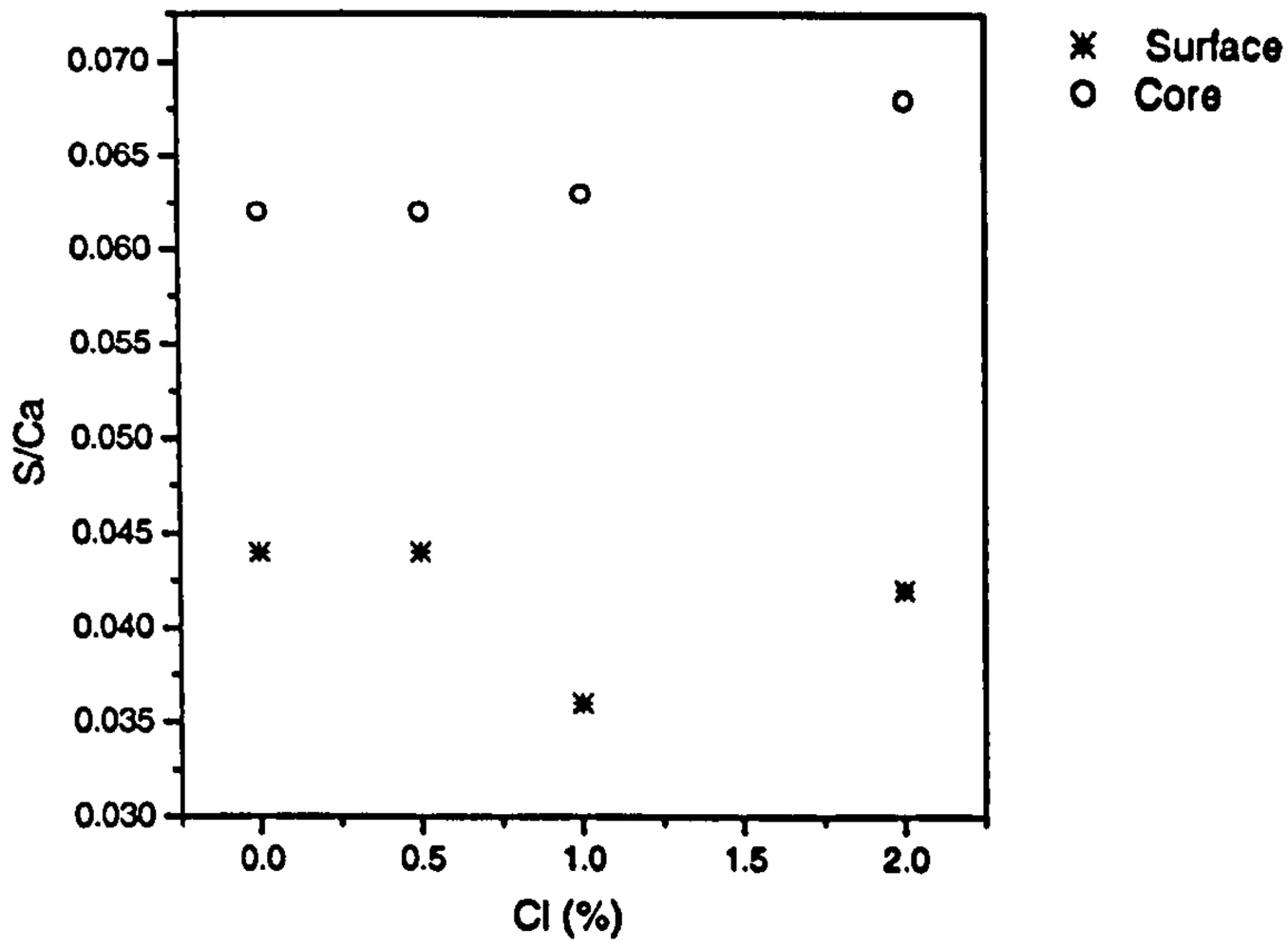

Figure 6.63: Mean S/Ca atomic ratio in 15%LF after 1 year in salt solution at 5°C

Indeed, Figure 6.64 seems to confirm such a trend between S/Ca and the unit cell parameter *c* and Cl^- concentration in solution. It can be seen that although a linear correlation (R^2=0.56) between the observed S/Ca (*) and the parameter *c* is very poor (△), this atomic ratio correlates (R^2=0.87) better with chloride concentration alone (○), but much better agreement (R^2=0.99) is found when using a combination of both *c* unit cell and Cl^-(○).

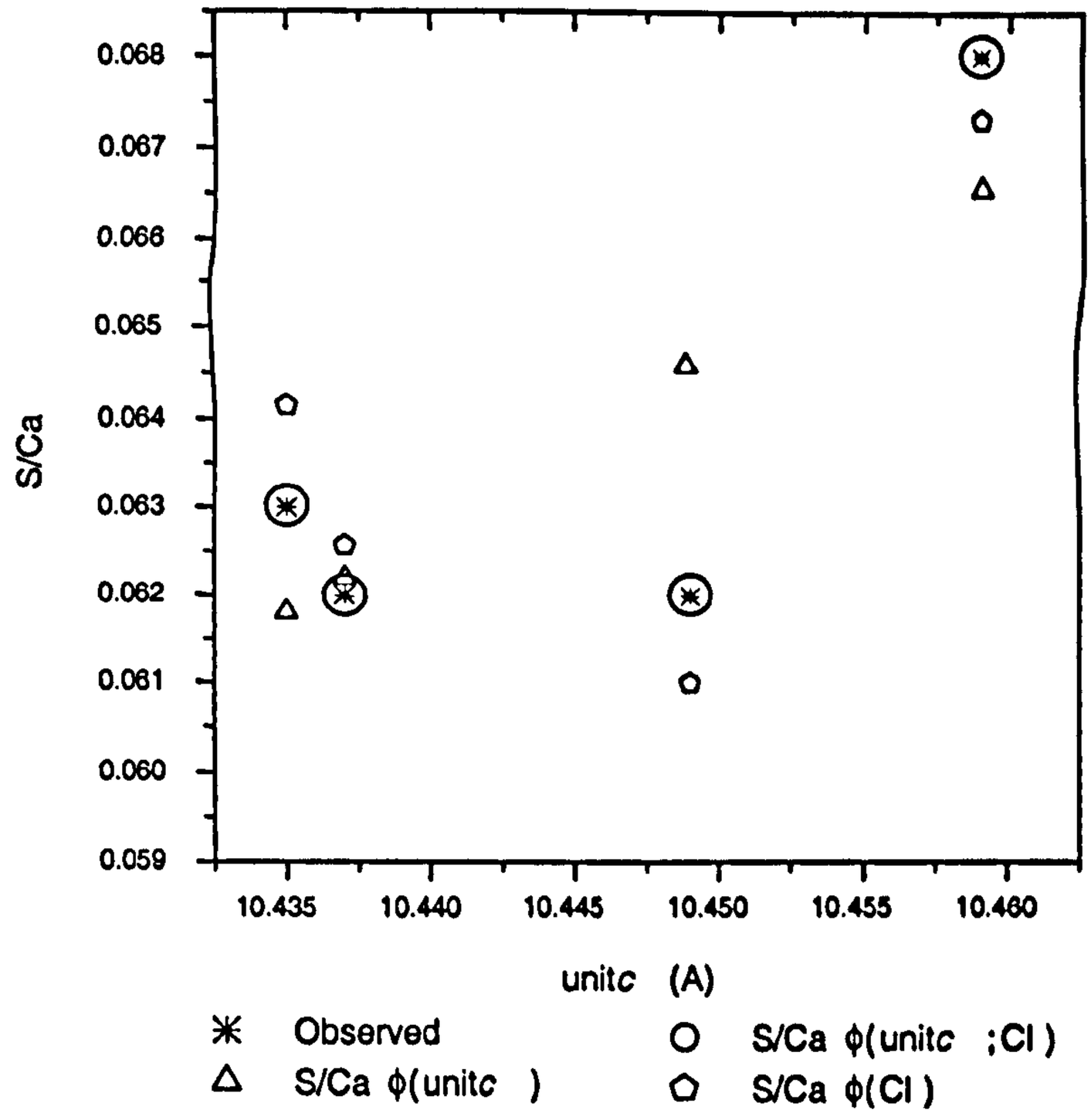

Figure 6.64: Correlation between S/Ca and unit C with and without including the factor Cl.

Therefore, the cement matrix composition deviates from its typical values due to the thaumasite form of sulfate attack, which appears to have damaged the matrix by:

(i) Incongruently dissolving the calcium and hydrosilica from the C-S-H structure, hence, the observed Si/Ca values are lower than those expected in conventional magnesium sulfate attack;

(ii) Possible destruction of the structure of ettringite and Friedel's salt which released their sulfate ions and chloride ions, respectively, and probably transformed into a hydrogarnet type phase,

(iii) Precipitation of thaumasite solid solution within the matrix on an intimate scale smaller than the resolution of the microscope;

(iv) The improved correlation between the Si/Ca and S/Ca plots with respect to $^{Net}Si_{500}$ and the *c* parameter by adding chloride to the model leads to the conclusion that chloride plays a role in the damage caused to CSH.

D. Chloride and magnesium profiles in mortar containing limestone filler immersed in combined sulfate and chloride solutions at 5°C.

Table 6-7 shows the average Cl^- and Mg^{2+} atomic ratios determined from QXMA in samples containing 15%LF in salt solution after 1 year at 5°C.

Table 6-7: shows Cl and Mg atomic ratios at the core and surface of 15%LF immersed in sulfate and combined sulfate and chlorides after 1 year at 5°C.

Sample	Atomic ratio	Surface		Core		Typical Values for CSH
		Mean	Sd_{Error}	Mean	Sd_{Error}	
15M5	Cl/Ca	0.006	0.001	0.011	0.001	Variable
	Mg/Ca	*0.013*	*0.003*	*0.016*	*0.004*	*0.030*
15M55	Cl/Ca	0.026	0.005	0.040	*0.011*	*Variable*
	Mg/Ca	0.010	0.003	0.007	0.002	0.030
15M105	Cl/Ca	0.024	0.004	0.060	0.009	Variable
	Mg/Ca	0.023	0.005	0.012	0.002	0.030
15M205	Cl/Ca	0.045	0.011	0.088	0.010	Variable
	Mg/Ca	0.020	0.005	0.011	0.002	0.030

It can be seen that the Cl/Ca ratio increases with chloride concentration in both surface and core regions, in a linear fashion. The rate of chloride binding is reduced in approximately 50% in the surface regions when compared to the core, as observed by the linear correlation model as shown in Figure 6.65.

Also, it can be seen in Figure 6.66 that although several points fell close the NaCl line at the surface, some points were predominantly chloride with much less sodium. This observation seems to be in agreement with the findings based on XRD in which no calcium chloroaluminate hydrate (Friedel's salt) had been detected at the surface (within the corroded material), but was detected in the core (bulk sample). Indeed, in the core, as can be seen in Figure 6.67, the chloride analyses were mostly distributed close to the Cl/Ca line rather than grouped with sodium around the NaCl line as in the surface region, which, again, appears to be in agreement with previous findings by XRD that chloride is bound within aluminate phases (see section 5.3.3-A). Indeed, it has been

confirmed that the chloride distribution correlates better with aluminates than with silicates in all solution (see Fig 6.47-6.48, 6.50-6.51, 6.53-6.54).

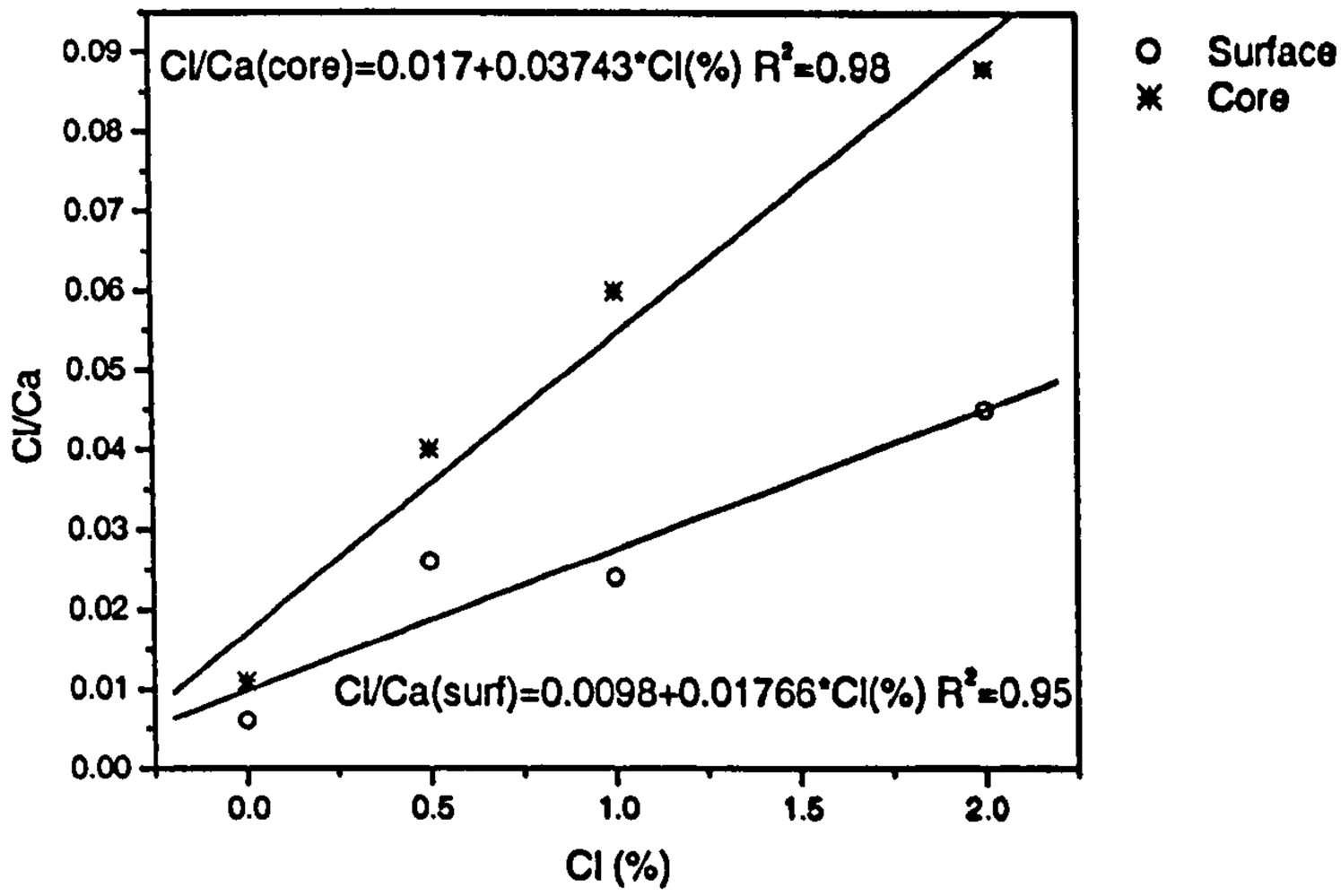

Figure 6.65: Chloride profile in 15%LF after 1 year at 5°C in salt solution.

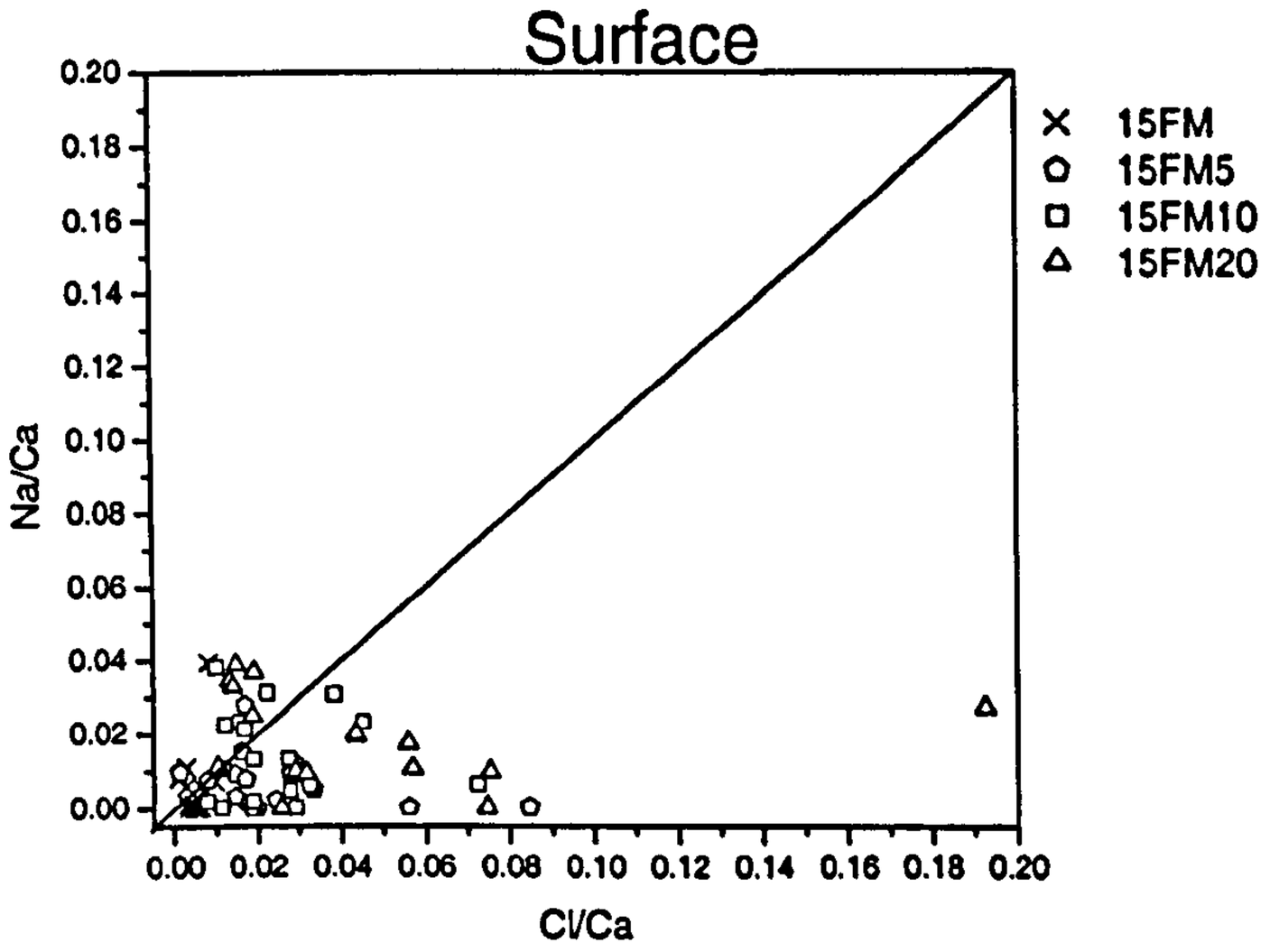

Figure 6.66: Sodium and chloride profile at the surface in 15%LF after 1 year at 5°C in salt solution.

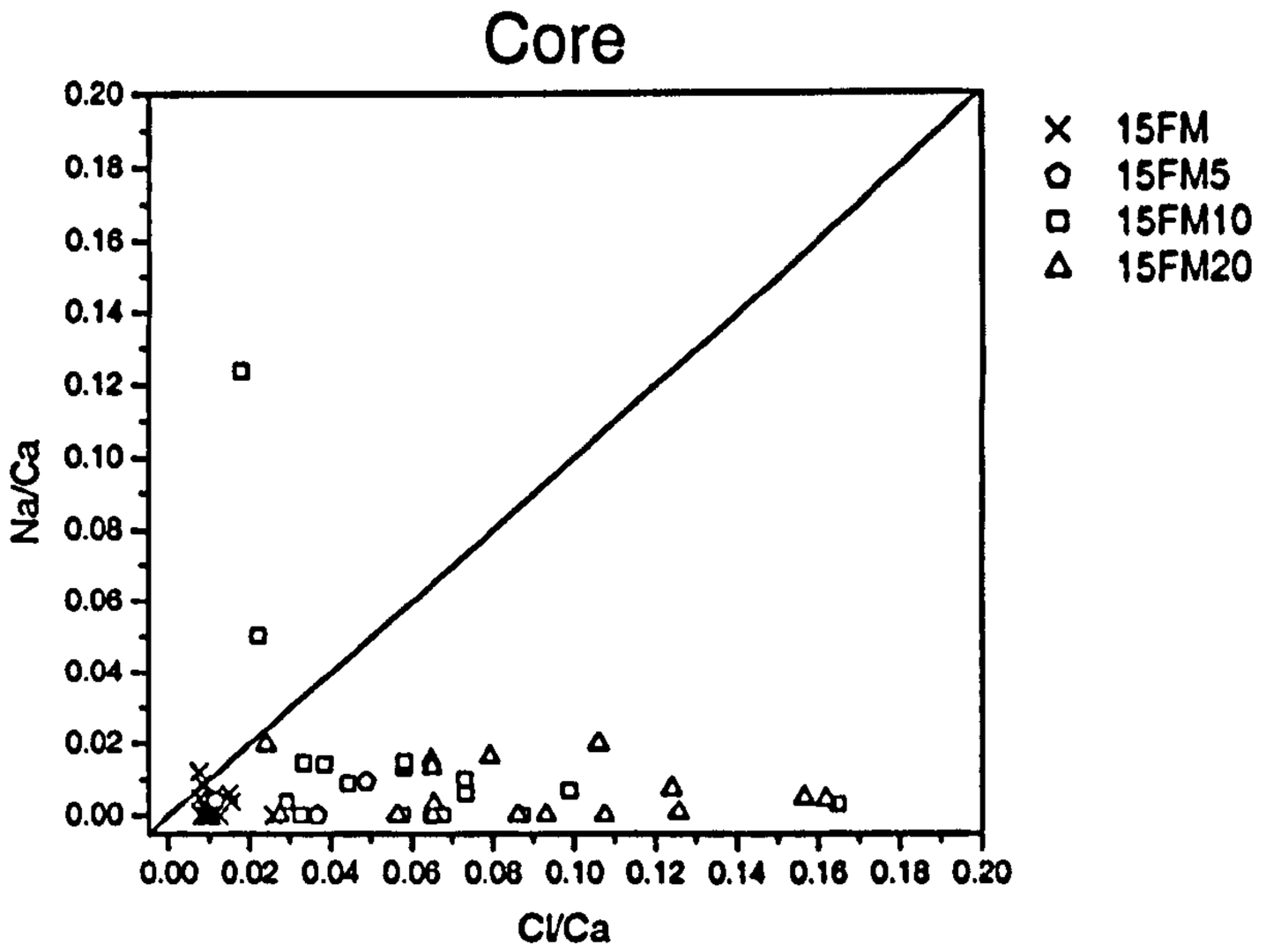

Figure 6.67: Sodium and chloride profile at the core in 15%LF after 1 year at 5oC in salt solution.

As far as the magnesium profile is concerned (Figure 6.68), the mean Mg/Ca ratio was found to be below 0.03. This appears to indicate that very little interaction (meaning the formation of magnesium silicate hydrate) occurred within the samples. Although this distribution was significantly scattered, the maximum value for Mg/Ca was 0.09, whereas most of the points were below 0.05 (Figure 6.55). Nevertheless, brucite has been identified within the corroded material but not in the bulk analysis. This observation confirms the very low diffusivity of magnesium in cement matrix and also that brucite is favoured to precipitate rather than MSH as calcium silicate hydrate would be engaged in thaumasite formation, which differentiates this mechanism of attack from the classical magnesium sulfate attack [48].

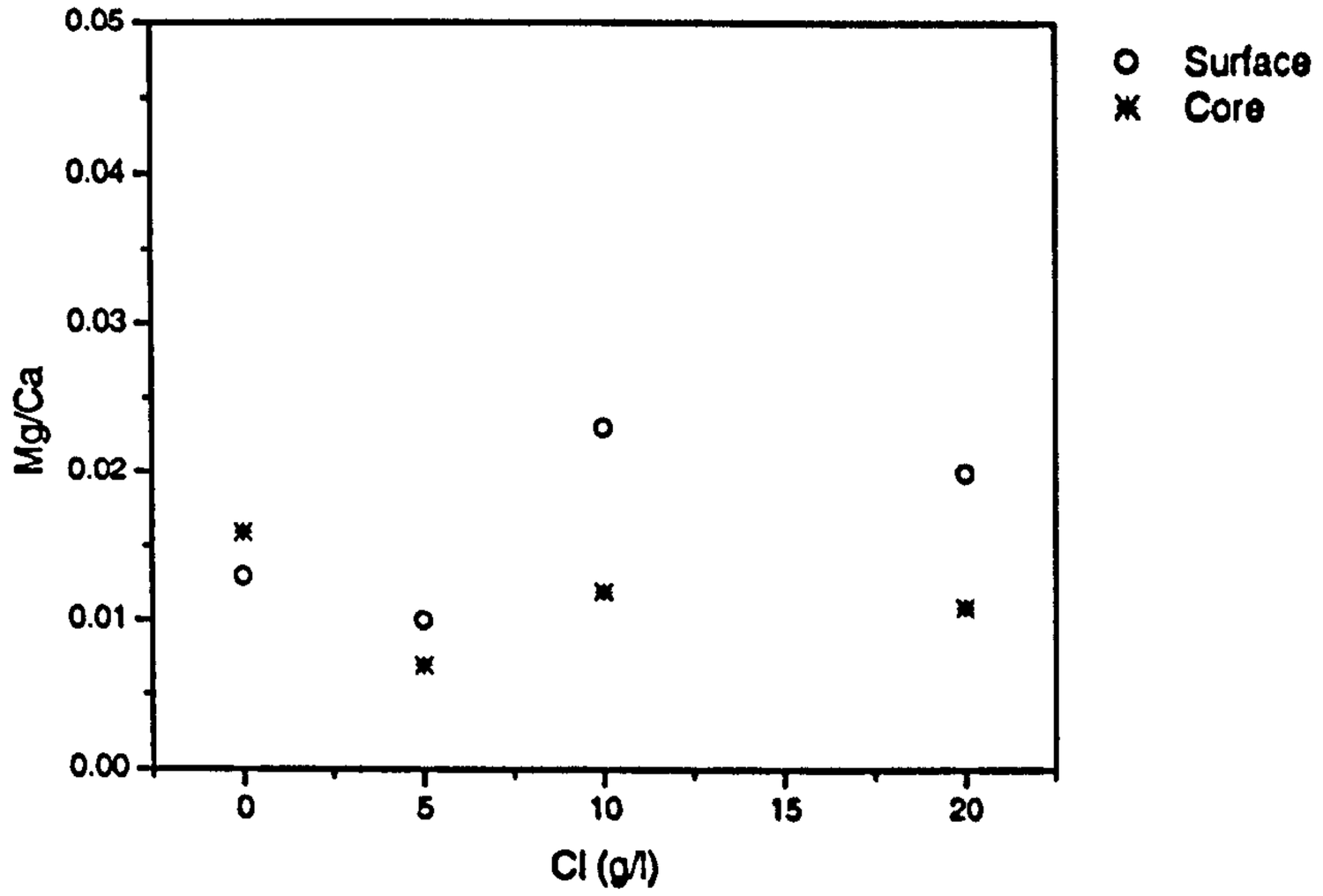

Figure 6.68:Magnesium profile at the surface in 15%LF after 1 year at 5oC in salt solution.

6.5. Conclusions

The combined action of chlorides and sulfates in the thaumasite form of sulfate attack has been investigated for the first time. Based on the results, it can be concluded that:

- The thaumasite form of sulfate attack (TSA) caused significant damage in samples with and without limestone filler after 1 year of immersion in sulfate and combined sulfate and chloride solutions at 5°C.

- The attack was marked by a progressive development of a dark grey continuous band (in BEI) at the surface, which occurred not only within the cement matrix but also around the surrounding aggregates, despite the presence or not of chloride in the sulfate solutions.

- Extensive cracks developed at the boundaries of such bands and the matrix, which demonstrates a loss in the binding properties of the matrix as chunks of mortar could be easily detached by hands when dried (The corroded material was white and mushy when wet).

- Whereas normal features of hydrated Portland cement were identified in the core of all samples, some unhydrated clinker grains, which were also attacked by the precipitation of thaumasite solid solution, were distributed

within a network of cracks that developed within the cement matrix at the surface.

- It appears that CSH dissolves incongruently in which it decalcifies and also loses its silicate, at the first stages of the attack, but congruently as total conversion into thaumasite takes place at advanced stages of TSA, as it becomes very pervasive.

- As for the chloride binding capacity, it appears that thaumasite has a very limited or non-existent capacity to interact with chloride because:

  (i) The unit cell parameters fell comfortably within the known *limits for thaumasite solid solutions*;

  (ii) The chloride content correlated well with the parameter *c*, which is affected by the sulfate to carbonate ratio within the unit cell. There seems to be an optimum chloride concentration in which a purer thaumasite precipitates. The minimum *c*, tends to vary linearly with carbonate and chloride content.

  (iii) Hence, it is more likely that such correlation seems to be better explained by an increased solubility of calcium carbonate. Since the low Cl/Ca ratio contradicts the hypothesis that Cl^- replaces either carbonate or sulfate within the crystal structure of thaumasite.

- The chemical attack suffered by the CSH was rather different from a classic magnesium sulfate attack. In TSA affected mortars, Si/Ca values of the matrix fell within the CSH-ettringite-thaumasite area, which is indicative of a mixture of solid solutions, rather than a conventional decalcification and intrusion of magnesium in the gel.

- The extent of chemical alteration was higher at the surface than at the core, but it also varied with chloride concentration, as indicated by a good correlation between Si content (obtained by both QXMA and IRS), and both carbonate and chloride contents.

- Reasonable correlation was also obtained with the damage assessed by the loss of mass and the moles of octahedral silica. Less damage was developed in samples immersed in 0.5%Cl^- and greater damage observed in 1.0%Cl^- in 15%LF samples. However greater mass loss was detected as the chloride concentration increased to 2.0%. Also, in these solutions, the correlation between the Si/Ca and $Si(OH)_6$ were both the lower and the higher, respectively.

- Although the Cl/Ca ratio increased with chloride concentration, the binding capacity was reduced in the corroded areas, due to the precipitation of thaumasite. Yet again, this observation points to the fact that the role chloride in TSA is primarily catalytic.

- Better correlation was obtained between the S/Ca ratio versus lattice parameter *c* and chloride concentration in solution. This observation can be explained by the fact that similar solid solution of the material that precipitated at the bottom of the containers and also precipitation within the hydrated cement paste.

- The levels of magnesium were mostly below the typical values for a sound cement matrix, which indicates that magnesium plays a different role in TSA than it does in classical magnesium sulfate attack, where the buffered pH action of brucite precipitation and MSH are responsible for the breakdown of the integrity of the matrix.

- The levels of sodium were also low, and were mostly identified in some precipitation of Halite (NaCl) since the Na/Cl ratio fell along its composition line at the surface.

- The effect of chloride concentration of 0.5%Cl^- on the chemical alteration on the specimen appears to confirm that the attack was slightly less intense than other salt concentrations. Nevertheless, TSA attacked the surface.

- The non-linearity of the effect of Cl^- observed appears to be associated with its catalytic role in TSA, in which greater solubility of carbonates competes with the slow kinetics of thaumasite precipitation.

Chapter Seven

Effect of Combined Chloride and Sulfate on TSA: Overall Discussion

7.1 Discussion

Ordinary Portland cement mortars containing calcium carbonate filler have been immersed in magnesium sulfate and combined sulfate and sodium chloride solutions at 5°C and 20°C. The discussion addresses the objectives of this current work:

- To investigate the changes in the microstructure of Portland cement mortars immersed in magnesium sulfate solution at 5°C for 5 years;

- To investigate the extent to which atmospheric carbonation affects the formation of thaumasite;

- To evaluate whether or not chloride plays any role in the formation of thaumasite;

- To study the effectiveness of metakaolin in Portland limestone cements exposed to sulfate solutions, and combined chloride and sulfate solutions at different temperatures;

- To assess whether or not the chemical composition of thaumasite is affected by the presence of chlorides;

- To analyse the effect of thaumasite on the chloride binding capacity of the cement matrix in cement, containing limestone filler.

7.1.1 The effect of carbonate content on the microstructural changes in Portland cement mortars as a result of TSA

There are at least four sources of carbonates in Portland cement concrete:

(ii) The cement itself as a minor additional constituent (*MAC*), or as filler replacing clinker [21];

(iii) The aggregates [14];

(iv) The bicarbonates in groundwater [15, 76, 82];

(v) The carbonation of the concrete during the construction process.

Although all carbonates can be considered responsible for the increased susceptibility of cementitious systems to TSA (section 4.4.1 and 4.4.5-Chapter 4 and [2, 76]), the contribution of each source depends on a combination of factors such as: solubility and kinetics of thaumasite precipitation, temperature, pH, and the presence of other ionic species such as dissolved carbon dioxide and also how the carbonates alter the cement matrix . For instance, the BRE Special Digest 1 [14] has introduced the aggregate carbonate range, which is an indicator of the level of carbonate permitted under conditions susceptible to TSA. This range permits more carbonates in the concrete depending if they have originated in the coarse aggregate or less if the have come from the fine aggregate.

At low temperatures, it has been observed that carbonates, either added as minor additional constituents (*MAC),* filler or coming from atmospheric carbonation promoted the precipitation of thaumasite in all Portland cement systems in this research (Chapter 4 and Chapter 5). Indeed, thaumasite was responsible for causing disruption of the cement matrix, with damage increasing with carbonate content.

Basically, whereas a certain degree of supersaturation of ions with respect to thaumasite nucleation could be expected when bicarbonate is the source, the presence of *MAC* filler distributed within the cement matrix appears to facilitate such nucleation by possibly reducing the thaumasite/solution interfacial energy. This reduction in the solid-liquid interfacial energy by the presence of a nucleation site has been discussed by Drever [82]. In the latter case, lower supersaturation can be expected for the nucleation of thaumasite, therefore, increasing the rate of its formation. Although there are other potential nucleation sites for thaumasite in the cement matrix, fine carbonate filler is

favoured because of its chemical compatibility with thaumasite, since it is the source of carbonates that differentiates TSA from conventional sulfate attack in cold sulfate environments. In the present research, carbonate filler was replaced and mixed with Portland cement. When interground with cement, it is possible that the size of the easily ground carbonate particles would tend to fall in the finest fraction of the cement [158], thus offering nucleation sites and increasing the chances for thaumasite attack.

Also, it was observed that thaumasite formation demands a highly alkaline cement pore solution inside the concrete (*see* section 5.3.4-Chapter 5), which increases the chances of thaumasite formation at deeper sites in limestone cements, where carbonates (CO_3^{2-}) would be already available inside the concrete either as *MAC* or filler. In the case of bicarbonate (HCO_3^{1-}) containing groundwater, TSA would progress from the surface inwards. Yet, in such a case, thaumasite precipitation can also be affected by the pH gradient of the concrete-groundwater interface, which could be buffered at levels below that necessary for thaumasite formation, by a strong dissolution of soluble hydration phases of the cement. However, the attack would expose fresh concrete, which would raise the pH and hence allow thaumasite to form. Also, another calcium carbonate phase (calcite or aragonite) could precipitate at the surface.

In general, all Portland cement mortar samples, with and without limestone filler, immersed in sulfate solution at 5°C predominantly developed thaumasite within one year (Chapter 5). A similar trend was also found in long-term specimens previously immersed in solutions of higher magnesium sulfate concentration (1.8%$MgSO_4$) at 5°C for 5 years, but it took more time for a significant amount of thaumasite to precipitate within one year. Only ettringite was found in the OPC control system after one year of immersion in such a high concentration, as reported by Hartshorn [69], but thaumasite became all pervasive and progressively advanced inwards, at the expense of the CSH and other phases such as ettringite, ferrite, and clinker grains. It appears that a higher concentration of magnesium in solution led to an early deposition of a brucite layer at the surface, which not only buffered the pH below 10.5 but also blocked pores that might have retarded the diffusion of ions into this mortar [50, 99], resulting in delayed formation of thaumasite. Indeed, Hartshorn [69] detected that mostly ettringite precipitated in the OPC control with 5% limestone filler samples after 1 year, but it was totally converted into thaumasite after 5 years, as reported by Torres et al. [13, 18] and as shown in Chapter 4, accompanied by extensive damage to the mortars.

Although thaumasite can form at higher temperatures [47, 124], and was observed to crystallise alongside ettringite at room temperature (20°C) in several conditions during this research (Figure 5.21, 5.27, 5.31 and Table 5.2), the effect of carbonate content and its source on the formation of carboante phases differed from the observations made at lower temperatures. Indeed, other carbonate phases such as calcite and aragonite (Figure 5.20-21 and 5.30-31), which readily precipitate at higher temperature, were found to be more abundant under these conditions than thaumasite. In such cases, carbonate phases would also precipitate alongside brucite at the surface and a beneficial blocking of pores could be expected [50, 99]. Because calcium carbonate-water equilibrium pH in groundwater appears to be low (8.48) [82] for thaumasite formation[70], a calcium carbonate layer at the surface of the concrete can thus reduce the chances of thaumasite precipitation, which requires alkaline solution (*see* 5.3.4-Chapter 5). Therefore, although a higher carbonate content would increase the risk of thaumasite formation at higher temperatures, the potential damage associated with TSA is remarkably reduced or even non-existent, depending on whether the carbonates would stay long enough in solution to allow thaumasite nucleation or precipitate as aragonite, for instance. However, a reduction in the temperature would revert the process towards thaumasite formation.

Finally, it appears that carbonate solubility and the kinetics of thaumasite nucleation seem to control the potential damage associated with the thaumasite form of sulfate attack. Hence, it is important to consider that the combined interaction of carbonate content, and other factors such as other ionic species in solution, can also adversely affect the susceptibility of cementitious systems to TSA, by increasing the availability of carbonate ions in solution.

7.1.2 The effect of atmospheric carbonation on the formation of thaumasite

As far as atmospheric carbonation is concerned, the formation of a carbonated low pH zone also seems to explain why thaumasite did not attack carbonated areas, but significant attack was found beneath the cement/carbonated layer in the core of samples exposed to air for 5 years prior to immersion in sulfate solution at cold temperature (*see* Figures 5.12-5.16). Indeed, the greater the width of the carbonated zone, the less the damage caused by thaumasite. Crammond [159] also observed that carbonation somehow protected concrete from the precipitation of thaumasite in the carbonated zones. In further studies, Collett et al. [76] examined the effect of carbonation as a potential source of carbonates for TSA. They also observed the formation of thaumasite beneath the cement/carbonated zone interface.

7.1.3 The role of chloride in TSA: Damage assessment, characterization of deterioration products and main factors

The presence of chlorides in sulfate containing solution does not inhibit the formation of thaumasite in Portland cement mortars (see Figures 5.5 and 5.7-5.9). The data presented in this research seems to indicate that the effect of chloride ions on thaumasite formation is predominantly catalytic, since an absence of chloride bearing phases has been detected among the deteriorated products (see section 5.3.3).

Indeed, it has been observed that the presence of chlorides and sulfates considerably increases the solubility of carbonates at low temperatures (Appendix II), and this appears to be the main factor affecting the formation of thaumasite in the presence of chlorides. In this case, the extra availability of carbonates would lead to a higher susceptibility for TSA because the carbonate species would precipitate as thaumasite. Indeed, whereas thaumasite was the main phase responsible for extensive damage in all mixes with and without limestone filler at low temperature (Figures 5.20, 5.26, 5.28, 5.30 and Table 5.2), calcium carbonate (aragonite) was abundantly deposited among the deterioration products at higher temperature (Figures 5.21, 5.27, 5.29, 5.31 and Table 5.2).

However, the increased solubility of carbonates alone cannot explain why 0.50%Cl^- concentration seemed to reduce the extent of attack in some samples (Figure 5.5, 5.18 and Table 5.5). Indeed, it was found by loss in mass experiments, and also by visual assessments (clearer in samples containing 15% limestone filler), that there seems to be an optimum concentration of chlorides in which the excess carbonate ions available in solution match the demand for thaumasite precipitation. In this case, greater damage can be expected (as in 1.0%Cl^-, for instance). When the concentration of chlorides is higher than such an optimum, it appears that carbonates would be needed to equilibrate the negative charge imbalance caused by the diffusion and reaction of chlorides inside the cement matrix of the sample [145]. This can possibly explain the reason why more aragonite was found whenever less thaumasite was detected, as at 20°C, and mostly at the surface of the samples. More evidence for this view will be presented when discussing the effect of chloride on the composition of thaumasite.

Therefore, it appears that the optimum chloride concentration in which more thaumasite is expected would depend on the level of carbonates in the solution. For

instance, a statistical model based on mass loss suggests that mortar samples containing only 5% limestone filler immersed in a solution containing 1.8% Cl^- and 0.6% SO_4^{2-} would develop similar mass loss due to TSA as a mortar containing 15% limestone filler in pure sulfate solution of the same concentration (Figure 5.18). This can have serious implications with regards to the performance of European Standard OPC, where incorporation of 5%LF is allowed, in underground concrete foundations.

In thaumasite-affected areas, no Friedel's salt has been detected (sections 5.3.3 and 6.3.3). This observation indicates that Friedel's salt, which dissolves in the presence of carbonates [105, 106], might also be unstable in the presence of thaumasite.

The adverse increase in the susceptibility of carbonate-containing Portland cement to TSA raises the question whether the presence of chlorides also affects the threshold levels specified for aggregate carbonate range and the aggressive chemical environment classes for concrete in aggressive groundwater specifications in the BRE digest for use of concrete in aggressive ground [14].

7.1.4 The use of metakaolin in mortar containing limestone filler to prevent TSA

Systems containing 10% metakaolin offered good resistance to TSA, despite the high limestone content of 15%, up to 1 year in salt solution at 5°C. Indeed, the effectiveness of metakaolin can be expected because it is a very reactive pozzolan, which consumes the soluble lime from the system and improves the refinement of the pores, which are important factors affecting the resistance of the cement to sulfate attack [160].

However, significant signs of damage were detected after 72 weeks of immersion in pure magnesium sulfate. The mode of attack seemed to be the conventional type of sulfate attack, with the precipitation of gypsum alongside ettringite, even at 5°C. Also, because other XRD peaks could be assigned to orthorhombic thaumasite (Figure 5.23), it was suspected that the precipitation of this thaumasite was also responsible for the attack. However, gypsum was the main phase responsible for the attack, and ettringite have also been identified. However both phases have been detected after one year, when no damage was detected (Table 5.2). Further analyses revealed that no octhahedral silicon was found (Figure 5.33). It was then suspected that thaumasite changed its symmetry to orthorhombic as happened in the case of a similar carbonate free thaumasite analogue, whose XRD pattern can be found under the PDF number 44-1413.

This mineral has not been reported as a deterioration product in sulfate attack, and also not considered as a possible transition symmetry in the ettringite-thaumasite solid solution. Furthermore, the disappearance of the Al-O-Si stretching wave band when the sample was damaged might possibly be correlated with the nature of the effect of metakaolin on the type of CSH formed in this mix. Although it is still not clear why no damage was identified in combined chloride and sulfate solutions, it seems that because metakaolin improved the chloride binding capacity of the matrix (higher deposition of Friedel's salt-Table 5.2) and chloride diffusion [161], the detrimental effect of free chloride in solution was reduced.

7.1.5 Composition of thaumasite in the presence of chlorides

The possibility of chloride interacting with thaumasite was investigated (section 6.3.2). As for the possibility of chlorides entering within the unit cell of thaumasite, it does not seem to occur since all the observed thaumasite lattice parameters comfortably fell within the limits for a thaumasite type of phase, and sometimes even below the values expected for the thaumasite end-member (section 6.3.2-C). The existence of afghanite, a mineral that (i) contains the same assemblage of chemical elements as in thaumasite plus chlorine, and also (ii) crystallises in similar symmetry [153], seems to indicate that chloride can replace carbonates in the crystal structure. However, such a hypothetical chloride- thaumasite analogue would have a Cl/Ca ratio higher than 0.33, much higher than any Cl/Ca ratio identified in the corroded matrix during this study (sections 6.3.2A-Band 6.4.2A-B).

In general, good correlation was found between the concentration of chlorides and the presence of octahedral silicon, the unit cell *c* parameter, and the bound sulfate in the cement matrix (sections 6.4.2A-C). Indeed, greater damage was observed in samples with a lower value of *c* and higher octahedral silicon content (Figures 5.5 and 6.23). Moreover, the data indicated a certain interaction between chloride and carbonate affecting the unit cell parameter *c* of thaumasite (section 6.4.2B, Figure 6.56). It appears that this precipitation would occur under a certain concentration (optimum) of soluble chloride in which thaumasite would have the lowest *c*, and that this optimum chloride concentration would decrease linearly with increasing carbonate content (Figure 6.57). Indeed, carbonates affect the cell parameter *c* in thaumasite because its planar structure reduces the height of the cell compared to the tethrahedral sulfate ions within the thaumasite crystal structure (Figure 6.24). Torres et al. [18] identified a linear trend in

which the higher the amount of carbonate filler content added in the mortar samples the lower the unit cell parameter *c*.

Once more, such trends also seem to provide evidence for the interaction of chlorides and carbonate, in which much higher levels of chloride diffusing and reacting inside the cement would demand more carbonate ions to equilibrate the unbalanced negative charge, hence, the lower carbonate/sulfate ratio in the thaumasite. Indeed, the less the carbonate/sulfate ratio of the thaumasite crystal structure, the higher the unit cell parameter *c*, hence, the structure would shift towards an ettringite solid solution phase. It has been proposed that the presence of carbonates is also responsible for helping to increase the coordination of silicon to six, which is characteristic of thaumasite [84].

Another aspect of the effect of the chloride on the matrix is that it can increase the local pH as it reacts with aluminates and with CSH gel to some extent [140, 145, 146]. Indeed, such an increase in pH is basically because bound chloride would unbalance the negative charge in pore solution, hence, hydroxyl and even carbonate ions are needed. However, the precipitation of solid phases containing sodium or magnesium would also compensate for the unbalanced charge. Both cations were found to have very limited diffusion into the samples, which were often extremely low (section 6.4.3D). In the case of magnesium, the levels were always smaller than that has been published as acceptable levels as found in unattacked cement matrixes [81]. Therefore, the local pH in the cement matrix that was observed to increase in the presence of chloride (section 5.4.5) should also need to be considered as another factor affecting the precipitation of thaumasite.

7.1.6 Chloride binding capacity and interaction in thaumasite attacked Portland cement matrix

As far as chloride interaction with the cement matrix is concerned, it has been found that thaumasite damaged areas at the surface bound less chloride than the core of mortar samples independent of chloride concentration (Chapter 6).

The thaumasite type of sulfate attack affected the nature of the CSH gel in some peculiar ways. The damaged areas at the surface in all solutions were characterised by the development of thaumasite dark grey bands at the surface and around the silicon aggregates, with the formation of a porous, cracked and altered CSH and some residual clinker grains in between (Figures 6.2, 6.6, 6.9 and 6.11). The Si/Ca ratio of the damaged CSH decreased towards the centre of the area between thaumasite-ettringite-

CSH gel lines in the Al/Ca-Si/Ca plots (Figures 6.36, 6.38, 6.40, 6.42). This observation is contrary to that connected with common decalcification of CSH as in conventional sulfate attack where the Si/Ca ratio tends to increase [48, 104]. A lower Si/Ca ratio would indicate a greater ability to bind chlorides, as has been reported by Beaudoin et al. [146]. Nevertheless, when the Si/Ca ratio was low, the chloride binding capacity of these corroded areas at the surface were always lower than those in the core (Table 6.7). This apparent contradiction could be explained by:

(iv) Some of the Si^{4+} detected by QXMA correlated with the octahedral silicate estimated by quantitative IR spectroscopy for the material at the surface of the specimens (Table 6.3 and Section 6.4.3-A). This observation indicates that some of the thaumasite that precipitated at the surface could also be intermixed with the attacked CSH.

(v) Another possibility is that the Si/Ca of CSH has a ratio lower than ca. 0.66, which could indicate a mixture of normal type of CSH and CH or even thaumasite [12], but could actually be an incongruently dissolved CSH, which was both decalcified and also had its hydrousilicate ions leaching out, thus contributing to thaumasite formation. This hypothesis will be addressed in section 7.1.8.

(vi) The data suggest that chloride seemed more prone to be bound by aluminate phases than with silicate phases (section 6.3.4). Indeed, whenever poor correlation was observed between the Cl/Ca and Si/Ca ratios, good correlation was found between those for Cl/Ca and Al/Ca ratios.

A lower chloride binding capacity of the thaumasite-affected areas can have serious implications as far as reinforcement corrosion is concerned. As the damage front penetrates inside the concrete, the previously bound chloride, and even chloride bearing phases, could release chlorides into pore solution. This trend has been observed in the present work in 15% limestone filler samples (section 6.3.4D).

7.1.7 Effect of pH on TSA

It has been reported that thaumasite formation needs an alkaline environment to precipitate (pH >10.5) [70], because thaumasite does not seem to form in conditions where ettringite is unstable (pH<10.7, [143]) and the solubility of bicarbonate ions decreases [76]. It has been also reported that the presence of chloride can not only

increase the local pH [140, 145], but it can also increase the stability of ettringite at pH as low as 9.5 [102].

Indeed, it has been observed that the pH increased as the level of chloride concentration increased, more at 5°C than at 20°C (section 5.4.5). Although this trend was observed in all mixes (Table 5.5), it was more evident in OPC with 15% limestone filler, where greater damage was also detected due to TSA (Figures 5.36-5.37). Some correlation was also found between both maximum pH increase and the relative mass of the specimens, whose variation reflected the degree of the attack visually observed as the binder of the cements was attacked and thaumasite was precipitated in the bottom of the containers. Indeed, the greater the damage, the higher the extent of pH increase after 197 days constantly immersed in salt solutions and after the first solution replenishment. After 357 days, no correlation was found, however, but the pH of all solutions at 5°C increased to near or above 12, in which thaumasite was also extensively found (Section 5.3.3). Despite the poor correlation coefficient of this approach, good agreement was found between the intensity of attack (Figures 5.5 and 5.18) and the maximum rate of pH increase (Figures 5.38 to 5.31, Table 5.5), especially in OPC and 15%LF mixes. This trend has been consistently confirmed throughout this research, despite the complexity of simultaneous chemical reactions occurring in these systems (Table 5.3), which adversely affects both pH and damage in different ways.

It appears that the need for solution with higher alkalinity in the formation of thaumasite seems also to be correlated with the solubility of silicate ions, especially amorphous hydrous-silicon as in CSH. Indeed, thaumasite becomes very pervasive as CSH decalcifies, dissolves and completely turns into thaumasite in the advanced stages of attack (Chapter 4). This was clearly marked by the formation of the dark grey bands within the cement matrix (CSH and clinker grains) and around the silica aggregate grains (Chapter 4 and section 6.3.1). Drever [82] reported that there is a significant increase in the solubility of the silicate ions when the pH is higher than 10. He also reported that even polymeric silicate ions can be found in very alkaline solution. Another aspect that corroborates with the pH threshold of ca. 10.5 is that the pH at the carbonate/bicarbonate equilibrium increases to 10.55 when the temperature is reduced to 5°C [82].

7.1.8 Mechanisms by which chloride affect thaumasite precipitation in Portland cement

A. Carbonate system

There can be several possibilities for thaumasite formation in Portland cement matrixes, which vary according to the cations of the dissolved sulfate, silicate and carbonate species and also in thaumasite formation. Several reaction paths are proposed, in which thaumasite is formed through the congruent dissolution of CSH in the presence of gypsum and portlandite [11, 84]. Although not very likely to be in equilibrium with sulfates, portlandite is sometimes presented as a reaction product [10]. The dissolution of ettringite is also reported to participate in the formation of thaumasite, in what is called the 'woodfordite' route [84]. In this later case, it still not clear whether ettringite would either offer a nucleation site for thaumasite or it undergoes a substitutional ion exchange resulting in thaumasite. The last topochemical mechanism is believed to be unlikely as the ettringite/thaumasite solid solution series involves some discontinuity [9, 62]. Both mechanisms can be as described in equation 7.1 [11] and equation 7.2 [10, 84]

.

$$C_3S_2H_3 + 4M\overline{S} + 2C\overline{C} + 3CH + 32H \rightarrow 2C_3S\overline{C}\,\overline{S}H_{15} + 2C\overline{S}H_2 + 4MH \quad (7\text{-}1)$$

$$C_3S_2H_3 + C_3A3C\overline{S}H_{32} + 2C\overline{C} + 4H \rightarrow 2C_3S\overline{C}\,\overline{S}H_{15} + C\overline{S}H_2 + AH_3 + 4CH \quad (7\text{-}2)$$

Recent investigation of the role of atmospheric carbonation [76] reported that a better depiction of thaumasite formation was provided when bicarbonates ($CH\overline{C}_2$) were included in the reaction, as shown in equations 7.3 and 7.4. In both cases, aggressive CO_2 ($\overline{C}^A$) is proposed to be generated, which results in further dissolution of any calcite in the system. The authors defined the amount of CO_2 required to establish calcium bicarbonate as stabilising CO_2 ($\overline{C}^s$).

$$C_3S_2H_3 + 2C\overline{S}H_2 + 2[CH\overline{C}_2\ (+\overline{C}^s)] + CH + 20H \rightarrow 2C_3S\overline{C}\,\overline{S}H_{15} + 2C\overline{C} + 2\overline{C}^A \quad (7\text{-}3)$$

$$2C_3S_2H_3 + C_3A3C\overline{S}H_{32} + 6[CH\overline{C}_2\ (+\overline{C}^s)] + CH + C\overline{S}H_2 + 16H \rightarrow 2C_3S\overline{C}\,\overline{S}H_{15} + 8C\overline{C} + AH_3 + 6\overline{C}^A \quad (7\text{-}4)$$

According to Eglinton [138], the greater the amount of aggressive CO_2 dissolved in solution, the more aggressive the solution since the pH is reduced, thus the dissolution

of any calcite added as filler or precipitated due to atmospheric carbonation in the cement would take place. Based on equation 7.5, Eglinton [138] proposes that the extrapolated values of aggressive CO_2 can be determined using the diagram shown in Figure 7.1.

$$CaCO_3 + H_2CO_3 = Ca(HCO_3)_2 \qquad (7.5)$$

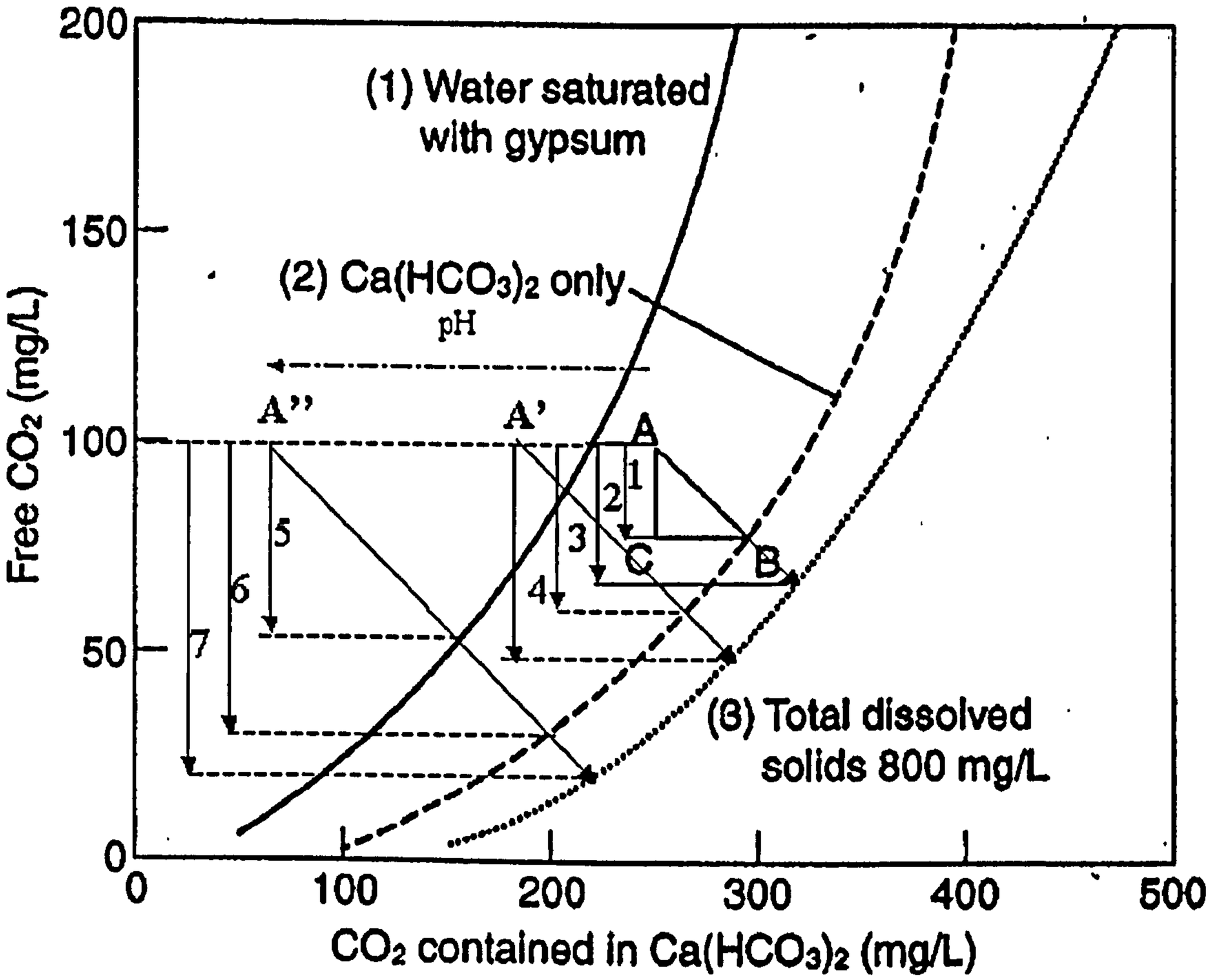

Figure 7.1: Modified equilibrium CO_2-$Ca(HCO_3)_2$ from Eglinton [138].

The line AB represents the reaction 7.4 in which two moles of bicarbonates is equivalent to one mole of free CO_2. Because the scale of calcium bicarbonate is twice that of free CO_2, the estimations of aggressive CO_2 can be done by drawing a 45 degree line (AB) from the free CO_2-CO_2 in calcium bicarbonate point until the line reaches the equilibrium curves of saturated gypsum (solid line 1), calcium bicarbonate $Ca(HCO_3)_2$ and water (dashed line 2), and also NaCl-containing solution (dotted line 3).

The points A, A' and A'' represent solution compositions with different amounts of calcium bicarbonate in the same amount of free CO_2. In very alkaline solutions, as required by thaumasite, the concentration of CO_3^{2-} is much higher than that of HCO_3^{1-} with the increase in pH [82]. Hence, the solution composition would shift from the point A to A'', for instance. Estimated values of aggressive CO_2 (vertical arrows 1

to 7) were determined using Eglinton [138] diagram for solutions with different bicarbonate concentration in the same free CO_2 content (points A, A' and A''), as shown in Figure 7.2.

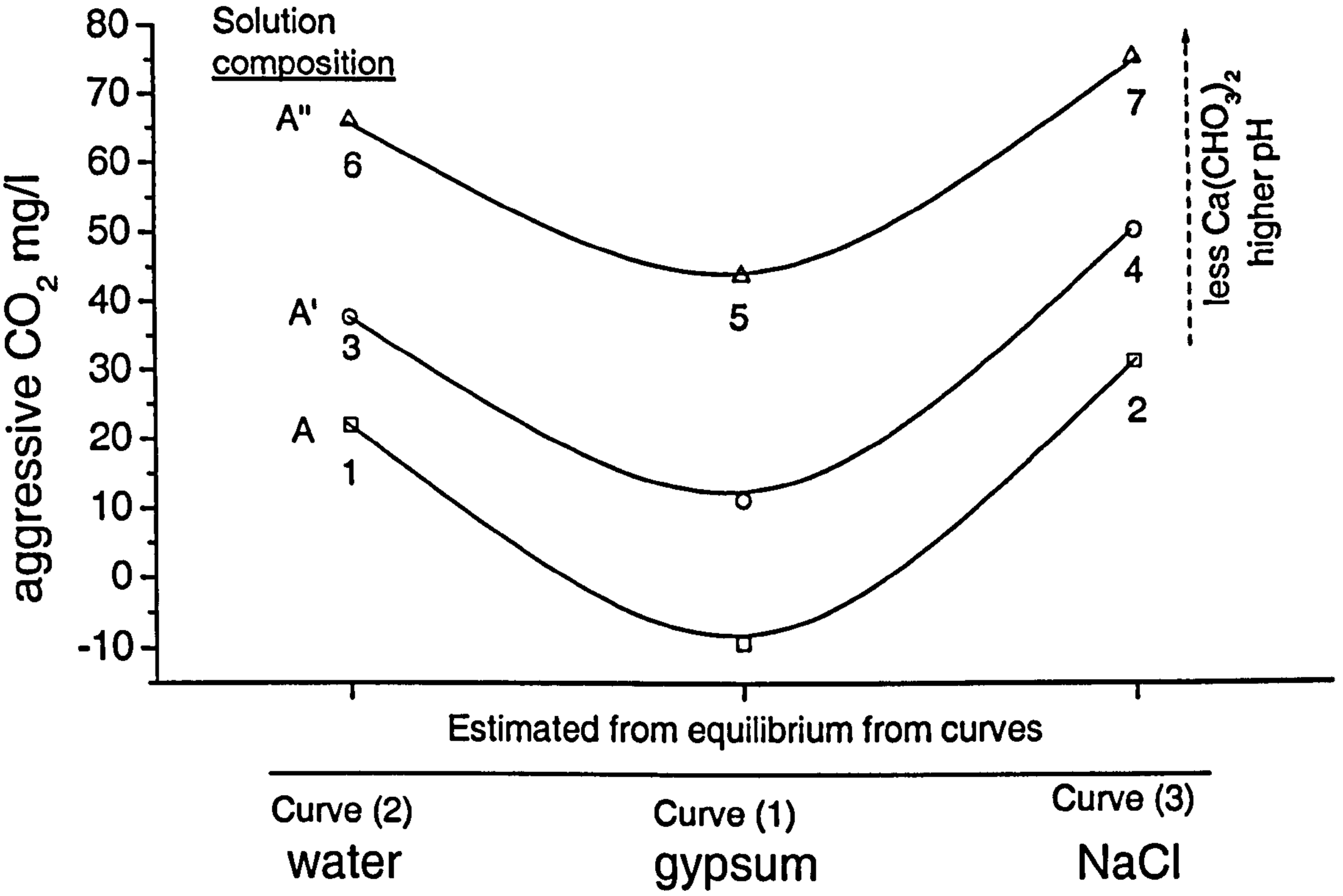

Figure 7.2: Etimated aggressive CO_2 using the modified equilibrium CO_2-$Ca(HCO_3)_2$ from Eglinton [138] in Figure 7.1. (Curve 1, 2 and 3 are shown in Figure 7.1)

It can be seen that the estimated amount of aggressive CO_2 is always higher in the sodium chloride-containing solution (points 2, 4 and 7) than in water (points 1,3 and 6) and saturated gypsum solution (points 3 and 4). This observation agrees with the findings on the solubility of calcite in sodium chloride solutions, especially at 5°C (Appendix II). Indeed, Eglinton [138] reported that the amount of free CO_2 that is necessary to stabilise $Ca(HCO_3)_2$ is reduced in the presence of chloride salts, thus the aggressiveness of the solution is increased by the higher activity of aggressive CO_2. The amount of aggressive CO_2 is reduced in solutions saturated with gypsum (curve 1), when compared to the other equilibrium lines (curve 2 and 3). A reduction in the concentration of Ca^{2+} ion concentration was also observed in this solution when gypsum was immersed in 0.50%Cl^- and 0.60%SO_4^{2-} (M5) (see Appendix II), in which case less damage was also observed (Figure 5.5). This might be correlated with a reduction in the

degree of the attack in M5 solution, as less aggressive CO_2 would be present to contribute to thaumasite formation.

Therefore, chloride ions also affect the carbonate system by increasing the activity of aggressive CO_2, which contributes to thaumasite formation (Chapter 5) by increasing the dissolution of calcite [76]

B. Silicate system

In this current research, in order to match some features identified in BEI-X-ray microanalysis, it was assumed that the CSH could only be partially dissolved via incongruent dissolution. In addition, chloride can possibly affect the composition of this CSH by:

(i) Increasing the chances of thaumasite precipitation due to a greater solubility of carbonates in solution;

(ii) Increasing the local pH in the cement pore solution.

There is some evidence to support the view of partial dissolution of the CSH due to the sulfate attack at the early stages reported in this thesis:

(i) A low Si/Ca ratio that indicates a sound CSH [12], should have a higher chloride binding capacity as postulated by Beaudoin et al. [146]. However, it was observed in this study that less chloride was bound in this type of CSH in thaumasite-affected areas at the surface than in the core (section 7.1.6). The matrix at the surface appeared severely cracked instead of showing the conventional features of a cement matrix (Figures 6.5 to 6.12). This type of matrix was always found at the surface within areas that were already detached from the bulk of the sample, indicating loss of bonding as in a sound CSH. Therefore, the lower Si/Ca ratio than 0.6 indicates a simultaneous dissolution of calcium and silicon. Indeed, although the Si/Ca ratio has been used to identify the type of CSH in the cement matrix [12], this parameter alone is not able to detect other features of the CSH such as chain length, which is also used to characterise this phase.

(ii) Although the detection of Si/Ca ratio by QXMA is also unable to detect the coordination of the Si^{4+}, the correlation between the silicon detected by

both techniques indicates that some octahedral silicon also precipitated within the CSH structure (section 6.4.3A). This observation confirms the view of a simultaneous dissolution of calcium and silicon leading to the Si/Ca values observed, in which thaumasite precipitated within the matrix.

(iii) Also, in some instances, hydrogarnet appeared to have precipitated within the CSH. Indeed, a higher Al/Ca ratio (c.a. 0.3 or greater) was detected within the damaged areas, whilst it was still within the expected levels for the CSH (0.08) in less attacked areas of the samples (section 6.4.3B).

C Catalytic role of chloride in thaumasite formation

Whether the direct or the via ettringite route is taken into account, it can be proposed that the reaction can be according to equations 7.5 and 7.6, respectively, in which CSH partially dissolves. The data indicate a small or zero chloride binding capacity of this thaumasite attacked CSH.

$$C_3S_2H_3 + C\bar{S}H_2 + \bar{C} + 11H \rightarrow \left|\begin{array}{l} Temp \sim low \\ pH > 10.55 \end{array}\right| C_3S\bar{C}\bar{S}H_{15} + C_1S_1H_1 \quad (7\text{-}5)$$

$$2C_3S_2H_3 + C_3A3C\bar{S}H_{32} + 2\bar{C} + 2H \rightarrow \left|\begin{array}{l} T \sim low \\ pH > 10.55 \end{array}\right| 2C_3S\bar{C}\bar{S}H_{15} + 2C_1S_1H_1 + C_3AH_6 + C\bar{S}H_2 \quad (7\text{-}6)$$

Both gypsum and the remaining attacked CSH ($C_1S_1H_1$), which may possibly be similar to suolunite (PDF 74-2248) can undergo further reaction with calcium carbonate at later stages, which will result in a total conversion of the chemically altered CSH into thaumasite, as seen in equation 7.7.

$$C_1S_1H_1 + C\bar{S}H_2 + C\bar{C} + 12H \rightarrow \left|\begin{array}{l} T \sim low \\ pH > 10.55 \end{array}\right| C_3S\bar{C}\bar{S}H_{15} \quad (7\text{-}7)$$

This sequence can possibly explain the occurrence of the dark grey band that developed at the surface and surrounding aggregate in all damaged samples, in which only thaumasite and siliceous aggregate could be detected in the advanced stages of the TSA (Figures 6.1-2, 6.5-6, 6.9 and 6.11). Another characteristic that marked the long-term attack was the total conversion of the matrix into thaumasite, as happened in high limestone content samples after 5 years in highly concentrated magnesium sulfate solution in which thaumasite became pervasive and dominated over the hydrated cement phases (Chapter 4). In early stages though, damaged CSH was always identified in the corroded area, which was often surrounded by the dark grey area that formed at

the surface and surrounding aggregate grains. The aggregate-cement transition zone is more porous than the matrix, hence, deposition of thaumasite at this site yields disruption due to the loss of binding capacity of the cement. The significance of an incongruent dissolution of CSH, with little binding capacity, is that significant damage can develop in the concrete without the need for total conversion into thaumasite. This can indicate that correlation between damage and quantitative analysis with respect to thaumasite alone may present some inconsistencies. However, such dissolution would cause a loss in the stiffness of the matrix. The view of a catalytic role for chloride in thaumasite formation can also be supported by:

(i) The instability of chloride-bearing phases, such as Friedel's salt, in solutions containing carbonates, which transforms into hydrogarnet according to equation 7.7 [105, 107].

Dissolution of FS:

$$C_3A.CaCl_2.H_{10} + CO_3^{2-} \rightarrow C_3AH_{6\,solid} + C\overline{C} + 4H + 2Cl^- \qquad (7\text{-}7)$$

(ii) Hydrogarnet is also unstable in carbonate systems, in which it turns into hydrous alumina or gibbsite [105].

Dissolution of hydrogarnet:

$$C_3AH_{6\,solid} + 3CO_3^{2-} \rightarrow AH_3 + 3C\overline{C} + 3H \qquad (7.8)$$

It is important to point out that, in these proposed reactions, it is assumed that portlandite (CH) is neither a reactant nor a reaction product, but it is necessary in helping to maintaining the pH at the alkaline level that favours thaumasite formation. Being very soluble in water at cold temperatures, portlandite can be primarily consumed in the early stages of the attack. Carbonation is also another possibility. Also, the dissolution of CSH supplies the lime and the silicon to the pore solution for the precipitation of thaumasite.

In the case of the via ettringite route, it is also important to emphasise that sulfate ions could also be released from the dissolution of ettringite itself, which explains its instability in thaumasite systems. Almost certainly, for that reason, ettringite was not identified in any corroded parts of the samples in the present research at 5°C, as it converted into thaumasite. This observation is more evident in samples subjected to a long exposure to cold sulfate attack, as reported in Chapter 4. In this case, although

ettringite was always identified as the main phase in systems containing little or no carbonate filler after one year [11, 69], only thaumasite was detected after 5 years [13, 18].

D. Summary

The presence of chloride was not considered in equations 7.5 to 7.7, because its role is considered to be primarily catalytic, since:

(i) The incorporation of chloride ions in solid solution within the crystal structure of thaumasite was found to be unlikely;

(ii) No chloride-bearing phases were identified within the corroded parts of the samples; and

(iii) The chloride binding capacity of the CSH gel was found to be reduced in the corroded areas of the cement matrix.

Hence, the effect of chlorides in the mechanism of thaumasite formation appears to be as follows:

1. The presence of chlorides increases the solubility of carbonates in solution, particularly if carbonates are added to the concrete as a replacement material or as aggregate;
2. The presence of chloride also appears to increase the local pH, hence, increasing the chances for thaumasite formation [140, 145] by increasing the solubility of hydrous silicate ions [82].
3. Moreover, as the presence of chloride ions that can increase the stability of ettringite at pH as low as 9.5 [132], it can also have given greater stability for thaumasite, mainly by supplying more carbonate ions in solution. Therefore, the same reaction path suggested in equations 7.5 to 7.7 can be applied to thaumasite susceptible systems containing chloride ions.

The overall effect depends on the combination between the solubility of carbonates and the kinetics of thaumasite formation, in which higher concentrations of chlorides would have a different effect on the carbonates. A hypothetical phase diagram is proposed in Figures 7.3 and 7.4 in which the role of chloride in the thaumasite formation is catalytic. The concentration of chlorides is hypothetical, so the test solutions marks are used for analogy purposes.

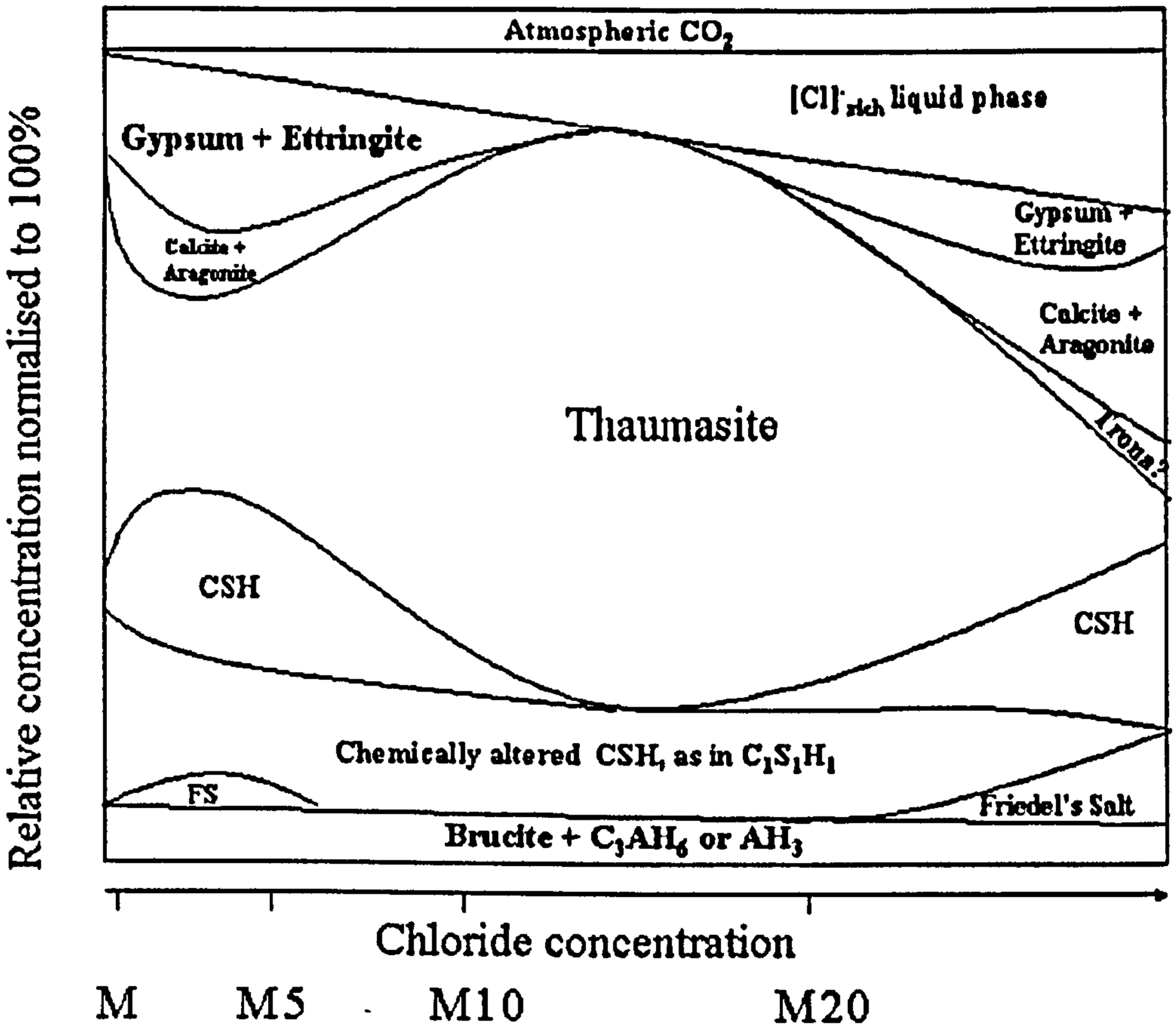

Figure 7.3: Schematic phase diagram in OPC-Calcite-Epsomite-NaCl-CO_2-H_2O at 5°C, (FS): Friedel's salt, (M): 0.6% SO_4^{2-}, (M5): 0.6% SO_4^{2-} +0.5%Cl^-, (M10): 0.6% SO_4^{2-} +1.0%Cl^-, (M20): 0.6% SO_4^{2-} +2.0%Cl^-.

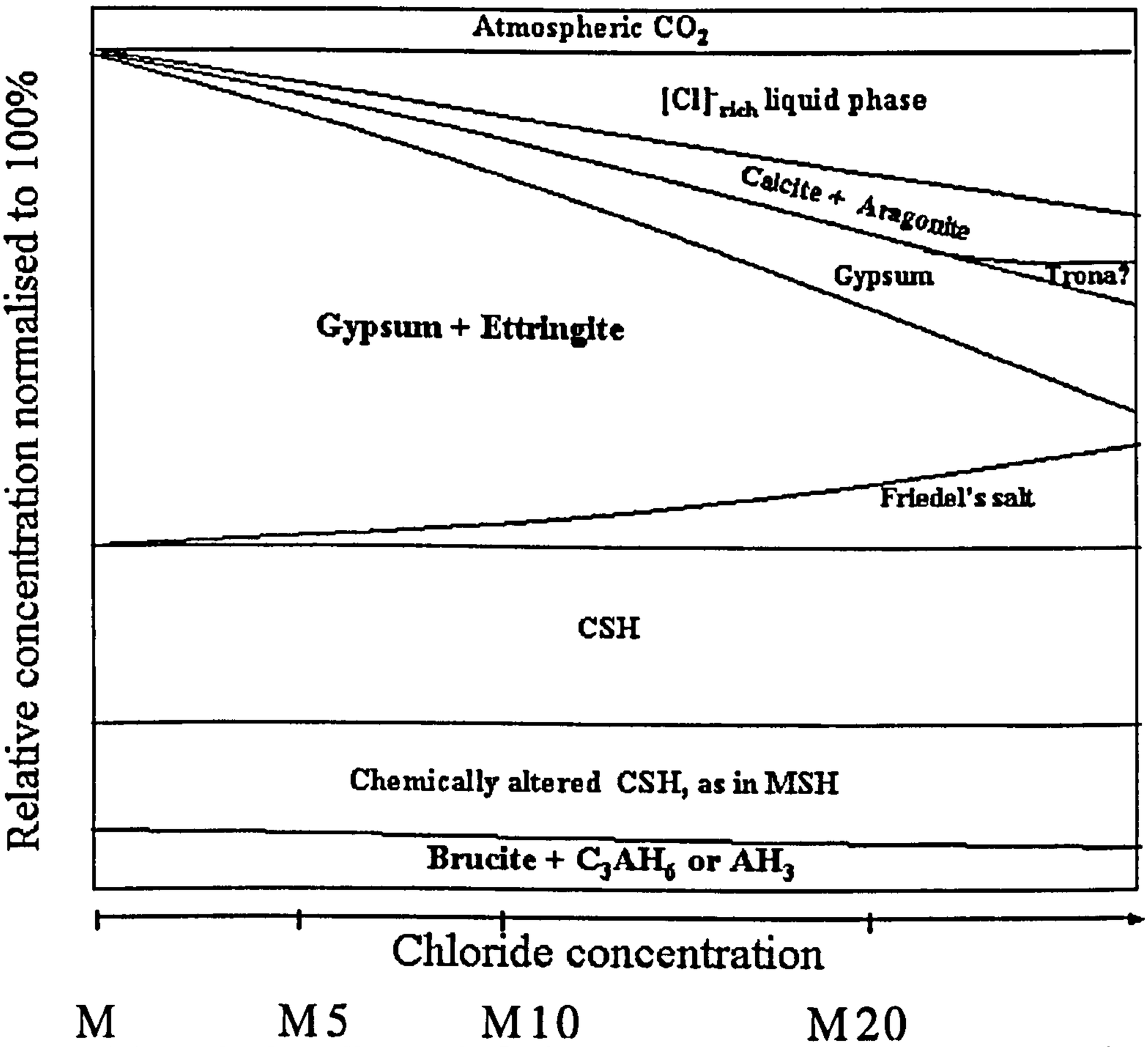

Figure 7.4: Schematic phase diagram in OPC-Calcite-Epsomite-NaCl-CO_2-H_2O at 20°C, (FS): Friedel's salt, (M): 0.6% SO_4^{2-}, (M5): 0.6% SO_4^{2-} +0.5%Cl^-, (M10): 0.6% SO_4^{2-} +1.0%Cl^-, (M20): 0.6% SO_4^{2-} +2.0%Cl^-.

From these phase diagrams, it is proposed that the precipitation of the carbonates, which increase in concentration, is affected by the presence of NaCl (section 7.1.8A), as calcite, aragonite or thaumasite would depend on the kinetics of the precipitation of each mineral. It is well established [82] that in certain marine conditions, high temperature and in the presence of magnesium ions, aragonite precipitates rather then calcite, even though the latter is the thermodynamic stable phase. Yet, the meta-stable aragonite is then observed even for geological periods of time. It is likely that similar kinetic considerations determine whether or not thaumasite precipitates instead of (or as well as) calcite or aragonite. Indeed, at low temperatures (5°C in this thesis), thaumasite was found to be more favourable to crystallise. At 20°C, where thaumasite formation is extremely slow, the carbonates would tend to precipitate as aragonite or calcite.

In the case that thaumasite does not precipitate, Friedel's salt remains in the system, despite the low temperature, as detected in the core of all the samples, but carbonate or hydrogarnet or hydrous alumina might precipitate. Providing the system is within the conditions for the stability of Friedel's salt, the effect of chloride can be seen as beneficial for at least two main reasons. First, it retards the formation of secondary ettringite formation, which can be expansive and detrimental in concrete. Second, it takes chlorides out of the pore solution, which improves the system with respect to chloride-induced corrosion, and also shifts the equilibrium line of carbonates so that less aggressive CO_2 is generated for each mole of carbonate stabilising calcium bicarbonate [138].

The apparent mitigation observed in M5 solutions appears to be explained by less aggressive CO_2 being generated in a calcium bicarbonate system along the gypsum equilibrium line (Figure 7.1) than along the NaCl equilibrium line for the same system. This ultimately reduces the aggressiveness of the system towards the dissolution of calcite, thus reducing the overall effect of the increase of carbonates in solution, and the sulfate phases would precipitate as gypsum and ettringite, and the carbonate phases would possibly precipitate as aragonite and calcite. The remaining sulfate and carbonates would also react to form thaumasite, but to a lesser extent.

With very high concentrations of sodium in solution, there is the possibility of the precipitation of trona, as has already been observed in field cases [130]. Nevertheless, this phase was not identified in any laboratory sample, as the concentration of sodium was found to be very low and associated with the presence of halite (NaCl) (Figure 6.6).

E. Damage assessment

In general, the potential damage associated with thaumasite formation was increased in the presence of chlorides according to the normogram presented in Figure 7.5. Greater corrosion was observed in samples immersed in chloride based solution, which resulted in greater rate of mass loss (Figure 5.18). However, this trend was not linear, which reveals that the complex interactions between carbonate, chloride and sulfate species affect the precipitation of some minerals. The main observations lead to:

- There is a pH threshold for thaumasite formation that controls the concentration of carbonates in solution, which seems to be around 10.55, below which the concentration of CO_3^{-2} and HCO_3^{-1} reduces practically below the saturation level needed for thaumasite nucleation;

- The potential carbonate increases as the chloride level increases, which is much more evident at lower than at higher temperatures (Zone III). Although the potential risk for TSA increases with chloride concentration, it seems to be controlled by the kinetics of thaumasite nucleation, solubility and kinetics of the carbonate precipitation. At higher concentrations of chlorides, the carbonate counter diffusion and the faster precipitation rate of aragonite and calcite, appears to reduce the chances of thaumasite formation, hence, reducing the potential damage (zone IV). Also, the effect of gypsum on the activity of aggressive carbonates, reducing the dissolution of calcium carbonate, also diminishes the potential damage caused by TSA at lower Cl^- concentrations (zone V). Therefore, levels of limestone in Portland cement that are believed to be safe with respect to TSA may not be so in the presence of chloride ions.

- At higher temperatures, the kinetics of other carbonate precipitation such as aragonite reduces the chance of thaumasite formation, since the kinetics of a thaumasite precipitation is very slow at this temperature level (zone I), hence, gypsum and ettringite would precipitate instead. As the level of chloride increase, Friedel's salt appears to mitigate the attack since it removes aluminate species from solution, eg. by reacting with monosulfate, and reduces the chance of the precipitation of secondary ettringite (Zone II).

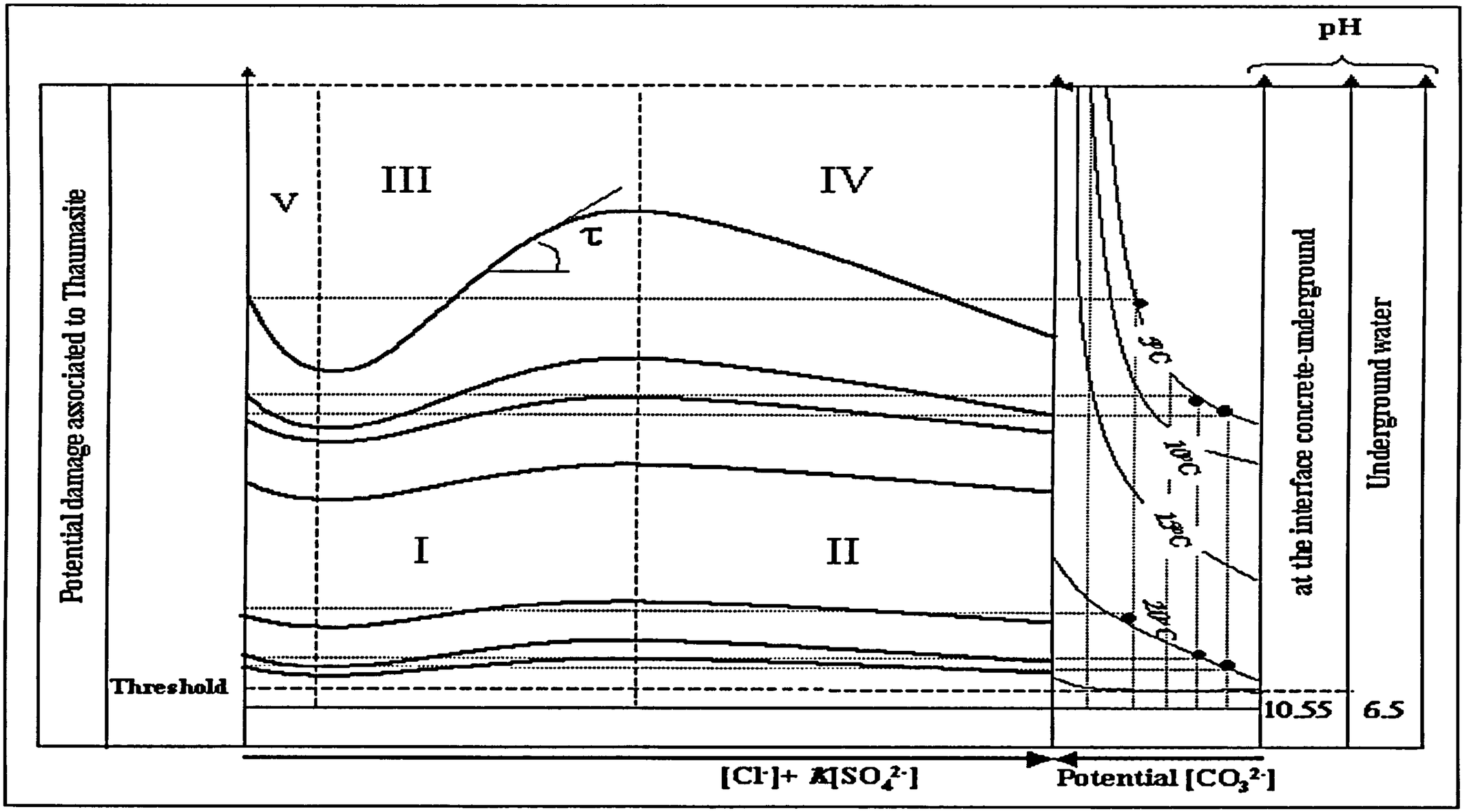

(τ=kinetics of calcite and aragonite precipitation+ calcite dissolution/Kinetics of thaumasite nucleation).

Figure 7.5: Overall damage assessment in samples immersed in combined sulfates and chlorides in this research.

Chapter Eight

Overall conclusions and recommendations for future work

8.1 Overall Conclusions

The main conclusions of this research are as follows:

- The effect of chloride ions on sulfate attack depends on the temperature, as it mitigates conventional sulfate attack at 20°C, but it increases the thaumasite form of sulfate attack (TSA) at 5°C.

- The presence of chloride ions in solution influences the thaumasite form of sulfate attack due to complex interactions between the carbonate cycle in solution, chloride concentration, stability of chloride-bearing phases and the alkalinity of the system;

- In sulfate solutions, the presence of carbonates, whether originating from a minor additional constituent in cement (*MAC*) or atmospheric carbonation will adversely affect the susceptibility of concretes to TSA, especially in the presence of chlorides;

- Although the solubility of carbonates increases with chloride concentration, the role of chloride in this mechanism of attack varies according to the temperature, which strongly affects both the solubility of the carbonate species and the kinetics of formation of carbonate-bearing phases, such as calcite, aragonite and thaumasite;

- Because the kinetics of thaumasite nucleation is drastically reduced at 20°C, carbonate is preferentially bound by other kinetically favourable phases such as calcite or aragonite, in the presence of magnesium species in solution;

- The aggressiveness of the deterioration process depends on the type of carbonate-bearing phase that precipitates. Whereas the crystallisation of

thaumasite causes strong deterioration of the cement matrix, the formation of aragonite or calcite does not seem to cause any detrimental effect.

- Unlike in seawater, where the pH is buffered by the equilibrium in the calcium carbonate, and brucite formation is extensive due to the high concentration of magnesium ions, the presence of chloride increased the pH of the solutions, especially at 5°C.

- The low concentration of sodium in the cement matrix is indicative that the local pH may well have increased as the absorption of these ions would counter-balance the rise in pH due to the adsorption and combination of chlorides in both the CSH and the aluminate phases;

- Because thaumasite requires an alkaline environment, atmospheric carbonation would reduce the pH in the carbonated area, which would prevent its formation, despite carbonation being a source of carbonates in itself. Nonetheless, only long-term carbonation prevented the formation of thaumasite in the carbonated zone of mortars containing limestone filler. Yet thaumasite precipitated immediately underneath the carbonated/non-carbonated interface and extensively in short-term carbonated samples;

- Even when carbonates are available in the cement pore solution, ettringite and gypsum precipitate at the early stages of the attack. However, these phases convert into thaumasite at the later stages of the attack. Hence, early identification of ettringite and gypsum as a result of sulfate attack does not mean that this assemblage will not undergo further reaction towards thaumasite when the right conditions are met, namely cool temperature and carbonate-rich pore solution. Thaumasite can eventually precipitate in concrete exposed to sulfates at 20°C if the pore solution is supersaturated with respect to carbonates for a long time;

- At advanced stages of the attack, thaumasite becomes all pervasive, and destroys all cementitious phases in the cement, such as CSH, residual clinker grains, where only the aggregate and thaumasite remain, hence, all binding properties are lost. Even Friedel's salt, which was abundantly found in the core of samples and in samples where thaumasite was not detected, becomes unstable in the presence of carbonates and was not found within thaumasite-affected areas;

- The presence of chlorides seems to accelerate the rate of thaumasite formation, as it increases both the alkalinity of the system and the concentration of carbonate ions in solution;

- At very high concentrations of chlorides, calcium carbonate phases may also precipitate, possibly because the diffusion of chlorides inside the concrete may induce a counter diffusion of carbonates (in the case of filler cements) to equilibrate the negative charges at the concrete-groundwater interface. Because the kinetics of the precipitation of other carbonate phases can prevail over the formation of thaumasite, the attack can be mitigated;

- The attack appeared to be mitigated at the chloride concentration of 0.5%. This can possibly be explained by a lower pH throughout the period of exposure, and also by changes in the solubility of gypsum and possibly lower aggressive CO_2 in solution at this Cl/SO_4 ratio;

- At 0.60% SO_4^{2-}, the critical chloride concentration in this thesis was found to be between 1.0%Cl^- and 2.0%Cl^-, which was most evident in mortar containing 15% limestone filler. This critical value was consistently observed in the visual damage of the specimens, the mass loss due to the attack, the composition of the thaumasite, and the features of the micro-analytical changes in the cement matrix of this mix;

- A statistical model suggests that the optimum chloride concentration in which thaumasite precipitates with the smallest *c* parameter is linearly proportional to the inverse of the carbonate content in the system. The higher the carbonate content, the lower the amount of chloride necessary for thaumasite to be formed with a composition close to that of the end-member of the solid solution series;

- The chloride binding capacity of thaumasite seems non-existent or extremely small because the thaumasite crystal structure tended to the thaumasite end-member of the solid solution series, in which the lower unit cell parameter *c* was found in chloride rather than in pure sulfate solutions, and also because the Cl/Ca ratio observed in all samples was below the theoretical value for a chloride-containing thaumasite analogue;

- The chloride binding capacity of the cement matrix is reduced in thaumasite-affected areas because the CSH incongruently dissolved as a result of a decalcification, loss of silicate ions, and the precipitation of thaumasite within the gel;

- The role of chloride in the thaumasite form of sulfate attack appears to be primarily catalytic, because chloride does not appear to enter into solid solution within thaumasite; the chloride-bearing phases are not stable in the presence of carbonates; and the chloride binding capacity of the cement matrix is reduced in thaumasite-affected areas. Thus, it is postulated that the mechanism of thaumasite formation in the presence of chlorides can be expressed according to equations 8.1 and 8.2. In these equations, portlandite is neither a reactant nor a reaction product of thaumasite formation, but it assists to maintain the solution at the high alkaline level required for this mechanism;

Attack on CSH:

Early stages:

$$C_3S_2H_3 + C\bar{S}H_2 + \bar{C} + 11H \rightarrow C_3SC\bar{S}H_{15} + C_1S_1H_1 \quad (8.1)$$

Completion:

$$C_1S_1H_1 + C\bar{S}H_2 + C\bar{C} + 12H \rightarrow C_3S\bar{C}\bar{S}H_{15} \quad (8.2)$$

Attack via ettringite:

$$2C_3S_2H_3 + C_3A3C\bar{S}H_{32} + 2\bar{C} + 2H \rightarrow 2C_3S\bar{C}\bar{S}H_{15} + 2C_1S_1H_1 + C_3AH_6 + C\bar{S}H_2 \quad (8.3)$$

- The absence of Friedel's salt within the corroded areas where thaumasite was the dominant phase can be explained by the instability of the former mineral in carbonate systems when it converts into hydrogarnet, which may also be unstable under these conditions (solution containing carbonate, sulfate and chloride ions at low temperature) as shown in equations 8.4 and 8.5:

Dissolution of Friedel's salt:

$$C_3A.CaCl_2.H_{10} + CO_3^{2-} \rightarrow C_3AH_6 + C\overline{C} + 4H + 2Cl^- \quad (8.4)$$

Dissolution of hydrogarnet:

$$C_3AH_6 + 3\overline{C}_{liq} \rightarrow AH_3 + 3C\overline{C} + 3H \quad (8.5)$$

- In general, the use of metakaolin suppressed TSA for the first year, mostly because of the dilution of the cement that was replaced by both metakaolin and limestone filler. The beneficial effects of the pozzolanic reactions (consumption of calcium hydroxide and improvements of the cement matrix) improved the pore structure, reducing the diffusion and alkalinity of the system;

- It is possible that metakaolin mitigated the detrimental effect of chlorides ions on TSA by increasing the chloride binding capacity;

- Because metakaolin containing mortar was attacked after 73 weeks of exposure to pure magnesium sulfate solution at 5°C, it is important to investigate the long-term durability of this blend. The type of attack was mostly conventional sulfate attack with the formation of gypsum and ettringite. However, it is still not clear whether the nature of the CSH formed in this mix was responsible for the precipitation of an orthorhombic type of thaumasite, with lower carbonate content;

- As far as the effect of combined chloride and sulfate on TSA is concerned, the potential susceptibility to TSA of systems containing calcium carbonates, either as limestone filler or from atmospheric carbonation, has increased, mostly because of an increase in the activity of carbonates in the presence of chlorides. The data suggest that in certain combinations of chlorides and sulfates, the potential damage in systems with low carbonate content can be increasingly greater than other systems containing higher content of limestone in pure sulfate solution. This can have serious implications for the specification of thresholds of sulfates and carbonates for durable concrete designed to resist TSA;

8.2 Recommendations for future research

- Because of the catalytic role of chlorides in the formation of thaumasite, it is important to assess how chlorides affect the thresholds of the Aggressive Chemical Environment for Concrete (ACEC) site classification and the Aggregate Carbonate Range (ACR), as defined in the BRE SD-1 [14], and also to develop a simplified thaumasite damage assessment diagram including ACEC, ACR and some ground water parameters including chlorides

- To investigate the performance of GGBS and SRPC in TSA prone conditions in the presence of chlorides.

    - These cements have different chloride binding capacities, hence, their overall performance will also be affected by the presence of chlorides

- To Investigate the kinetics, transport and reaction modelling in Portland cement in Cl-(Mg,Ca,Na)SO_4-$CaCO_3$-H_2O-CO_2 systems at different temperatures

- Usefulness of energy-wave propagation non-destructive techniques (NDT) in detecting onset and damage caused by TSA in cementitious systems.

    - A pilot study during the present investigation on the use of NDT has identified that the energy dissipated by damping mechanisms can be a good tool in prediction the onset of thaumasite, as the cement matrix loses its superficial stiffness, that can affect the response of the structure, which could be analysed as a composite beam with an external damper layer

- Investigate the performance of other cement replacement materials in TSA prone environments to compare their effects with those observed in the presence of metakaolin.

    - Analyses on the delayed attack on metakaolin-containing mortar suggests that there may be some sort of interaction within the CSH structure, because of the absence of the Al-O-Si vibrational bands in the corroded samples that were observed prior to the attack.

- Determine the crystal structure of thaumasite-ettringite solid solution in $CaO\text{-}Cl\text{-}SO_4\text{-}CaCO_3\text{-}H_2O\text{-}CO_2$ systems at different temperatures.

References

1. Bickley, J.A., *The repair of Arctic structures damaged by thaumasite.* Cement and Concrete Composites, 1999. **21**(2): p. 155-158.
2. *Department of the Environment, Transport and the Regions. The thaumasite form of sulfate attack: risks, diagnosis, remedial works and guidance on new construction. Report of the Thaumasite Expert Group, DETR, London, January 1999.* 1999.
3. Hagelia, P., Sibbick, R. G., Crammond, N. J. and Larsen, C. K., *Thaumasite and secondary calcite in some Norwegian concretes.* Cement and Concrete Composites, 2003. **25**(8): p. 1131-1140.
4. Romer, M., L. Holzer, and M. Pfiffner, *Swiss tunnel structures: concrete damage by formation of thaumasite.* Cement and Concrete Composites, 2003. **25**(8): p. 1111-1117.
5. Stark, D.C., *Occurrence of thaumasite in deteriorated concrete.* Cement and Concrete Composites, 2003. **25**(8): p. 1119-1121.
6. Crammond, N.J., *Thaumasite in failed cement mortars and renders from exposed brickwork.* Cement and Concrete Research, 1985. **15**(6): p. 1039-1050.
7. Collepardi, M., *Degradation and restoration of masonry walls of historical buildings.* Materials and Structures, 1990. **23**: p. 81-102.
8. Regourd, M., Bissery, P.; Evers, G.; Hornain, H.; Mortureax, B., *Ettringite et thaumasite dans le martier de la digue du port de Cherbourg.*, in *Annales ITBTP*. 1978. p. 358: 876-880.
9. Crammond, N.J., *The thaumasite form of sulfate attack in the UK.* Cement and Concrete Composites, 2004. **25**(8): p. 809-818.
10. Bensted, J., *Thaumasite -- background and nature in deterioration of cements, mortars and concretes.* Cement and Concrete Composites, 1999. **21**(2): p. 117-121.
11. Hartshorn, S.A., J.H. Sharp, and R.N. Swamy, *Thaumasite formation in Portland-limestone cement pastes.* Cement and Concrete Research, 1999. **29**(8): p. 1331-1340.
12. Taylor, H.F.W., *Hydration of Portland cement.* 2nd ed. Cement Chemistry. 1997, London: Thomas Thelford.
13. Torres, S.M., Sharp, J. H., Swamy, R. N., Lynsdale, C. J. and Huntley, S. A., *Long term durability of Portland-limestone cement mortars exposed to magnesium sulfate attack.* Cement and Concrete Composites, 2003. **25**(8): p. 947-954.
14. *BRE Special Digest 1, Concrete in aggressive ground. Building Research Establishment, Watford, UK.* 2001.
15. Wimpenny, D. and D. Slater, *Evidence from the highways agency thaumasite investigation in Gloucestershire to support or contradict postulated mechanisms of thaumasite formation (TF) and thaumasite sulfate attack (TSA).* Cement and Concrete Composites, 2003. **25**(8): p. 879-888.
16. Slater, D., M. Floyd, and D.E. Wimpenny, *A summary of the Highways Agency Thaumasite Investigation in Gloucestershire: the scope of work and main findings.* Cement and Concrete Composites, 2003. **25**(8): p. 1067-1076.
17. Sibbick, T., D. Fenn, and N. Crammond, *The occurrence of thaumasite as a product of seawater attack.* Cement and Concrete Composites, 2003. **25**(8): p. 1059-1066.
18. Torres, S.M., Kirk, C. A., Lynsdale, C. J., Swamy, R. N. and Sharp, J. H., *Thaumasite-ettringite solid solutions in degraded mortars.* Cement and Concrete Research, 2004. **34**(8): p. 1297-1305.

19. Mayfield, L.L., *Limestone additions to Portland cement-An Old Controversie Revised*, in *Carbonate additions to cement*, P. Klieger, Hooton, R.D., Editor. 1990, American Society for Testing Materials. p. 3-13.
20. Moir, G., ed. *Minor additional constituents: Permitted types and benefits.* Eurocements. Impact of ENV 197 on Concrete Constructions., ed. R.K.D.a.M.R. Jones. 1994, E&FN Spoon: London. 37-56.
21. *BS EN 197-1Cement—part 1: composition, specications and conformity criteria for common cements.*, B. Standards and Institution, Editors. 2001: London.
22. Poitevin, P., *Limestone aggregate concrete, usefulness and durability.* Cement and Concrete Composites, 1999. **21**(2): p. 89-97.
23. Hooton, P. and M.D.A. Thomas, *The Use of Limestone in Portland Cement: Effect on Thaumasite Form of Sulfate Attack.* 2002, Portland Cement Association: Illinois, USA.
24. Capiteli, V.C. and M. Florindo, eds. *The influence fo limestone additions on the sulfur trioxide content in Portland cement.* Carbonate Additions to Cement. AST STP 1064, ed. R.D.H. P. Klieger. 1990, American Society for Testing and Materials: Philadelphia. 30-40.
25. CEMBERAU, *Climate Change, Cement and the EU.*, C.T.E.C. Association, Editor. 1998. p. 1-11.
26. Davidovits, J., *Global Warming Impact on the Cement and Aggregates Industries.* WORLD RESOURCE REVIEW, 1994. **6**(2): p. 263-276.
27. Sharp, J.H., Lawrence, C. D., Yang, R.D., *Calcium aluminate cements-Low energy cements, special cements or what?* Adv. Cement Research, 1999. **11**(1): p. 3-13.
28. Soroka, I. and N. Setter, *Calcareous fillers and the compressive strength of portland cement.* Cement and Concrete Research, 1976. **6**(3): p. 367-376.
29. Soroka, I. and N. Setter, *The effect of fillers on strength of cement mortars.* Cement and Concrete Research, 1977. **7**(4): p. 363-476.
30. Neville, A.M., *Properties of Concrete*. 4th ed. 1995, London: Peason Education Ltd. 844.
31. Hartshorn, S.A., R.N. Swamy, and J.H. Sharp, *Engineering porperties and structural implications of Portland limestone cement mortar exposed to magnesium sulfate attack.* Adv. Cem. Research, 2001. **13**(1): p. 31-46.
32. Kakali, G., Tsivilis, S., Aggeli, E. and Bati, M., *Hydration products of C3A, C3S and Portland cement in the presence of CaCO3.* Cement and Concrete Research, 2000. **30**(7): p. 1073-1077.
33. Ohba, Y., Nakamura, A. , Lee, J.K. , Sakai, E. and Daimon, M. *Influence of $CaCO_3$ on the hydration of various types of calcium aluminates with unhydrite.* in *Proc. 10th International Congress on the Chemistry of Cement.* 1997. Gothenburg, Sweeden.
34. Klemm, W. and L.D. Adams, eds. *An investigation of the formation of carboaluminates.* Carbonate additions to cement, ed. P.K.a.R.D. Hooton. Vol. Special Technical Publication STP 1064. 1990, ASTM-commitee C-1 on cement. 60-72.
35. Monteiro, P.J.M., J.C. Maso, and J.P. Ollivier, *The aggregate-mortar interface.* Cement and Concrete Research, 1985. **15**(6): p. 953-958.
36. Péra, J., S. Husson, and B. Guilhot, *Influence of finely ground limestone on cement hydration.* Cement and Concrete Composites, 1999. **21**(2): p. 99-105.
37. Tasong, W.A., J.C. Cripps, and C.J. Lynsdale, *Aggregate-cement chemical interactions.* Cement and Concrete Research, 1998. **28**(7): p. 1037-1048.
38. Fischer, R. and H.-J. Kuzel, *Reinvestigation of the system C4A.nH2O --- C4A.CO2.nH2O.* Cement and Concrete Research, 1982. **12**(4): p. 517-526.

39. Hornain, H., Marchand, J. , Duhot, V. and Regourd, M.M., *Diffusion of chloride ions in limestone filler blended cement pastes and mortars.* Cement and Concrete Research, 1995. **25**(8): p. 1667-1678.
40. Zelic, J., Krstulovic, R., Tkalcec, E. and Krolo, P., *Durability of the hydrated limestone-silica fume Portland cement mortars under sulphate attack.* Cement and Concrete Research, 1999. **29**(6): p. 819-826.
41. Irassar, E.F., M. González, and V. Rahhal, *Sulphate resistance of type V cements with limestone filler and natural pozzolana.* Cement and Concrete Composites, 2000. **22**(5): p. 361-368.
42. Heikal, M., H. El-Didamony, and M.S. Morsy, *Limestone-filled pozzolanic cement.* Cement and Concrete Research, 2000. **30**(11): p. 1827-1834.
43. Tsivilis, S., Batis, G. , Chaniotakis, E., Grigoriadis, Gr. and Theodossis, D., *Properties and behavior of limestone cement concrete and mortar.* Cement and Concrete Research, 2000. **30**(10): p. 1679-1683.
44. Matthews, J.D., *Performance of limestone filler cement concrete*, in *Euro-Cements: Impact of ENV 197 on Concrete Constructions*, R.K. Dhir, M.R. Jones, Editor. 1994, E&FN Spoon: London.
45. Bonavetti, V., et al., *Influence of initial curing on the properties of concrete containing limestone blended cement.* Cement and Concrete Research, 2000. **30**(5): p. 703-708.
46. Hooton, R.D., *Effects of Carbonate Additions on the Heat of Hydration and Sulfate Resistance of Portand Cements.*, in *Carboate additions to cement.*, P.K.a. D.R.Hooton., Editor. 1990, ASTM STP 1064: Philadelphia, USA. p. 73-81.
47. Hartshorn, S.A., J.H. Sharp, and R.N. Swamy, *The thaumasite form of sulfate attack in Portland-limestone cement mortars stored in magnesium sulfate solution.* Cement and Concrete Composites, 2002. **24**(3-4): p. 351-359.
48. Bonen, D., and Cohen, M.D., *Magnesium sulfate attack on portland cement paste — II. Chemical and mineralogical analyses.* Cement and Concrete Research, 1992. **22**(4): p. 707-718.
49. Santhanam, M., M.D. Cohen, and J. Olek, *Mechanism of sulfate attack: A fresh look: Part 1: Summary of experimental results.* Cement and Concrete Research, 2002. **32**(6): p. 915-921.
50. Buenfeld, N.R. and J.B. Newman, *The development and stability of surface layers on concrete exposed to sea-water.* Cement and Concrete Research, 1986. **16**(5): p. 721-732.
51. Clark, B.A. and P.W. Brown, *The formation of calcium sulfoaluminate hydrate compounds: Part I.* Cement and Concrete Research, 1999. **29**(12): p. 1943-1948.
52. Clark, B.A. and P.W. Brown, *The formation of calcium sulfoaluminate hydrate compounds: Part II.* Cement and Concrete Research, 2000. **30**(2): p. 233-240.
53. Tikalski, P.J., et al., *Redefining cement characteristics for sulfate-resistant Portland cement.* Cement and Concrete Research, 2002. **32**: p. 1239-1246.
54. Taylor, H.F.W., C. Famy, and K.L. Scrivener, *Delayed ettringite formation.* Cement and Concrete Research, 2001. **31**(5): p. 683-693.
55. Kelham, S., *The effect of cement composition and fineness on expansion associated with delayed ettringite formation.* Cement and Concrete Composites, 1996. **18**(3): p. 171-179.
56. Kuzel, H.-J., *Initial hydration reactions and mechanisms of delayed ettringite formation in Portland cements.* Cement and Concrete Composites, 1996. **18**(3): p. 195-203.
57. Yang, R. and N.R. Buenfeld, *Microstructural identification of thaumasite in concrete by backscattered electron imaging at low vacuum.* Cement and Concrete Research, 2000. **30**(5): p. 775-779.

58. Lachowski, E.E., S.J. Barnett, and D.E. Macphee, *Transmission electron optical study of ettringite and thaumasite.* Cement and Concrete Composites, 2003. **25**(8): p. 819-822.
59. Lawrence, C.D., *Sulfate attack on concrete.* Magazine of Concrete Research, 1990. **42**: p. 249-264.
60. Osborne, G.J., *The durability of SRPC/GGBS concretes in aggressive sulphate, acid and marine environments, , (editors),, , , pp. . 1994*, in *Eoru-cements: impact of ENV 197 on contrete constructions*, R.K. Dhir, Jones, M.R., Editor. 1994, E&FN Spon ltd: London. p. 169-182.
61. Gollop, R.S.a.T., H. F. W., *Microstructural and microanalytical studies of sulfate attack. I. Ordinary portland cement paste.* Cement and Concrete Research, 1992. **22**(6): p. 1027-1038.
62. Barnett, S.J., D.E. Macphee, and N.J. Crammond, *Extent of immiscibility in the ettringite-thaumasite system.* Cement and Concrete Composites, 2003. **25**(8): p. 851-855.
63. Crammond, N.J., *The thaumasite form of sulfate attack in the UK.* Cement and Concrete Composites, 2003. **25**(8): p. 809-818.
64. Erlin, B. and D.C. Stark, *Identification and occurrence of thaumasite in concrete.*, H.R. Record, Editor. 1966. p. 108–13.
65. Barnett, S.J., Adam, C. D., Jackson, A. R. W. and Hywel-Evans, P. D., *Identification and characterisation of thaumasite by XRPD techniques.* Cement and Concrete Composites, 1999. **21**(2): p. 123-128.
66. Barnett, S.J., Adam, C.D., Jackson, A.R.W. and Hywel_Evans, P.D., *Identification and characterization of thaumasite by XRPD techniques.* J. Materials Science, 2000. **35**: p. 4109-4114.
67. Bickley, J.A., R.D. Hooton, and J. Balinski. *Thaumasite related deterioration of concrete structures.* in *Proceeding of Malhotra Symposium on Concrete Technology.* 1994. San Francisco.
68. Longworth, T.I., *Contribution of construction activity to aggressive ground conditions causing the thaumasite form of sulfate attack to concrete in pyritic ground.* Cement and Concrete Composites, 2003. **25**(8): p. 1005-1013.
69. Hartshorn, S.A., *Sulfate attack of Portland limestone cements*, in *PhD in Mechanical Engineering*. 1998, The University of Sheffield: Sheffield. p. 214.
70. Gaze, M.E. and N.J. Crammond, *The formation of thaumasite in a cement:lime:sand mortar exposed to cold magnesium and potassium sulfate solutions.* Cement and Concrete Composites, 2000. **22**(3): p. 209-222.
71. Barker, A.P. and D.W. Hobbs, *Performance of Portland limestone cements in mortar prisms immersed in sulfate solutions at 5 [deg]C.* Cement and Concrete Composites, 1999. **21**(2): p. 129-137.
72. Kakali, G., Tsivilis, S., Skaropoulou, A., Sharp, J. H. and Swamy, R. N., *Parameters affecting thaumasite formation in limestone cement mortar.* Cement and Concrete Composites, 2003. **25**(8): p. 977-981.
73. Tsivilis, S., Kakali, G., Skaropoulou, A., Sharp, J. H. and Swamy, R. N., *Use of mineral admixtures to prevent thaumasite formation in limestone cement mortar.* Cement and Concrete Composites, 2003. **25**(8): p. 969-976.
74. Justnes, H., *Thaumasite formed by sulfate attack on mortar with limestone filler.* Cement and Concrete Composites, 2003. **25**(8): p. 955-959.
75. Hobbs, D.W., *Thaumasite sulfate attack in field and laboratory concretes: implications for specifications.* Cement and Concrete Composites, 2003. **25**(8): p. 1195-1202.
76. Collett, G., Crammond, N. J., Swamy, R. N. and Sharp, J. H., *The role of carbon dioxide in the formation of thaumasite.* Cement and Concrete Research. **In Press.**

77. Brunauer, S. and D.L. Kantro, *The hydration of Tricalcium Silicate and beta-Dicalcium Silicate from 5oC to 50oC.*, in *The Chemistry of cements.*, H.F.W. Taylor, Editor. 1964, Academic Press Inc. Ltd.: London. p. 287-309.
78. Escalante-García, J.I. and J.H. Sharp, *The microstructure and mechanical properties of blended cements hydrated at various temperatures.* Cement and Concrete Research, 2001. **31**(5): p. 695-702.
79. Miller, F.M. and F.J. Tang, *The distribution of sulfur in present-day clinkers of variable sulfur content.* Cement and Concrete Research, 1996. **26**(12): p. 1821-1829.
80. Yang, R. and J.H. Sharp, *Hydration characteristics of Portland cement after heat curing: I, Degree of hydration of the anhydrous cement phases.* J. Am. Ceram. Soc, 2001. **84**(3): p. 608-614.
81. Taylor, H.F.W., *Distribution of sulfate between phases in Portland cement clinkers.* Cement and Concrete Research, 1999. **29**(8): p. 1173-1179.
82. Drever, J.I., *The Geochemistry of Natural Waters. Surface and Ground water Environments.* 3rd ed. ed. 1997: Prentice Hall Ltd. 420-421.
83. Hill, J., Byars, E. A., Sharp, J. H., Lynsdale, C. J., Cripps, J. C., and Zhou, Q., *An experimental study of combined acid and sulfate attack of concrete.* Cement and Concrete Composites, 2003. **25**(8): p. 997-1003.
84. Bensted, J., *Thaumasite--direct, woodfordite and other possible formation routes.* Cement and Concrete Composites, 2003. **25**(8): p. 873-877.
85. Gaze, M.E., *The effects of varying gypsum content on thaumasite formation in a cement:Lime:Sand mortar at 5 [deg]C.* Cement and Concrete Research, 1997. **27**(2): p. 259-265.
86. Crammond, N.J. and P.J. Nixon. *Deterioration of concrete foundation piles as a result of thaumasite formation.* in *6th International Conference on Durability of Building Materials.* 1993. Japan.
87. Gollop, R.S. and H.F.W. Taylor, *Microstructural and microanalytical studies of sulfate attack III. Sulfate-resisting portland cement: Reactions with sodium and magnesium sulfate solutions.* Cement and Concrete Research, 1995. **25**(7): p. 1581-1590.
88. van Aardt, J.H.P. and S. Visser, *Thaumasite formation: A cause of deterioration of portland cement and related substances in the presence of sulphates.* Cement and Concrete Research, 1975. **5**(3): p. 225-232.
89. Ludwig, U. and S. Mehr. *Distruction of historical buildings by the formation of ettringite and thaumasite.* in *8th International Congress on the Cement Chemistry.* 1986. Rio de Janeiro.
90. Morales, R.T. *The sulfate reistant Portland cement are not the ultimate answer to the problem of sulfate attack.* in *8th International Congress on the Chemistry of Cement.* 1986. Rio de Janeiro, Brazil.
91. Knudsen, T., *Thaumasite. Its stability amd formation. A literature review report.*, in *Eurocare-thaumasite.* 1990, Eureka Project. p. 1-21.
92. Collepardi, M., *Thaumasite formation and deterioration in historic buildings.* Cement and Concrete Composites, 1999. **21**(2): p. 147-154.
93. Irassar, E.F., Bonavetti, V. L., Trezza, M. A., Gonzalez, M. A., *Thaumasite formation in limestone filler cements exposed to sodium sulphate solution at 20°C.* Cement and Concrete Composites. **In Press.**
94. Al-Amoudi, O.S.B., M. Maslehuddin, and Y.A.B. Abdul-Al, *Role of chloride ions on expansion and strength reduction in plain and blended cements in sulfate environments.* Construction and Building Materials, 1994. **9**(1): p. 25-33.
95. Bothe, J.V.J. and P.W. Brown, *PhreeqC modeling of Friedel's salt equilibria at 23±1 °C.* Cement and Concrete Research, 2004. **34**(6): p. 1057-1063.

96. Hobbs, D.W. and M.G. Taylor, *Nature of the thaumasite sulfate attack mechanism in field concrete.* Cement and Concrete Research, 2000. **30**(4): p. 529-533.
97. Eden, M.A., *The laboratory investigation of concrete affected by TSA in the UK.* Cement and Concrete Composites, 2003. **25**(8): p. 847-850.
98. Ben-Yair, M., *The effect of chlorides on concrete in hot and arid regions.* Cement and Concrete Research, 1967. **4**(3): p. 405-416.
99. Conjeaud, M.L., *Mechanism of Sea water attack on Cement Mortar.* 1978(SP 65-3): p. 39-61.
100. Al-Amoudi, O.S.B., *Attack on plain and blended cements exposed to aggressive sulfate environments.* Cement and Concrete Composites, 2002. **24**(3-4): p. 305-316.
101. Csizmadia, J., G. Balázs, and F.D. Tamás, *Chloride ion binding capacity of aluminoferrites.* Cement and Concrete Research, 2001. **31**(4): p. 577-588.
102. Damidot, D., Glasser, F. P. *Thermodynamic Investigation of the $CaO-Al_2O_3-CaSO_4-CaCl_2-H_2O$ system at 25°C and the Influence of Na_2O.* in *10th international congress on the chemistry of cement: Performance and durability of cementitious materials.* 1997. Gothenburg,Sweden.
103. Midgley, H.G.a.I., J. M., *The penetration of chlorides into hardened cement pastes.* Cement and Concrete Research, 1984. **14**(4): p. 546-558.
104. Gollop, R.S. and H.F.W. Taylor, *Microstructural and microanalytical studies of sulfate attack. I. Ordinary portland cement paste.* Cement and Concrete Research, 1992. **22**(6): p. 1027-1038.
105. Scrivener, K.L., Capmas, A., *Calcium aluminate cement*, in *Lea's Chemistry of Cement and Concrete*, P.C. Hewlett, Editor. 1998, Butterworth Heinemann: Oxford. p. 760-763.
106. Goñi, S. and A. Guerrero, *Accelerated carbonation of Friedel's salt in calcium aluminate cement paste.* Cement and Concrete Research, 2003. **33**(1): p. 21-26.
107. Suryavanshi, A.K. and R. Narayan Swamy, *Stability of Friedel's salt in carbonated concrete structural elements.* Cement and Concrete Research, 1996. **26**(5): p. 729-741.
108. Jones, M.R., McCarthy, M.J., Dhir, R.K. *Chloride Ingress and Reinforcement Corrosion in Carbonated and Sulphated Concrete.* in *Corrosion and Corrosion Protection of Steel in Concrete.* 1994. Sheffield: Sheffield Academic Press.
109. Lukas, W., *Substitution of Si in the lattice of ettringite.* Cement and Concrete Research, 1976. **6**(2): p. 225-233.
110. Wakeley, L.P. and D.M. Roy, *Experimental concretes for sealing radioactive-waste repositories in evaporite strata.* Cement and Concrete Research, 1983. **13**(1): p. 97-106.
111. Brown, P.W. and S. Badger, *The distributions of bound sulfates and chlorides in concrete subjected to mixed NaCl, MgSO4, Na2SO4 attack.* Cement and Concrete Research, 2000. **30**(10): p. 1535-1542.
112. Diamond, S., *Thaumasite in Orange County, Southern California: an inquiry into the effect of low temperature.* Cement and Concrete Composites, 2003. **25**(8): p. 1161-1164.
113. Hagelia, P., et al., *Thaumasite and secondary calcite in some Norwegian concretes.* Cement and Concrete Composites, 2003. **25**(8): p. 1131-1140.
114. Monsoni, S., M. Longhi, and M. Collepardi. *The influence of pozzolanic additions on the concrete resistance to CaCl2 attack.* in *CANMET/ACI Interantional Conference on Advances in Concrete Technology.* 1992. Athens, Greece.
115. Chatterji, S., *Mechanism of the CaCl2 attack on portland cement concrete.* Cement and Concrete Research, 1978. **8**(4): p. 461-467.

116. Bertsson, L. and S. Chandra, *Damage of concrete sleepers by calcium chloride.* Cement and Concrete Research, 1982. **12**(1): p. 87-92.
117. Higgins, D.D., *Increased sulfate resistance of ggbs concrete in the presence of carbonate.* Cement and Concrete Composites, 2003. **25**(8): p. 913-919.
118. Higgins, D.D. and N.J. Crammond, *Resistance of concrete containing ggbs to the thaumasite form of sulfate attack.* Cement and Concrete Composites, 2003. **25**(8): p. 921-929.
119. Hill, J., Byars, E. A., Sharp, J. H., Lynsdale, C. J., Cripps, J. C., and Zhou, Q., *An experimental study of combined acid and sulfate attack of concrete.* Cement and Concrete Composites, 2003. **25**(8): p. 997-1003.
120. Nobst, P. and J. Stark, *Investigations on the influence of cement type on thaumasite formation.* Cement and Concrete Composites, 2003. **25**(8): p. 899-906.
121. Mulenga, D.M., J. Stark, and P. Nobst, *Thaumasite formation in concrete and mortars containing fly ash.* Cement and Concrete Composites, 2003. **25**(8): p. 907-912.
122. Smallwood, I., S. Wild, and E. Morgan, *The resistance of metakaolin (MK)-Portland cement (PC) concrete to the thaumasite-type of sulfate attack (TSA)--Programme of research and preliminary results.* Cement and Concrete Composites, 2003. **25**(8): p. 931-938.
123. Zevin, L. and G. Kimel, *Quantitative X-ray Diffractometry*, ed. I. Mureinik. 1995, New York: Springer-Verlag New York, Inc. 372.
124. Macphee, D.E., and Barnett, S.J., *Solution properties of solids in the ettringite--thaumasite solid solution series.* Cement and Concrete Research. **In Press.**
125. Jones, I.P., *Chemical microanalysis using electron beams*, ed. I.P. Jones. 1992, London: The Institute of Materials. 241.
126. Kleinbaum, D.G., K.L. Kupper, and K.E. HMuller, *Applied Regression Analysis and Other Multivariate Methods.* 1988, Massachusetts: PWS-KENT Publishing Company. 718.
127. Crammond, N., *The occurrence of thaumasite in modern construction - a review.* Cement and Concrete Composites, 2002. **24**(3-4): p. 393-402.
128. Crammond, N. and M. Halliwell. *The thaumasite form of sulfate attack in concretes containing a source of carbonate ions.* in *2nd Symposium Advances in Conc Tech,*. 1995: ACI, P154-19.
129. Novak, G.A. and A.A. Colville, *Efflorescent mineral assemblages associated with cracked and degraded residential concrete foundations in Southern California.* Cement and Concrete Research, 1989. **19**(1): p. 1-6.
130. Brown, P.W. and A. Doerr, *Chemical changes in concrete due to the ingress of aggressive species.* Cement and Concrete Research, 2000. **30**(3): p. 411-418.
131. Lukas, W., *Betonzerstorung durch SO3-angriff unter bildung von thaumasit und woodfordit.* Cement and Concrete Research, 1975. **5**(5): p. 503-517.
132. Damidot, D., Stronach, S., Kindness, A., Atkins, M. and Glasser, F. P., *Thermodynamic investigation of the CaO---Al2O3---CaCO3---H2O closed system at 25[deg]C and the influence of Na2O.* Cement and Concrete Research, 1994. **24**(3): p. 563-572.
133. Glasser, F.P., A. Kindness, and S.A. Stronach, *Stability and solubility relationships in AFm phases: Part I. Chloride, sulfate and hydroxide.* Cement and Concrete Research, 1999. **29**(6): p. 861-866.
134. Edge, R.A. and H.F.W. Taylor, *Crystal structure of thaumasite, (Ca3 Si (O H)6 (H2 O)12) (S O4) (C O3).* Acta Crystallographica Section B, 1971. **27**(3): p. 594-601.

135. Barnett, S.J., Macphee, D. E., Lachowski, E. E. and Crammond, N. J., *XRD, EDX and IR analysis of solid solutions between thaumasite and ettringite.* Cement and Concrete Research, 2002. **32**(5): p. 719-730.
136. Farmer, V.C. The infrared spectra of minerals (Mineralogical Society monographs-4). 1974, London: Mineralogical Society.
137. Regourd, M.M., *Cement Made from Blastfurnace Slag*. 4 ed. Lea's Chemistry of Cement and Concrete, ed. P.C. Hewlett. 1998, Oxford: Butterworth Heinemann. 1057.
138. Eglinton, M., *Resistance of Concrete to Destructive Agencies*, in *Lea's Chemistry of Cement and Concrete*, P.C. Hewlett, Editor. 1998, Reed Educational and Professional Publishing Ltd.: Oxford.
139. Birnin-Yauri, U.A., and Glasser, F. P., *Friedel's salt, Ca2Al(OH)6(Cl,OH)·2H2O: its solid solutions and their role in chloride binding.* Cement and Concrete Research, 1998. **28**(12): p. 1713-1723.
140. Glasser, F.P., *Chemistry of the alkali-aggregate reaction*, in *The Alkali-aggregate reaction in concrete*, R.N. Swamy, Editor. 1992, Blackie and Son Ltd: London. p. 336.
141. Courard, L., Darimont, A., Schouterden, M., Ferauche, F., Willem, X. and Degeimbre, R., *Durability of mortars modified with metakaolin.* Cement and Concrete Research, 2003. **33**(9): p. 1473-1479.
142. Wild, S., J.M. Khatib, and A. Jones, *Relative strength, pozzolanic activity and cement hydration in superplasticised metakaolin concrete.* Cement and Concrete Research, 1996. **26**(10): p. 1537-1544.
143. Gabrisova, A., J. Havlica, and S. Sahu, *Stability of calcium sulphoaluminate hydrates in water solutions with various pH values.* Cement and Concrete Research, 1989. **21**(6): p. 1023-1027.
144. Monteiro, P.J.M. and P.K. Mehta, *Interaction between carbonate rock and cement paste.* Cement and Contrete Research, 1985. **16**(2): p. 127-134.
145. Suryavanshi, A.K., J.D. Scantlebury, and S.B. Lyon, *Mechanism of Friedel's salt formation in cements rich in tri-calcium aluminate.* Cement and Concrete Research, 1996. **26**(5): p. 717-727.
146. Beaudoin, J.J., Ramachandran, V. S. and Feldman, R. F., *Interaction of chloride and C---S---H.* Cement and Concrete Research, 1990. **20**(6): p. 875-883.
147. Jones, M.R., Macphee,D. E., Chudek, J. A., Hunter, G., Lannegrand, R., Talero, R. and Scrimgeour, S. N., *Studies using 27Al MAS NMR of AFm and AFt phases and the formation of Friedel's salt.* Cement and Concrete Research, 2003. **33**(2): p. 177-182.
148. Odler, I., *Hydration, Setting and Hardening of Portland Cement*, in *Lea's Chemistry of Cement and Concrete*, P.C. Hewlett, Editor. 2001, Butterworth Heinemann: Oxford. p. 241-297.
149. Jensen, O.M., A.M. Coats, and F.P. Glasser, *Chloride ingress profiles measured by electron probe micro analysis.* Cement and Concrete Research, 1996. **26**(11): p. 1695-1705.
150. Young, R.A., *The Rietveld Method*, ed. I.U.o. Crystalography. 2000, Oxford: Oxford University Press. 298.
151. Barnett, S.J., C.D. Adam, and A.R.W. Jackson, *An XRPD profile fitting investigation of the solid solution between ettringite, Ca6Al2(SO4)3(OH)12.26H2O, and carbonate ettringite, Ca6Al2(CO3)3(OH)12.26H2O.* Cement and Concrete Research, 2001. **31**(1): p. 13-17.
152. Barnett, S.J., Halliwell, M. A., Crammond, N. J., Adam, C. D. and Jackson, A. R. W., *Study of thaumasite and ettringite phases formed in sulfate/blast furnace*

slag slurries using XRD full pattern fitting. Cement and Concrete Composites, 2002. **24**(3-4): p. 339-346.
153. Ballirano, P.B., E.;Maras, A.;Merlino, S., *Crystal structure of afghanite, the eight-layer member of the cancrinite-group: evidence for long-range Si, Al ordering.* European Journal of Mineralogy, 1997. **-**: p. 21-30.
154. Rastsvetaeva, R.K., Pobedimskaya, E.A., Terent'eva, L.E. and Sapozhnikov, A.N., *Structural features of afganite and its place among cancrinite group minerals.* Kristallografiya, 1993. **38**: p. 94-103.
155. Busing, W.R., *An interpretation of the structures of alkaline earth chlorides in terms of interionic forces.* Transactions of the American Crystallographic Association, 1970. **6**(57-72.).
156. Dalibart, M. and J. Derouault, *Les composes de coordination des halogenures d'aluminium: mise au point sur leurs proprietes structurales et les methodes d'analyses: Coordination compounds with aluminum halides: review of their structural properties and of their characterization by vibrational and NMR spectroscopies.* Coordination Chemistry Reviews, 1986. **74**: p. 1-51.
157. Harris, A.W., Manning, M.C., Tearle, W.M. and Tweed, C.J., *Testing of models of the dissolution of cements—leaching of synthetic CSH gels.* Cement and Concrete Research, 2002. **32**: p. 731–746.
158. Tsivilis, S., Chaniotakis, E., G. Kakali and G. Batis, *An analysis of the properties of Portland limestone cements and concrete.* Cement and Concrete Composites, 2002. **24**(3-4): p. 371-378.
159. Crammond, N.J., Halliwell, M. A. and Higgins, D. D. *The use of groundblastfurnace slag to avoid the thaumasite form of sulfate attack: four year results.* in *Conference on Sustainable Construction into the Next Millennium: Environmentally Friendly and Innovative Cement-Based Materials.* 2000. Joao Pessoa, Brazil.
160. Khatib, J.M. and S. Wild, *Sulphate Resistance of Metakaolin Mortar.* Cement and Concrete Research, 1998. **28**(1): p. 83-92.
161. Asbridge, A.H., G.A. Chadbourn, and C.L. Page, *Effects of metakaolin and the interfacial transition zone on the diffusion of chloride ions through cement mortars.* Cement and Concrete Research, 2001. **31**(11): p. 1567-1572.

Appendix I

Statistical analyses of Relative Mass Loss, carbonate and chloride content

Multivariate statistical analysis was performed to study the significance of the selected parameters and their possible interactions on the relative mass of the cubes after immersion in salt solutions for 1 year. The main factors were calcium carbonate filler replacing clinker (Cc=0, 5 and 15%) and chloride in solution as NaCl (Cl= 0, 5, 10 and 20g/l). The equations and tables for the multivariate statistical analyses are published in Kleinbaum et al. [126].

A. Statistical analyses with single variables calcium carbonate (Cc) and chloride content (Cl)

The first analysis, regression coefficients and analysis of variance (ANOVA) shown in table V-1 to V-2, considers calcium carbonate content.

Table V-1: Linear regression of samples in salt solutions using parameter Cc (Figure 5.18)

Independent:	Column(Cc) -> Column(Cc)			
Dependent:	Column(Rmass)			
Parameter	Value	Error	t-Value	Prob>|t|
Constant	-0.43555	0.47678	-0.91354	0.38478
Cc	1.36932	0.51043	2.68271	0.02509
R-Square(COD)	Adj. R-Square	Root-MSE(SD)		
0.44434	0.3826	0.10991		

Despite the parameter Cc being statistically significant (Prob>t=0.025), the regression correlation is poor (R^2=0.44), hence, indicating a poor correlation between the relative mass detected and the content of calcium carbonate alone.

Table V-3 to V-4 show the linear regression and analysis of variance when considering the factor Cl alone.

Table V-3: Linear regression of samples in salt solutions using parameter Cc (Figure 5.18)

Independent:	Column(Cl) -> Column(Cl)			
Dependent:	Column(Rmass)			
Parameter	Value	Error	t-Value	Prob>|t|
Constant	0.90859	0.05937	15.30392	<0.0001
Cl	-0.00789	0.00513	-1.53986	0.15798
R-Square(COD)	Adj. R-Square	Root-MSE(SD)		
0.20852	0.12058	0.13117		

The factor Cl is also statistically significant, but the between the relative mass and chloride content is even poorer than with calcium carbonate factor (R^2=0.21).

B. Statistical analyses with multiple variables calcium carbonate (Cc), chloride content (Cl)

Obviously, the variation of the mass at 5°C was not linear, hence, poor correlations were already expected (Figure 5.17). The non–linearity can be associated with complex interactions, with carbonates and chlorides playing inter-related ore distinct roles. In the multiple variable approach, each factor Cc and Cl were analysed up to the third order polynomial, and also both factors together.

Table V-4 and V-5 show the statistical multivariable analysis of carbonate content (Cc) and chloride content (Cl), respectively.

Table V-4: Multivariate regression of samples in salt solutions using the factor Cc (Figure 5.18)

Independent:	Column(Cc) -> Column(Cc3)			
Dependent:	Column(Rmass)			
Parameter	Value	Error	t-Value	Prob>|t|
Constant	0.91093	1.14794	0.79353	0.45352
Cc	-0.01523	7.27934E6	-2.09248E-9	1
Cc2	0.06492	1.94116E6	3.34438E-8	1
Cc3	-0.00347	97057.82829	-3.57077E-8	1
R-Square(COD)	Adj. R-Square	Root-MSE(SD)		
	2.29589			

Table V-4: Multivariate regression of samples in salt solutions using the factor Cl (Figure 5.18)

Independent:	Column(Cl) -> Column(Cl3)			
Dependent:	Column(Rmass)			
Parameter	Value	Error	t-Value	Prob>|t|
Constant	0.83224	0.06985	11.9141	<0.0001
Cl	0.07589	0.04775	1.58932	0.15601
Cl2	-0.01132	0.00746	-1.51728	0.17298
Cl3	3.62931E-4	2.63435E-4	1.37769	0.21073

R-Square(COD)	Adj. R-Square	Root-MSE(SD)
0.47625	0.25179	0.12099

Although the non-linear analyses also did not show good correlation for both Cc and Cl polynomials, it can be seen that the variation of relative mass can be better fitted when the factor chloride (Cl) is used than by using calcium carbonate content (Cc) alone, which errors were extremely high.

C. Statistical analyses with multiple variables calcium carbonate (Cc), chloride content (Cl) and interactions between both factors.

Another attempt was made to fit the relative mass (Rmass) variation using both factors carbonate content (Cc) and chloride content (Cl) as well as other interaction between these two factors (CcCl). Table V-5 shows the best-fit statistical model identified.

Table V-5: Multiple Regression of Model 1 on samples in salt solutions at 5°C (Figure 5.18).

Independent:	Column(Cl) -> Column(Cl3)			
Dependent:	Column(rm5)			
Parameter	Value	Error	t-Value	Prob>|t|
Constant	0.90714	0.02332	38.8965	<0.0001
Cl	0.07064	0.0147	4.80665	0.00298
Cc2	-8.98801E-4	1.08978E-4	-8.24754	1.71746E-4
Cl2	-0.01001	0.0023	-4.35206	0.00481
Cl3	3.10501E-4	8.12596E-5	3.8211	0.00875

R-Square(COD)	Adj. R-Square	Root-MSE(SD)
0.95755	0.92924	0.03721

(Rmass): relative mass; (Cl): chloride concentration; (Cc): limestone filler content.

It can be seen that the multivariate correlation coefficient (R^2=0.958) significantly increased with the inclusion of both factors. Also, the analysis of variance (ANOVA), as shown in table V-6, indicates that this model is fit for predictions, as the calculated

Fisher value ($F_{4.6}$=33.83) is significantly higher than the tabulated value ($F_{4.6}$=0.0003) (Kleinbaum et al. [126]).

Table V-6: ANOVA of Model 1 on samples in salt solutions at 5°C.

Item	Degrees of Freedom	Sum of Squares	Mean Square	F Statistic
Model	4	0.18734	0.04684	33.83277
Error	6	0.00831	0.00138	
Total	10	0.19565		

Prob>F
2.96311E-4

According to this model, the relative mass observed after one year of immersion in salt solution can be explained according to the Equation V-1, in which both chlorides and carbonates influenced the performance of the test mortar mixes at 5°C.

$$Rmass = \underset{\pm 0.02}{0.907} + \underset{\pm 0.015}{0.071}\,Cl - \underset{\pm 0.002}{0.01}\,Cl^2 + \underset{\pm 0.00008}{0.003}\,Cl^3 - \underset{\pm 0.0001}{0.0009}\,Cc^2$$

Table V-7 and V-8 show another attempt to improve the statistical model by introducing the factor (CcCl).

Table V-7: Multiple Regression of Model 2 on samples in salt solutions at 5°C.

Independent: Column(Cl) -> Column(Cl3)
Dependent: Column(rm5)

Parameter	Value	Error	t-Value	Prob>|t|
Constant	0.89557	0.03434	26.08235	<0.0001
Cl	0.06927	0.01703	4.06815	0.01525
Cc2	-0.00135	6.11166E-4	-2.21032	0.09159
Cl2	-0.00965	0.00268	-3.60763	0.0226
CcCl	-6.38435E-6	2.66872E-4	-0.02392	0.98206
Cc	0.00739	0.01	0.73879	0.50104
Cl3	2.96336E-4	9.49643E-5	3.12049	0.03551

R-Square(COD)	Adj. R-Square	Root-MSE(SD)
0.96285	0.90713	0.04263

(Rmass): relative mass; (Cl): chloride concentration; (Cc): limestone filler content.

Table V-8: ANOVA of Model 2 on samples in salt solutions at 5°C.

Item	Degrees of Freedom	Sum of Squares	Mean Square	F Statistic
Model	6	0.18838	0.0314	17.27946
rror	4	0.00727	0.00182	
Total	10	0.19565		

Prob>F
0.00788

The introduction of the combined factor CcCl did not bring any significant improvement to the statistical model. The multivariate correlation slightly improved (R2=0.963), but the Fisher value significantly decreased ($F_{6.4}$ =17.28).

C. Samples at 20°C

The best model for samples immersed at 20oC is shown in Table V.9 and equation V-1.

Table V.9: Multiple Regression of best model for samples in salt solutions at 20°C.

Independent: Column(Cl) -> Column(Cc)
Dependent: Column(rm5)

Parameter	Value	Error	t-Value	Prob>|t|
Y-Intercept	1.13035	0.0425	26.59775	<0.0001
Cl	0.00801	0.00857	0.93404	0.39316
Cc2	-0.00123	7.45182E-4	-1.64612	0.16066
Cl2	-1.81639E-4	3.83508E-4	-0.47363	0.65573
CcCl	-7.31548E-4	3.32714E-4	-2.19873	0.07922
Cc	0.02265	0.01223	1.85185	0.12325

R-Square(COD)	Adj. R-Square	Root-MSE(SD)
0.64155	0.28309	0.05314

Table V.10: ANOVA of best model for samples in salt solutions at 20°C.

Item	Degrees of Freedom	Sum of Squares	Mean Square	F Statistic
Model	5	0.02527	0.00505	1.78976
Error	5	0.01412	0.00282	
Total	10	0.0394		

Prob>F
0.26922

D. Summary

Statistical analyses were carried out to determine the significance of the main factors affecting the relative mass response calculated for mortar mixes containing limestone immersed in salt solutions for 1 year at 5°C (Figure 5.17).

It has been shown that the best fit was obtained by the introduction of both factors calcium carbonate replacing clinker (Cc) and chloride content in solution (Cl). The best statistical model for samples at 20°C was found with the Equation V-1, and the best model for samples at 5°C can described by the Equation V-2, with the correlation coefficient of 0.64 and 0.96, respectively. The predicted relative mass contours for samples immersed at 20°C and 5°C can be seen in Figure 5.18 and 5.19 in Chapter 5, respectively.

$$Rmass20 = \underset{\pm 0.04}{1.13} + \underset{\pm 0.009}{0.008}\,Cl - \underset{\pm 0.00038}{0.00018}\,Cl^2 - \underset{\pm 0.00033}{0.0007}\,Cc.Cl + \underset{\pm 0.00033}{0.0227}\,.Cc - \underset{\pm 0.0007}{0.00123}\,Cc^2 \quad \textbf{(V-1)}$$

$$Rmass5 = \underset{\pm 0.02}{0.907} + \underset{\pm 0.015}{0.071}\,Cl - \underset{\pm 0.002}{0.01}\,Cl^2 + \underset{\pm 0.00008}{0.003}\,Cl^3 - \underset{\pm 0.0001}{0.0009}\,Cc^2 \quad \textbf{(V-2)}$$

Appendix II

Water solubility of calcite and gypsum in different chloride concentrations and temperatures

Introduction

The observations obtained by XRD and IRS suggest that chlorides and temperature may affect the solubility of sulfate species, carbonates and, indeed, other minerals in the pore solution of cementitious systems. Indeed, Drever [82] showed that chloride increases the solubility of carbonates, as shown in Figure AII-1. However, He also pointed out that sodium can precipitate as trona ($Na_2.CO_3.NaHCO_3.2H_2O$), hence, reducing the concentration of calcium carbonates in solution.

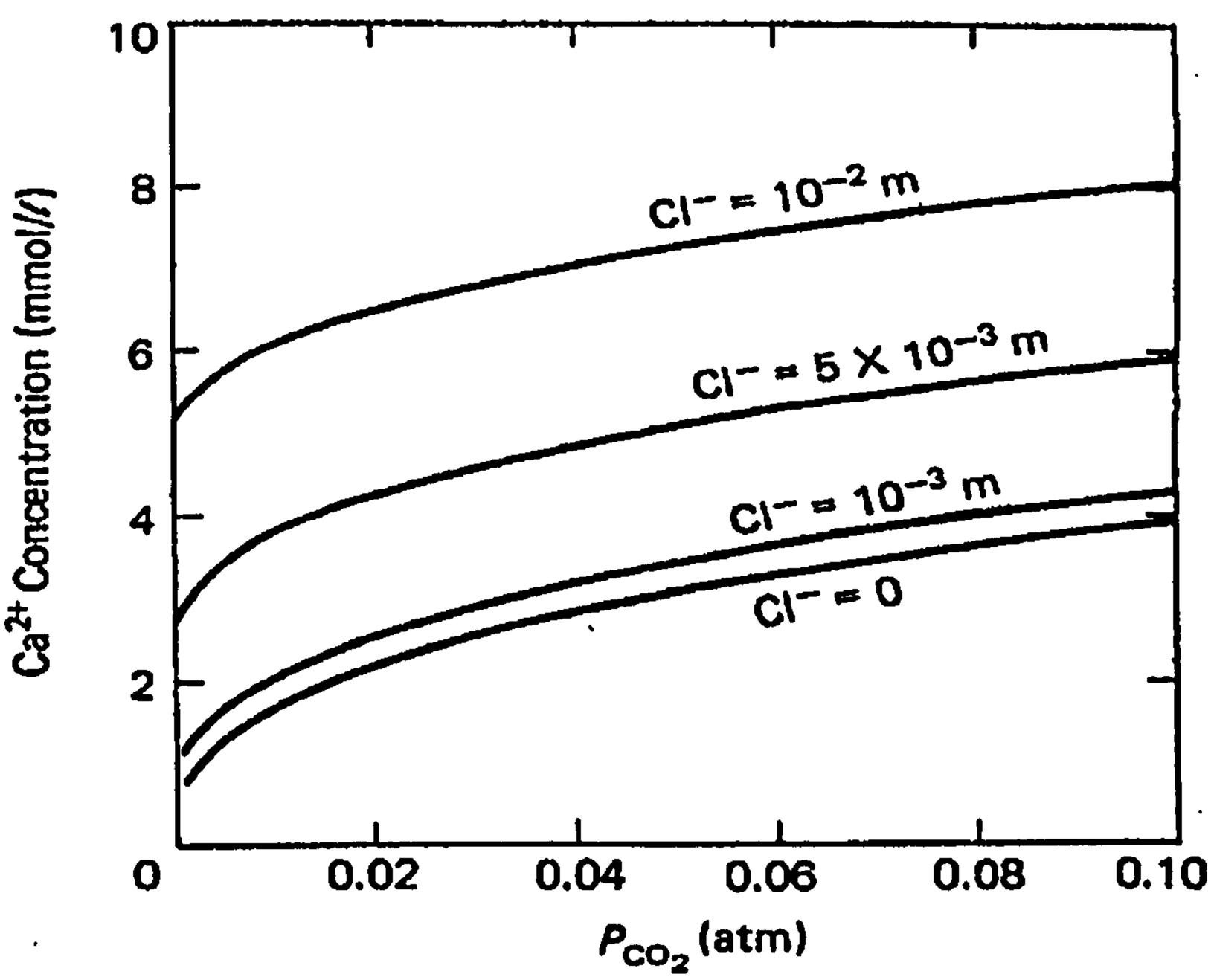

Figure AII 1: Calcium concentration as a function of P_{CO2} and Cl^- at 25°C, as shown in [82].

In order to investigate the effect of each salt solution selected in the scope of this thesis, a small-scale experiment was designed to assess whether the water solubility of

calcite and gypsum changes in the presence of combined magnesium sulfate and sodium chloride solutions at 5°C and 20°C.

Methodology

A known mass of these salts were mixed in high purity, deionised and demineralised water, in the concentrations of the designed solutions applied to the cement mortars according to Table AII-1. The solids were totally dispersed in water and manually agitated on a daily basis for one week. After that, the samples were analysed by ion chromatography for anions and cations, with special attention to calcium, since either calcite or gypsum are the sole source of calcium ions in these systems. In order to account for the dissolution of calcite in the salt solutions, the vials also contained atmospheric CO_2. This procedure was used in order to simulate the actual environment in the mortar containers, in which CO_2 was always present in this research.

Table AII.1: Salt concentration in solution.

WATER SOLUBILITY OF INORGANIC MATERIALS AT DIFFERENT TEMPERATURES AND SALT CONCENTRATIONS						Calculated Concentrations (ppm)	
Solution		Amount in (g/10ml)					
		Calcium carbonate	Calcium sulfate	Epsom salt	Sodium chloride	SO_4^{2-}	Cl^-
20°C	1	2.00	0.00	0.00000	0.00000	0.00	0.00
	2	0.00	0.50	0.00000	0.00000	1440.00	0.00
	3	2.00	0.00	0.15480	0.08410	6031.17	5128.05
	4	2.00	0.00	0.15480	0.16530	6031.17	10079.27
	5	2.00	0.00	0.15400	0.33070	6000.00	20164.63
	6	0.00	0.50	0.15490	0.08160	7475.06	4975.61
	7	0.00	0.50	0.15460	0.16630	7463.38	10140.24
	8	0.00	0.50	0.15490	0.33008	7475.06	20126.83
5°C	9	2.00	0.00	0.00000	0.00000		0.00
	10	0.00	0.50	0.00000	0.00000	1440.00	0.00
	11	2.00	0.00	0.15480	0.08387	6031.17	5114.02
	12	2.00	0.00	0.15400	0.16510	6000.00	10067.07
	13	2.00	0.00	0.15490	0.33110	6035.06	20189.02
	14	0.00	0.50	0.15490	0.08240	7475.06	5024.39
	15	0.00	0.50	0.15480	0.16620	7471.17	10134.15
	16	0.00	0.50	0.15460	0.32990	7463.38	20115.85

Results

1 Gypsum

It can be seen from Figure AII-2, that the water solubility of gypsum in pure water (Cl ppm =0) was not very much affected by reduction in the temperature in pure water, as already reported [12]. In the presence of salts, gypsum solubility was also not very much affected within the concentrations of the selected solutions of this thesis. Exception is made to the Cl^- concentration of 5g/l and 6g/l SO_4^{2-} (Clppm=5000), in which the amount of calcium in solution again reached its minimum at both 5 and 20°C. The combination of low temperature and increased chloride concentration showed the same non-linear trend as observed by other techniques (visual inspection, mass loss and x-ray microanalyses). This solubility trend seems to be in agreement with that reported by Damidot and Glasser [132], that the solubility of gypsum in equilibrium with the system $CaO-Al_2O_3-CaSO_4-CaCl_2-H_2O$ at 25°C decreases as the concentration of chlorides increases in solution. Therefore, the sulfate ions would precipitate as gypsum in this range of chloride concentrations.

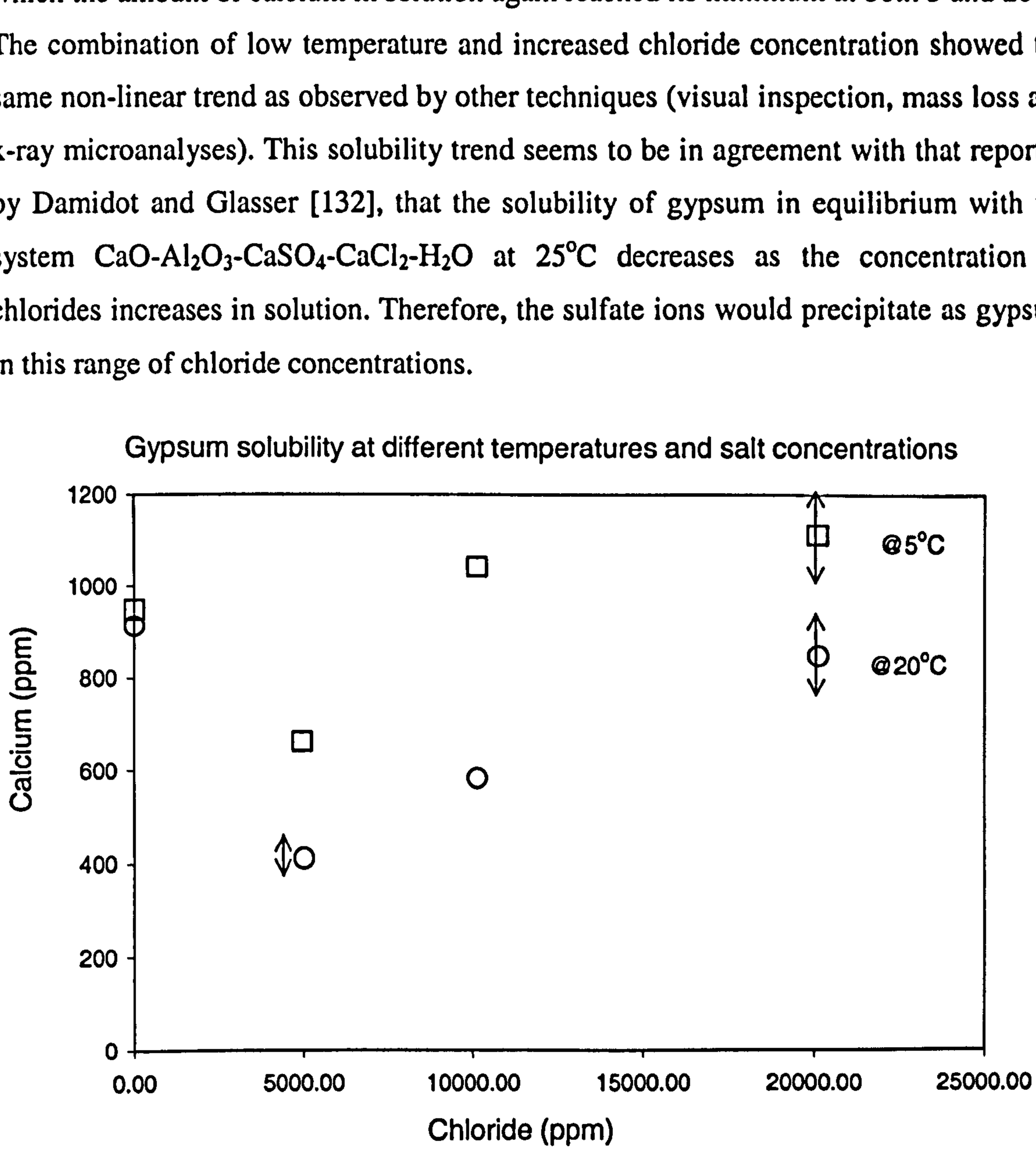

Figure AII 2: Calcium concentration of $CaSO_4$-NaCl-$MgSO_4$-H_2O-CO_2 system at 20°C and 5°C.

2 Calcite

Figure AII-3 shows the concentration of Ca^{2+} ions in solution is significantly affected by temperature and also by chloride concentration.

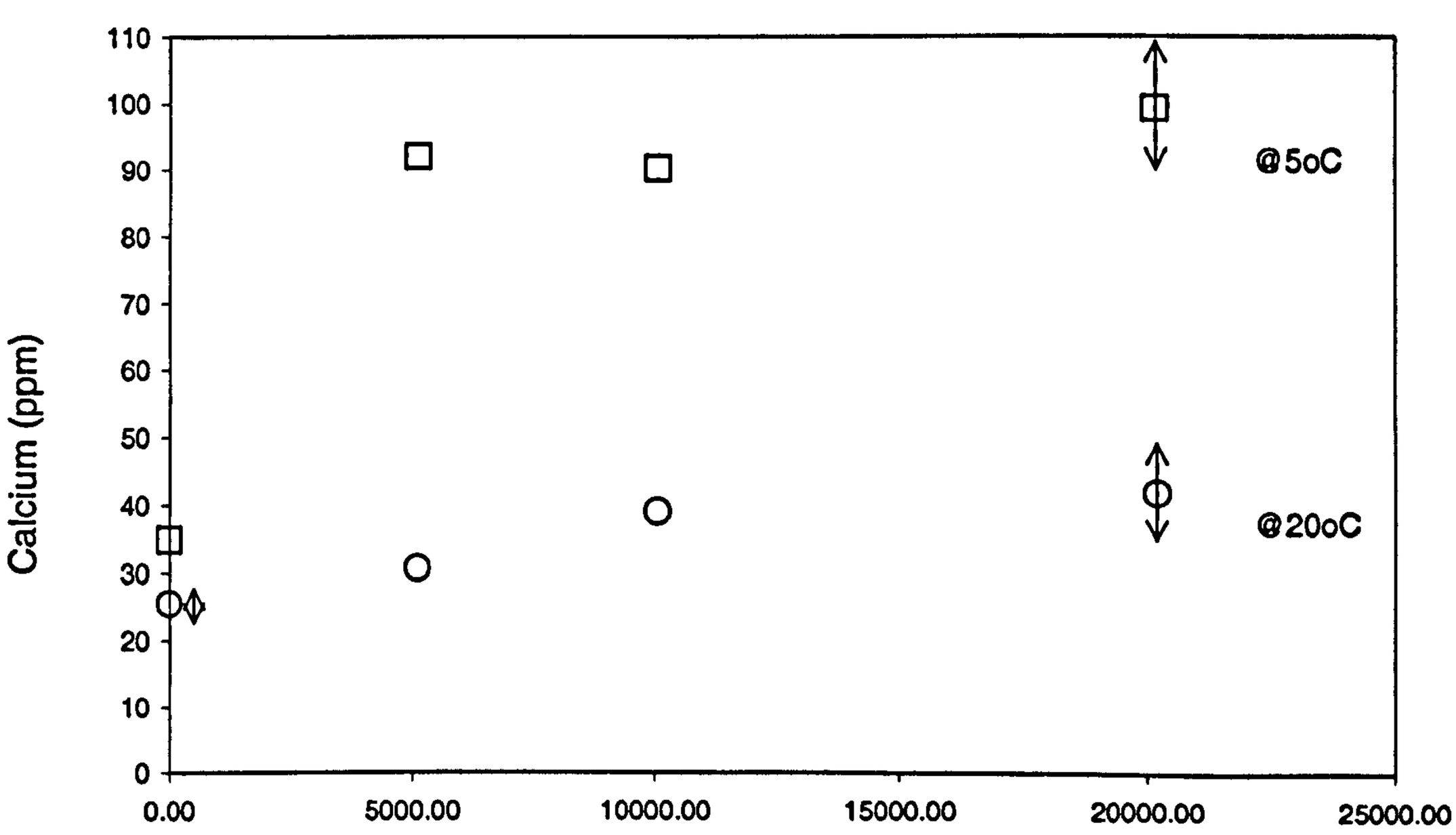

Figure AII 3: Calcium concentration of $CaCO_3$-NaCl-$MgSO_4$-H_2O-CO_2

As far as water solution is concerned, Eglinton [138] reported that 62.7 ppm of calcite is released in water in the presence of air (CO_2 pressure of 0.03%). This represents a calcium concentration of 26.55 ppm, at 18°C. In Tasong et al. [37], the calcium concentration released by calcite in water at 70°C was reported to be 30.0 ppm, but it stabilised at 25.0 ppm after 1 month. The values observed in water at 5°C and 20°C were 34.9 and 25.5 ppm, respectively, which are not only consistently similar to the expected values reported by these authors, but with the expected increase in calcium concentration due to the decrease in temperature [82].

As far as salt concentrations are concerned, the increase in the solubility of calcite can be clearly seen, since the calcium concentration reached up to 99.4 ppm and 41.0 ppm at 5 and 20°C, respectively, at 20000 ppm Cl^-.

Discussion

Figure AII-4 shows the variation of the calcium concentration relative to the calcium released in water at 20°C, according to Equation AII-1.

$$[Ca^{2+}] \text{ normalised to water @20°C: } X(\%) = \frac{100\{[Ca^{2+}]_{x,s,t} - [Ca^{2+}]_{x,w20°C}\}}{[Ca^{2+}]_{x,w20°C}} \quad \text{(AII-1)}$$

$[Ca^{2+}]$	concentration of Ca^{2+}	s	salt solution
x	calcite or gypsum	t	temperature
W_{20^oC}	water at 20°C		

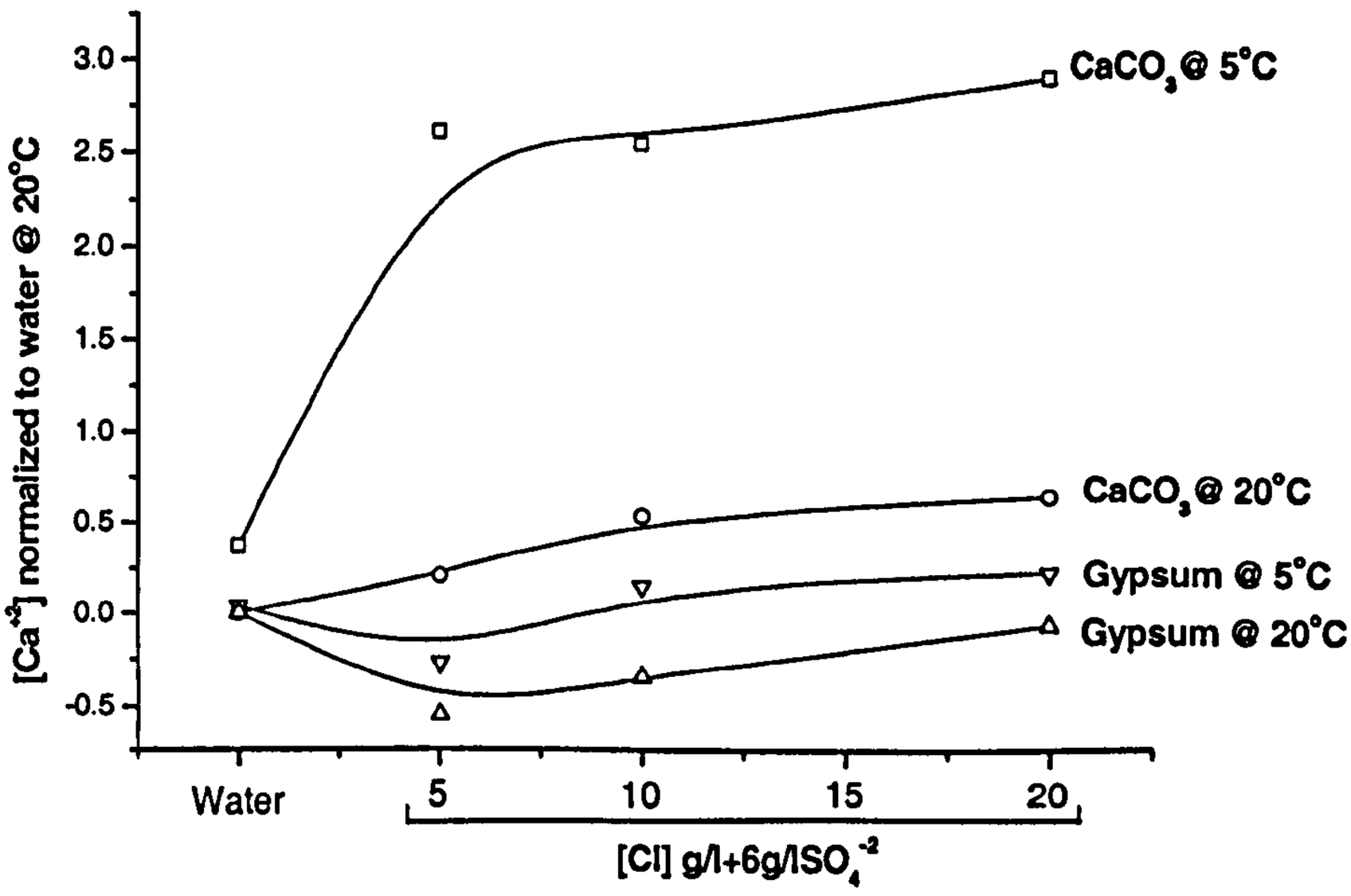

Figure AII 4: Relative concentration of calcium in $CaSO_4$-NaCl-$MgSO_4$-H_2O-CO_2 and $CaCO_3$-NaCl-$MgSO_4$-H_2O-CO_2 systems at 20°C and 5°C.

It can be seen that chloride ions affected the solubility of gypsum only slightly. However, the solubility of calcite increased as the level of chloride increased. This effect appears to be strongly controlled by temperature. The concentration of calcium was more than twice as high in combined sulfate and chloride solutions as in pure water at 5°C, and also 50% higher at 20°C.

However the presence of the combined species sodium, sulfates and magnesium did not seem to reduce the availability of calcium in solution. It is important to consider that carbonates can be bound by carbonate-containing phases other than thaumasite, such as dolomite ($CaMg(CO_3)_2$), aragonite ($CaCO_3$), trona ($NaHCO_3.Na_2CO_3.2H_2O$) or even the more soluble nahcolite ($NaHCO_3$) [12]. These sodium carbonate minerals have already been reported as a result of sulfate attack affected areas, at temperatures higher than 15°C [130]. However, the concentrations of Na^+ and Cl^- in all solutions fell along the line, which Na/Cl atomic mass ratio (0.66) is equivalent to the calculated atomic mass ratio for NaCl (0.65), as seen in Figure AII-5.

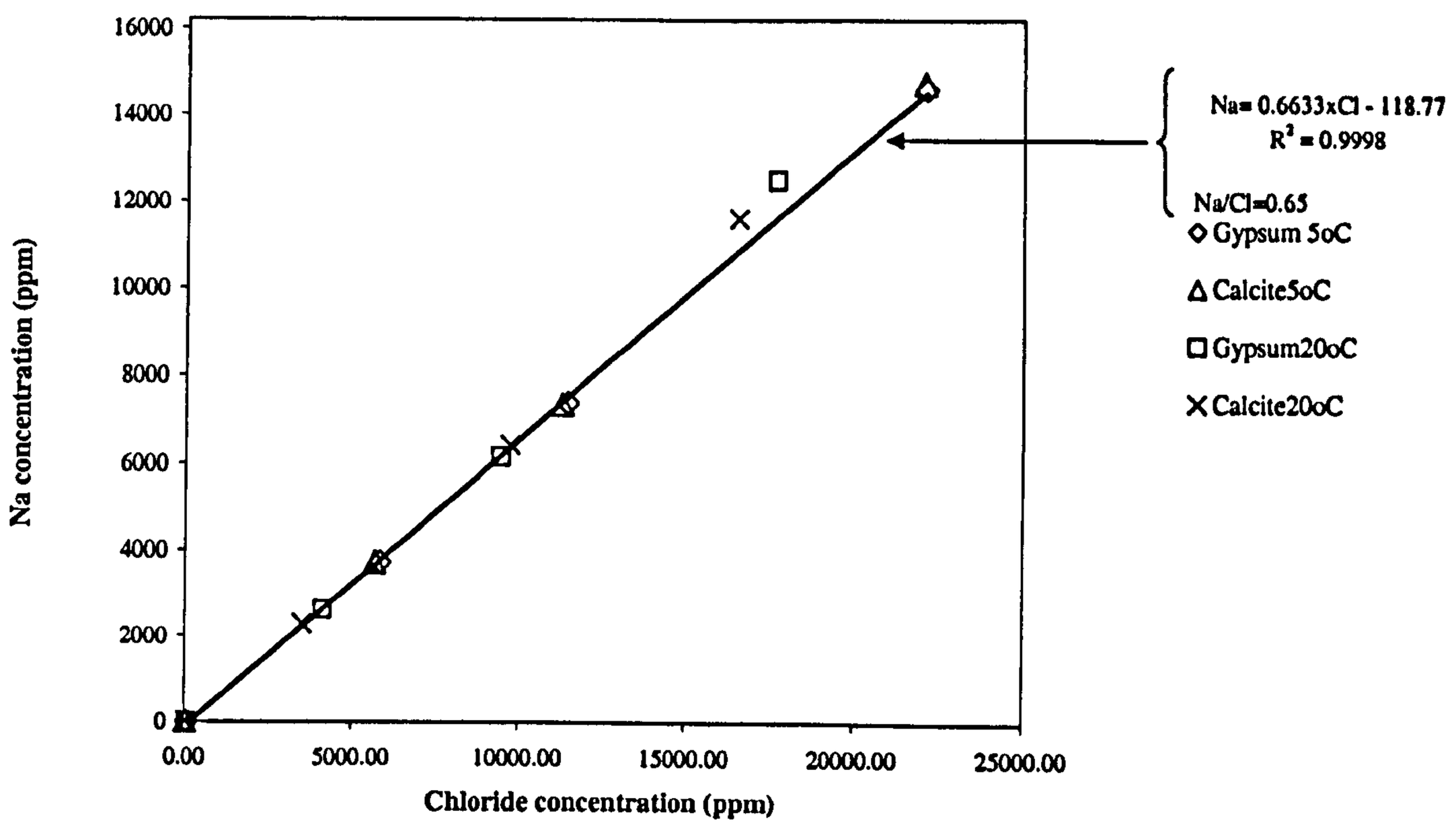

Figure AII-5: Concentration of sodium and chloride ions in water containing NaCl, epsomite, calcite and gypsum at different temperatures.

This shows that the chloride activity was the same as that of sodium, hence, indicating that no sodium carbonate phase precipitated in these solutions. In the cases observed in this thesis, aragonite ($CaCO_3$) precipitated favorably, especially at higher temperatures where the formation of thaumasite is slower. Hence, less thaumasite would be expected if the precipitation of any of these sodium or calcium carbonate minerals was kinetically faster than thaumasite.

These observations provided explanation for detrimental role that chlorides play in the formation of thaumasite, by affecting calcite solubility in the presence of atmospheric CO_2, especially at lower temperatures. Whether chloride affects calcite solubility more than atmospheric CO_2 dissolution cannot be concluded here. However, it is observed that chloride concentration increases both mechanisms of carbonate

supply to Portland cement systems, either by limestone filler already inside the concrete or via diffusion. This effect is more pronounced at lower temperatures (5°C), which can possibly explain the interactions observed in previous chapters. In pore solution chemistry, higher carbonate release would represent higher potential for thaumasite formation. This indicates that carbonate contents that are currently considered as not harmful in terms of TSA risk assessment, based on experiments in which chlorides were not involved, may have their carbonate activity doubled in the presence of chloride and other primary known risk factors. Of course, other factors such as the presence of other alkalis such as Na^+, which can reduce the solubility of calcite with the precipitation of sodium carbonate phases, must be considered as well.

Conclusion

The following conclusions can be drawn from this study:

- The presence of chloride ions affects the solubility of calcite and gypsum;
- Gypsum is slightly affected at both temperatures, but its solubility appears to decrease at the chloride concentration of 0.5%Cl^- and 0.6%SO_4^{2-};
- The solubility of calcite strongly increases in the presence of salt solutions, especially at lower temperatures (5°C), in which it reached double that in pure water;
- It is not clear whether the dissolution of calcite was more affected by the presence of sodium chloride or by the concentration of aggressive CO_2 that appears to increase with the presence of NaCl in solution (see section 7.1.8A).

A thorough investigation on the activity concerning a number of significant ions is needed, since adverse effects can be expected in the equilibrium of the thaumasite, ettringite, gypsum and cement pore solution composition.